NASA SP-320

STOL TECHNOLOGY

A conference held at
AMES RESEARCH CENTER
Moffett Field, California
October 17–19, 1972

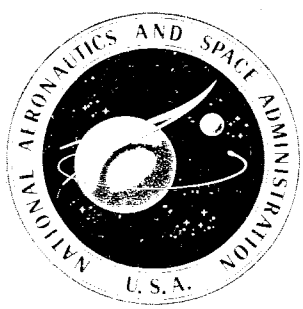

NATIONAL AERONAUTICS AND SPACE ADMINISTRATION

NASA SP-320

STOL TECHNOLOGY

A conference held at
NASA Ames Research Center
Moffett Field, California
October 17–19, 1972

Prepared by Langley Research Center

Scientific and Technical Information Office 1972
NATIONAL AERONAUTICS AND SPACE ADMINISTRATION
Washington, D.C.

For sale by the National Technical Information Service
Springfield, Virginia 22151 -- Price $6.00

PREFACE

This compilation consists of papers presented at a conference on STOL Technology sponsored by the National Aeronautics and Space Administration at its Ames Research Center, October 17-19, 1972. The presentations were made in sessions subdivided according to subject matter as follows: (1) Short-Haul Transportation Systems, (2) Aerodynamics, (3) Loads, (4) Flight Dynamics, (5) Operational Aspects, (6) Quiet STOL Propulsion, and (7) Jet Powered-Lift Noise Technology.

Contributors of the papers presented were NASA authors from the Ames Research Center, the Flight Research Center, the Langley Research Center, and the Lewis Research Center. Contributions were also made by authors or coauthors from the Federal Aviation Administration and the U.S. Army Air Mobility Research and Development Laboratory.

CONTENTS

LOADS

Session Chairman: Homer G. Morgan

FLIGHT DYNAMICS

Session Chairman: Seth B. Anderson

OPERATIONAL ASPECTS

Session Chairman: Robin K. Ransone

SHORT-HAUL TRANSPORTATION IN THE 1980's

By Leonard Roberts
NASA Ames Research Center

INTRODUCTION

The purpose of this paper is to review some of the thinking that leads to the identification of STOL aircraft as a means of improving and expanding short-haul air transportation in the United States. This thinking has been influenced to a great extent by the Department of Transportation and by the industry (the airlines and the airframe manufacturers) and the results of a number of their studies, several of which are still going on, have been made available. These studies provide a means of evaluating whether current technical programs are aimed in the right direction. They also point out the broader tradeoff that must be made between technology, economics, and the environmental factors that have become increasingly important in recent years. Paper no. 2, by Thomas L. Galloway, will discuss the characteristics of several candidate short-haul aircraft; and paper no. 3, by Elwood C. Stewart, will discuss the corresponding system analysis, including the economic and environmental factors. Additional references to previous work are to be found in the Bibliography.

For future short-haul air transportation, it is necessary to consider both the traffic demand and the air-system capacity required to accommodate it. These considerations lead to an estimate of the extent to which the future air system is likely to experience congestion and to the means of alleviating such congestion. The relative effectiveness of CTOL and STOL aircraft in providing relief from congestion and the relative costs then provide a measure of the usefulness of STOL aircraft to short-haul transportation.

TRAFFIC DEMAND AND AIR-SYSTEM CAPACITY

Figure 1 is a summary of traffic demand forecasts until the year 1995 and is based upon projections made by the Air Traffic Control Advisory Committee (ATCAC) and the Air Transport Association (ATA). This is a semilogarithmic plot and the growth rate in air traffic demand, as indicated by the shaded band, is between 10 percent and 12 percent per annum. Traffic demand is expected to reach 500 million passengers per year by 1980 and to double again during the 1980's. This growth in demand for air travel should not be surprising, since by 1980 the average American will be able to travel between any two points in the continental United States for less than 1 percent of his annual salary. However, actual growth in air travel can take

place only if the capacity of the air system undergoes a corresponding growth. In this regard the experience of the last decade suggests that very few new large airports will be built; thus any major expansion of capacity must be accomplished by other means.

The use of conventional aircraft to the greatest extent permitted will undoubtedly continue, and figure 2 summarizes some of the ways that may be used to expand the capacity of the CTOL system. First the number of passengers per aircraft can be increased by the introduction of wide-body aircraft and by increasing the load factor from the current level of 55 percent to perhaps 65 percent. It is estimated that these two changes would expand the current air-system capacity by 80 and 18 percent, respectively. Taken together this would double the number of passengers without increasing the number of aircraft. Beyond that, the number of aircraft can be increased, both by rescheduling aircraft movements to avoid peaking and by reducing separation between aircraft. This would further increase the capacity of the air system by about 50 percent. This increase in capacity is compared with the growth in demand in figure 3. Despite the increase, capacity will cease to keep up with demand after about 1980. The result will be severe congestion of the airways and the air system more generally. This would have the effect of reducing demand, of course, but this is hardly a satisfactory solution.

It should be pointed out that the assumptions made with regard to increasing capacity may be overly optimistic in view of the following offsetting factors:

The introduction of wide-body aircraft must take into account the substantial investment that exists in the current narrow-body aircraft.

Increases in load factor to levels approaching 65 percent are generally accompanied by a reduction in the quality of service to the traveling public. Elimination of traffic peaks may have the same effect.

Finally, separation distances may be constrained by the trailing-vortex hazard, and reductions in aircraft spacing may be difficult to achieve in practice.

If these difficulties are indeed encountered, traffic demand may exceed the air-system capacity before 1980. Perhaps more significantly, even if additional capacity can be provided, the amount of traffic passing through the airport and ground access system at major hubs will triple in the process and the problem is merely passed on to the land side of the airport.

Thus, the probable situation faced by CTOL transportation in the 1980's can be summarized in these terms: Demand will greatly exceed airport capacity; congestion and increased air-travel costs will result; short-haul traffic will be displaced from major airports. Evidently by the end of this decade the means of redistributing air traffic to provide relief for the major airports must be found and must be in a way that is economically and environmentally acceptable.

It is clear that new short-haul aircraft and additional short-haul airports will be required and it is in this context that the costs and the benefits of STOL aircraft must be considered.

COSTS AND BENEFITS OF STOL AIRCRAFT

With respect to costs, figure 4 shows the variation of direct operating cost (DOC) as field length is reduced from 4000 feet (1200 m) to 1500 feet (450 m). These DOC's are conservative in the sense that they are the highest costs found in the studies to be reported in paper no. 2 by Thomas L. Galloway. The increase in DOC for the STOL requiring a field length of 4000 feet (1200 m) over the level enjoyed by CTOL (approximately $1\frac{1}{2}$¢/mile) is a result of achieving a lower noise level of 95 EPNdB for the STOL aircraft. Further increases in DOC for the STOL aircraft result from increasing engine costs (increased thrust/weight) as field length is reduced. In practice it may be possible to offset some of this increase in DOC through reductions in indirect operating costs for STOL aircraft, although such reductions are not assumed in this paper.

Presumably the DOC increases depicted in figure 4 would be reflected in the fare structure, and figure 5 depicts the extent to which typical fares could increase. Here, fare is shown as a function of trip distance and the solid line labeled CTOL (no congestion) corresponds to the current CAB rates of \$12 plus 6.3¢/mile. Also shown is the band corresponding to STOL aircraft requiring field lengths between 4000 and 1500 feet (1200 and 450 m) and having DOC's between 3¢/mile and 5¢/mile.

The STOL fares are higher than CTOL fares, as expected. The most likely alternative to STOL, however, is a congested CTOL system, and assuming that the costs of congestion are reflected in the fares, the resulting CTOL fare levels may be substantially higher than those enjoyed by current CTOL passengers. These "congested" fare levels are shown in the shaded region at the upper left-hand part of figure 5. The lower boundary to this region is based on a fare that includes the cost of an average delay of 24 minutes per flight, corresponding to a traffic demand that exceeds capacity by 10 percent. (The airlines' experience of congestion in 1968 showed that a cost of \$30 per passenger was incurred for each hour of delay, so that a 24-minute delay would cost about \$12 per passenger.)

The point is that even with only a 10 percent excess demand over capacity, the resulting delays would cause CTOL fares to exceed those of a STOL system operating from alternate airports. Of course, the ability of a STOL system to relieve air congestion will depend on how many secondary airports can be made available. In this regard, it should be recognized that the area impacted by noise can be reduced, and therefore the number of quiet STOL airports increased, by going to aircraft with the capability for

shorter field lengths. Thus both the costs and the benefits increase as field length is reduced.

The nature of the tradeoff that must be made between costs and benefits is shown in figure 6; the 400-mile fare and the percentage of airports (from a typical sample) which could contain the 95-EPNdB contour are shown as a function of aircraft field-length capability. The fare, shown on the vertical scale, varies in the range of $43 to $51 and increases as the aircraft field length decreases. On the other hand, the percentage of airports that can be used also increases as the field length decreases, on the basis of the criterion that an airport is acceptable if the 95 EPNdB contour is entirely contained within its boundaries.

There are two points to be made. First, on the basis of this criterion, only 40 percent of the airports can accommodate an airplane requiring a field length of 4000 feet (1200 m), whereas 90 percent of the airports can accommodate the STOL requiring a field length of 2000 feet (600 m). Second, for further reductions to field lengths below 2000 feet (600 m), the costs increase rapidly without the benefit of many new airports becoming available. Evidently further consideration should be given to the region near the knee of the curve, between 3000 and 2000 feet (900 and 600 m), in order to establish the best field length for short-haul aircraft.

CONCLUDING REMARKS

Several conclusions can be drawn from the considerations that have been summarized in this paper. A comparison of anticipated demand for air travel with the capacity of the air system suggests that growth in air transportation will be limited in the 1980's by severe congestion. Thus, new aircraft and additional airports will be required to permit a redistribution of traffic away from major airports. The availability of additional airports, however, will depend on the aircraft noise level and field-length capability. Such conclusions, of course, depend on certain assumptions and many of these will not be validated until a number of questions are resolved.

Among these questions are: What growth in travel demand will actually occur over the next decade? What increases in CTOL capacity can be realized? How can the airport access problems be resolved? How quiet can STOL aircraft be made? What is the likelihood of adding STOL airports to the system?

The answers to many of these questions will depend on how rapidly the STOL technology is advanced, particularly in the areas of quiet propulsive lift and in the use of avionics for flight-path control. And, of course, it is the primary purpose of this conference to report some of the recent advances that have been made in these areas. It has been the intention of this paper to provide a reminder of both the potential of STOL aircraft

and some of the problems that must be resolved before they can become part of the nation's air transportation system. The technology and application of these aircraft will be discussed in detail in the ensuing papers.

BIBLIOGRAPHY

1. Anon.: Civil Aviation Research and Development Policy Study – Report. NASA SP-265, 1971. (Also available as DOT TST-10-4.)

2. Anon.: Civil Aviation Research and Development Policy Study – Supporting Papers. NASA SP-266, 1971. (Also available as DOT TST-10-5.)

3. Air Transport Association of America, 1970 Air Transport Facts and Figures, Washington, D.C.

4. Transportation Association of America, Transportation Facts and Trends, 7th Edition, April 1970, Washington, D.C.

5. Civil Aeronautics Board, Handbook of Airline Statistics, 1969 Edition, U.S. Government Printing Office, Washington, D.C., 1970.

6. Anon.: R&D Plan To Increase Airport and Airway System Capacity – Program Description. AD 707 186, FAA, May 1970.

7. Loftin, Laurence K., Jr.: Aeronautical Vehicles – 1970 and Beyond. AIAA Paper No. 70-1262, Oct. 1970.

TRAFFIC DEMAND
1965 - 1995

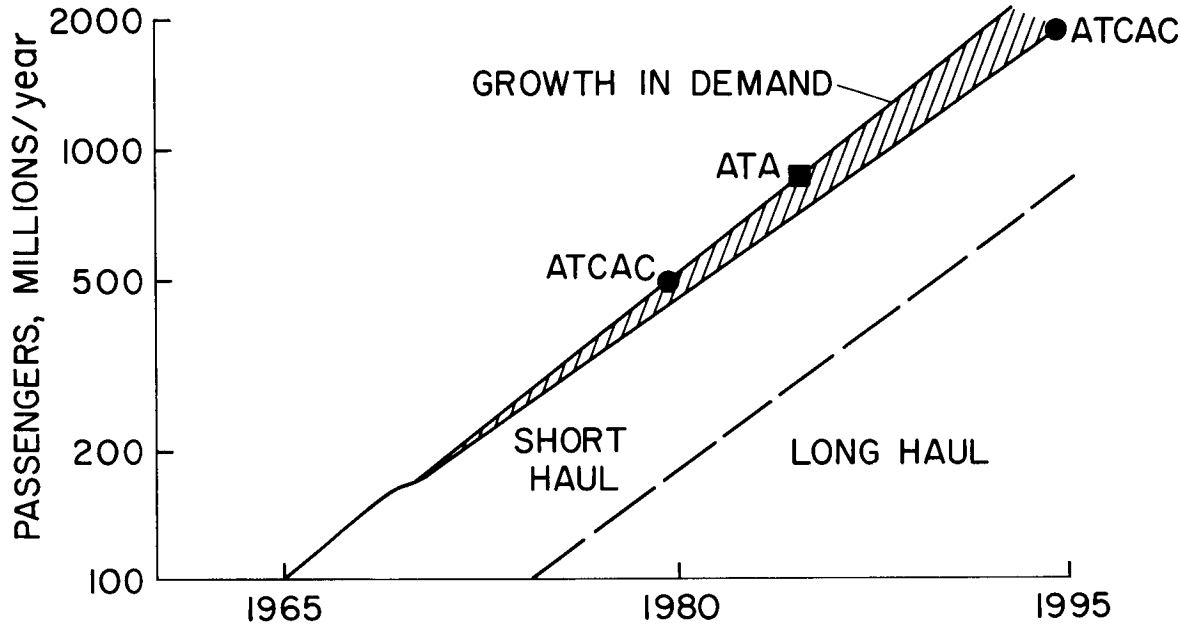

Figure 1

POSSIBLE INCREASE IN CTOL CAPACITY

INCREASE PASSENGER/AIRCRAFT

- ALL WIDE BODY AIRCRAFT 80%
- LOAD FACTOR OF 65 percent 18%

INCREASE NUMBER OF AIRCRAFT

- ELIMINATE TRAFFIC PEAKS 25%
- REDUCE SEPARATION DISTANCE 25%

Figure 2

TRAFFIC DEMAND/AIRPORT CAPACITY

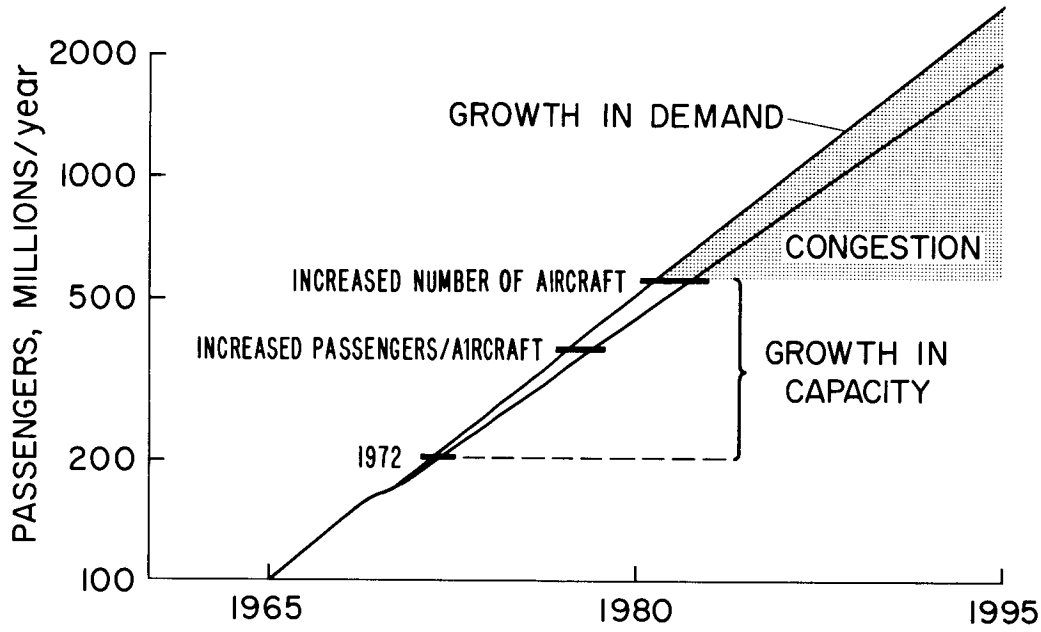

Figure 3

COST OF REDUCED FIELD-LENGTH CAPABILITY

100 PASSENGER AIRCRAFT

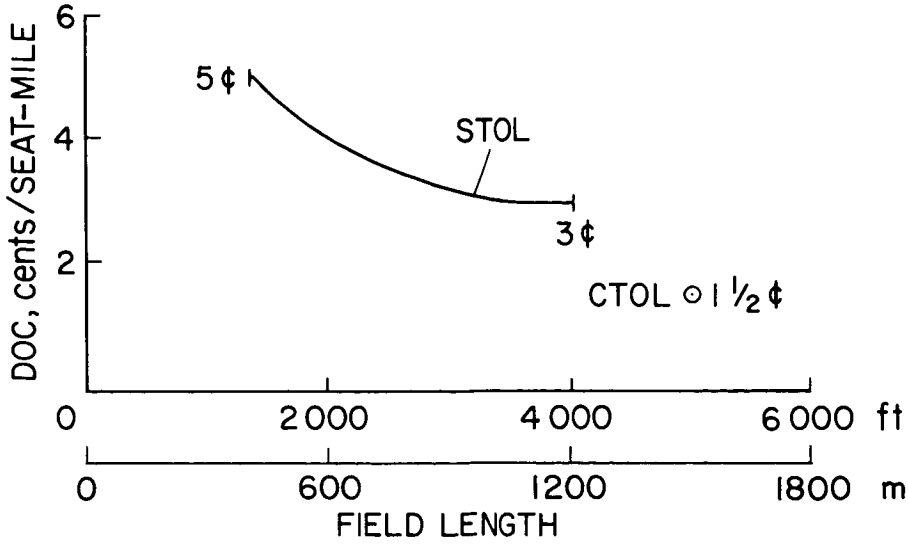

Figure 4

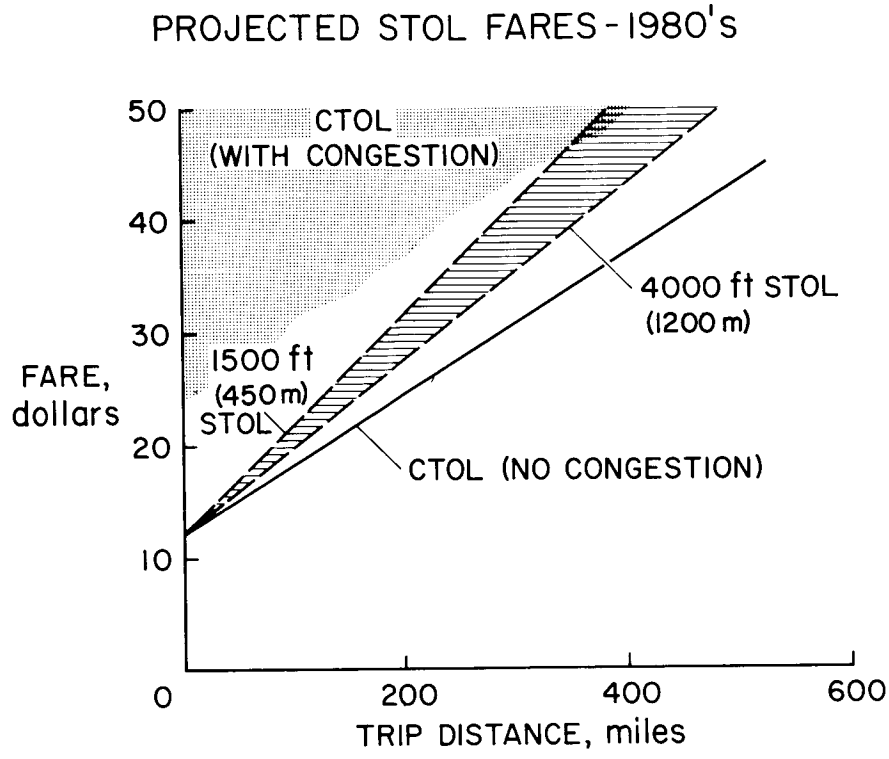

Figure 5

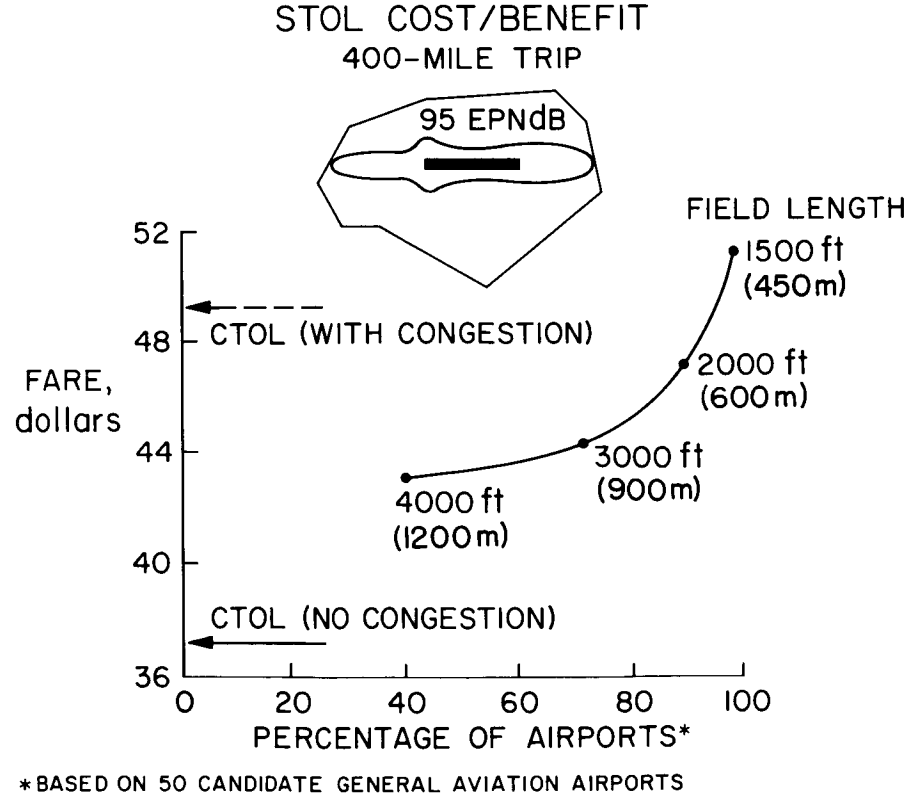

Figure 6

FUTURE SHORT-FIELD AIRCRAFT

By Thomas L. Galloway
NASA Ames Research Center

INTRODUCTION

Quiet short take-off and landing aircraft are being proposed for improving short-haul air transportation. Several turbofan-powered aircraft concepts for obtaining short-field performance have been investigated in the past. NASA currently has two contracts with industry to study quiet-turbofan short-field aircraft in short-haul air transportation systems. The contractors are Lockheed and McDonnell Douglas. Paralleling these studies are STOL propulsion system studies by Allison and General Electric. The propulsion studies are discussed in paper no. 33 by Robert J. Denington, Robert W. Koenig, Michael R. Vanco, and David A. Sagerser.

The Lockheed and Douglas studies are divided into two phases with the following objectives:

(1) Determine the relationships between quiet-turbofan STOL aircraft characteristics and the economic and social viability of short-haul air transportation.

(2) Identify critical technology and technology-related problems to be resolved in successful introduction of representative STOL short-haul systems.

(3) Define representative aircraft configurations, their characteristics, and the costs associated with their development and operation.

(4) Identify desirable technology advances for improving STOL short-haul systems.

Phase I, completed in October 1972, was an evaluation of potential concepts aimed at defining a reasonable number of configurations for detailed analysis of phase II. This meets the first part of objective (1). The detailed analysis of phase II, which will be completed in May 1973, in addition to detailed aircraft design, will investigate in depth the economic, social, and technological factors associated with STOL systems. This meets the remaining objectives outlined above. This paper draws mainly on data generated during the phase I portion of the studies to evaluate short-field concepts.

AIRCRAFT PARAMETRIC EVALUATION

The aircraft will be evaluated on the basis of performance, noise, weight, and direct operating cost. With regard to performance, the field length, wing loading, and thrust characteristics of the lift concepts will be investigated. The noise level of

95 PNdB at a 500-ft (150-m) sideline was a design requirement and its effect on direct operating cost will be evaluated. Weight and direct operating cost will be evaluated on the basis of field length, passenger size, and lift concept.

There are many potential design concepts that can be considered in the parametric evaluation. A matrix of aircraft using various high-lift systems and design parameters was considered during phase I of the studies.

Five lift systems were included and a range of design parameters investigated, as outlined below:

Propulsive lift concepts –

- Externally blown flap (EBF)
- Upper-surface blown jet flap (OTW)
- Augmentor wing (AW)
- Internally blown jet flap (IBF)

Aerodynamic lift concept –

- Mechanical flap (MF)

Design parameters –

- Passenger capacity: 50, 100, and 200
- Field length: 1500, 2000, and 3000 ft (450, 600, and 900 m); sea level, 95° F (308 K)
- Cruise Mach number: 0.70, 0.75, and 0.80
- Range: 500 nautical miles (926 km)
- Noise: 95 PNdB at 500-ft (150-m) sideline

The design parameters listed above were investigated for each lift concept. The aircraft in this parametric analysis all had four engines and used conventional aircraft technology. The feasibility of twin-engine configurations as well as the use of composite materials on some of the concepts is being investigated in the second phase of the studies.

REPRESENTATIVE CONFIGURATIONS

Figures 1 to 6 illustrate representative aircraft configurations for three of the propulsive lift concepts – the EBF, the OTW, and the AW. The contractor associated with the configuration is identified in each figure. These configurations show different design philosophies but, since they are not to the same scale, direct comparisons are not appropriate.

The externally blown flap designs of figures 1 and 2 are characterized by high-bypass-ratio engines. Lockheed used the siamese engine arrangement to reduce nacelle interference effects and ease the engine-out problem whereas Douglas used the more

conventional engine arrangement. The over-the-wing configurations are shown in figures 3 and 4. Again, the Lockheed design has the high-bypass-ratio engines in a siamese arrangement on a high-wing configuration, whereas the Douglas design has a low wing with separated engines. The augmentor-wing configurations are shown in figures 5 and 6. These two configurations are similar and are distinguished from the externally blown flap configurations by their smaller diameter, lower bypass ratio engines.

DESIGN METHODOLOGY

The design methodology used in evaluating the matrix of potential designs was to determine the design that had the minimum direct operating cost and met the particular field length, cruise, and mission requirements. The methodology also allowed for the evaluation of the various engine cycles from the propulsion studies to determine the cycle that minimized direct operating cost.

The methodology is shown schematically in figure 7. For a given field length, design range, passenger size, and lift concept, the thrust-weight ratio (T/W) required for the design to meet the various requirements is shown as a function of wing loading (W/S). The solid lines represent the take-off and landing thrust requirements for the given field length. The position of these lines depends on aerodynamic characteristics of the lift system and thrust lapse rate of the engine cycle. The cruise thrust requirement is represented by the dashed line. Two dashed lines are shown to represent different cruise thrust requirements as might be affected by increasing cruise Mach number (inc. M) or decreasing engine fan pressure ratio (dec. FPR).

Also shown in figure 7 is the resulting direct operating cost (DOC) of the potential designs as a function of wing loading. The direct operating cost follows the trend of the cruise-thrust-requirement curve. Since it is desired to have a design that minimizes direct operating cost, this means that the design which matches the field length and cruise thrust requirements is the minimum-direct-operating-cost design. Such designs are indicated by the symbols in figure 7 for the two conditions.

AIRCRAFT EVALUATION RESULTS

Using the methodology previously described, the various concepts were evaluated on a consistent basis. The results will be discussed in this section of the paper.

Consider, first, the relationship between field length and wing loading shown in figure 8. The two bands presented represent the general trend in wing loading for the designs investigated in the study. The field lengths shown in this figure and in the figures that follow are based on the requirements of Federal Air Regulations, Part 25, for sea-level, 95° F (308 K) conditions (ref. 1). For ride qualities comparable to current

jet aircraft, it is desirable to be at or above an 80-psf (3.8-kN/m^2) wing loading. For the powered-lift concepts, this can be accomplished for field lengths of 2000 ft (600 m) or more. For the mechanical flap, field lengths of 3500 ft (1050 m) or more would be required unless a ride-smoothing or gust-alleviation system is incorporated in the design. Except for the Lockheed OTW concept, all the powered-lift concepts investigated fell within the shaded band. The Lockheed OTW concept showed the potential of obtaining wing loadings 20 to 30 percent higher than the powered-lift region. However, at the time of analysis, the data base was very limited. It is felt that when the data are analyzed in detail and the appropriate corrections are made for wing planform, engine installation, and forward speed, the data will be similar to those for the other externally blown systems.

The thrust requirements for the concepts will be investigated by taking a fixed field length of 2000 ft (600 m). Figure 9 shows the thrust-weight ratio required for the mechanical flap, externally blown flap, and augmentor wing as a function of wing loading. The shaded regions represent the trend in thrust requirements for the three concepts. The mechanical flap is limited to wing loadings below 50 psf (2.4 kN/m^2) to meet the landing requirements. The EBF has high thrust requirements – at wing loadings between 60 and 75 psf (2.9 and 3.6 kN/m^2) to meet the take-off requirement and above 75 psf (3.6 kN/m^2) to meet the landing requirement. The augmentor wing has the lowest thrust requirements and is take-off critical for all wing loadings shown. The shaded bands represent many potential designs. The symbols in figure 9 are the designs that minimize direct operating cost and meet both the field length and cruise requirements.

All things being equal, moving toward the lower right-hand corner of figure 9 should result in lighter vehicles. However, all things are not equal, and the weights for the powered-lift concepts are quite similar, as shown in figure 10. In this figure, gross weight is shown as a function of field length for the 100-passenger-size aircraft. The powered-lift concepts shown by the shaded bands and the mechanical flap shown by the solid lines represent designs which minimize direct operating cost. As a point of reference, the take-off weight of a DC-9 airplane performing the same mission (100 passengers and 500 nautical miles (926 km)) is about 96 000 lb (427 kN).

As can be seen in figure 10, there is a difference in weight between the two contractor designs. Through an independent in-house analysis, the factors that contribute to these differences have been identified as shown in figure 11. With the design parameters of M = 0.75, 100 passengers, and 2000-ft (600-m) field length, the Lockheed and Douglas designs of an EBF configuration were simulated by the sizing and performance program. The bar on the left in each group represents the simulated Lockheed design, whereas the bar on the right represents the simulated Douglas design. The thrust per engine differed by 14 000 lb (62 kN) and the gross weight by 45 000 lb (200 kN). The second bar of each group accounts for that part of the difference resulting from differences in engine installation losses and drag during cruise. Higher drag estimates and

larger engine losses resulted in the Douglas design having higher thrust requirements for cruise. This led to higher wing loadings and higher thrust loadings to meet both the cruise and field-length requirements. (Compare fig. 7.) The difference in drag and engine installation losses accounted for one-half of the thrust difference and one-seventh of the weight difference. The third bar in each group in figure 11 accounts for that part of the difference resulting from differences in weight estimating factors. This difference was mainly in the subsystems area of furnishing, hydraulics, electrical, electronics, and cabin environment. These differences accounted for three-fourths of the gross-weight difference and one-half of the thrust difference.

The increasing trend in gross weight with reducing field length and in the difference between contractor designs shown in figure 10 is also reflected in direct operating cost as shown in figure 12. Direct operating cost in cents per available seat statute mile (ASSM) is shown as a function of field length for the 100-passenger-size vehicles. The powered-lift concepts can all be represented by the narrow bands and show a sharp increase below a field length of about 2000 ft (600 m). The smaller, 50-passenger concepts which were investigated had DOC's at or above 5 cents per seat mile, whereas the 200-passenger-size concepts had DOC's below the 100-passenger-size vehicles. The DOC's shown in figure 12 are higher than those for current short-haul aircraft. However, it must be remembered, current aircraft have lower thrust-weight ratios, have unit costs based on past development programs, and are noiser than the short-field concepts represented in figure 12.

A measure of the relative effect of low noise and short-field length on direct operating cost is shown in figure 13. This figure shows the direct operating cost of various design points normalized to a design with noise characteristics similar to current short-haul aircraft, 113 PNdB at 500-ft (150-m) sideline. When the design must meet the noise requirement of 95 PNdB at 500 ft (150 m), the DOC increases by about 30 percent. The increasing trend with reducing field length is the same as was previously shown.

Up to this point, the comparisons have mainly considered 100-passenger-size vehicles. To get a feel for the appropriate passenger size, the return on investment (ROI) was used as a screening parameter. Figure 14 shows the results for a typical high-density market. Each grouping represents a field length, a range of passenger sizes, and a range of cruise Mach numbers (M_{CR}). ROI, in the context used here, measures the ability of the aircraft to return to the investor the value of the investment, plus a profit, over a designated life span. ROI is decreasing as field length is reduced due to the increasing DOC. The 50-passenger vehicles have significantly lower ROI's than the 100- to 200-passenger size because of high DOC's, with the optimum occurring at about 150 passengers regardless of field length. ROI was not sensitive to cruise Mach number for the range of Mach numbers investigated.

CONCLUSIONS

In summary, the following conclusions are reached regarding future short-haul aircraft having short-field capability:

1. Propulsive lift concepts cannot be separated on the basis of direct operating cost.

2. The noise constraint of 95 PNdB strongly influenced direct operating cost.

3. Fifty passenger and 1500-ft (450-m) field-length vehicles have high direct operating costs.

4. The 150-passenger-size aircraft appears optimum for high-density markets.

5. Significant uncertainties exist in estimating aerodynamic and propulsion performance, and weight which indicates additional work is needed to fully understand these areas.

These conclusions are those that result from only analyzing the vehicles. How these vehicles fit into a short-haul air-transportation system that is socially and economically viable are highlighted in the companion papers by Leonard Roberts (paper no. 1) and Elwood C. Stewart (paper no. 3).

REFERENCE

1. Anon.: Airworthiness Standards: Transport Category Airplanes. FAR Pt. 25, FAA, Feb. 1, 1965.

EBF CONFIGURATION

LOCKHEED

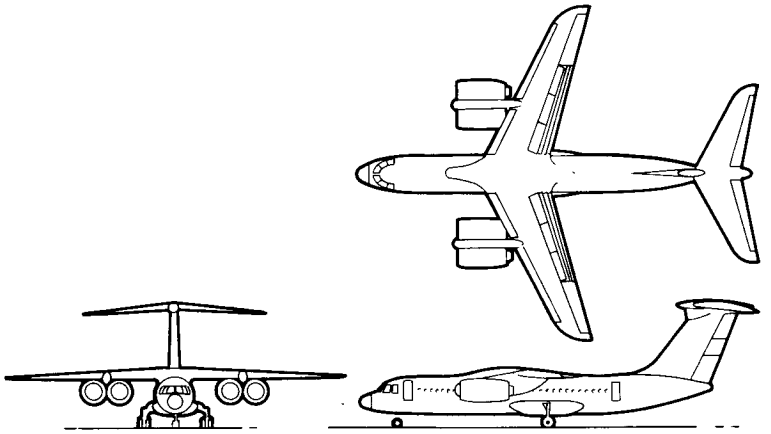

Figure 1

EBF CONFIGURATION

DOUGLAS

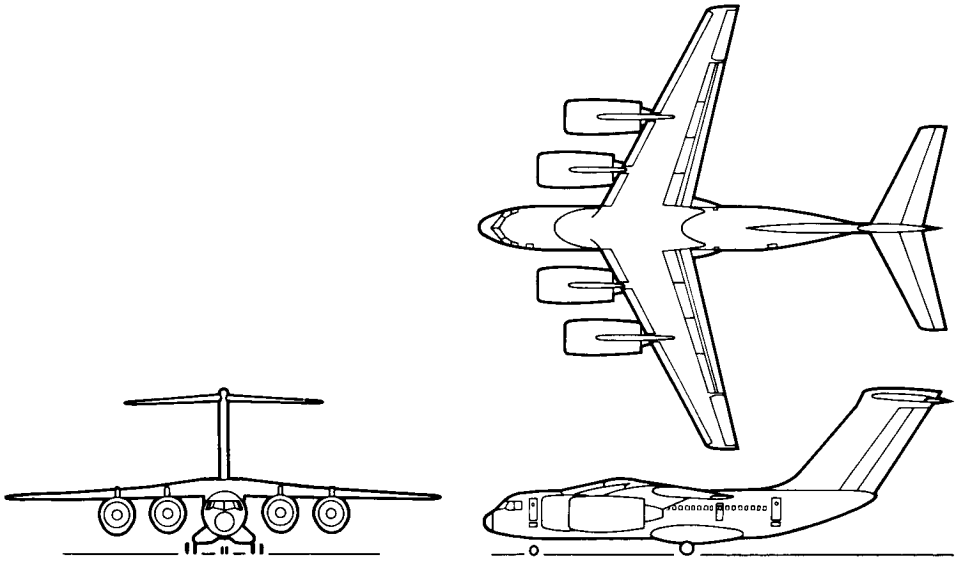

Figure 2

OTW CONFIGURATION

LOCKHEED

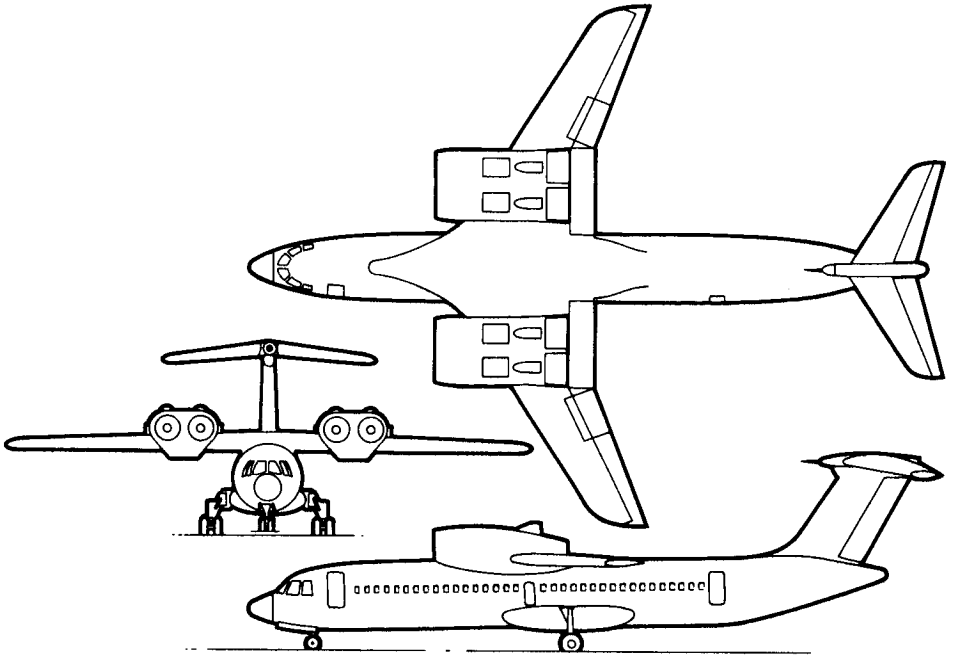

Figure 3

OTW CONFIGURATION

DOUGLAS

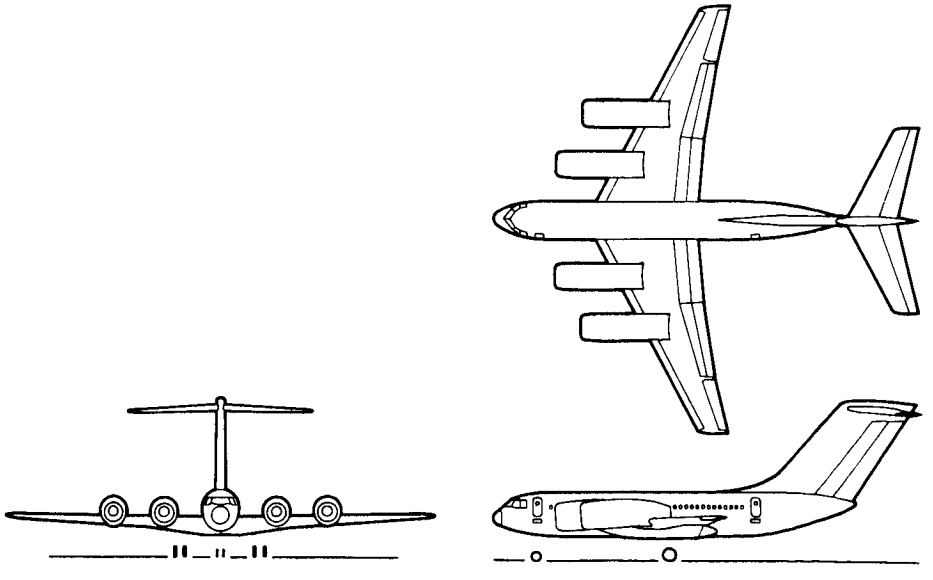

Figure 4

AW CONFIGURATION

LOCKHEED

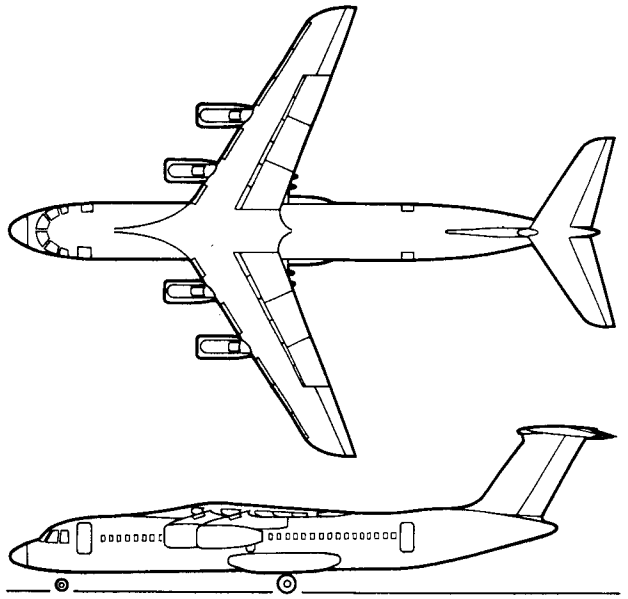

Figure 5

AW CONFIGURATION

DOUGLAS

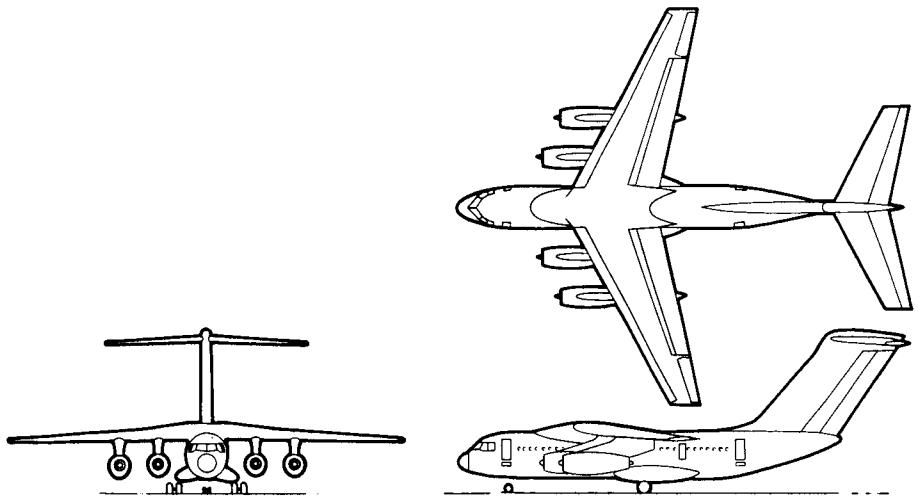

Figure 6

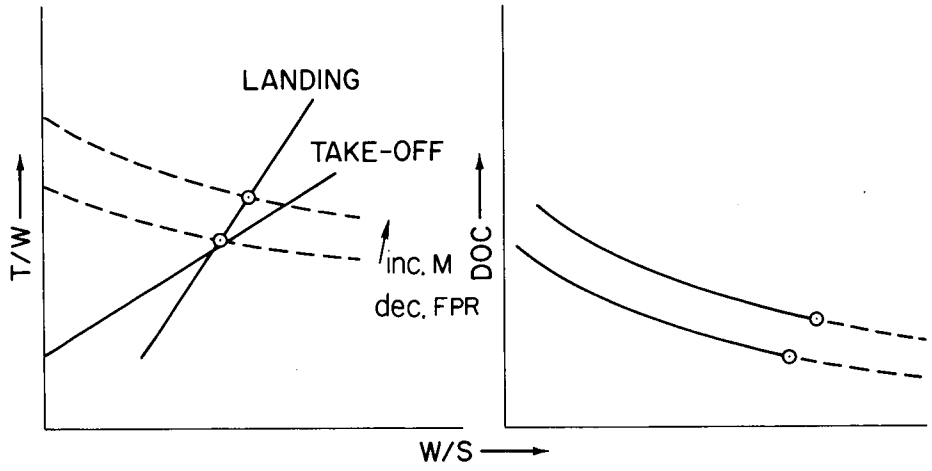

Figure 7

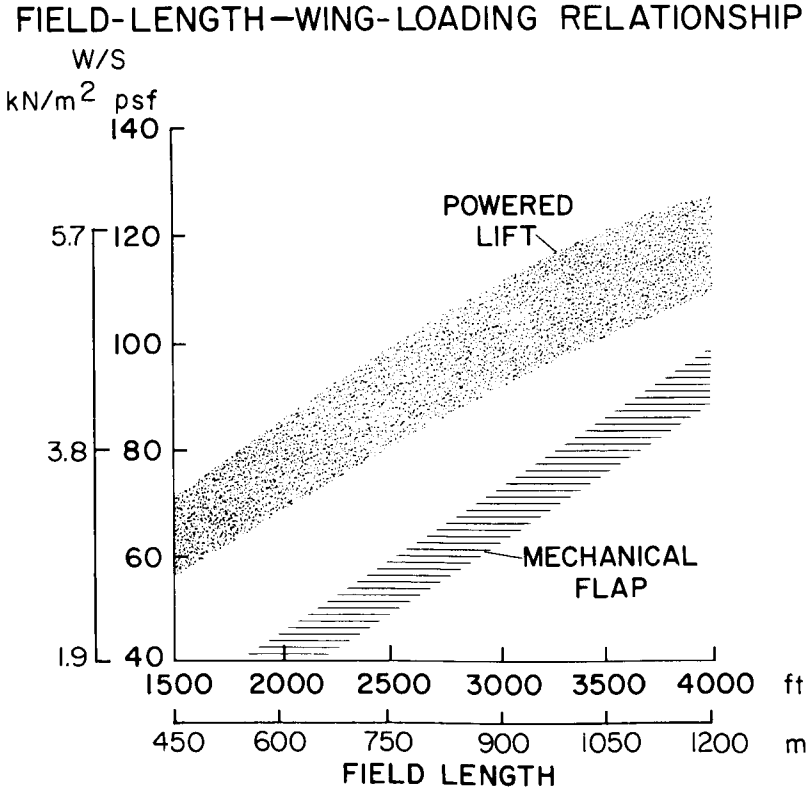

Figure 8

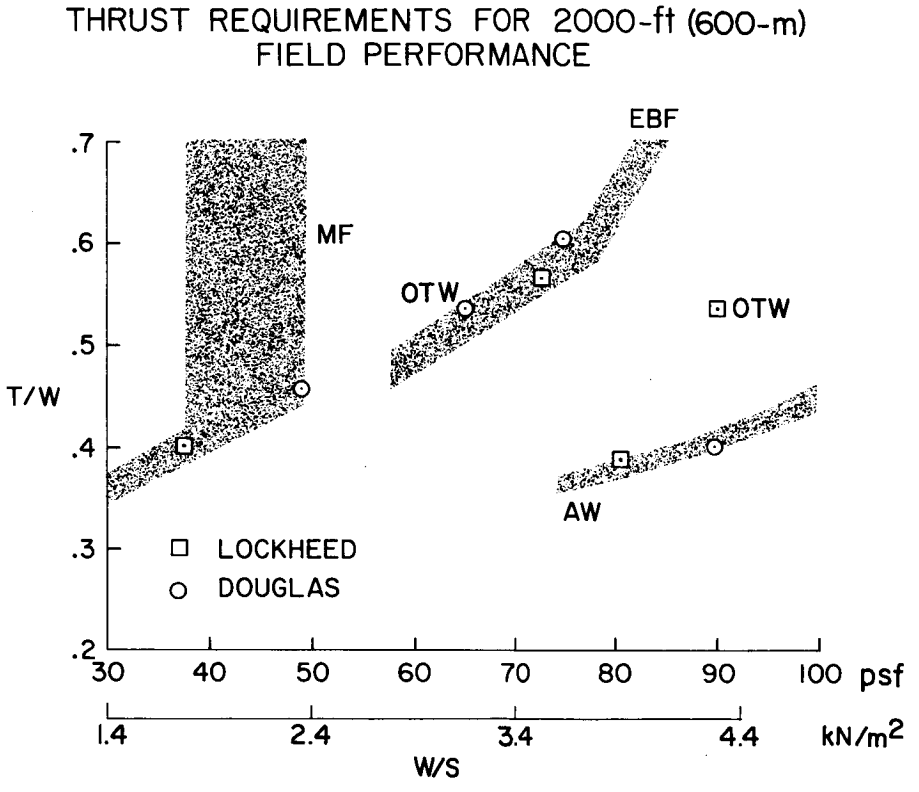

Figure 9

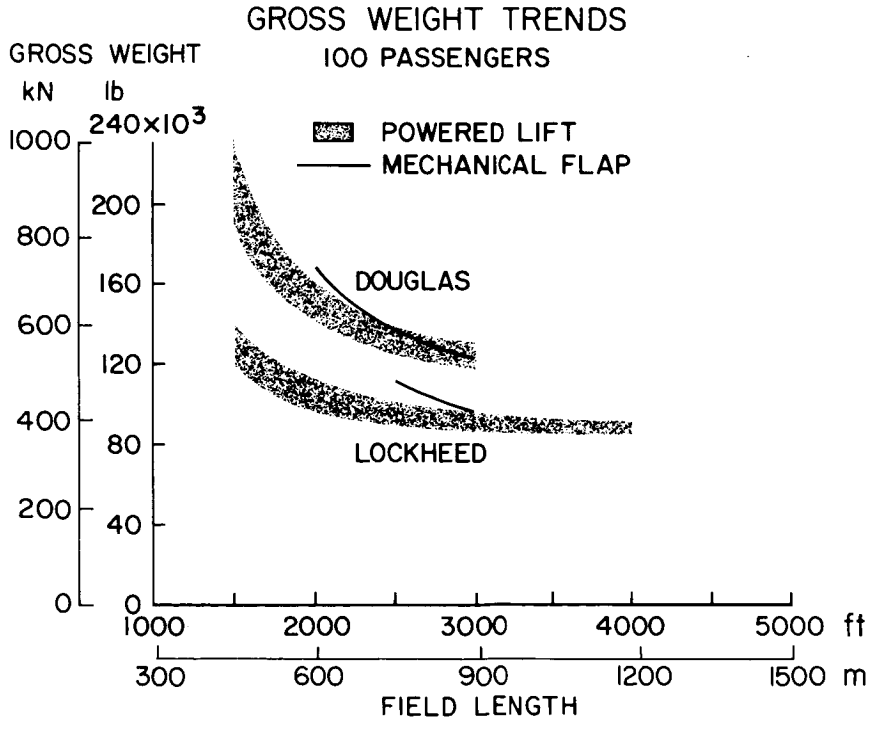

Figure 10

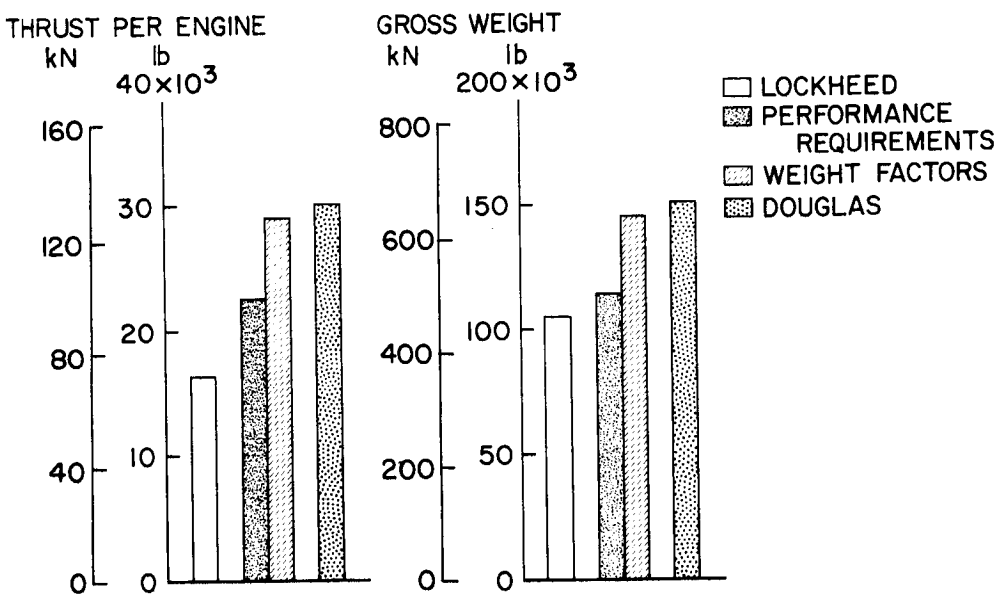

Figure 11

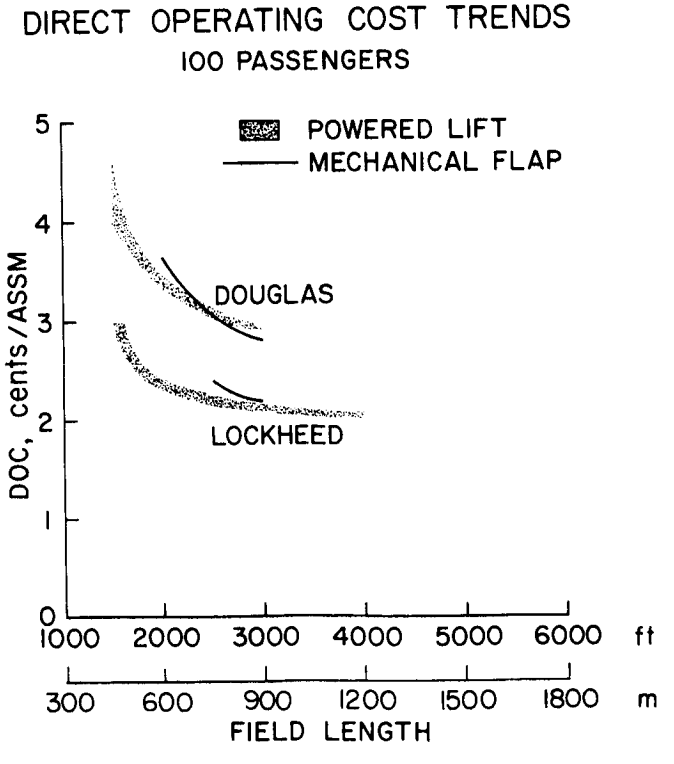

Figure 12

DOC SENSITIVITY

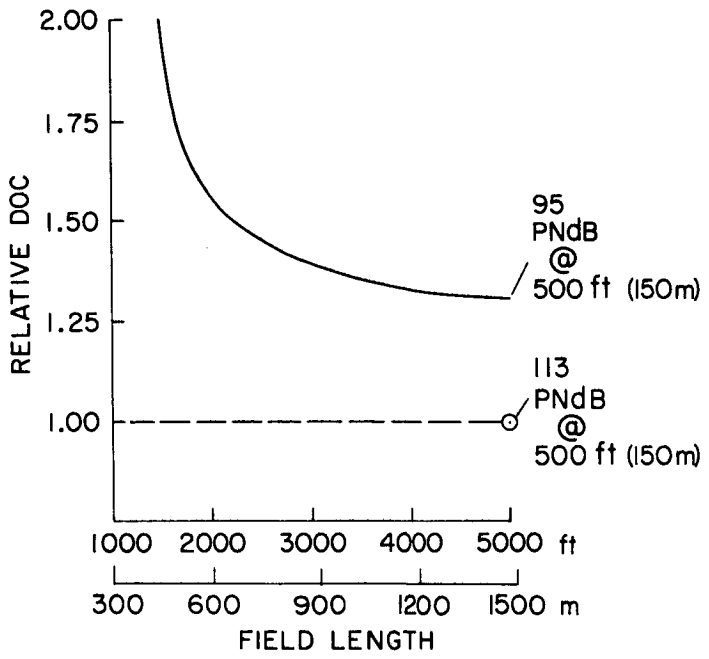

Figure 13

RETURN ON INVESTMENT SENSITIVITY

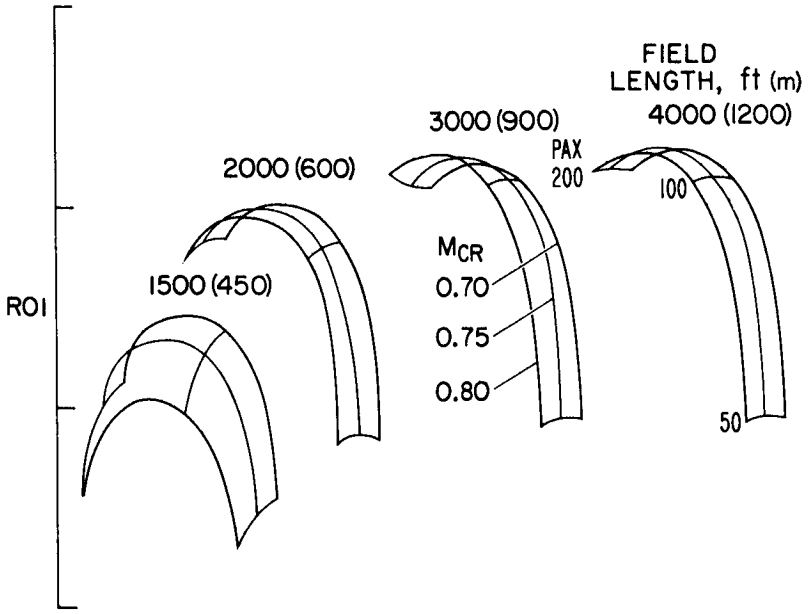

Figure 14

ECONOMIC AND ENVIRONMENTAL ASPECTS OF STOL TRANSPORTATION

By Elwood C. Stewart
NASA Ames Research Center

INTRODUCTION

Some interim results of a systems study of STOL transportation will be discussed in this paper. These results are based on a study being done by The Aerospace Corporation for the Ames Research Center. However, since the study is currently only half completed, the discussion will be in the nature of a progress report. An attempt will be made to present an overview of the study and its objectives and some of the results that are beginning to emerge.

The systems study to be discussed herein concerns the question of the impact of advanced STOL aircraft in meeting the needs of a short-haul transportation system. By careful consideration of the objectives which the short-haul system should achieve, it is believed that evaluation should be made in terms of the following criteria:

1. Service to the passenger
2. Economic viability
3. Environmental criteria
    a. Community noise
    b. Ground and air decongestion
    c. Air pollution

The first item, service to the passenger, is best measured in terms of the number of passengers the system will attract and is of obvious importance if the system is to serve a useful purpose. Economic viability is readily measured in terms of the return on investment (ROI); interest will center on different levels of return on investment in order to cover the range between the maximum level permitted by regulating agencies and a low level which would correspond to subsidized operation. The environmental criteria to be considered include the impact of STOL system noise on the community surrounding the airports, the ground and air decongestion which might be achieved at the major CTOL hubs, and the effect on air pollution.

METHODOLOGY

To accomplish the preceding objectives, the characteristics of the advanced STOL aircraft and its operational capabilities will be of obvious importance and interest. However, this is clearly not sufficient, since the aircraft is only part of a much

larger system with which it must interface. This larger system, which is to be considered in the analysis, is shown in figure 1. On the left is the transportation system with its major components, the traveler, the existing transportation, and the proposed new STOL system. The first step in the methodology involves modeling these components of the transportation system, followed by an arena analysis. A description of these topics is beyond the intended scope herein, but it is important to note that the analysis is based on a competitive situation between various combinations of modes in which the traveler is assumed to select the least-cost alternative (including value of time). Although a great many results of interest can be obtained from the analysis, interest herein will center on the STOL system performance. For this purpose the three figures of merit or criteria discussed earlier are shown for the STOL system. The unique feature of the methodology to be used here is that three of the figures of merit, passengers carried, return on investment, and noise impact, are used as feedbacks to the STOL system. The remaining two figures of merit, congestion and pollution, are merely evaluated since it is anticipated that they will be benefits which will increase with the number of passengers carried. The three feedback loops are used in an optimization procedure to alter all the available STOL system parameters to achieve a desired objective. This objective is to maximize the number of passengers carried with a constraint on the return on investment. The noise impact is inherently included in the optimization through the economics, as will be discussed subsequently.

The STOL system parameters which can be utilized to accomplish the optimization are important to note. They consist of the following:

1. Aircraft concept
2. Aircraft size
3. Fleet size
4. Changes in aircraft technology
5. Curved, steep flight paths
6. Location of STOLports
7. Service paths
8. Land use
9. Fare levels

Most of these variables are self-explanatory. The first five are concerned with the aircraft and its capabilities; item 4 refers to technological changes such as reduced noise and reduced field length capability. In item 7 "service paths" refers to a route between any two ports. Item 8 is intended to represent the use of land surrounding the airport so as to be compatible with the actual noise levels.

GUIDELINES

There are several important guidelines for the study which need discussion. First, the study is directed toward a 1980 time period to correspond to the time at which the congestion problem is predicted to become critical as discussed in paper no. 1 by Leonard Roberts. Second, the STOL system will be assumed to utilize existing general-aviation airports or perhaps new airports if necessary. Thus the STOL system operates independently of the major hubs which currently process the short-haul traffic. For this reason some degree of decongestion of the major hubs would be expected. Third, various ground costs are charged to the STOL system economics. These include new or improved terminals to process the passenger demand determined by the optimization analysis, new or improved runways to handle the number and sizes of aircraft determined by the analysis, and the cost of noise buffer zones surrounding the airport so as to be compatible with the noise levels. And finally, the noise is to be measured by NEF, or noise exposure factor, corresponding to generally accepted practice in the United States and Europe.

The arenas to which the analysis is being applied are illustrated in figure 2. As can be seen, they consist of four cities in the California Corridor, three cities in the Midwest Triangle, and four cities in the Northeast Corridor. These arenas have been selected because they cover the spectrum of travel patterns likely to be encountered in the United States. Figure 3 illustrates the differences in these travel patterns.

The STOL aircraft to be used in the short-haul system studies are intended to cover a variety of parametric changes. In this paper, however, the results for one particular aircraft will be given. Some of the characteristics of this aircraft are shown in figure 4, and they are included in the spectrum of aircraft characteristics discussed in paper no. 2 by Thomas L. Galloway.

PRELIMINARY RESULTS

With the preceding information as background, some of the preliminary results of the optimization analysis utilizing the above STOL aircraft in the California Corridor can now be discussed. Of importance will be the various figures of merit shown in figure 1. The first result is shown in figure 5. Here the maximum number of daily passengers (departures and arrivals) which can be carried as a function of return on investment and vehicle size is given in carpet plot form. This plot is the result of the optimization analysis and must be interpreted carefully. Each point on the plot is an optimum point achieved by varying the STOL system parameters. For example, to achieve a 7.5-percent return on investment with a 100-passenger aircraft, all the available STOL system parameters have been varied to attract the maximum number of passengers, in this case 22 000

per day. Along the 100-passenger-capacity line, the number of passengers carried decreases as the return on investment increases. This is because, for example, the optimum fare increases and the optimum fleet size decreases in order to meet the increased return on investment. It might be noted that the discontinuity in the plot is due to the required addition of a third crew member.

There are several significant observations to be made from figure 5. With regard to vehicle size, it can be seen that the results are relatively insensitive to vehicle capacities between 100 and 200. This is important because it allows freedom to base the choice of vehicle size on other considerations. For example, from the community acceptance viewpoint the smaller 100-passenger aircraft might be preferable. Another observation is that positive values of return on investment are achieved. The 7.5-percent line is typical of what is actually achieved by successful short-haul air carriers, while the 10.5-percent line represents an upper bound established by the Public Utilities Commission. The effect of subsidizing the operation is a significant increase in the number of passengers carried, as can be seen by the lines for lower return on investment. A final observation is that the number of passengers which the STOL system can attract is substantial. How substantial is best answered by comparison with the traffic carried by the other modes, that is, by examining the modal split.

The modal split between the various modes will be illustrated for the point in figure 5 corresponding to the 10.5-percent return on investment and the 200-passenger aircraft. The result for the Los Angeles-San Francisco part of the California Corridor both with and without STOL is shown in figure 6. Here it is seen that the STOL system has captured about one-third of the total traffic, and that there has been little impact on car, rail, and bus traffic. The major impact is on the CTOL mode, and this traffic has been reduced by about a factor of 3. This reduction is believed to be beneficial to the CTOLports. It might be interpreted as a decongestion effect, although a better interpretation would be that this reduction in short-haul CTOL traffic represents available capacity that can be used to meet the increasing long-haul demand expected in the early 1980's as discussed in paper no. 1 by Leonard Roberts. This beneficial effect on the CTOLports would be magnified when the aircraft rather than passenger traffic is considered. For example, the elimination of a short-haul aircraft from the CTOL hub would mean that a much larger long-haul aircraft could be used and that the passenger-carrying capacity of the CTOL hub would be correspondingly increased. It is worth emphasizing that these results are preliminary in nature and that a more thorough evaluation is required.

The modal split effects just discussed are conservative from the viewpoint that the return on investment was 10.5 percent. These effects are more pronounced when the return on investment is decreased to a lower figure of 8 percent. Results for this case indicate that the STOL system would then capture 38 percent of the total, whereas the CTOL short-haul traffic would be reduced by a factor of 4.

Next some results obtained regarding community noise impact will be discussed. Two approaches based on different assumptions are being considered. One assumption is that noise buffer zones can be purchased so that the land use will be compatible with the actual noise levels. An alternate assumption is that such noise buffers cannot be purchased because of the social and environmental restrictions.

On the basis of the assumption that noise buffer zones are to be purchased, an examination is being made of the noise impact on the total system. To illustrate the methodology being used and the results emerging, an example airport, the Concord-Buchanan airport, is shown in figure 7. Shown here are the airport boundary, the two runways, and the surrounding zoning pattern as indicated by the codes. Each of the irregular-shaped areas corresponds to a different land value, with the higher priced residential land being generally in the southwestern portion of the map. Also shown in the figure is the general-aviation straight-line flight pattern, landing from the north and departing toward the south. A curved STOL flight pattern, which has been determined to be desirable for minimum noise impact, is indicated by the approach coming from the northwest and departing to the west; thus the planned residential zones are largely avoided. This STOL path also descends at a steep angle of 7.5^{o} and departs at 10^{o}. From these paths and the mix of aircraft, it is possible to determine the various NEF noise contours of interest, namely 30, 35, and 40 NEF corresponding to acceptable levels for residential, commercial, and manufacturing uses, respectively. These contours when superimposed on the land zones enable one to determine the total dollar value of the land (excluding the airport) for which the acceptable noise levels are exceeded. This dollar value is the manner in which the noise impact is used in the feedback loop shown in figure 1.

Results of the noise analysis just described are given in figure 8. The impact of the projected general-aviation operations for 1980 is shown as the horizontal line and is about $3 million. The effect of superimposing STOL operations is indicated by the two lowest curves. Note that the effects of aircraft size and number of operations over the entire range shown have a small dollar impact compared with the general-aviation impact. The number of operations actually required, as determined by the optimization analysis, indicated 10 operations would be sufficient at this port; even the busiest ports required no more than 40 operations. Thus for the required number of operations, the impact is only a fraction of a million dollars. Allowing the noise level to increase by 6 EPNdB does not increase the impact greatly over the ranges cited.

There are several reasons which account for these results. First, the single-flight noise contours in terms of EPNdB are small as a result of the basically quiet aircraft characterized by the noise levels in figure 4 and the steep flight paths possible with the STOL aircraft. The steep flight paths for ascent or descent tend to widen the noise contours rather than lengthening them as with conventional flight paths; therefore, the noise

contours tend to be confined better to the airport boundaries. Second, the effect of multiple operations on the NEF contours is small because the number of operations required to optimize the total system performance is small.

The dollar impact of noise can perhaps be put in better perspective by comparing these noise impact costs with the total system costs. Total system costs for a system optimized for a 100-passenger-size aircraft have been determined to include the total aircraft fleet costs, the terminal costs, and costs for airfield improvements or new airfields. Such costs are in excess of $200 million, and therefore the noise impact costs are small in comparison.

The above results alone are obviously not conclusive because of their port-dependent nature. Although the same pattern is emerging for some of the other ports used in this study, these preliminary conclusions regarding noise impact should be interpreted cautiously until the analysis for all ports is complete.

Regarding the second assumption that noise buffer zones cannot be purchased, only a preliminary examination has been made. From an analysis of 115 existing general-aviation airports in the California Corridor and Midwest Triangle, the number of airports which would just enclose the 95 EPNdB noise contour has been determined, and the results are shown in figure 9. Here the number of such ports is shown as a function of the field-length capability of the aircraft. Aircraft requiring long field lengths have relatively long noise footprints. As field-length capability is shortened the footprint becomes smaller, and more ports would contain the noise footprints so that the curve rises. Note that even at 1500 feet (460 meters) aircraft capability, there are still nearly half of the ports which would not enclose the noise contour. The number of ports required and the corresponding field-length capability of the aircraft can be determined only by a total systems analysis in the context of figure 1. However, it is clear that the information of figure 9 would be an input to the systems study. For example, the number of ports available (the ordinate) would influence the convenience of the STOL system to the traveler, and hence ultimately affect the figures of merit in figure 1, that is, the passenger-carrying capability and the economic viability. The aircraft field-length capability (the abscissa) would influence the economics of the systems analysis because of the greater cost to achieve shorter field-length capability. Thus the best point to choose in figure 9 needs further study in which the information of figure 9 is incorporated into the complete systems analysis illustrated in figure 1.

PRELIMINARY CONCLUSIONS

The preliminary conclusions that have been reached thus far in the study for a 1980 short-haul system in the California Corridor can be itemized as follows:

1. Attainable STOL technology could result in a short-haul transportation system which is economically viable and which would attract a large number of people.

2. Aircraft sizes between 100 and 200 passengers have little effect on passenger demand.

3. Under the assumption that noise buffers can be purchased for compatible land use, preliminary results indicate that noise impact costs for 95-EPNdB aircraft are negligible compared with the general-aviation impact and the other STOL system costs. However, analysis for all the ports in the various arenas needs to be completed before definitive conclusions can be drawn.

4. Under the assumption that noise buffers cannot be purchased because of social and environmental restrictions, port availability and very short field-length aircraft capability may be critical issues and need further study.

5. The required volume of STOL traffic at the general-aviation airports is small. Large increases in the number of operations could accommodate future short-haul demand growth in the 1980's.

6. The STOL system would enable a significant expansion in the long-haul traffic from major CTOL hubs.

METHODOLOGY

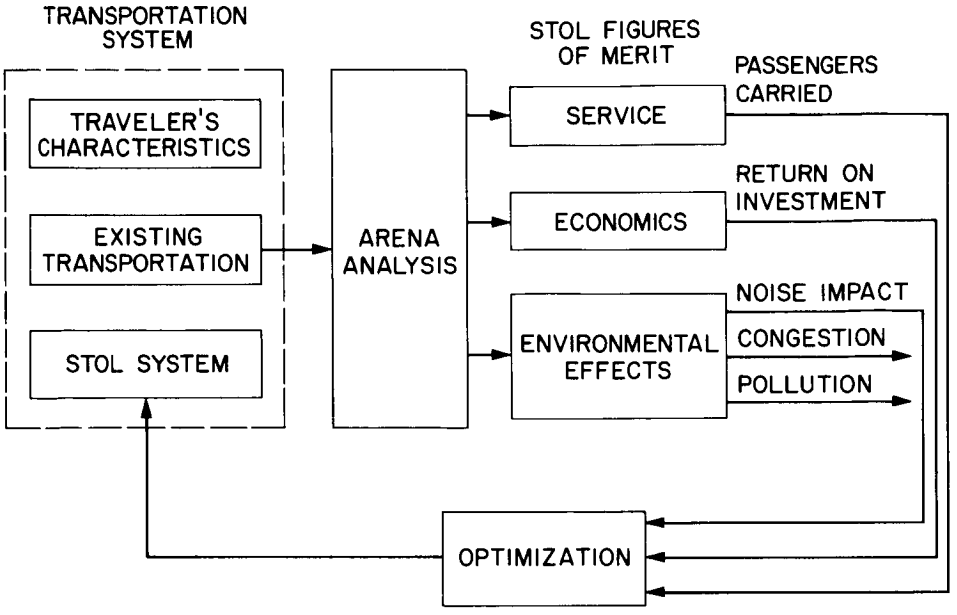

Figure 1

SHORT-HAUL STOL TRANSPORTATION SYSTEM STUDY ARENAS

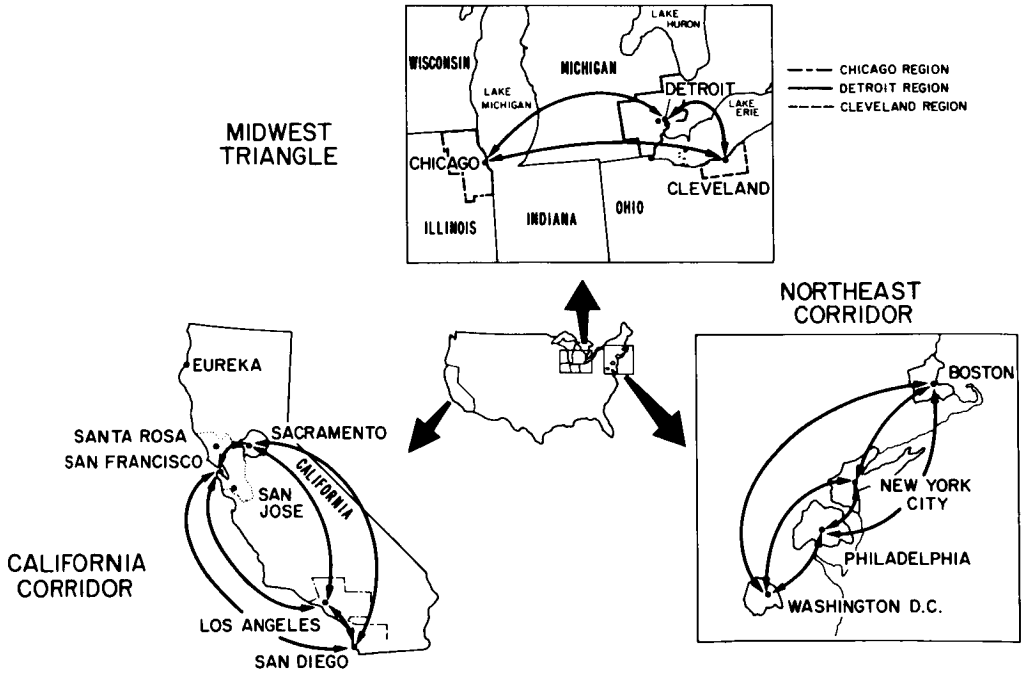

Figure 2

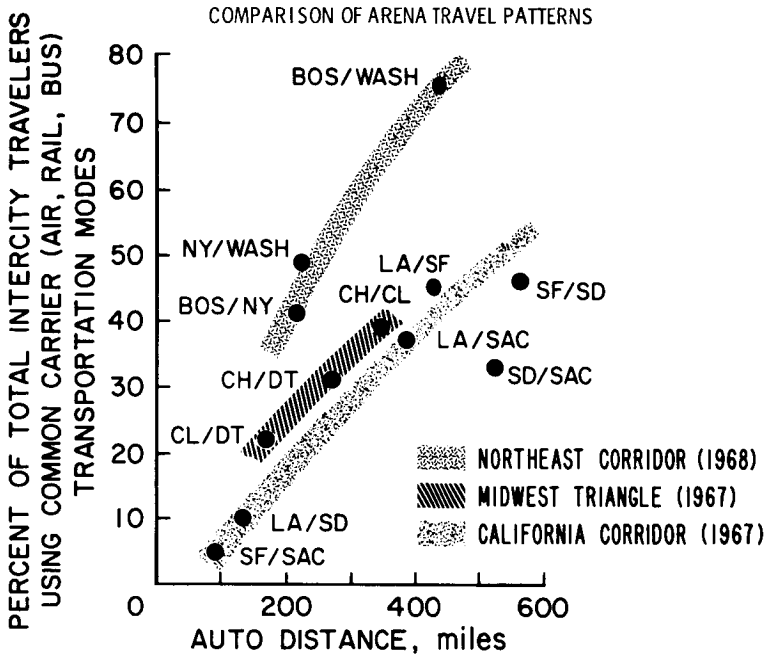

Figure 3

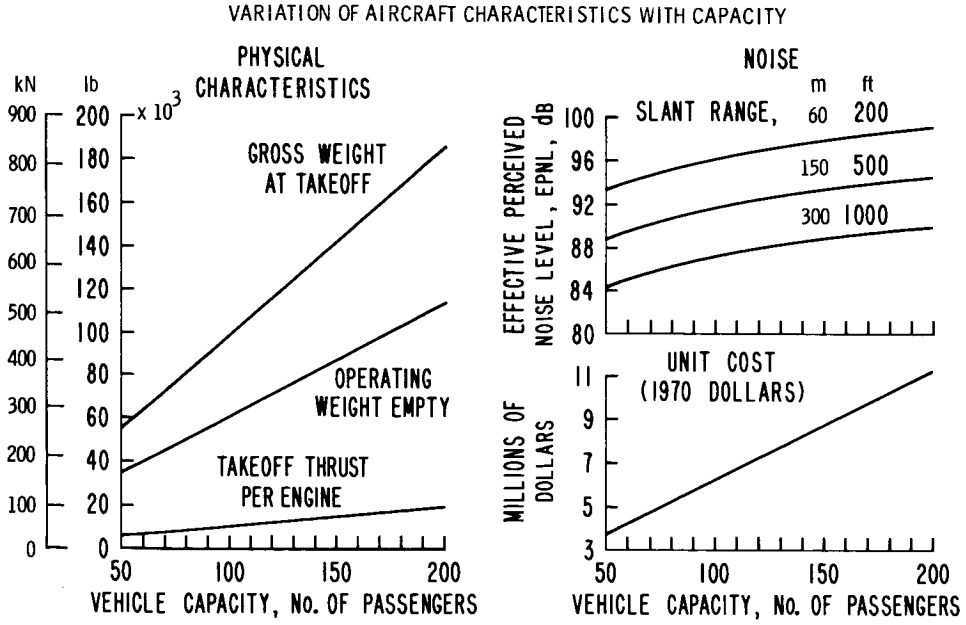

Figure 4

EFFECT OF VEHICLE CAPACITY AND RETURN ON INVESTMENT ON PASSENGER PATRONAGE

CALIFORNIA CORRIDOR

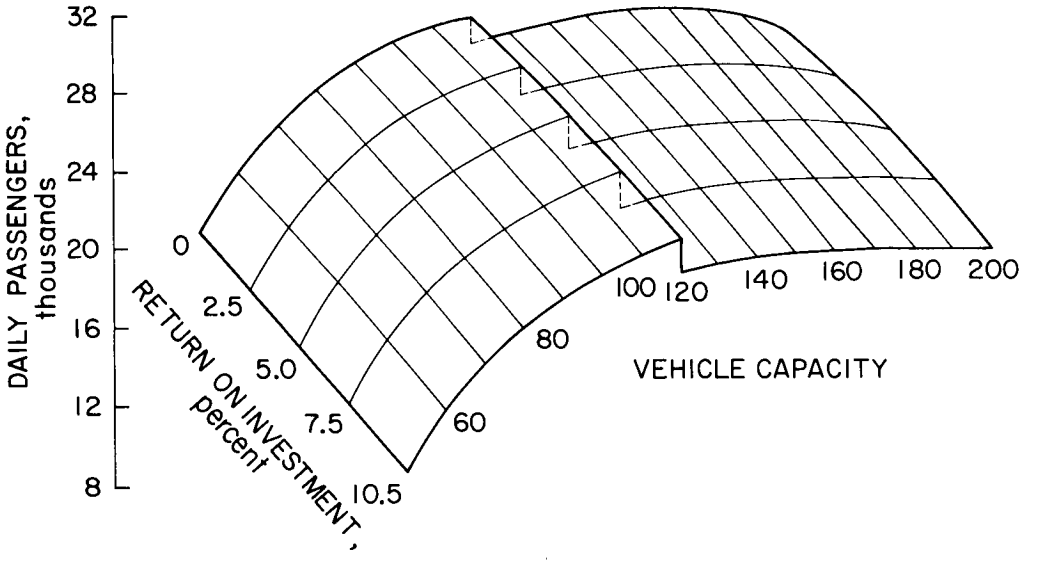

Figure 5

IMPACT OF STOL ON 1980 MODAL SPLIT

EXAMPLE RESULTS FOR LOS ANGELES–SAN FRANCISCO

200 PASSENGERS ROI = 10.5%

MODE	ONE-WAY FARE	PASSENGER TRIPS PER DAY	
		WITHOUT STOL	WITH STOL
STOL	17.94	———	12,290
CTOL	16.50	16,510	5,760
CAR	——	20,740	19,580
BUS	13.50	770	580
RAIL	16.00	380	190
TOTAL		38,400	38,400

Figure 6

CONCORD-BUCHANAN AIRPORT SURROUNDING LAND USE ZONES
WITH STOL & CTOL ROUTES

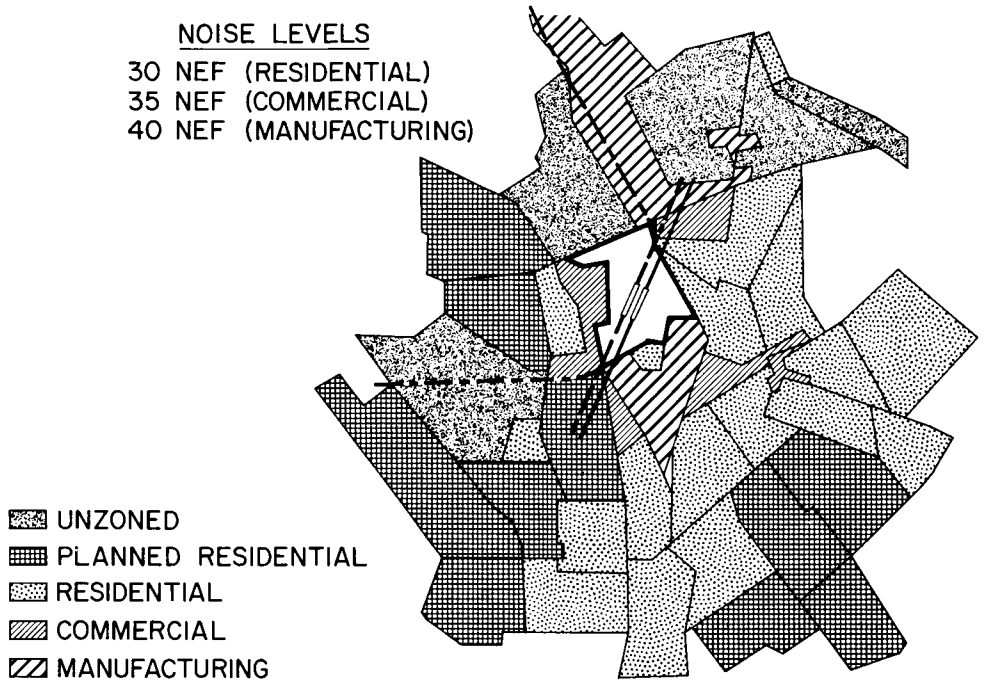

Figure 7

DOLLAR VALUE OF NOISE IMPACTED LAND FOR
CONCORD-BUCHANAN AIRPORT

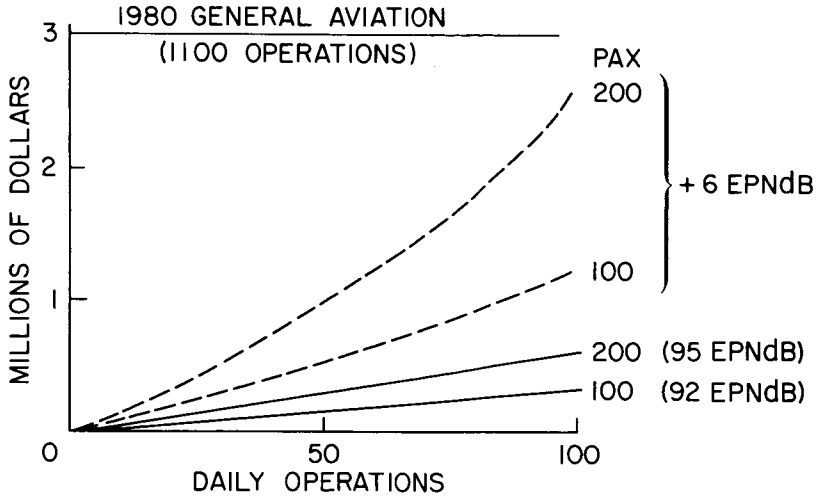

Figure 8

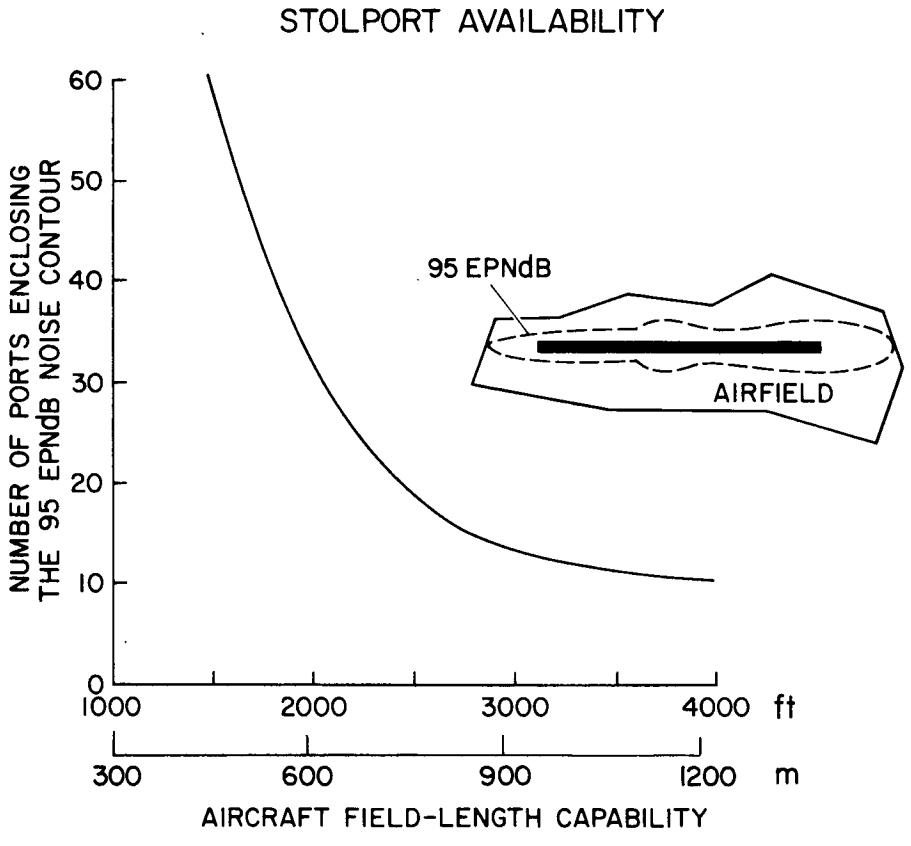
STOLPORT AVAILABILITY
NUMBER OF PORTS ENCLOSING THE 95 EPNdB NOISE CONTOUR
60
50
40
30
20
10
0
95 EPNdB
AIRFIELD
1000
2000
3000
4000
ft
300
600
900
1200
m
AIRCRAFT FIELD-LENGTH CAPABILITY
NOTE: 115 AIRFIELDS IN CALIFORNIA CORRIDOR AND MIDWEST TRIANGLE

Figure 9

OVERVIEW OF TECHNOLOGY SESSIONS

By Bradford H. Wick
NASA Ames Research Center

There are two objectives to be accomplished by this overview. First, STOL aircraft technology development will be related to the requirements for an expanded and improved short-haul system, and then the scope of the conference will be related to the STOL technology developments. Figure 1 lists the items to be covered. First the systems requirements will be summarized; then the principal aircraft requirements will be identified; and, finally, the status of STOL technology development and the scope of the technology efforts covered by this conference will be outlined.

The requirements for an expanded and improved short-haul system are summarized in a qualitative way in figure 2. They are subdivided into three categories: (1) Those for better short-haul service, (2) those that would make short-haul a better neighbor, and (3) the "hold-the-fort" requirements, which relate to the comfort, safety, reliability, and economics offered by CTOL short-haul aircraft.

What are the STOL aircraft requirements that will be needed to satisfy these system requirements? Figure 3 lists some of the more important ones derived from aircraft and system studies. They are grouped according to the system requirements. The short-field requirement responds to the better-service and better-neighbor requirements through increasing the number of potentially acceptable airport sites. The noise requirement offers the possibility of realizing the use of the potential airport sites without intruding with respect to community noise and land usage. A question mark is shown after the noise requirement, since it is probably the most uncertain of the aircraft requirements shown. The flight-path-angle requirements are based on considerations of noise alleviation, obstacle clearance, and separation of the aircraft operations from the community. A few of the aircraft requirements for retaining certain desirable CTOL features are listed next. The high-wing-loading requirement is suggested by considerations of ride quality, cruise performance, and gross weight. The requirement for a turbofan type of propulsion system is based on considerations of performance, passenger preference, and reliability. The number of engines is related to aircraft size, economics, and engine-out operating margins. For the 100-passenger aircraft, economics would dictate the smaller number of engines; whereas, for some propulsive-lift systems, the larger number of engines may be required to provide adequate engine-out margins. The bypass ratio and ratio of thrust to gross weight correspond to values for short-haul CTOL aircraft. The STOL aircraft will require a higher thrust-weight ratio and a bypass ratio that depends upon the propulsive-lift system.

With these STOL aircraft requirements identified, the needed aircraft technology will be considered. What has been established by technology efforts to date and what is being developed by ongoing efforts will be examined. The developments that are essential will be distinguished from those that are desirable. Figure 4 provides a qualitative assessment of the status of STOL aircraft technology. The efforts to date have clearly established the effectiveness of several propulsive-lift concepts. High wing lift can be provided for short-field operations, and the terminal-area flight paths can be steeper and more tightly curved for STOL aircraft than for CTOL.

Further efforts in four areas are essential to the successful use of the propulsive-lift STOL aircraft. The critical areas are the development of quiet propulsion and propulsive-lift systems. The challenge is in providing quiet systems that will be acceptable with respect to performance and complexity. The demands on aircraft systems technology will be greater for the propulsive-lift STOL aircraft than they have been for CTOL. These demands are the result of the short-field flight-path requirements, the lift-thrust interactions of the propulsive-lift STOL aircraft, and ground effects during flare and landing. The task will be to provide the required levels of stabilization and flight-path precision without compromising flight safety and without requiring undue systems complexity. The technology developments must obviously be accompanied by the development of design criteria and operating procedures.

Advances in structures and materials technologies are not identified as essential to the initial introduction of propulsive-lift STOL aircraft into short-haul service. This conclusion is suggested by the preliminary results of the aircraft and system studies discussed in the preceding papers. Methods of estimating structural weights clearly need further attention.

The lower part of figure 4 identifies areas in which efforts are desirable for improving the efficiency of STOL aircraft. Advances in technology should show greater economic benefits for STOL than for CTOL because of the much greater coupling effects of the aircraft technologies in the case of STOL. For example, an improvement in propulsive-lift efficiency could lead to interrelated reductions in thrust and in gross weight. There could be an associated reduction in the magnitude of the noise suppression problem, which could lead to further interrelated reductions in thrust and gross weight. Advances in structures and materials technologies could also have a cascading effect. The economic benefits of structural weight reductions will be dependent upon the cost of advanced materials and the techniques for their fabrication.

Before proceeding to the outline of the scope of the technology sessions, the effectiveness of propulsive lift will be compared with the effectiveness of aerodynamic lift alone (that is, lift provided by a very effective mechanical flap system). Figure 5 shows a band of predicted values of wing loading for propulsive-lift STOL. These are compared

with predicted wing loadings for the aerodynamic-lift STOL and the wing loading for an existing aerodynamic-lift CTOL. The band of wing loadings for the propulsive-lift STOL was derived from values for the externally blown flap and the augmentor-wing concepts. These results show that propulsive-lift systems can, indeed, provide wing loadings in the range required from considerations of ride quality, cruise performance, and gross weight. Because of the noise problem of the propulsive-lift STOL, attention is being given to the aerodynamic-lift STOL aircraft which incorporates a control system to provide acceptable ride qualities.

The aircraft characteristics required to provide the high-lift short-field capability also provide the STOL aircraft with the capability of flying curved paths that are steeper and tighter than those for CTOL aircraft. This capability offers benefits with respect to noise alleviation and airspace usage in the terminal area.

The noise-alleviation benefits of the steeper flight paths are illustrated in figure 6. The noise footprint area is shown increasing to the right, flight-path steepness increasing vertically, and field length increasing to the left. The take-off case is illustrated here, but the landing case would be similar. A reduction in field length provides a sizable reduction in the noise footprint. The tighter curved flight-path capability of the STOL transport offers a greater possibility of avoiding areas that are particularly noise sensitive.

The greater flight-path capability of the STOL as compared with the CTOL aircraft offers reductions in the airspace requirements in the terminal area. This potential benefit is illustrated in figure 7. The terminal area corridors for the two types are compared to the same scale in the lower part of the figure. The STOL corridors are shown to an enlarged scale (by a factor of 5) in the top part of the figure. In addition to requiring less airspace, the STOL aircraft also is able to use more of the available airspace.

Figure 8 outlines the scope of the STOL technology efforts covered by this conference. The technology areas are shown on the left, and the respective technology sessions are shown on the right. The technology developments identified during the preceding discussion of the status of STOL technology are listed under the appropriate technology areas.

It can be seen from the outline that the conference reports on the critical development problems, presents design data for several technology areas, and describes efforts to provide desirable improvements in systems performance.

Not previously described, but of key importance, is the development of airworthiness standards for propulsive-lift STOL aircraft. A paper in the Operational Aspects session reports on the FAA program to provide criteria for use in completing the development of the standards.

In conclusion, it should be emphasized that the individual papers in the conference are in the nature of progress reports on recently completed work and on the planning of future efforts in STOL aircraft technology. To put the papers in perspective, each session chairman will present a brief overview of his particular technology area. The attention is concentrated on STOL aircraft for the high-density short-haul system. The most promising type of STOL aircraft for this mission is the turbofan-powered propulsive-lift type. Since this type is also of primary interest for military missions, the technology results will have applicability to the military missions. There is a limit to the applicability, however, because of differences in operational requirements and constraints. It is also expected that the results presented in this conference will have some applicability to the low-density short-haul mission.

SHORT-HAUL SYSTEM REQUIREMENTS AND STOL TECHNOLOGY

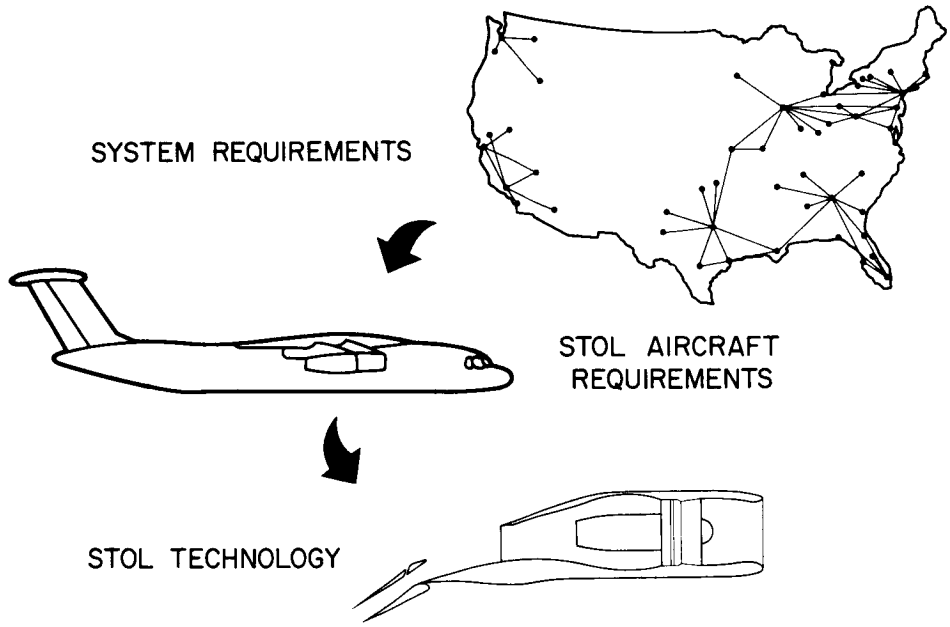

Figure 1

SHORT-HAUL SYSTEM REQUIREMENTS

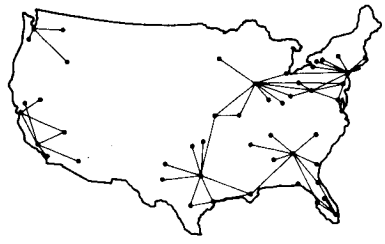

- BETTER SERVICE
  - INCREASED CAPACITY
  - REDUCED ACCESS TIME
  - REDUCED TRIP TIME
- BETTER NEIGHBOR
  - REDUCED NOISE IMPACT
  - REDUCED POLLUTION
  - REDUCED GROUND CONGESTION
  - MINIMUM LAND USAGE
- RETAIN GOOD FEATURES
  - JET TRANSPORT COMFORT
  - JET TRANSPORT SAFETY AND RELIABILITY
  - JET TRANSPORT ECONOMICS

Figure 2

STOL AIRCRAFT REQUIREMENTS

- BETTER SERVICE AND NEIGHBOR -
  - FIELD LENGTH, ft (m) — 1500-2500 (450 - 750)
  - NOISE, EPNdB AT 500ft (150 m) — 95 (?)
  - FLIGHT PATH ANGLES, deg
    - TAKE-OFF — 12 TO 17
    - LANDING — -6 TO -7.5

- RETAIN GOOD FEATURES (OF CTOL)
  - WING LOADING, lb/ft^2 (kN/m^2) — 80 - 100 (3.8 - 4.8)
  - CRUISE MACH NO. — 0.7 - 0.8
  - RANGE, n. mi — 400 - 600
  - NO. OF PASSENGERS — 100 - 200
  - TURBOFAN PROPULSION
    - NO. OF ENGINES — 2 - 4
    - BYPASS RATIO — 5 - 6
    - THRUST / GROSS WEIGHT — 0.3

Figure 3

STATUS OF STOL AIRCRAFT TECHNOLOGY

ESTABLISHED:

- EFFECTIVE PROPULSIVE LIFT CONCEPTS
  - HIGH LIFT FOR SHORT FIELD LENGTHS
  - FLIGHT PATH STEEPNESS AND CURVATURE

BEING DEVELOPED:

- QUIET PROPULSION
- QUIET PROPULSIVE LIFT
- EFFECTIVE & ACCEPTABLE AIRCRAFT SYSTEMS
- DESIGN CRITERIA & OPERATING PROCEDURES

} ESSENTIAL

- MORE EFFICIENT PROPULSIVE LIFT CONCEPTS
- LESS COMPLEX PROPULSION/LIFT SYSTEMS
- IMPROVED STRUCTURES & MATERIALS
- IMPROVED CRUISE PERFORMANCE

} DESIRABLE

Figure 4

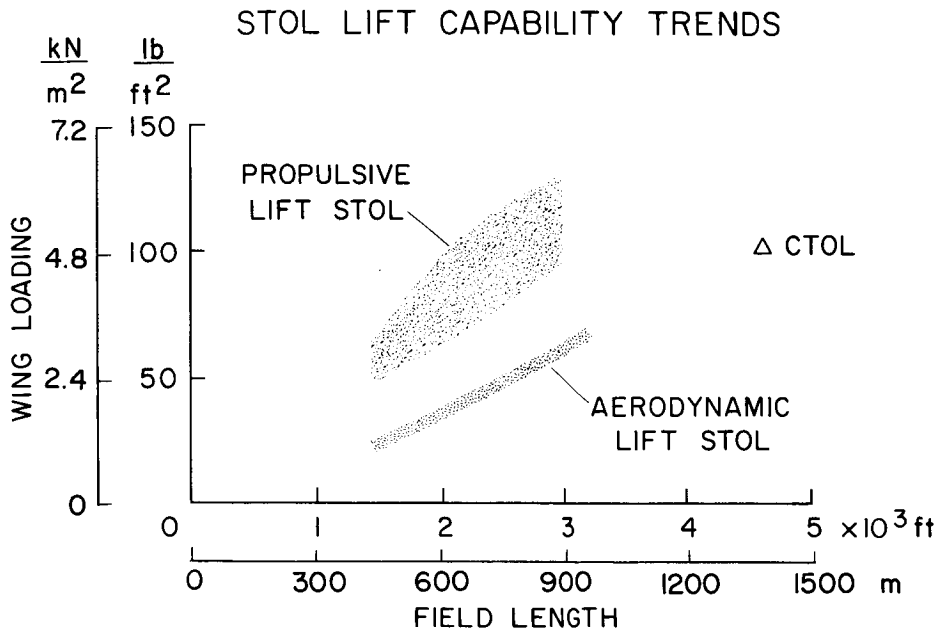

Figure 5

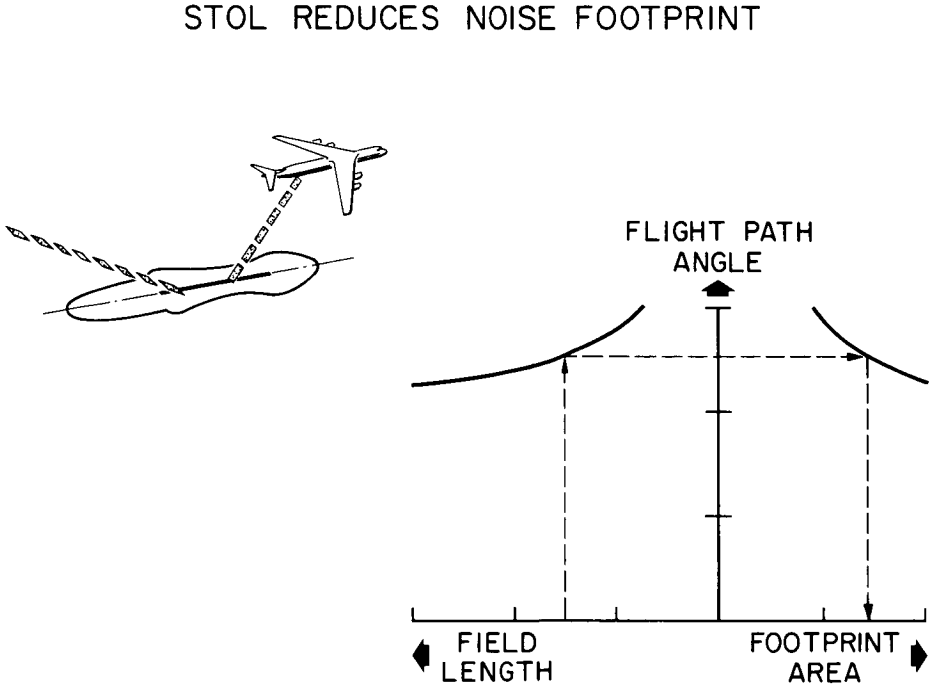

Figure 6

STOL REDUCES TERMINAL AIRSPACE REQUIREMENTS

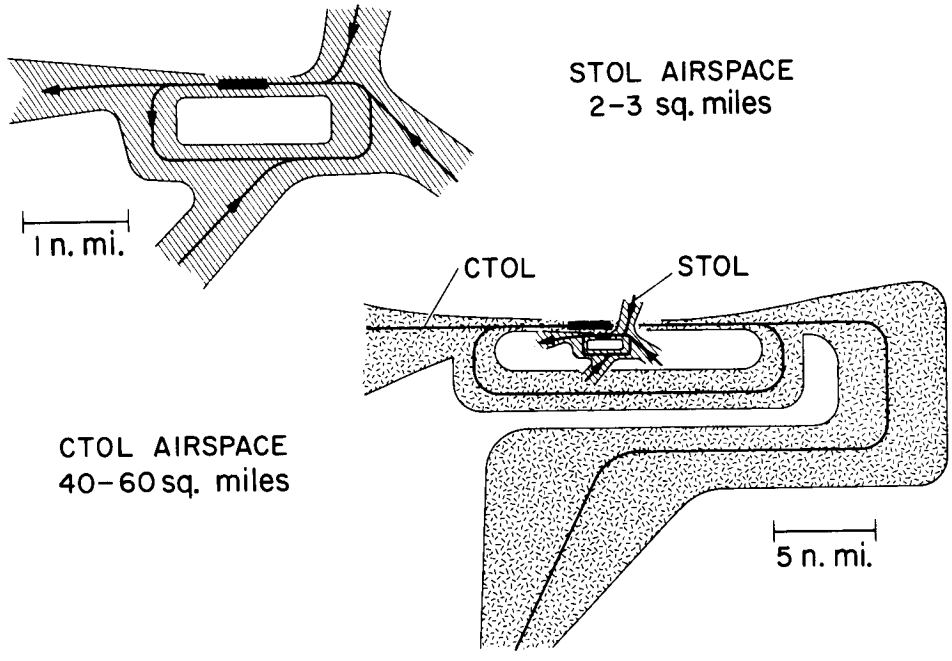

Figure 7

SCOPE OF STOL AIRCRAFT TECHNOLOGY CONFERENCE

TECHNOLOGY AREA	SESSION
● PROPULSIVE LIFT SYSTEM • LOW NOISE, DESIGN DATA, EFFICIENCY	AERODYNAMICS/QUIET PROPULSION
● PROPULSION SYSTEM • LOW NOISE, DESIGN DATA, PERFORMANCE	QUIET PROPULSION
● STRUCTURES • DESIGN DATA	LOADS
● AIRCRAFT SYSTEMS • PERFORMANCE, DESIGN DATA	FLIGHT DYNAMICS/OPERATIONS
● OPERATING PROCEDURES • FLIGHT PATH CONTROL, TERMINAL AREA CONTROL	FLIGHT DYNAMICS/OPERATIONS
● AIRWORTHINESS STANDARDS	OPERATIONS

Figure 8

AERODYNAMIC AND PERFORMANCE CHARACTERISTICS OF EXTERNALLY BLOWN FLAP CONFIGURATIONS

By William G. Johnson, Jr.
NASA Langley Research Center

INTRODUCTION

The development of a jet-powered STOL transport has resulted in reexamination of the various powered-lift concepts. The externally blown flap (EBF) has long been recognized as one of the ways to produce the high lift required for STOL operations. As shown in figure 1, the EBF concept uses the engine exhaust flow to produce an incremental lift on the wing by a direct deflected-thrust vector and by flow through the flap slots which increases the circulation and thereby enhances the lift-producing capabilities of the total lifting system.

The purpose of this paper is to present some of the characteristics of EBF powered lift. To predict the aerodynamic performance of a particular EBF configuration, the contributions to lift of the various components of the total powered lift need to be understood. In this paper, specific effects such as the induced aerodynamics, the static turning, the flap span and deflection, and the engine size and flap chord are examined.

5

SYMBOLS

A	aspect ratio
b	wing span, m
c_f	total flap chord, m
C_D	drag coefficient, $\frac{\text{Drag}}{q_\infty S}$
C_L	lift coefficient, $\frac{\text{Lift}}{q_\infty S}$
$C_{L,o}$	power-off lift coefficient
$C_{L,\Gamma}$	circulation lift coefficient

$C_{L,trim}$ trimmed lift coefficient

C_μ thrust coefficient, $\frac{\text{Gross static thrust}}{q_\infty S}$

d_F diameter of fan cowl exit, m

EBF externally blown flap

q_∞ free-stream dynamic pressure, N/m^2

S wing area, m^2

α angle of attack, deg

δ_j jet deflection angle, arc tan $\frac{\text{Normal force}}{\text{Axial force}}$, deg

η flap turning efficiency, $\frac{\text{Resultant force}}{\text{Static thrust}}$

DISCUSSION

Some lift and drag data recently obtained from a typical externally blown double-slotted flap configuration are shown in figure 2. The data are presented as plots of C_L as a function of α and of C_D for the range of thrust coefficient from 0 to approximately 4. At any constant angle of attack, there is considerable variation in lift coefficient with thrust coefficient.

This variation is shown in figure 3 where the total EBF lift is broken into the various components. These components can be related to the sample data in figure 2 in the following manner. The unpowered lift $C_{L,o}$ developed by the total lifting system is plotted as circular symbols. The deflected-thrust component $C_\mu \sin(\alpha + \delta_j)\eta$ depends on how much of the engine thrust is directed into lift and how well. If all the thrust could be directed into lift with no turning losses, the thrust contribution to lift in coefficient form would equal the corresponding C_μ value since the lift and thrust are nondimensionalized by the same factors. The remainder is the powered circulation lift component $C_{L,\Gamma}$. It is the difference between the sum of the unpowered-lift and deflected-thrust components and the total lift. For example, the sum of the power-off lift coefficient and the thrust contribution to lift, represented by any value of C_μ, is considerably less than the power-on lift coefficient which corresponds to that particular thrust level.

A measure of the static EBF turning effectiveness is needed to study the effects of the deflected thrust on the induced aerodynamics. Such a measure is shown in figure 4 where the normal force divided by the static thrust is plotted against the longitudinal force divided by the static thrust. These forces are measured statically or at zero forward speed. For the flaps-up condition, or no jet turning, δ_j would equal 0^o and the longitudinal force would about equal the static thrust, which indicates, as might be expected, no turning losses. As the jet is deflected by the flap system, there are resulting losses. The higher the turning, the greater the losses as indicated by the band. This band includes most of the available EBF data with the data from the more efficient flap systems located along the top edge. The EBF generally uses conventional engines and flap systems. The relatively sharp dropoff in efficiency for the higher turning angles is the price to be paid for using a simple turning system.

The contributions to EBF lift were shown in figure 3. A breakdown of the EBF drag shows a similar deflected-thrust component which uses the cosine function. Removal of these deflected-thrust components from the total lift and drag leaves values of circulation lift and drag which might be expected to follow the trends of circulation aerodynamics. The resulting characteristics of the circulation lift and drag could possibly provide a means of estimating the power-on lifting performance of the EBF system. In figure 5, the process for removing the deflected-thrust components is shown by using the solid symbol for a reference. The result is the complete collapse of the power-on and power-off lift-drag polars to a band of circulation lift and drag. This band of thrust-removed lift-drag polars is shown in figure 6 for both take-off and landing flaps. The data are plotted as thrust-removed lift (total measured lift minus thrust contribution to lift) as a function of the thrust-removed drag (total measured drag minus thrust contribution to drag). The data show that these collapsed power-on thrust-removed lift-drag polars follow the same trend as the traditional induced-drag parameter $C_L^2/\pi A$. Since the comparison with the induced-drag parameter is intended only to show the trends of the collapsed data and not the absolute magnitude of the drag, the value of the profile drag $C_{D,o}$ was set equal to 0 and the value of the Oswald wing efficiency factor e was set equal to 1.

Although the direct deflected-thrust contributions have been removed from these data, an additional variation of the thrust-removed lift, or total circulation lift, exists as a function of thrust. This variation is plotted in figure 7 which shows the effect of the static turning on the total circulation lift $C_{L,\Gamma} + C_{L,o}$ (refer back to fig. 3 for the relationship of these parameters). By using different engine configurations on the double-slotted flap model, from which all previously shown data were obtained, and a triple-slotted flap model, different levels of static turning were obtained without a physical change to the high-lift system itself. The relative values of the static turning parameter $\sin(\alpha + \delta_j)\eta$ are plotted as bar graphs for each flap system. The data show that the total

circulation lift is directly related to this parameter; that is, the highest level of this parameter produced the highest level of circulation lift and similarly for the other levels.

In figure 8, the effects of flap span and deflection are shown for the untrimmed and trimmed conditions. Lift coefficient is plotted against drag coefficient for take-off and landing flap deflections and for a range of thrust coefficient from 0 to approximately 4. The solid line represents the full-span flap extending from the fuselage to the wing tip and the broken line represents the partial-span flap or inboard two-thirds of the full-span flap.

For both the untrimmed and trimmed data, there is very little span effect for either flap deflection. Both spans even exhibit approximately the same maximum lift capability. The only effect of trimming the data is the expected reduction in lift due to the lift-trim penalty.

To look at the effects of engine size, the double-slotted and triple-slotted flap models were tested with several different engines. Shown in figure 9 are the combinations of engine sizes and flap configurations. These combinations are compared in terms of the parameter d_F/c_f where d_F is the diameter of the fan cowl exit and c_f is the total flap chord measured from the leading edge of the first flap element to the trailing edge of the last element. In terms of bypass ratio, these engines would represent bypass ratios of about 4, 6, and 10 on the double-slotted-flap configuration and bypass ratios of about 6 and 10 on the triple-slotted-flap configuration looking from top to bottom. All the wind-tunnel tests were conducted with a large-chord leading-edge slat on the wing outboard of the engine; the broken lines indicate that there was no leading-edge slat immediately behind the engine. The data for these configurations are shown in figure 10 where the effects of engine size and flap chord are shown for a thrust coefficient of 4. These data show that the engine tested as the middle-size engine on the double-slotted-flap model and as the smaller engine on the triple-slotted-flap model gives considerably better performance than the largest engine for both flap systems. This higher performance is not unexpected considering the extension of the flap into the engine exhaust flow. The larger engine probably has a portion of its exhaust flow passing under the flap system without being contained and turned. This lack of turning results in a lower lift being produced. If the capability of the flap system to contain the flow is the only consideration, the smallest engine on the double-slotted-flap system would be expected to be more effective. One explanation for its lower effectiveness is that this engine has a tighter core of exhaust flow which possibly is not spreading as well as that of the middle-size engine even though it is being contained and turned. Although spreading and containment are only two of the several parameters that could be considered, the largest engine whose flow can be fully contained and turned by the flap system seems to give the best lift-producing performance.

Since high noise levels for the powered-lift concepts have become a matter of major concern, multilobe noise-suppression nozzles have been suggested as a means of reducing the EBF noise. These nozzles were tested on the triple-slotted-flap model shown in figure 11 to determine their lift-producing capabilities. In figure 12, the results of this investigation are shown. These data show a lower lift performance for the noise-suppression nozzles. The lower performance was indicated in the static turning and can probably be attributed to the larger diameter of exhaust flow core for the noise-suppression nozzles. This result is similar to that found with the engine size comparison in figures 9 and 10. The data (fig. 12) show, however, that the noise-suppression nozzles could be used to develop the lift required for STOL if the flap system is designed to consider the engine-exhaust flow characteristics.

CONCLUSIONS

The study of some of the characteristics of EBF powered lift and how such effects as the induced aerodynamics, static turning, flap span and deflection, and engine size and flap chord contribute to these characteristics has resulted in several basic conclusions, as follows:

1. The induced aerodynamics, in particular the induced drag from powered-lift concepts, follow conventional aerodynamic trends.

2. The total circulation lift can be related to the static turning.

3. The use of high-bypass-ratio engines will probably require increased flap size to retain powered-lift effectiveness.

EXTERNALLY BLOWN FLAP

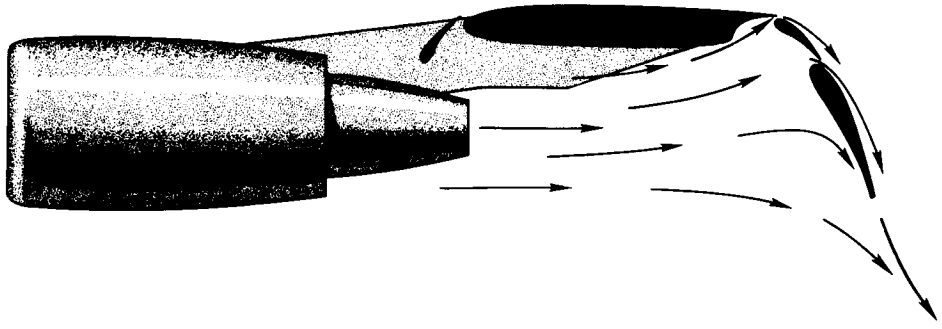

Figure 1

TYPICAL DATA FOR EBF CONCEPTS

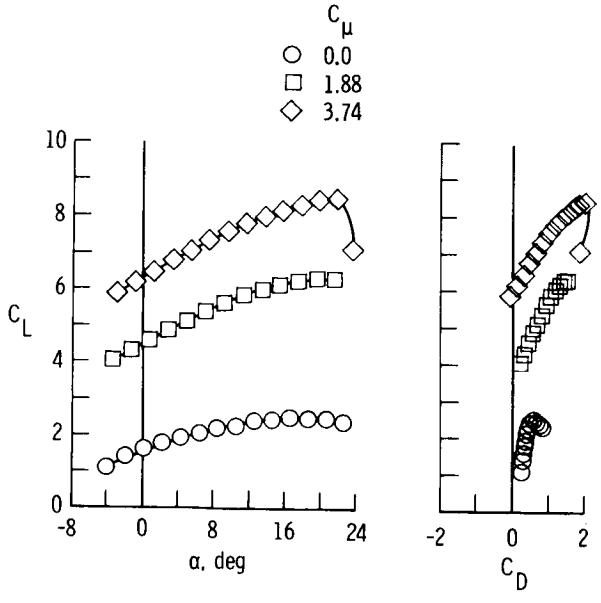

Figure 2

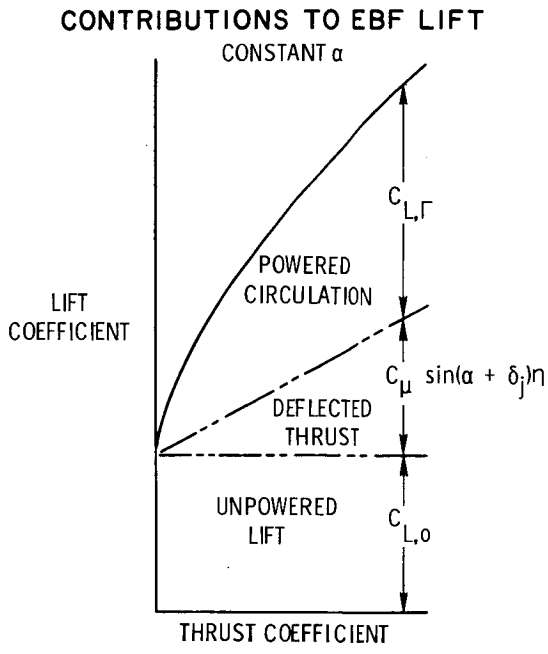

Figure 3

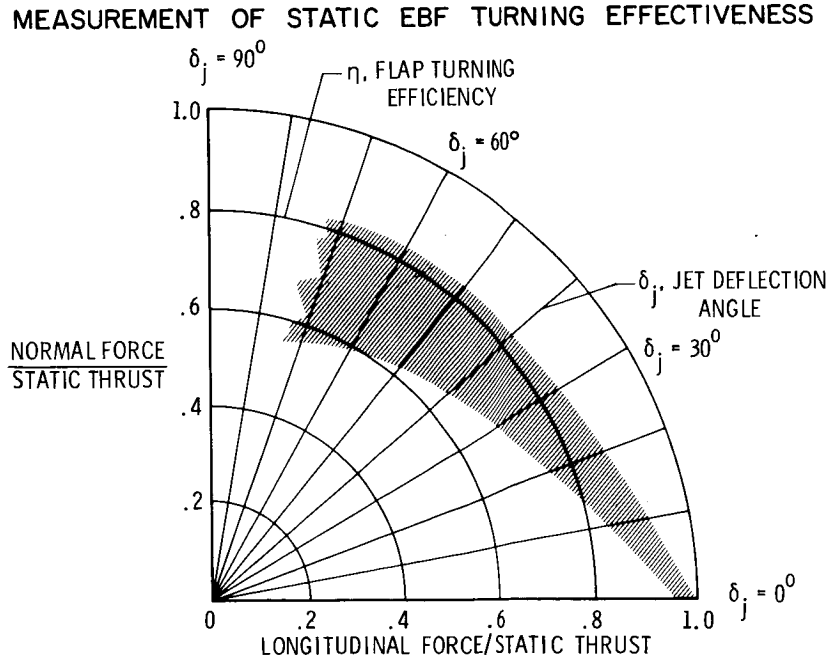

Figure 4

REMOVAL OF DIRECT THRUST CONTRIBUTIONS

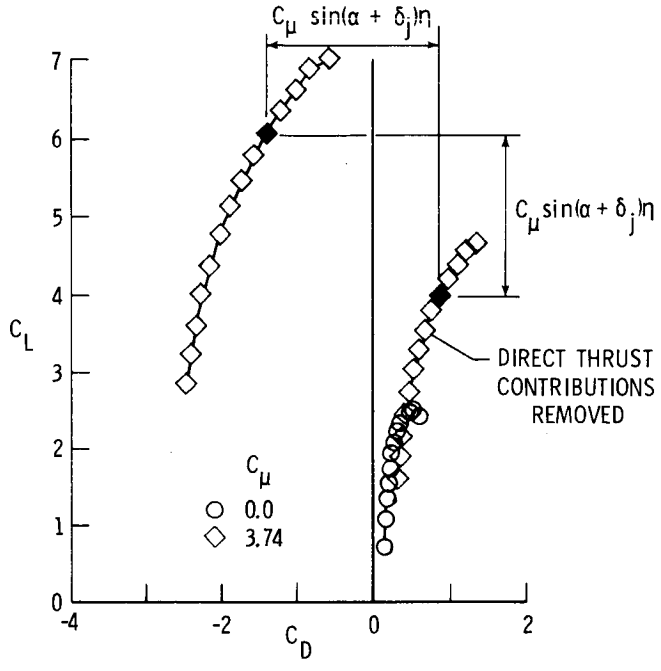

Figure 5

THRUST-REMOVED LIFT-DRAG POLARS

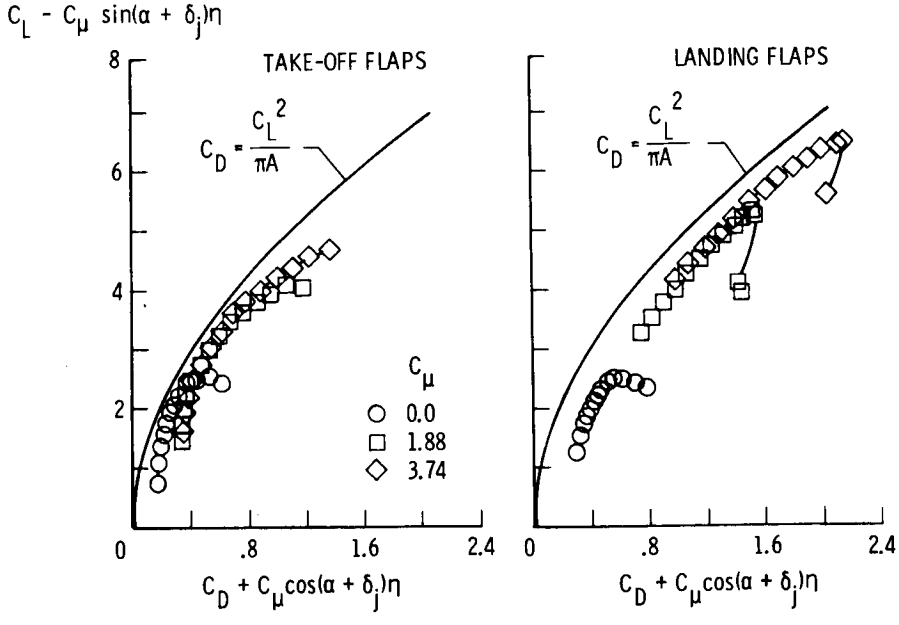

Figure 6

EFFECT OF STATIC TURNING EFFECTIVENESS ON TOTAL CIRCULATION LIFT

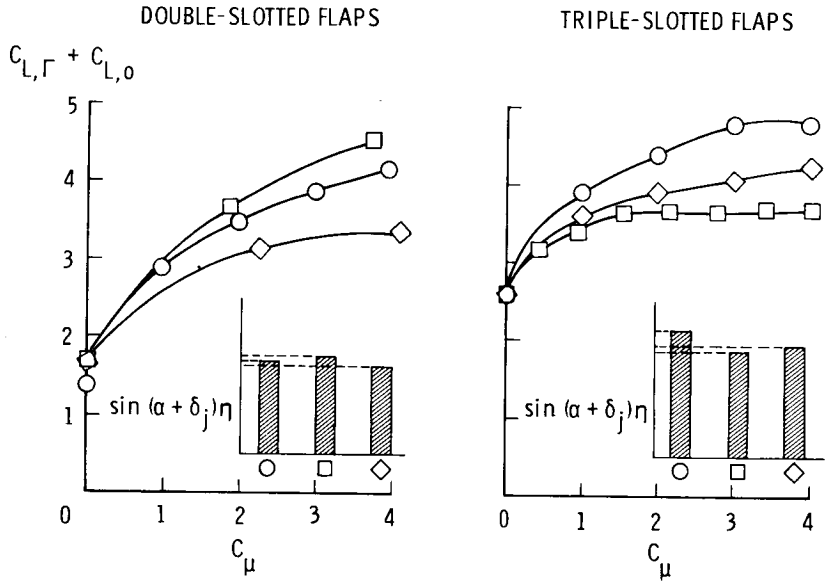

Figure 7

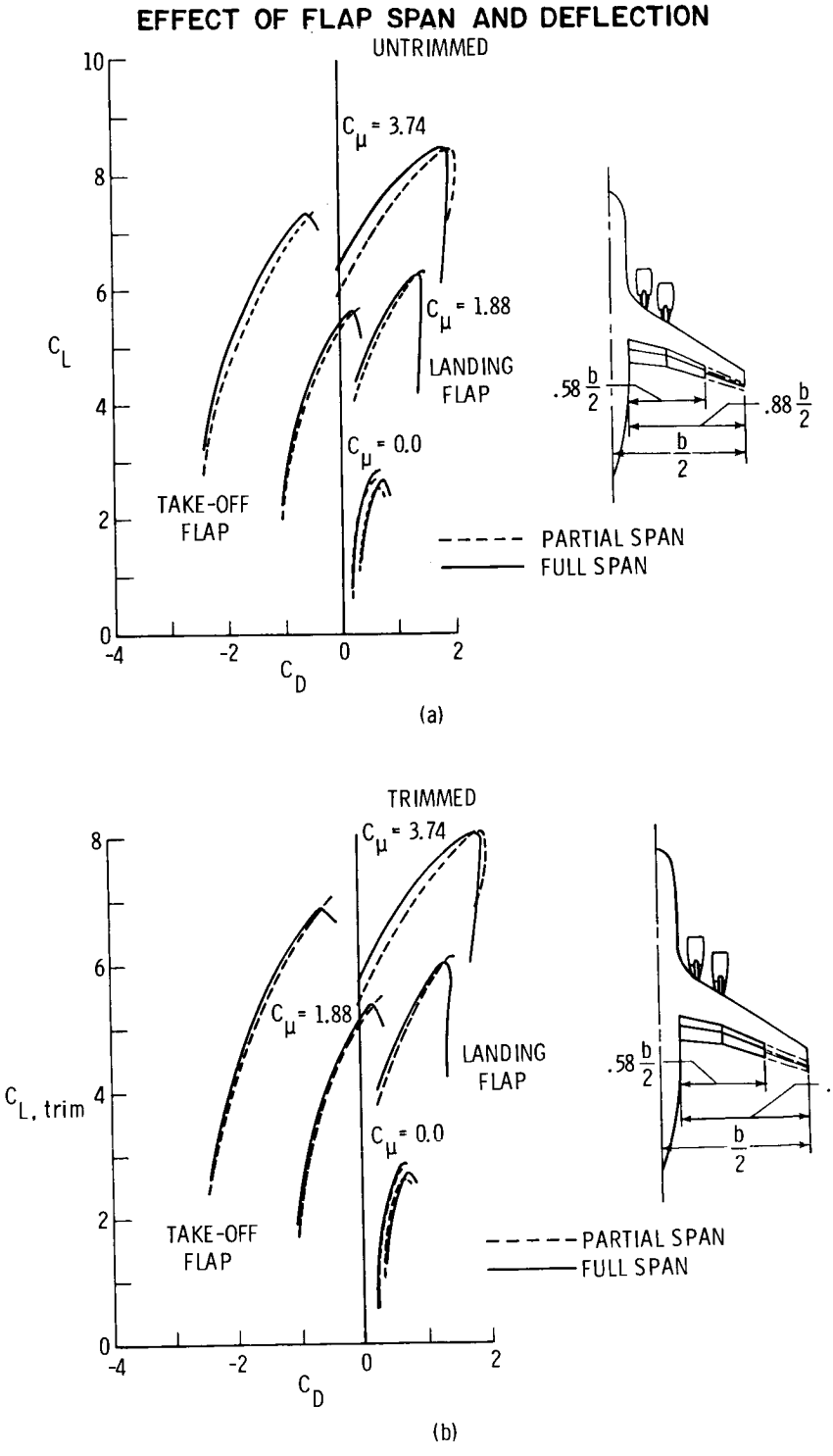
EFFECT OF FLAP SPAN AND DEFLECTION
UNTRIMMED
C_L
C_D
C_μ = 3.74
C_μ = 1.88
C_μ = 0.0
LANDING FLAP
TAKE-OFF FLAP
.58 b/2
.88 b/2
b/2
PARTIAL SPAN
FULL SPAN
(a)
TRIMMED
$C_{L,\,trim}$
C_μ = 3.74
C_μ = 1.88
C_μ = 0.0
LANDING FLAP
TAKE-OFF FLAP
.58 b/2
.88 b/2
b/2
PARTIAL SPAN
FULL SPAN
(b)

Figure 8

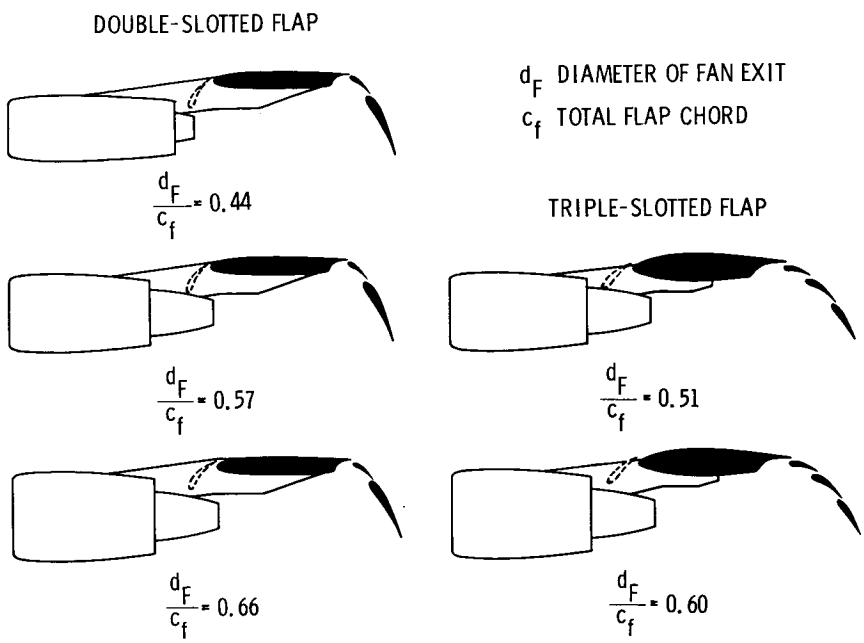

Figure 9

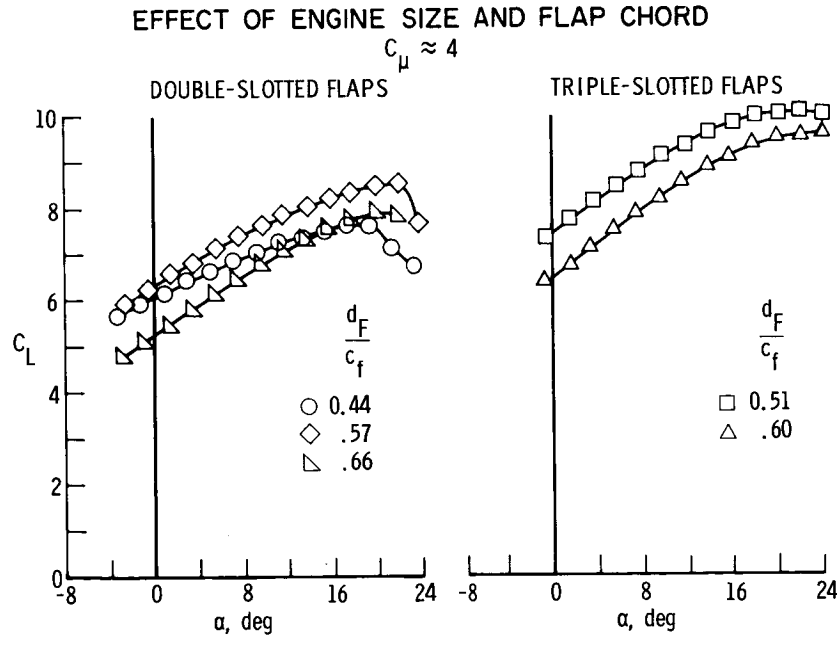

Figure 10

NOISE-SUPPRESSION-NOZZLE INVESTIGATION

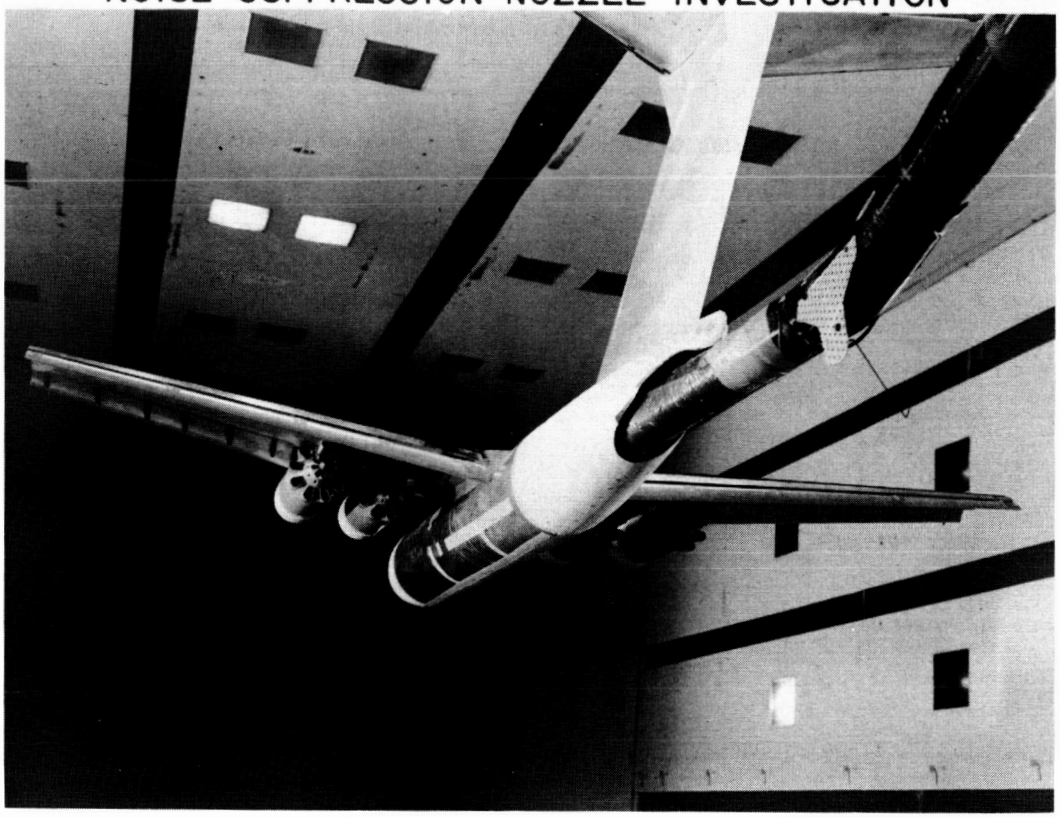

Figure 11

RESULTS OF NOISE-SUPPRESSION-NOZZLE INVESTIGATION

$C_\mu \approx 4$

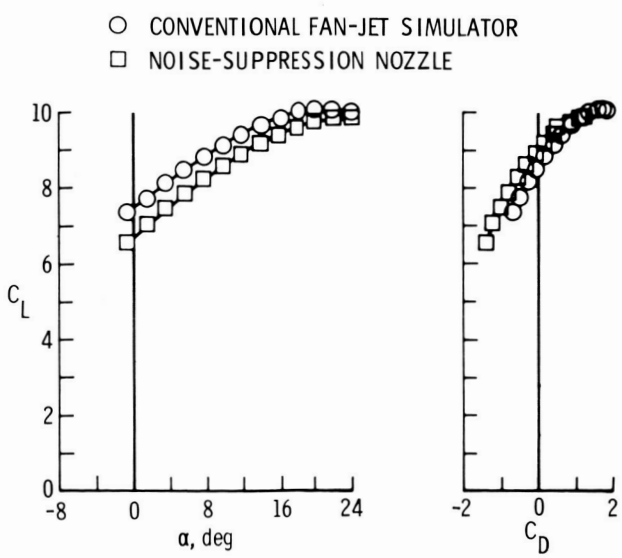

Figure 12

STABILITY AND CONTROL OF EXTERNALLY BLOWN FLAP CONFIGURATIONS

By Lysle P. Parlett
NASA Langley Research Center

SUMMARY

This paper summarizes the results of wind-tunnel investigations on the stability and control characteristics of externally blown jet-flap configurations and identifies certain problems and points out some of the solutions to the problems. Conventional wind-tunnel tests and free-flight model tests have shown that longitudinal trim and stability can be achieved by a properly located horizontal tail of sufficient size, and that lateral trim in the engine-out condition can be produced by combinations of differential flap, spoiler, and rudder deflection. Free-flight model tests have revealed a lightly damped Dutch roll lateral oscillation, and have shown that the oscillation can be stabilized by use of artificial damping.

INTRODUCTION

Considerable effort has been directed over the last several years toward the study of aerodynamic and stability and control characteristics of externally blown jet-flap configurations. This work came about because the relative mechanical simplicity and good aerodynamic performance made the concept attractive for use on STOL aircraft configurations. Early work (ref. 1) documented the high potential of the concept for STOL performance; later investigations (refs. 2 to 4) however brought to light serious problems such as pitch trim and longitudinal stability at high lift, and lateral trim in an engine-out condition. The problems of pitch trim and of longitudinal stability (see refs. 2 to 4) are common to all powered-lift STOL systems. The problem of engine-out lateral trim is shared to some extent by other concepts, but is very serious for externally blown flap (EBF) configurations (see refs. 4 to 6). Although data for the present paper are based on research done on the EBF concept, a number of the points brought out will apply also to other STOL concepts. Data presented in the figures are based on the results of conventional static force tests. The dynamic characteristics of an EBF configuration, as shown by free-flight model tests, will be described briefly in qualitative terms.

SYMBOLS

b	wing span, meters
C_L	lift coefficient, $\frac{L}{qS}$
C_l	rolling-moment coefficient, $\frac{l}{qSb}$
C_{l_β}	effective dihedral parameter, $\frac{\partial C_l}{\partial \beta}$
ΔC_L	lift loss coefficient due to failure of one engine
ΔC_l	rolling-moment coefficient due to failure of one engine
C_m	pitching-moment coefficient, $\frac{M_Y}{qS\bar{c}}$
C_n	yawing-moment coefficient, $\frac{M_Z}{qSb}$
C_{n_β}	directional stability parameter, $\frac{\partial C_n}{\partial \beta}$
C_μ	engine gross-thrust coefficient, $\frac{T}{qS}$
c	wing chord length, meters
$\bar{c}$	length of mean aerodynamic chord, meters
h	tail height above wing-chord plane, meters
i_t	incidence of horizontal tail, positive when leading edge is up, deg
L	lift, newtons
l	tail moment arm, meters, or rolling moment, positive right wing down, N-m
M_Y	pitching moment, positive nose up, N-m

M_Z yawing moment, positive nose right, N-m

q free-stream dynamic pressure, N/m^2

S wing area, $meters^2$

T total engine gross thrust, newtons

$T_{1/2}$ time required for Dutch roll oscillation to damp to one-half amplitude, sec

y moment arm to inoperative engine, meters

α angle of attack, deg

β sideslip angle, positive nose left, deg

ϵ downwash angle measured relative to free stream, deg

ω_d damped frequency of Dutch roll oscillation, rad/sec

$1 - \frac{\partial \epsilon}{\partial \alpha}$ downwash factor

Abbreviations:

c.g. center-of-gravity location

M.A.C. mean aerodynamic chord

DISCUSSION

Longitudinal Characteristics

Provision of adequate trim in pitch is more of a problem for all STOL concepts than for conventional aircraft, but the problem is particularly severe for the EBF concept. The source of the problem is illustrated in figure 1. The plot is for a high-lift condition and shows the variation of pitching moment with angle of attack for several thrust levels. These data are tail-off data and thus, of course, the curves have an unstable slope; the significant point, however, is that very large diving moments are produced at high thrust settings. These diving moments are the result of the center of lift being located so far rearward (approximately 60 percent $\bar{c}$).

The significance of these diving moments in terms of tail size required for trim is shown in figure 2. The figure shows the tail size required for trim as a function of tail lift coefficient following the procedure outlined in reference 2. This plot was prepared by assuming that the wing is operating at a maximum lift coefficient of 8, that the tail moment arm is 3.5 wing chords, and that the static margin is 10 percent. Any given point on the curve represents some compromise between tail area and complexity. Without any high-lift devices, tail areas of over 40 percent of the wing area would be required. With some combination of elevator and leading-edge high-lift device, the tail area required would still be about 35 percent, a value nearly double that required by conventional airplanes. If, by fuller use of high-lift technology, the tail lift coefficients are made approximately equal to the wing lift coefficients, the tail size can be reduced to that of conventional airplanes.

Figures 1 and 2 have shown that there is a large pitching moment to be trimmed and that a large tail is required for trim; figure 3 shows another aspect of the tail design problem – that the tail location is also important in considering the tail contribution to stability. Figure 3 is based on a powered-lift approach condition, and presents a plot of pitching-moment coefficient against angle of attack for two horizontal-tail locations. The tail-off curve is taken from figure 1. At low angles of attack the tail in a high rearward position makes a noticeable but inadequate contribution to the stability of the complete configuration. At high angles of attack, the contribution of the tail actually becomes destabilizing. If the same tail is moved forward and upward, it now produces stability for the complete configuration through the angle-of-attack range up to slightly over 15°. The stabilizing effects of this high forward tail become weaker as angle of attack increases, but the loss in stability is much more gradual than when the tail was in the rearward location.

Figure 4 shows why the high forward tail position was more favorable from stability considerations. This figure is based on smoke-flow studies and illustrates the vortex flow setup by a wing operating in a powered-lift condition. The tip vortices do not trail straight backward but are drawn in sharply toward the center line of the airplane. At high angles of attack, such as shown in the drawing, the rearward tail enters a region of powerful downwash, and the result is a serious loss of stability. The high forward tail, however, would be farther from the more intense parts of the vortex flow, and would retain its stabilizing effect in spite of its shorter moment arm.

Surveys have been made of the downwash angles in the region of the horizontal tail and this information is summarized in figure 5 in terms of the variation of downwash factor $1 - \frac{\partial \epsilon}{\partial \alpha}$ with thrust coefficient for three horizontal-tail locations. Figure 5 shows that regardless of the location, the tail loses some effectiveness as power is increased,

but the high forward tail retains its stabilizing effect much better than the others at high thrust levels. However, some cases have been found in which a low tail was as stabilizing as a high one; the stability is dependent on the vortex pattern which, in turn, is influenced by wing lift distribution. If the tail can be kept out of the vortex, it can retain stability, and experience has shown that a high forward tail is clear of the vortex area more often than a low tail is.

The influence of tail location on trim characteristics is shown in figure 6, which is a plot of pitching moment against thrust coefficient at constant wing angle of attack and tail incidence. The low tail produces markedly less change in pitching moment with change in thrust than does the high tail, evidently because the powerful downwash at the low tail position produces a nose-up pitching moment which approximately balances the nose-down pitching moment of the wing as power is increased. Apparently, then, the low tail has the more desirable characteristics of providing trim with least incidence change, although figure 5 showed that the high tail might be preferable if stability is an important consideration. The trim and stability characteristics of a horizontal tail have been shown to be largely dependent on its location, but more work is needed before these characteristics can be predicted from a knowledge of wing lift intensity and distribution.

Lateral Characteristics

Figure 7 shows the effect of thrust on two lateral static stability derivatives, the directional stability and the effective dihedral. As thrust is increased, the directional stability parameter C_{n_β} also increases because of the increased velocity past the vertical tail. The effective dihedral is positive and becomes more positive because of the increase in wing lift-curve slope at high thrust. Although the static stability increases with increasing thrust, the net effect is a decrease in dynamic stability, as shown in figure 8.

Presented in figure 8 is a plot of the Dutch roll oscillation characteristics of an EBF configuration in terms of the damping parameter $1/T_{1/2}$ and the damped frequency parameter ω_d. The boundaries are taken from a recent AGARD publication outlining STOL handling criteria. (See ref. 7.) For the power-off condition, the Dutch roll behavior of the EBF would be considered unsatisfactory but acceptable. When power is applied, the dynamic characteristics deteriorate seriously and become very nearly unacceptable. Calculations indicate that to produce satisfactory Dutch roll characteristics of an EBF configuration, the basic damping in roll and in yaw would have to be doubled. More detailed information on the Dutch roll problem will be presented in later papers based on simulator studies.

Another major lateral problem is that of restoring trim in the event of failure of one engine. This problem, of course, involves both roll and yaw, the roll being the more

critical in an approach condition. In an effort to establish the magnitude of the problem in roll, an attempt has been made to correlate the rolling moment with the lift loss which accompanies failure of one engine. The results of this correlation are shown in figure 9, which is a plot of engine-out rolling moment against engine-out lift loss. If it is assumed that the lift loss is concentrated at the spanwise station of the dead engine, the calculated rolling moments would fall along the dashed line. However, when the rolling moments are actually measured, it is found that they are almost invariably smaller than would have been calculated. This result indicates that the center of lift induced by this engine is inboard of the engine. Therefore the moments are not as large as would be expected, but they are still large enough to require special attention.

One means by which these moments can be controlled is shown in figure 10, which is a plot of rolling-moment coefficient against lift coefficient for a configuration having a four-engine thrust-weight ratio of 0.6. In four-engine operation the rolling moments would, of course, be zero, and a maximum lift coefficient of about 9 could reasonably be expected. With the failure of one outboard engine, the thrust-weight ratio would fall to 0.45, and the maximum lift coefficient would then become about 7.0, approximately what it would be in four-engine operation at three-quarters thrust, but the out-of-trim rolling moments would be very large. These moments can, however, be trimmed out by full-span differential flap deflection without an excessive lift penalty. The additional moments produced by spoiler deflection would then be available for maneuvering in roll.

The directional problems associated with engine-out operation are shown in figure 11, which is a plot of the yawing-moment coefficients that correspond to the rolling moments presented in figure 10. The no-control moment is large enough to be a problem in itself, but the differential flap deflection which was so effective in producing roll trim has such a large adverse effect on the yaw that directional trim can now be produced only by full use of some device like a blown or slotted rudder. It has been found, however, that deflecting only the midspan element of the flap differentially produces favorable yaw. The rolling effectiveness of these midspan elements is shown in figure 12, which is essentially the same as figure 10 except that the rolling moment due to differential midspan flap deflection is shown, and the spoiler increment is now added to the midspan flap curve. The figure shows that differential deflection of the midspan elements produces about three-quarters of the roll that the full-span flaps produced. These midspan elements, then, have virtually trimmed the aircraft in roll and have produced a yawing moment which is within the trim capability of a conventional rudder.

Dynamic stability and control studies of the EBF concept have been made with the free-flight model technique which has proved useful in previous research in pointing out problem areas which might have been overlooked in conventional testing.

The model which was built for the flight tests is shown in figure 13. It has a span of 3.05 meters (10 ft) and is powered by four 15.24-cm (6-in.) diameter jet engine simulators driven by compressed air. Slots and appropriate tubing in the model provided boundary-layer control, when desired, over the wing leading edge, ailerons, and rudder. The horizontal tail was equipped with a Krueger flap, and the elevator deflection was a constant 50^{o}. The control surfaces were deflected by remotely controlled pneumatic actuators. Longitudinal control was produced by deflecting the entire horizontal tail; lateral control was produced by spoilers, ailerons, and rudder.

The free-flight technique is illustrated in figure 14. This figure shows the model being flown without restraint in the 9- by 18-meter (30- by 60-ft) open-throat test section of the Langley full-scale tunnel and remotely controlled about all three axes by human pilots. Pneumatic power and electric control signals are supplied to the model through the flexible trailing cable, which is made up of wires and light plastic tubes. The pilots perform various experiments with the model controls, and note the dynamic response of the model.

The results of the free-flight model tests showed that with all engines operating and with artificial damping about all three axes, the model was easy to fly even at angles of attack of 24^{o}, very near the stall. Without artificial damping, however, the model exhibited a lightly damped Dutch roll oscillation which was easily excited by use of rudder control. With one outboard engine inoperative, the model was trimmed laterally through the use of differential flap, spoilers, and rudder; and with artificial damping again applied, the model was still easy to fly. This result indicated that the dynamic behavior with one engine inoperative was not greatly different from that of four-engine operation. Transient motions following an engine failure were not studied in the model flight tests, but were investigated in simulator studies reported in paper no. 14 by David A. Kier, William Grantham, Bruce E. Powers, and Luat T. Nguyen.

CONCLUDING REMARKS

The results of stability and control work on the EBF can be summarized briefly as follows: a large horizontal tail is required for adequate trim and a high forward tail location appears best for stability; satisfactory solutions to the engine-out lateral trim problem have been developed, and stability augmentation will probably be required for adequate Dutch roll damping.

REFERENCES

1. Campbell, John P.; and Johnson, Joseph L., Jr.: Wind-Tunnel Investigation of an External-Flow Jet-Augmented Slotted Flap Suitable for Application to Airplanes With Pod-Mounted Jet Engines. NACA TN 3898, 1956.

2. Johnson, Joseph L., Jr.: Wind-Tunnel Investigation of the Static Longitudinal Stability and Trim Characteristics of a Sweptback-Wing Jet-Transport Model Equipped With an External-Flow Jet-Augmented Flap. NACA TN 4177, 1958.

3. Parlett, Lysle P.; and Shivers, James P.: Wind-Tunnel Investigation of an STOL Aircraft Configuration Equipped With an External-Flow Jet Flap. NASA TN D-5364, 1969.

4. Parlett, Lysle P.; Freeman, Delma C., Jr.; and Smith, Charles C., Jr.: Wind-Tunnel Investigation of a Jet Transport Airplane Configuration With High Thrust-Weight Ratio and an External-Flow Jet Flap. NASA TN D-6058, 1970.

5. Freeman, Delma C., Jr.; Parlett, Lysle P.; and Henderson, Robert L.: Wind-Tunnel Investigation of a Jet Transport Airplane Configuration With an External-Flow Jet Flap and Inboard Pod-Mounted Engines. NASA TN D-7004, 1970.

6. Parlett, Lysle P.; Greer, H. Douglas; Henderson, Robert L.; and Carter, C. Robert: Wind-Tunnel Investigation of an External-Flow Jet-Flap Transport Configuration Having Full-Span Triple-Slotted Flaps. NASA TN D-6391, 1971.

7. Anon.: V/STOL Handling. I - Criteria and Discussion. AGARD Rep. No. 577, Dec. 1970.

PITCHING-MOMENT CHARACTERISTICS

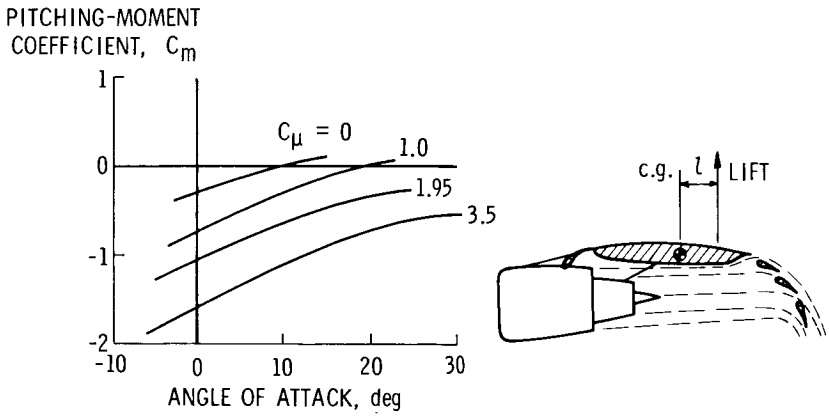

Figure 1

HORIZONTAL-TAIL REQUIREMENTS

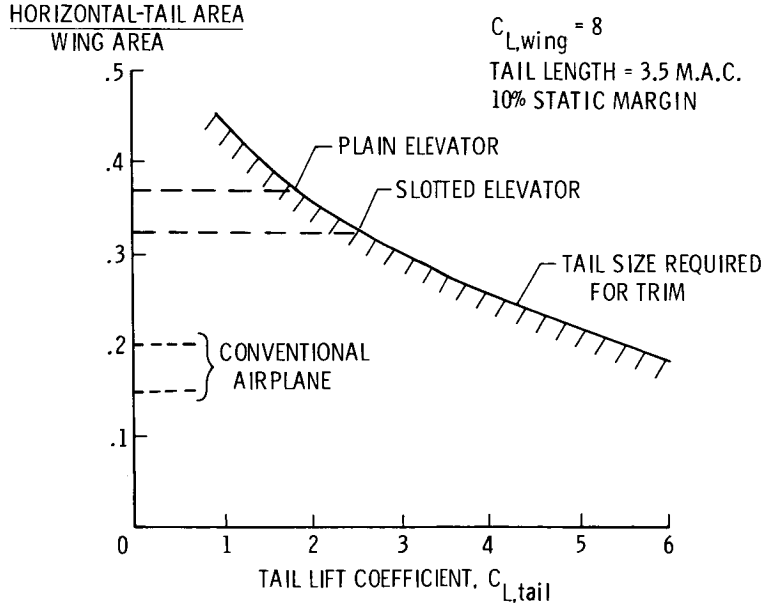

Figure 2

LONGITUDINAL STABILITY

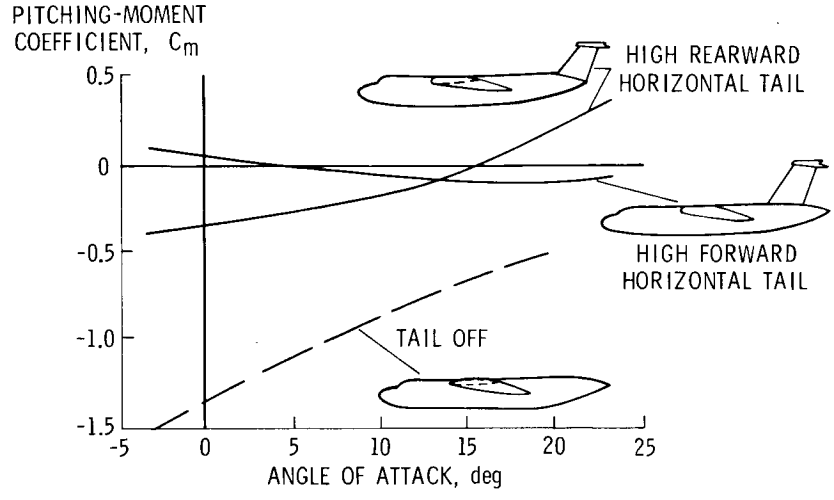

Figure 3

WING VORTEX FLOW

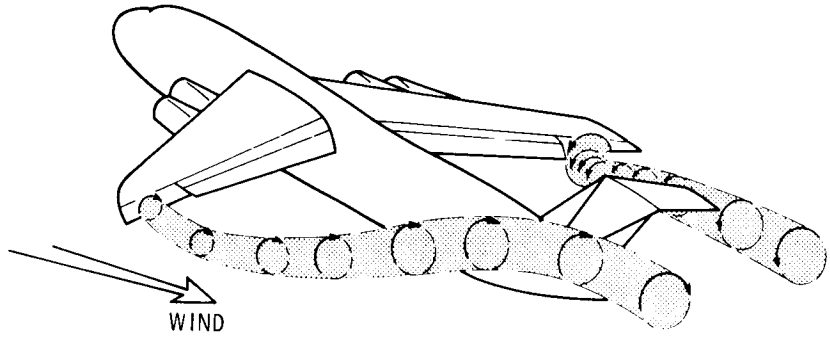

Figure 4

DOWNWASH CHARACTERISTICS

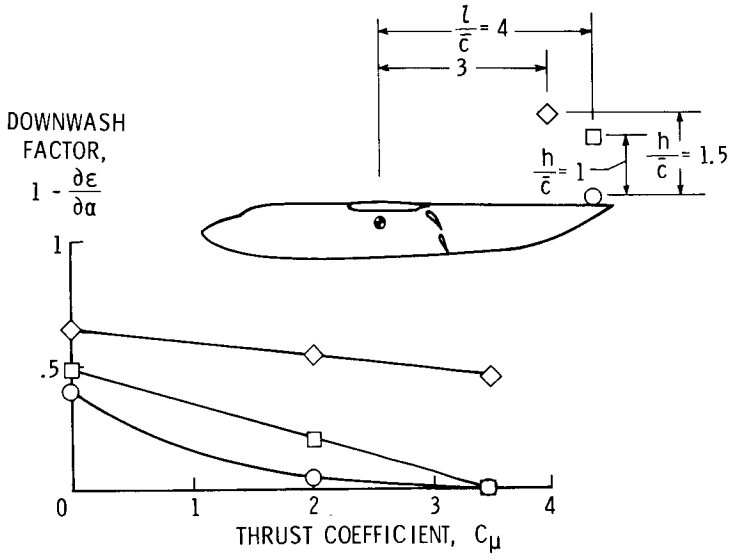

Figure 5

TRIM CHARACTERISTICS

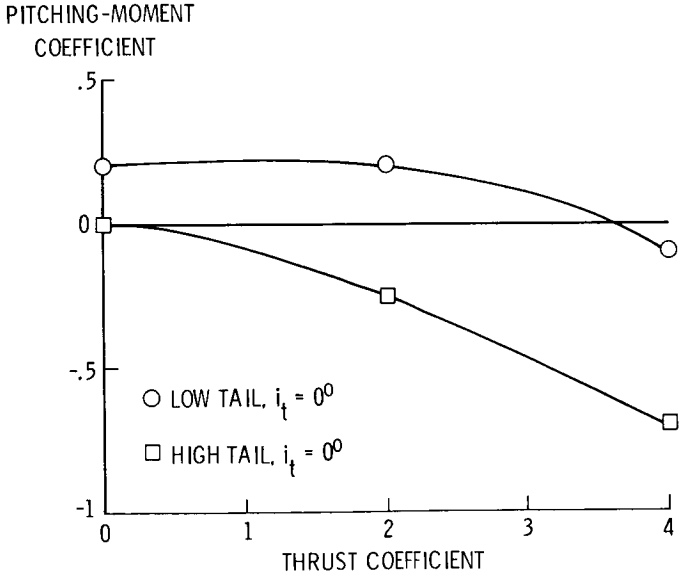

Figure 6

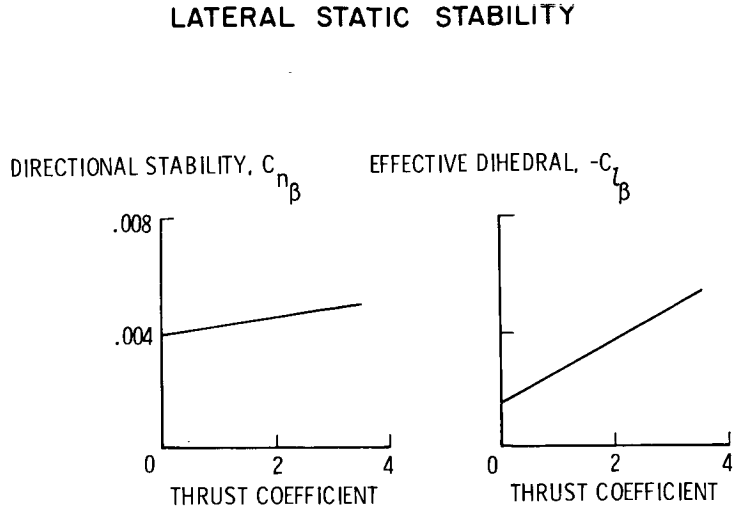

Figure 7

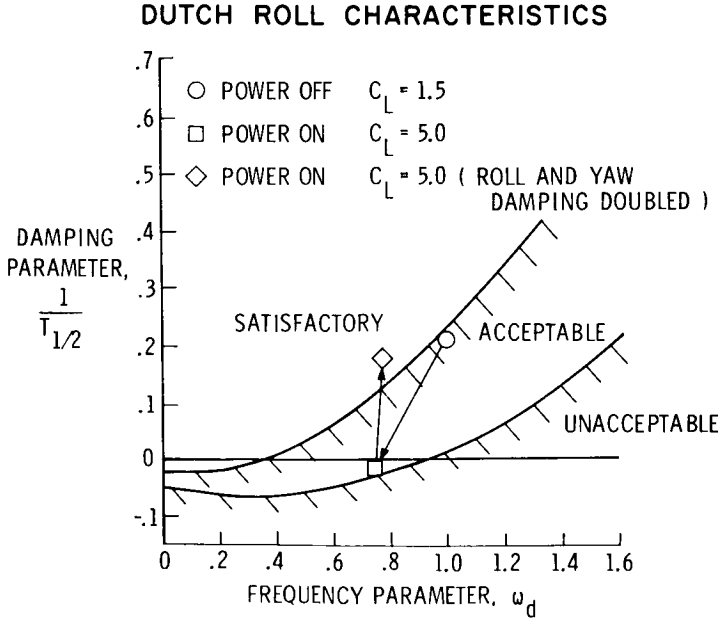

Figure 8

ENGINE-OUT ROLLING MOMENTS

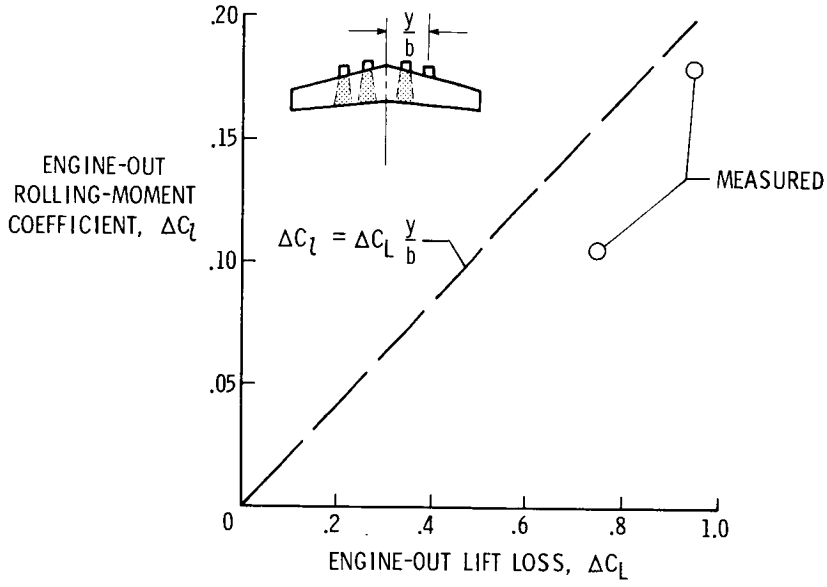

Figure 9

LATERAL TRIM WITH FULL-SPAN DIFFERENTIAL FLAP

OUTBOARD ENGINE OUT

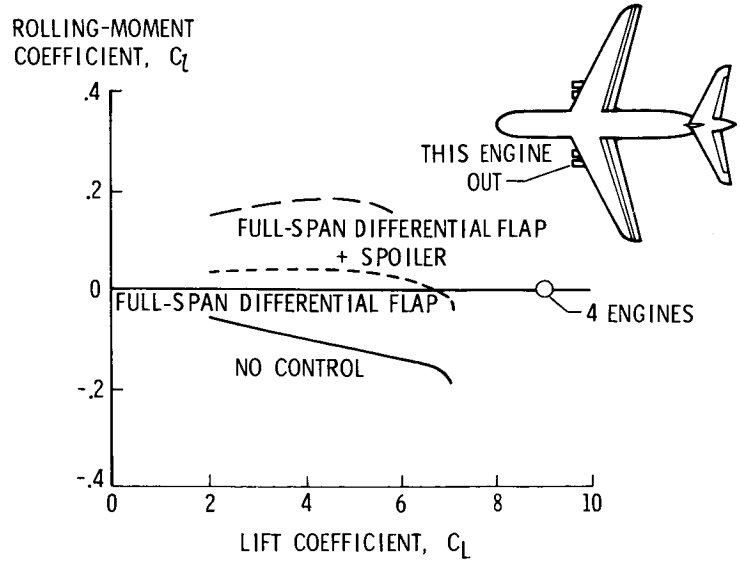

Figure 10

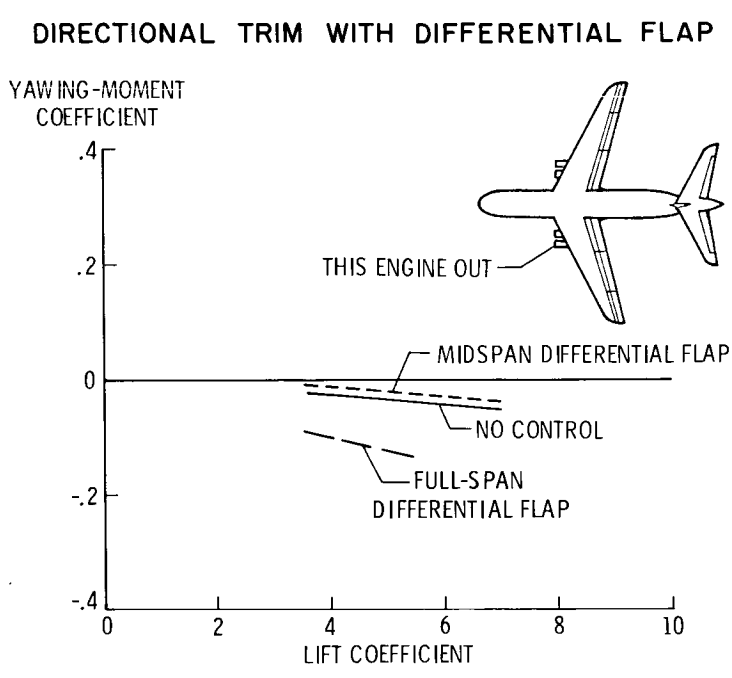

Figure 11

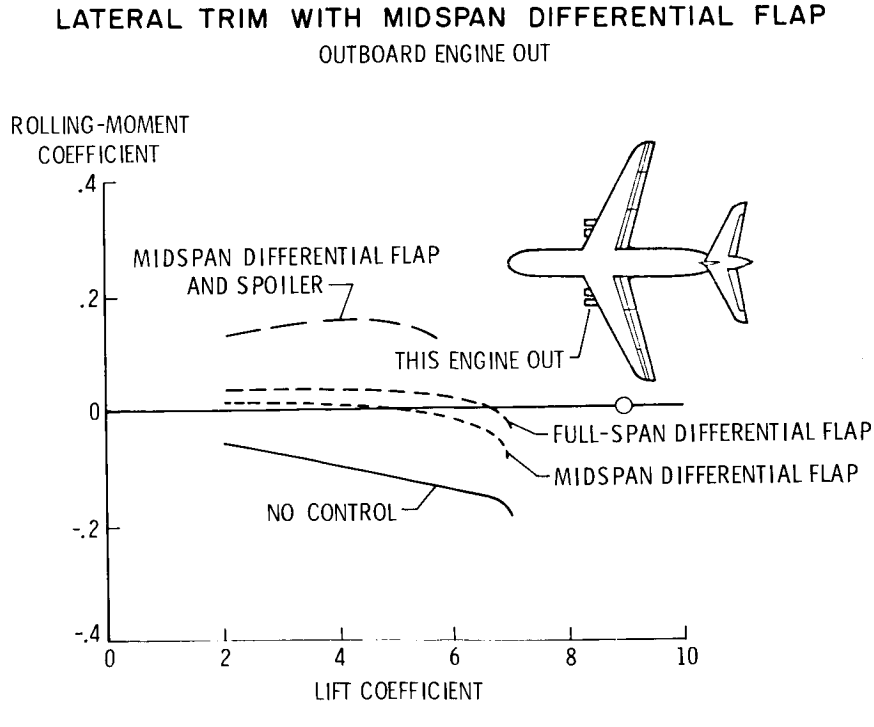

Figure 12

FREE-FLIGHT MODEL

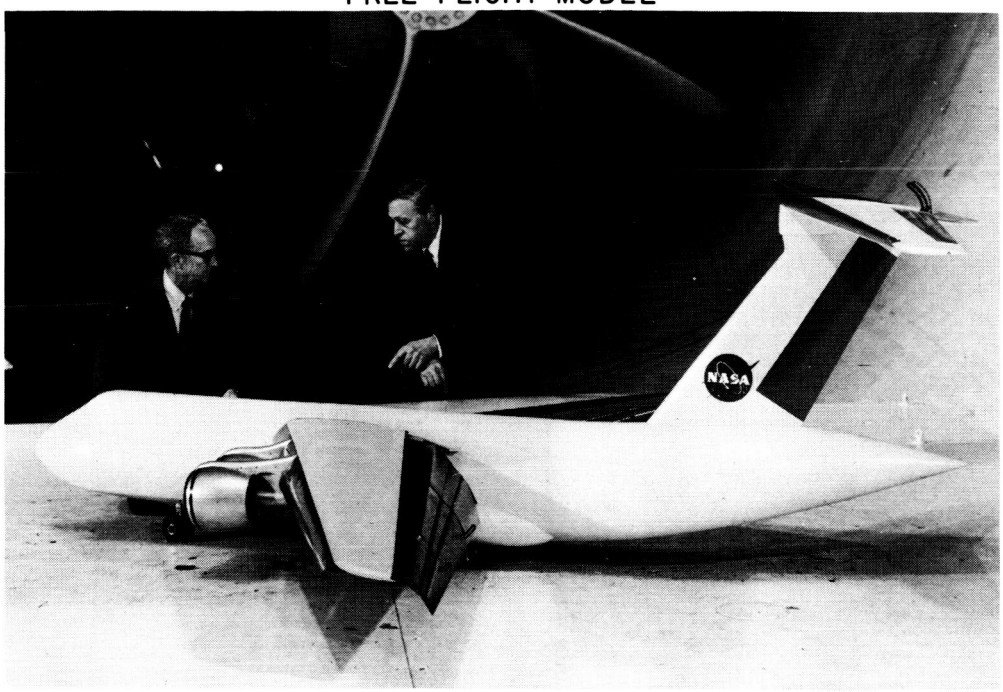

Figure 13

FREE-FLIGHT TEST TECHNIQUE

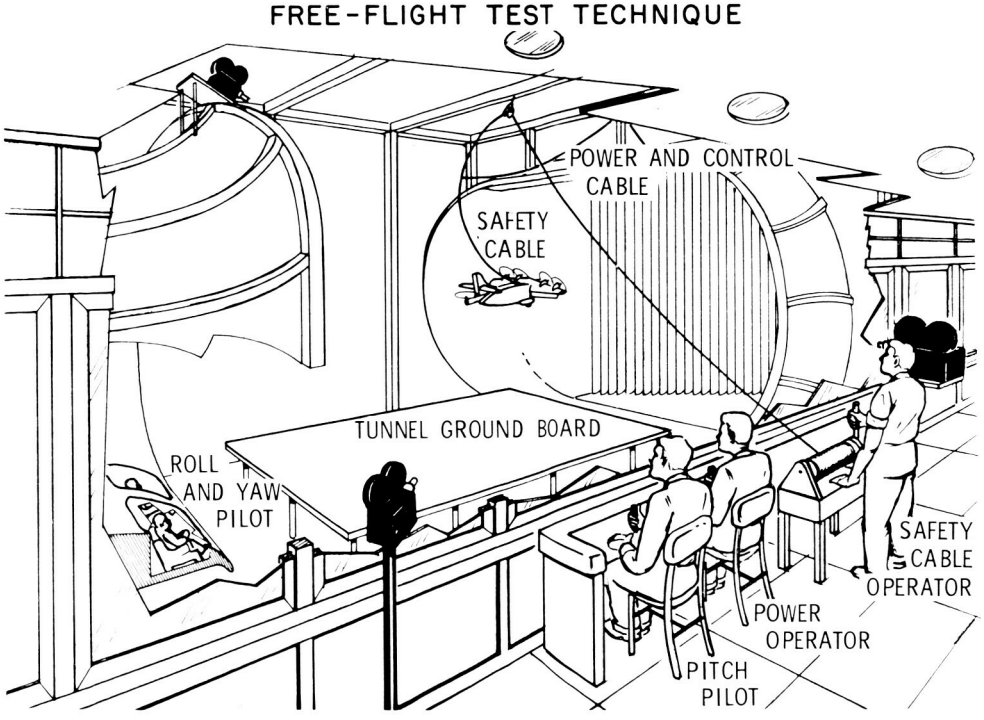

Figure 14

AERODYNAMIC CHARACTERISTICS OF A SWEPT AUGMENTOR WING

By David G. Koenig
NASA Ames Research Center

and

Michael D. Falarski
U.S. Army Air Mobility R&D Laboratory

SUMMARY

A brief outline of augmentor wing research sponsored by Ames Research Center is presented and is followed by a discussion of large-scale wind-tunnel test results for a swept augmentor wing configuration. The results showed that the augmentor wing could be applied to high-speed swept wing designs with little adverse effect on either the basic performance of the augmentor or the longitudinal characteristics, including maximum lift and stall. Three lateral control devices were shown to be effective and ground effect was measured for several complete aircraft configurations.

INTRODUCTION

As part of continuing research and development of the augmentor wing powered high-lift systems, tests have been made recently on a swept augmentor wing. Although the augmentor performed well on simple unswept wing planforms, there were significant questions concerning the adverse effects of sweep and taper ratio on augmentor wing performance. Design studies have shown that angles of sweep up to 25° would be required in order to maintain sufficient wing thickness to enclose the required ducting as well as to maintain the required cruise Mach numbers for augmentor wing aircraft.

Areas which could be adversely affected by this sweep are as follows: Augmentor performance – particularly at airspeed – could be affected by sweeping the augmentor inlet with respect to the local flow coming from the wing upper surface. Aircraft performance near 1g flight would be affected by adverse effects on basic forces and moments in view of previous experience in the application of other high-lift devices to swept wings. Characteristics at high angle of attack such as maximum lift and stall could be adversely affected by sweep. And, finally, lateral stability and control and ground effect are items which must be documented for use in design studies.

The wind-tunnel test program using a large-scale swept wing model was designed to answer questions in the areas just mentioned. Results will be summarized in this paper following a brief outline of augmentor wing research at Ames Research Center.

NOTATION

b	wing span, m (ft)
c	wing chord, m (ft)
$\bar{c}$	mean aerodynamic chord, m (ft)
C_D	drag coefficient, $\frac{\text{Drag}}{qS}$
C_{J_I}	total isentropic jet thrust coefficient, including augmentor, aileron BLC, and fuselage BLC, $\frac{F_I}{qS}$
C_L	lift coefficient, $\frac{\text{Lift}}{qS}$
C_l	rolling-moment coefficient, $\frac{\text{Rolling moment}}{qSb}$
C_m	pitching-moment coefficient, $\frac{\text{Pitching moment}}{qS\bar{c}}$
C_n	yawing-moment coefficient, $\frac{\text{Yawing moment}}{qSb}$
C_p	pressure coefficient, $\frac{p_l - p_\infty}{q}$
F	force of augmentor measured on static test, N (lb)
F_I	isentropic jet thrust, N (lb)
F_{nozzle}	force of primary nozzle, N (lb)
h	distance from ground to model wing chord plane at $\alpha = 0^o$, N (ft)
p_l	wing surface static pressure, N/m^2 (psf)
p_∞	free-stream static pressure, N/m^2 (psf)
q	free-stream dynamic pressure, N/m^2 (psf)
S	wing area, m^2 (ft^2)

T/W	ratio of total static engine thrust to aircraft weight
α	model angle of attack, deg
β	angle of sideslip, deg
δ_a	aileron deflection, deg
δ_f	augmentor deflection, augmentor centerline rotation from wing chord plane, deg
δ_{th}	engine residual thrust nozzle rotation, 0 when nozzle is parallel to wing chord plane, deg

BACKGROUND

The augmentor wing has been studied as a powered high-lift device which can be integrated with the aircraft propulsion system to improve the landing and takeoff characteristics of STOL aircraft. Work was started with unswept wing configurations in order to simplify the study of augmentor performance at forward speed. This was also a promising configuration which could result in a flight-test vehicle that could be built economically. A sketch of one of the more recent unswept-augmentor-wing-model configurations is shown in figure 1. Results of wind-tunnel tests on these configurations are presented in references 1 and 2. It was found that the aerodynamics of the configuration were good, particularly the longitudinal stability and control characteristics.

The augmentor wing was then chosen as the powered high-lift system for use on the NASA flight research vehicle. This aircraft is being flight tested, and initial flight-test results are discussed in paper no. 20 by Hervey C. Quigley and Richard F. Vomaski.

Work on advanced augmentor wing configurations has been continuing in order to improve augmentor performance and reduce noise of the augmentor wing. These subjects are also discussed in subsequent papers. Advanced augmentor wing concepts are being integrated into aircraft design studies and should be sufficiently generalized to help in the direction of future research and development. Some initial results in this effort are presented in references 3 to 6.

A significant part of this work is the study of the cruise augmentor wing. This is basically a thrust augmentor used as a propulsion device for aircraft at cruise. Two cruise augmentor wing programs are being sponsored by Ames Research Center. One is included in a contract with The Boeing Company and the other is a joint effort of the

United States and Canada. Each program has a different approach, but either design could lead to reduced weight and simplification of augmentor-wing-aircraft lift-propulsion systems.

The remainder of this paper summarizes results of recent tests in the Ames 40- by 80-foot wind tunnel. During the last 2 years, tests in and out of ground effect were made in a joint effort between the United States and Canada. The test data for these tests are presented in references 7, 8, and 9 and are summarized in the following discussion.

MODEL AND TEST DESCRIPTION

Figure 2 shows the model planform superimposed on the configuration used in a previous unswept wing test. The wing was swept 27.5° and had a slightly larger aspect ratio than the unswept wing. The wing had a taper ratio of 0.3 and an average section thickness of 0.115 compared with 0.4 and 0.16, respectively, for the unswept wing. As with the unswept wing the model had blown ailerons, used a full-span slat for leading-edge stall control, and was equipped with provisions for BLC across the top of the fuselage to control root stall. Further description of the model is presented in references 7, 8, and 9.

Photographs of the models are shown in figures 3, 4, and 5. Figures 3 and 5 show the model equipped with 4 JT15D powered nacelles to simulate unvectored residual thrust of the engine. The model is shown in figure 4 equipped with J85 nacelles. The nozzles for each of these nacelles swiveled from thrusting back parallel with the nacelle centerline to 30° forward of vertical. For the out-of-ground-effect tests the model was installed near the center of the wind-tunnel test section. The model was tested near the floor of the wind tunnel to simulate the effect of ground as shown in figures 4 and 5.

A comparison of the augmentor configuration with a previous configuration used on the unswept wing is shown in figure 6. The primary difference was the elimination of the slot on the flap. Bench tests of 2D models made prior to installation of the augmentor model indicated that augmentation ratios F/F_I were decreased from a maximum of 1.39 to 1.37 by eliminating this slot.

RESULTS AND DISCUSSION

Augmentor Performance

Prior to the wind-tunnel tests, the augmentation of the fully assembled augmentor was measured with the model on a static test stand. The results are summarized in figure 7 and are presented in more detail in reference 8. Augmentation ratio shown is the ratio of augmentor measured thrust to the nozzle thrust measured with the augmentor

removed. The maximum values of augmentation ratio of 1.43 and 1.33 for the 2D and large-scale model, respectively, compare well when it is considered that no attempt was made to optimize the augmentor after it was installed on the large-scale model. This comparison between the bench tests and complete model static tests was similar to corresponding comparisons for the unswept model, and it can therefore be concluded that there were no major adverse effects of sweep on static augmentor performance. Preliminary analysis of augmentor performance at forward speed indicated that here no performance was not adversely affected by sweep. Further discussion of the augmentor performance at forward speed is included in paper no. 8 by Thomas N. Aiken.

Longitudinal Characteristics

A comparison of two sets of basic data for the unswept and swept wing configurations is presented in figure 8 for the models with tail off. The ailerons were deflected 45° and 30° for the unswept and swept wings, respectively, the augmentor flap was 50°, and the jet coefficient was 0.8. It is evident that the lift and drag characteristics are similar, with the lift-curve slope and maximum lift the same and the slope of the drag curve being of the same shape. A comparison of the moment data shows that both curves are close to linear and if the moment center for the swept wing model were moved back $0.07\overline{c}$ the two sets of moment data could be superimposed.

The effects of sweep on lift as functions of power and flap deflection are shown in figures 9 and 10 for zero angle of attack as well as maximum lift. The flap lift increments as well as the maximum lift obtained for the swept wing are seen to bracket the values measured for the unswept wing; thus, the effects of power on the lift were the same for the two models. One significant difference appeared in maximum lift (fig. 10); values decreased for the unswept wing as flap deflection increased and remained about the same for the swept wing.

The basic stalling characteristics were different from those of the unswept wing for some wing configurations in that the swept wing generally stalled first at the wing tips whereas the unswept wing generally stalled at the root and fuselage blowing boundary-layer control improved maximum lift for that case (see ref. 2). For the swept wing the effect of symmetric aileron deflection on stall is shown in figure 11 for the landing flap setting $(\delta_f = 70^{\circ})$. The C_{m_α} curves in the upper portion of the figure show pitch-up occurred for the $\delta_a = 30^{\circ}$ and 45° settings. The tendency to pitch up was eliminated up to 32° angle of attack by reducing the aileron droop to 15°. The reason for this is shown by the variation with spanwise location of pressure coefficient on the wing at 0.07c which may be used as a qualitative spanwise load distribution along the wing. The data show a loss in loading at the wing tip and a slight gain in lift at the root. Tendency to pitch up or an adverse stalling characteristic can therefore be reduced by undrooping the

ailerons. As may be seen from the lift data of references 7 and 8, reducing δ_a from 45^o to 15^o reduces $C_{L_{max}}$ by only 0.25.

During the investigations of references 7 and 8, three tail heights were considered for the tail lengths indicated in figure 2. The heights ranged from the extended wing chord plane to $1.4\bar{c}$ above the chord plane. Downwash data were obtained for all three tail positions and tail-on force and moment data are available for the two higher positions. For both of these positions, the stability and control characteristics of the complete aircraft configurations were excellent. As an example, the effect of power on trim is shown in figure 12 for a moment center located at 35 percent chord. The data are chosen for trim lift values of 3.5 and 5.2 for the takeoff and landing flap deflections, respectively, for the condition of 1g flight. As shown, the effect of power was slight for values of T/W of 0.3 and 0.4 and, although not shown, this conclusion is valid for a much larger range of T/W. Also, for the lift range shown, static stability was not influenced greatly by power.

During the tests reported in references 8 and 9, nacelle-wing interference effects were measured, particularly with the powered nacelle configurations shown in figures 4 and 5. In augmentor wing designs, between 40 and 80 percent of the engine thrust is ducted to the augmentor and the remainder is exhausted under the wing. The nacelle-wing interference effects were measured over a thrust range representing these distributions, or thrust splits, and typical results are shown in figure 13 for the four-nacelle configuration with no thrust deflection. The lift and drag values for the takeoff flap setting $(\delta_f = 40^o)$ are presented as functions of augmentor jet thrust C_{J_I} for nacelles off and two thrust splits. The lift and drag coefficients are those resulting after the gross engine thrust has been subtracted. For the higher values of C_{J_I}, the lift for the 60-40 (engine-augmentor) split was 11 percent below the nacelle-off values but a significant portion of this was also measured for the 33-67 split. A split of 25-75 is being seriously considered for some current augmentor wing designs, and for these the adverse effects of both nacelle and residual thrust could probably be considered small. It is believed that adverse effects of residual thrust could be further reduced by slight downward deflection of the jet.

Lateral Characteristics

Lateral stability and control characteristics of the swept augmentor wing model are presented in references 7 and 8. It was shown that both C_{l_β} and C_{n_β} were linear with augmentor thrust and comparable to those of wings equipped with other powered high-lift systems. The lateral control methods investigated proved to be effective, and control options are summarized in figure 14. The data are presented in terms of rolling-moment and yawing-moment increment obtained while one side of each control is cycled. The values were found to be additive except where the aileron is moved together with the spoiler

of the same side since the spoiler reduced the effectiveness of the aileron. An interesting combination of the devices would be the use of the spoilers in conjunction with the augmentor throttling for a fixed symmetrical aileron droop where, as shown by the yawing-moment data, the yawing-moment inputs would tend to cancel and to produce little or no yawing moment due to roll control.

Ground Effect

The ground effect of the model was measured by using the wind-tunnel test-section floor as a fixed ground board with the model installed as shown in figures 4 and 5. Results of the measurements are shown in figures 15 and 16 for the cases of the basic wing and two nacelles installed (configuration of fig. 4), respectively. The lift data are presented for constant angle of attack which represents an aircraft touchdown attitude, and the drag data are shown for a typical approach lift value. The measurements showed that below a value of $C_{J_I} = 0.6$, ground effect was negligible. For values of C_{J_I} above 0.6, the adverse effect on lift increased with C_{J_I} to a value representing a 10-percent reduction in lift. The ground effect on drag for a constant lift coefficient was found to be negligible. It should be noted that these effects were due to reducing ground height $1.34\bar{c}$ which would be approximately wheel height at touchdown.

CONCLUDING REMARKS

In summary, it was found that the augmentor wing could be applied to a high-speed swept wing configuration and result in favorable longitudinal and lateral characteristics. There were found to be no major adverse effects of sweep on augmentation ratio or on basic lift, drag, and moment characteristics; maximum lift and the stall were mild but could be controlled by proper choice of symmetrical aileron droop.

Investigations of the lateral characteristics of the swept augmentor wing indicated that three controls were effective and a system was possible having no yawing-moment input.

Ground effect measurements showed a small adverse effect on lift when ground height was reduced to 1.34 chords or wheel height.

REFERENCES

1. Koenig, David G.; Corsiglia, Victor R.; and Morelli, Joseph P.: Aerodynamic Characteristics of a Large-Scale Model With an Unswept Wing and Augmented Jet Flap. NASA TN D-4610, 1968.

2. Cook, Anthony M.; and Aiken, Thomas N.: Low-Speed Aerodynamic Characteristics of a Large-Scale STOL Transport Model With an Augmented Jet Flap. NASA TM X-62,017, 1971.

3. O'Keefe, J. V.; and Kelley, G. S.: Design Integration and Noise Studies for Jet STOL Aircraft. Vol. I – Program Summary. D6-40552-1 (Contract NAS2-6344), Boeing Co., May 1972. (Available as NASA CR-114471.)

4. Roepcke, F. A.; and Kelley, G. S.: Design Integration and Noise Studies for Jet STOL Aircraft. Vol. II – System Design and Evaluation Studies. D6-40552-2 (Contract NAS2-6344), Boeing Co., May 1972. (Available as NASA CR-114472.)

5. Campbell, J. M.; Lawrence, R. L.; and O'Keefe, J. V.: Design Integration and Noise Studies for Jet STOL Aircraft. Vol. III – Static Test Program. D6-40552-3 (Contract NAS2-6344), Boeing Co., May 1972. (Available as NASA CR-114473.)

6. Wang, T.; Wright, F.; and Mahal, A.: Design Integration and Noise Studies for Jet STOL Aircraft. Vol. IV – Wind Tunnel Test Program. D6-40552-4 (Contract NAS2-6344), Boeing Co., May 1972. (Available as NASA CR-114474.)

7. Falarski, Michael D.; and Koenig, David G.: Aerodynamic Characteristics of a Large-Scale Model With a Swept Wing and Augmented Jet Flap. NASA TM X-62,029, 1971.

8. Falarski, Michael D.; and Koenig, David G.: Longitudinal and Lateral Stability and Control Characteristics of a Large-Scale Model With a Swept Wing and Augmented Jet Flap. NASA TM X-62,145, 1972.

9. Falarski, Michael D.; and Koenig, David G.: Longitudinal Aerodynamic Characteristics of a Large-Scale Model With a Swept Wing and Augmented Jet Flap in Ground Effect. NASA TM X-62,174, 1972.

UNSWEPT WING MODEL

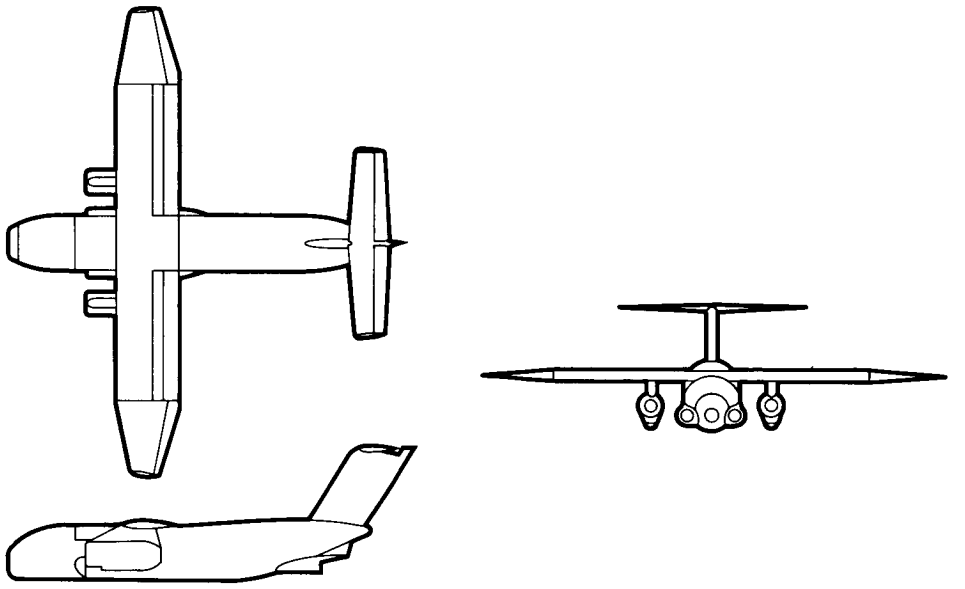

Figure 1

COMPARISON OF SWEPT AND UNSWEPT WING MODEL CONFIGURATIONS

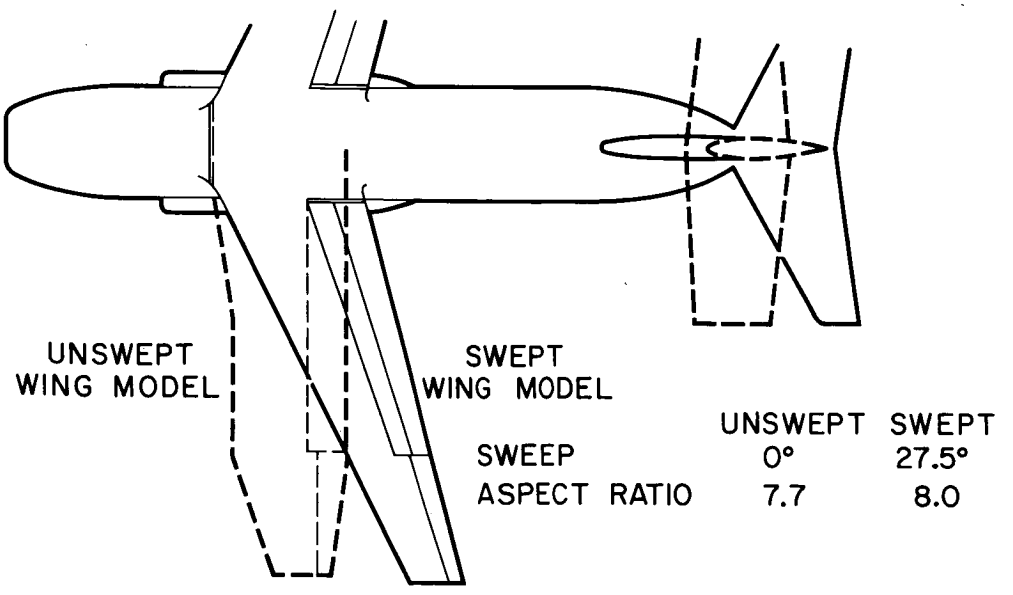

Figure 2

SWEPT WING MODEL INSTALLED IN THE
40-BY 80-FOOT WIND TUNNEL

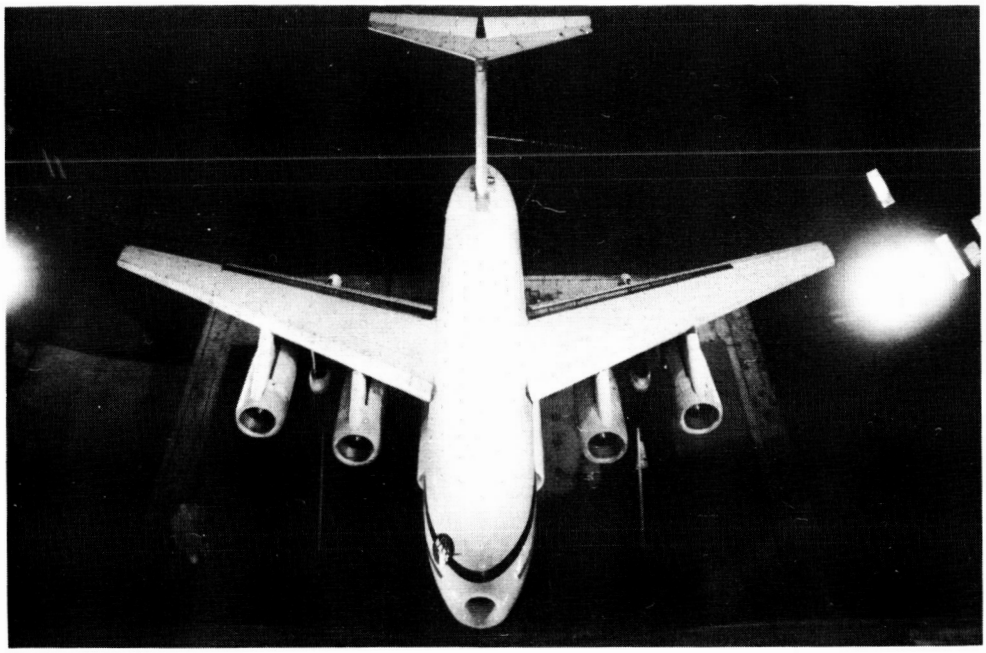

Figure 3

AUGMENTOR WING MODEL INSTALLED IN WIND
TUNNEL FOR GROUND EFFECT TESTS

J85 NACELLES

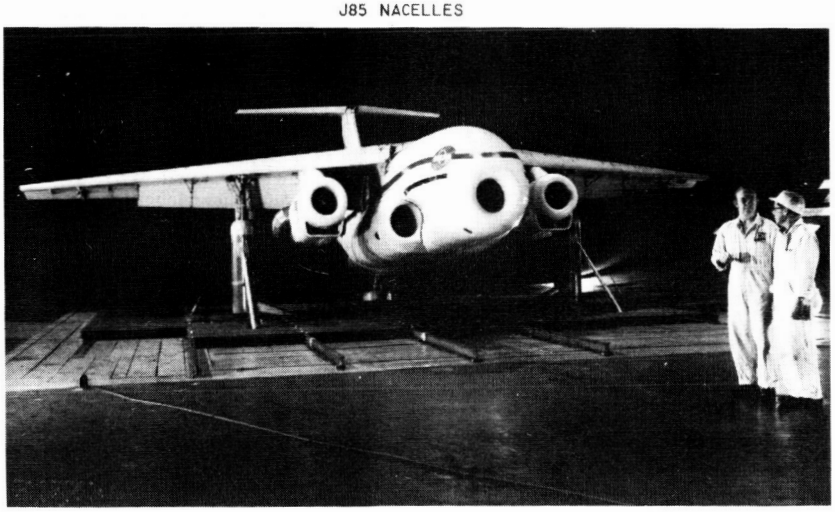

Figure 4

AUGMENTOR WING MODEL INSTALLED IN WIND TUNNEL FOR GROUND EFFECT TESTS

JT15D NACELLES

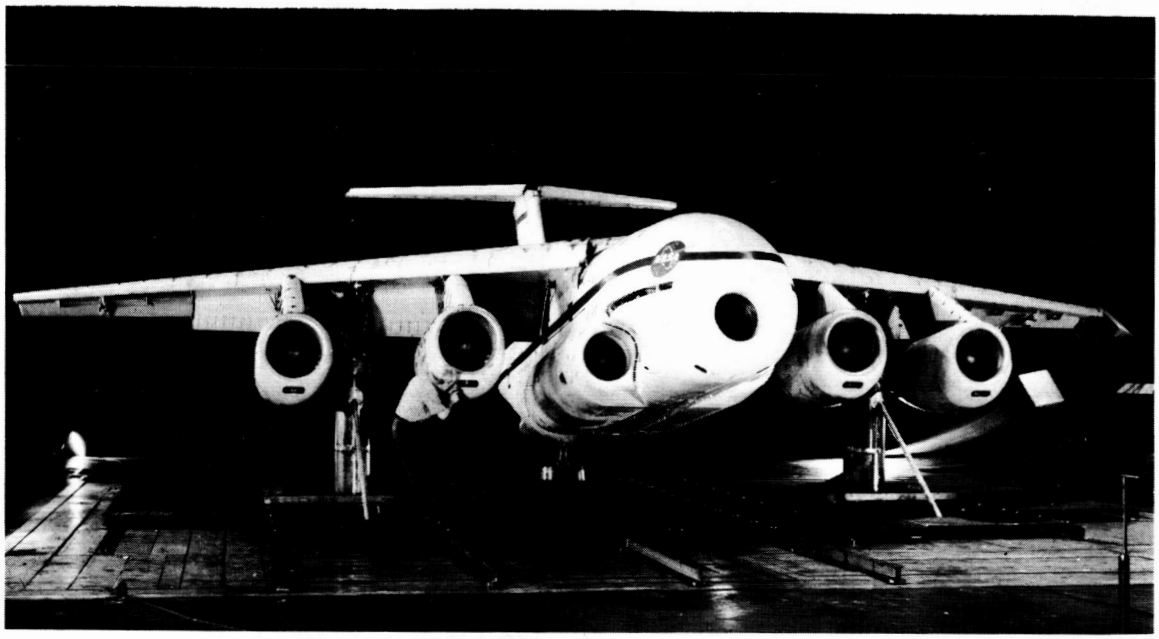

Figure 5

STREAMWISE SECTION OF AUGMENTOR FLAP

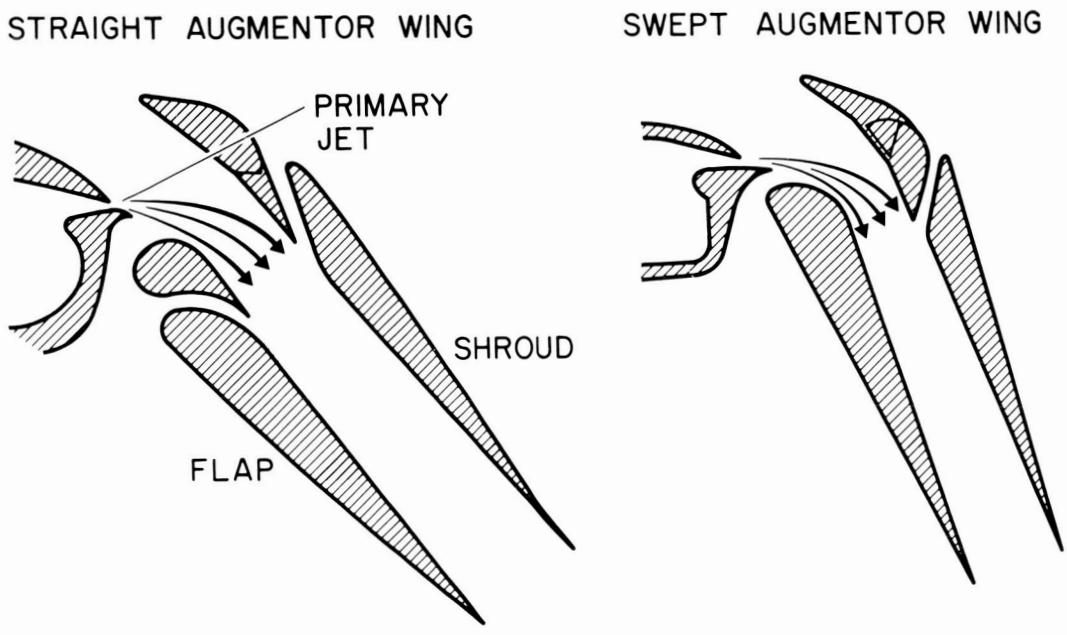

Figure 6

AUGMENTOR STATIC PERFORMANCE FOR SWEPT WING

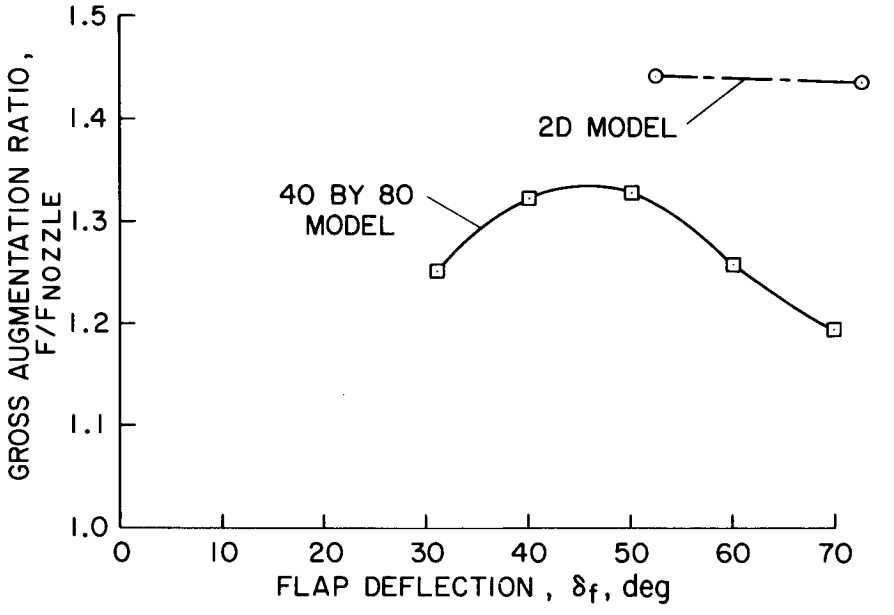

Figure 7

UNSWEPT AND SWEPT WING COMPARISON
LONGITUDINAL CHARACTERISTICS

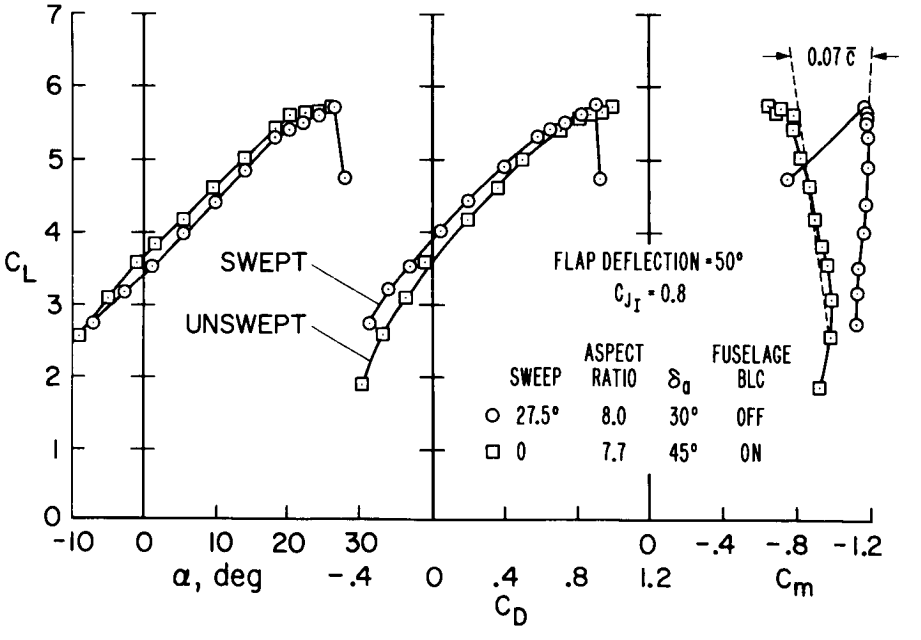

Figure 8

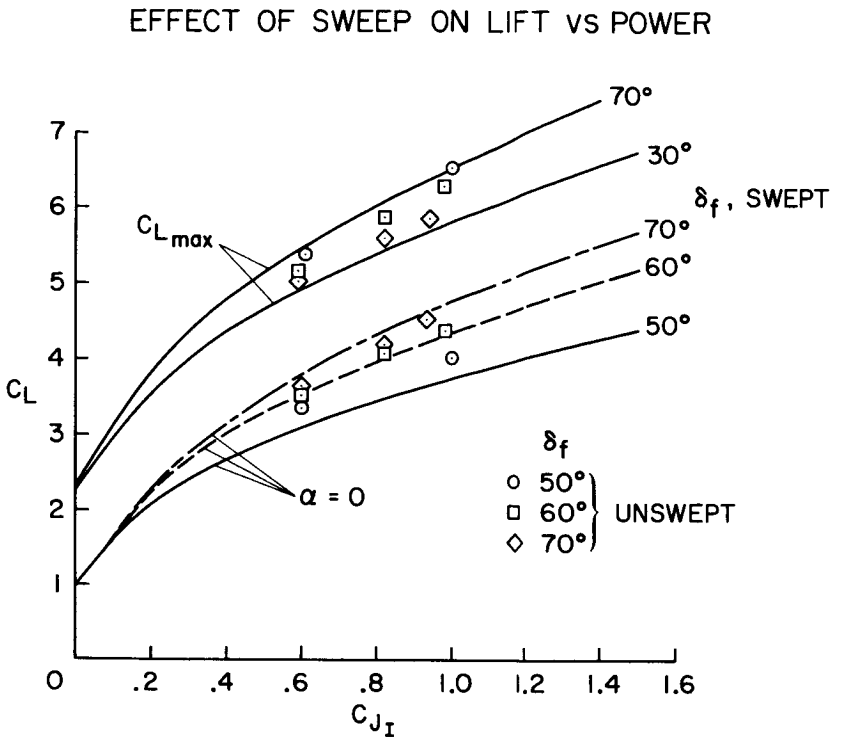

Figure 9

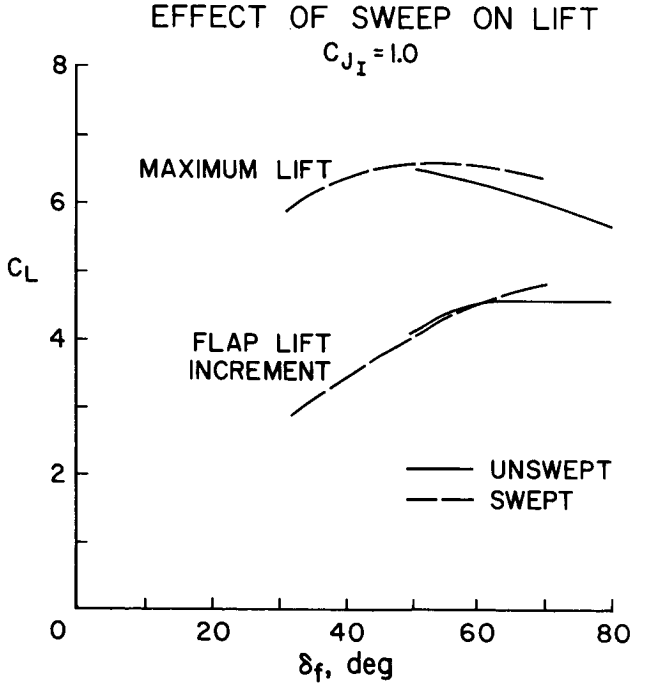

Figure 10

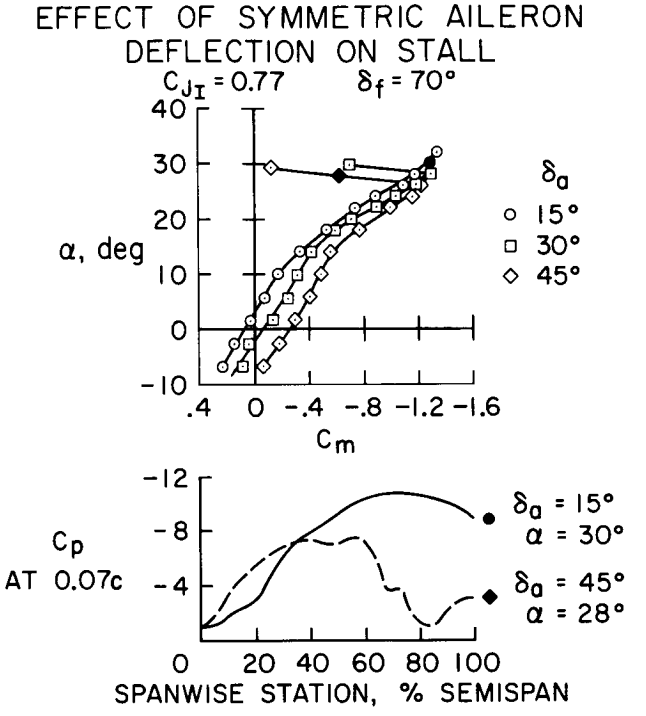

Figure 11

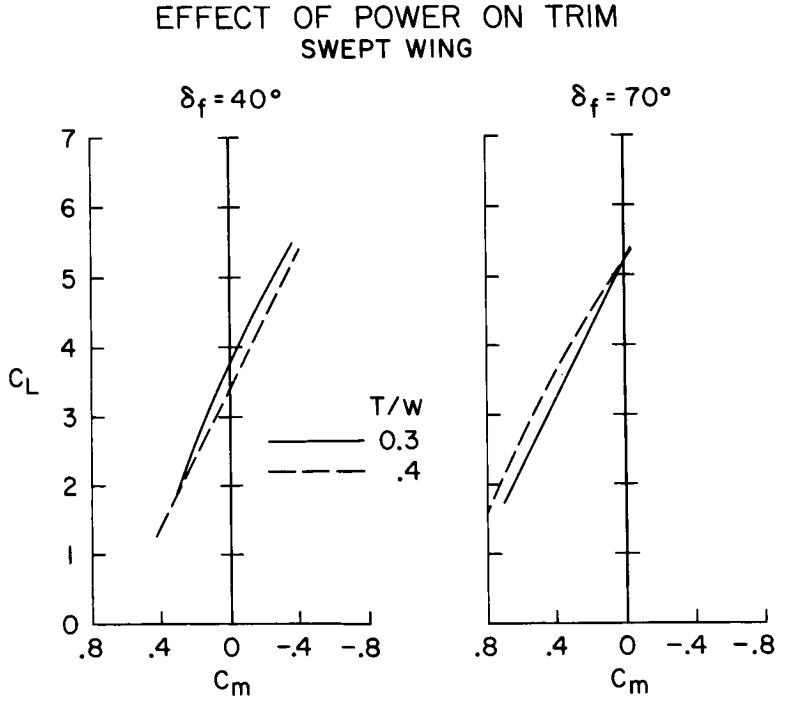

Figure 12

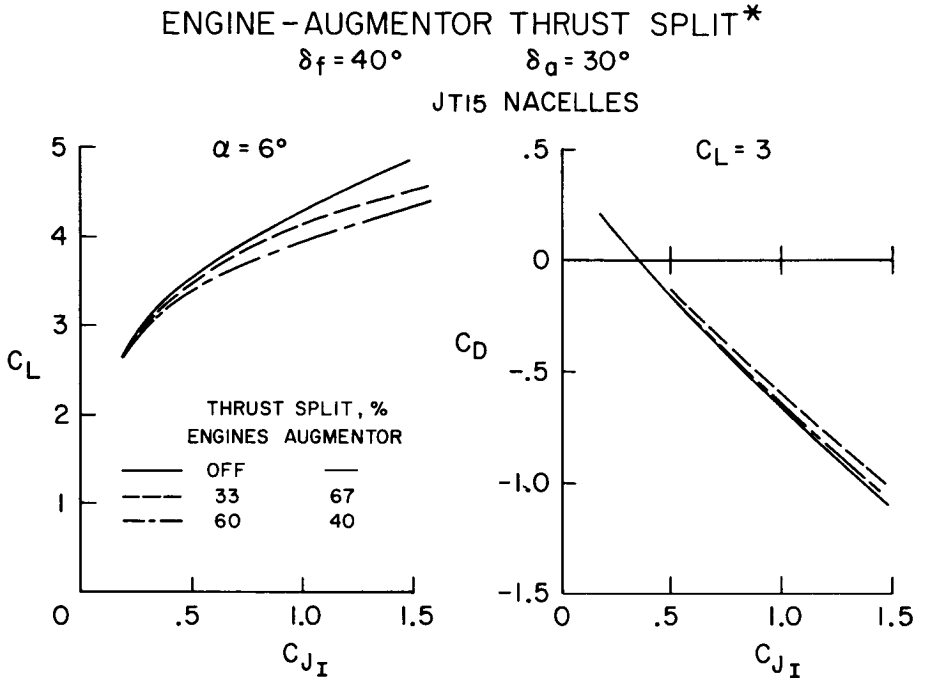

*MEASURED DURING GROUND EFFECT TESTS AT 2.04 CHORDS GROUND HEIGHT

Figure 13

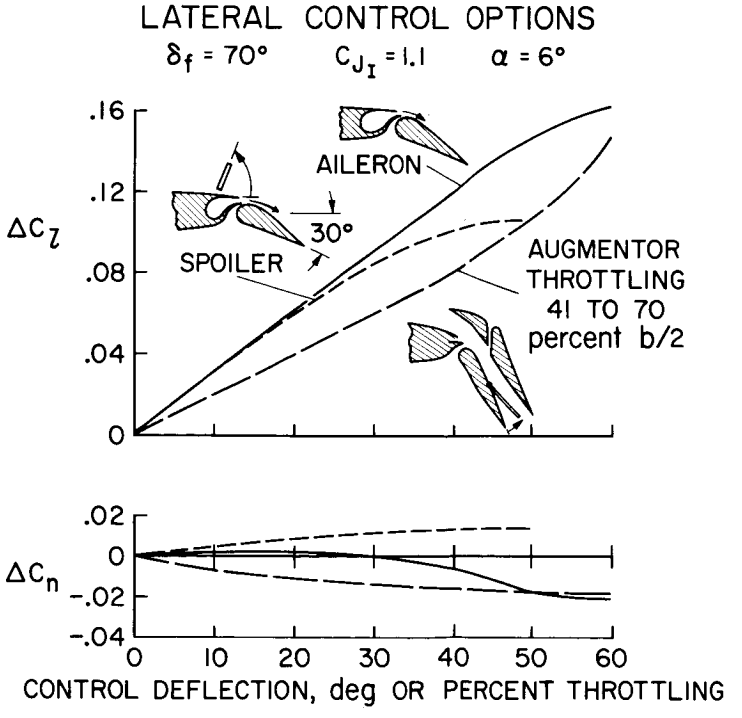

Figure 14

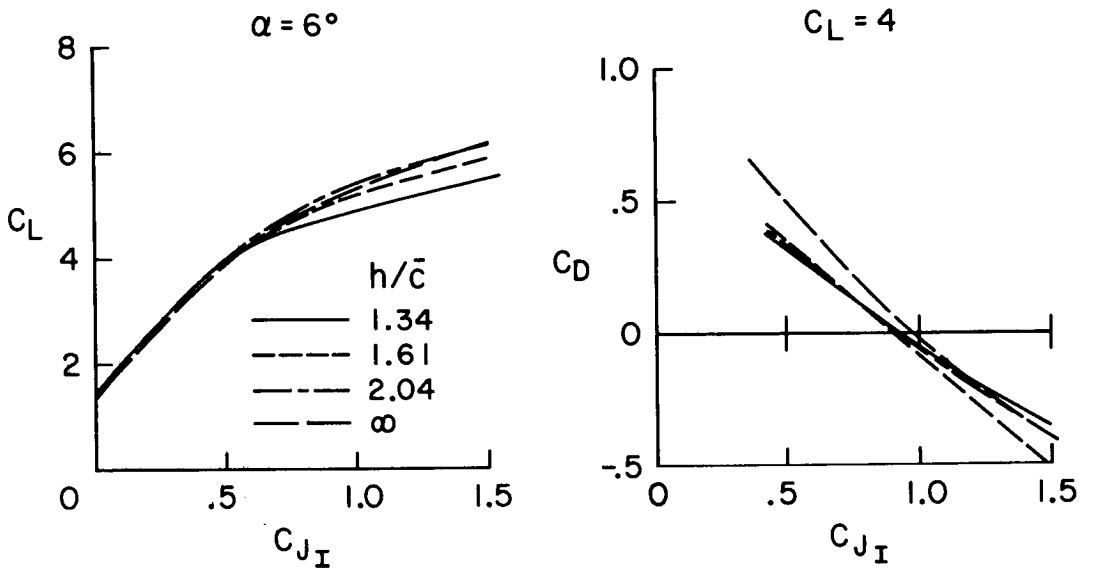

Figure 15

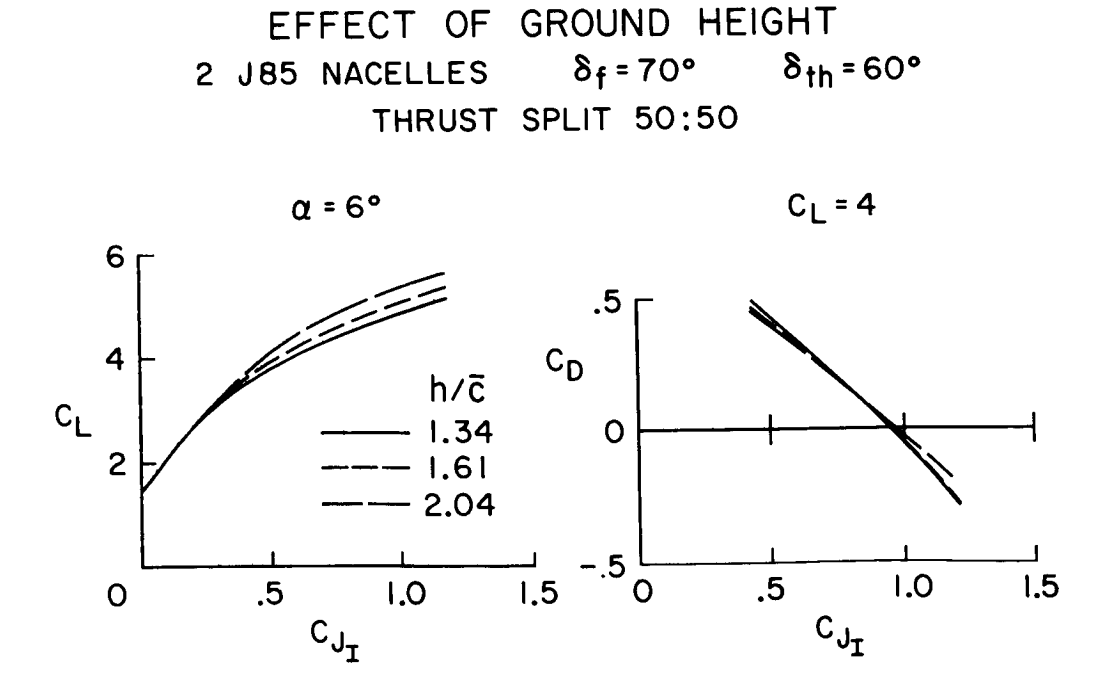

Figure 16

ADVANCED AUGMENTOR-WING RESEARCH

By Thomas N. Aiken
NASA Ames Research Center

SUMMARY

Results of research on advanced augmentors are discussed. Research concerned with performance has indicated that: (1) Augmentors with lobe-type nozzles give higher thrust augmentation than those with slot-type primary nozzles, (2) the thrust of augmentor wings at forward speed is greater than that of internally blown flaps for the speed range of interest, and (3) the optimum augmentor geometry at forward speed may be different from the optimum static geometry. Analysis of augmentor-wing data has shown that the data may be correlated by accounting for the augmentation and entrainment in defining a net thrust coefficient.

INTRODUCTION

Research programs have been conducted both by contractors and by NASA to improve augmentor performance and reduce the noise of the augmentor. This paper will cover only the performance aspects of these studies; however, noise reduction was the major driving force of the study. Specifically, the topics to be covered in this paper are thrust augmentation performance of augmentors designed to be quiet, a comparison of thrust available from conventional jet flaps and the augmentor wing, and thrust correlating parameters.

SYMBOLS

C_D drag coefficient

$C_{D,i}$ induced drag coefficient

$C_{D,o}$ profile drag coefficient

C_J nozzle jet thrust coefficient, $\frac{\text{Nozzle thrust}}{q_\infty S}$

$C_{J,net}$ net jet thrust coefficient, $\phi C_J - 2C_q$

C_L lift coefficient

C_q secondary mass flow coefficient, $\frac{\text{Secondary mass flow}}{\rho_\infty V_\infty S}$

h average nozzle height, cm (in.)

ℓ flap length, cm (in.)

$\dot{m}$ mass flow rate, kg/sec (lbm/sec)

q_{JET} nozzle jet dynamic pressure, N/m^2 (lb/ft^2)

q_∞ free-stream dynamic pressure, N/m^2 (lb/ft^2)

S wing reference area, m^2 (ft^2)

V velocity, m/sec (ft/sec)

ϕ thrust augmentation ratio, $\frac{\text{Augmentor thrust}}{\text{Nozzle thrust}}$

ρ density, kg/m^3 ($slugs/ft^3$)

Subscripts:

primary nozzle

secondary free-stream air entrained by augmentor

∞ free stream

RESULTS AND DISCUSSION

Development of the slot-type augmentor, shown in figure 1, was begun in the early 1960's by the Canadian Defence Research Board and De Havilland Aircraft of Canada. During the latter part of the 1960's, research on a large scale was conducted at the Ames Research Center with joint Canadian-NASA sponsorship. This work produced an effective augmentor that was appropriate for flight testing but, with the growing emphasis on noise, was too noisy. Research to reduce noise led to studies of multielement nozzles.

Static Performance

At Ames Research Center the performance of multielement nozzles has been studied. This effort led to the nozzle depicted in figure 2. This nozzle has a small continuous slot as well as discrete vertical lobes. Other multielement nozzles may have vertical lobes alone and may have different height and spacing values. The basic difference between the characteristics of the nozzles in figures 1 and 2 is that the lobe nozzle improves mixing by distributing the primary flow over much of the inlet, whereas the slot nozzle is limited to mixing obtained by natural jet spreading.

The maximum static thrust augmentation for the two types of nozzles is shown plotted against the nondimensional mixing length in figure 3. Data for the upper curve were obtained from references 1 to 4 and the present investigation. The lower curve was extracted from some unpublished data. The figure shows that lobe nozzle augmentors give higher thrust augmentation than slot nozzle augmentors at a given value of mixing length.

System studies reported in references 1 to 4 indicate that a typical, quiet, 150-passenger, augmentor-wing STOL would have as much thrust as possible in the nozzles and a resultant nondimensional mixing length of about 50. At that value, figure 3 shows that lobe nozzles give a 50-percent increase in augmentation or a 10-percent increase in thrust compared with slot nozzles.

The manner in which the lobe nozzles increase the thrust augmentation is shown in figure 4, a plot of the exit velocity profiles for the two types of nozzles. Both nozzles are canted 30^{o} so that there is no turning within the augmentor. The primary momentum is approximately the same for each nozzle.

An integration of the two curves would show that the lobe nozzle has greater momentum and mass flow, hence greater thrust augmentation and secondary flow entrainment, than the slot nozzle. Also, because the profile for the lobe nozzle is more uniform, the lobe is more efficient than the slot nozzle and gives greater thrust augmentation per entrained flow.

The static noise characteristics of lobe nozzles are better than those of slot nozzles and are shown in detail in paper no. 31 by Falarski, Aoyagi, and Koenig.

Forward Speed

At forward speed, the augmentor wing is basically an internally blown flap (IBF), hence one would expect their characteristics to be similar. There are, however, two basic differences. First, the augmentor wing lacks strong boundary-layer control on the upper shroud surface, which may lead to shroud flow separation at high flap angles.

Second, the addition of a shroud causes thrust augmentation and secondary flow entrainment much like a propulsive device.

The effect of this last difference is shown in figure 5. This is a plot of nondimensional thrust as a function of nondimensional forward speed for an augmentor wing and an internally blown flap at identical conditions. The data are from references 1 to 4. The shroud forms an ejector and thereby increases thrust at low forward speeds. This thrust due to the augmentor falls off with forward speed due to secondary flow momentum drag. However, for the range of forward speeds from static to takeoff, the augmentor wing has greater net thrust than the internally blown flap. This would result in a smaller required installed thrust for a given mission.

The effect of adding a shroud is also shown in figure 6. The figure shows drag polars from references 1 to 4. All the polars are at the same nozzle thrust coefficient C_J but are at different forward speeds and pressure ratios (PR). The figure indicates that C_J is a reasonable correlating parameter at low forward speeds and pressure ratios, but fails at the higher values of each.

The drag characteristics of the augmentor wing are dependent on the net thrust or the gross augmented thrust minus the secondary flow inlet momentum. The momentum drag can be calculated if it is assumed that the augmentation and entrainment do not change with forward speed, only with pressure ratio, so that the static values may be used. Values of static augmentation and entrainment as a function of pressure ratio are shown in figure 7 for the data in figure 6.

Figure 8 shows the drag equation for the augmentor wing; $C_{D,o}$ and $C_{D,i}$ are the profile and induced drag coefficients, respectively. If the assumptions are correct, subtracting the effects of the augmentor, $-\phi C_J + 2C_q$, from the data of figure 6 should collapse the data to a single line since they have identical profile and induced drags. The right-hand plot of figure 8 indicates that the assumptions were correct. The drag polars are nearly identical; thus, the difference in the drag polars of figure 6 was due to the differences in $\phi C_J - 2C_q$ or $C_{J,net}$ caused by changes in augmentation and entrainment with pressure ratio.

These results indicate that static augmentor results can be used to adjust data for the effect of pressure ratio if $C_{J,net}$ is used for the correlating parameter. This, of course, applies only to data from the same augmentor configuration.

Turning now to lift characteristics, figure 9 shows the effect of some geometry changes on the lift of an augmentor wing at a high flap angle. The normal configuration is similar to the augmentor of reference 5, but with a lobe nozzle. Both lowering the shroud (moving it rearward relative to the flap) and closing the lower gap (practical only

with a lobe nozzle) improve the lift characteristics. Closing the lower gap also improves the lift at low flap angles. Static augmentation is reduced with both these changes.

CONCLUSIONS

From the results and discussion contained in this paper, the following conclusions can be made:

1. Lobe nozzles give higher augmentation than slot nozzles.

2. The thrust of an augmentor wing at forward speed is greater than that of an internally blown flap for the range of interest of thrust coefficients.

3. Augmentor wing drag data should be correlated with a net jet thrust coefficient to account for the augmentation and entrainment.

4. Optimum augmentor geometry at forward speed may be different from optimum static geometry.

REFERENCES

1. O'Keefe, J. V.; and Kelley, G. S.: Design Integration and Noise Studies for Jet STOL Aircraft. Vol. I – Program Summary. D6-40552-1 (Contract NAS2-6344), Boeing Co., May 1972. (Available as NASA CR-114471.)

2. Roepcke, F. A.; and Kelley, G. S.: Design Integration and Noise Studies for Jet STOL Aircraft. Vol. II – System Design and Evaluation Studies. D6-40552-2 (Contract NAS2-6344), Boeing Co., May 1972. (Available as NASA CR-114472.)

3. Campbell, J. M.; Lawrence, R. L.; and O'Keefe, J. V.: Design Integration and Noise Studies for Jet STOL Aircraft. Vol. III – Static Test Program. D6-40552-3 (Contract NAS2-6344), Boeing Co., May 1972. (Available as NASA CR-114473.)

4. Wang, T.; Wright, F.; and Mahal, A.: Design Integration and Noise Studies for Jet STOL Aircraft. Vol. IV – Wind Tunnel Test Program. D6-40552-4 (Contract NAS2-6344), Boeing Co., May 1972. (Available as NASA CR-114474.)

5. Falarski, M. D.; and Koenig, D. G.: Longitudinal and Lateral Stability and Control Characteristics of a Large-Scale Model With a Swept Wing and Augmented Jet Flap. NASA TM X-62,145, 1972.

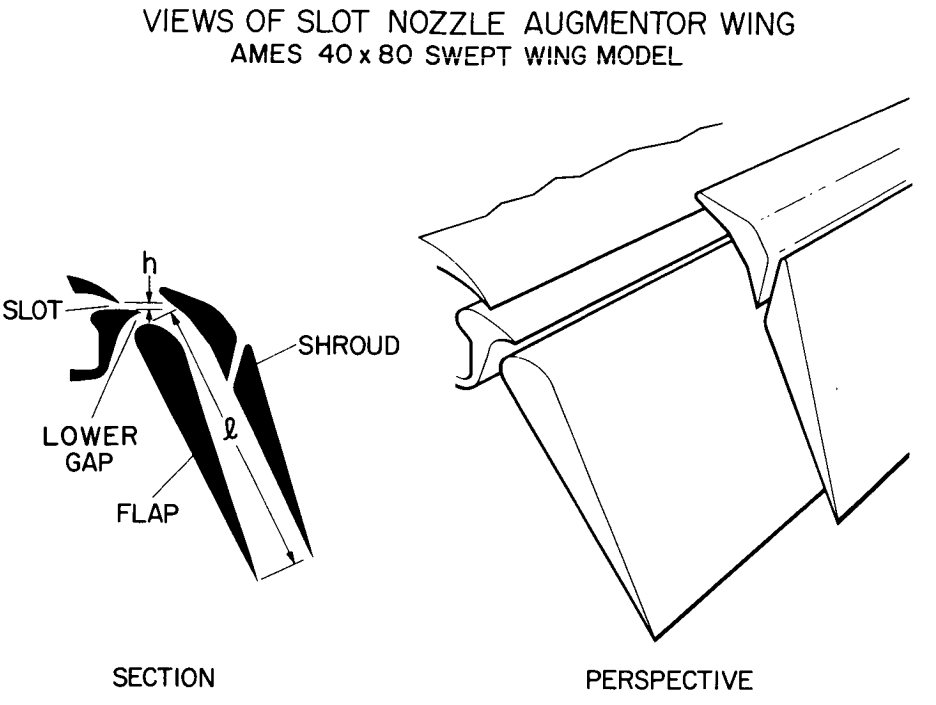

Figure 1

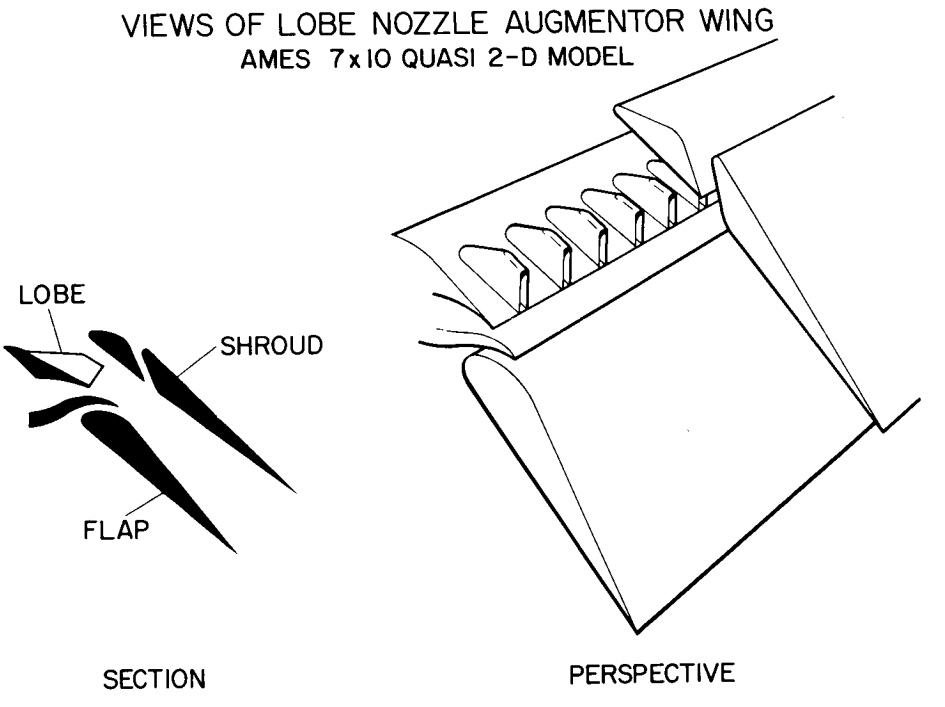

Figure 2

EFFECT OF MIXING LENGTH ON THE MAXIMUM STATIC THRUST AUGMENTATION OF TWO NOZZLE TYPES

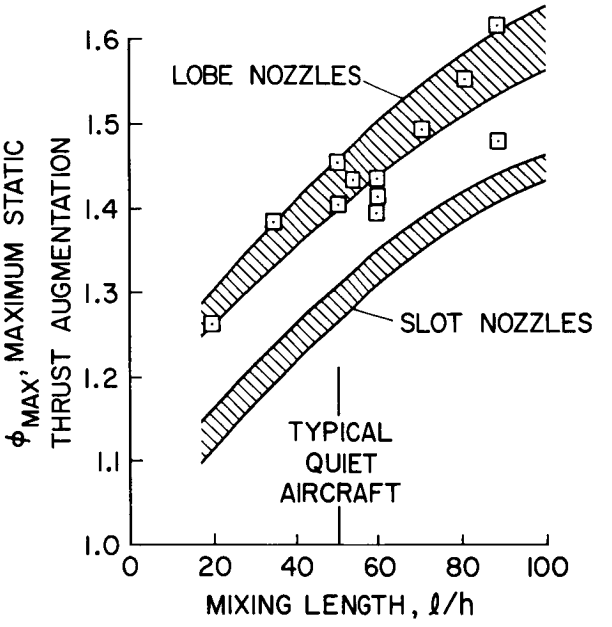

Figure 3

EXIT VELOCITY PROFILES FOR TWO NOZZLES
FLAP ANGLE = 30°

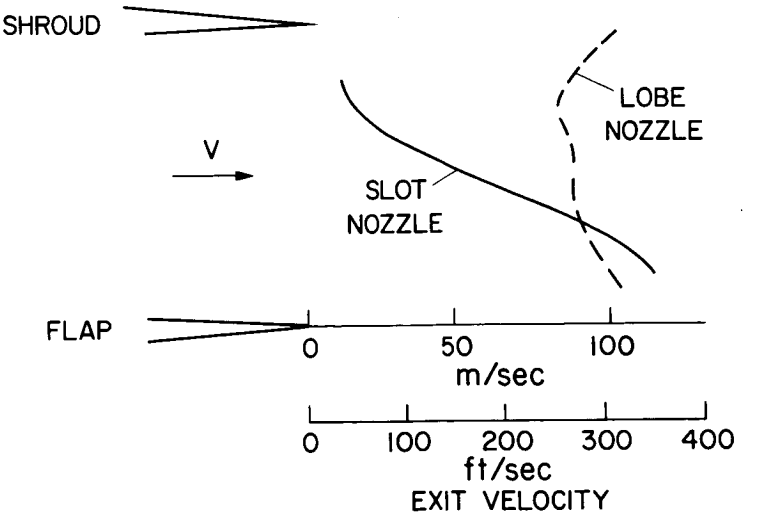

Figure 4

COMPARISON OF THRUST LAPSE FOR AUGMENTOR WING AND IBF

$C_L = 3$, FLAP ANGLE = 30°, NOZZLE PRESSURE RATIO = 2.3

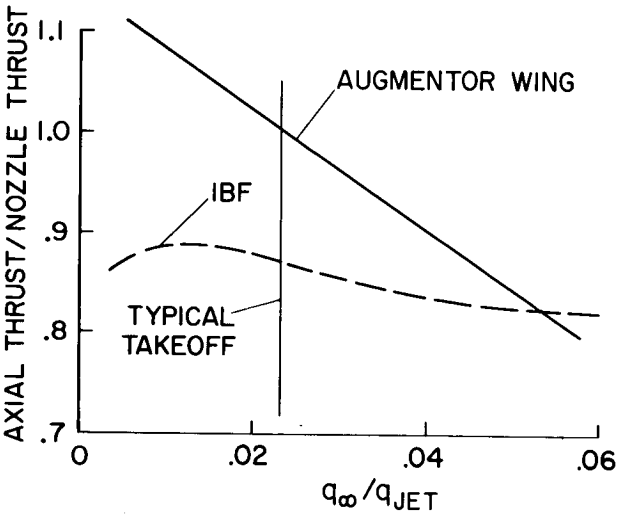

Figure 5

DRAG POLARS OF AN AUGMENTOR WING AT SEVERAL FORWARD SPEEDS AND PRESSURE RATIOS

SLOT NOZZLE, FLAP ANGLE = 30°, $C_J = 0.8$

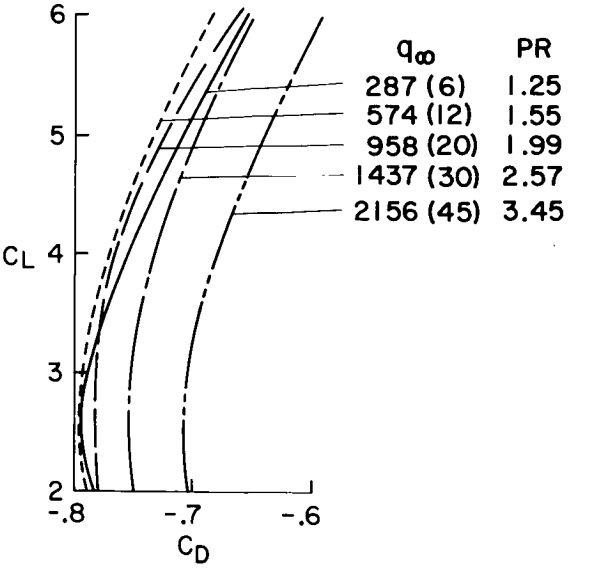

Figure 6

STATIC AUGMENTATION AND ENTRAINMENT CHARACTERISTIC OF SLOT NOZZLE AUGMENTOR WING

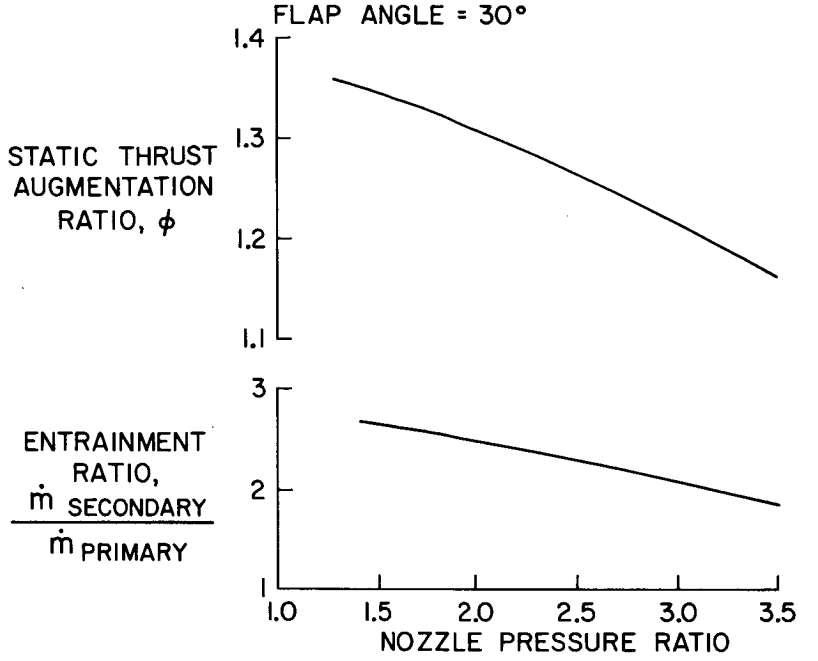

Figure 7

DRAG EQUATION OF AUGMENTOR WING

$$C_D = -\phi C_J + 2C_q + C_{D,o} + C_{D,i}$$

$$2C_q = \frac{V_\infty \text{ (SECONDARY MASS FLOW)}}{q_\infty S}$$

ϕ, C_q ARE COMPUTED USING STATIC DATA

CORRELATION OF DRAG POLARS

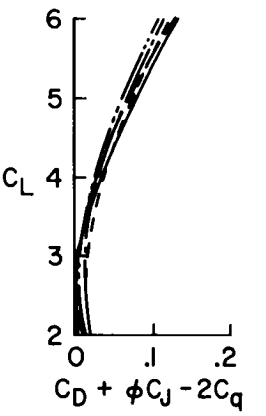

Figure 8

EFFECT OF GEOMETRY CHANGES ON LIFT CHARACTERISTICS OF AUGMENTOR WING

LOBE NOZZLE, FLAP ANGLE = 60°, ANGLE OF ATTACK = 0°

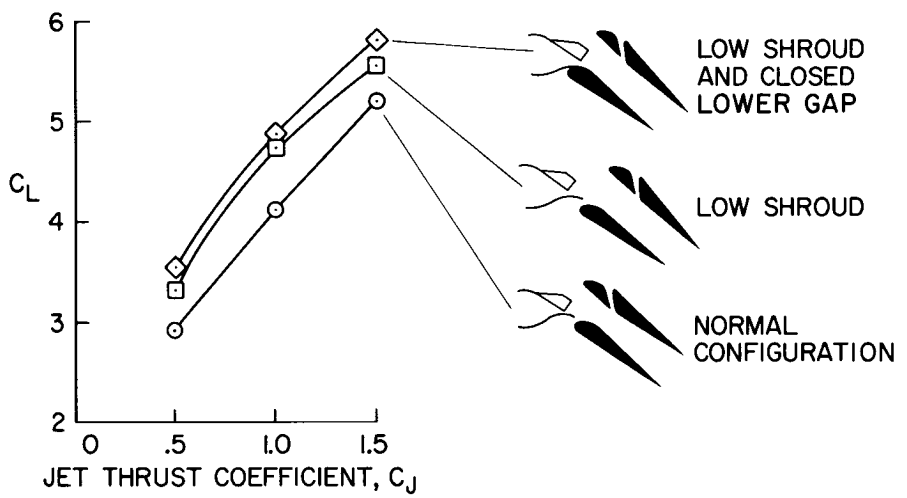

Figure 9

AERODYNAMICS OF THE UPPER SURFACE BLOWN FLAP

By Arthur E. Phelps III
Langley Directorate, U.S. Army Air Mobility R&D Laboratory

SUMMARY

This paper summarizes the results of some preliminary wind-tunnel investigations made to provide fundamental aerodynamic information on the upper surface blown jet-flap concept incorporating high-bypass-ratio turbofan engines. The results of the investigation have shown the concept to have aerodynamic performance generally similar to that of other externally blown high-lift systems. A few of the more critical problems associated with this concept have been identified and preliminary solutions to some of these problems have been found. These results have proven to be sufficiently encouraging to warrant continuation of fundamental research efforts on the concept.

INTRODUCTION

Although the upper surface blown jet-flap (USB) concept is presently receiving a considerable amount of attention in STOL research, it is worthwhile to note that this is not a new idea. During the latter part of the 1950's, some preliminary aerodynamic and noise investigations were performed at Langley Research Center on the models shown schematically in figure 1. (See refs. 1 and 2.) The aerodynamic model had a partial-span plain flap located behind the engine nacelle and employed a wide, thin exhaust nozzle to distribute the exhaust flow more or less evenly along the flap span. At the same time that these aerodynamic studies were being performed, a series of investigations were made to measure the noise levels associated with various types of jet flaps, one of which was an upper surface blown type generally similar to that used in the aerodynamic model. (See fig. 1.) The results of the aerodynamic investigations suggested that the USB concept could provide the high lift necessary for efficient STOL operation, and the noise studies indicated that the USB concept was not only generally quieter than the other concepts under study, but also that the wing tended to act as a noise shield. As was the case with all the other jet-flap schemes, however, there was little interest in the idea at that time, primarily because of the lack of suitable powerplants. The turbojet engines of that day had very hot exhaust temperatures, and their heavy weight made them impractical for providing the high thrust required for STOL applications. With the increasing emphasis on quiet STOL aircraft and the availability of lightweight, high-bypass-ratio turbofan engines, attention has once again been focused on the upper surface blown jet flap as a promising candidate for STOL applications.

SYMBOLS

b	wing span, meters
C_D	drag coefficient, Drag/qS
C_L	lift coefficient, Lift/qS
ΔC_L	lift loss due to failure of one engine
$C_{L,trim}$	trim lift coefficient
C_l	rolling-moment coefficient, l/qSb
C_m	pitching-moment coefficient, $M/qS\bar{c}_w$
C_μ	engine gross-thrust coefficient, T/qS
c	local wing chord, meters
$\bar{c}_t$	horizontal-tail mean aerodynamic chord, meters
$\bar{c}_w$	wing mean aerodynamic chord, meters
i_t	horizontal-tail incidence angle, degrees
l	rolling moment, positive right wing down, newton-meters
M	pitching moment, positive nose up, newton-meters
q	free-stream dynamic pressure, newtons/meter^2
S	wing area, meters^2
T	engine gross thrust, newtons
y	moment arm to inoperative engine, meters
δ_f	flap deflection angle, degrees

ABBREVIATIONS

EBF externally blown jet flap

USB upper surface blown jet flap

DISCUSSION

General Aerodynamic Considerations

Recent work has been directed at providing fundamental aerodynamic information on the USB concept incorporating modern, high-bypass-ratio turbofan engines; and some preliminary work was conducted on the semispan model shown in figure 2 (ref. 3). This model featured a full-span plain trailing-edge flap, a full-span leading-edge Krueger flap, and a two-engine powered nacelle simulating a high-bypass-ratio turbofan-engine installation. The essential difference between this model and the aerodynamic model of figure 1 was that the installation of the high-bypass-ratio engines resulted in a very thick jet which proved to be difficult to turn. It was known from previous work (ref. 4) that a number of critical parameters are involved in effective jet turning; among them is the ratio of jet thickness to turning radius. For the configuration of figure 2, the jet thickness for the basic nacelle proved to be too large, and it was necessary to thin the jet in order to turn the exhaust flow. The device used for this purpose was simply a flat deflector plate attached to the nacelle exit in such a way that the exhaust flow was directed down toward the top of the wing.

Figure 3 has been prepared to show the interrelation of some of the parameters involved in effective turning, and shows schematically the relationship between the engine pressure ratio and the ratio of jet thickness to turning radius for the static turning case. This figure indicates that good turning can be obtained with thicker exhaust jets through the use of engines with lower pressure ratios (high bypass ratios). Consequently, the use of these modern engines does not require the very thin jet sheet needed for turbojet installations of the type simulated on the earlier models. Unfortunately, the installation of low-pressure-ratio engines in a more or less conventionally shaped nacelle generally results in an exhaust-jet thickness that is still too high for good turning performance, and some additional thinning is necessary. Figure 4 shows schematically a few methods that have been studied for improved turning efficiency.

The first method, and the one which was used on the semispan model of figure 2, is simply the use of a flat deflector attached to the top of the nacelle exit in such a way as to direct the exhaust flow down toward the top of the wing. The exhaust jet is free to expand and spread spanwise, but is effectively thinned enough to provide good turning performance. A second technique is the use of a nacelle with a fishtail-type planform. That

is, the nozzle has a high aspect ratio with an exit designed to have the proper height for effective turning and is flared in plan to maintain the required exit area. This arrangement differs from the deflector technique in that the exhaust flow is confined to a specific region of the wing span and does not spread spanwise. A third alternative is the use of a turning vane located above the flap knee and extending spanwise a sufficient distance to capture and turn the exhaust flow. This method forces the jet to turn, but has the disadvantage of relatively high noise and low efficiency. Such an arrangement has recently been tested at Langley, and these results are presented by Danny R. Hoad in paper no. 10. Another method, not shown in figure 4, is that of boundary-layer control at the knee of the trailing-edge flap. This method has proven effective for turning the jet exhaust, even for relatively thick exhaust jets. (See ref. 3.)

In order to illustrate more clearly the effect of the exhaust deflector, figure 5 has been prepared to show schematically the nature of the exhaust flow behind the basic nacelle and the nacelle with a deflector attached. It should be noted that these sketches show the wind-on characteristics, since these have proven to be more serious than the static characteristics. As the jet exhaust exits the basic nacelle, the sides of the jet sheet tend to roll up into vortices. As soon as the flow begins to turn over the flap, the jet begins to contract and continues to do so until it leaves the flap trailing edge. At this point the side vortices have become fairly large and powerful, and their effect is to greatly reduce the portion of the flap span affected by the exhaust jet. Placing a deflector on the nacelle, however, spreads the exhaust flow spanwise an appreciable distance at the nacelle exit. Although the jet still tends to contract as it follows the flap, considerably more of the span is affected by the jet sheet, and much improved turning performance is realized.

Longitudinal Characteristics

The aerodynamic lift characteristics of the semispan model of figure 2 are shown in figure 6 as a plot of lift coefficient against angle of attack for three different power settings. For a thrust coefficient of about 4, a maximum lift coefficient of about 10.5 was obtained, whereas the power-off maximum lift coefficient was about 2.5. This power increment in lift is generally comparable with that obtained for other external-flow, jet-augmented, high-lift systems.

The results of these preliminary tests led to the testing of the full-span model shown in figure 7. This model had a tapered wing with the leading edge swept 30°; four engines mounted at 27 and 42 percent semispan; a full-span, 0.19c leading-edge slat; and a double-slotted trailing-edge flap, the inboard portion of which was covered by a thin piece of sheet metal to provide a smooth, large-radius, upper surface contour. The engine nozzles were essentially of the fishtail type, although the top of the exit nozzle was contoured so that the exhaust-flow center line was deflected downward toward the top of the wing in front of the

flap knee. The horizontal tail shown in dashed lines was not optimized, but was tested only to investigate potential stability and control problems.

The static turning performance of the model for two flap settings, 55^{o} and 35^{o}, is shown in figure 8 along with turning data for an EBF model having the same flap settings, and serves to indicate the relative efficiency of the flap systems in turning the exhaust jet. The radial lines indicate the turning angle; and the arcs show the ratio of resultant force to thrust, which is a measure of the efficiency of the system. Generally speaking, the USB model showed good turning and somewhat higher efficiency than the EBF model, although this USB configuration did not turn the flow completely for the 55^{o} flap setting. This relatively good turning is reflected in the wind-on data shown in figure 9. These data are shown in the form of trim-lift drag polar plots for the full-span model along with corresponding plots for the semispan model of figure 2 and a typical EBF model. On this plot, negative drag coefficients imply accelerating flight or climb, and positive drag coefficients indicate descent. The introduction of the EBF model data here is intended to provide only a qualitative comparison of the performance of the USB model with that of another external-flow powered-lift STOL concept. These data show that the upper surface blown jet flap as tested provided aerodynamic performance generally comparable with that of the EBF configuration shown.

Some interest has recently been expressed in a two-engine airplane, primarily for reasons of simplicity and economy. In order to investigate briefly the performance of such an arrangement, a twin-engine configuration was tested by removing the outboard engines from the four-engine model. The results of these tests are shown in figure 10 as trim-lift drag polar plots for a jet thrust coefficient of 2 and for both the two- and four-engine configurations. The solid lines show the performance with the basic 0.19c leading-edge slat, and the dashed line shows the performance of the twin-engine configuration with a 0.25c slat. This comparison has been made only to show what modifications were required of the two-engine configuration to match the performance of the basic four-engine version and suggests, for this particular model, that the two-engine arrangement might require more leading-edge treatment.

Longitudinal Stability and Trim

Figure 11 is a plot of pitching moment against angle of attack for both the tail-on and the tail-off configurations for the model of figure 7. These data are plotted for a jet thrust coefficient of 4.0 and a flap setting of 55^{o}, as this condition provided the most powerful untrimmed diving moments. The horizontal tail is located $1.5\bar{c}_{w}$ above and $3.5\bar{c}_{w}$ aft of the center of gravity, a position that has proven successful for other jet-flap concepts. The data show that sufficient tail power is available to trim the large tail-off diving moments and that the model was generally stable with the horizontal tail as tested. At the higher angles of attack, the tail appears to have lost some of its effectiveness for

providing stability, evidently because it has moved into the powerful vortex field discussed by Lysle P. Parlett in paper no. 6.

Engine-Out Lateral Characteristics

Figure 12 is a plot of rolling-moment coefficient against angle of attack for both the two- and four-engine configurations of the full-span model for a flap deflection of 55^{o}, a thrust-weight ratio of 0.45, and the left outboard engine inoperative. Similar data for an EBF configuration having the same engine positions and thrust-weight ratio have been shown on the four-engine curve to give an idea of the relative magnitude of the engine-out moments. One method that has been suggested for relieving these rolling moments is to open the flap slots behind the failed engine, and allow the flap to operate as a conventional slotted flap, which would presumably be more efficient than the unslotted flap. These data indicate that this technique had only a relatively small effect on the engine-out rolling moments for the present configuration; in fact, in the case of the four-engine arrangement, the rolling moments actually increased when the flap slots were opened. Inasmuch as these are only preliminary tests and only a few data have been obtained concerning this problem, no conclusions should be drawn yet regarding the advisability of opening the flap slots behind a failed engine as a means of relieving the engine-out rolling moments.

In connection with the engine-out problem, some calculations were performed to correlate the rolling moments with the engine-out lift loss, and the results are shown in figure 13. The solid line represents the rolling moments obtained by multiplying the loss in lift by the distance to the dead engine, and the data points shown are the measured rolling moments. The fact that the measured moments are less than the computed moments indicates that the effective moment arm is not as great as the actual distance to the dead engine.

CONCLUSIONS

The results of recent wind-tunnel investigations on the upper surface blown jet-flap concept incorporating high-bypass-ratio turbofan engines have shown the concept to have aerodynamic performance generally similar to other externally blown high-lift systems. These results have proven to be sufficiently encouraging to warrant continuation of fundamental research efforts. As a part of this future research, tests are planned in the Langley full-scale tunnel with a large upper surface blown flap model powered with jet engines in order to obtain information on possible effects of scale and hot jet exhaust.

REFERENCES

1. Maglieri, Domenic J.; and Hubbard, Harvey H.: Preliminary Measurements of the Noise Characteristics of Some Jet-Augmented-Flap Configurations. NASA MEMO 12-4-58L, 1959.

2. Turner, Thomas R.; Davenport, Edwin E.; and Riebe, John M.: Low-Speed Investigation of Blowing From Nacelles Mounted Inboard and on the Upper Surface of an Aspect-Ratio-7.0 35^{o} Swept Wing With Fuselage and Various Tail Arrangements. NASA MEMO 5-1-59L, 1959.

3. Phelps, Arthur E.; Letko, William; and Henderson, Robert L.: Low-Speed Wind-Tunnel Investigation of a Semispan STOL Jet Transport Wing-Body With an Upper-Surface-Blown Jet Flap. NASA TN D-7183, 1973.

4. Lowry, John G.; Riebe, John M.; and Campbell, John P.: The Jet-Augmented Flap. Preprint No. 715, S.M.F. Fund Paper, Inst. Aeronaut. Sci., Jan. 1957.

EARLY NASA UPPER SURFACE BLOWN JET-FLAP MODELS

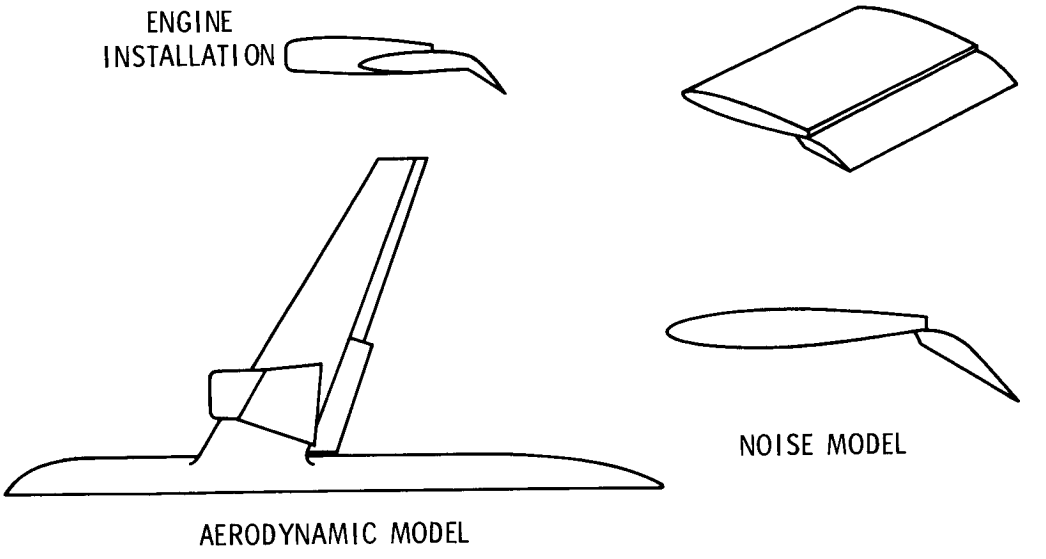

Figure 1

GENERAL RESEARCH SEMISPAN MODEL

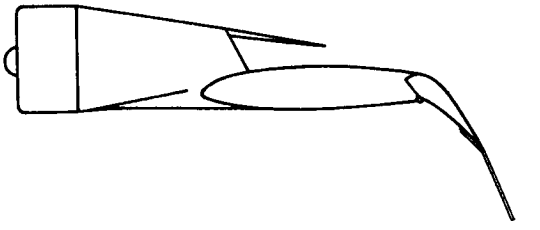

TYPICAL SECTION THROUGH ENGINE NACELLE

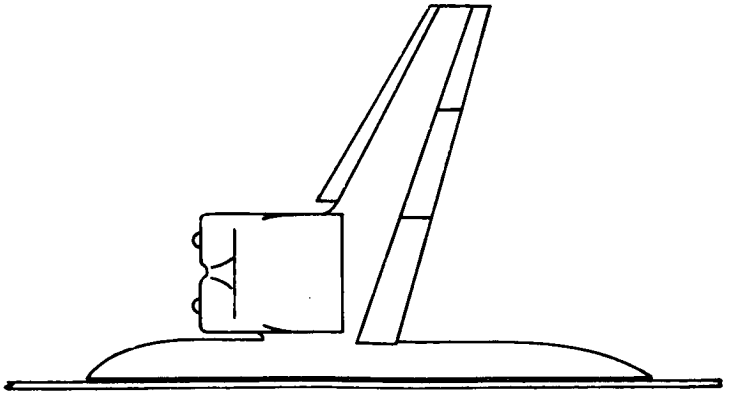

Figure 2

STATIC TURNING OF UPPER SURFACE BLOWN JET FLAP

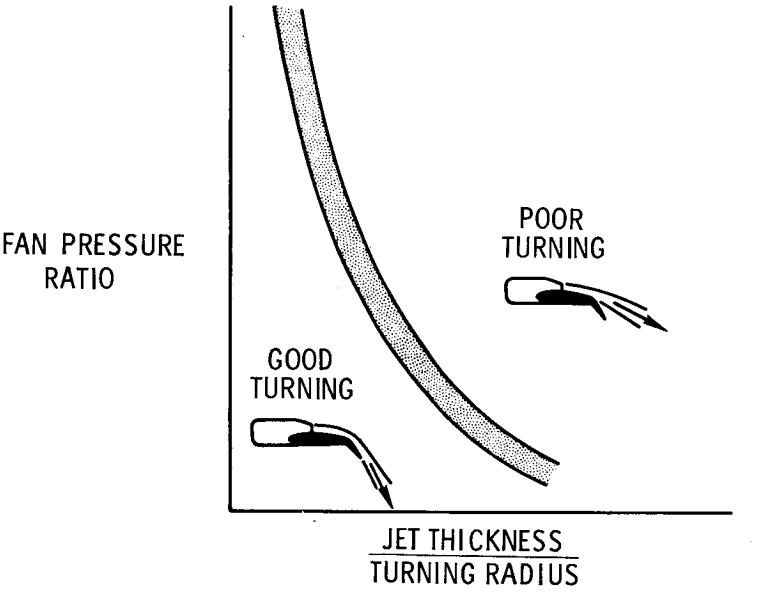

Figure 3

METHODS TO IMPROVE TURNING

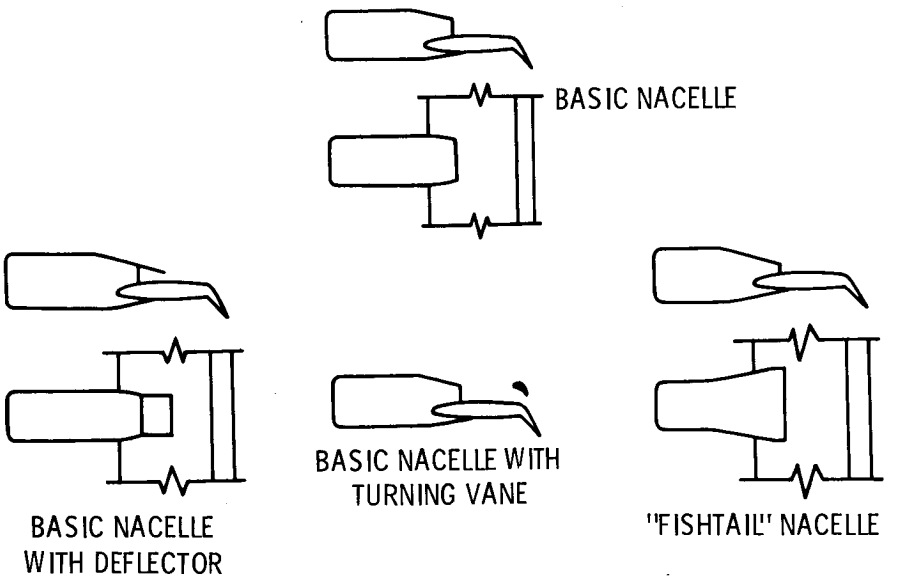

Figure 4

EFFECT OF NACELLE EXIT

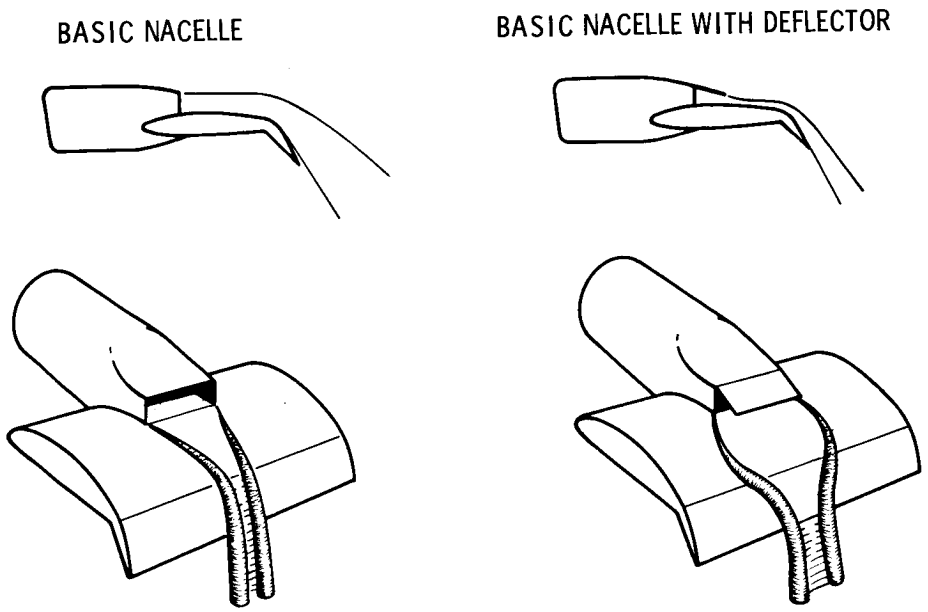

Figure 5

LIFT CHARACTERISTICS OF SEMISPAN MODEL

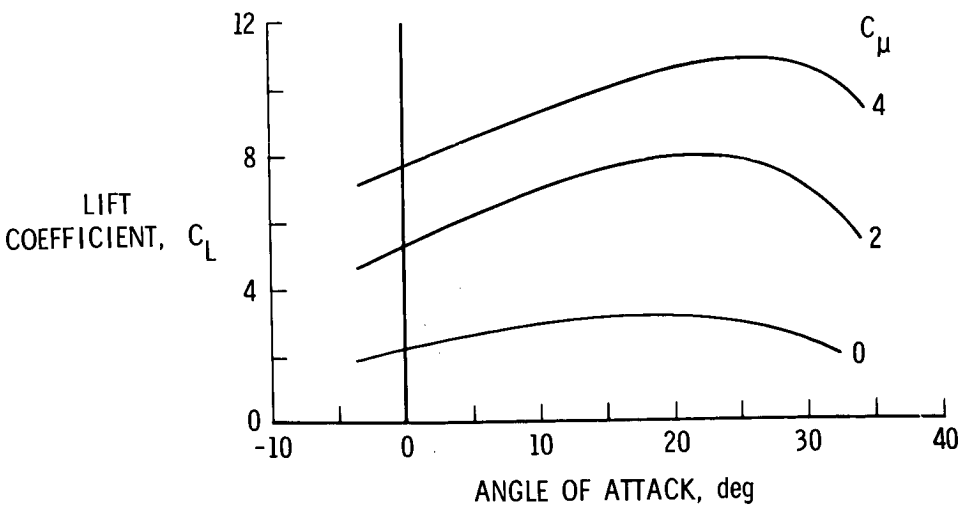

Figure 6

FULL-SPAN UPPER SURFACE BLOWN JET-FLAP MODEL

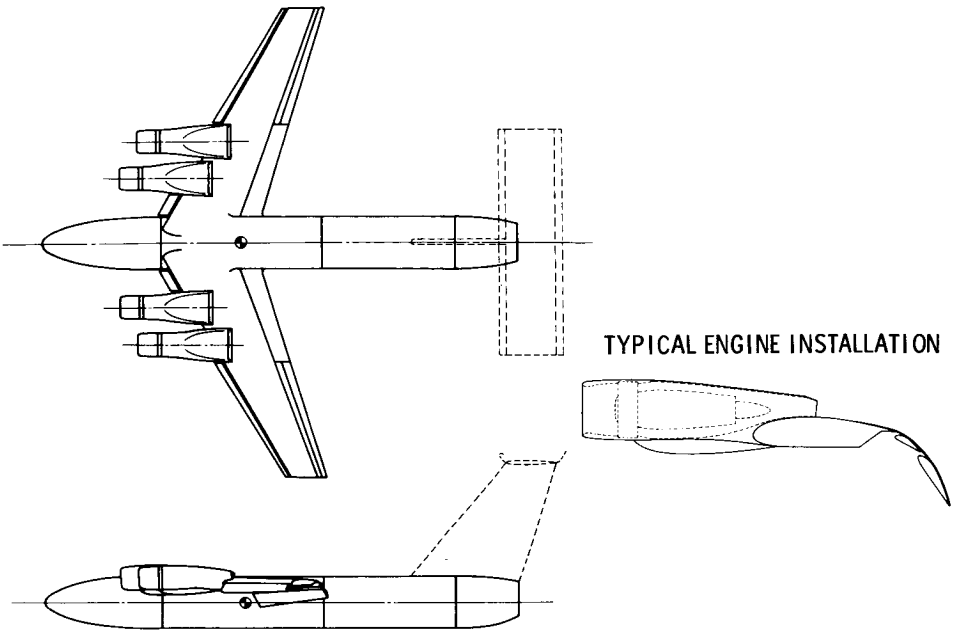

Figure 7

TURNING EFFICIENCY AND TURNING ANGLE

FULL-SPAN MODEL

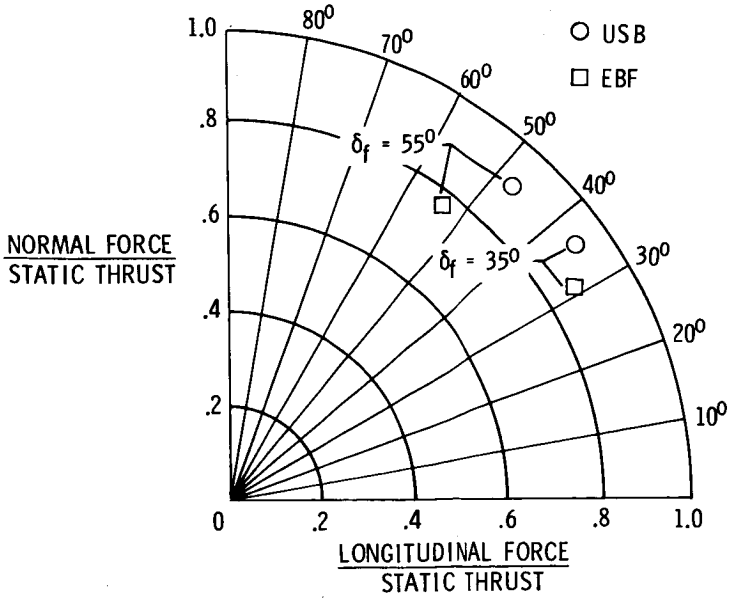

Figure 8

COMPARISON OF LIFT-DRAG CHARACTERISTICS

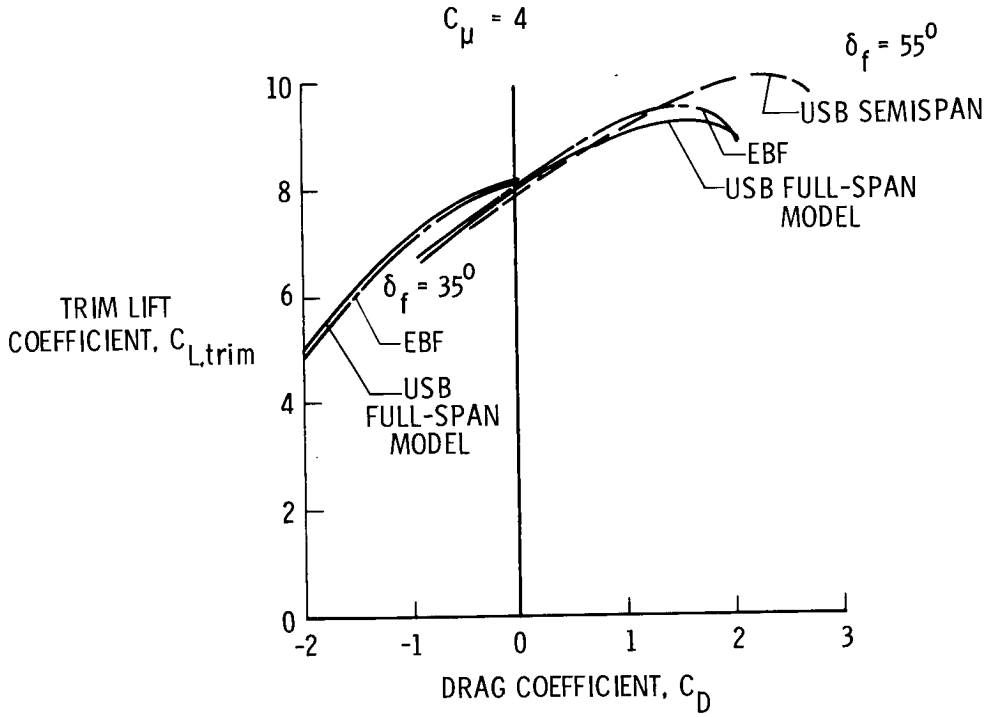

Figure 9

LIFT-DRAG CHARACTERISTICS

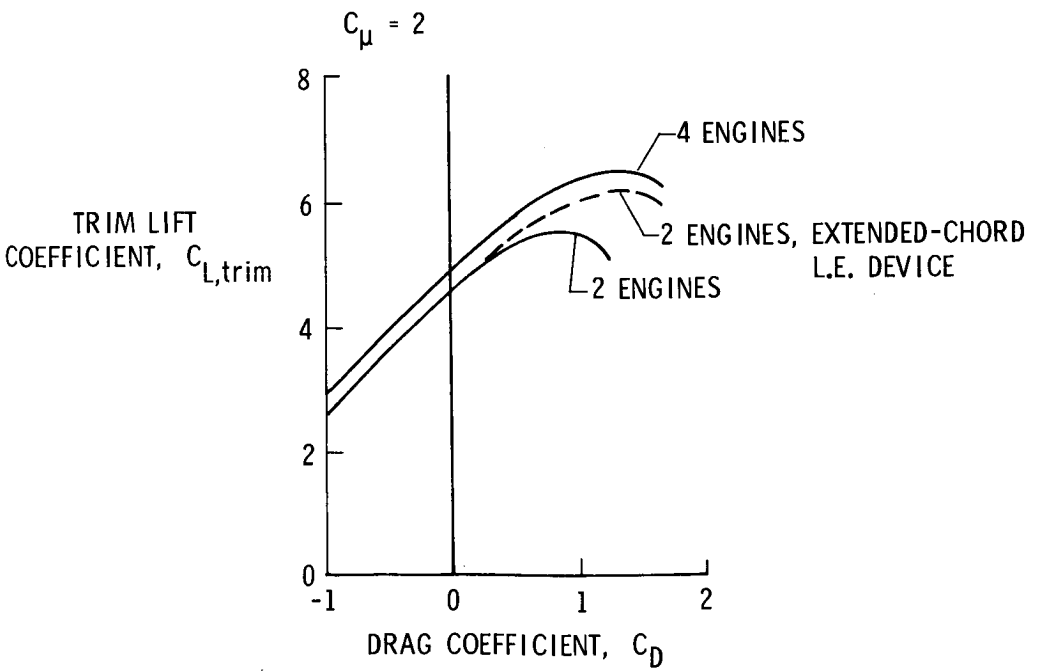

Figure 10

LONGITUDINAL AERODYNAMIC CHARACTERISTICS

$C_\mu = 4$

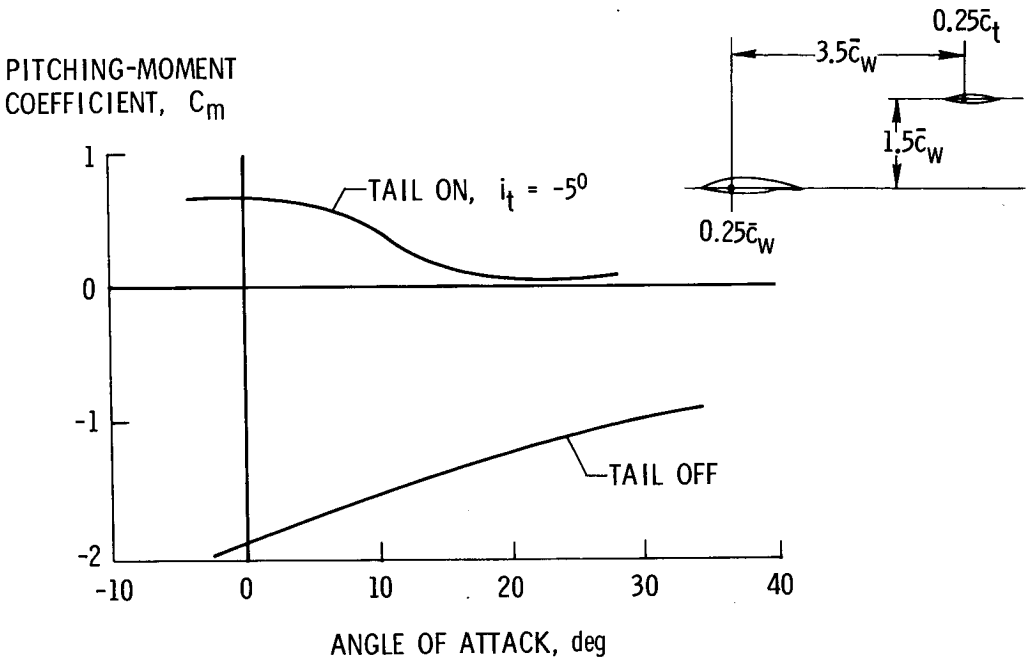

Figure 11

LATERAL AERODYNAMIC CHARACTERISTICS

LEFT ENGINE INOPERATIVE

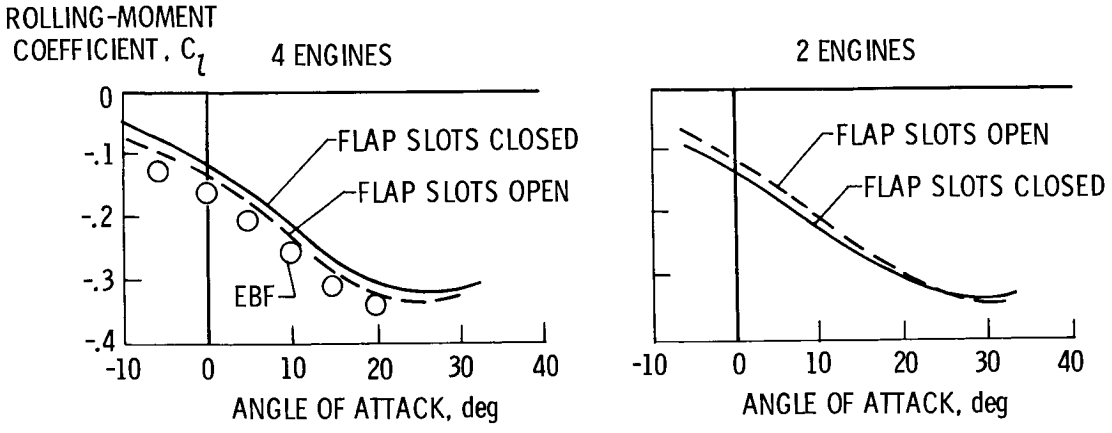

Figure 12

ENGINE-OUT ROLLING MOMENTS

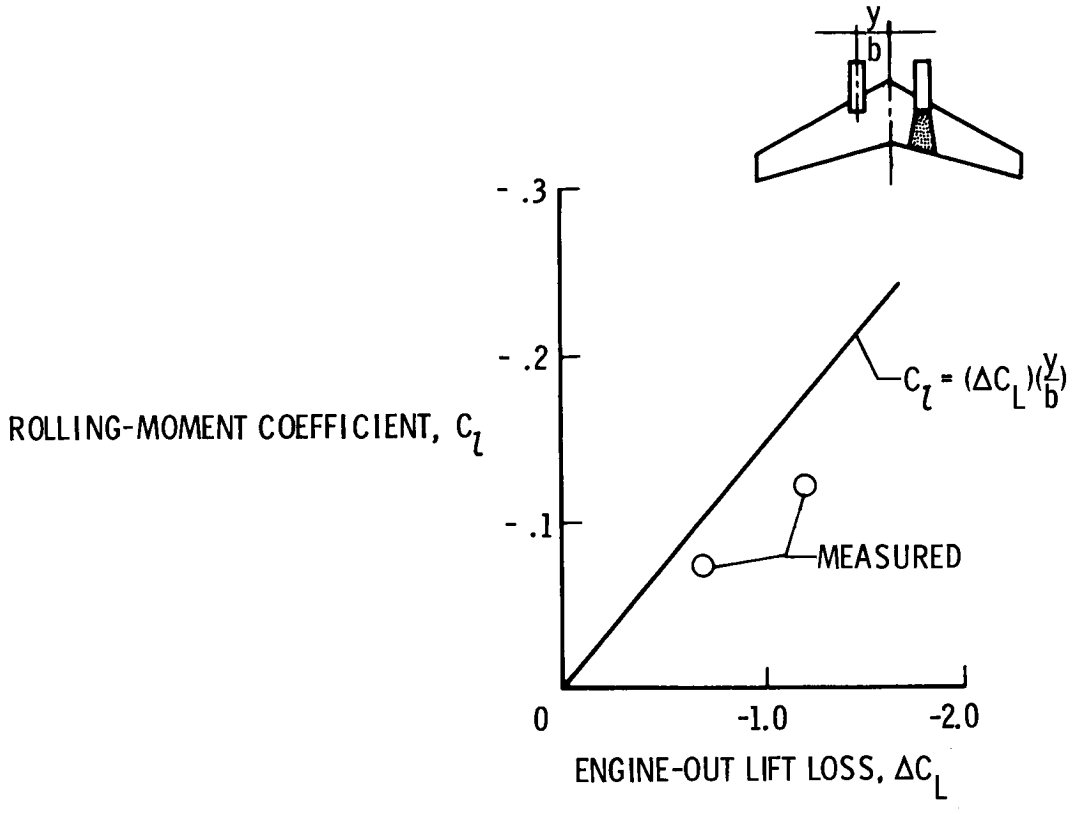

Figure 13

COMPARISON OF AERODYNAMIC PERFORMANCE OF SEVERAL STOL CONCEPTS

By Danny R. Hoad
Langley Directorate, U.S. Army Air Mobility R&D Laboratory

INTRODUCTION

Numerous concepts have been suggested to provide the necessary high lift required for STOL missions, both military and civilian. The purpose of this paper is to present the results of a series of Langley V/STOL tunnel investigations on two basically similar models. These investigations were designed to provide data for a systematic direct comparison of five of the concepts considered. Since the concepts were based on similar model characteristics, complete optimization of all the concepts was impossible. In fact, each concept has its own degree of optimization, but none have been extensively optimized for performance. It must also be understood that in this paper only aerodynamic characteristics are compared. Any other comparison among the concepts is beyond the scope of this paper.

SYMBOLS

C_D drag coefficient, $\frac{\text{Drag}}{q_\infty S}$

C_L lift coefficient, $\frac{\text{Lift}}{q_\infty S}$

$C_{L,max}$ maximum lift coefficient

C_m pitching-moment coefficient, $\frac{\text{Pitching moment}}{q_\infty S\bar{c}}$

C_μ thrust coefficient, $\frac{\text{Thrust}}{q_\infty S}$

$\bar{c}$ mean aerodynamic chord of plain wing, meters (ft)

q_∞ free-stream dynamic pressure, newtons/meter^2 (lbf/ft^2)

S wing area, meters^2 (ft^2)

T thrust, newtons (lbf)

T/W	ratio of installed thrust to total aircraft weight
V	approach velocity, knots
W	total aircraft weight, newtons (lbf)
W/S	wing loading, kilonewtons/meter^2 (lbf/ft^2)
α	angle of attack, degrees
γ	glide slope, degrees
δ_f	flap deflection, degrees
$\delta_{f,L}$	landing flap deflection, degrees
$\delta_{f,T}$	take-off flap deflection, degrees
δ_j	jet deflection angle, degrees

DISCUSSION

The five STOL high-lift concepts considered are shown in figure 1. The configuration shown in figure 1(a) incorporates three of the concepts: the externally blown flap, the deflected thrust with double-slotted flaps, and the upper surface blown flap. The configuration shown in figure 1(b) incorporates the other two concepts: the internally blown flap and the augmentor wing. The deflected-thrust configuration has its engine exit located at 75 percent of the local wing chord. Preliminary data obtained from a study of a series of longitudinal nozzle positions indicated that this would be the best position to locate the engine exit in both the take-off and landing configurations. This upper surface blown flap has been discussed by Arthur E. Phelps in paper no. 9. This configuration uses the upper-surface vane to help turn the flow over the wing in the landing mode. The two models in figure 1 differ only in wing thickness. The configuration in figure 1(a) has a wing with a thickness ratio of 0.093 and that in figure 1(b) has a wing with a thickness ratio of 0.17. The thicker wing is necessary to provide space for the internal ducting required for the internally blown concepts shown in figure 1(b). All the data presented were obtained from unpublished results of tests made in the Langley V/STOL tunnel.

The flap static turning effectiveness of four of the five concepts is presented in figure 2. The thrust is defined as the total thrust provided by the propulsive system with

flaps removed. The landing configurations have flap deflections ranging from 55^{o} to 65^{o}, and the take-off configurations have flap deflections of 30^{o} and 35^{o}. The deflected-thrust concept is not shown since this concept depends on thrust vectoring rather than on the flap system to provide the turning angles required for high lift. One measure of the relative merit of the concepts can be obtained from this figure. The relatively low thrust recovery and jet turning angles of the externally blown concepts are especially noticeable in the landing mode. The rather large jet turning angles of the internally blown concepts are appreciably higher than their respective flap deflections; this indicates that the flow stays attached to the upper surface of the flap whose trailing-edge upper-surface angle is approximately 17^{o} relative to the flap chord line. Data were recently obtained for the augmentor-wing model only in the landing mode. These data are only preliminary and further modifications will probably improve the characteristics of this model.

Tail-off basic aerodynamic data for all concepts are shown in figures 3(a) to 3(c). Figure 3(a) presents data for the three externally blown concepts in the take-off mode with a flap deflection of 35^{o}. For the deflected-thrust concept, the preliminary data mentioned previously indicated that the combination of nozzle position and jet deflection angle providing the best performance in the take-off mode should be at 75 percent of the local wing chord and 45^{o} relative to the wing chord. Very little difference among the concepts is seen in the lift curves except that the externally blown flap provides somewhat greater lift at the higher angles of attack. The lift-drag polars are also quite similar. For clarity, the curves for $C_{\mu} = 2$ were omitted from the pitching-moment data. These data show that at $C_{\mu} = 4$ the deflected-thrust configuration has the least amount of negative pitching moment because the direct deflected jet is low and ahead of the flap system.

Figure 3(b) presents the tail-off basic aerodynamic data for the three externally blown concepts in the landing mode. The preliminary data for the deflected-thrust concept in the landing mode indicated that the best performance could be achieved by deflecting the engine exit 85^{o} relative to the wing chord. The externally blown flap and upper surface blown flap configurations develop approximately the same range of lift coefficient at $C_{\mu} = 2$. In the limited test program on the upper surface blown flap model, the optimum conditions required to keep the flow attached at higher thrust coefficients were not found. The data should approximately match those for the externally blown flap configuration on the basis of the previous discussion of the upper surface blown flap concept in paper no. 9. In contrast to the data in the take-off mode, the data for the deflected-thrust concept in the landing mode reveal that this configuration does not induce as much circulation lift as do the other two configurations at $C_{\mu} = 2$ and 4. The lift-drag polars indicate that all the configurations have the positive drag necessary for descent in the high-lift range. The pitching-moment data show that the deflected-thrust configuration has the largest negative pitching moment at the higher thrust coefficient because the jet deflection

angle is so high. Reducing this jet deflection angle would reduce this pitching moment but would also reduce the lift and descent capability.

Figure 3(c) presents the tail-off basic aerodynamic data for the two internally blown concepts in the landing mode. The aerodynamic characteristics for this augmentor-wing configuration have been compared with data for a similar model tested at the Ames Research Center, and the data are generally in agreement. The difference in the lift-coefficient values of these two configurations at $C_\mu = 1.0$ and 1.5 can probably be attributed to the 5^o difference in flap deflection. Also, it is interesting to note that approximately the same amount of lift can be generated by the internally blown configurations with one-half the thrust coefficient required for the externally blown flap and the upper surface blown flap configurations (figs. 3(b) and 3(c)). Both of the internally blown configurations have the positive drag necessary for descent and both have approximately the same descent capability. For clarity, the curves for $C_\mu = 1$ were omitted from the pitching-moment data. These data show that at the high thrust coefficient the augmentor-wing configuration has slightly more negative pitching moment.

In order to make direct comparisons of all five concepts, the basic aerodynamic longitudinal data were used to determine the landing and take-off trimmed lift coefficients. These data are shown in figure 4 as a function of thrust coefficient. For the purposes of this paper, a speed margin of 20 percent or a lift-coefficient margin of 44 percent was used for the landing configuration, and a speed margin of 15 percent or a lift-coefficient margin of 32 percent was used for the take-off configuration. Data for the augmentor-wing concept in the take-off mode are not shown because these data have not yet been obtained with the model. This test program is now in progress. In the landing mode, the internally blown flap and the augmentor-wing configurations require the least amount of thrust to obtain a given lift coefficient. The externally blown flap and the upper surface blown flap configurations require more thrust, and the deflected-thrust configuration requires the most. The dashed line represents the expected values of the upper-surface blown flap configuration at the higher thrust coefficients. Again, this is based on the discussion in paper no. 9 of the comparability of the upper-surface blown flap concept with the externally blown flap concept. In the take-off mode, it can be seen in figure 4 that for a given lift coefficient, the range of thrust required is smaller than that in the landing mode. The internally blown flap configuration again requires the least amount of thrust; similar data would be expected for the augmentor-wing concept for take-off.

For a 609.6-meter (2000 ft) runway, a STOL aircraft with a 3.83-kilonewton/meter^2 (80 lbf/ft^2) wing loading would land at a lift coefficient of about 4.2 and take off at a lift coefficient of about 3.2. Comparing these concepts at these lift coefficients in figure 4 reveals that all the STOL configurations require more thrust to develop the lift coefficient

needed to land than to develop the lift coefficient needed to take off. By extending this thrust coefficient required to net thrust-to-weight ratio required, a comparison can be made with some commonality among the concepts in approach glide slope and speed.

Figure 5 provides this comparison as the net thrust-to-weight ratio plotted against the wing loading of the aircraft. The concepts are compared in the landing mode with a 20-percent speed margin, a descent glide slope of 6°, and an approach velocity of 75 knots. The net thrust-to-weight ratios required for the internally blown flap and the augmentor-wing configurations are much less than those required for the other three configurations throughout the range of wing loading. The deflected-thrust configuration requires a substantially higher net thrust-to-weight ratio than do the externally blown flap and the upper surface blown flap configurations. It should be emphasized that the results shown in figure 5 are based only on aerodynamics and that the type of propulsion system required for the different concepts has not been considered. When the propulsion aspect is considered, the differences between the internally blown and externally blown concepts become much smaller.

CONCLUDING REMARKS

The results of this comparison of five of the STOL concepts considered have provided an insight into the feasibility of each concept. The most complex systems require the least amount of net thrust, and the least complex systems require the most amount of net thrust. It should be kept in mind that, although this comparison is based on data obtained with models having closely similar geometric characteristics, none of the models have been optimized to the extent required for a detailed quantitative performance comparison.

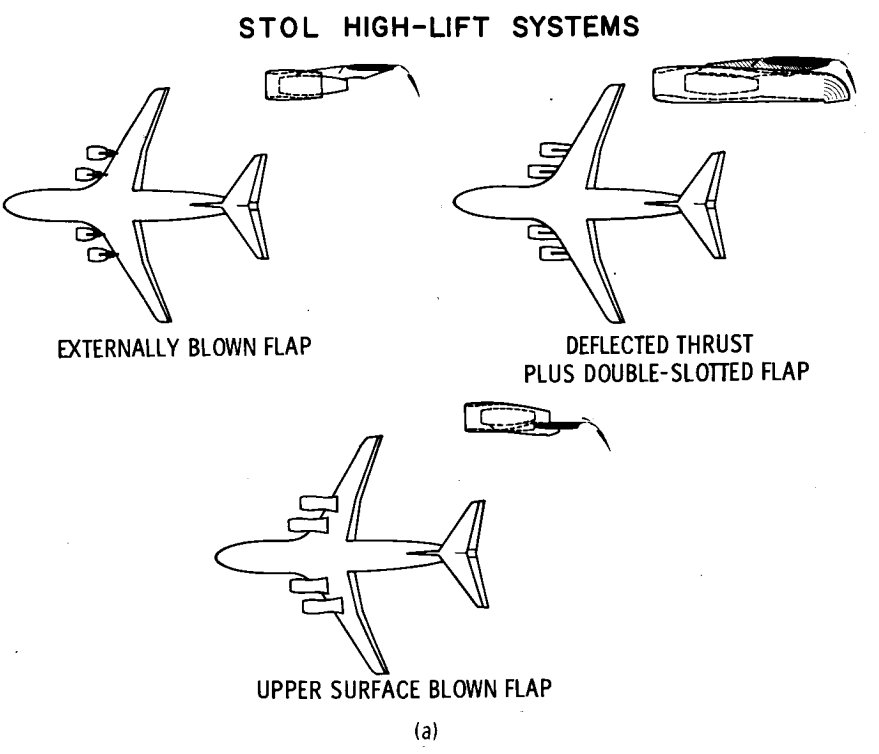
STOL HIGH-LIFT SYSTEMS
EXTERNALLY BLOWN FLAP
DEFLECTED THRUST
PLUS DOUBLE-SLOTTED FLAP
UPPER SURFACE BLOWN FLAP
(a)

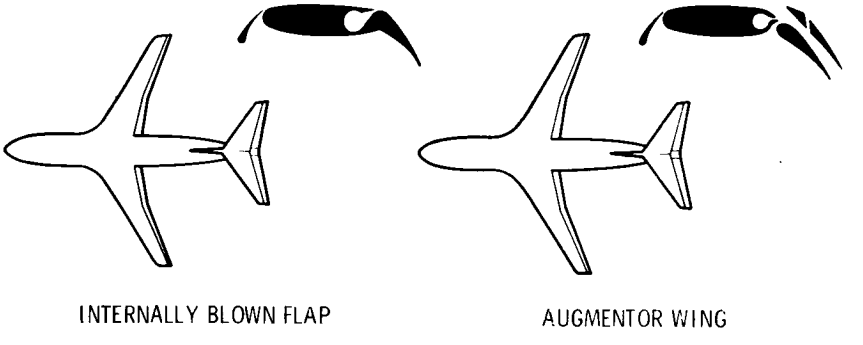
INTERNALLY BLOWN FLAP
AUGMENTOR WING
(b)

Figure 1

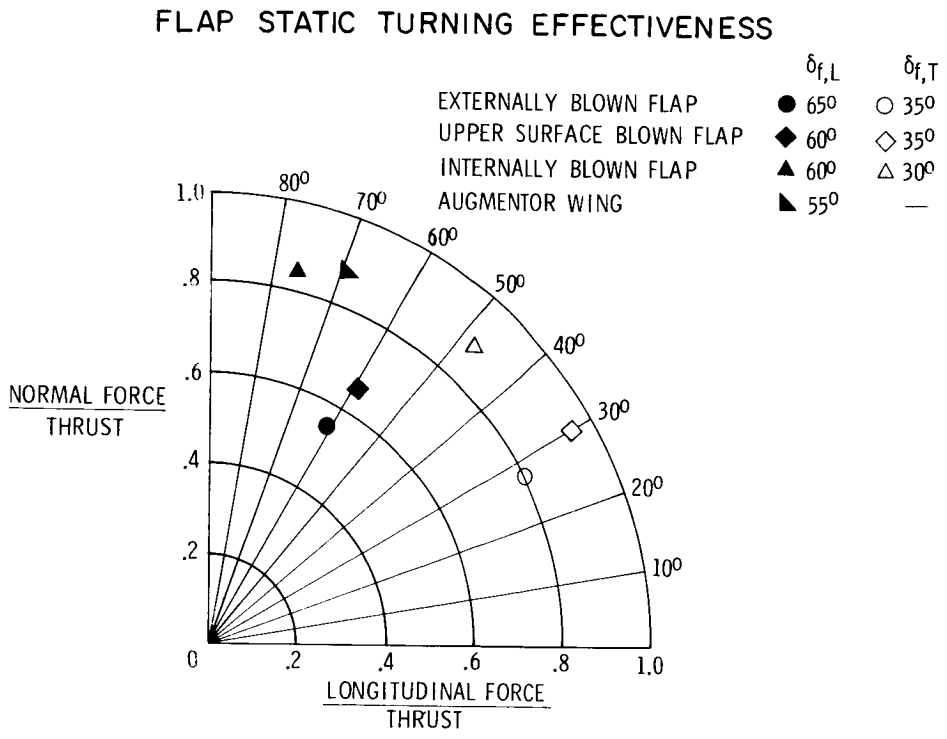

Figure 2

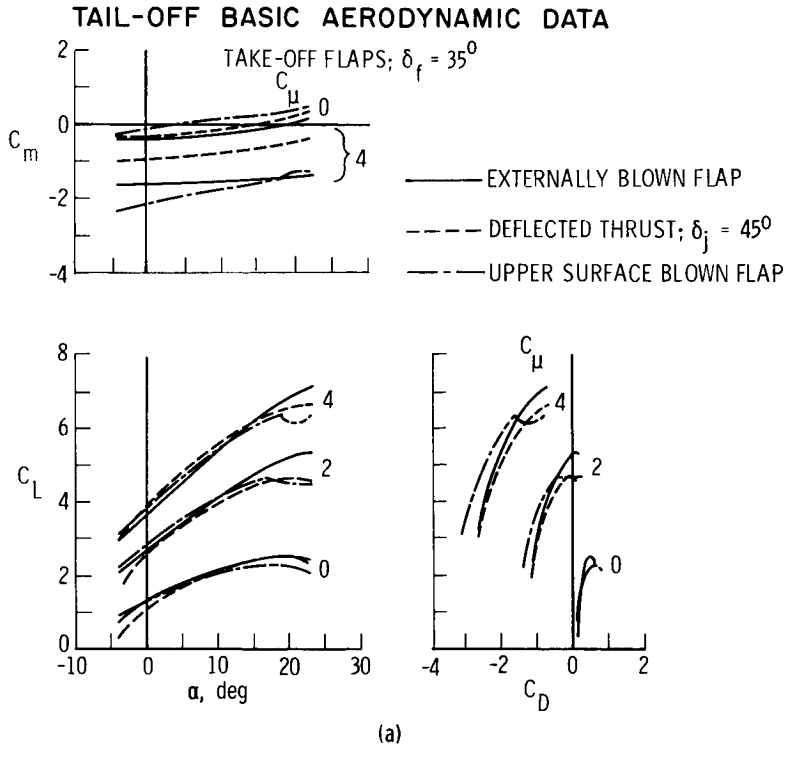

Figure 3

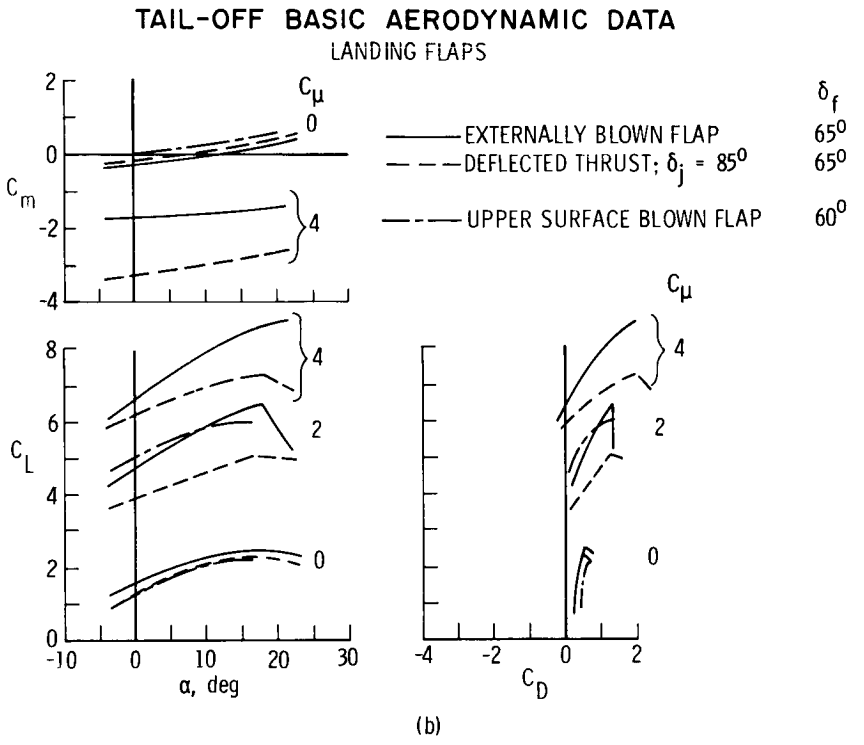

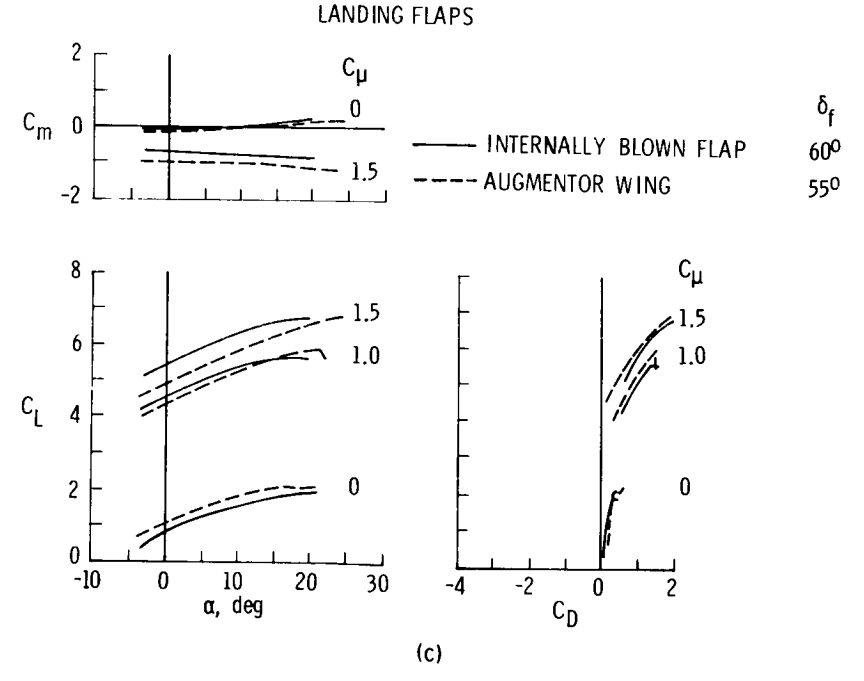

Figure 3 – Concluded

TRIM LIFT COEFFICIENTS

TYPICAL SPEED MARGINS

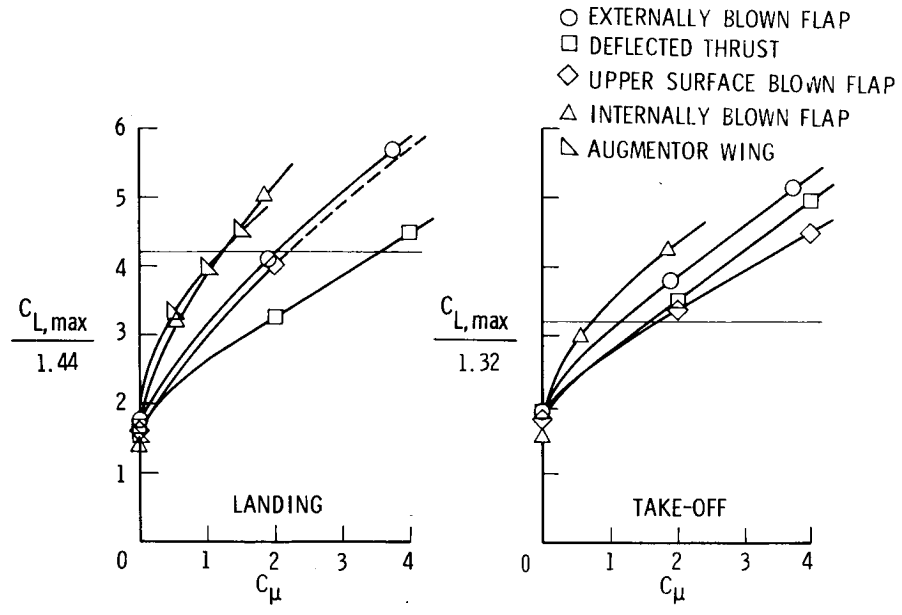

Figure 4

NET THRUST-TO-WEIGHT RATIO REQUIRED

LANDING FLAPS WITH 20% SPEED MARGIN; $\gamma = -6^0$; V = 75 knots

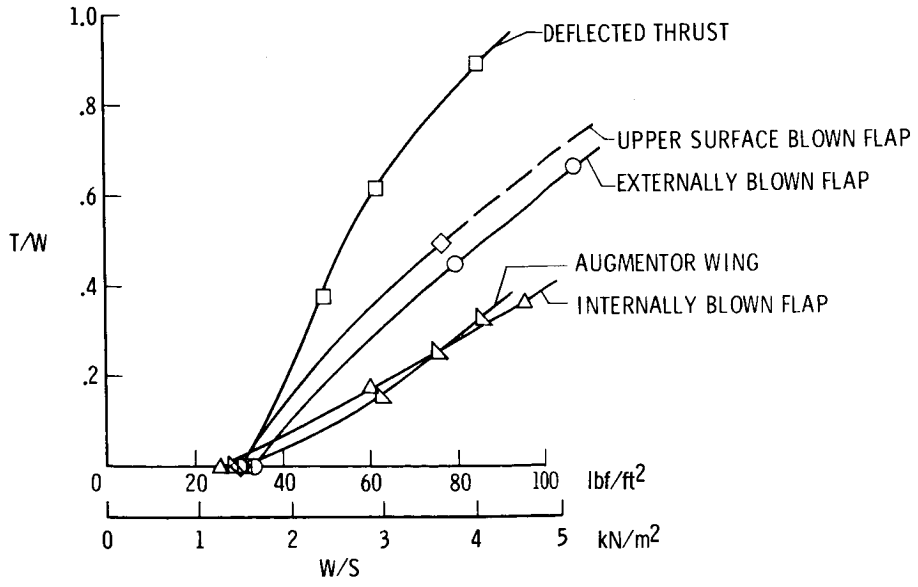

Figure 5

AERODYNAMIC LOADS MEASUREMENTS ON EXTERNALLY BLOWN FLAP STOL MODELS

By George C. Greene and Boyd Perry III
NASA Langley Research Center

SUMMARY

The externally blown flap powered-lift concept has some real and potential flap loads problems which are due to the impingement of the engine exhaust on the flap system. In this paper, the problem of large static and dynamic loads on the flap system and the flap thermal environment are discussed. Recent data are presented in each of these areas.

INTRODUCTION

The major loads problem areas for the externally blown flap (EBF) concept are large static loads, low-frequency structural response, and high temperatures. The problem of large static loads behind the engines is inherent in the externally blown flap concept. Analytic techniques for predicting flap load distributions are still under development and do not give satisfactory results, especially for large flap deflections. Experimental data have been collected on a few models for use in the estimation of design static loads and validation of prediction techniques. However, these data have not been formally published. Therefore, very little NASA data are available to the designer. Experimental data have been obtained on the three models shown in cross section in figure 1. The two small-scale models have comparable dimensions of about 20 cm, and the large-scale model is about an order of magnitude larger. The large-scale model was extensively instrumented for loads measurements. Details of this model and its instrumentation are given subsequently.

Flap response to unsteady pressure loading is a potential problem area since at the present neither the structural characteristics nor the unsteady pressure loadings on a typical flap system are well defined. At the present time, the only data available are from boilerplate models. In addition to measurements on the large-scale model shown in figure 1, unsteady pressure measurements have been made at the Lewis Research Center on a large-scale wing section with a two-element flap configuration similar to the small-scale configuration shown in the upper right corner of figure 1. These tests on the two-element flap configuration were conducted primarily to determine noise characteristics and to assess the high-frequency panel fatigue problem.

Very little effort has been expended in assessing the relatively low-frequency response of the whole flap system to unsteady pressure loading.

Flap temperatures are another potential problem for the EBF concept. At high flap deflections, the engine flow impinges directly on the flap system. On the large-scale model, flap temperatures were measured in the region behind the engines. Small-scale models used simulated engines and did not yield any temperature data.

SYMBOLS

C_p pressure coefficient

C_μ static thrust coefficient

c_n section normal-force coefficient

x/c chord fraction

α angle of attack, degrees

$\Phi(f)$ power spectral density, $(N/m^2)^2/Hz$ or g^2/Hz

MODEL DESCRIPTION

Figure 2 shows the model mounted in the Ames 40- by 80-foot wind tunnel. The model has an 11.6-m (38-ft) wing span and a full-span, triple-slotted flap system. The region of exhaust impingement on the flap system can be seen behind the engines. The flap system and the relative position of the engines can be seen better in figure 3. The engines, which had a bypass ratio of 3, extend back to about the wing leading edge. The flap system was made up of three flap elements and was instrumented for measuring static pressure distribution and unsteady pressure loading, flap response, and flap temperatures in the region behind the engines. Chordwise static pressures were measured on each flap element at 10 span stations. High-frequency pressure transducers were mounted in each flap behind the inboard engine to measure the unsteady pressure loading. Accelerometers were mounted in each flap element near the root and also behind the inboard engine to measure flap response. Temperature was measured by using thermocouples and temperature-sensitive paints in the region behind the engines.

RESULTS AND DISCUSSION

Before the data from the large-scale model are discussed, consider a chordwise pressure distribution from tests at the Langley Research Center of the small-scale model shown on the left of figure 1. This model has three flap elements, a vane and two flaps, but the flap geometry is substantially different from the large-scale-model flap geometry. Figure 4 shows the pressure distribution on the small-scale-model flap system at a spanwise position influenced by the engine although not directly behind it. Pressure coefficient is plotted against the local chord location for each flap element. These data from the small-scale model are shown to illustrate the effect of configuration differences on the flap loading. Note that the loading on the third element or trailing flap is more than twice as large as the loading on either the vane or leading flap.

Chordwise pressure distributions are also available for the large-scale model. However, in order to present a clearer picture of the flap loading, the chordwise pressure distributions were integrated so that the spanwise variation of the loads could be presented. Figure 5 shows the spanwise variation of normal-force coefficient for each of the three flap elements on the large-scale model. Section normal-force coefficient is plotted against the semispan fraction for the nominal landing flap deflections of $15^{\circ}/35^{\circ}/55^{\circ}$ and model angle of attack of 16°.

The thrust coefficient is 4.0 which corresponds to a high-power approach condition. The spanwise shape of the loading curve is typical of the EBF concept, with peak loads corresponding to the engine locations. For this configuration, the peak loads on the second flap are nearly as large as the loads on the third flap. Outboard of the engines, the third flap has the lowest loading of the three. Recall that figure 4, for the small-scale model, indicated loads much higher on the third flap element than on the others. These data indicate, therefore, that great care should be exercised in using data from one configuration to predict loads on another configuration, even a similar configuration.

Spanwise loads data are available for all three flap elements as a function of several parameters. However, the spanwise loading on only one flap element, the third, is used to illustrate their effects. Figure 6 shows the effect of engine power setting and wing angle of attack on the third-flap loads. Normal-force coefficient is plotted against the semispan fraction for two angles of attack, 4° and 16°, for thrust coefficients of 0, 2.3, and 4.0. The lower curve shows the unpowered flap loading. This loading is about the level expected on conventional transport aircraft flaps. The increase in flap loading is shown for thrust coefficients of 2.3 and 4.0. For a thrust coefficient of 4.0, the loading behind the engines is increased by about an order of magnitude over the unpowered case. Angle-of-attack effects on the third-flap loads are minor compared to the effect of power setting, as can be seen by comparing peak loads at the same power setting.

The effect of flap deflection on the loads on the third flap is shown in figure 7. The third-flap normal-force coefficient is plotted against semispan fraction for take-off and landing flap deflections at a thrust coefficient of 4 and an angle of attack of 16°. For the landing flap deflections, the engine core impinges directly on the third flap. For the take-off flap deflections, the core passes beneath the flaps and the loads are significantly lower. For the landing flap deflections, the peak loads are about $1\frac{1}{2}$ times as large as the take-off flap loads.

Now consider the area of dynamic loads. Figure 8 shows unsteady pressure and flap acceleration power spectra for the first-flap-element, landing flap deflection. Power spectral density is plotted as a function of frequency in both cases. Note that it is a linear frequency scale. The data represent the input and response information for a constant engine-power setting with the wind on in one case and with the wind off in the other. There are two points to be made with this figure. First, the unsteady pressure or input power spectral density for both conditions decreases with increasing frequency with no predominant peaks. The response spectrum, however, is characterized by large peaks. This indicates that the structure is vibrating in its natural modes. For this boilerplate model, the first mode at 75 Hz is higher than would be expected for a flight-weight structure. Since the input power may be greater at the lower frequencies, one must consider the possibility of vibratory loads on a flight-weight structure.

Note the great similarity between the data for the two conditions, that is, with a constant power setting but with the wind on in one case and with it off in the other. These results indicate that the engines have a much larger effect on the unsteady pressures than the wind-tunnel velocity. It appears, therefore, that future tests of flight-weight flap structures might be performed on a static test stand rather than in a wind tunnel.

The final problem area to be discussed is the flap temperature environment. Figure 9 shows the temperature distribution on the lower surface of the flap system. The conditions correspond approximately to approach flap and power settings. Small regions on the third flap sustained temperatures approaching the engine tailpipe temperature (about 825 K). These temperatures should represent a worst-case condition since these engines had a bypass ratio of 3 compared to bypass ratios of 6 or more planned for STOL aircraft. Increasing the bypass ratio should lower these temperatures. Some preliminary temperature measurements at the Flight Research Center on an engine with a bypass ratio of 6 indicated that the maximum temperatures would be reduced to about 500 K. Of course, 500 K may still be too high for materials such as aluminum and the composites. Mixing nozzles, which forcibly mix the cool bypass air with the engine exhaust, can bring the maximum temperatures down to acceptable levels. However, mixing nozzles can be noisy and noise is also a problem. Other possible solutions include deflecting the hot exhaust jet away from the flap system or limiting flap deflections so that the exhaust does

not impinge on the flap system. Any solution of this temperature problem could also have a major effect on performance.

CONCLUDING REMARKS

In summary, previous small-scale-model data have shown large static loads on the flap system behind the engines. The large-scale-model tests confirmed the magnitude of these loads and indicated that the relative loading of each flap element depends on the engine-wing-flap geometry.

Flap response measurements indicated that the unsteady pressure loading excited the natural vibration modes of the flap system on this model. Since this was a boiler-plate model, the only conclusion that can be drawn is that the possibility of large vibration loads must be considered for a flight-weight structure. The similarity of the unsteady pressure and flap response spectra for the wind-off and wind-on cases indicated that it may be possible to realistically test flight-weight flap structures on a static test stand rather than endure the extra costs and scheduling problems associated with large-scale wind-tunnel tests.

And, finally, there is a potential flap-temperature problem which if not resolved might preclude the use of materials such as aluminum and the composites in the flap structure.

MODEL CONFIGURATIONS

SMALL-SCALE MODELS

LARGE-SCALE MODEL

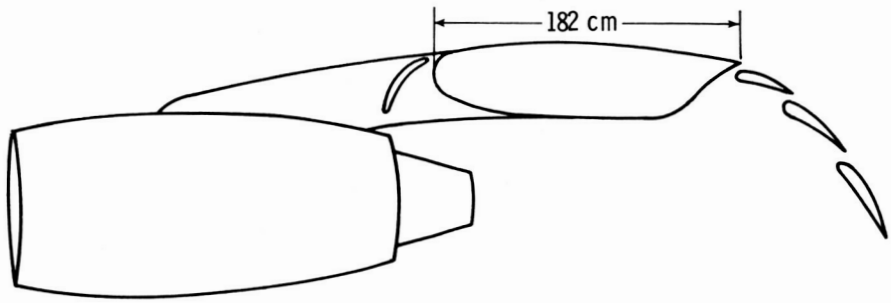

Figure 1

11.6-meter (38-FOOT) WIND-TUNNEL MODEL

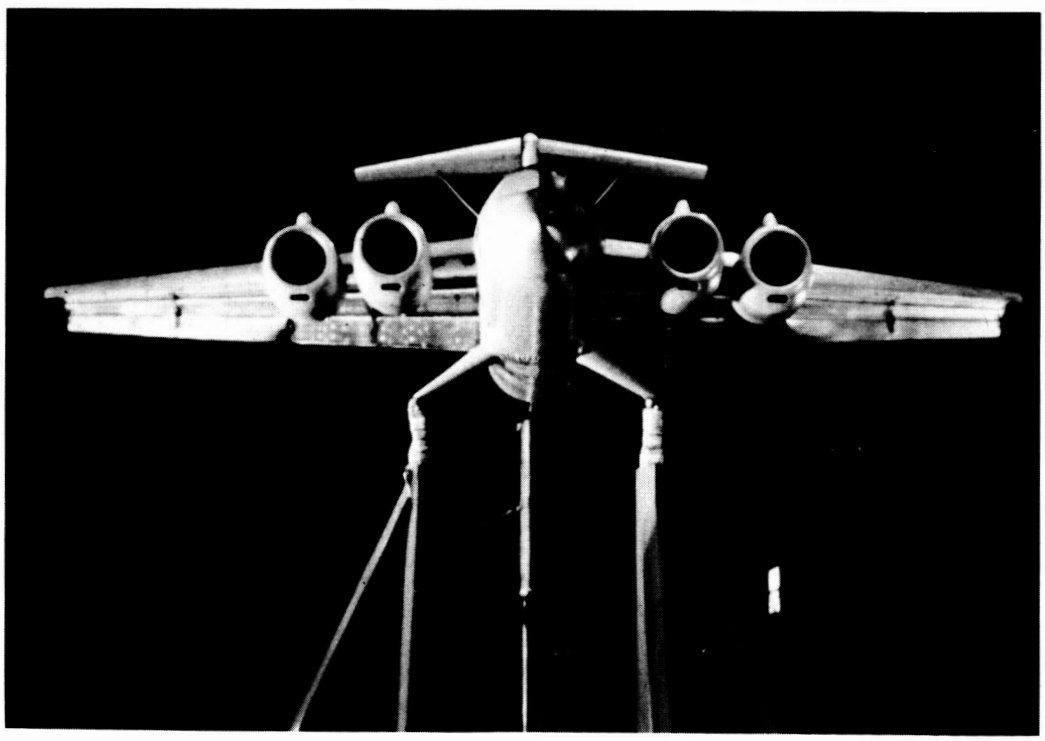

Figure 2

FLAP SYSTEM

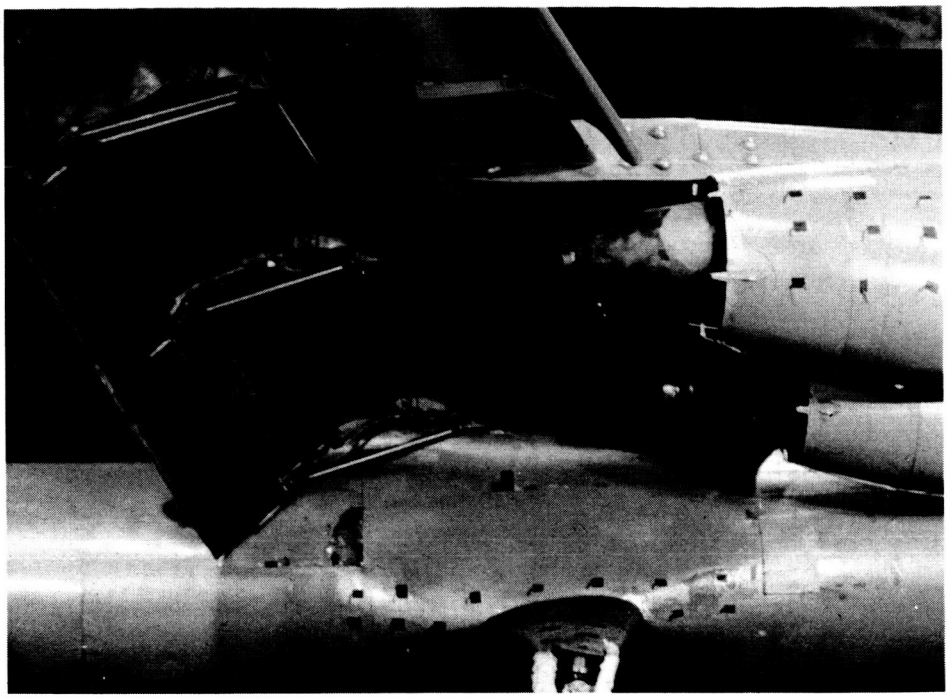

Figure 3

FLAP PRESSURE DISTRIBUTION

SMALL-SCALE MODEL

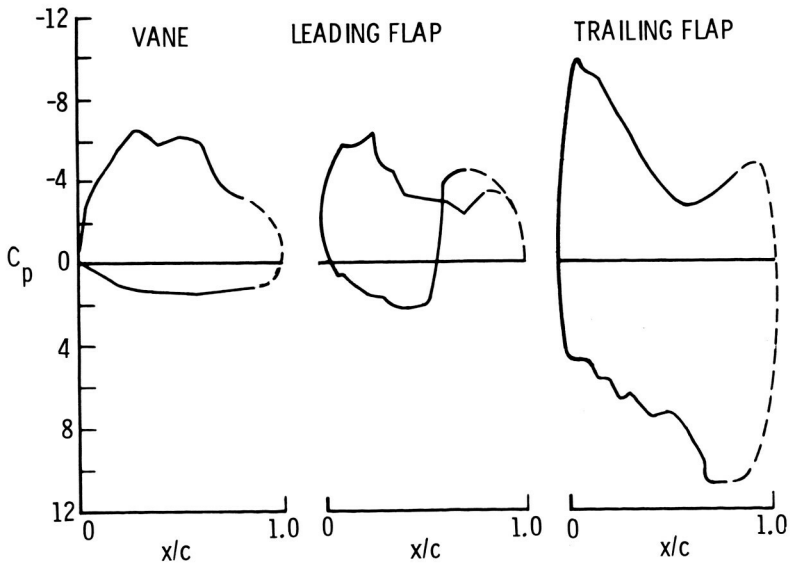

Figure 4

SPANWISE VARIATION OF FLAP NORMAL FORCE

LANDING FLAPS ($15^0/35^0/55^0$)

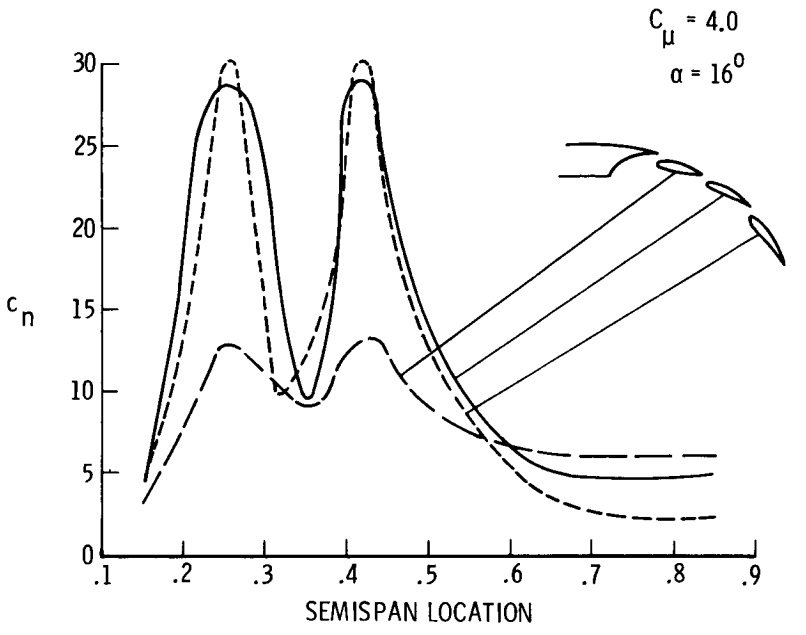

Figure 5

EFFECT OF POWER ON THIRD-FLAP LOADS

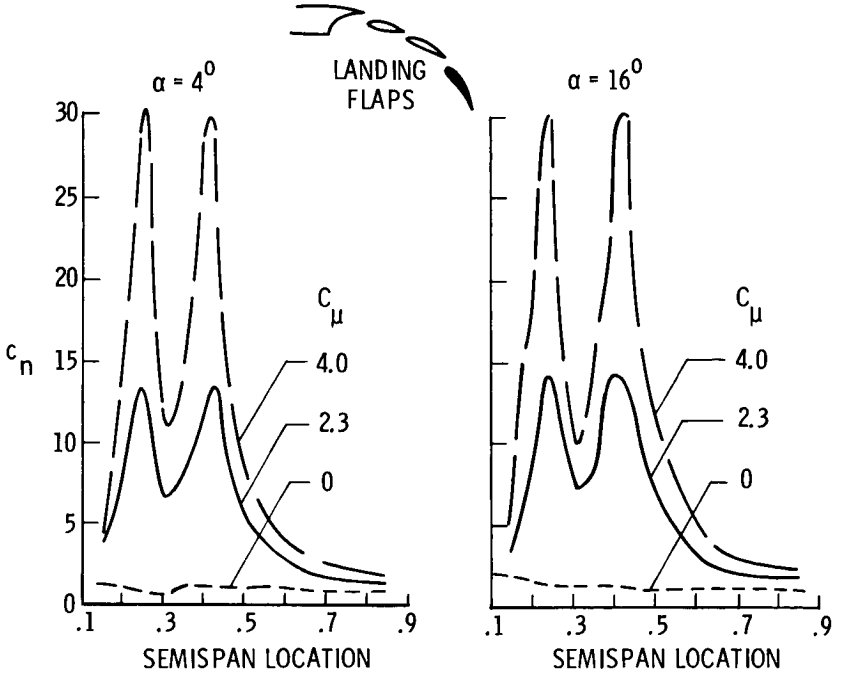

Figure 6

EFFECT OF FLAP DEFLECTION ON THIRD-FLAP LOADS

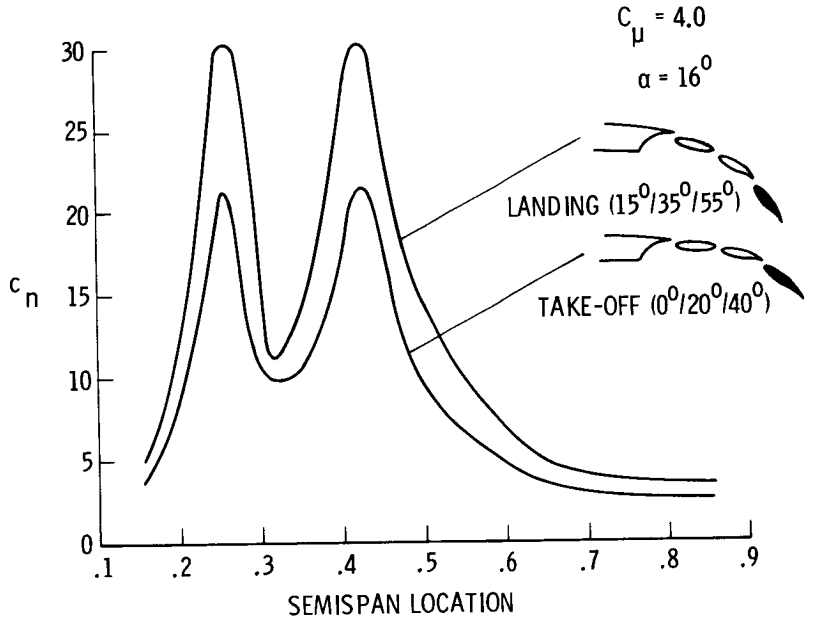

Figure 7

PRESSURE AND ACCELERATION POWER SPECTRA

CONSTANT POWER SETTING

—— WIND ON (C_μ = 4.0)

----- WIND OFF

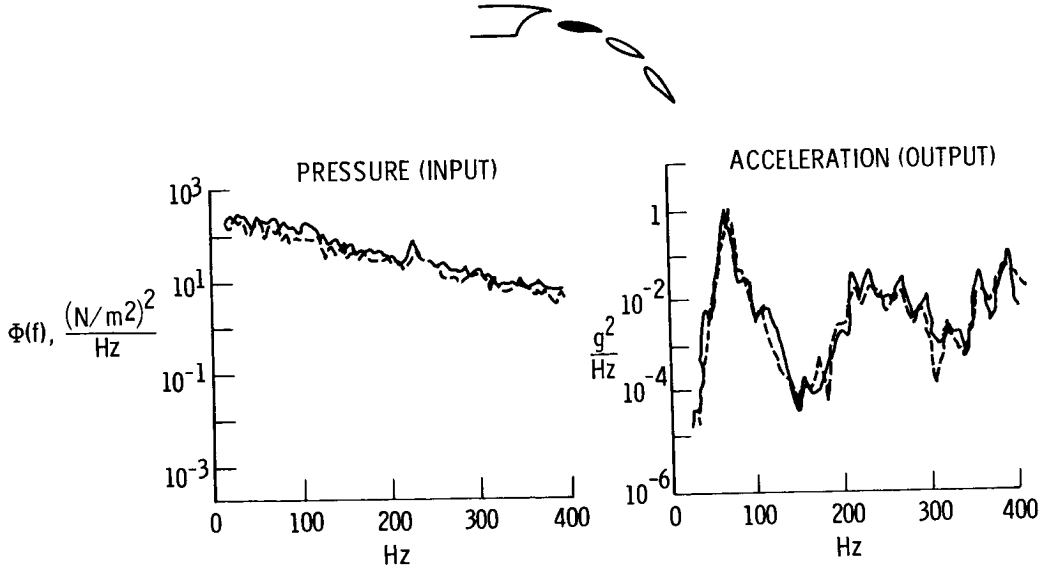

Figure 8

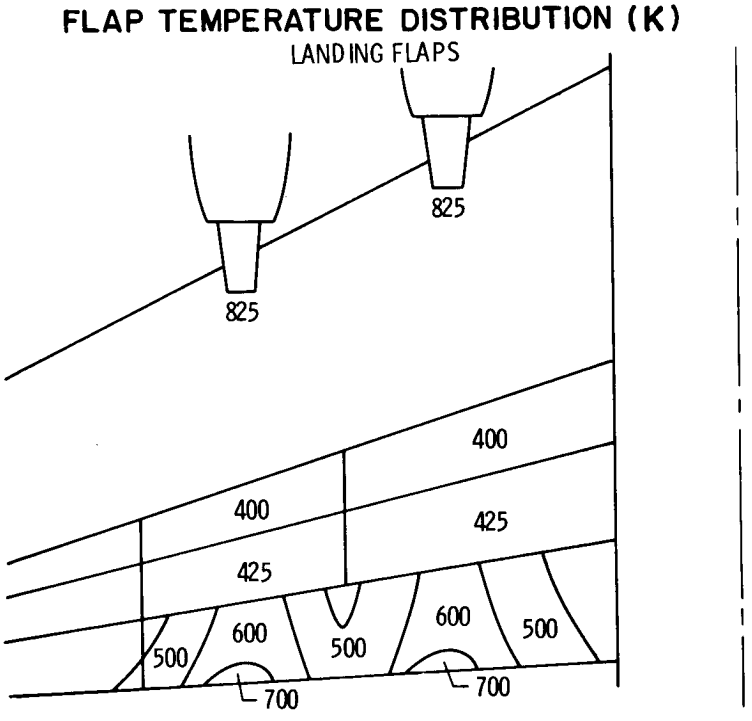
FLAP TEMPERATURE DISTRIBUTION (K)
LANDING FLAPS
825
825
400
400
425
425
600
600
500
500
500
700
700

Figure 9

EXTERNALLY BLOWN FLAP DYNAMIC LOADS

By Donald L. Lansing, John S. Mixson, Thomas J. Brown *,
and Joseph A. Drischler
NASA Langley Research Center

12

SUMMARY

This paper presents some of the principal results obtained in three series of measurements of fluctuating surface pressures induced on externally blown flaps by jet impingment. Large- and small-scale models and hot- and cold-flow tests are considered. The discussion sets forth scaling parameters and consistent features of the root-mean-square values and spectra of the loading. Implications of these results with regard to sonic fatigue are indicated.

INTRODUCTION

The powered-lift systems being considered for use on commercial STOL vehicles generate additional lift by deflecting the exhaust flow of a turbulent jet with the aid of one or more turning flaps. For these systems large areas of the wing and flap surfaces are immersed within the jet exhaust. Consequently, these surfaces are subjected to high-intensity fluctuating loads which have the potential for inducing high vibration levels and sonic fatigue.

There is very little information presently available on flap loads. This lack of information poses a serious problem for the aircraft designer who must provide structural integrity in an adverse environment with minimum weight. The purpose of this paper is to call attention to several sources of information on flap loads and to give a brief summary of the current state of knowledge.

SYMBOLS

D	bypass nozzle diameter
f	frequency, Hz
M	jet center-line Mach number at exit
N_{Str}	Strouhal number, Df/u_j

* Langley Directorate, U.S. Army Air Mobility R&D Laboratory.

p_{rms} root-mean-square value of fluctuating component of pressure

q_j jet center-line dynamic pressure at exit

u_j jet center-line velocity at exit

$\Pi(N_{Str})$ one-third-octave band power spectrum

SOURCES OF LOADS AND LOADS DATA

Figure 1 shows the principal sources of turbulent pressure fluctuations on externally blown flaps. The sources of turbulence are: upstream disturbances such as combustion processes, the mixing region of the core and bypass nozzle exhaust, boundary layers on flap and wing surfaces, regions of separated flow which may occur when flaps are deflected to high angles of attack, and high-velocity air passing through slots. The turbulence scale and intensity and the associated dynamic loading actions are different in each of these flow regions. The type of loading action to which any part of the wing-flap system is exposed depends upon the geometric arrangement of the configuration, such as the engine location and number of flaps, and upon operating conditions, such as angle of attack, forward speed, and engine power setting. Thus, a great diversity of loading conditions is likely to be encountered during the operation of an externally blown flap.

There are three principal sources of data on dynamic loads on externally blown flaps: the large-scale cold-jet model tested at the Lewis Research Center, shown in figure 2; the 11.6-m- (38-ft-) span hot-jet STOL model tested in the Ames 40- by 80-foot wind tunnel, shown in figure 3; and the small-scale cold-jet model tested by Bolt Beranek and Newman, Inc., Cambridge Laboratory, shown in figure 4. This paper presents a sampling of some of the results of these tests.

The Lewis Research Center tests which were carried out by Walter J. Kreim and Robert H. Dorsch are discussed first.

LEWIS RESEARCH CENTER TESTS

Figure 2 is a photograph of the test arrangement. This is a 1/2-scale model of a double-slotted flap. The engine exhaust was simulated with a nozzle having a bypass ratio of six and using air at ambient temperature. Tests were conducted at four core jet Mach numbers of 0.52, 0.71, 0.90, and 1.10 and without forward speed.

Nine surface pressure transducers were positioned on the wing and flaps along the nozzle center line as indicated by the circular and square symbols in the sketch at the

bottom of figure 5. The values of the dynamic pressure coefficient measured at these locations are plotted at the top of the figure above the corresponding transducer location. The dynamic pressure coefficient is the ratio of p_{rms}, the root-mean-square value of the fluctuating component of the pressure, to the dynamic pressure q_j at the exit of the core jet. The fluctuating component of pressure is defined to be the actual time varying pressure minus the static pressure.

It was found that the rms levels at all transducers except one scaled on the jet dynamic pressure q_j. With this exception, each data point represents results for four jet Mach numbers. The exceptional transducer is located on the lower surface of the second flap near the jet center line. The largest pressures were always measured here, with values of p_{rms}/q_j ranging from 0.066 at $M = 0.52$ to 0.126 at $M = 1.1$. High loads were also measured at other positions on the lower flap surfaces and on the upper surface of the second flap. The high loads on the upper surface of the second flap are probably the result of the turbulence produced by the flow passing through the slot between the flaps.

Examples of one-third-octave power spectra of the surface pressure are shown in figure 6. The spectra are divided by the square of the jet dynamic pressure and are plotted against the Strouhal number $N_{Str} = Df/u_j$ based on bypass nozzle diameter D and the core jet exit velocity u_j. The range of frequencies corresponding to this range of Strouhal numbers depends, of course, upon D and u_j. For this model the frequency range is about 50 to 50 000 Hz. When plotted in this form, the four spectra at each of transducers A and B collapse into the hatched regions labeled A and B, respectively. This type of normalization has been used for a variety of other flow-induced dynamic loads. Thus, although the collapse of data is not unexpected, it is gratifying to see that it also holds for flap loads.

The spectral shapes at the two transducers are significantly different. The peaked spectrum is typical of spectra measured at all lower surface transducers whereas the broad spectrum with more high-frequency content is typical of all the upper surface measurements. The peak in the lower surface spectra occurs at frequencies ranging from about 100 Hz at $M = 0.52$ to 300 Hz at $M = 1.10$. The spectra are broadband in nature and are therefore capable of exciting many structural modes.

The high-frequency portion of the lower surface spectra falls off at about the inverse 1.3 power of the Strouhal number. The line drawn through the hatching is a simple approximation to the decay which could be useful for analytical purposes and which will be used subsequently to compare these data with the Ames Research Center data.

It is of interest to point out that spectra measured on the lower surface of a 1/15-scale-model flap by Bolt Beranek and Newman, Inc., have essentially the same shape as the spectra labeled B in figure 6, have a peak at the same Strouhal number

(about 0.4), and have dynamic pressure coefficients comparable to those shown in figure 5. This agreement indicates compatibility between large- and small-scale experiments with regard to lower surface pressure spectra and overall levels.

AMES RESEARCH CENTER TESTS

Figure 3 is a photograph of the 11.6-m- (38-ft-) span STOL model in the Ames 40- by 80-foot tunnel. As discussed in paper no. 11 by George C. Greene and Boyd Perry III, this is a half-scale model of a triple-slotted flap. Since JT15D engines were installed on the model and operated during the tests, the flow over the flap surfaces is hot. Figures 7 and 8 show results of the intensity and spectra of surface pressure measured on this model for take-off flap setting (30^{o} on the third flap). For the data shown here, the maximum temperatures, which occurred on the third flap, never exceeded 425 K (300^{o} F).

Figure 7 shows the range of values of the dynamic pressure coefficient as a function of angle of attack for a forward speed of 19 m/sec (61 ft/sec), and two core jet velocities of 205 m/sec (674 ft/sec) and 286 m/sec (938 ft/sec). As indicated by the sketch at the right, measurements were made at three pressure transducers, one on the lower surface of each of the flaps along the engine center line. The solid line through the stippled region separates the data taken on the second flap, which fall in the upper part of the region, from the data taken on the first and third flaps, which fall in the lower portion. The general variation in dynamic pressure coefficient is first a decrease up to small positive angles of attack and then an increase with further increase in angle of attack. There is considerable scatter of the data within each of the regions. The normalization with core jet exit dynamic pressure q_j is not as effective here as for the Lewis Research Center tests. The variation of dynamic pressure coefficient with angle of attack shown in this figure does not apply to all test conditions.

The range of values of the dynamic pressure coefficient shown in figure 7 is comparable to the range measured in the Lewis tests (see fig. 5) and is representative of the majority of the Ames data for take-off flaps. However, as will be noted later, there is a minority of data which gives considerably higher pressure coefficients of about 0.1 and 0.3.

One-third octave power spectra of the surface pressures are shown as a function of Strouhal number in figure 8. These spectra were taken on the lower surface of the second flap at take-off flap setting with a jet velocity of 286 m/sec (938 ft/sec) and forward speed of 19 m/sec (61 ft/sec). Spectra for all five angles of attack, -8^{o}, 0^{o}, 8^{o}, 16^{o}, and 24^{o}, fall in the shaded region. The data collapse is quite good at Strouhal numbers greater than about 0.5. The rate of falloff of the spectra with Strouhal number is the same as for the Lewis tests. There is some scatter in the low-frequency end of the spectrum. The amount of scatter and the shape of the spectrum in this frequency range have been found

to depend upon transducer location. At this transducer the spectra appear to level off at low frequencies. At other transducers the spectra may drop off at low Strouhal numbers as in the Lewis tests or may continue to increase as Strouhal number decreases.

BOLT BERANEK AND NEWMAN, INC., TESTS

Figures 7 and 8 have shown the intensity and spectra of the dynamic loads at isolated positions along the jet center line, but not enough transducers were used in either of these tests to provide any insight into the spanwise distribution of loads. This kind of data was taken on the 1/15-scale model shown in figure 4. This model is a partial-span section geometrically similar to the wing and flaps on the Ames STOL model. This triple-slotted flap was blown with a circular convergent nozzle using air at ambient temperatures. The model was tested by Bolt Beranek and Newman, Inc., as part of a contract effort to study noise suppression methods on flaps. The circles along the leading edge, trailing edge, and midspan of the under side of the flaps indicate the locations at which surface pressures were measured. The results of this study are presented in reference 1.

From these measurements it is possible to begin to form a picture of the load distribution over the flaps. The inferred distributions for approach and take-off flap settings are shown in figures 9 and 10, respectively. The relative intensity of the loading is indicated by various types of shading. The absolute levels of fluctuating pressure are of the same order as those measured in the Lewis tests. Both figures show that there are large areas of the flap off the jet center line which are exposed to high dynamic loads. The third flap generally has the largest area exposed to high loads. There are pockets of high and low loading scattered over the flaps in a way which is not simply related to the geometry of the engine-wing-flap system. In particular, the highest loads do not always occur on the jet center line.

SUMMARY OF DATA AND IMPLICATIONS

Figure 11 shows the range of dynamic pressure coefficients measured in the three experiments previously described and the range of jet Mach numbers for the investigation. Also shown for comparison are dynamic pressure coefficients measured in a simple wall jet (ref. 2) and in a free jet (ref. 3). With the exception of a few high values obtained in the Ames tests, maximum dynamic pressure coefficients measured so far on STOL models and in wall jets fall in the range from 0.10 to 0.15. Thus, with only these few exceptions, an upper bound of about 0.2 can be placed on the maximum value of p_{rms}/q_j. This bound appears to be independent of Mach number. The values of jet exit dynamic pressure for the three STOL model experiments range from about 9.6 kN/m^2 (200 lb/ft^2) to 47.9 kN/m^2

(1000 lb/ft^2). Therefore, a value of the dynamic pressure coefficient of 0.2 corresponds to root-mean-square values of surface pressure from about 1.9 kN/m^2 (40 lb/ft^2) to 9.6 kN/m^2 (200 lb/ft^2). The similarities of the spectral shapes obtained from the three STOL models were pointed out previously. Thus, the principal conclusion of this paper is that consistent results for several gross features of flap loads are being obtained from large- and small-scale models and hot- and cold-flow tests. It is, therefore, believed that these common features can be extrapolated to full scale with considerable confidence.

It is desirable in concluding this paper to place flap loads in context with other types of dynamic loads and point out possible implications of the loading levels observed with regard to the design of externally blown flaps.

Figure 12 presents a comparison of representative sound pressure levels of several sources of acoustic loading on aircraft structures. The sound pressure levels are expressed in decibels (dB). Based on past experience, it is known that sonic fatigue becomes a consideration in aircraft structural design when the levels begin to exceed about 130 dB. This lower limit is not absolute, as indicated by the vertical shading between the horizontal bars. Sonic fatigue is a major consideration as the levels approach 160 dB. The top four loading actions have been associated with sonic fatigue on aircraft structures. Since flap loads are seen to be of a comparable order of magnitude and have a broadband spectrum capable of exciting many modes, one is led to the conclusion that blown flaps may also be subject to sonic fatigue which would then become an important consideration in the detailed design of powered-lift systems.

REFERENCES

1. Hayden, Richard E.; Kadman, Yoram; and Chanaud, Robert C.: A Study of the Variable Impedance Surface Concept as a Means for Reducing Noise From Jet Interaction With Deployed Lift-Augmenting Flaps. Rep. No. 2399 (Contract No. NAS1-9559-18), Bolt Beranek and Newman Inc., [1972]. (Available as NASA CR-112166.)

2. Strong, D. R.; Siddon, T. E.; and Chu, W. T.: Pressure Fluctuations on a Flat Plate With Oblique Jet Impingement. NASA CR-839, 1967.

3. Fuchs, H. V.: Measurement of Pressure Fluctuations Within Subsonic Turbulent Jets. J. Sound & Vib., vol. 22, no. 3, June 8, 1972, pp. 361-378.

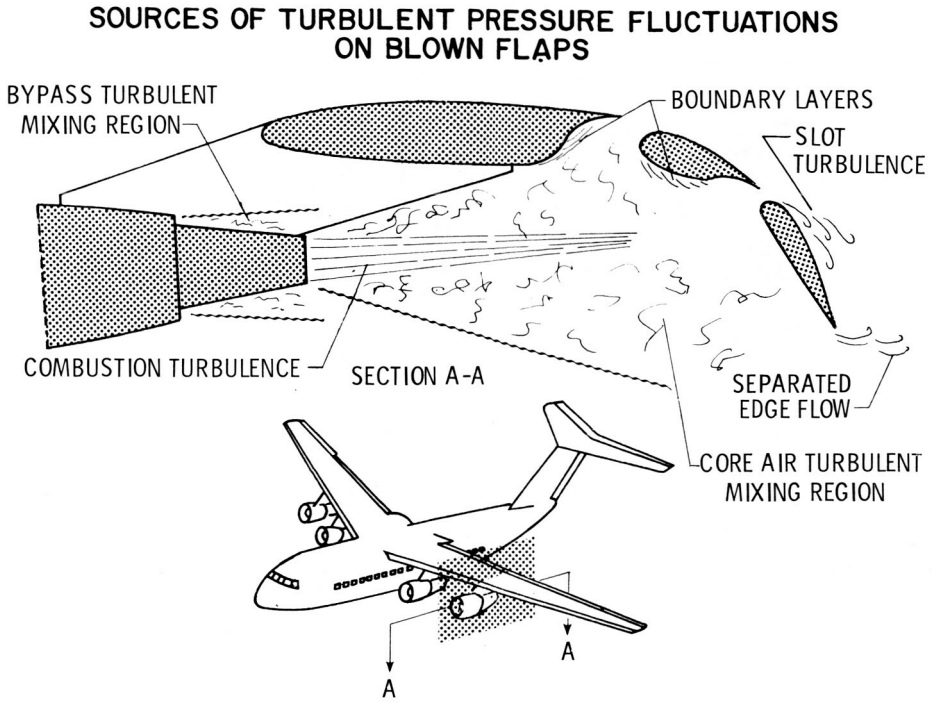

Figure 1

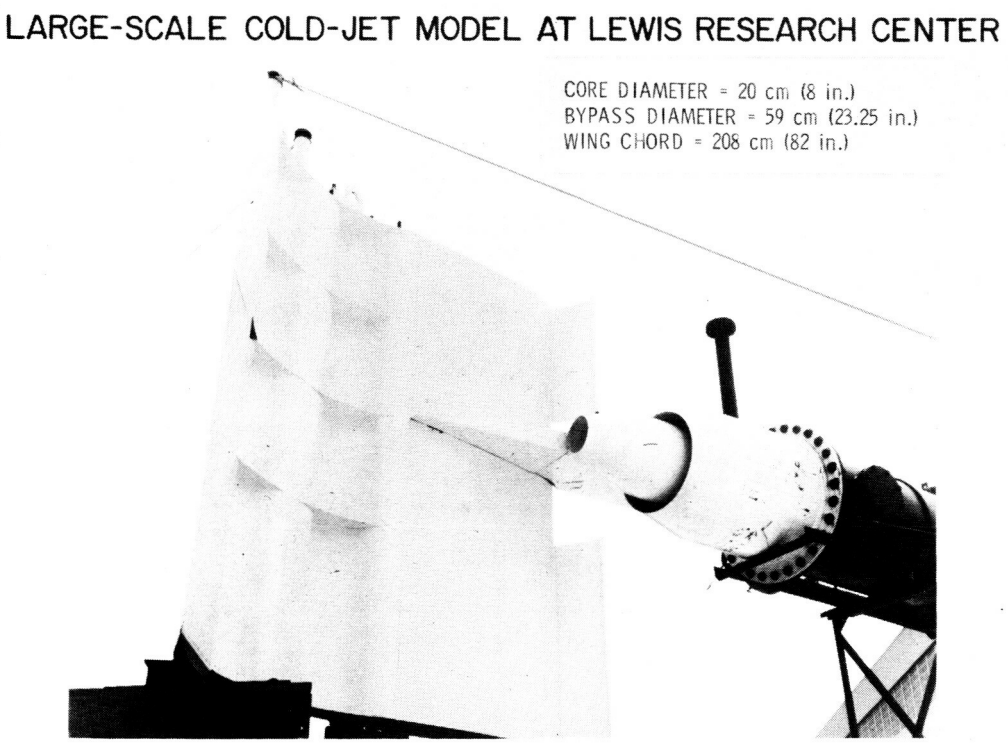

Figure 2

11.6-m- (38-ft-) SPAN HOT-JET STOL MODEL AT AMES RESEARCH CENTER

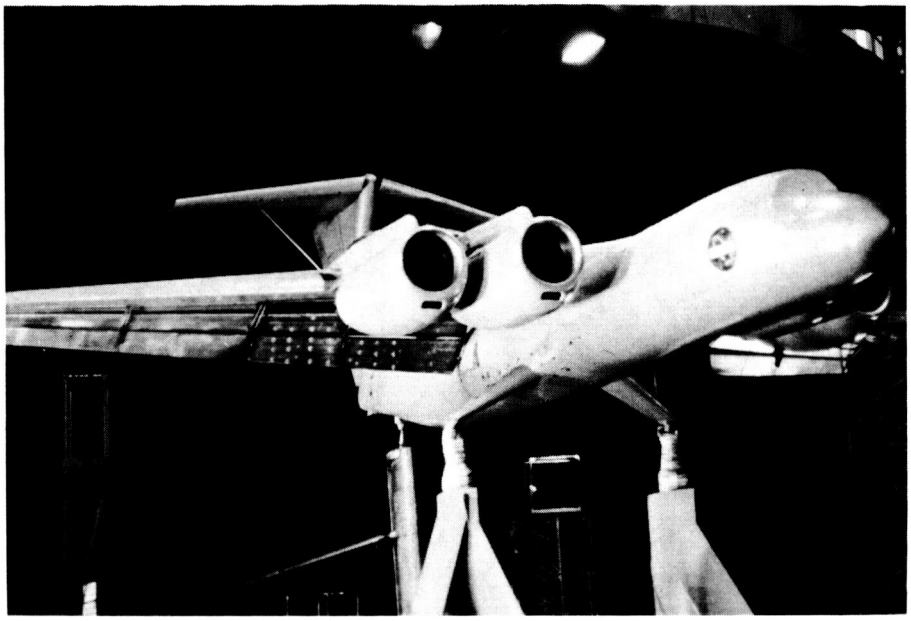

Figure 3

SMALL-SCALE COLD-JET MODEL AT BOLT BERANEK AND NEWMAN, INC., CAMBRIDGE LABS

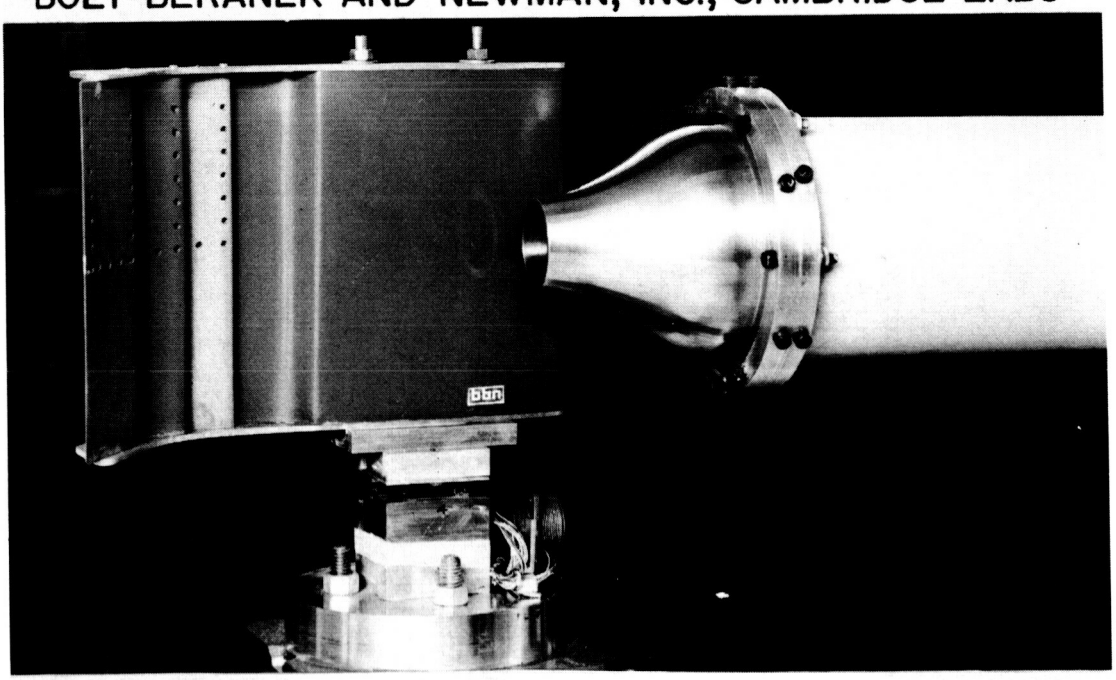

JET DIAMETER = 4.4 cm (1.75 in.) WING CHORD = 28 cm (11 in.)

Figure 4

CHORDWISE DISTRIBUTION OF DYNAMIC PRESSURE

LARGE-SCALE COLD-JET EBF MODEL

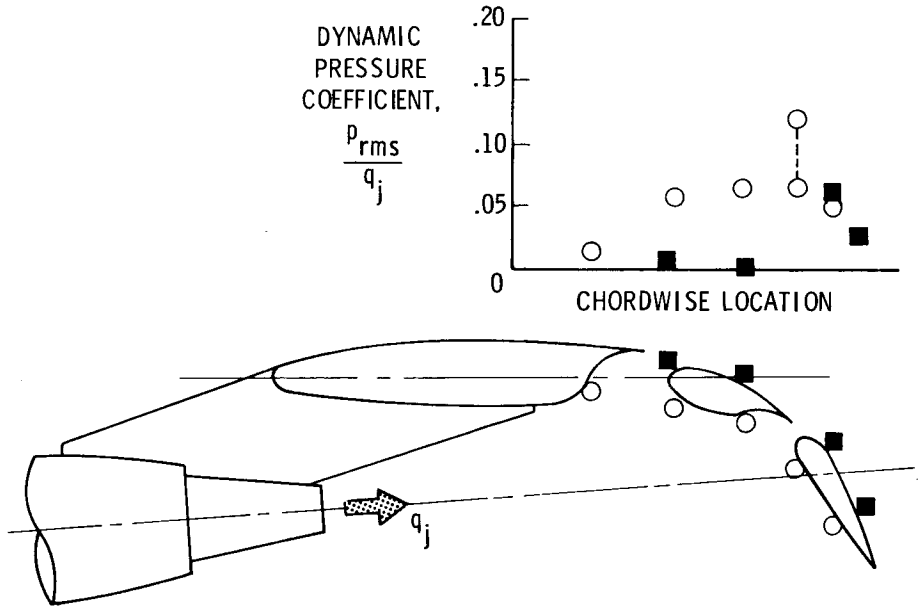

Figure 5

POWER SPECTRA OF SURFACE PRESSURE

LARGE-SCALE COLD-JET EBF MODEL

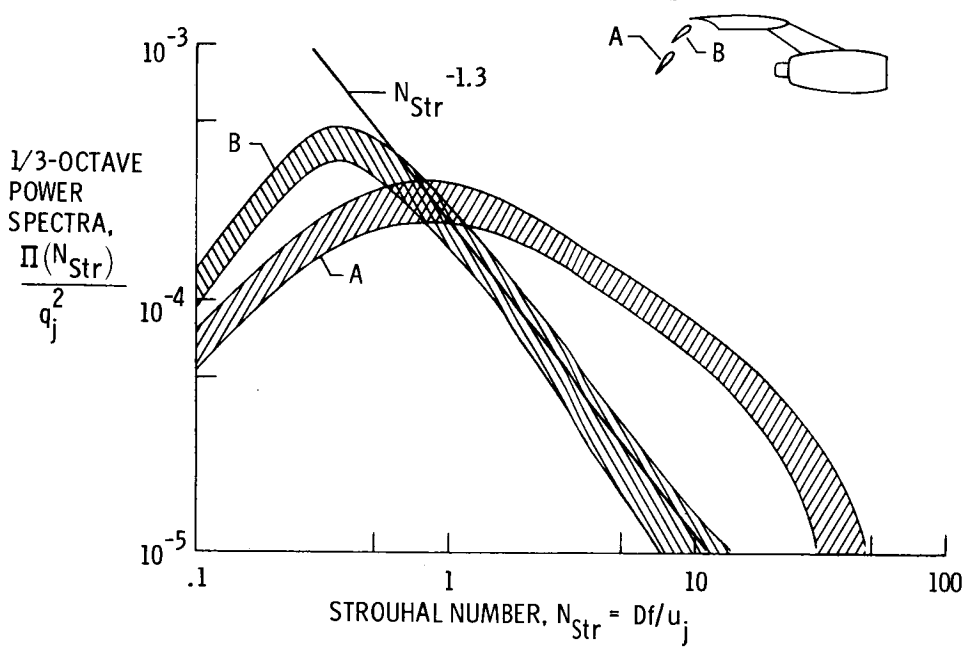

Figure 6

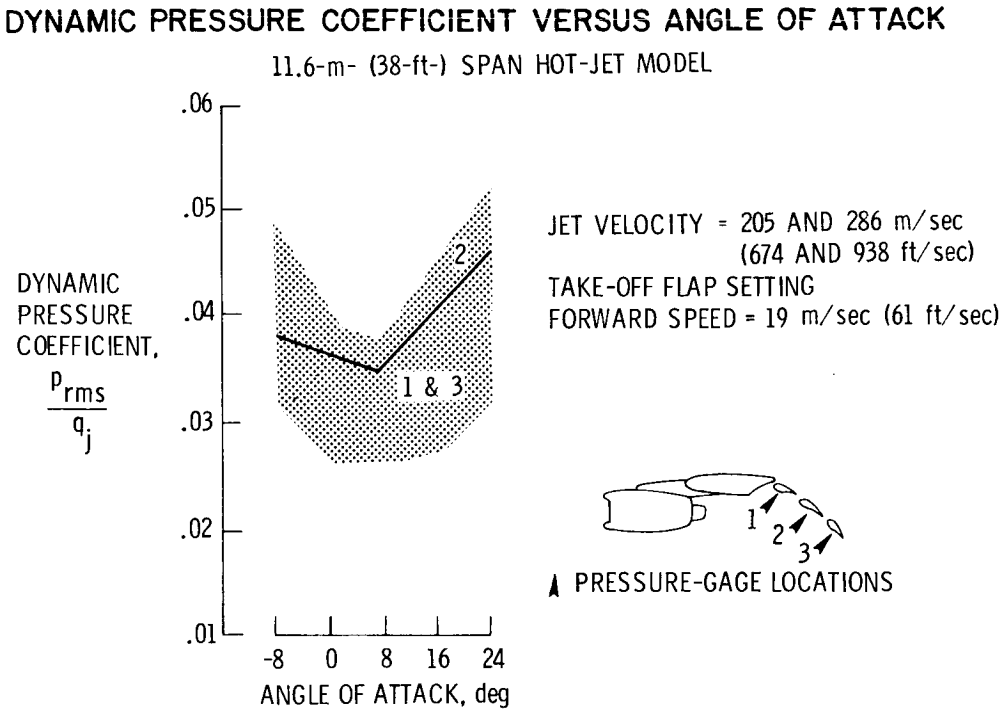

Figure 7

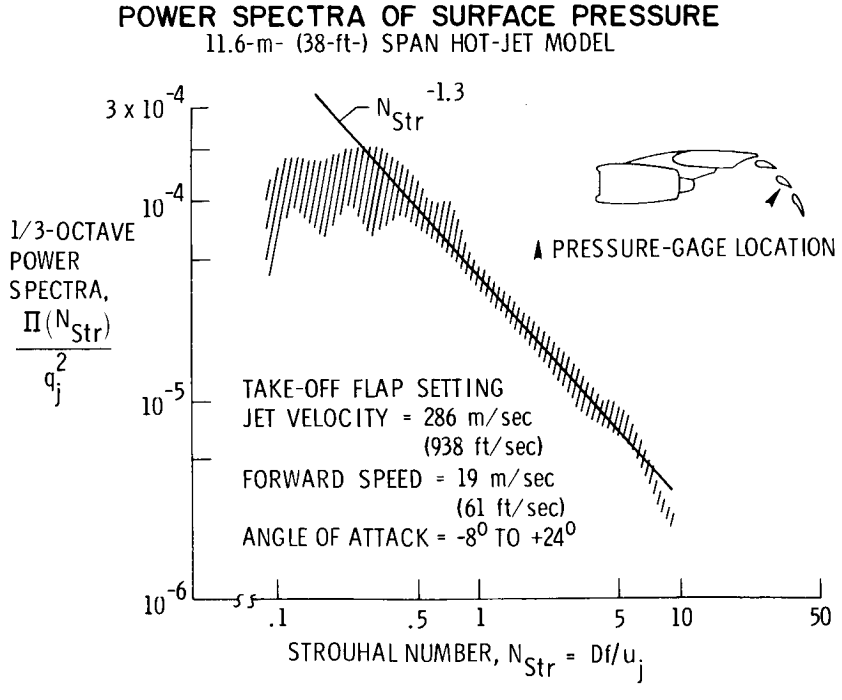

Figure 8

INFERRED DISTRIBUTION OF DYNAMIC SURFACE PRESSURE
APPROACH FLAP SETTING

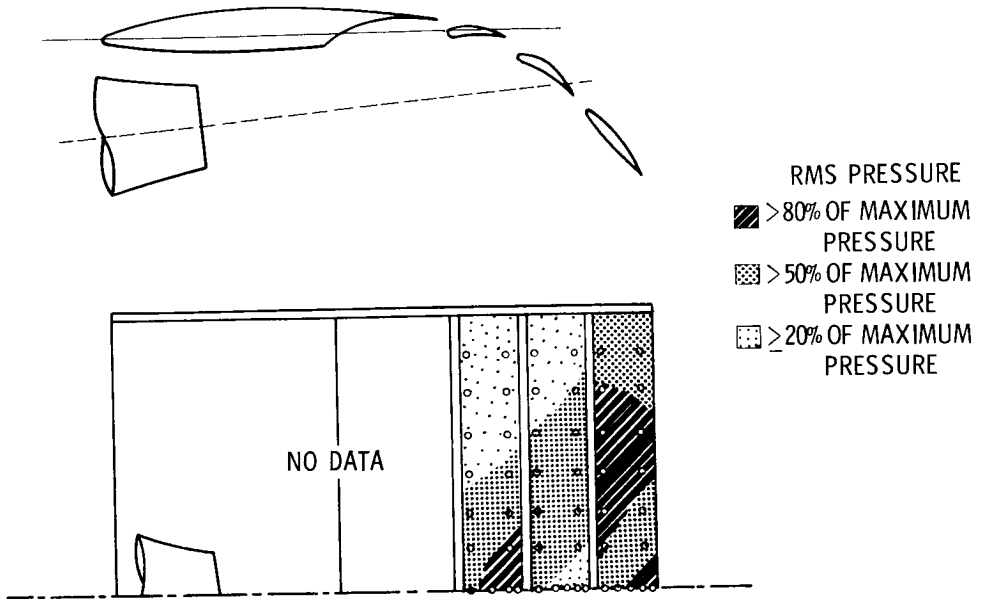

Figure 9

INFERRED DISTRIBUTION OF DYNAMIC SURFACE PRESSURE
TAKE-OFF FLAP SETTING

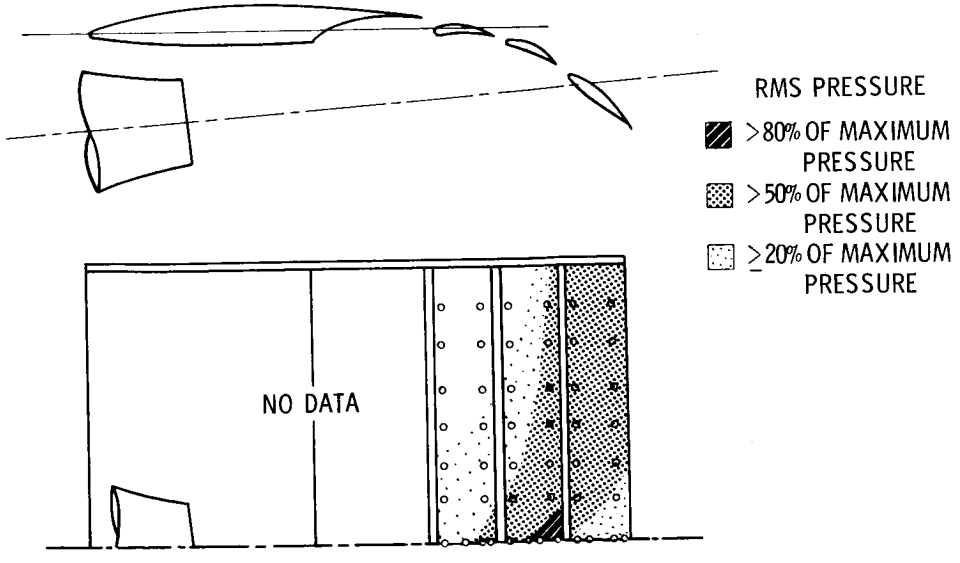

Figure 10

COMPARISON OF DYNAMIC PRESSURE COEFFICIENTS

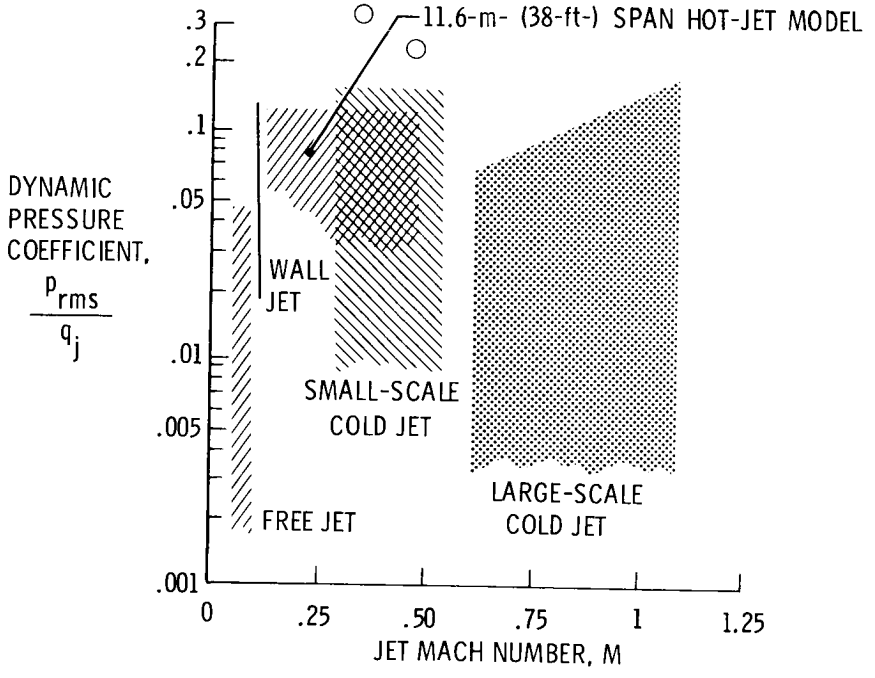

Figure 11

SOUND PRESSURE LEVELS OF ACOUSTIC LOADING ON AIRCRAFT STRUCTURES

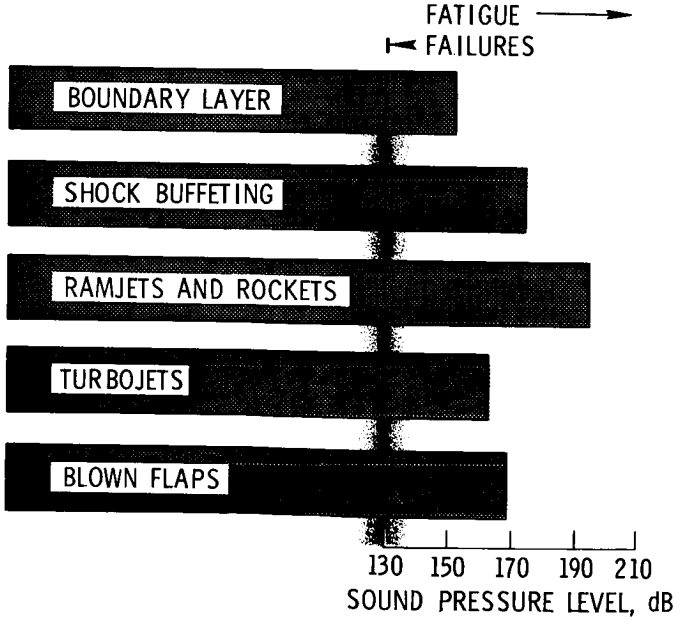

Figure 12

SURVEY OF WING AND FLAP LOWER-SURFACE TEMPERATURES AND PRESSURES DURING FULL-SCALE GROUND TESTS OF AN EXTERNALLY BLOWN FLAP SYSTEM

By Donald L. Hughes
NASA Flight Research Center

13

SUMMARY

Full-scale ground tests of an externally blown flap system were made using the wing of an F-111B airplane and a CF700 engine. Pressure and temperature distributions were determined on the undersurface of the wing, vane, and flap for two engine exhaust nozzles (conical and daisy) at several engine power and engine/wing positions. The tests were made with no airflow over the wing. The leading-edge wing sweep angle was fixed at 26°, the angle of incidence between the engine and the wing was fixed at 3°, and the tests were conducted with the flap retracted, extended and deflected 35°, and extended and deflected 60°. The integrated local pressures on the undersurface of the flap produced loads approximately three times as great at the 60° flap position as at the 35° flap position. With both nozzle configurations, more than 90 percent of the integrated pressure loads were contained within ±20 percent of the flap span centered around the engine exhaust centerline. The maximum temperature recorded on the flaps was 218° C (424° F) for the conical nozzle and 180° C (356° F) for the daisy nozzle.

INTRODUCTION

The need for a commercial air transport which is economically sound and which can operate out of conveniently located airports with short landing strips is widely recognized. The Government is taking steps to help develop a short take-off and landing (STOL) airplane which would meet these requirements. To achieve short take-off and landing distances without sacrificing the high wing loading needed for passenger ride comfort or the ability to maintain high cruise speeds, an augmented-lift device must be used.

An externally blown flap system of augmented lift is being considered for use on an experimental NASA STOL airplane. In this system, the primary thrust engines are close to the undersurface of the wing, so that when the flaps are lowered the jet exhaust impinges on the flap. Additional lift results from increased circulation about the wing and from the change in momentum of the deflected jet stream.

A survey of the areas of engine-exhaust-flow impingement on the flap and wing of an externally blown flap system is needed to determine the spanwise pressure distribution as well as the actual flap loads and temperatures generated. Although some attempts to obtain pressure distributions on a wing and flap system have been made by using scale models in wind tunnels, little has been done with full-scale wings and engines in an environment free of wind-tunnel interference effects. To provide such wing pressure data, the NASA Flight Research Center instrumented the wing of an F-111B airplane that was mounted vertically and adjacent to a CF700 turbofan engine on a ground-test fixture. The wing and engine were so positioned that the jet exhaust impinged on the flap when the flap was extended. The tests were conducted with no airflow over the wing other than that induced by the engine exhaust jet.

SYMBOLS

Physical quantities in this report are given in the International System of Units (SI) and parenthetically in U.S. Customary Units. The measurements were taken in U.S. Customary Units. Factors relating the two systems are presented in reference 1.

D	diameter of nozzle, m (in.)
F_p	pressure load obtained by integration of local pressures on undersurface of flap or vane, N (lbf)
p	local pressure, N/m^2 (lbf/in^2)
p_o	ambient static pressure, N/m^2 (lbf/in^2)
x	distance along engine centerline from nozzle face to flap surface (fig. 2), m (in.)
y	distance from centerline of engine exhaust at nozzle face to wing surface (fig. 2), m (in.)

TEST CONFIGURATION

Wing

The inboard half of an F-111B left wing was mounted vertically on a movable platform installed on an engine run-up ramp at Edwards Air Force Base, CA (fig. 1). The position of the wing with respect to the engine exhaust nozzle could be varied in several

ways (fig. 2): distance from the nozzle to the flap (longitudinally), distance from the nozzle to the wing (laterally), angle of incidence between the engine and wing, and angle of leading-edge sweep. All the test data presented were obtained with the flaps in three positions: retracted, extended and deflected 35°, and extended and deflected 60°. (Flap positions are referred to as retracted, 35°, and 60°.) The 60° flap position was not normal for the F-111B wing, and for this setting the flaps were held in a special support fixture mounted on the upper surface of the wing at the normal flap rail locations. Figure 3 shows the undersurface of the wing with the flaps in the 35° position. The test results presented were obtained with the wing leading-edge sweep angle set at 26°.

Engine

A General Electric CF700 turbofan engine was mounted in a fixed position on the thrust stand adjacent to the wing (fig. 1). A bellmouth inlet and an acoustically treated exhaust duct which terminated in one of two interchangeable exit nozzles were connected to the engine. Closeup photographs and schematic drawings of both the daisy and conical exit-nozzle configurations are shown in figure 4, along with nozzle diameters and areas. The conical nozzle was sized to provide approximately the same thrust as the daisy nozzle.

Wing/Engine Relationships

Wing, flap, and nozzle positions and their relationships are shown in figure 2. All the test data were obtained with an angle of incidence between the engine and wing of approximately 3°. The longitudinal distances x from the nozzle to the point of jet impingement on the 60° flap position were set at approximately 3, 4, and 5 conical nozzle diameters. These longitudinal positions were then used as fixed positions for both nozzles regardless of changes in flap position or movement of the wing closer to the engine. The closeness of the wing to the nozzle, y, was fixed at a common centerline for each nozzle configuration, as shown in figure 2.

Measured Thrust

The thrust of the engine with each exhaust-nozzle configuration installed was measured by using the thrust table and its underground balance system. The thrust of the engine was measured to higher values with the flaps at the 60° position than with the flaps at the 35° position; consequently, no data are presented above 12 010 N (2700 lbf) for any of the 35° flap configurations.

INSTRUMENTATION

Static-pressure ports were installed on the underside of the wing, vane, and flap, providing low-response steady-state pressures in a grid, as shown in figure 3. No pres-

sure or flow measurements were made on the upper surface of the wing, vane, or flap. In three of the static-pressure ports on the flap, on or near the centerline of jet-exhaust impingement, high-response transducers were mounted so that their diaphragms were flush with the surface of the flap (fig. 3). These transducers were capable of withstanding the high temperatures of the jet exhaust. Temperature measurements were obtained at each static-pressure port by means of surface-mounted thermocouples.

RESULTS

Pressure and Temperature Profiles

Pressure and temperature data obtained during the ground tests of the externally blown flap system were plotted on scale drawings of the test wing at corresponding recording locations. Lines of equal pressure or temperature were then drawn between the plotted data points. A typical set of pressure-ratio contours with the flap at the 60^{o} position for the daisy nozzle configuration is shown in figure 5. Temperature and pressure contour drawings of this type were made for each stabilized data run and were used to determine the effects of exhaust impingement quantitatively. The pressure contours were also integrated for each stabilized data run to determine the overall pressure load on the undersurface of the flap and vane. The wing surface pressure and temperature contours did not reveal any unusual or extreme values like those on the flaps and vanes. Consequently, no analysis was made of the wing surface.

The effect of engine thrust on the maximum pressure ratios recorded on the flap for the conical and daisy nozzle configurations is shown in figure 6. The maximum pressure ratios recorded on the flap with the conical nozzle are higher over the range of thrust than the pressures recorded with the daisy nozzle. This result indicates a greater concentration or focusing of exhaust pressure with the conical nozzle configuration. This concentration is confirmed in figure 7, which shows that the maximum temperatures recorded on the flap are higher with the conical nozzle than with the daisy nozzle. With a jet exhaust-gas exit temperature of 315^{o} C (600^{o} F), the maximum temperature recorded on the flap was 218^{o} C (424^{o} F) for the conical nozzle and 180^{o} C (356^{o} F) for the daisy nozzle. It should be noted that these maximum temperatures occurred with no flow over the wing and flap; under actual flight conditions the temperatures would probably be lower.

Undersurface Flap Loads

The load experienced by the undersurface of the flap as a result of engine-exhaust impingement, called F_p, was determined by integrating the static-pressure contour data for each steady-state data run at flap positions of 35^{o} and 60^{o}. With the flaps retracted, the load on the flaps was essentially zero.

Typical curves of undersurface flap load as a function of flap position are shown in figure 8 for an engine thrust setting of approximately 12 010 N (2700 lbf) and a longitudinal distance x of 3 diameters for both the conical and daisy nozzle configurations. Even though the values of F_p at the 35° and 60° flap positions varied somewhat with the different nozzle configurations, figure 8 shows that for both configurations the loads on the undersurface of the flap at the 60° position are approximately 3 times as great as those at the 35° flap position.

The effect of longitudinal nozzle position on F_p at a comparable engine thrust of 12 010 N (2700 lbf) is shown in figure 9. Moving the nozzle closer to the flap caused only slight increases in flap loads with both nozzle configurations and both the 35° and 60° flap positions.

The effect of measured engine thrust on F_p is shown in figure 10 for the conical nozzle configuration at two nozzle locations with the flaps in the 60° position. The data show that as the measured engine thrust increases, F_p for the flap and vane also increases fairly linearly except at maximum thrust. It is possible that this pressure variance occurs as the engine is moved closer to the flap because of the expansion of the exhaust-gas plume from the conical nozzle, which could cause the loss of large amounts of exhaust gas (which were not monitored) through the opening between the flap and vane.

The percentage distribution of F_p over the span of the flap for both nozzle configurations at maximum recorded flap pressure loads is shown in figure 11. The distribution of the spanwise flap load was determined by dividing the flap into 10 segments of equal length and integrating the faired pressures in each segment. The load on each 10-percent segment of the span was calculated as a percentage of the total load for each configuration. The conical nozzle tended to concentrate most of the pressure load on one 10-percent segment of the flap, but the daisy nozzle spread the pressure load more evenly over more than one segment. For the conical nozzle configuration, a maximum F_p of 37 percent was concentrated on one 10-percent segment of the flap near the engine exhaust centerline. The F_p produced by the daisy nozzle configuration was about 30 percent on two adjacent 10-percent flap segments straddling the engine exhaust centerline. For both nozzle configurations, more than 90 percent of the spanwise F_p on the flap was within ±20 percent of the flap span centered around the engine exhaust centerline.

Dynamic-Pressure Measurements

Power-spectral-density traces obtained for the high-response pressures on the flap surface were analyzed over the frequency range from 5 hertz to 500 hertz for many of the steady-state data runs. Attempts were made to correlate the power spikes in the power-spectral-density curves from each data run with the fan or core rotor speeds and the blade passage frequencies. Figure 12 shows power-spectral-density traces obtained from one

of the high-frequency-response pressure transducers on the surface of the flap. The data were obtained with the daisy nozzle at $x = 5$ diameters for a range of rotor speeds from approximately 77 to 121 rps for the fan rotor and approximately 200 to 250 rps for the core rotor. The value of the frequency of the peak in each power-spectral-density curve does not vary as much as the rotor speed (50 rps). Therefore, the peak frequencies in the power-spectral-density traces are not related to fan rotor speed, core rotor speed, or blade passage frequency; they are probably some form of panel flutter or resonance.

CONCLUDING REMARKS

Pressure and temperature data were measured on the undersurface of an F-111B wing, vane, and flap which were used in conjunction with a CF700 engine to simulate an externally blown flap system. The angle of incidence between the engine and the wing was fixed at 3° during the tests, and there was no airflow over the wing. Two engine-exhaust nozzles (conical and daisy) and several wing/engine positions, engine thrust levels, and flap positions were used.

The maximum temperatures recorded on the surface of the flap, 180° C (356° F) for the daisy nozzle and 218° C (424° F) for the conical nozzle, occurred with an exhaust-gas exit temperature of approximately 315° C (600° F).

Pressure loads on the undersurface of the flaps were approximately 3 times as great at the 60° flap position as at the 35° flap position and were concentrated within ± 20 percent of the flap centered around the exhaust centerline for both nozzle configurations. The flap pressure loads were measured with no airflow over the wing or flap and would consequently be additional to the normal flap pressure loads experienced in flight.

The daisy nozzle configuration spread the pressure load more evenly over the surface of the flap than the conical nozzle configuration for comparable engine thrust settings, resulting in higher overall pressure loads and lower temperatures on the undersurface of the flap.

REFERENCE

1. Mechtly, E. A.: The International System of Units – Physical Constants and Conversion Factors (Revised). NASA SP-7012, 1969.

TEST INSTALLATION

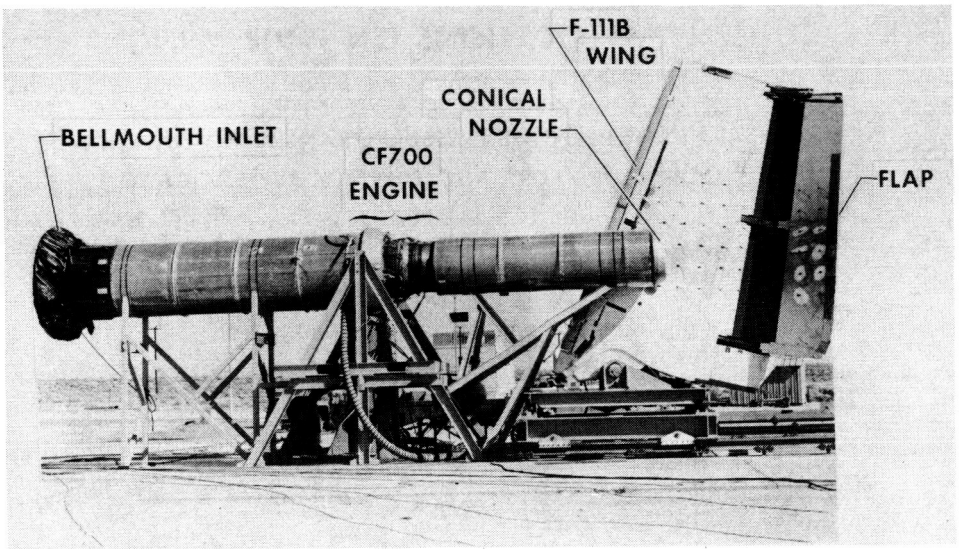

Figure 1

WING, FLAP, AND NOZZLE RELATIONSHIPS

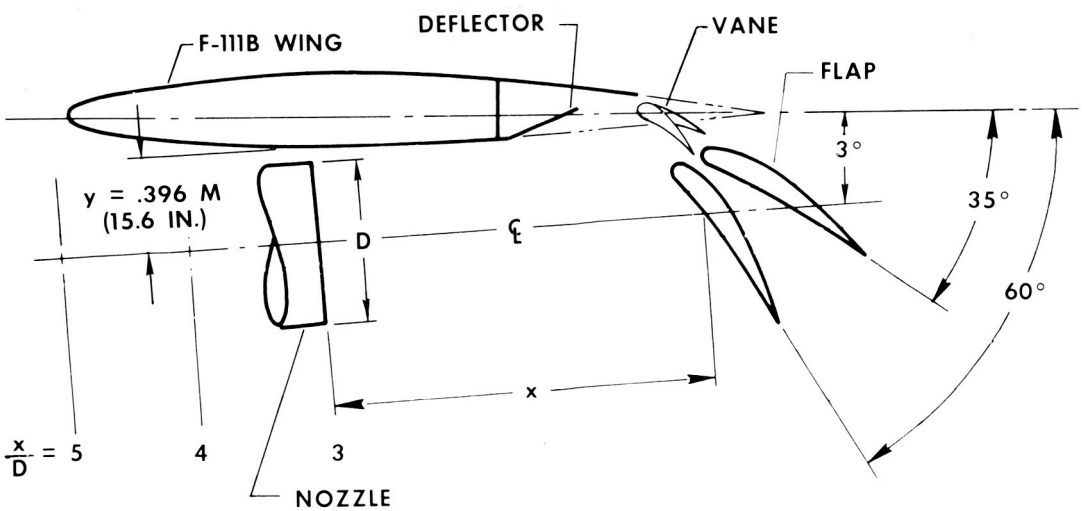

Figure 2

SENSOR LOCATIONS ON F-111B WING

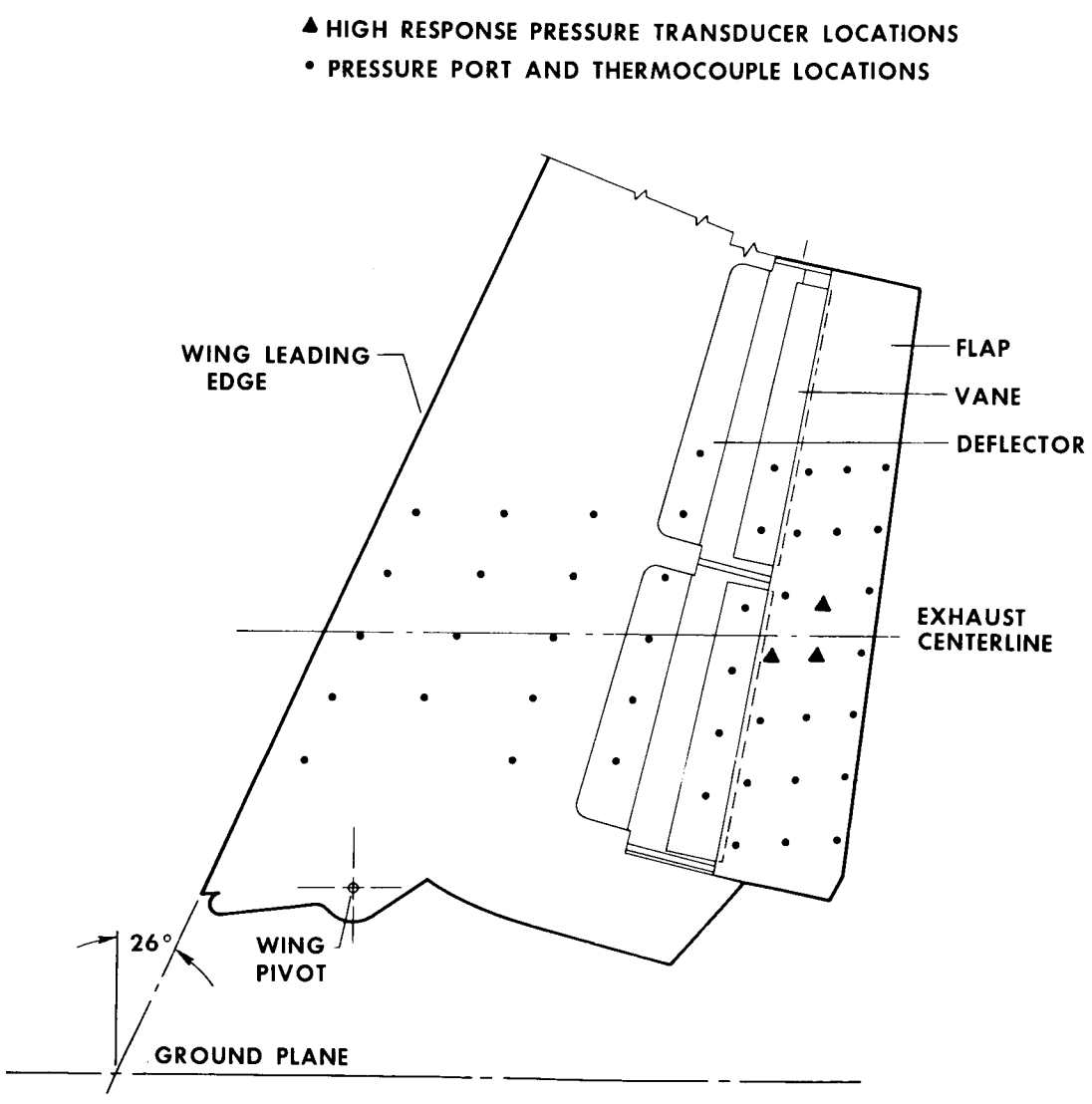

Figure 3

COMPARISON OF EXIT NOZZLES

DAISY NOZZLE

(AREA = .224 M^2 (347 IN^2))

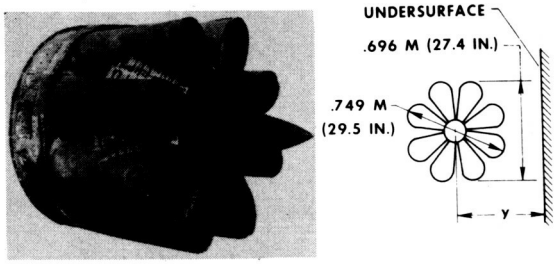

CONICAL NOZZLE

(AREA = .243 M^2 (377 IN^2))

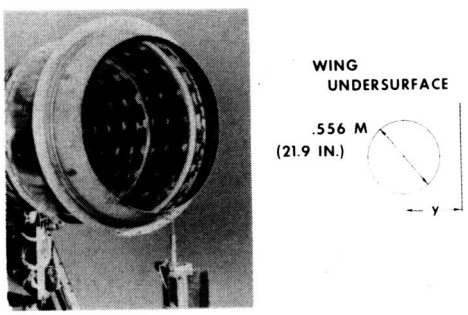

Figure 4

PRESSURE CONTOUR LINES

FLAP DEFLECTED 60°

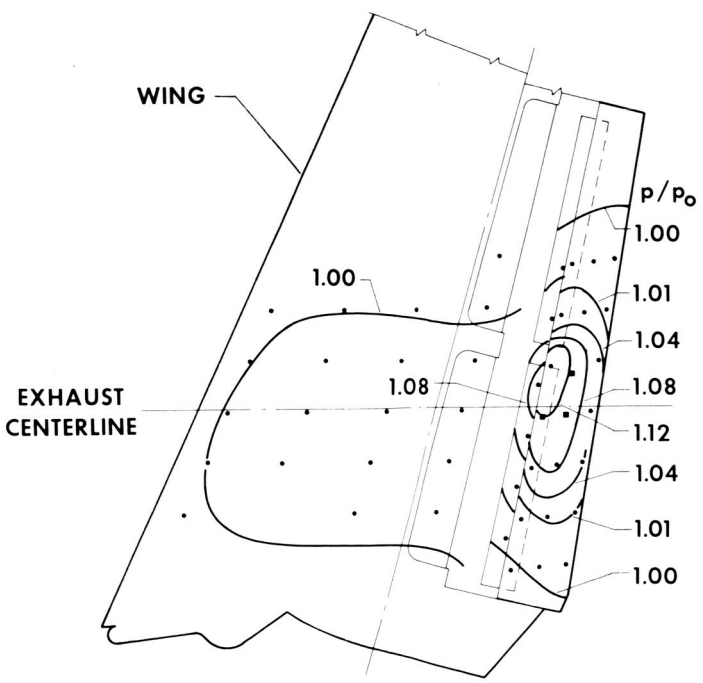

Figure 5

EFFECT OF ENGINE THRUST ON MAXIMUM RECORDED PRESSURES

$\frac{x}{D} = 3$

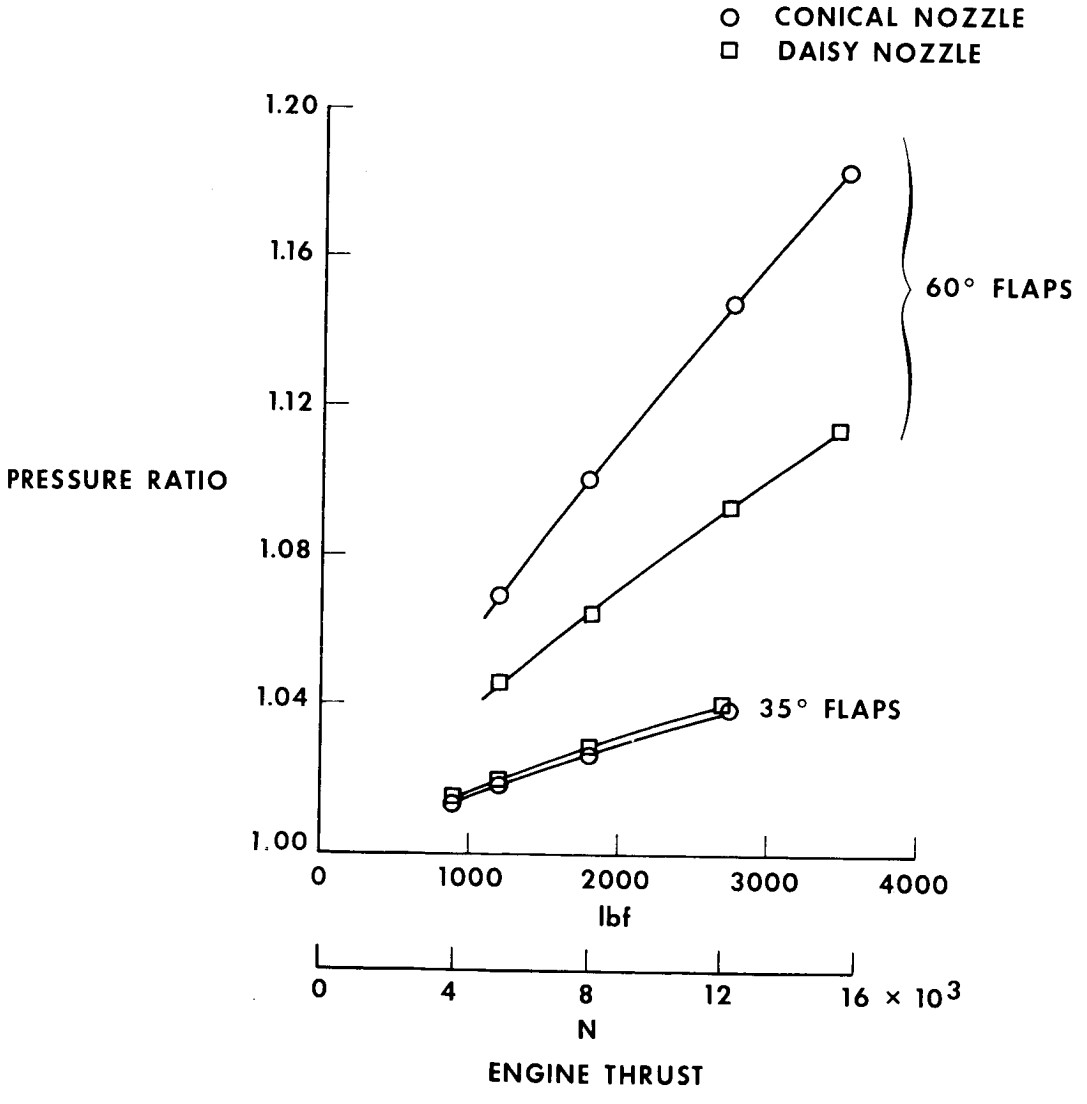

Figure 6

EFFECT OF ENGINE THRUST ON MAXIMUM RECORDED TEMPERATURES

$\frac{x}{D} = 3$

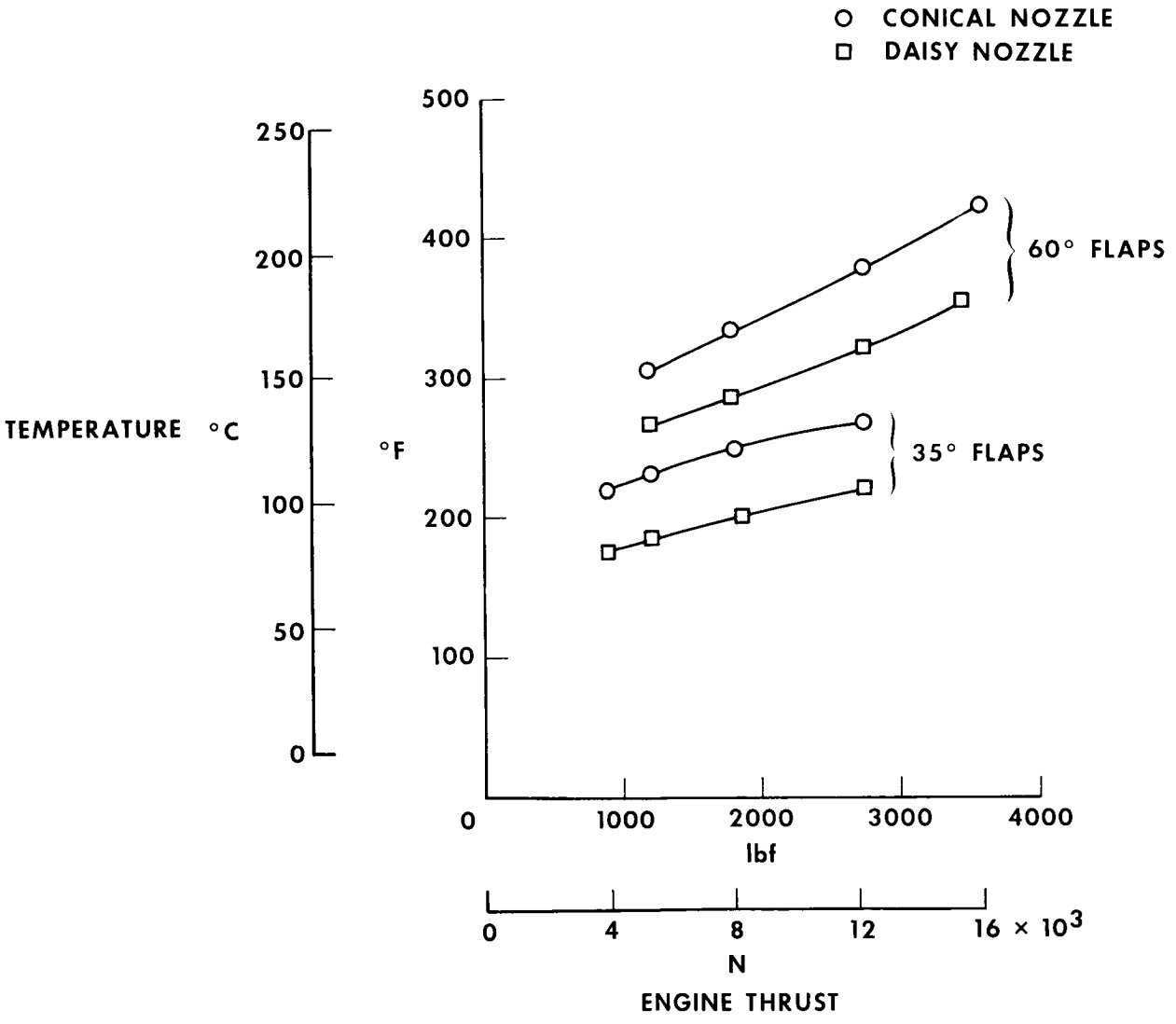

Figure 7

EFFECT OF FLAP POSITION ON FLAP LOADS

$\frac{x}{D}$ = 3, THRUST = 12 010 N (2700 LBF)

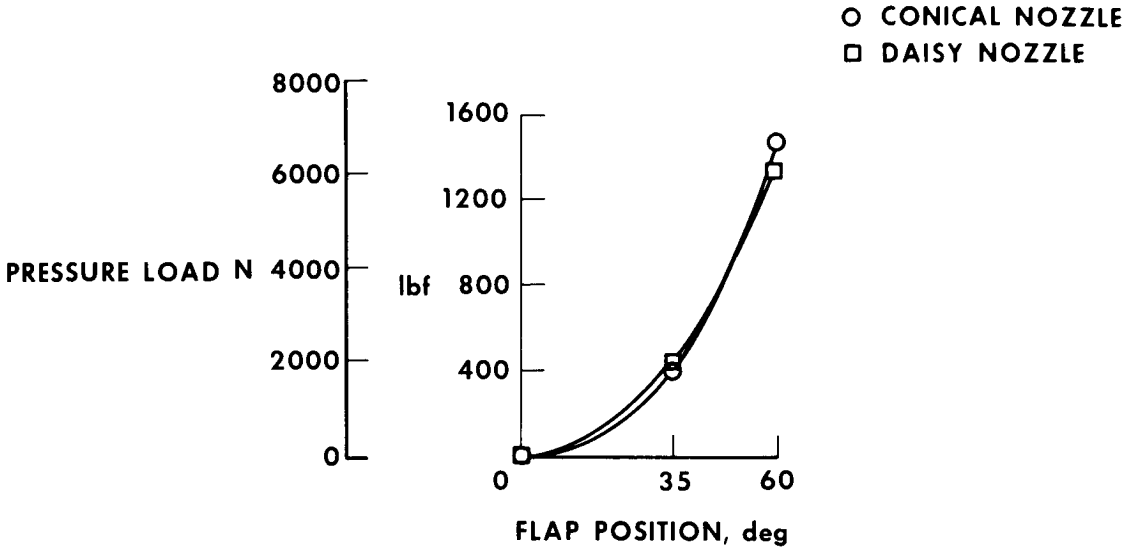

Figure 8

EFFECT OF NOZZLE POSITION ON FLAP LOADS

THRUST = 12 010 N (2700 LBF)

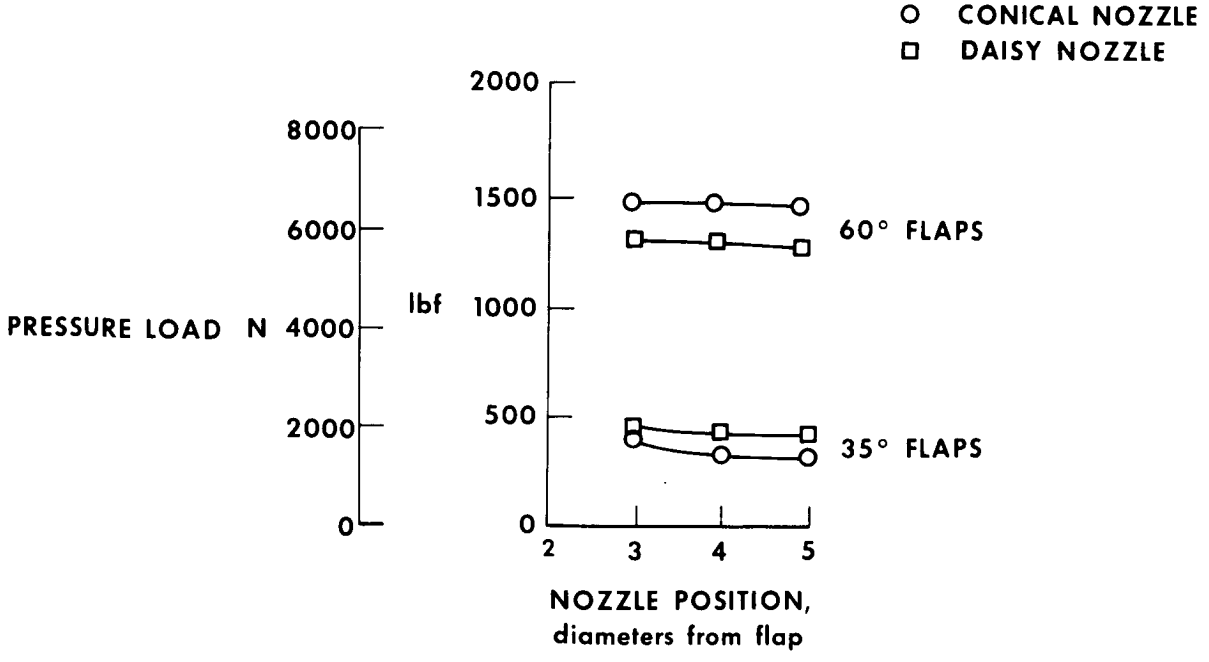

Figure 9

EFFECT OF ENGINE THRUST ON FLAP AND VANE LOADS

CONICAL NOZZLE WITH 60° FLAPS

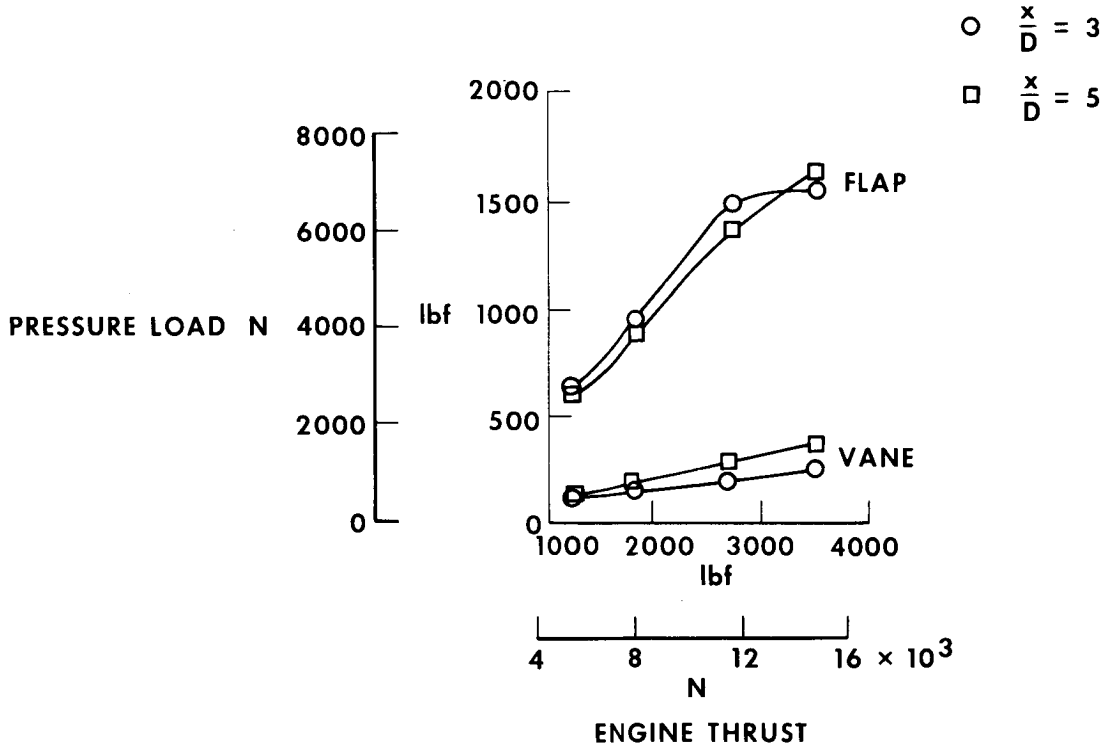

Figure 10

DISTRIBUTION OF FLAP LOAD OVER FLAP SPAN

MAXIMUM FLAP PRESSURE LOAD, THRUST = 15 569 N (3500 LBF), 60° FLAPS

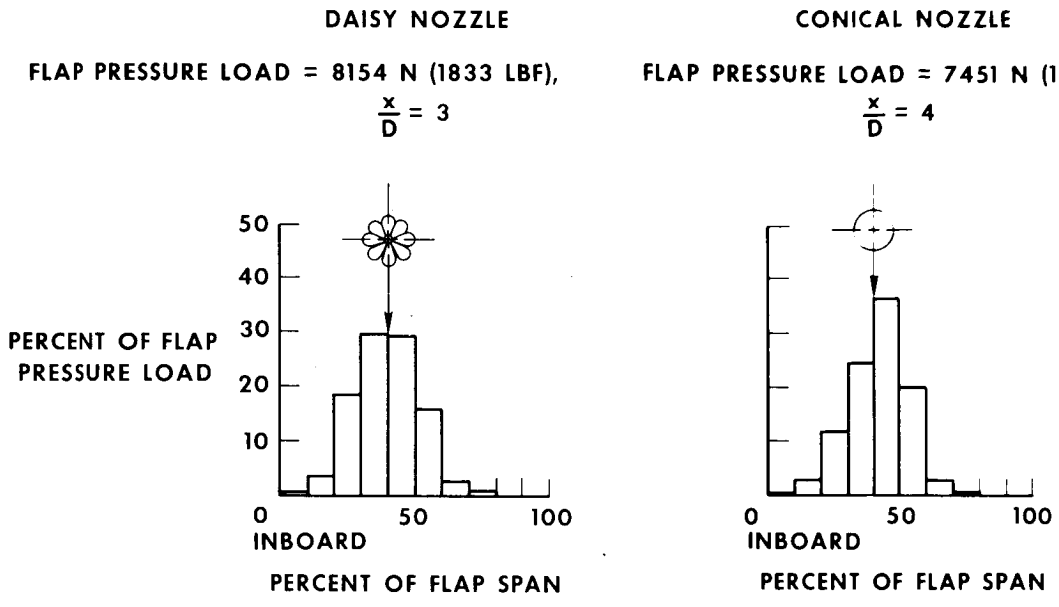

Figure 11

EFFECT OF ENGINE ROTOR SPEED ON POWER SPECTRAL DENSITY OF FLAP PRESSURE

35° FLAPS, $\frac{x}{D}$ = 5, DAISY NOZZLE

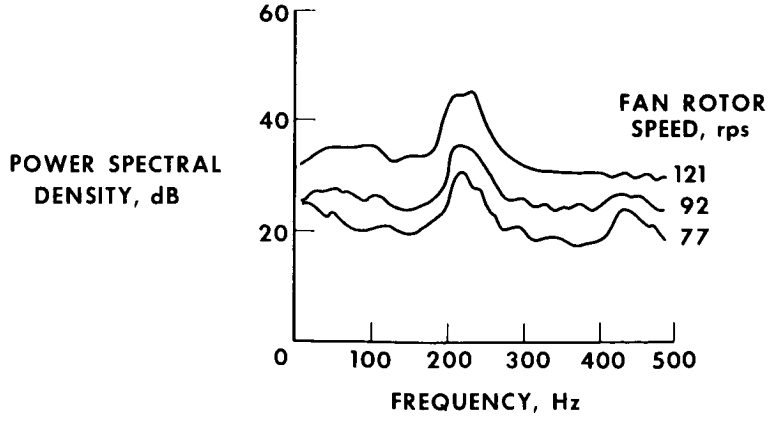

Figure 12

SIMULATOR EVALUATION OF THE FLYING QUALITIES OF EXTERNALLY BLOWN FLAP AND AUGMENTOR WING TRANSPORT CONFIGURATIONS

By David A. Kier, Bruce G. Powers,
NASA Flight Research Center

and

William D. Grantham, and Luat T. Nguyen
NASA Langley Research Center

SUMMARY

Concurrent simulations of powered-lift STOL transport aircraft having either an externally blown flap configuration or an augmentor wing configuration were conducted by the Langley and Flight Research Centers. Three types of simulators of varying sophistication were used: a simple fixed-base simulation with a simple visual display, a more complex fixed-base simulation using a realistic transport cockpit and a high-quality visual display, and a six-degree-of-freedom motion simulator that had a realistic transport cockpit and a sophisticated visual display.

The unaugmented flying qualities determined from these simulations were rated as unacceptable for both the externally blown flap and augmentor wing configurations. The longitudinal, lateral-directional, and single-engine-failure characteristics were rated satisfactory with extensive augmentation, including pitch and roll command systems, flight-path (or speed) augmentation, turn coordination, and effective yaw damping. However, the flare and landing characteristics from any approach glide-path angle in excess of 4^{o} were rated as unsatisfactory but acceptable.

INTRODUCTION

The National Aeronautics and Space Administration and its predecessor, the National Advisory Committee for Aeronautics, have conducted wind-tunnel tests on jet-powered STOL aircraft since 1956. (See ref. 1.) More recent wind-tunnel tests of the jet-powered-lift concept were performed on two configurations: the externally blown flap and the augmentor wing. (See refs. 2 to 8.) Data from these tests indicate that by using these concepts, approach lift coefficients on the order of 4 to 5 are readily attainable and thus good short field performance is possible.

Several simulations based on these wind-tunnel test data were conducted to evaluate the flying qualities of this class of aircraft. (See refs. 9 to 11.) References 9

and 10 were concerned with large externally blown flap configurations in the 113 750-kilogram (250 000-pound) class, and reference 11 dealt with a twin-engine, modified augmentor wing Buffalo aircraft.

To evaluate the flying qualities of a four-engine STOL aircraft of the 22 750-kilogram (50 000-pound) class configured with either an externally blown flap or augmentor wing concept, studies were conducted concurrently during the past several years by the Flight and Langley Research Centers. Three simulators were used to evaluate the flying qualities of this class of aircraft: a relatively simple fixed-base simulator (at the Flight Research Center (FRC)); a sophisticated fixed-base simulator (at the Langley Research Center (LaRC)); and a sophisticated six-degree-of-freedom motion simulator (in cooperation with and at the Ames Research Center (ARC)). Various analytical techniques were used to complement the simulations. The evaluation of the externally blown flap configurations was based on data from references 4 and 5 and the evaluation of the augmentor wing configuration, on data from references 6 to 8.

This paper presents an evaluation of the basic flying qualities of the test configurations and describes the control system concepts developed for improving the flying qualities. It also includes the results of engine-failure investigations.

TEST CONFIGURATIONS

Externally Blown Flap Configuration

The basic externally blown flap configuration was a "spread-engine" (ref. 4), triple-slotted flap, high-winged transport with a large T-tail (fig. 1(a)). References 4 and 5 describe the wind-tunnel configuration in detail. The physical characteristics of the simulated externally blown flap aircraft are presented in table 1. It should be noted that the configurations simulated on the FRC and ARC simulators were identical in test configuration, control system, and mass characteristics, whereas the LaRC simulation used a similar but slightly different configuration.

Longitudinal control was provided by the horizontal stabilizer, either alone or in conjunction with the elevator. On the LaRC configuration, the elevator remained fixed with respect to the stabilizer; on the FRC configuration, the elevator was geared to the stabilizer so that at full trailing-edge-up stabilizer, the elevator was at 50° trailing edge up, and at full trailing-edge-down stabilizer, the elevator was at 10° trailing edge down. For lateral control, flaperons and spoilers were used on the LaRC configuration; ailerons, flaperons, and spoilers were used on the FRC configuration. Directional control was provided by a rudder equipped with boundary-layer control on the LaRC configuration; on the FRC configuration, a double-hinged, slotted rudder was used for yaw control. Direct-lift control was provided on both configurations by symmetric spoiler deflection, and drag

modulation was provided by using symmetric deflections of the third element (most rearward) of the inboard flap segment.

Turbofanjet performance characteristics were based on the General Electric TF34-GE-2 turbofan engine (ref. 12) with a bypass ratio of 6 to 1 and a maximum uninstalled, sea-level static thrust of 41 296 newtons (9280 pounds). To accommodate the low noise requirements for STOL aircraft, the four engines were throttled to provide an installed thrust of 30 037 newtons (6750 pounds) per engine at take-off. Higher thrust levels were permitted for emergency conditions where noise constraints would not apply.

Augmentor Wing Configuration

References 6 to 8 provided the data base for simulating the augmentor wing configuration illustrated in figure 1(b).

Longitudinal and directional control were provided in the same manner as for the FRC augmentor wing configuration. Roll control was provided by ailerons with boundary-layer control and by spoilers.

Drag modulation and direct-lift-control test data were not available for use in the simulation of the augmentor wing configuration; however, thrust vectoring, augmentor choke deflection, and symmetric spoiler deflections can provide these features. So for this simulation, direct-lift control and drag modulation were evaluated by using the same incremental data used for the externally blown flap configurations.

The engines used for the augmentor wing configuration were four Lycoming ALF 502A engines (31 150 newtons (7000 pounds) nominal thrust) modified with high-power extraction turbines and operated in a derated condition. The normal derated thrust level for one engine was 20 470 newtons (4600 pounds), of which 16 465 newtons (3700 pounds) was from the fan. The fan air was collected and ducted to the wing nozzles. With assumed losses, this system provided approximately 14 100 newtons (3170 pounds) of thrust per engine at the wing nozzles. As for the externally blown flap configuration, additional thrust (approximately 8900 newtons (2000 pounds) per engine) was available for emergency conditions.

Mass Characteristics

The weight and inertial data used in this study are presented in table 2. As shown, the mass characteristics of the two configurations (externally blown flap and augmentor wing) were different for identical weights. These differences were due primarily to slight empennage differences which changed the inclination of the principal axis and to the greater weight of the wing of the augmentor wing configuration.

SIMULATOR DESCRIPTION

All three simulation setups used six-degree-of-freedom equations. The LaRC setup is described in reference 10, and the ARC moving-base simulator is described in reference 11. The FRC simulation was a hybrid six-degree-of-freedom fixed-base setup. The aerodynamic equations were solved in a digital computer, and the control system was simulated by an analog computer. The cockpit control force, damping, and linearity were infinitely variable over a wide range. The values used were selected as being representative of this class of aircraft. The control wheel had a four-position ("coolie cap") trim button, a direct-lift-control command button (two-position, spring-loaded to zero), and an intercom button. Rudder trim was obtained from a center console switch.

The visual display switch was generated by a point source system. A model of Edwards Air Force Base and Rogers Dry Lake with its runway complex and surrounding area was used in the visual display. The visual display had poor resolution characteristics at low altitudes. Height judgment for flare and other low altitude maneuvers was difficult below approximately 31 meters (100 feet) and virtually impossible below approximately 15 meters (50 feet). To aid the pilot in judging height, a simulated radar altimeter readable to the nearest 0.3 meter (1 foot) below 61 meters (200 feet) was installed.

Conventional cockpit instruments were used, including an FD-108 flight director (computer controlled) and indicators for angle of attack, angle of sideslip, airspeed, normal acceleration, power setting, control position, and rate of climb; and ILS crosspointers and a conventional altimeter. To evaluate the effects of in-flight engine failures, an engine could be failed either from the cockpit or from the analog computer console. An engine failure affected the pitch, roll, and yaw axes, reduced the thrust by 25 percent, and activated the "emergency" roll control (flaperons) on the externally blown flap configuration.

TEST PROCEDURES

The basic evaluation task for all three simulations was a simulated ILS approach. The test procedures were classified generally into four tasks:

(1) In level flight, or comfortably within the operational envelope, evaluate the four-engine aircraft at various flap positions (representative of approach, landing, and take-off setting) with the stability augmented aircraft and various control systems at several power settings.

(2) Perform simulated ILS approaches with four engines at different speeds with various levels of control system augmentation, including go-arounds at various altitudes for approximately one-third of the runs.

(3) Determine, as well as possible, the 1g stall and minimum control speeds of these configurations.

(4) Evaluate engine failure characteristics and controllability; repeat tasks 1, 2, and 3 with an engine failure during the run.

During the study, the pilots were asked to evaluate the handling qualities, stability, and controllability of the various configurations while they were performing these tasks.

RESULTS AND DISCUSSION

The results to be discussed were selected to provide an overview of some of the major problems encountered with powered-lift STOL aircraft.

Longitudinal Characteristics

Basic unaugmented airplane.- The basic unaugmented airplane longitudinal characteristics for all configurations were judged to be only marginally acceptable; that is, they were given pilot ratings of 6 to 7 on the Cooper-Harper rating scale (ref. 13). The major objections were: poor flight-path stability and speed control; the relatively high frequency (approximately 20 sec), lightly damped phugoid oscillation; sluggish pitch response; and large trim changes associated with changes in flaps, power, and airspeed.

The first two problems (poor flight-path stability and speed control, and the high-frequency phugoid oscillation) are amplified in STOL aircraft. A high degree of coupling between attitude, speed, and flight-path angle is typical of operation on the "back side" of the power-required curve and, for the test configurations, resulted in an unstable relationship between flight path and speed. Compounding this problem was a relatively high frequency (short period), lightly damped phugoid oscillation which caused the aircraft to oscillate about the desired speed and flight-path angle.

Figure 2 presents the flight envelope for the externally blown flap configuration in terms of flight-path angle and airspeed with loci of constant angles of attack and airplane pitch attitude superimposed. If it is assumed that the airplane were approaching at an airspeed of 75 knots and a flight-path angle of -5°, the angle of attack would be approximately 5° and the aircraft attitude would be essentially zero. If the pilot found that the aircraft was dropping approximately 2° below the glide slope and he wanted to correct up to the glide slope at constant speed, an increase in power of approximately 12 percent accompanied by a 3° decrease in angle of attack and a 1° decrease in pitch attitude would be required. Also, an increase in airspeed of 5 knots at constant flight-path angle would require a 5-percent reduction in power and a pushover to decrease angle of attack by 2° and pitch attitude by approximately 1.5°. In general, it can be said that power controls the flight path and attitude controls the airspeed. This piloting technique is the exact

opposite of that used in conventional transport approaches and of the intuitive correction, that is, power controls airspeed and attitude controls flight-path angle. However, as illustrated by the power reduction required to increase airspeed at constant flight-path angle, the high degree of coupling further complicated the piloting task.

The same type of analysis can be applied to the augmentor wing configuration, with essentially the same results.

Military specification 8785B (ref. 14) provides a criterion for flight-path stability in terms of the slope of the constant power curves expressed as the change in flight-path angle per knot change in airspeed. Figure 3 compares the characteristics of the two configurations with this criterion at several airspeeds. As shown, the externally blown flap configuration exceeds the minimum acceptable level at any airspeed below 79 knots, and the augmentor wing configuration exceeds the requirement at speeds below 73 knots. However, the rate of decreasing stability or increasing instability for the augmentor wing configuration is considerably higher than that for the externally blown flap configuration. The second part of the criterion establishes a level for the rate of change of stability. The externally blown flap configuration barely exceeds this requirement, whereas the augmentor wing configuration exceeds it by a wide margin. Translating this characteristic into piloting difficulties, it would seem that small corrections in flight path would be easier to accommodate on the augmentor wing configuration (less unstable characteristics) than on the externally blown flap configuration, but large changes would be more difficult (larger variation in stability levels).

The second major difficulty in the longitudinal mode was the relatively high frequency (short period), lightly damped phugoid oscillation. With a period of less than 20 seconds and a damping ratio of less than 0.02, this easily excited phugoid made flying precise ILS approaches extremely difficult. A time history of a typical phugoid oscillation is shown in figure 4 for the augmentor wing configuration. The speed excursions were in excess of 10 knots and the rate of climb varied in excess of 180 m/min (600 ft/min). The externally blown flap configuration exhibited similar characteristics.

When the pilot had to contend with the "back side" approach characteristics in combination with the adverse phugoid characteristics in turbulence, the ILS task became very difficult.

Augmented handling qualities.- If the longitudinal control system were to perform all the desired functions and correct the deficiencies in the longitudinal handling qualities, it was determined that some type of command system would be required. Accordingly, attitude, rate, and C^* (a combination of pitch rate and normal acceleration) systems were evaluated. All three systems provided good pitch response characteristics and alleviated the large pitch trim changes, but the attitude command provided the most precise control characteristics and was rated as the best overall system. A simplified

block diagram of the attitude command system is shown in figure 5. By proper gain selection, an attitude command system was provided with rate stabilization. With the system, the pilots' assessment of the longitudinal handling characteristics improved to 4 to 5.

However, the undesirable back side of the power curve characteristics, although alleviated somewhat, were still a source of complaint by the pilots. In an attempt to correct this deficiency, several speed—flight-path augmentation systems were evaluated. Simple speed stability augmentation using auto-throttle and direct-drag control provided good speed control during the approach when the system time constants were relatively low. The direct-drag control-surface-actuation rate had to exceed 5°/sec and the engine response characteristics had to be less than 0.8 second. With slower surface actuation rates, the system could be saturated and rate limited. By using the simple speed augmentation, the pilots' ratings improved further to 3 to 4. The pilots indicated that their major remaining objection was that precise flight-path control was a two-control task, that is, using the control column and the direct-lift control on the thumb switch. Thus, the direct-lift control was integrated with the column position and speed augmentation as shown in simplified form in figure 6. Use of this system resulted in further improvement in the pilots' ratings to 2 to 3.

Flare and touchdown.- One of the most significant problems encountered during these simulations was the inability to perform the flare so that the touchdown sink rates were reasonable and the touchdown was within the desired zone. Flaring powered-lift STOL aircraft with precision proved to be difficult. Table 3 compares some of the parameters for a STOL and CTOL flare and touchdown maneuver. The target touchdown sink rate for these maneuvers was 0.65 to 1.0 m/sec (2 to 3 ft/sec). The table illustrates that for the STOL airplane in a steep 7.5° glide slope approach, the change in sink rate from the approach condition to touchdown is more dramatic, the time is considerably shorter, and the distance traveled is considerably less than that for the conventional take-off and landing (CTOL) aircraft. Some of these same relative effects may be observed in a comparison of the parameters for the STOL aircraft in a 4° glide slope and the CTOL aircraft. The STOL flare is then characterized as a short, rather abrupt maneuver as compared with the CTOL flare. Although the data shown in table 3 for the STOL airplane are for an externally blown flap configuration, the discussion is applicable to either an externally blown flap or an augmentor wing STOL configuration. Complicating the situation further are the highly negative ground effects that the STOL configuration experiences and the inability to generate the necessary energy to flare by only rotating the airplane. Wind-tunnel tests have indicated that the powered-lift externally blown flap and augmentor wing configurations will encounter lift losses in ground effect on the order of 6 percent to 12 percent for the configurations tested. Also, the aerodynamic lift increases that can be obtained by rotating the airplane to reasonable angles of

attack are not sufficient to arrest the sink rate to the desired levels. This condition indicates that another source of energy will be required to provide the lift increase necessary to flare the aircraft.

Power increases on the order of 10 percent at flare initiation were attempted but, because of lag in engine response, the timing of the power change became critical, and even with the aid of the simulated radar altimeter, the pilot still had difficulty in flaring precisely. Flaring with power and rotation could have achieved the target touchdown sink rate, but the maneuver was difficult and a small error in timing the initiation of the two controls resulted in not arresting the sink rate sufficiently or "ballooning" and missing the touchdown zone. As table 3 shows, the timing is critical and very short. The pilot must anticipate the onset of the ground-induced lift losses and compensate in 4 to 6 seconds, depending on the approach glide slope.

The direct-lift control spoilers offered another alternate source to control lift without the large lags associated with power increases. Unfortunately, in order to generate the large lift increments required, the spoilers had to be up-rigged excessively. If the performance penalty caused by the up-rigged spoilers can be tolerated, using direct-lift control in the flare works well. Again, the timing of the input becomes critical.

It appears that a combination of devices may be required to successfully complete the flare, which could further complicate the maneuver. One solution may be to use a segmented approach, that is, translating from a 7.5° glide slope to 4° at approximately 65 meters (200 feet) height. This problem can probably be resolved only by flight test. In general, the flare and landing characteristics from any approach glide-path angle in excess of 4° were rated as unsatisfactory but acceptable.

Lateral-Directional Characteristics

Basic unaugmented airplane.- The unaugmented handling qualities of the two test configurations were rated as unacceptable; that is, they had pilot ratings of 8 to 9. The major objections were: unacceptably large sideslip excursions with any roll control input; low Dutch roll damping; a highly divergent spiral mode; and low apparent roll damping.

Figure 7 is a time history of a 15° wheel angle lateral step input illustrating the two characteristics most objectionable to the pilots. For the basic airplane, the sideslip moves first in the proverse direction, and thus indicates the proverse yaw generated by the spoilers. Then, as the roll rate increases, a highly adverse yaw dominates the response. After the roll rate has reached a more or less stable level, the lightly damped, fairly long period Dutch roll oscillation becomes apparent. But the Dutch roll excursions are oscillating about an apparent steady-state sideslip angle of approximately 7°. This offset is attributable to the yawing moment generated by the roll rate, known as the N_p

effect. The pilots found this N_p effect highly objectionable and believed it could easily cause pilot-induced oscillations during attempts to correct or precisely control the response. The dashed line illustrates the response of the fully augmented vehicle to the same wheel input. With a roll-rate command system, a constant roll rate proportional to wheel deflection is commanded. With effective yaw damping and a turn coordination system to eliminate the N_p effect, the angle-of-sideslip trace remains at essentially zero.

Augmented handling qualities.- As with the longitudinal axis, it was determined that some type of command system would be required in the roll axis and that the yaw axis would require extensive stability augmentation. In the roll axis, both rate and attitude command systems were evaluated. The roll-attitude command system was determined from pilot comments to be the best overall system. A simplified block diagram of this system is shown in figure 8. By appropriate gain selection, the system provides attitude command with rate stabilization. The attitude command could have possibly been eliminated in smooth air, but it greatly enhanced turbulence response and engine failure control.

For normal operation with the four-engine externally blown flap configuration, the flaperons were not used for roll control. When they were added, the roll-control power was found to be excessive for normal operation and caused roll-control sensitivity problems. Attempts were made to phase the roll-control devices with wheel deflection, but the pilots preferred the system illustrated in figure 8 for implementing the total roll-control systems.

The yaw-control system that provided the best overall lateral-directional pilot ratings used an aileron-to-rudder interconnect with roll rate, yaw rate, and roll angle feedbacks. (See fig. 9.) Feedback of roll angle was used in combination with the yaw rate to approximate a rate-of-change-of-sideslip-angle damper for additional yaw damping. Roll-rate feedback was used to compensate for the N_p effect and to act as a turn coordinator. The interconnect provided additional turn coordination by correcting the yaw effects of roll-control surface displacement.

When the roll attitude command and the "best" yaw stability augmentation system (SAS) were used, the pilot ratings improved from 8 to 9 for the unaugmented lateral-directional characteristics to 2 to 3 for the augmented airplane.

Engine-Out Characteristics

The engine-out characteristics of the externally blown flap configuration involve a critical design condition, especially in roll and yaw control, whereas an engine failure for the augmentor wing configuration is primarily a performance problem with only minor impact on stability and control. Because the augmentor wing concept used ducted air distributed essentially even across the flap span, an engine failure would not cause an

asymmetry in lift or drag through the powered-lift mechanism. Thus, an engine failure would not result in a major handling deficiency. The nonducted core exhaust thrust could produce asymmetries, especially if thrust vectoring is used, but this asymmetry would not be unduly severe. The core exhaust amounts to less than 20 percent of the total engine thrust, or about 4900 newtons (1100 pounds) of thrust. During the simulations, the pilots had no difficulty in controlling an engine failure on the fully augmented augmentor wing configuration, and the engine failure controllability was rated as 2 to 3 in the take-off or landing configuration.

An engine failure in an externally blown flap configured aircraft is critical for roll or yaw control, or both, because major asymmetries are encountered which produce large rolling or yawing moments, depending on the configuration. In a high-lift landing configuration, an engine failure would produce large lift asymmetries which would cause large rolling moments; in a high-thrust take-off configuration, an engine failure would cause large thrust asymmetries which would induce severe yawing moments. The magnitude of these moments for the simulated externally blown flap configuration, in the form of degrees of displacement in 2 seconds, is illustrated in figure 10. Also shown are the roll-control requirements for level 1 operation from reference 14 and the yaw-control requirements for normal operation from reference 15. As indicated, at a 75-knot approach speed, the engine-failure-induced roll angle reaches approximately 43^{o} in 2 seconds, whereas the level 1 requirement calls for a total control-surface-induced roll angle capability of 50^{o} in 2 seconds. Therefore, after trimming an engine-out rolling moment, little roll control would be left for maneuvering. The pilots considered this control margin to be unacceptable. The minimum acceptable control margin required the roll-control power to be increased to at least 135 percent over the engine-failure-induced moment at the nominal approach speed. Comparable results were found in the yaw axis for the take-off configuration; that is, a control power margin of at least 30 percent to 35 percent was required over the engine-failure-induced yawing moment at the reference take-off speed.

A time history of a number 1 (left outboard) engine failure for the externally blown flap configuration on the approach (fig. 11) illustrates the pilot's ability to control the engine-out condition and continue the landing with all augmentation on. The maximum vertical displacement from the glide slope was less than 4 meters (12 feet) and the maximum lateral displacement from the localizer center was less than 8 meters (25 feet). The pilot rated the task as 2.5. However, the engine-out condition presented problems in touching down within the designated touchdown zone with a touchdown sink rate of less than 1 m/sec (3 ft/sec). The touchdown sink rates could not be reduced below 1.5 m/sec (5 ft/sec), and the pilots reported that landing the aircraft was difficult, with a moderately high workload.

Comparison of Simulator Results

As previously stated, data and control systems used in the FRC and ARC simulators were identical, but slightly different data and control systems were used in the LaRC simulators. The FRC simulation had a simple fixed-base cockpit and visual display; the LaRC simulation also had a fixed-base setup but with a realistic transport cockpit and a sophisticated video presentation of a STOLport model; and the ARC simulation had a sophisticated six-degree-of-freedom motion simulator with a sophisticated visual display. Also, the same pilots participated in the FRC and ARC evaluations, but the LaRC pilots based their evaluations only on the LaRC simulation. A comparative summary of the simulator results for the externally blown flap configuration is shown in figure 12. There was generally fair-to-excellent agreement in the pilot ratings of the various characteristics for both the augmented and unaugmented airplanes.

The pilot ratings from the FRC simulation for the flare and landing are not shown because this simulation was not believed to be of sufficient quality to provide an adequate simulation in this area.

The results of the FRC and ARC simulations (in which the same pilots were used) show that even though the motion simulation generally provided better pilot ratings than the simple fixed-base setup, the ratings were only slightly better. However, the pilots reported that they could become more involved in the motion simulation than in the fixed-base simulation because of its greater realism.

CONCLUDING REMARKS

Two concurrent six-degree-of-freedom simulations of powered-lift STOL aircraft flying qualities were conducted by the Langley and Flight Research Centers. The Langley simulation considered only an externally blown flap configuration and used a fixed-base simulator with a realistic transport cockpit and good visual display. The Flight Research Center simulation considered two powered-lift concepts – the externally blown flap and augmentor wing – each of which was evaluated on two separate simulators using the same data base and control systems. One simulation was conducted at the Flight Research Center using a simple fixed-base cockpit and visual display, and the other simulation was conducted at the Ames Research Center using a sophisticated six-degree-of-freedom motion simulator with a realistic transport cockpit and a high-quality visual display. There was generally good agreement between the three simulations in terms of pilot opinion of the handling qualities characteristics.

The study indicated that both high-wing-loading, powered-lift STOL configurations evaluated would require substantial command and stability augmentation in all axes to provide satisfactory handling qualities. In the pitch axis, a pitch-attitude command system

was rated best by the pilots. Also, because of the high degree of flight-path instability, commonly referred to as operation on the "back side" of the power-required curve, both configurations required speed or flight-path augmentation, or both, to provide satisfactory characteristics.

The lateral-directional mode required a relatively sophisticated turn coordination feature in the directional control system to eliminate the large amounts of sideslip generated by any roll rate. Also, the directional axis required yaw-rate damping and pseudo-time-rate-of-change-of-sideslip damping. The roll augmentation found to be most effective was a roll-attitude command system; a roll-rate command proved to be adequate, but the attitude command was rated best by the pilots.

The final part of the landing approach, the flare and landing, was a persistent problem. To flare these configurations from a glide-path angle of 4^{o} or greater, the approach required an abrupt maneuver that had to be accomplished in only 5 to 6 seconds. Aggravating this flare problem was the high negative ground effect characteristic of STOL aircraft. It appeared that some form of pilot-assist mode would be required in the flare, either spoilers or a control-system command feature. Flaring with power alone was not an acceptable technique. In general, the flare and landing characteristics from any glide-path angle in excess of 4^{o} were rated as unsatisfactory but acceptable.

Maintaining the glide slope and localizer after the loss of a critical engine during the landing approach posed no problem for the pilot with either the fully augmented externally blown flap or augmentor wing configurations.

REFERENCES

1. Campbell, John P.; and Johnson, Joseph L., Jr.: Wind-Tunnel Investigation of an External-Flow Jet-Augmented Slotted Flap Suitable for Application to Airplanes With Pod-Mounted Jet Engines. NACA TN 3898, 1956.

2. Parlett, Lysle P.; Fink, Marvin P.; and Freeman, Delma C., Jr. (With appendix B by Marion O. McKinney and Joseph L. Johnson, Jr.): Wind-Tunnel Investigation of a Large Jet Transport Model Equipped With an External-Flow Jet Flap. NASA TN D-4928, 1968.

3. Freeman, Delma C., Jr.; Grafton, Sue B.; and D'Amato, Richard: Static and Dynamic Stability Derivatives of a Model of a Jet Transport Equipped With External-Flow Jet-Augmented Flaps. NASA TN D-5408, 1969.

4. Parlett, Lysle P.; Greer, H. Douglas; Henderson, Robert L.; and Carter, C. Robert: Wind-Tunnel Investigation of an External-Flow Jet-Flap Transport Configuration Having Full-Span Triple-Slotted Flaps. NASA TN D-6391, 1971.

5. Grafton, Sue B.; Parlett, Lysle P.; and Smith, Charles C., Jr.: Dynamic Stability Derivatives of a Jet Transport Configuration With High Thrust-Weight Ratio and an Externally Blown Jet Flap. NASA TN D-6440, 1971.

6. Koenig, David G.; Corsiglia, Victor R.; and Morelli, Joseph P.: Aerodynamic Characteristics of a Large-Scale Model With an Unswept Wing and Augmented Jet Flap. NASA TN D-4610, 1968.

7. Cook, Anthony M.; and Aiken, Thomas N.: Low-Speed Aerodynamic Characteristics of a Large-Scale STOL Transport Model With an Augmented Jet Flap. NASA TM X-62,017, 1971.

8. Falarski, Michael D.; and Koenig, David G.: Aerodynamic Characteristics of a Large-Scale Model With a Swept Wing and Augmented Jet Flap. NASA TM X-62,029, 1971.

9. Grantham, William D.; Deal, Perry L.; and Sommer, Robert W.: Simulator Study of the Instrument Landing Approach of a Heavy Subsonic Jet Transport With an External-Flow Jet-Flap System Used for Additional Lift. NASA TN D-5862, 1970.

10. Grantham, William D.; Sommer, Robert W.; and Deal, Perry L.: Simulator Study of Flight Characteristics of a Jet-Flap STOL Transport Airplane During Approach and Landing. NASA TN D-6225, 1971.

11. Rumsey, P. C.; Spitzer, R. E.; and Glende, W. L. B.: A Design Support Simulation of the Augmentor Wing Jet STOL Research Aircraft. Doc 6-24806-1 (Contract NAS 2-6025), Boeing Co., Jan. 1972. (Available as NASA CR-114 435.)

12. Anon.: TF34-GE-2 Turbofan Engine. Model Specification E1130. Gen. Elec. Co., Feb. 28, 1968.

13. Cooper, George E.; and Harper, Robert P., Jr.: The Use of Pilot Rating in the Evaluation of Aircraft Handling Qualities. NASA TN D-5153, 1969.

14. Anon.: Flying Qualities of Piloted Airplanes. Mil. Specif. MIL-F-8785B(ASG), Aug. 7, 1969.

15. Anon.: Recommendations for V/STOL Handling Qualities. AGARD Rep. 408A, Oct. 1964.

TABLE 1.- PHYSICAL CHARACTERISTICS OF THE TEST CONFIGURATIONS

	FRC externally blown flap	LaRC externally blown flap	FRC augmentor wing
Wing –			
Area, m^2 (ft^2)	55.8 (600)	78.4 (843)	55.8 (600)
Aspect ratio	7.3	7.3	8.0
Span, m (ft)	21.4 (66.2)	25.2 (78)	21.4 (69.3)
Taper ratio	0.34	0.34	0.30
Sweep at quarter chord, deg	27.5	27.5	27.5
Dihedral, deg	-3.5	-3.5	0
Incidence at mean aerodynamic chord, deg	4.5	4.5	0
Root thickness, percent chord	14	14	12.5
Tip thickness, percent chord	11	11	10.5
Mean aerodynamic chord, m (ft)	3.16 (9.8)	3.78 (11.74)	3.06 (9.5)
Airfoil section:			
Root	NACA 63_2A214	NACA 63_2A214	RAE 104
Tip	NACA 63_2A211	NACA 63_2A211	RAE 104
Flap span, percent semispan	61.7	61.7	82.3
Flap hinge axis, percent chord	78.0	78.0	68.5
Ailerons:			
Span, percent semispan	28.1	----------	9.4
Hinge axis, percent chord	78.0	----------	68.0
Travel, deg	0 to 60	----------	-10 to +45
Spoilers:			
Span, percent semispan	57	73	9
Percent chord	10	10	10.5
Deflection, deg	0 to 60	0 to 60	0 to 60
Horizontal tail –			
Area, m^2 (ft^2)	19.1 (205)	----------	14.8 (159)
Aspect ratio	5.3	5.3	4.5
Span, m (ft)	10.6 (33)	----------	8.5 (26.5)
Sweep at leading edge, deg	29	29	25
Elevator hinge axis, percent chord	73	73	60
Elevator travel, deg	-10 to 50	0 to 50	±30
Tail incidence, deg	±10	±10	±10
Volume coefficient	1.0	1.0	.99
Tail arm length, m (ft)	9.75 (28.7)	----------	11.55 (35.8)
Vertical tail –			
Area, m^2 (ft^2)	11.2 (120)	----------	8.1 (87)
Aspect ratio	1.66	1.66	1.4
Volume coefficient	0.09	0.09	0.075
Rudder hinge axis, percent chord	57	57	60
Rudder travel, deg	±45	±40	±45
Engine location –			
Inboard, percent semispan	22	22	22
Outboard, percent semispan	42	42	42

TABLE 2.- WEIGHT AND INERTIAL CHARACTERISTICS OF TEST CONFIGURATIONS

	FRC externally blown flap	LRC externally blown flap	FRC augmentor wing
Weight, kg (lb)	21 792 (48 000)	25 070 (55 100)	21 792 (48 000)
Center-of-gravity location, percent, mean aerodynamic chord	40	40	25
Moments of inertia, kg-m^2 (slug-ft^2):			
I_X	288 785 (213 000)	331 103 (244 212)	291 497 (215 000)
I_Y	315 223 (232 500)	334 637 (246 819)	312 308 (230 350)
I_Z	545 710 (402 500)	675 677 (461 482)	541 642 (399 500)
Product of inertia, kg-m^2 (slug-ft^2):			
I_{XZ}	42 233 (31 150)	27 690 (20 423)	35 250 (26 000)

TABLE 3.- COMPARISON OF FLARE PARAMETERS FOR TYPICAL CTOL AND STOL AIRPLANES

Airplane	Approach condition			Flare initiation altitude		Distance used		Time of flare, sec	Time in ground effect, sec
	Velocity, knots	Rate of climb,							
		m/sec	ft/sec	m	ft	m	ft		
CTOL Glide slope = -2.8°	125	-3	-10	15	50	692	2269	11.4	[a] 15
Externally blown flap STOL Glide slope = -7.5° Glide slope = -4.0°	75 75	-5 -3	-16 -9	13 9	43 29	172 227	563 744	4.8 6.0	[b] 4.1 [b] 6.3

[a] Time in positive ground effect.

[b] Time in negative ground effect.

EXTERNALLY BLOWN FLAP CONFIGURATION

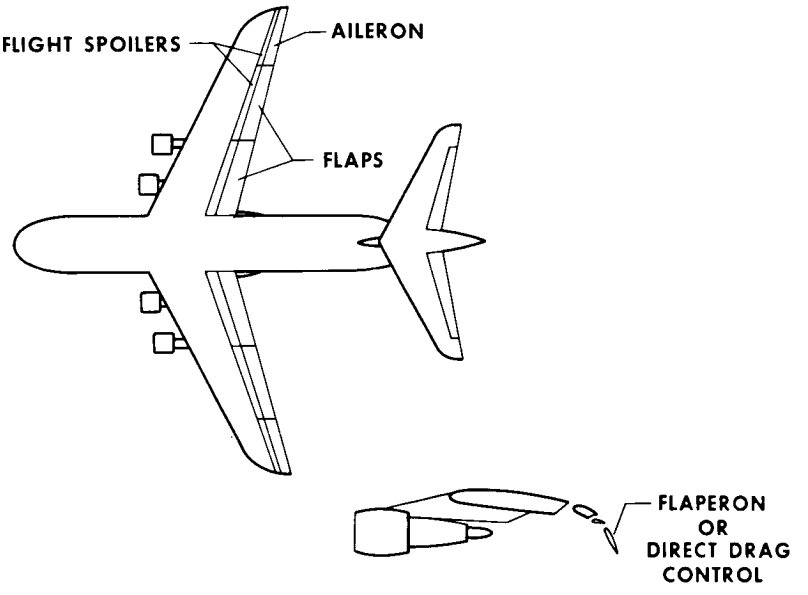

Figure 1(a)

AUGMENTOR WING CONFIGURATION

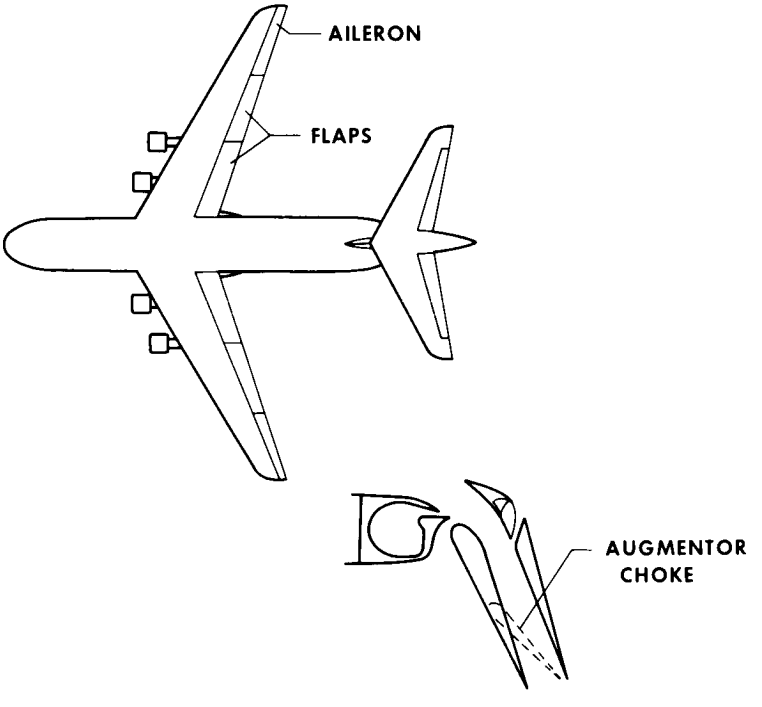

Figure 1(b)

EXTERNALLY BLOWN FLAP FLIGHT-PATH STABILITY CHARACTERISTICS

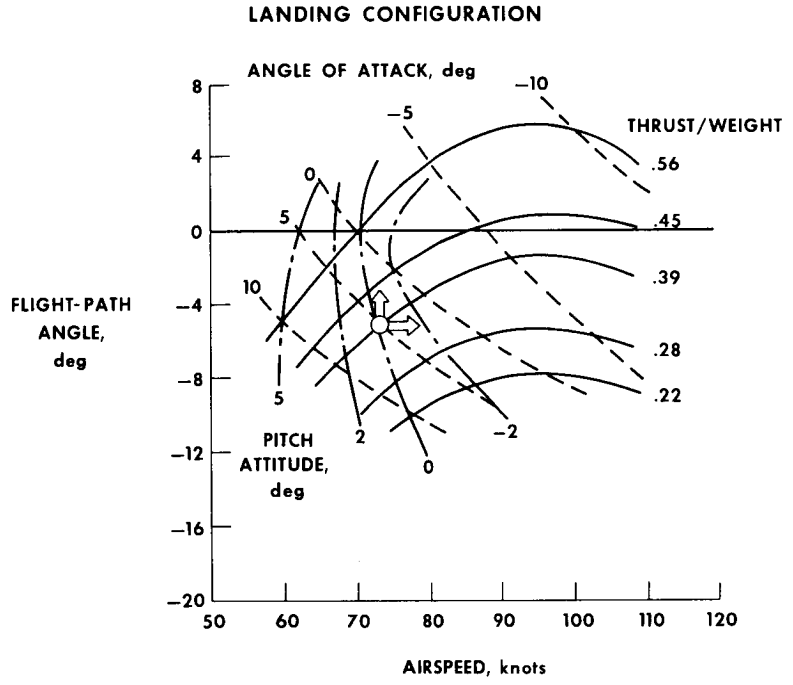

Figure 2

FLIGHT-PATH STABILITY CHARACTERISTICS

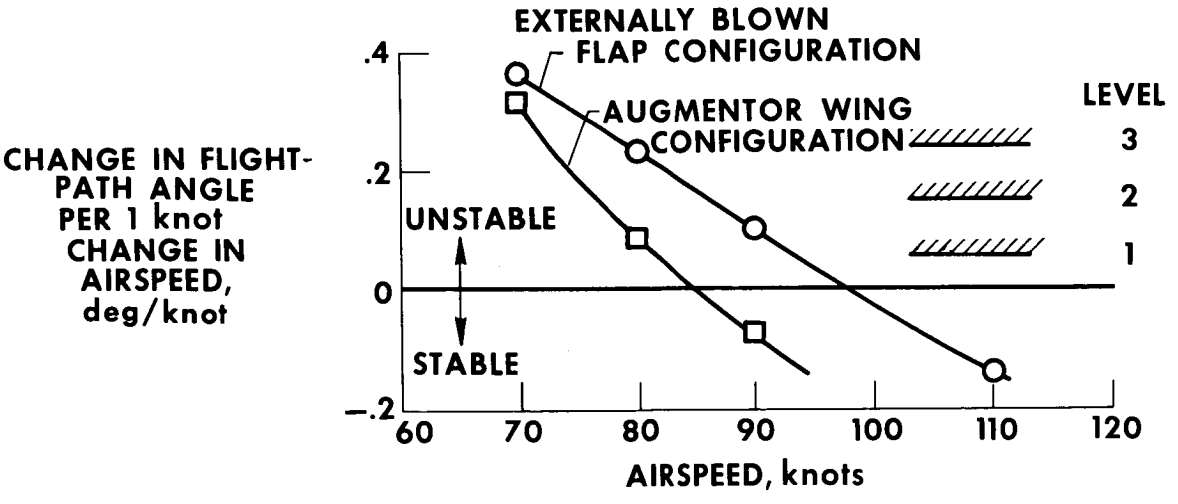

Figure 3

TIME HISTORY OF A LONGITUDINAL PULSE

AUGMENTOR WING, LANDING CONFIGURATION

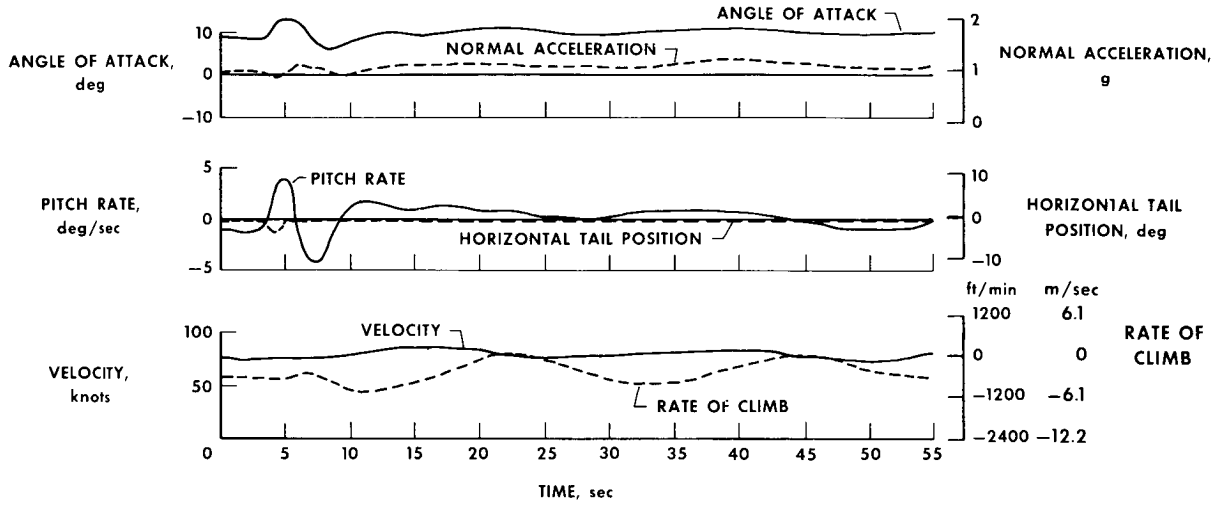

Figure 4

PITCH CONTROL SYSTEM BLOCK DIAGRAM

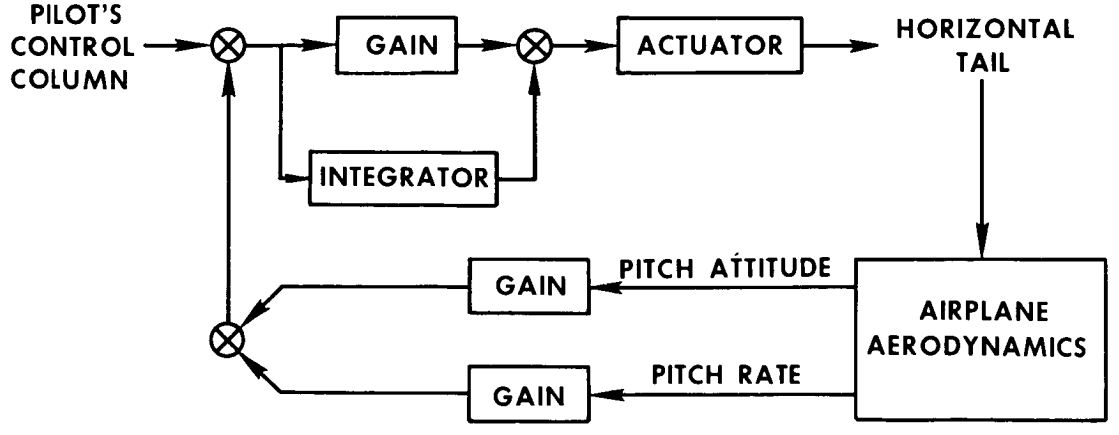

Figure 5

FLIGHT-PATH AUGMENTATION BLOCK DIAGRAM

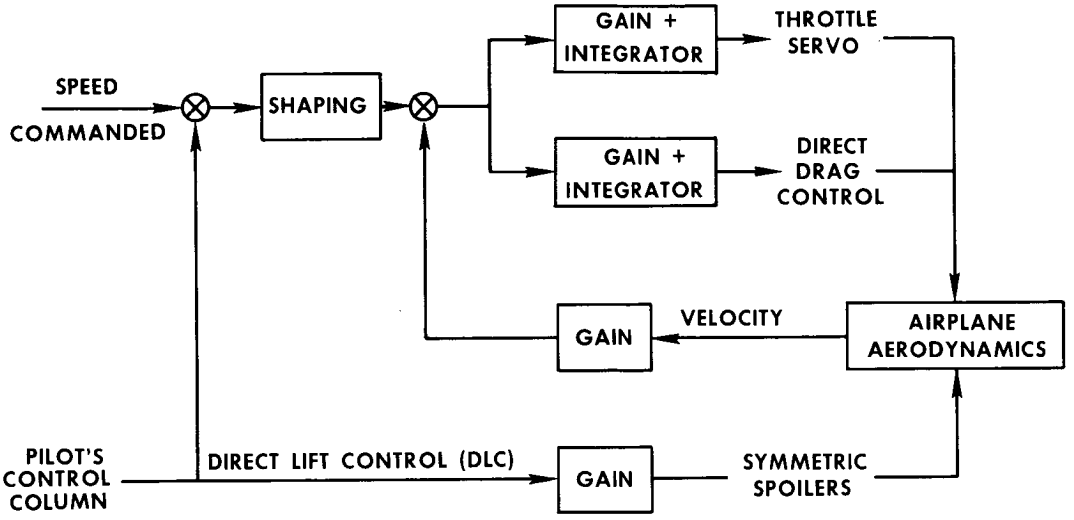

Figure 6

TIME HISTORY OF AN AILERON STEP

EXTERNALLY BLOWN FLAP LANDING CONFIGURATION

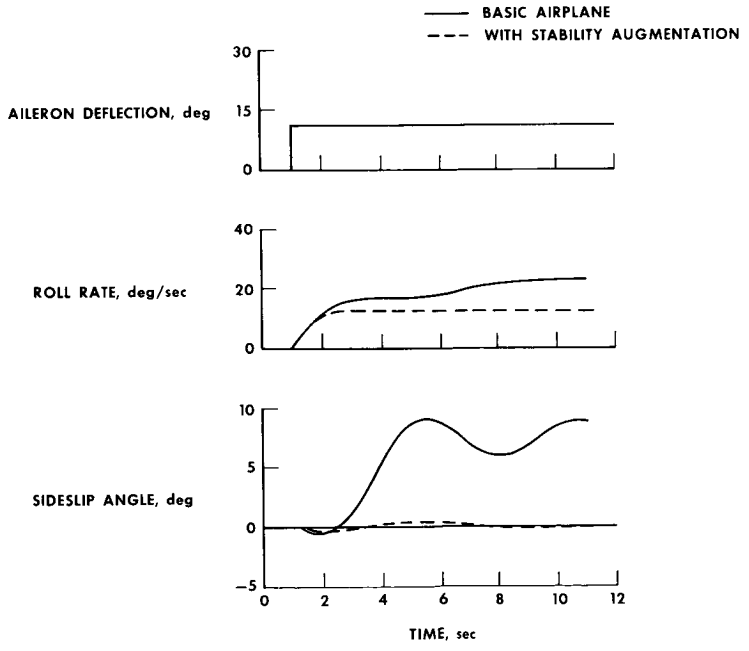

Figure 7

ROLL CONTROL SYSTEM BLOCK DIAGRAM

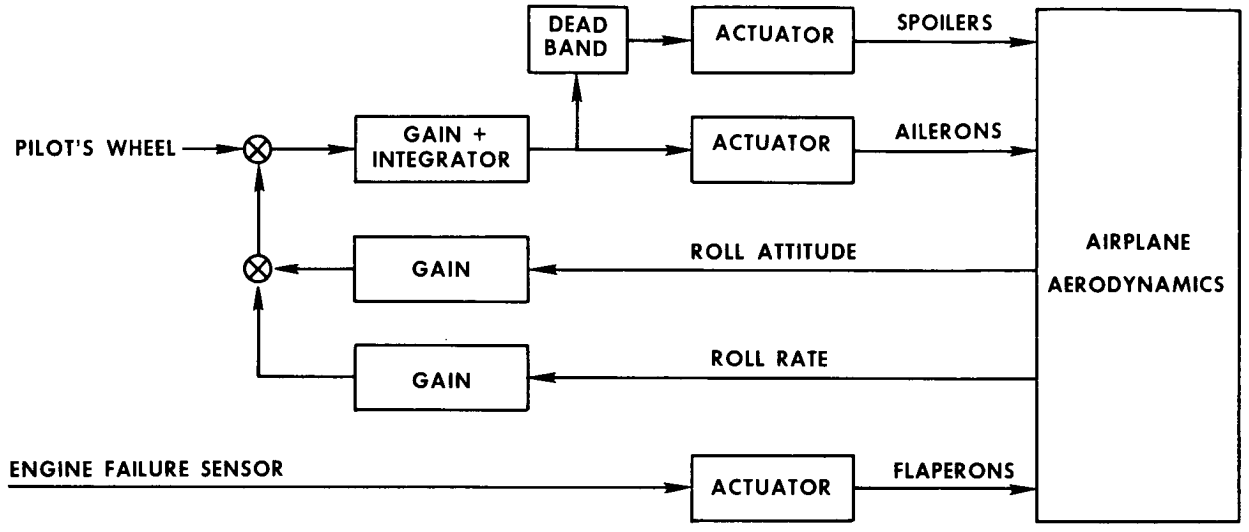

Figure 8

YAW CONTROL SYSTEM BLOCK DIAGRAM

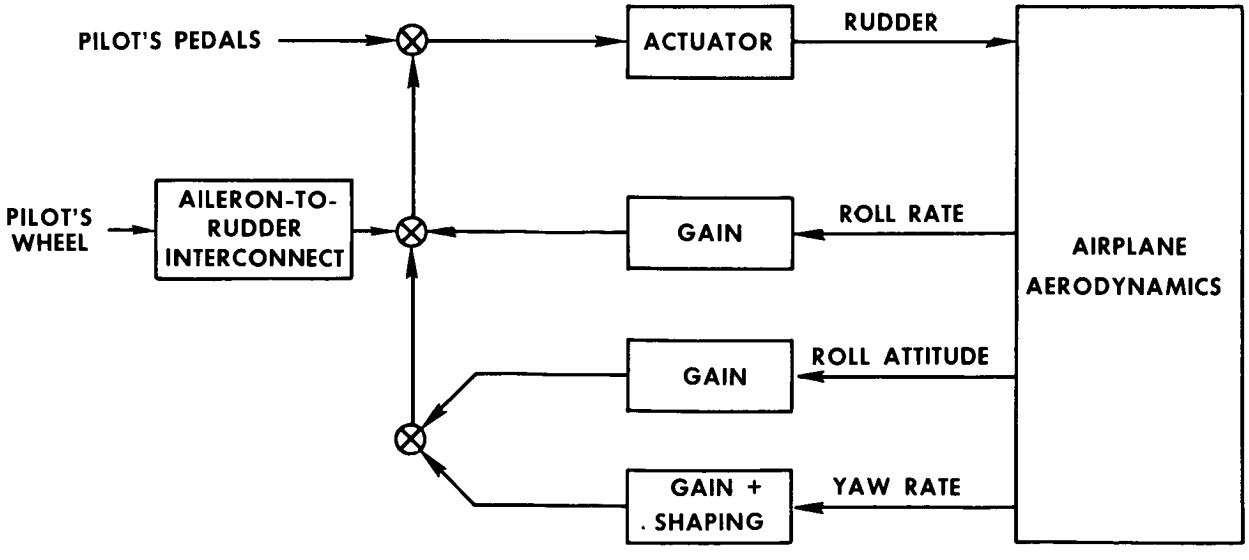

Figure 9

BANK AND YAW ANGLES GENERATED DUE TO AN OUTBOARD ENGINE FAILURE
EXTERNALLY BLOWN FLAP CONFIGURATION

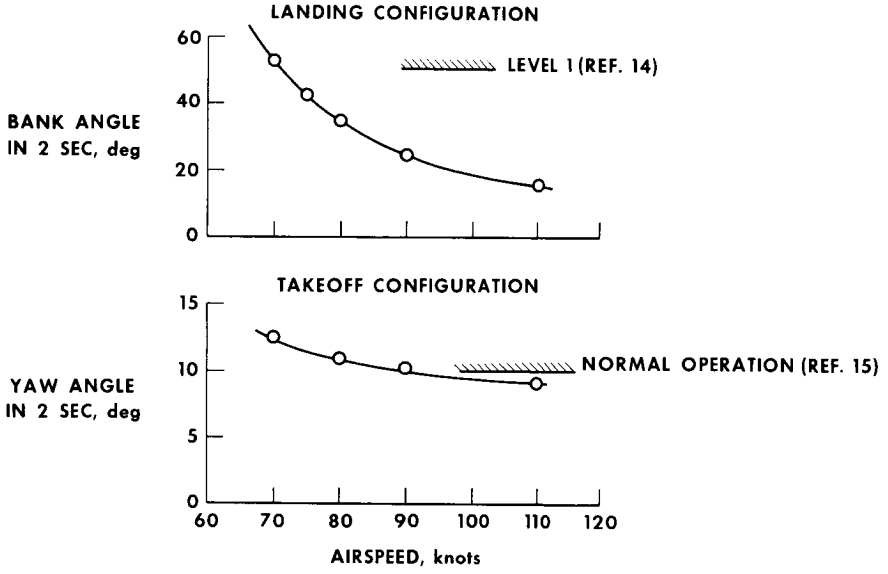

Figure 10

EXCURSIONS EXPERIENCED AFTER FAILURE OF AN OUTBOARD ENGINE
STABILITY AUGMENTATION ON

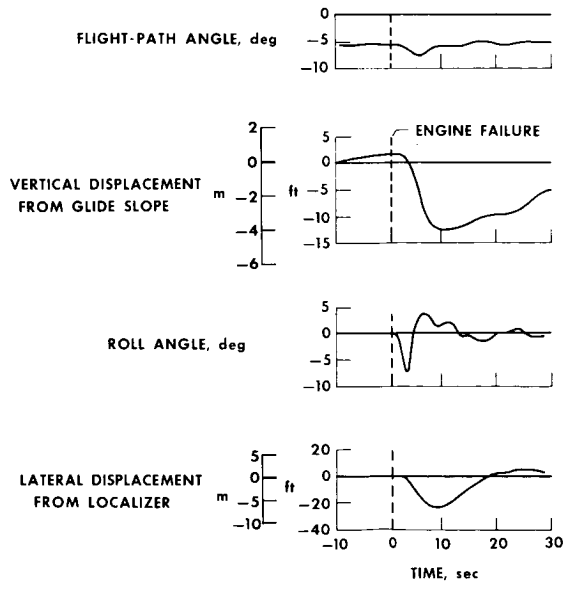

Figure 11

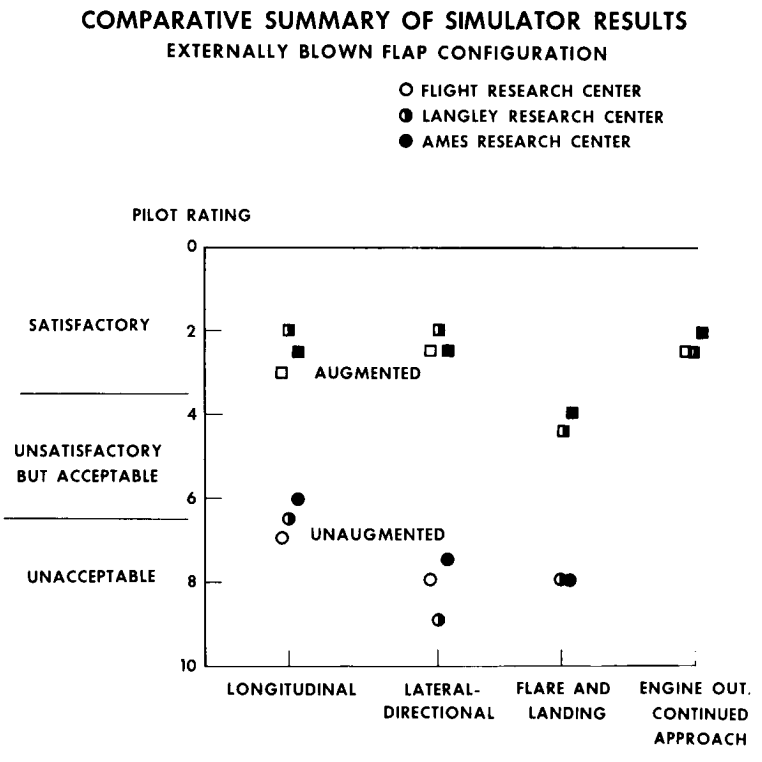
COMPARATIVE SUMMARY OF SIMULATOR RESULTS
EXTERNALLY BLOWN FLAP CONFIGURATION
O FLIGHT RESEARCH CENTER
◑ LANGLEY RESEARCH CENTER
● AMES RESEARCH CENTER
PILOT RATING
0
2
4
6
8
10
SATISFACTORY
UNSATISFACTORY BUT ACCEPTABLE
UNACCEPTABLE
AUGMENTED
UNAUGMENTED
LONGITUDINAL
LATERAL-DIRECTIONAL
FLARE AND LANDING
ENGINE OUT, CONTINUED APPROACH

Figure 12

FLIGHT-PATH AND AIRSPEED CONTROL FOR THE STOL APPROACH AND LANDING

By James A. Franklin and Robert C. Innis
NASA Ames Research Center

SUMMARY

Analytical investigations and piloted moving base simulator evaluations were conducted for manual control of flight path and airspeed for the approach and landing of a powered lift jet STOL aircraft. Flight-path and airspeed response characteristics were described analytically and were evaluated for the simulation experiments which were carried out on a large motion simulator (FSAA) at Ames Research Center. The response characteristics were selected and evaluated for a specified path and speed control technique. These characteristics were the initial flight-path response, flight-path overshoot, flight-path—airspeed coupling in response to a change in thrust, and the sensitivity of airspeed to pitch-attitude changes. Results are presented in the form of pilot opinion ratings and commentary, substantiated where appropriate by response time histories and aircraft states at the point of touchdown.

15

INTRODUCTION

Manual control of a transport category aircraft which is capable of operation at speeds associated with the STOL flight regime and which utilizes significant amounts of power to augment its basic aerodynamics is generally more difficult than control of a conventional transport aircraft operating at higher speeds. Considering the longitudinal control problem, pitch-attitude, flight-path, and airspeed response are all adversely affected by the low speed, high wing loading, and high inertias typical of the STOL transport category vehicle. Use of conventional controls such as elevator (or pitching-moment control) and power are likely to produce rather unconventional behavior as a result of

sluggish pitch-attitude response and strong excitation of the phugoid mode

sluggish flight-path response to attitude changes

operation on the backside of the thrust-required curve

large changes in lift and drag with engine power setting

significant coupling between flight path and airspeed with either attitude or power changes

changes in operating margins with airspeed and angle of attack

These differences demand a reexamination of the basis on which transport category aircraft should be designed from a stability and control and handling qualities viewpoint. It becomes necessary to consider more carefully the pilot's control technique and the vehicle response characteristics which define longitudinal handling-qualities criteria. It may be necessary as well to establish new criteria which relate to vehicle behavior not addressed in the current literature.

In response to these needs, an analytical and experimental study has been carried out to explore some of the problems of flight-path and airspeed control for the STOL approach and landing. The purpose of the analytical study was to describe the features which characterize flight-path and airspeed response as they appear to the pilot and to identify the contributions to these response characteristics of the aircraft's configuration and the flight condition at which it is operated. The experimental study was conducted to allow pilots to evaluate the significance of these response characteristics to their ability to fly the STOL approach and landing. The discussion which follows summarizes the results of the analytical study and presents the experimental results in some detail.

FLIGHT-PATH AND AIRSPEED RESPONSE CHARACTERISTICS

In defining the salient features of flight-path and airspeed response, it is assumed that the primary controls available to the pilot are the pitch-attitude and engine thrust controls. Attitude must be controlled tightly either by the pilot or with assistance of a command augmentation system (such as that described in ref. 1) to achieve reasonable path and speed precision. Control of thrust gives the pilot a powerful means of changing the aircraft's lift and drag characteristics (hence its flight path and speed) through the augmentation of the aircraft's basic aerodynamics by flow of fan air and jet exhaust over or through the wing flap system.

Both pitch attitude and thrust can significantly affect flight-path and airspeed response. Different techniques can be hypothesized regarding the manner in which the pilot utilizes these controls. Therefore, it is necessary to determine which control technique the pilot is likely to select before the path and speed response characteristics of importance to him can be defined. A typical example of the behavior of a powered lift STOL aircraft, such as illustrated in figure 1, demonstrates this point.

The response to an attitude change at constant thrust is shown in figure 1(a). The nose-up attitude change produces flight-path response typical of that for operation on the backside of the thrust-required curve, in that flight path initially shallows but eventually steepens. Such behavior, as is well known, makes attitude a rather poor control of flight path in the approach. However, airspeed response is conventional, and attitude offers reasonable control over speed providing the harmony between the two is satisfactory.

For an increase in thrust with attitude held constant shown in figure 1(b), flight path responds quickly with the long term change determined by specific configuration characteristics. On the other hand, speed response is decidedly adverse in that the airplane decelerates for an increase in thrust. Thrust thus appears to be an appropriate control for flight path and a rather poor control for speed. Accordingly, for the path and speed response characteristics illustrated, the pilot can be expected to use attitude to control airspeed and thrust to control flight path. With the control technique specified, it is possible to define the characteristics of the aircraft's response, when operated with this technique, that could be of importance to the pilot for manual control of the STOL approach and landing.

Based on the nature of the flight path and airspeed response to thrust shown in figure 1, the features which appear to need consideration to characterize the aircraft's behavior are

the initial response of flight path which indicates how quickly a path correction can be initiated

the relationship of the long term to short term change in flight path, as illustrated by the amount of overshoot in the response, which indicates how predictable the pilot can make the path correction

the extent of coupling of airspeed with flight path, as reflected by the amount of speed change accompanying the change in flight path, which indicates the amount of attention the pilot must devote to path and speed control and the extent to which he must continuously control path and speed, closed loop, to achieve the precision required for the landing approach

The response parameters which reflect this behavior are indicated in figure 2. Initial flight-path response is represented by the time constant τ_γ, which is described by the initial slope $d\Delta\gamma/dt$ and the peak response $\Delta\gamma_{max}$. Flight-path overshoot is reflected in the ratio $\left(\Delta\gamma_{max}/\Delta\gamma_{ss}\right)_{\Delta T}$. Flight-path—airspeed coupling is described by the ratio of steady-state speed and path changes $\left(\Delta V_{ss}/\Delta\gamma_{ss}\right)_{\Delta T}$. Short-term speed changes tend to be of small enough magnitude to be ignored when compared with the long-term speed changes.

Speed control, as was noted previously, is accomplished through changes in pitch attitude. In this case, the steady-state speed change for a given change in attitude $\Delta V_{ss}/\Delta\theta$ is the factor of interest and can be considered a control sensitivity of sorts. Assuming that pitch attitude is controlled tightly, these path and speed response characteristics may be defined in terms of the aircraft's X- and Z-axis (or drag and lift) derivatives due to speed, angle of attack, and thrust. These derivatives are predominantly determined by flight condition, wing loading, and efficiency of the high lift system, that is,

X_u axial velocity damping; a function of trim drag coefficient, trim airspeed, and wing loading (may be augmented by autospeed control)

X_α drag due to lift; a function of trim airspeed, wing loading, and induced drag

Z_u vertical force coupling with axial velocity; a function of trim airspeed

Z_α vertical velocity damping; a function of lift-curve slope, trim airspeed, and wing loading

$X_{\delta_T}/Z_{\delta_T}$ effective thrust line inclination $\theta_T = \cot^{-1}\left(-X_{\delta_T}/Z_{\delta_T}\right)$

Thus, the choice of landing-field length and cruise Mach number (which dictate landing-approach speed, flight-path angle, and wing loading) and the design of the high lift system (which defines the thrust turning effectiveness of the flap) will determine the aircraft's longitudinal handling qualities for the approach and landing.

EXPERIMENTAL PROGRAM

Description of the Simulation

A ground-based flight simulation of a powered lift jet STOL aircraft was used as a basis for piloted evaluation of the flight path and airspeed response characteristics described in the previous section of this paper. The simulation facility utilized was the Ames Research Center Flight Simulator for Advanced Aircraft (FSAA), a large motion facility with a high-resolution visual display. The vehicle on which the simulation was based was the Augmentor Wing Research Aircraft, a modified De Havilland of Canada C-8A Buffalo airframe incorporating an augmentor flap system for generating high lift coefficients for high wing loading STOL operation and deflected hot thrust to permit operation on steep flight paths. The aircraft is described in reference 2. A real-time digital model of the aircraft's aerodynamics and flight control system was programed as described in reference 3 for the XDS-Sigma 8 computer assigned to the FSAA facility. The static aerodynamic characteristics were derived as shown in reference 4 from model tests of the vehicle in the Ames 40- by 80-foot wind tunnel. Rotary derivatives were estimated by using jet flap theory where appropriate. Supporting data for these derivatives are unpublished although the models themselves appear in reference 4. Jet engine acceleration-deceleration characteristics were modeled to represent the results shown in reference 4.

The longitudinal flight control system provided for pitch-axis command augmentation and alteration of the vehicle's longitudinal-force characteristics through the use of vectored thrust. Pitch control was accomplished through hydraulic actuators driving the aircraft's existing elevator-spring tab system. Augmentation commands to the control actuator were provided in series with the pilot's control column inputs. Longitudinal-force control was achieved by vectoring the engines' hot thrust about a trim position deflected 90^{o} to the approach path. Thrust vectoring was accomplished by driving the engine's exhaust nozzles with commands composed of airspeed, angle of attack, and throttle position error signals. For thrust vectoring of $\pm 15^{o}$ about the 90^{o} trim condition, effective alteration of the basic aircraft's X_u, X_α, and X_{δ_T} derivatives was possible with no corresponding contribution to the respective Z-axis force characteristics.

Variations in X_u, X_α, and X_{δ_T} were used to alter the flight-path and speed response characteristics. Configurations were selected to permit independent evaluations of the path response time constant τ_γ and speed response to attitude $\Delta V_{ss}/\Delta\theta$ for essentially no flight-path overshoot or flight-path—speed coupling. Flight-path overshoot $\left(\Delta\gamma_{max}/\Delta\gamma_{ss}\right)_{\Delta T}$ and path—speed coupling $\left(\Delta V_{ss}/\Delta\gamma_{ss}\right)_{\Delta T}$ were also evaluated with path time constant and speed-attitude response held at fixed values. It was not possible to separately assess the effects of flight-path overshoot and flight-path—speed coupling when only X-axis force derivatives were varied. These two characteristics tend to be strongly interrelated, and variations in either one produced by alterations in X-axis force derivatives are reflected in the other. This interrelationship is illustrated in figure 3 where the solid line indicates the range of configurations evaluated in the simulation program. Some degree of independence between the path overshoot and path—speed coupling characteristics could have been achieved through variations in Z-axis force derivatives such as Z_u and Z_α. The range over which overshoot and coupling characteristics might be considered independent for the powered lift category of STOL aircraft is cross-hatched in this figure. This independence comes about through variations in Z_u and Z_α attributed to reasonable ranges of wing loading and approach speed. Configurations selected for the simulation program (indicated by the solid line with Z_u and Z_α held constant) were distributed through the region of practical importance in a manner to provide an appreciation of the influence of reasonable variations in path overshoot and path—speed coupling on handling qualities for the STOL approach.

Evaluation Task and Experimental Data

For the approach and landing, the pilot assumed control of the aircraft with it trimmed and configured for descent on the glide slope and alined with the localizer. The

approach was made to a 457-meter (1500-foot) STOL runway, with touchdown zone markings as indicated in figure 4. The aircraft was trimmed at 396 meters (1300 feet) for descent on a 7.5^{o} glide slope at an airspeed of 60 knots. Flaps were set at 65^{o}, hot thrust was vectored 90^{o} to the aircraft's reference waterline, and power was set corresponding to 28.4 kilonewtons (6380 pounds) of hot thrust. Lateral-directional stability augmentation, including roll damping, spiral mode stabilization, Dutch roll damping, and turn coordination, was utilized to improve control of bank angle, heading, and sideslip to prevent these factors from influencing the pilot's evaluation.

Two Ames experimental test pilots participated in the program. During the approach, the pilots introduced their own disturbances, offsets, and abuses as a means of evaluating each configuration. Both VFR and IFR evaluations were performed. Approach guidance was provided by raw ILS glide slope and localizer error information. Pilot ratings and commentary based on the Cooper-Harper scale were obtained for each configuration with regard to its handling qualities during the approach. Separate ratings for the landing flare were not obtained; however, qualitative comments on the aircraft's handling during the flare as compared with handling during the approach were noted.

DISCUSSION OF RESULTS

In the discussion to follow, pilot's evaluations of flight-path and airspeed control will be presented for the landing approach. A separate commentary on landing flare characteristics is included in a section at the end of the discussion.

Flight-Path and Airspeed Control

The influence of flight-path and airspeed response to thrust is considered first, with attention given first to the effect of initial flight-path response. Pilot ratings are shown in figure 5 for a range of flight-path time constants τ_{γ}. The results are presented for minimal flight-path overshoot and flight-path—airspeed coupling. Pilot ratings appear to be insensitive to variations in τ_{γ} over the range of configurations tested. The results are understandable in light of the evaluation task. During the approach, extremely rapid path corrections are not required and, as the pilots indicate, can readily be made for the various configurations shown in figure 5. As indicated in reference 5, bandwidths required for closed-loop path control are on the order of 0.5 to 1.0 radian/sec. For these configurations, and with the effects of engine acceleration-deceleration included, the required path control bandwidths can be achieved for the configurations investigated with little demand for compensation by the pilot.

It should be noted, that these configurations were evaluated for an optimized throttle sensitivity of $Z_{\delta_T} = -0.08$ g/inch. No variations in Z-axis characteristics were made

for the various configurations. Although an increase in vertical velocity damping Z_α/V_o could quicken the initial path response, it was not evaluated in this program. As is indicated subsequently in the discussion of flare characteristics, some quickening of path response such as could be achieved through Z_α augmentation would be beneficial to flare control.

Flight-path overshoot $\Delta\gamma_{max}/\Delta\gamma_{ss}$ and flight-path—speed coupling $\Delta V_{ss}/\Delta\gamma_{ss}$ are two characteristics of response to thrust which, as has been previously noted, were not evaluated independently in this program. They are strongly interrelated due to their mutual sensitivity to changes in longitudinal (X-axis) force characteristics such as trim drag, drag due to lift, and thrust inclination. However, this interrelationship is typical of powered lift STOL aircraft in general as was shown in figure 3 and the evaluation of mutual changes in these two parameters which was conducted in this program offers insight into their influence on path and speed control for this category of aircraft. Results are presented in figure 6, with pilot ratings plotted against the path—speed coupling parameter $\left(\Delta V_{ss}/\Delta\gamma_{ss}\right)_{\Delta T}$. The path—speed coupling influence was identified by the pilots as the primary factor in their evaluation and rating and, hence, was felt to be the relevant parameter for interpreting the data.

It is apparent that path—speed coupling has a pronounced effect on pilot ratings of path—speed control. In particular, a significant degradation in ratings can be noted for values of $\left(\Delta V_{ss}/\Delta\gamma_{ss}\right)_{\Delta T}$ in excess of -3 knots per degree. The adverse nature of the speed response to a flight-path change with thrust is illustrated in the inset diagram at the left of figure 6, where an increase in thrust to shallow the path causes the aircraft to decelerate, in turn washing out the intended path correction. Such behavior is particularly undesirable in that the strongly coupled response demands that the pilot pay considerable attention to path and speed control and to work in a continuous, coordinated, closed-loop fashion with attitude and thrust to achieve adequate precision of path and speed control. Furthermore, the attitude control technique required for holding speed constant while making a path correction with thrust is unnatural. It requires the pilot to lower the nose to hold speed while attempting to climb and vice versa. For these two reasons, strong path—speed coupling can make the aircraft unacceptable for flying the STOL approach.

To conclude the discussion of flight-path and airspeed control for the approach, it is necessary to determine the significance of speed behavior in response to its primary control, pitch attitude. The significance of speed control with attitude is indicated in figure 7. Pilot ratings for variations in the speed response parameter $\Delta V_{ss}/\Delta\theta$ are plotted for otherwise favorable values of τ_γ and $\left(\Delta V_{ss}/\Delta\gamma_{ss}\right)_{\Delta T}$. Variations in speed sensitivity to attitude have only a modest effect on pilot ratings. As might be expected the pilots objected, although not too strongly, to insensitive or to excessively sensitive

speed response to attitude changes. Poor harmony between speed and attitude either required excessive attitude changes for ordinary speed control or an unnecessarily fine touch on attitude to avoid objectionable speed excursions. Proper harmony seems to dictate a speed-attitude sensitivity on the order of $\Delta V_{ss}/\Delta\theta$ between -1.5 and -2.5 knots per degree.

Flare Control

The pilots did not specifically evaluate the flare maneuver as distinct from the landing approach. However, specific comments were made on flare characteristics where appropriate and it is on these comments that the following discussion is largely based.

It is evident from the results of this program as well as for those reported in references 1, 6, and 7 and by James L. Hassell, Jr., and Joseph H. Judd in paper no. 16 that the two-control flare (that is, where thrust is used to augment the flare by attitude) does not produce consistent STOL landing performance, either in terms of touchdown precision or low sink rates. A compilation of data of landing precision in terms of sink rate and point of touchdown for all of the configurations evaluated in this program is presented in figure 8. These data were obtained from experimental runs where the pilot's objective was to achieve the best landing performance possible rather than to carry out an evaluation of the aircraft's handling qualities. The pilots sought to land the aircraft within the touchdown zone and, if possible, at a sink rate of 1.8 m/sec (6 ft/sec) or less. The scatter in landing precision data of figure 8 speaks for itself. Touchdown sink rates, with one exception, exceeded 1.5 m/sec (5 ft/sec) and most landings were made at sink rates from 2.4 to 3 m/sec (8 to 10 ft/sec). Separation of the data into sets of configurations which could isolate effects of flight-path time constant and airspeed response to attitude (which includes the influence of frontside or backside operation) offers no further enlightenment. Data are presented in this form in figure 9, and there are no discernible trends with respect to landing precision, touchdown sink rate, or airspeed.

It can be questioned whether STOL operation should require minimizing sink rate at touchdown. The conceivable bounds for sink rate probably lie somewhere between a 0.9 m/sec (3 ft/sec) lower limit comparable to CTOL operation and a 3.7 to 4.3 m/sec (12 to 14 ft/sec) upper limit defined by the nominal approach flight-path angle and airspeed. Without attempting to place the results of this program in an acceptable or unacceptable category as regards landing impact, it can be said that landings performed on the simulator have produced sink rates somewhere halfway between these two limits.

It should be emphasized that the problem of achieving accurate landings at low sink rates does not stem from a lack of capability of the basic aircraft, that is, the capability for generating the normal load factors to curve the flight path to terminate the approach

at the proper position and vertical velocity. The potential for generating normal acceleration $\Delta\alpha_z$ is more than adequate if aircraft rotation and an increase in power are both used. Instead, the problem is that of controlling this load factor so as to generate it quickly and precisely for performing the flare. In this program, no sophisticated control schemes were investigated for flare, such as control interconnects (e.g., column to throttles) or Z_α augmentation. The basic aircraft's controls for short-term flight-path changes were evaluated and, as with the other referenced powered lift STOL simulations, they were found to be inadequate for the task.

The foregoing remarks must be qualified as applying to the control technique (described elsewhere in this paper) which was used by the pilots to perform the flare and landing. Furthermore, it must be borne in mind that the ability to satisfactorily produce the motion and visual cues crucial to the pilot for performing this maneuver is always in question when a ground-base simulator is used. Not withstanding the motion capability of the FSAA and the visual resolution capability of the Redifon system, the evaluation pilots harbored doubts of their ability to judge altitude, sink rate, and normal acceleration and to use these cues effectively in controlling the aircraft through the flare. However, even with these qualifications of the experimental results, it is felt that their interpretation for the purpose of distinguishing between significant and inconsequential contributions to the flare and landing is valid.

It should also be evident from the results of this program that path and speed control characteristics which are favorable for the approach are not necessarily favorable for control through the flare to landing. In particular, flight-path response time constants which have been shown in figure 5 to be satisfactory for the approach do not permit path corrections to be accomplished quickly enough for the flare. A sample time history of a STOL landing is presented in figure 10 for the configuration having the best path and speed control characteristics for the approach. The time frame for the flare, from the point at which the pilot initiates the maneuver with the elevator to touchdown, is 3 seconds. For any control to be useful for path corrections within this time frame, the corrections must be initiated and stabilized within approximately 2 seconds. Such response implies equivalent first-order time constants on the order of 0.75 to 1.0 second. Neither the dynamics of the basic airframe, which responds at frequencies on the order of 0.3 radian/sec to either attitude or thrust changes, or the engine dynamic response, which requires 1.5 to 2.0 seconds to stabilize following a commanded thrust change, offers the kind of response demanded. Clearly a need exists for utilizing the potential existing in the basic aerodynamics and reserve thrust to achieve the desired flare capability. The solution most likely lies with quickened engine acceleration characteristics and augmentation of the aircraft's vertical velocity damping Z_α/V_0. So far as speed response and control is concerned, it could be speculated that the characteristics of speed response to thrust, which were judged adverse for the approach, may not be so objectionable for the flare.

The time span over which the speed change can occur does not allow for significant changes in speed considering the speed response time constants involved. Speed response to attitude changes is likely to be important to the pilot in order that he can rely on a reasonable and predictable speed bleed off through the flare to touchdown.

The final point to be made is that the successful use of two controls to accomplish the flare demands that one of the controls be identified as primary and the other control be relegated to a secondary or supporting role. Throughout this program and during other STOL simulations at Ames as well, the evaluation pilots virtually unanimously expressed a preference for a single control with which to perform the flare. Their motivation was the desire to simplify the flare technique so as to be able to get consistent results in real operational use. If a single control which has these features [1] cannot be devised and if, as a result, two controls must be used, the pilots would prefer to be able to initiate the flare with the primary control and to use it for flight-path corrections as required throughout the flare. The primary control could either be attitude or power and it should have the quick time response previously indicated. The secondary control would be used in an open-loop or preprogramed manner to assist the flare and would not be used further to perform corrections to the flare. As the pilots indicate, they cannot simultaneously use two controls in a closed-loop fashion to accomplish the flare and at the same time have confidence in their ability to get consistently good landing performance.

CONCLUSIONS

The conclusions which can be drawn from the experimental program are qualified, where appropriate, by the technique used by the pilot to control flight path and airspeed during the landing approach. Further qualification of the results obtained for the landing flare are imposed by the ability to adequately reproduce on the simulator the motion and visual cues important to the pilot for performing this maneuver.

With these qualifications, the following conclusions can be made as a result of the analytical and simulation studies of flight-path and airspeed control for powered lift STOL aircraft:

1. With pitch attitude stabilized and for flight-path control with thrust and airspeed control with pitch attitude, the characteristics which define flight-path and airspeed

---

[1] The control must also be suitable for use during the approach and for wave-offs, for adapting to engine failures, and, at the same time, be highly reliable and easily maintained.

response as they appear to the pilot are

initial flight-path time constant in response to thrust

overshoot in flight-path response to thrust

flight-path—airspeed coupling defined by the change in speed following a path correction with thrust

airspeed change due to a change in attitude

2. For flight-path and airspeed control during the approach and over a range of configuration characteristics appropriate to powered lift STOL

flight-path—airspeed coupling is the dominant influence on handling qualities

speed sensitivity to pitch attitude has a moderate influence on handling qualities

initial flight-path time constant has a negligible effect over the range investigated $(1.5 < \tau_\gamma < 7 \text{ sec})$

3. Flare characteristics are not necessarily predictable based on their counterparts for the approach. The ability to draw firm conclusions regarding desirable flare characteristics is restricted by the quality of the flare simulation. Nevertheless, it is likely that

compared with flight-path control on the approach, quicker flight-path response will be required to achieve the landing precision required for STOL field lengths and touchdown sink rates less than 1.8 m/sec (6 ft/sec)

more sophisticated control schemes, such as control integration and vertical velocity damping augmentation, will be required to realize the inherent potential of the basic aircraft's aerodynamics and reserve thrust for performing the flare

REFERENCES

1. Franklin, James A.; and Innis, Robert C.: Longitudinal Handling Qualities During Approach and Landing of a Powered Lift STOL Aircraft. NASA TM X-62,144, 1972.

2. Quigley, Hervey C.; Sinclair, S. R. M.; Nark, Theodore C., Jr.; and O'Keefe, Jack V.: A Progress Report on the Development of an Augmentor Wing Jet STOL Research Aircraft. [Preprint] 710757, Soc. Automot. Eng., Sept. 1971.

3. Cleveland, William B.; Vomaske, Richard F.; and Sinclair, S. R. M.: Augmentor Wing Jet STOL Research Aircraft Digital Simulation Model. NASA TM X-62,149, 1972.

4. Rumsey, P. C.; and Spitzer, R. E.: Simulator Model Specification for the Augmentor Wing Jet STOL Research Aircraft. D6-26065TN (Contract NAS2-6025), Boeing Co., Dec. 1971. (Available as NASA CR-114434.)

5. Ashkenas, Irving L.; and Craig, Samuel J.: Multiloop Piloting Aspects of Longitudinal Approach Path Control. ICAS Paper No. 72-46, Aug.-Sept. 1972.

6. Grantham, William D.; Nguyen, Luat T.; Patton, James M., Jr.; Deal, Perry L.; Champine, Robert A.; and Carter, C. Robert: Fixed-Base Simulator Study of an Externally Blown Flap STOL Transport Airplane During Approach and Landing. NASA TN D-6898, 1972.

7. Allison, R. L.; Mack, M.; and Rumsey, P. C.: Design Evaluation Criteria for Commercial STOL Transports. D6-40409 (Contract NAS2-6344), Boeing Co., June 1972. (Available as NASA CR-114454.)

FLIGHT PATH AND AIRSPEED RESPONSE

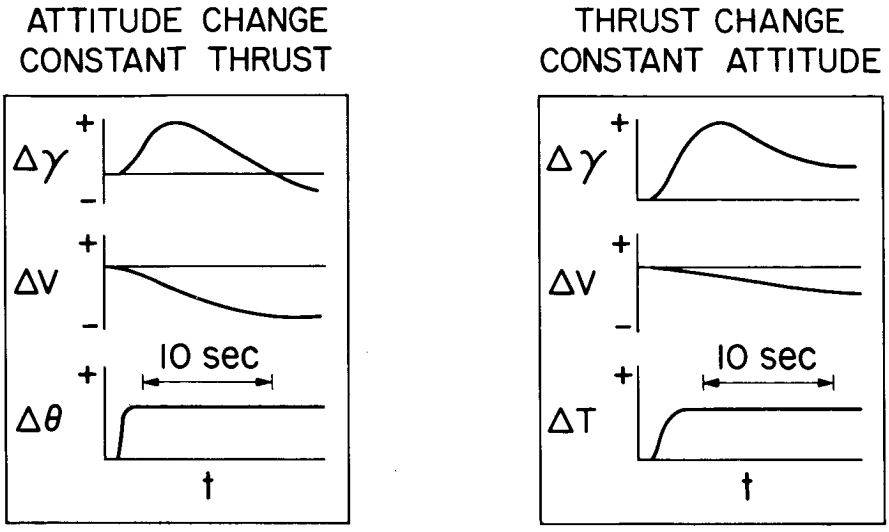

Figure 1

FLIGHT-PATH AND AIRSPEED RESPONSE TO THRUST

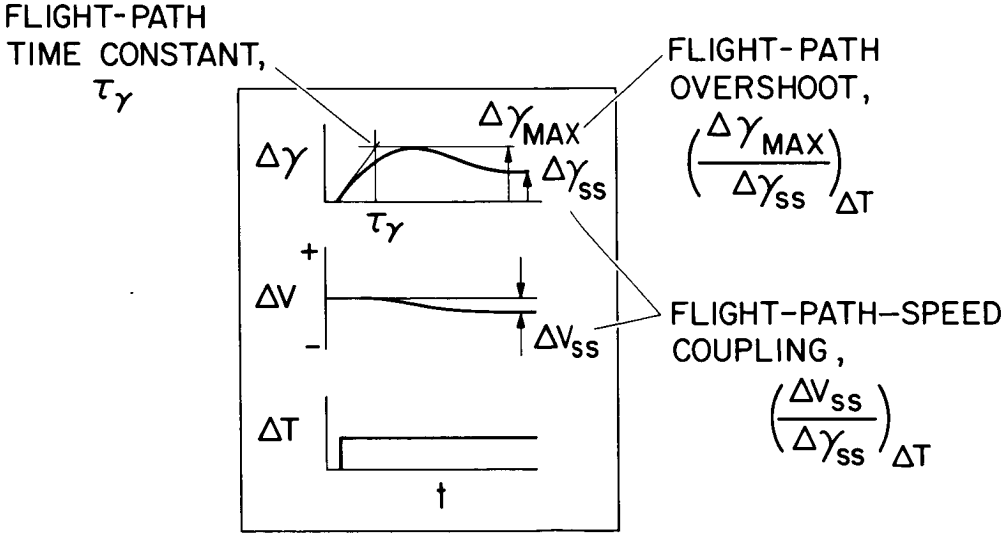

Figure 2

INTERRELATION OF FLIGHT-PATH OVERSHOOT AND FLIGHT-PATH—SPEED COUPLING PARAMETERS

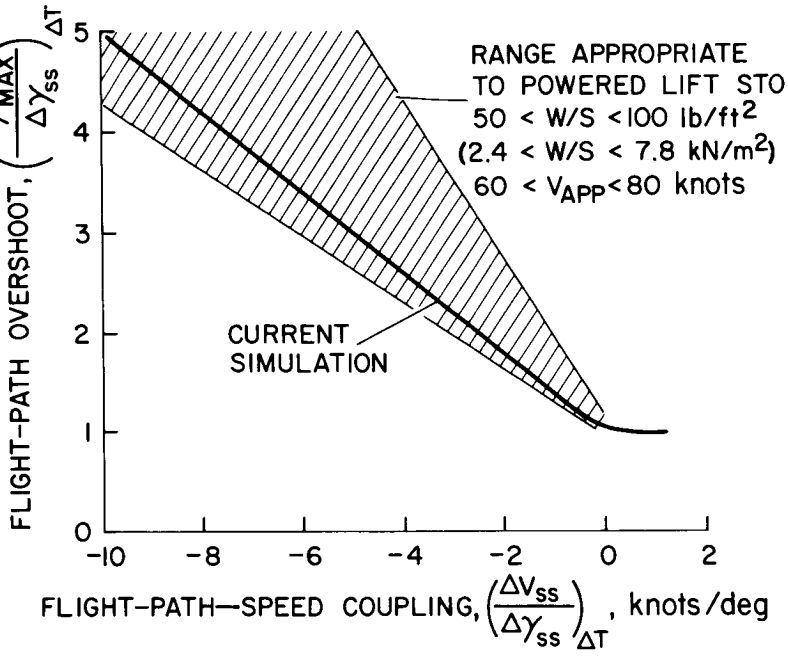

Figure 3

SIMULATION TASK

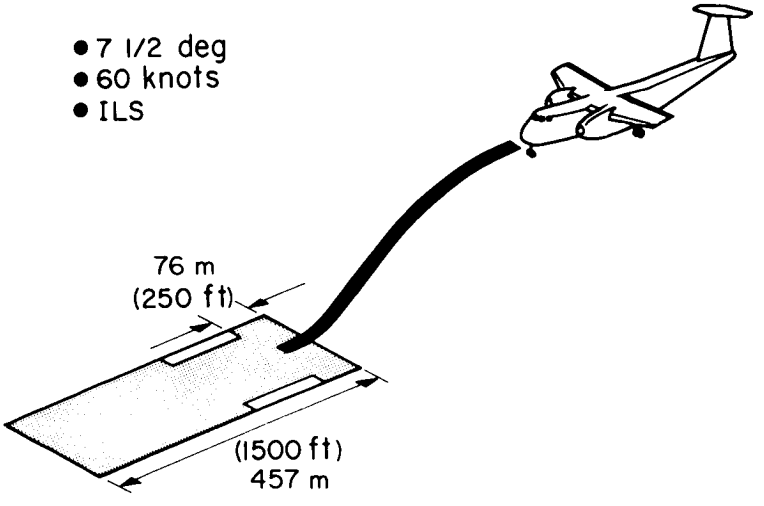

Figure 4

INFLUENCE OF FLIGHT-PATH TIME RESPONSE

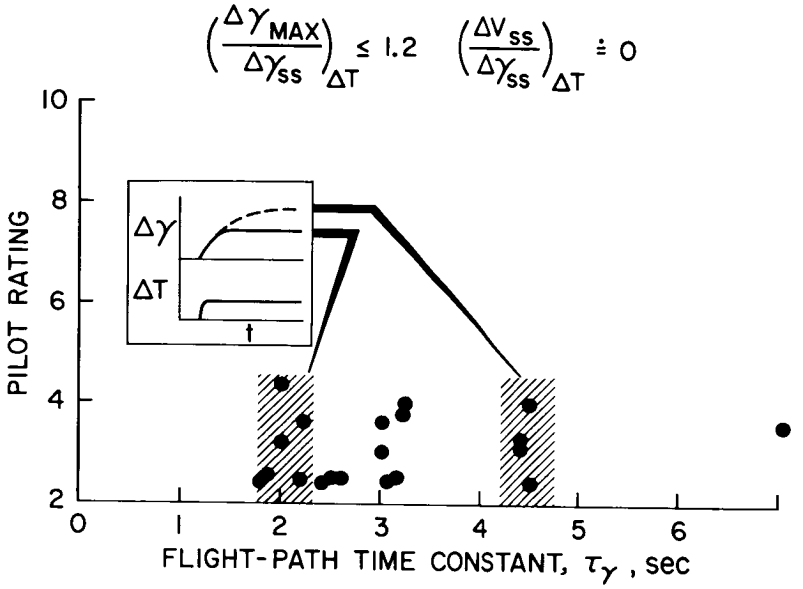

Figure 5

INFLUENCE OF FLIGHT-PATH—AIRSPEED COUPLING DUE TO THRUST

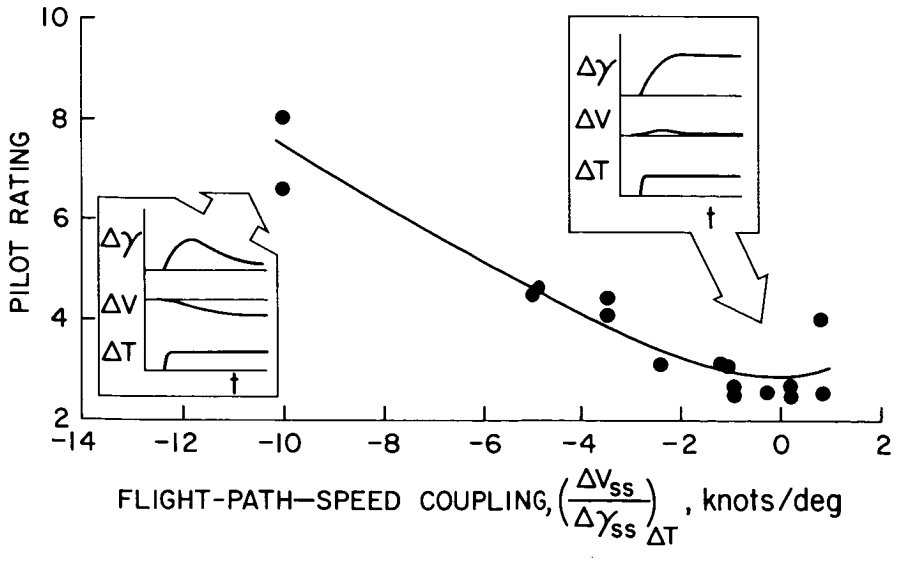

Figure 6

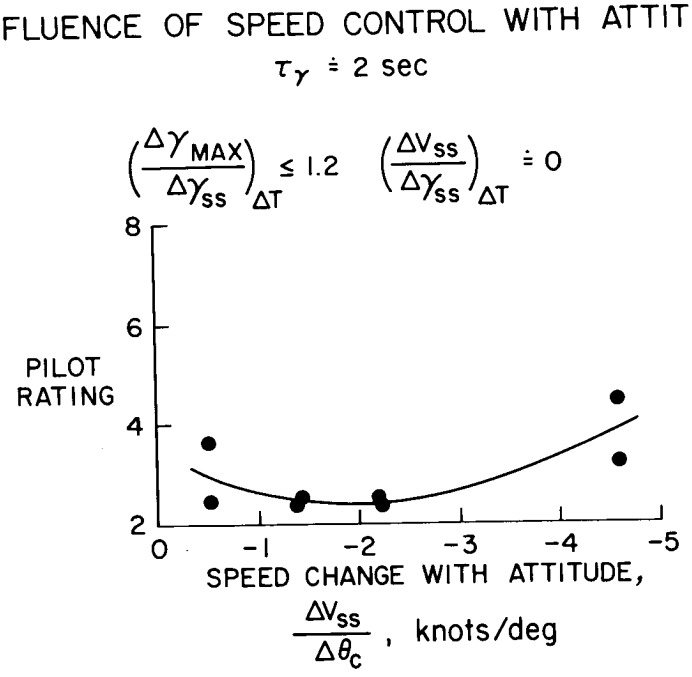

Figure 7

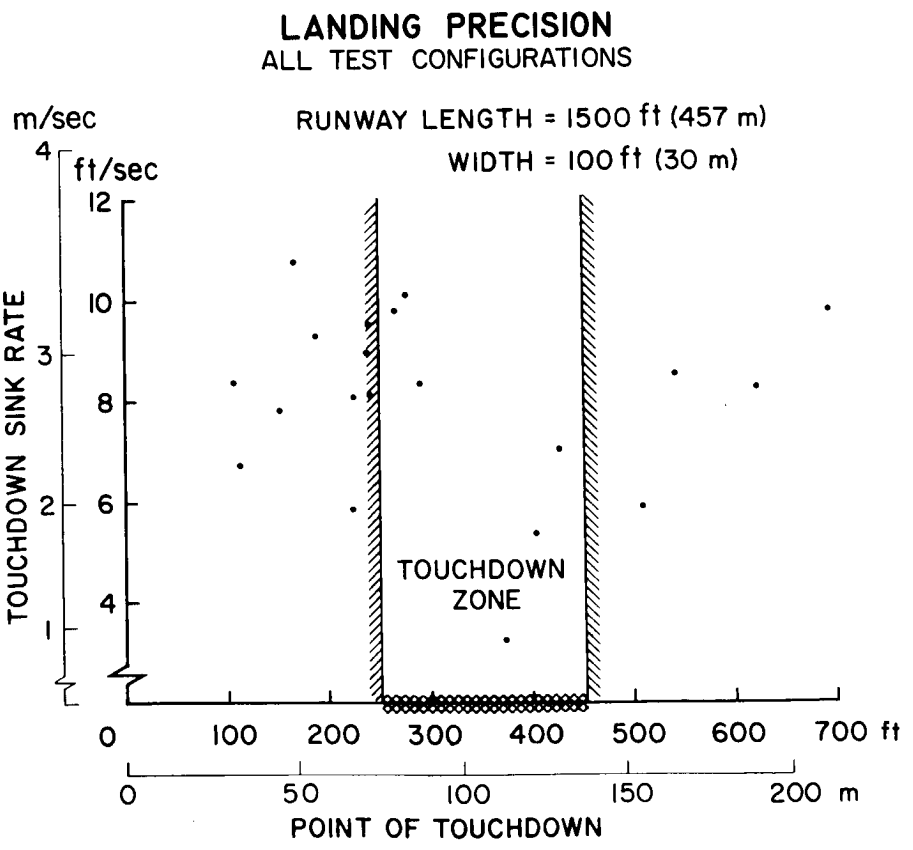

Figure 8

EFFECTS OF FLIGHT-PATH RESPONSE TO THRUST AND SPEED RESPONSE TO ATTITUDE ON LANDING PRECISION

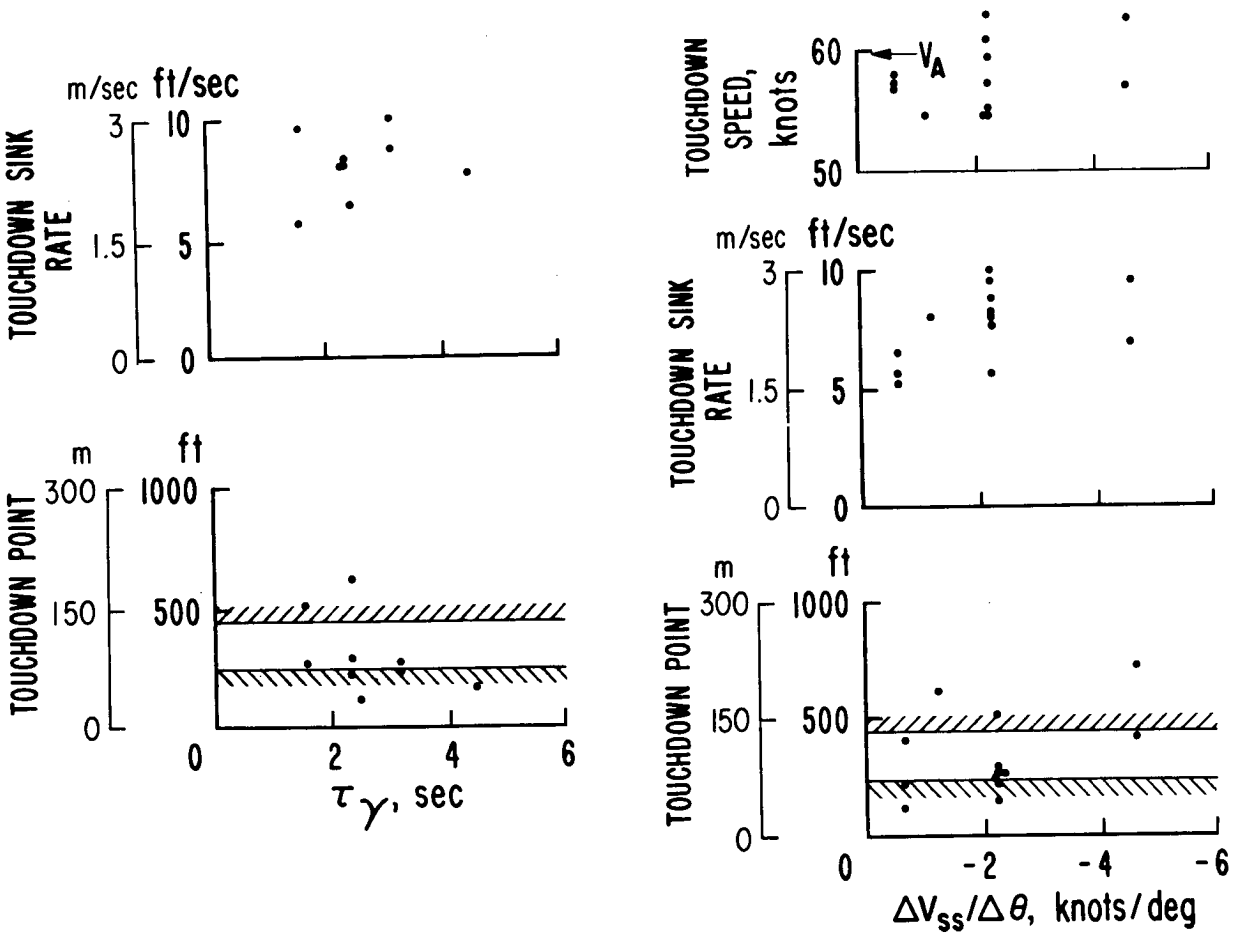

Figure 9

EXAMPLE STOL LANDING

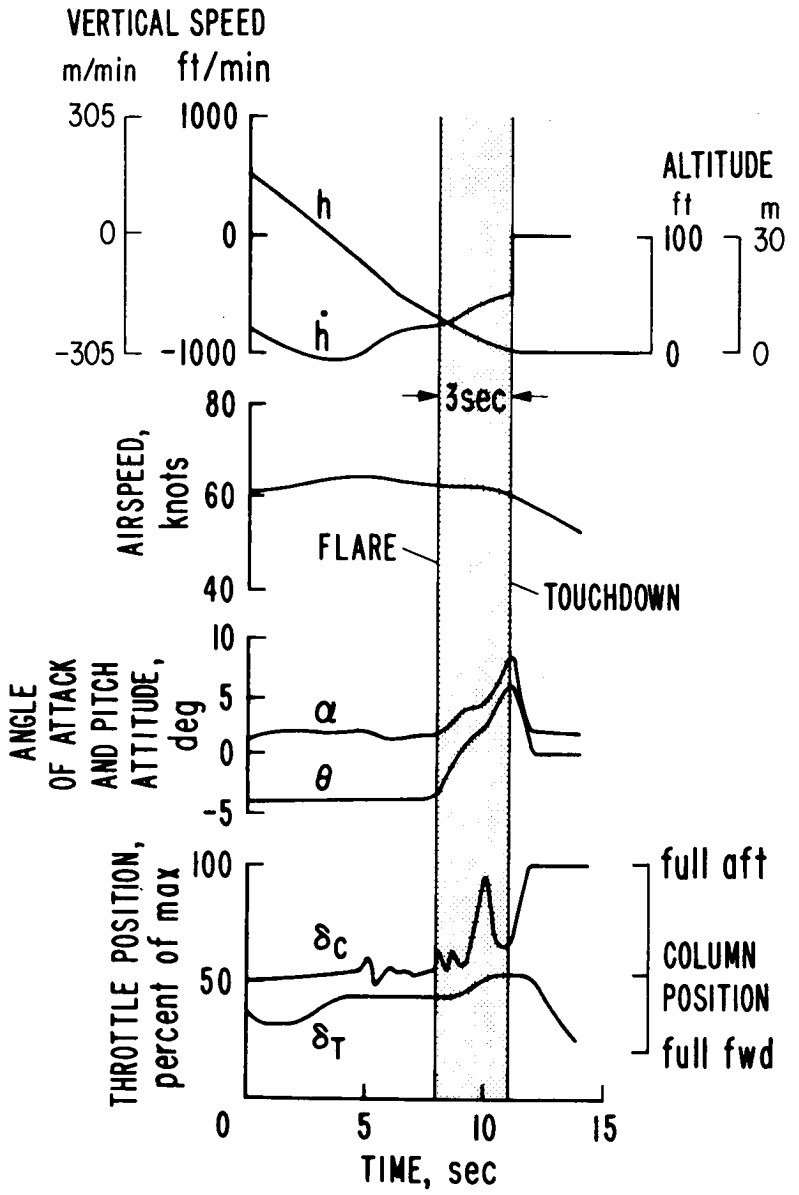

Figure 10

STUDY OF GROUND PROXIMITY EFFECTS ON POWERED-LIFT STOL LANDING PERFORMANCE

By James L. Hassell, Jr., and Joseph H. Judd
NASA Langley Research Center

SUMMARY

Data from wind-tunnel measurements are presented to show the magnitude of "adverse ground effects" on the longitudinal aerodynamic coefficients of a powered-lift STOL airplane. A steady-state analysis shows the changes in thrust and angle of attack required during the landing approach and flare as the airplane flies close to the ground.

The piloting problems that these ground effects may create were investigated with an in-flight simulator to find the consequences of lift loss during the landing-flare maneuver for a STOL transport. Flight tests were made at Princeton University using the variable stability Navion setup with STOL transport aerodynamics and control responses and were flown at design approach speeds and descent conditions. Although nearly all landings were made with ground contact in the designated touchdown zone, the sink rate at touchdown was higher than the generally accepted values for conventional aircraft. Landing-task difficulty was greater for the low-wing STOL configuration than for the high-wing STOL configuration because of the increased adverse ground effects produced by the closeness of the low-wing position to the ground during the landing flare.

16

INTRODUCTION

For conventional aircraft, ground effect produces a buoyancy characteristic during landing that is easily detectable by pilots. Wind-tunnel research on powered-lift models has indicated an exactly opposite effect commonly called "suckdown" as shown in reference 1. Concern over the consequences of this adverse ground effect on landing powered-lift STOL aircraft has led to the studies reported herein.

Briefly, these studies consist of the analysis of wind-tunnel test results of a powered-lift STOL transport model in and out of ground effect and the consequences of the changing aerodynamic characteristics on the capability of the aircraft to perform the landing-flare maneuver. In order to account properly for dynamic behavior during approach and landing, an investigation was undertaken with an airborne simulator which incorporated the powered-lift STOL transport aerodynamic and mass characteristics and which was capable of providing proper ground effect inputs. Some

important results of the in-flight simulation such as the influence of the ground effects on landing, comparisons of high- and low-wing STOL configurations, and the effect of a stability augmentation system (SAS) are presented.

SYMBOLS

b	wing span
C_L	lift coefficient
$C_{L,\infty}$	lift coefficient out of ground effect
$C_{L,trim}$	STOL transport lift coefficient in longitudinal trim
h	height of wing mean chord above ground
h'	height of flap trailing edge above ground
S	wing area
T	engine gross thrust
T/W	STOL transport thrust-weight ratio
W	STOL transport weight
W/S	STOL transport wing loading
$\ddot{\theta}$	angular acceleration in pitch

EFFECT OF GROUND PROXIMITY ON LONGITUDINAL AERODYNAMIC COEFFICIENTS

Figure 1 shows typical longitudinal aerodynamic data, lift, drag, and pitching-moment coefficients measured on an externally blown flap STOL transport model in the Langley V/STOL tunnel above a moving-belt ground plane. These test results are for flaps set to a landing deflection of 60° on a four-engine high-wing configuration. Data are presented to compare the out-of-ground-effect case with the in-ground-effect case.

For this powered-lift condition, ground effect causes a loss of lift, a reduction in drag, and a nose-down change in pitching moment.

Lift loss due to ground effect is plotted against wing height above the ground for several values of lift coefficient in figure 2. The variation of the lift coefficient with height was obtained by using the empirical relationship

$$\frac{\text{Lift in ground effect}}{\text{Lift out of ground effect}} = \left\{ \frac{1}{1 + \dfrac{0.000293\, C_{L,\infty}{}^2}{\sqrt{\left(\dfrac{h'}{b}\right)^2 + \left[4\left(\dfrac{h'}{b}\right)^2\right]^2}}} \right\}^2$$

This relationship was based on a Boeing-developed expression from a simple-image horseshoe-vortex analysis, modified to use the height of the flap trailing edge h' instead of the wing chord height h and fitted to the measured data of reference 1. The lift loss due to ground effect increases as wing height above the ground is reduced and the severity of the lift loss increases with increasing lift coefficient. The dashed line in figure 2 is representative of the wing height at touchdown for high-wing configurations. For powered-lift STOL airplanes operating at lift coefficients less than 3, the lift losses are minor. STOL transports, however, are projected to operate at approach lift coefficients as high as 4 to 5 where lift losses in ground effect are higher.

Figure 3, which was taken from reference 2, gives the relationship between landing field length and wing loading as a function of approach lift coefficient. This figure illustrates the reason lift coefficients of 4 to 5 are of interest. It can be seen that conventional jet transports operating at approach lift coefficients of 1.5 to 1.8 and with higher wing loadings have field-length requirements greater than 1200 meters (4000 feet). Low wing loading aircraft can, of course, operate into much shorter airports – approaching light aircraft capability. But to achieve STOL field-length capability with wing loadings of the order of 3800 to 4800 N/m^2 (80 to 100 lb/ft^2) requires approach at lift coefficients of 4 or higher.

The data presented in figures 1 to 3 were measured on a four-engine STOL transport with externally blown flaps. Figure 4 shows the lift losses due to ground effect for several powered-lift concepts such as the tilt wing, straight- and swept-wing conventional jet flaps, and the externally blown flap. (See refs. 1, 3, 4, and 5.) It is seen that the ground effects are independent of the type of powered-lift system used to produce the lift. The agreement of these data insures confidence that the current study of STOL ground effects during landing is applicable to other STOL concepts.

INFLUENCE OF ADVERSE GROUND EFFECTS ON THE LANDING FLARE

To understand better the problems associated with landing a powered-lift STOL, figure 5 presents part of a flight-path envelope for the out-of-ground-effect condition. These curves were derived from wind-tunnel tests of an externally blown flap STOL configuration with a flap deflection of 60^{o}. Flight-path angle is plotted against trimmed lift coefficient for several values of aircraft thrust-weight ratio indicated by the solid curves, and for a range of angles of attack indicated by the dashed curves. Point A is a typical approach condition corresponding to a 6^{o} glide-path angle at a lift coefficient of 4.2. To perform a flare from this approach condition, instantaneous normal acceleration can be obtained either by increasing throttle setting, by increasing angle of attack, or by a combination of the two. But, as indicated by figure 6, the influence of ground effect causes the flight-path envelope to shrink and shift to the upper left, and reflects both the lift loss and the reduction in drag. Point A of the original out-of-ground-effect envelope shifts to point B on the in-ground-effect envelope and indicates a steady-state descent angle of about 3^{o} for the case where the pilot does nothing – that is, if both throttle and angle of attack are held constant. Lift coefficient has decreased from 4.2 to about 3.8. Of course, an aircraft could not reach this steady-state condition corresponding to an abrupt increase in speed in the short time involved in the landing flare. Also, the pilot is going to take some positive action to generate normal acceleration for the flare, such as increasing power or angle of attack or both.

Point C represents the effect of increasing the angle of attack while holding the throttle constant and corresponds to the same lift coefficient in ground effect as point A for the out-of-ground-effect approach condition. The lift loss due to ground effect has been recovered, and the aircraft ends up with a steady-state condition in ground effect at the same speed as on approach but at a descent angle about half as steep as the original approach condition.

Point D represents the case where power is increased while angle of attack is held constant and corresponds to the same value of lift coefficient as the original approach condition. The increase in power has recovered the lift loss due to ground effect, and the STOL transport ends up with a steady-state condition in ground effect with zero flight-path angle.

The main point of this discussion is that despite the lift loss due to ground effect, when either increased power or angle of attack is used to flare the aircraft, rate of sink can be arrested. Zero flight-path angle should be achievable either with a reasonable power increase alone or with a combination of increased power and angle of attack.

FLIGHT SIMULATION OF APPROACH AND LANDING OF A FOUR-ENGINE STOL TRANSPORT

The STOL ground-effects problem could not be adequately assessed with ground-based simulators. Visual displays on the best ground-based simulators lack resolution and realism for those last few feet above the runway that are so important to judging when to initiate the flare. Therefore, a decision was made to investigate the problem of powered-lift STOL ground effects with an in-flight simulation so that more could be learned about the consequences of lift loss during the landing flare maneuver. Figure 7 illustrates the STOL transport configuration selected for this simulation study. It is about the same size and weight as the NASA projected QUESTOL aircraft, has a wing loading of 3600 N/m^2 (75 lb/ft^2), and a thrust-weight ratio of about 0.6. It is shown here as a high-wing configuration; however, both high- and low-wing configurations were simulated. Figure 8 shows the lift loss associated with the high- and low-wing configurations used in the simulation. The high-wing configuration experiences a lift loss of about 10 percent at ground contact, whereas the low-wing configuration at ground contact may lose as much as 25 percent.

The in-flight simulation was carried out under contract with Princeton University using the variable stability Navion shown in figure 9. This vehicle was chosen for several reasons: Its variable stability features could be adjusted to represent the STOL transport dynamic characteristics properly. A representative STOL stability augmentation system providing attitude command functions could be incorporated. The Navion could be flown at the actual approach speed and descent condition of interest in this study. The flap could be slaved to a sensitive onboard radar altimeter to simulate properly the lift losses due to ground effects. This radar altimeter could also be interconnected with the throttle and elevator of the Navion to simulate changes in drag and pitching moment due to ground effect.

Figure 10 illustrates the simulated STOLport and flight-test pattern. Runway markings were provided to establish a 60-meter (200-foot) long touchdown zone. Visual approach aids were set up to enable the pilots to hold the 6° approach angle. Tests consisted of setting up the approach condition about 2.4 kilometers (1.5 miles) out at an altitude of about 260 meters (850 feet) above ground level, holding the 6° approach angle down to a point where the flare was initiated, and then attempting to touch down in the designated landing zone as softly as possible. All landings were touch and go, so no evaluation of landing rollout was made. Pilots were asked to rate the landing task difficulty on the Cooper scale; and measurements were taken to determine rate of sink at touchdown, and the landing dispersion. Both Princeton and NASA test pilots were involved in the flight tests.

RESULTS OF IN-FLIGHT SIMULATION OF THE LANDING OF A FOUR-ENGINE STOL TRANSPORT

Some of the variables evaluated during the flight simulation of the approach and landing of a STOL transport are

(1) No ground effects

(2) High- and low-wing ground effects

(3) Longitudinal control power

(4) Longitudinal SAS on and off

(5) With and without atmospheric turbulence

(6) Engine thrust-response lag characteristics

(7) Three- and four-engine cases

Results related to items (1) to (4) are discussed in detail but first a few brief comments on items (5) to (7) are appropriate: Turbulence aggravated the landing task and caused poorer pilot ratings because of the increased workload. Thrust-response lag had to be kept low, especially for landings made by using only power to generate normal acceleration. A thrust-response time constant of 0.4 second was found to be the maximum permissible for this case. This time constant was found to be acceptable if the flare maneuver consisted of, first, the use of power, followed by an increase in angle of attack. This flare technique turned out to be the preferred method for landing the simulated STOL airplane because the pilots used the control column as a vernier in the flare maneuver after the throttle had been advanced to a preselected level. Sufficient thrust was available to perform powered flare with only three engines operating so that the additional thrust with four engines did not have any effect on either landing performance or task difficulty. The handling of lateral-directional asymmetries due to a failed engine, however, were not a part of this simulation. The rest of this paper will deal with landing performance for the three-engine thrust cases to compare various levels of ground effects, the effect of control power, and the effect of longitudinal stability augmentation.

Figure 11 shows a comparison of landing performance with and without simulated ground effects. These results were obtained for the "SAS on" condition – that is, the longitudinal stability augmentation system provided good frequency and damping characteristics; and longitudinal control was augmented with an attitude-command—attitude-hold function. Touchdown dispersion is plotted against rate of sink at touchdown. The pilots attempted to land within the 60-meter (200-foot) zone, and to touch down as softly as possible. With no ground effect, landings were made at low touchdown sink rates and within the landing zone. With high-wing ground effects, touchdown sink rates were considerably

higher – some landings with sink rates as high as 1.8 or 2.1 m/sec (6 or 7 ft/sec). Also, several landings were outside the touchdown zone. The main effect of the more severe ground effects for the low-wing case was somewhat harder touchdowns – over 2.4 m/sec (8 ft/sec) on one landing, and somewhat less dispersion.

The effect of SAS failure on landing performance is shown in figure 12. The data for the "SAS on" condition are the same as those presented in figure 11. The data for SAS off were obtained with the longitudinal SAS and the attitude-command—attitude-hold function inoperative. In general, the SAS-off landings showed somewhat more dispersion and slightly higher touchdown sink rates, especially for the simulated low-wing ground effects case. One landing exceeded 2.7 m/sec (9 ft/sec), and several landings were considerably short of the touchdown zone.

Figure 13 shows the effect of longitudinal control power for the high-wing ground effects case with SAS off. AGARD recommendations call for a minimum of 0.4 ranging up to 0.6 rad/sec^2. The landing results shown on the left were obtained with a value of $\ddot{\theta}$ of 0.26 – a value less than the AGARD minimum. Sink rates at touchdown ranged up to almost 2.4 m/sec (8 ft/sec) although most of the landings were made within the touchdown zone. The landings shown on the right were for a pitch control power higher than AGARD recommendations – 0.78 rad/sec^2. The marked improvement in landing performance is evident – only one landing exceeded 1.5 m/sec (5 ft/sec) sink rate; and the landing dispersion pattern for the most part is concentrated in the middle of the touchdown zone.

Figure 14 summarizes the effect of several variables on the pilot ratings of the landing task difficulty using the Cooper scale – low numbers are satisfactory and high numbers are unacceptable. All these results apply to landings using thrust corresponding to the three-engine emergency condition. In the first comparison, the severity of ground effect is shown to be a significant factor. These results were with SAS on. Task difficulty was rated $2\frac{1}{2}$ to $3\frac{1}{2}$ with no ground effects; and the ratings deteriorated to the order of 4 to $5\frac{1}{2}$ with low-wing ground effects. In the second comparison of figure 14, the effect of longitudinal SAS is shown to be an even more significant factor. Results are given for both the high-wing and low-wing cases. These results may be interpreted as the loss of SAS causing a deterioration of 2 to $2\frac{1}{2}$ points in pilot rating. In the last comparison of figure 14, longitudinal control power is shown to have a relatively minor effect on pilot rating. The results are for the SAS-off condition where any effects would not be masked by the SAS itself. Low control power was only about 1/2 point worse than high control power.

CONCLUDING REMARKS

Analysis of wind-tunnel data for a four-engine powered-lift STOL transport indicated the possibility that adverse ground effects might be a problem during the landing of the aircraft. The results of the flight simulation of approach and landing of a powered-lift STOL transport at a lift coefficient of 4.2 show that the ground effects may degrade the landing performance and the pilot rating of the landing-task difficulty. However, satisfactory ratings were obtained for the high-wing configuration when adequate stability augmentation was provided. Although nearly all landings were made with ground contact in the touchdown zone, the vertical sink rate at touchdown was higher for the STOL transport than the normal value of about 1 m/sec (3 ft/sec) for conventional transport aircraft. Landing task difficulty was increased for the low-wing STOL configuration as compared with the high-wing configuration because of the increased ground effects produced by the closeness of the low wing position to the ground during the landing flare.

REFERENCES

1. Vogler, Raymond D.: Wind-Tunnel Investigation of a Four-Engine Externally Blowing Jet-Flap STOL Airplane Model. NASA TN D-7034, 1970.

2. Wick, Bradford H.; and Kuhn, Richard E.: Turbofan STOL Research at NASA. Aeronaut. & Astronaut., vol. 9, no. 5, May 1971, pp. 32-50.

3. Goodson, Kenneth W.: Ground Effects on a Four-Propeller Tilt-Wing Configuration Over a Fixed and Moving Ground Plane. NASA TN D-3938, 1967.

4. Goodson, Kenneth W.: Effect of Ground Proximity on the Longitudinal, Lateral, and Control Aerodynamic Characteristics of a Tilt-Wing Four-Propeller V/STOL Model. NASA TN D-4237, 1967.

5. Turner, Thomas R.: A Moving-Belt Ground Plane for Wind-Tunnel Ground Simulation and Results for Two Jet-Flap Configurations. NASA TN D-4228, 1967.

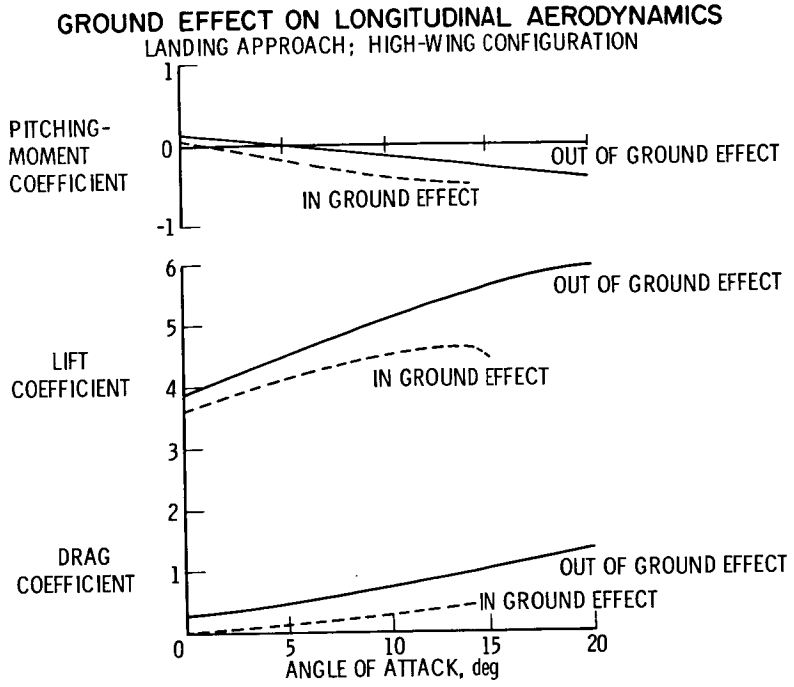

Figure 1

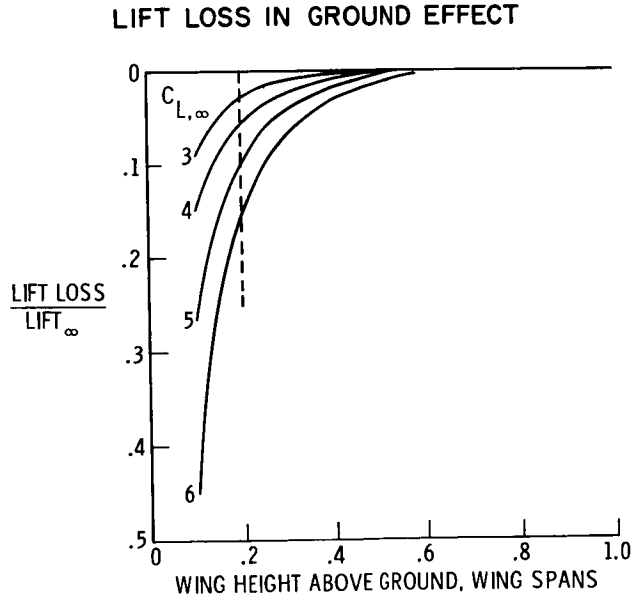

Figure 2

EFFECT OF LIFT COEFFICIENT ON AIRPLANE LANDING CHARACTERISTICS

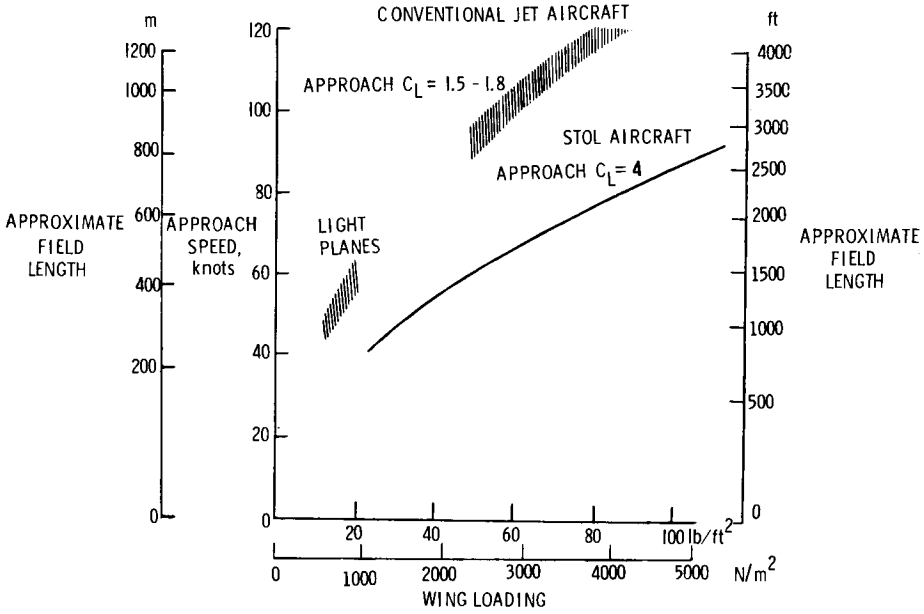

Figure 3

EFFECT OF CONCEPTS ON LIFT LOSS IN GROUND EFFECT

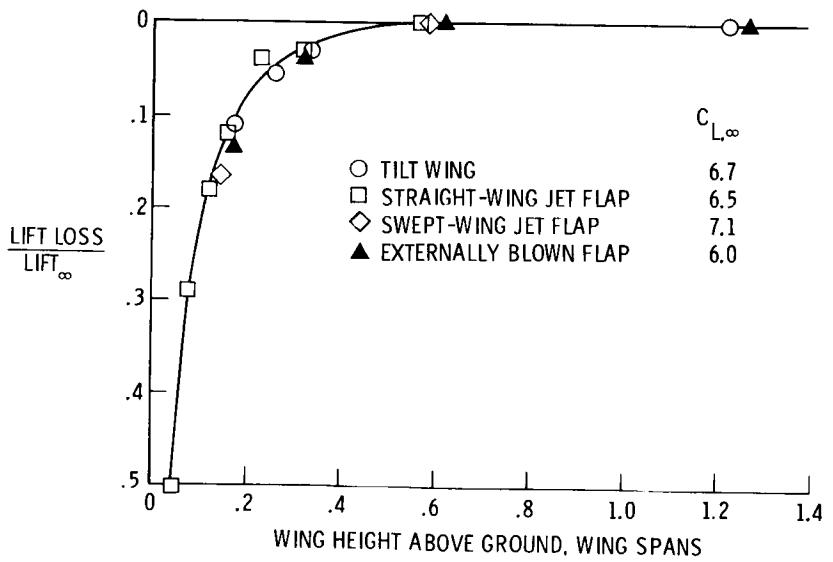

Figure 4

FLIGHT-PATH ENVELOPE OUT OF GROUND EFFECT

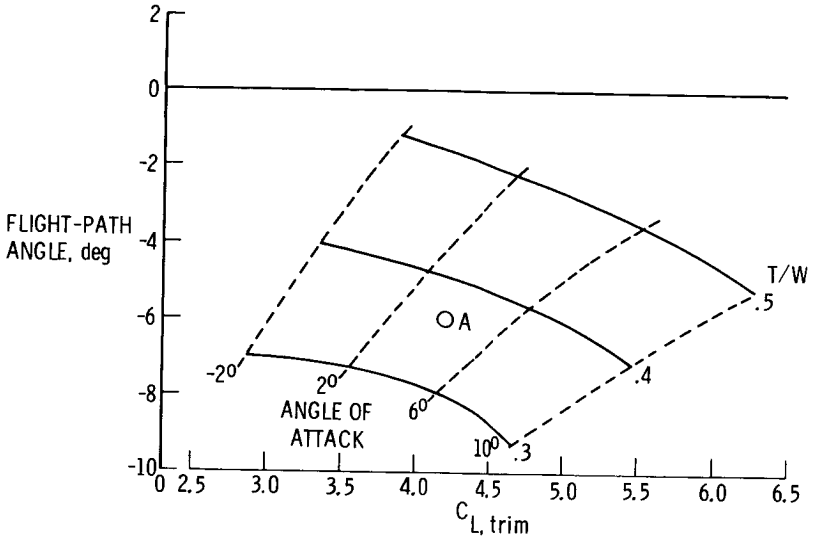

Figure 5

FLIGHT-PATH ENVELOPE IN GROUND EFFECT

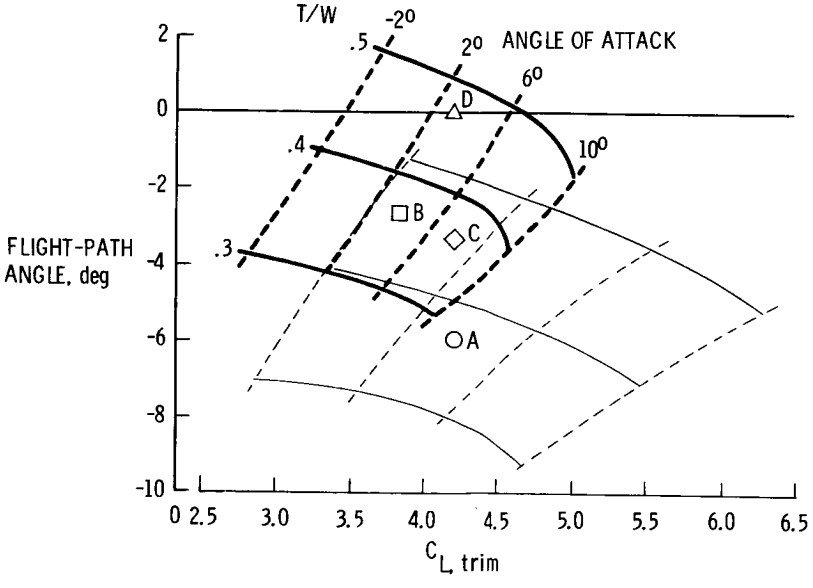

Figure 6

POWERED-LIFT STOL CONFIGURATION USED IN GROUND EFFECTS STUDY

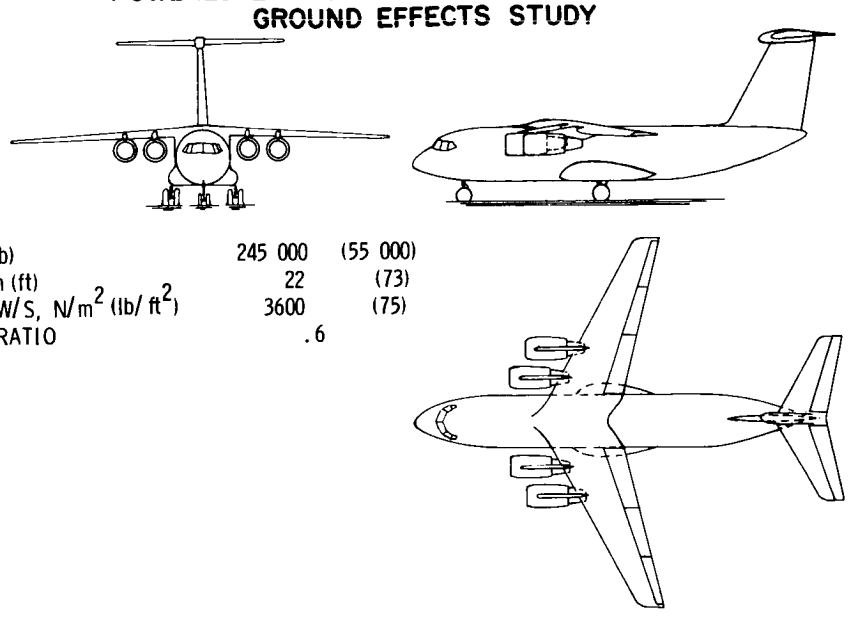

WEIGHT, W, N (lb)	245 000	(55 000)
WING SPAN, b, m (ft)	22	(73)
WING LOADING, W/S, N/m^2 (lb/ft^2)	3600	(75)
THRUST-WEIGHT RATIO	.6	

Figure 7

EFFECT OF WING HEIGHT ON LIFT LOSS IN GROUND EFFECT

$C_{L,\infty} = 4.5$

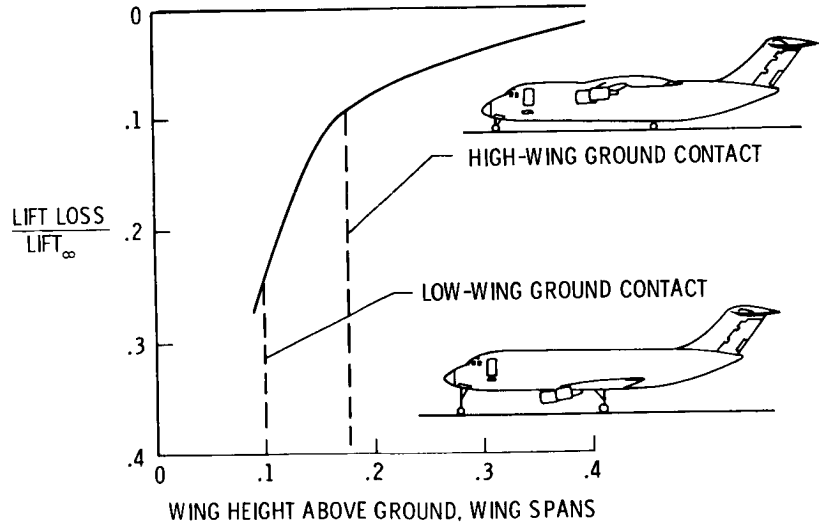

Figure 8

Figure 9

SIMULATED STOLPORT AND FLIGHT-TEST PATTERN

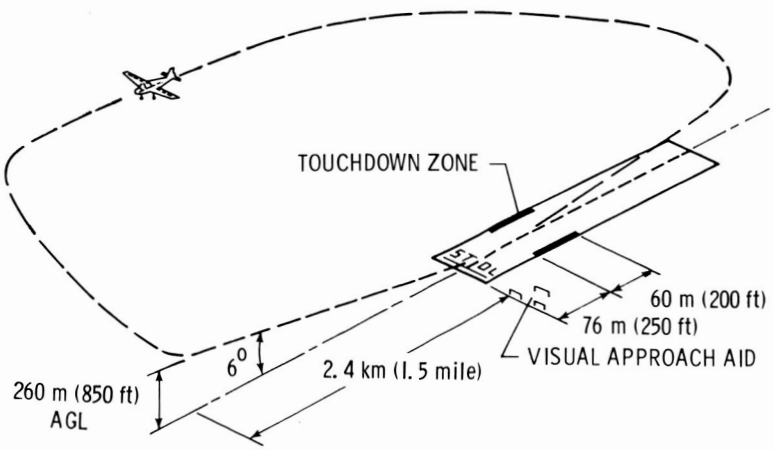

Figure 10

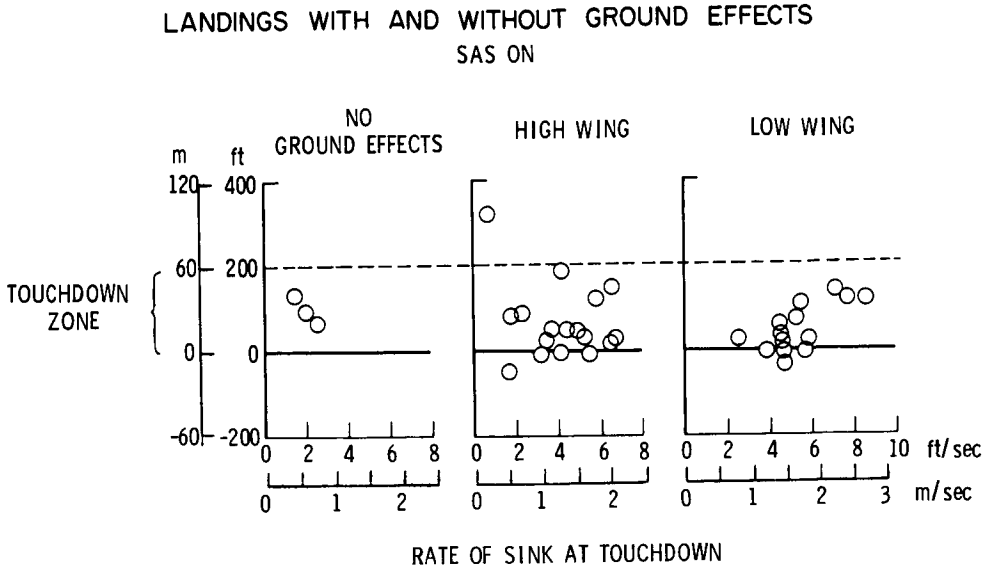

Figure 11

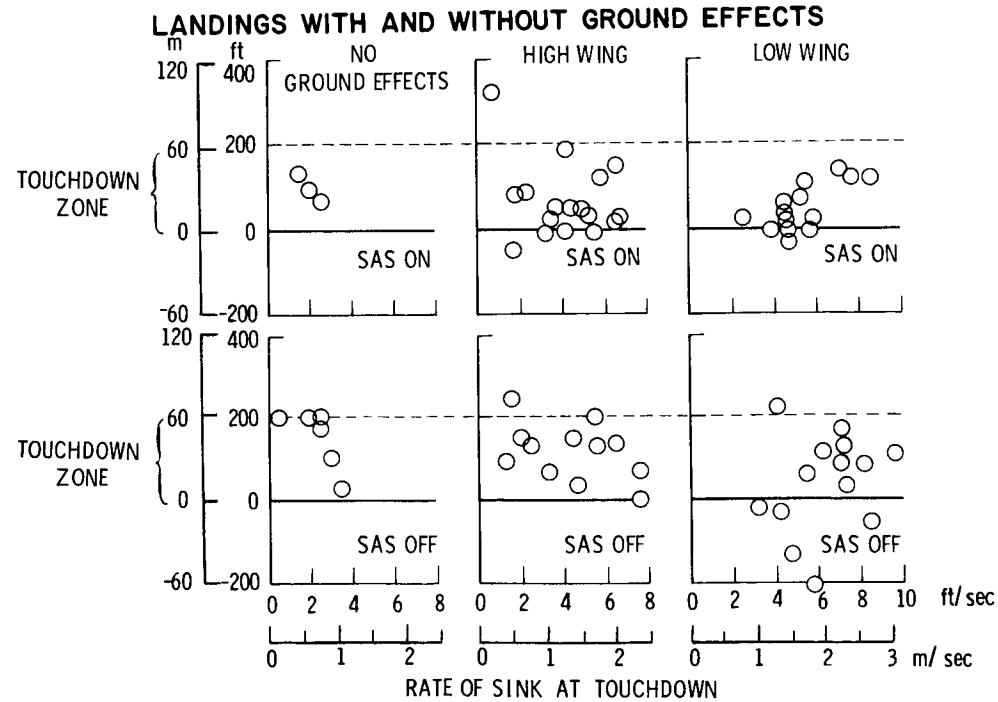

Figure 12

LANDINGS WITH HIGH-WING GROUND EFFECTS

SAS OFF

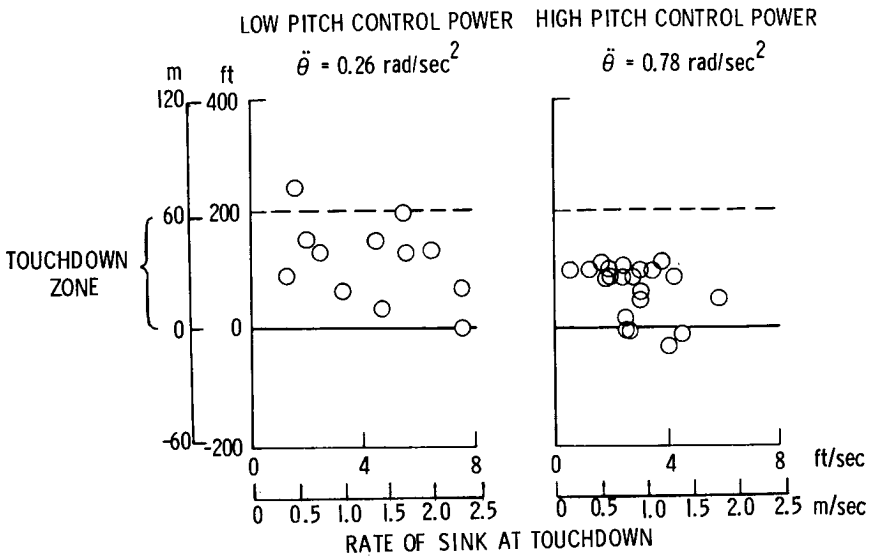

Figure 13

EFFECT OF LANDING SIMULATION VARIABLES ON PILOT RATING (COOPER SCALE)

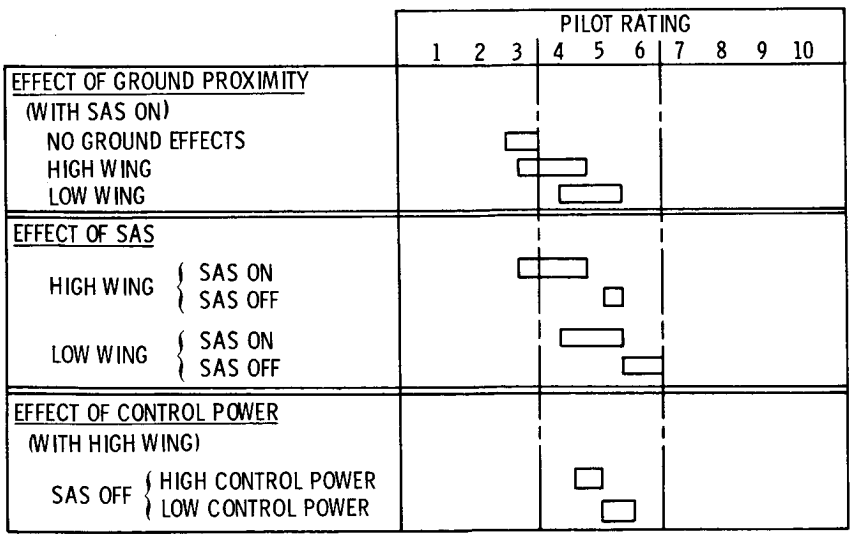

Figure 14

STATUS OF STOL RIDE QUALITY AND CONTROL

By D. William Conner and W. Elliott Schoonover, Jr.
NASA Langley Research Center

INTRODUCTION

Use of jet transports by all first level carriers and many second level carriers has established high standards of ride quality which the traveler now expects on all airlines, large or small. Conventional jet transports, however, are not always practical for all passenger-carrying situations. In designing new aircraft which will accommodate these special situations, a question naturally arises concerning the relative importance given ride quality by the passengers. This question was addressed in depth at an NASA sponsored symposium on vehicle ride quality held at the Langley Research Center in July 1972 (ref. 1).

Figure 1 presents the findings of a traveler-opinion survey conducted in a study for NASA by the University of Virginia (paper 11 of ref. 1). Asked the importance of various factors associated with transportation, travelers rated these 10 as the most important. They are listed according to average rating.

Safety and reliability rank at the top in importance followed by time saving and convenience. Ride quality is considered equal in importance to cost and is rated between "Somewhat important" and "Very important." The remaining four factors have a lesser rating. This nonquantitative opinion-type information certainly must be used with some care in its influence on research programs or aircraft specifications. It does, however, provide considerable food for thought concerning factors which may influence traveler acceptance and use of a particular vehicle system.

Ride quality is a general term relating to the degree of well-being felt by the passenger and comprises many factors, some psychological and some physiological. The following ride-quality factors were rated important by travelers queried in the University of Virginia opinion survey:

Motion and vibration
Cabin noise
Cabin temperature
Change in cabin pressure
Seat comfort

Motion and vibration is a factor which affects the whole aircraft. Noise, temperature, change in pressure, and seat comfort relate to conditions within the cabin which generally can be adequately addressed by existing technology. The factor of motion and

vibration presently is not so amenable to treatment and is the principal subject of discussion in this paper.

Compared with jet CTOL airliners, what is the relative level of motion and vibration which could be expected of STOL vehicles? Figure 2 graphically illustrates the situation. The peak vertical acceleration in g units is presented as a function of occurrence in percent time measured over extended periods of cruise flight for a 130-passenger Boeing 727 jet CTOL vehicle and a 52-passenger Breguet 941 turboprop STOL aircraft (data from ref. 2). The STOL vehicle experienced maximum acceleration peaks of at least twice the magnitude of those of the jet CTOL aircraft; the incidence of any given peak acceleration was many times greater for the STOL vehicle. Peak lateral accelerations, which were also measured but are not presented herein, showed the same relative differences between the two vehicles. Certainly the ride of the STOL aircraft could be expected to be much rougher than that of the jet CTOL aircraft. It should be noted that the STOL aircraft was cruising at a lower altitude and a lower speed than the CTOL aircraft, which undoubtedly influenced ride quality. Such differences in operation, however, would probably be the normal situation in air carrier use of these two types of vehicles. The wing loading for the Breguet 941 was less than one-half that of the Boeing 727 and this may have influenced the response. However, for equal wing loadings, weights, and flight speeds, STOL vehicles tend to have a greater response to gusts than CTOL vehicles because of the inherently larger tail surface areas required for trim and stability. See, for example, figure 21 of reference 3.

Figure 3 illustrates the technology areas which are being addressed in this paper. As indicated on the left side of the figure, inputs to the aircraft are transmitted through and modified by the aircraft; this causes motions at the seat which, in turn, cause a reaction by the passenger. One technology area of interest concerns ride-smoothing systems which can be used to modify the motions at the seat caused by given perturbing inputs. The other technology area concerns ride-quality criteria which define, in quantitative terms, seat motions or vibrations that are, or are not, acceptable to passengers.

RIDE-QUALITY CRITERIA

Meaningful and comprehensive ride-quality criteria suitable for designing transport aircraft presently do not exist. The bulk of prior effort in developing criteria has been directed toward ground vehicle application and has been limited to only a few degrees of freedom. Figure 4(a) presents reduced-comfort boundaries which have been proposed by the International Standards Organization and are presently being circulated for approval to representatives of the various member nations of the organization (paper 9 of ref. 1). It should be emphasized that NASA is not proposing or endorsing these standards. The boundaries, which are a distillation of the results of many prior studies, are expressed

in terms of rms acceleration as a function of frequency. Acceleration levels below the boundaries are rated acceptable and those above the boundaries are rated unacceptable. Boundaries are given for vertical and lateral motions only and are shown for a 1-hour exposure period. A family of such boundaries differing in magnitude has been proposed for other exposure periods. The boundaries shown are for single-degree-of-freedom conditions and may shift when more than one degree of freedom is involved (paper 5 of ref. 1). It should be noted that emphasis has been placed on defining boundaries in the higher frequency or "vibration" domain with no boundary proposed below 1 Hz, which may be dubbed the "motion" domain. Such a cut-off is typical of previously proposed criteria; in fact, some criteria do not extend below 5 Hz.

Figure 4(b) presents the relation of the aircraft situation to the proposed boundaries. At the bottom of the figure is shown the frequency range of principal sources of aircraft motion: namely, flight maneuvers, pilot-induced oscillations, and response to turbulence. (These data are from paper 9 of ref. 1.) These motions occur in the very low frequency range, generally below 1 Hz. The figure also shows a motion-sickness region known to exist at frequencies below 1 Hz (paper 1 of ref. 1). This region is not covered by the ISO draft standard which addresses principally the problem of minimizing discomfort from resonances of various parts of the body in the frequency range from 5 to 15 Hz. Obviously, a need exists for criteria which extend down to at least 0.1 Hz. Also, since an aircraft is subject to angular motions of considerable magnitude, angular degrees of freedom need to be considered as well. (See paper 11 of ref. 1.) Aeronautical interests have only recently addressed this technology area.

One investigation discussed in the symposium on vehicle ride quality relates directly to STOL ride-quality criteria and was carried out for NASA by Princeton University (paper 4 of ref. 1). Exploratory flight experiments were conducted with a variable stability Navion shown in figure 5. The Navion, specially outfitted to serve as an in-flight simulator, was also used in the investigation discussed in paper 16 by James L. Hassell and Joseph H. Judd. In the ride-quality investigation, the aircraft responses being simulated were those of a blown flap STOL transport having a 3.4-kN/m^2 (70 lb/ft^2) wing loading and operating at a 70-knot approach speed. Two pilots alternated as a passenger in the rear seat of the aircraft and rated the quality of ride for closely controlled motions of the aircraft. A pilot's opinion of ride comfort in the close quarters of this aircraft admittedly may not be exactly that of the average passenger in an airliner, but it should provide qualitative information useful in pointing out areas where more refined experiments are needed.

The principal results of this study are briefly noted. Ride discomfort occurred when the aircraft response to moderate isotropic turbulence input exceeded $0.05g_{rms}$ in vertical motion which is in general accord with the ISO proposed reduced-comfort bound-

ary. Ride discomfort also occurred when rms angular velocity response to turbulence exceeded 5^{o}/sec in yaw velocity or 13^{o}/sec in roll velocity. Also, when repeated S-turns were made in level flight and smooth air, ride discomfort occurred when rms roll rates exceeded 20^{o}/sec. There are two points to be made from these results. First, ride-quality considerations may impose some restrictions on the magnitude and kind of terminal area maneuvers (such as those that involve rather tight turns and high roll angles) which are being considered for STOL operations. Second, the results conclusively indicate that criteria are needed which include more than just vertical and lateral motions.

The following factors are being investigated in detail by NASA in developing comprehensive ride-quality criteria:

(1) Vertical and lateral acceleration effects down to very low frequencies

(2) Longitudinal deceleration (limited principally to runway braking conditions)

(3) Roll, pitch, and yaw angular velocities and/or accelerations

(4) Effects of duration and randomness of disturbances in aircraft due to turbulence or gust inputs and time between disturbance occurrences

Time between disturbances is important since a passenger's reaction to disturbances is influenced by the immediate past history of events.

(5) Interactive effects between the various degrees of freedom of motion, between motion and cabin environment, and between motion and visual cues

(6) Types and percentages of travelers satisfied

Information must be obtained in a manner which can be related to the traveling public and to what percentage are satisfied with the ride for a given degree of disturbance. It is impossible to satisfy all of the travelers all of the time; therefore, the aim is to develop criteria which can be applied by the user for his particular goal of percentage satisfaction.

Investigations of ride-quality criteria are being carried out by NASA at the Langley Research Center and at the Flight Research Center. At Langley, the investigations utilize commercial carrier vehicles and research aircraft and three ground-based motion and vibration simulators. One of these simulators (fig. 6) was designed specifically for ride-quality studies. The reduced-scale model, temporarily situated on the left, shows the type of mechanism which provides motions in three degrees of freedom, the segment of the passenger compartment, and a passenger seat. The test subject compartment, here shown with the front wall removed, realistically simulates a segment of an airliner interior. Either four first-class seats or six tourist-class seats can be accommodated. At the Flight Research Center, the investigations utilize the variable-stability general-purpose airborne simulator (GPAS). Details of these simulators and plans for their use in ride-quality studies are given in papers 12 and 13 of reference 1.

RIDE-SMOOTHING SYSTEMS

Ride-smoothing systems may be employed to reduce the motions at the seat. Passive control systems can be effective within limits, but the real payoff in comfort is offered by active control systems. Presently, analysis indicates that active control systems (ACS) can provide a substantial degree of ride smoothing. For example, see reference 4. The required performance of the ACS components needed is within the current technology. Considerable in-flight service experience with active control systems used in applications other than for ride control is being obtained. The B-1 bomber will incorporate an active control system for ride smoothing of the pilot's compartment.

A STOL ride-control development program has been initiated with the objective of generating ride-control technology through development and evaluation of an active control system specifically designed to provide ride smoothing on a STOL vehicle. Although much can be learned through analysis, there are deficiencies in technology for translating analysis results into operating hardware. The general approach being followed is to select an existing STOL vehicle for trial and then carry out a study to establish feasibility of a control system or systems to smooth the ride and generate system trade-off data. If the results of the study appear sufficiently attractive, a system will then be designed and installed. It will be evaluated first by flight testing and then by airline use. Use by an airline requires an FAA certificated aircraft. Therefore, selection of a vehicle for study becomes narrowed by the need for an existing certificated STOL aircraft. The De Havilland Twin Otter, shown in figure 7, was selected as the one airplane which most appropriately meets these requirements. It carries 20 passengers and has a maximum wing loading of 1.4 kN/m^2 (30 lb/ft^2). A somewhat larger aircraft with heavier wing loading would have been preferred, but no such certificated STOL vehicle is presently in use in this country.

The first phase of this program is now underway and consists of several parts. A mathematical model of the aircraft dynamic response to inputs has been derived and exercised to determine the ride-quality characteristics of the basic vehicle and is presently being used to evaluate various candidate active control systems which vary in complexity and provide various degrees of ride smoothing. Also to be evaluated are weight and volume penalties, ease of certification, and system cost. From this evaluation study, trade-off information will be available for several systems. The study by The Boeing Company, Wichita Division, was started in July 1972 and is not yet completed.

The gust response characteristics of the basic aircraft are presented in table I. For three flight conditions, the rms responses have been calculated for the gust input levels indicated. During gusty flight conditions, only about 1 percent of the gusts exceeds these values. Even though exact criteria for ride comfort are lacking, response would probably

not be objectionable if below $0.03g_{rms}$ in the vertical direction, if below $0.015g_{rms}$ in the lateral direction, and if below 4^{o}/sec rms for each of the three angular velocities. Only pitch, roll, and yaw velocity response levels are considered to be acceptably low. Accordingly, system studies are being directed principally toward reduction of the vertical and lateral responses.

The studies have progressed sufficiently to illustrate some results. The vertical responses that can be obtained with three different ride-control systems are presented in table II. As in table I, the rms response to a 1-percent-exceedance gust input has been calculated for take-off, cruise, and landing conditions. The first system consisted of using ailerons (40 percent authority) deflected in the same direction rather than differentially. When compared with the characteristics of the basic aircraft, the system response was decreased substantially in the take-off and cruise modes but only slightly in the landing approach mode with flaps deflected. Adding the elevator (25 percent authority) further decreased the response for take-off and cruise but did not alter response for landing. Adding a biased spoiler to the system in the landing approach mode did effect a decrease in response but not as much as desired. Results to date appear promising. As the program progresses and more is learned, the technology will be factored into studies with newer and more advanced STOL vehicles.

CONCLUDING REMARKS

Ride quality for STOL aircraft is considered to be an important factor in passenger acceptance. A need exists for development of comprehensive and meaningful ride-quality criteria, and an NASA program is now underway for such criteria development. Ride quality may impose restrictions on the magnitude and kind of terminal-area maneuvers that have been considered for STOL operations. These restrictions generally would involve the angular degrees of freedom for which exploratory flight studies indicate upper boundaries will probably be dictated by ride-quality considerations. The ride quality of STOL aircraft can be improved by use of active control systems. Such systems for smoothing the ride are considered to be within the present state of the art, and only technology details and demonstration need to be carried out.

REFERENCES

1. Anon.: Symposium on Vehicle Ride Quality. NASA TM X-2620, 1972.

2. Conner, D. William: Ride Quality – An Increasingly Important Factor in Transportation Systems. Paper presented at 1971 International IEEE Conference on Systems, Networks, and Computers (Oaxtepec, Mexico), Jan. 1971.

3. Marks, M. D.; and Carpenter, D. O.: Low Speed Handling Characteristics of the STOL Aircraft. AIAA Paper No. 70-1332, Oct. 1970.

4. Holloway, R. B.; Thompson, G. O.; and Rohling, W. J.: Prospects for Low Wing-Loading STOL Transports With Ride Smoothing. J. Aircraft, vol. 9, no. 8, Aug. 1972, pp. 525-530.

TABLE I.- CALCULATED GUST RESPONSE OF BASIC AIRCRAFT

[Gust input: 2.0 m/sec rms vertical; 2.0 m/sec rms lateral]

Flight mode	Vertical acceleration, g_{rms}	Lateral acceleration, g_{rms}	Pitch, roll, and yaw velocities, deg/sec
Take-off	0.088	0.021	<2.2
Cruise	.125	.028	
Landing	.101	.045	

TABLE II.- CALCULATED EFFECTS OF RIDE-CONTROL SYSTEM

Flight mode	Vertical response, g_{rms}, to gust input			
	No RCS	Aileron	Aileron + elevator	Aileron + elevator + spoiler
Take-off	0.088	0.048	0.029	0.029
Cruise	.125	.045	.022	.022
Landing	.101	.082	.082	.055

RELATIVE IMPORTANCE OF RIDE QUALITY

FROM TRAVELER SURVEYS

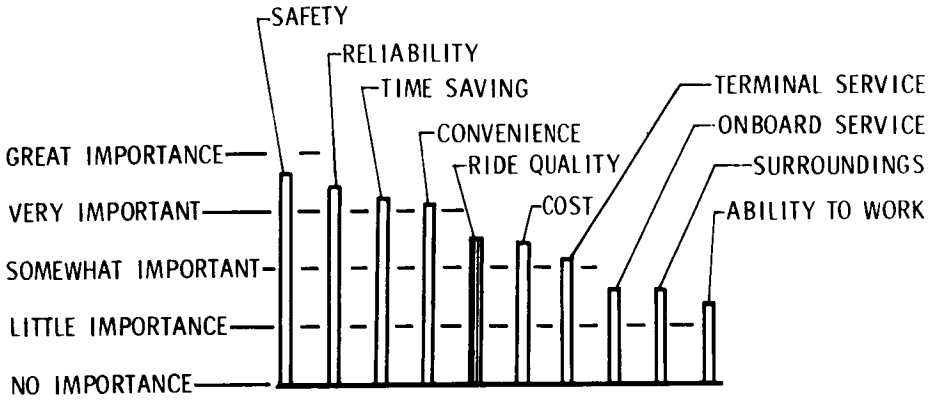

Figure 1

INCIDENCE OF MOTION AND VIBRATION

CRUISE CONDITION

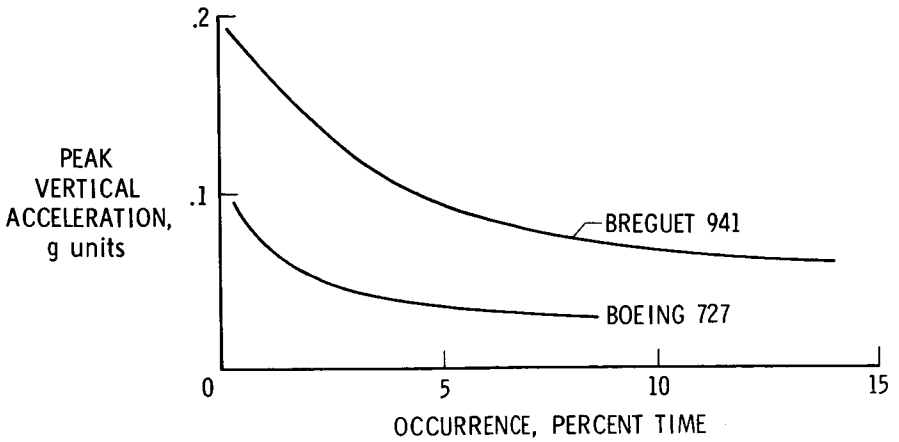

Figure 2

TECHNOLOGY AREAS PRESENTLY ADDRESSED
FOR MOTION AND VIBRATION

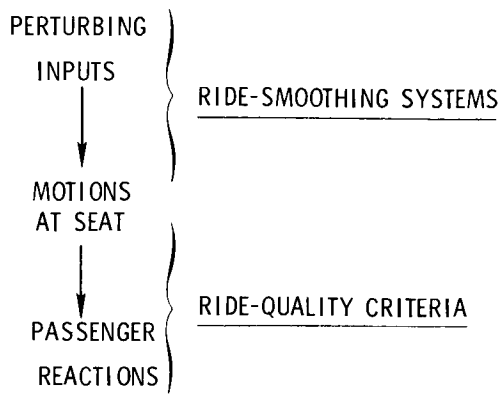

Figure 3

PROPOSED REDUCED-COMFORT BOUNDARIES

ISO DRAFT INTERNATIONAL STANDARD 2631
(1-HOUR EXPOSURE CONDITION)

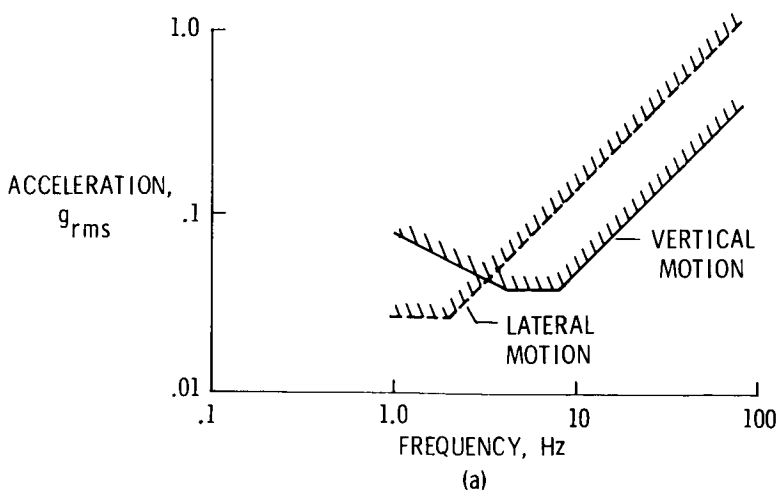

Figure 4

PROPOSED REDUCED-COMFORT BOUNDARIES

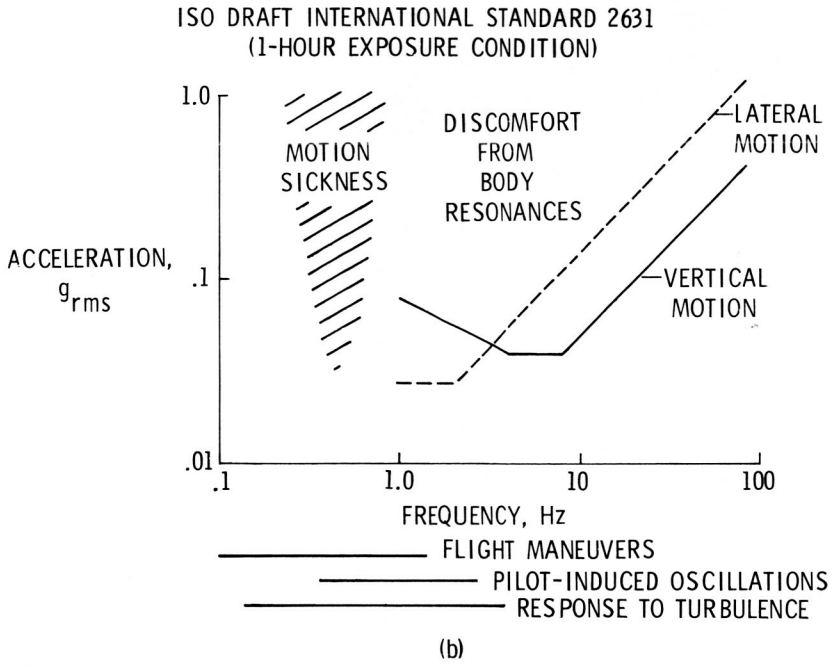

(b)

Figure 4 – Concluded

NAVION IN-FLIGHT SIMULATOR

Figure 5

LANGLEY PASSENGER RIDE-QUALITY APPARATUS

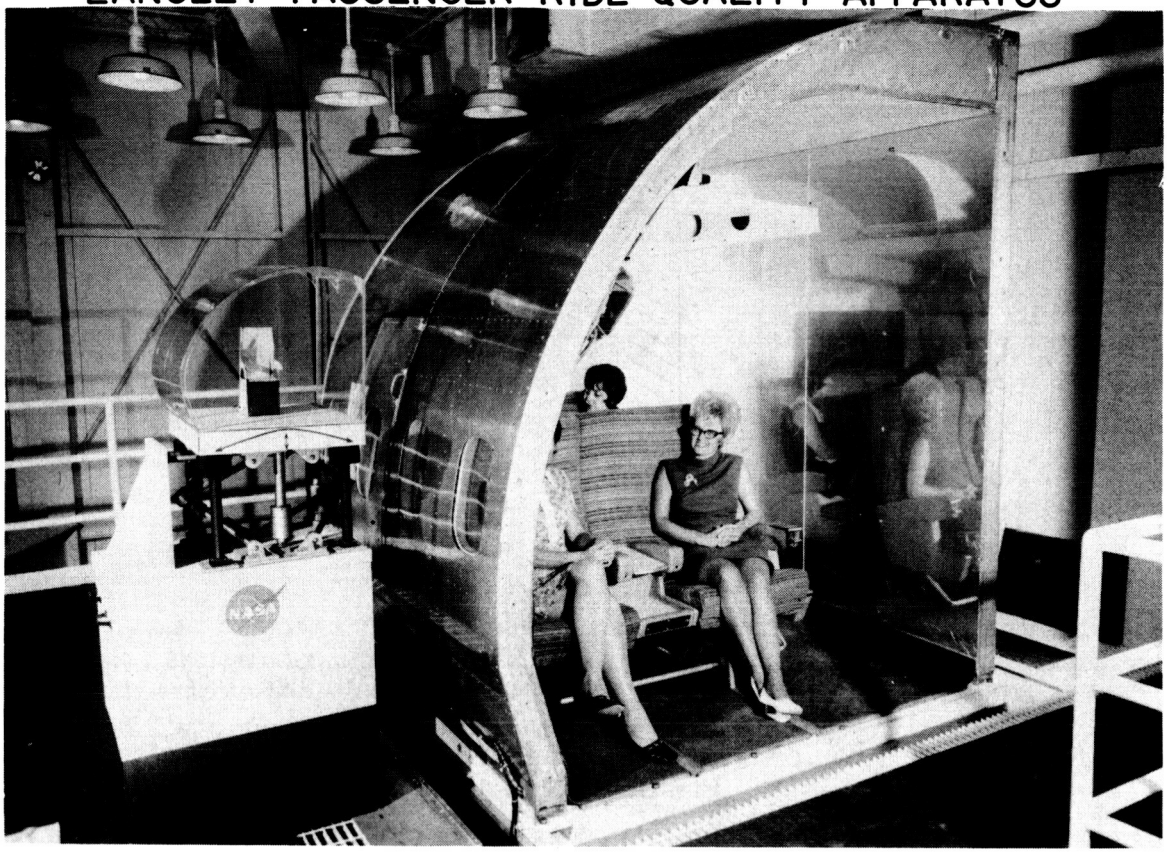

Figure 6

TWIN OTTER AIRCRAFT

Figure 7

HEAD-UP DISPLAYS FOR STOL VISUAL APPROACHES

By Everett A. Palmer
NASA Ames Research Center

and

Fred W. Cronn
San Jose State University

SUMMARY

A simulation study was conducted to determine the effectiveness of a simple head-up display in improving glide-slope tracking performance during steep visual approaches in a STOL aircraft. The head-up display featured an attitude-stabilized horizon bar and glide-slope reference bar parallel to and 7.5^{o} below the horizon bar. On some approaches a flight-path marker symbol showing the projected ground impact point was also displayed. Half of the approaches were flown in a conventional mode in which the pilot changed pitch attitude to correct for height errors. The remaining approaches were flown in a direct-lift mode in which the pilot modulated thrust to change the flight-path angle without pitching the aircraft.

Use of the head-up display resulted in a large increase in glide-slope tracking precision when compared with approaches made without the display. The addition of the flight-path marker symbol resulted in a further but smaller increase in precision. There were no significant differences between the two control modes for either of the displays.

INTRODUCTION

During a visual landing approach, a pilot needs two kinds of continuous information: (1) the present aircraft position relative to the glide-slope approach angle and (2) flight-path vector information which tells him where he is going. Two variations of a head-up display (HUD) which depicted the glide-slope and flight-path angles were evaluated in this study. The objective was to determine the capability of the HUD to aid the pilot in maintaining a desired glide-slope angle to the runway in a simulated STOL aircraft during night visual approaches.

Previous HUD studies can be classified into two basic areas. The first area is directed toward the effectiveness of the HUD as a guidance system in nonvisual approaches. The second area, which requires less complex HUD symbology, concerns its application as an electronic aid for insuring consistently safe visual approaches. This study is concerned with the second area.

Without electronic assistance many accidents have occurred during visual approaches, most of them occurring at night. During the first 8 years of commercial jet operations approximately 16 percent of the major accidents occurred during night visual approaches over unlighted terrain or water toward well-lighted cities and airports. (See ref. 1.) The night visual problems associated with present-day aircraft operations are amplified in STOL aircraft operations because of the slower speeds, steeper approach angles, and other factors.

Although the visual problems will be increased in future planned STOL aircraft operations, certain visual cues used today will still remain a basic part of the problem. A visual cue used for determining altitude error from a specified glide-slope angle is illustrated in figure 1. It is the perceived distance of the runway aim point below the horizon. This distance appears to remain constant throughout the approach when the aircraft is maintained exactly on the glide slope because the angle of elevation from the aim point is constant. The angle of elevation (glide-slope angle) also is equivalent to the depression angle of the aim point below the horizon. If the pilot adjusts his flight path so that the depression angle of the aim point below the horizon remains constant, he will maintain a constant glide-slope angle. That this cue or other cues to glide-slope angle are not always adequate is attested to by the number of accidents which occur during nonprecision visual approaches.

STOL aircraft visual approaches will result in additional visual problems with an increased need for precise glide-slope tracking. The steeper approach angle (7.5° instead of 3°) causes the distance between the horizon and runway aim point to be larger which is expected to cause estimates of small changes in glide-slope angle to be more difficult. The visual problem is further aggravated by the planned location of STOLports near or within cities. Substantial blocking of the true horizon reference may occur because of nearby high-rise buildings. The city light patterns at night with many elevated lights also may cause the pilot to make glide-slope corrections in relation to an invalid true horizon reference. This condition has been shown to occur in earlier simulator studies. (See refs. 2 and 3.) The head-up display evaluated in the present study was designed to portray both a gyro-stabilized true horizon reference and a 7.5° glide-slope reference to counter these visual problems. The glide-slope reference was provided by a pitch- and roll-stabilized glide-slope reference bar (dashed bar in fig. 2) that was parallel to and 7.5° below the true horizon. The display showed the pilot that he was on a 7.5° glide slope to the ground points superimposed by the glide-slope reference bar.

Concurrent with determining the aircraft position relative to the glide-slope angle, the pilot must determine where his flight-path vector is taking him so he can make appropriate pitch corrections to maintain or return to the desired glide-slope angle. Two visual cues used to determine his flight-path vector are (1) expansion cues and (2) aircraft pitch attitude.

Figure 3 shows that as an aircraft descends on the final approach, all points on the ground appear to expand outward from the one point where the aircraft flight-path vector intersects the ground. Longitudinal changes in the location of this point relative to the runway aim point tell the pilot that his flight-path angle has changed. Experimental studies (ref. 4) have shown that it is difficult for pilots to use the expansion cue because of the low angular rates of expansion until the aircraft is close to the runway. The slow approach speeds of STOL aircraft further reduce the usefulness of this cue to flight-path angle because the expansion rate will be even less. For these reasons the head-up display also incorporated a flight-path marker symbol (the ◇ in fig. 2) which superimposed the point where the flight-path vector intersected the ground.

In present-day conventional aircraft, pitch attitude furnishes an indirect visual cue to flight-path angle. Changes in flight-path lag approximately 0.5 sec behind changes in pitch attitude. In the steady state, the two changes are separated by the trim angle of attack. Therefore, where the aircraft is pointing is a useful cue as to where it is actually going.

STOL aircraft may employ direct-lift control to vary flight-path angle directly without the need to first change the aircraft's pitch attitude. The flight-path response is typically quicker with direct-lift control than with the more conventional control mode, but a problem may exist in that the pilot no longer can use pitch attitude as a cue to flight-path angle. It was hypothesized that the head-up display of flight-path angle would be of more use for a direct-lift control mode than for a conventional attitude control mode. For this reason two types of aircraft control, conventional and direct lift, were used in the display evaluation.

In the experiment, approaches were flown with (1) no head-up display, (2) head-up display with glide-slope reference, and (3) a head-up display with attitude, glide slope, and flight-path angle information. Two types of control techniques, conventional and direct lift, were used with each display condition. The six display-control mode combinations were evaluated by measures of pilot performance, loading-task measures of pilot workload, and pilot opinion.

TEST EQUIPMENT

Cockpit

A fixed-base simulator was used for this evaluation. The control column and wheel were spring loaded. The throttle levers were mounted on an overhead panel as in the augmentor wing STOL aircraft. No panel instruments were provided because the experimental objective was to evaluate only the information the pilot derived from his view of the runway and the head-up display.

Aircraft Dynamics

Simplified linear dynamics of the augmentor wing jet STOL research aircraft dynamics were used. A longitudinal stability augmentor system and automatic speed control were included. The conventional dynamics incorporated a pitch-rate-command attitude-hold system. For the direct-lift dynamics, the pitch attitude was stabilized and the throttle was used by the pilot to provide direct lift. In both cases the airspeed was automatically maintained at 60 knots by the nozzle control. Figure 4 shows the transfer functions from control to flight-path angle for each of the control techniques.

Visual System and Head-Up Display

The visual system consisted of a collimating lens system and a 53-cm (21-in.) cathode ray tube (CRT) display. A general-purpose computer graphics system was programed to display a dynamic perspective night view of a STOLport and its surrounding terrain. Figure 2 shows the pilot's view of the STOLport and HUD during an approach. The HUD consisted of (1) a horizon bar, (2) a glide-slope reference (GSR) bar at 7.5^{o} below and parallel to the horizon bar, (3) an aircraft symbol which displayed the aircraft pitch and roll attitude, and (4) the flight-path marker (FPM) symbol which showed the intersection with the ground of the aircraft flight-path vector. The HUD symbology was drawn directly on the CRT by the computer graphics system and viewed through the same collimating optics as the night scene. Perfect signals were used to position the display symbology in exact alinement and registration with the perspective view of the runway.

PROCEDURES

Pilots

Four airline pilots with extensive backgrounds in instrument flying were selected to participate in the experiment.

Experimental Design

Each of the four pilots completed eight approaches for data within twelve experimental conditions (three displays for two control techniques and two workloads). The pilots were divided into two groups. One group flew the conventional control mode first while the second group flew the direct-lift mode of control first. The presentation order of display-workload conditions was counterbalanced between pilots and between groups. The pilots flew one practice and two data sessions under each control technique. Each pilot flew four approaches in each of six display-workload combinations within each session. A total of 384 data approaches were flown in the experiment.

Winds

From each block of four approaches a headwind was selected randomly without replacement from the set of 0,0,5, and 5 m/sec (0,0,10, and 10 knots). Simulated turbulence on all flights consisted of u and w gusts with root-mean-square (rms) magnitudes of 0.8 m/sec and 0.4 m/sec (1.6 knots and 0.8 knot).

Flight Profiles

At the beginning of each approach, the simulated aircraft was positioned 3000 m (9850 ft) from the runway aim point at an altitude of 395 m (1300 ft) on a 7.5° glide slope to the runway aim point. The aircraft was trimmed to a -7.5° flight-path angle through the air mass. The pilots were instructed to maintain a 7.5° glide slope until runway touchdown. Upon landing, each pilot was presented a display of his glide-slope height errors at four points along the approach.

Extra Workload Task

A loading task was used in this study to accentuate the differences in performance between displays. The task consisted of an "X" and a digital count in the upper left-hand corner of the display. (See fig. 2.) At the start of the flights in which this task was used, a line appeared randomly in one of the four quadrants defined by the "X" and remained in that position until the four-way trim button on the control wheel was pushed toward that quadrant. The line was then removed and returned after 0.5 sec in another randomly selected quadrant. The number to the right of the "X" was incremented once every 1.4 sec. Every time the pilot responded correctly the count was decremented. The pilots were required to keep the count below 5 or the main display would disappear. This task resulted in a combination forced and self-paced task. The minimum average response rate was forced but the pilot could establish his own scan rate to the secondary task.

Performance Measures and Statistical Analysis

Figure 5 illustrates the four 250-m (820-ft) intervals of the approach in which data were recorded. The three dependent variables were root-mean-square height error from the 7.5° glide slope, standard deviation (STD) of sink rate, and STD of control movement (column or throttle). The independent variables for the analysis of variance for root-mean-square altitude error* and STD of sink rate were three displays, two control techniques, two headwinds, two workload levels, four pilots, and four data collection intervals. For the variable STD of control, separate analyses were calculated for each

*For the statistical analysis, the logarithm of the root-mean-square altitude error was analyzed to compensate for nonnormality in the data.

control technique. When the analyses indicated that the main effects were significantly different, then paired comparison tests were conducted. In the following discussion the terms "significant" and "marginally significant" refer to statistical significance levels of 0.01 and 0.05, respectively.

Debriefing

At the end of the study each pilot completed a debriefing questionnaire and rated the displays and dynamics on a display attentional workload scale.

RESULTS AND DISCUSSION

Approach Precision

Figure 6 shows the effect of displays and headwinds on average root-mean-square altitude error. The plotted data are averaged over control techniques, workload levels, pilots, intervals, and replications. There was a very large and significant improvement in approach precision with the head-up display incorporating the glide-slope reference bar. Root-mean-square altitude error decreased by a factor of six from 14.3 m to 2.3 m (47 ft to 7.5 ft). When the flight-path marker symbol was included, there was a further, but only marginally significant, decrease in altitude error to 1.7 m (5.6 ft). The approach precision with either HUD is equivalent to performance for conventional aircraft during precision instrument approaches. The presence of the 5-m/sec (10-knot) headwind caused a significant reduction in performance only during approaches made with no head-up display. Both HUD allowed the pilots to compensate completely for the headwind.

Figure 7 shows the effect of displays and control techniques on average root-mean-square altitude error. There was no significant difference between the two control techniques for any of the displays. Specifically, there was no evidence to support the hypothesis that the flight-path marker symbol would result in a larger improvement in approach precision with the direct-lift control technique than with the more conventional control techniques. One reason for this finding may be that the glide-slope reference bar allowed the pilots to estimate both the magnitude of the glide-slope error and the rate of change of glide-slope error. The flight-path marker provided more precise information on the rate of change of glide-slope error but since both control techniques had a reasonable flight-path response, this greater precision may not have helped as much as if the dynamic response were slower. A second reason is that the direct-lift control technique resulted in a faster flight-path response than the pitch-control technique. This effect can be seen by examining the transfer functions in figure 4. Therefore, the lead provided by the flight-path marker on glide-slope error was not as important with the direct-lift dynamics as with the more conventional dynamics.

Performance with both head-up displays improved significantly as the range to the runway decreased. This result was to be expected since the display indicated a glide-slope error which increased in sensitivity at closer ranges. Approach precision with no HUD degraded until measurement interval 3 and then improved as the range to the runway decreased. There were generally large corrections made between measurement interval 1 and the runway threshold.

The pilots were also significantly different but the trends in performance improvement on the three displays were the same for all pilots.

Approach Smoothness

The standard deviation of sink rate provides a measure of the smoothness of the approach. Figure 8 shows the effect of displays and control techniques on the average standard deviation of sink rate. Sink-rate variability was significantly larger on approaches made with the basic HUD than on approaches made with no HUD or with the HUD including the flight-path marker. With no HUD, the approach was smooth because the pilot had poor information on where he was and therefore did not make numerous flight-path corrections. With the basic HUD, the pilots had better glide-slope information and, consequently, made more flight-path corrections to stay on the path and to correct for the wind turbulence. Finally, the flight-path marker allowed the pilot to make smaller more precise flight-path corrections and thereby to fly a smoother approach.

Figure 8 depicts the only significant interaction between displays and control technique found in this experiment. On the no HUD approaches the STD of sink rate was 44 percent greater for the direct-lift control technique. This difference was not found for approaches with the HUD; thus, it lent support to the preceding explanations that the glide-slope error rate information available from the glide-slope reference bar was adequate and that the more precise rate information provided by the flight-path marker was not a requirement.

Neither headwinds nor pilots were significantly different; sink-rate variability increasing as the range to the runway decreased. This condition results from the pilot naturally tightening up his control and making more frequent flight-path corrections to stay on the glide slope.

Pilot Workload

The experimental measures relative to pilot workload were (1) the extra workload task, (2) the standard deviation of control position, and (3) pilot ratings of display attentional workload. The extra workload task required the pilots to look away from the runway and display on the average of once every 1.4 sec. On approaches with the extra

task and either of the head-up displays, the root-mean-square altitude error increased slightly, but this increase was not enough to be statistically significant. No display or control technique was sensitive to the partial visual attention caused by the extra task. The lack of significant differences indicates that the approach workload with any of the displays or control techniques was low enough to allow a demanding extra task to be added without degrading the performance.

For the conventional control technique, control activity as measured by the standard deviation of column position was significantly greater for the two head-up displays. Figure 9 shows that control activity nearly doubled on approaches flown from either of the head-up displays. Figure 10 shows a similar trend with the direct-lift control technique for more control activity with the basic head-up display, but this difference was not significant. The interaction between pilots and displays was significant. In general, the pilots were physically working harder with the head-up displays but this extra work allowed them to increase their approach precision by a factor of 6 to 8.

As with the other measures, the pilots and the measurement intervals were significantly different. For both control techniques, control activity nearly doubled from interval 4 to interval 1.

Pilot ratings of display attentional workload without the extra task for both control techniques are shown in figure 11. The changes in rating from no HUD to basic HUD are somewhat mixed. Pilots 1 and 4 rated the basic HUD as being more demanding and pilots 2 and 3 said it was equally or less demanding. As shown in figures 9 and 10, all pilots except pilot 3 with the direct-lift dynamics had a higher physical workload as measured by control activity with the basic HUD. However, the HUD should have made it easier to estimate glide-slope errors which may account for the lower workload ratings for two of the pilots. When the flight-path marker was added, the ratings dropped or stayed the same. Adding the flight-path marker did not significantly increase the rating (fig. 11) or the control activity (figs. 9 and 10).

Pilot Interviews

All pilots felt that the glide-slope reference bar was very helpful in staying on the glide slope. They felt the flight-path marker was helpful and allowed them to make more precise corrections but that it was not as important as the glide-slope reference bar. However, three pilots preferred the HUD with the flight-path marker and only one preferred the basic HUD. All pilots preferred the direct-lift dynamics. All pilots felt the HUD should contain additional information. Pilot 1 wanted airspeed; pilot 2, altitude; pilot 3, sink rate; and pilot 4, altitude and sink rate. All pilots felt that the simulated night scene was good to excellent during the approach.

CONCLUDING REMARKS

A simulation study was conducted in which airline pilots flew steep STOL visual approaches with and without a simple head-up display. Approach performance was evaluated as a function of the type of head-up display (HUD), headwinds, control technique, extra workload task, and pilots. The results indicated that approaches with the basic head-up display containing a pitch- and roll-stabilized glide-slope reference bar 7.5^{o} below the horizon had one-sixth the altitude error as approaches flown with no head-up display. Glide-slope tracking errors with the head-up display were equivalent to the performance that would be expected on a precision instrument approach. The workload with the head-up display was higher but approach precision was better.

The addition of the flight-path marker symbol which depicts where the aircraft flight-path vector intersects the ground resulted in a further but much smaller increase in precision. Approaches flown with the head-up display incorporating the flight-path marker tended to be smoother and the pilots rated them as being less demanding than approaches with the basic head-up display. There was no indication that the flight-path marker would aid the direct-lift control technique any more than it would aid the conventional control technique.

REFERENCES

1. Anon.: Night Visual Approaches. Pilots Safety Exchange Bulletin 69-101/102, Flight Safety Foundation, Inc., Feb.-Mar. 1969.

2. Kraft, Conrad L.; and Elworth, Charles L.: Flight Deck Work Load and Night Visual Approach Performance. AGARD-CP-56, Dec. 1969, pp. 11-1 – 11-14.

3. Palmer, Everett A.: Night Visual Approaches - Pilot Performance With and Without a Head-Up Display. NASA TM X-62,188, 1972.

4. Palmer, Everett A.: Experimental Determination of Human Ability To Perceive Aircraft Aim Point From Expanding Gradient Cues. Paper presented at 40th Annual Scientific Meeting, AMA, May 1969.

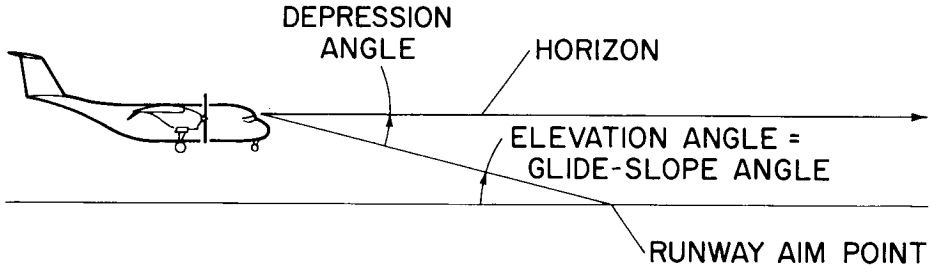

(a) Side view.

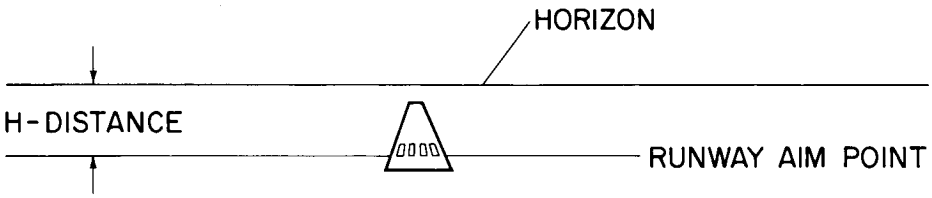

(b) Pilots forward view.

Figure 1.- Visual information on altitude error from a specified glide-slope angle.

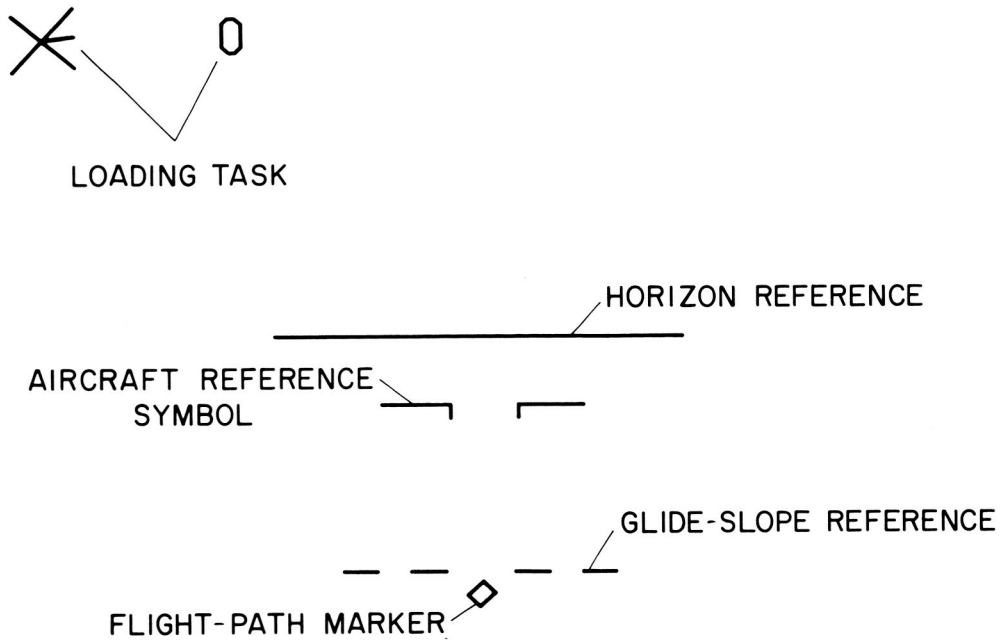

(a) Display symbology.

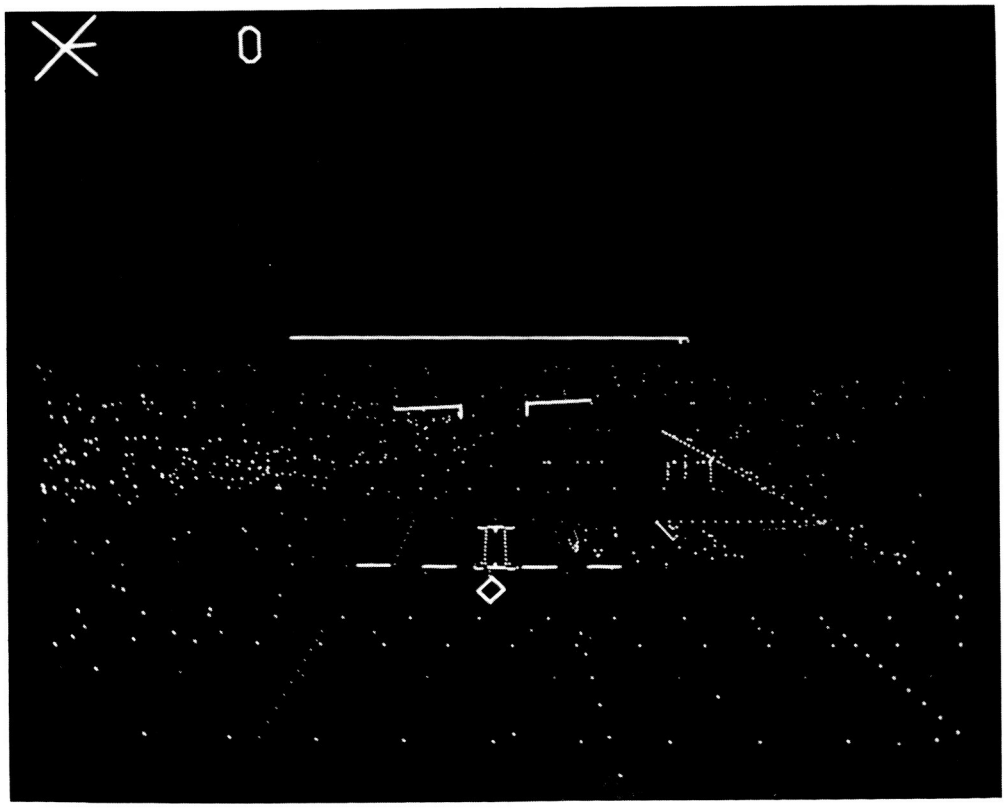

(b) Photograph of display.

Figure 2.- Head-up display and night view of STOL runway and surrounding city lights.

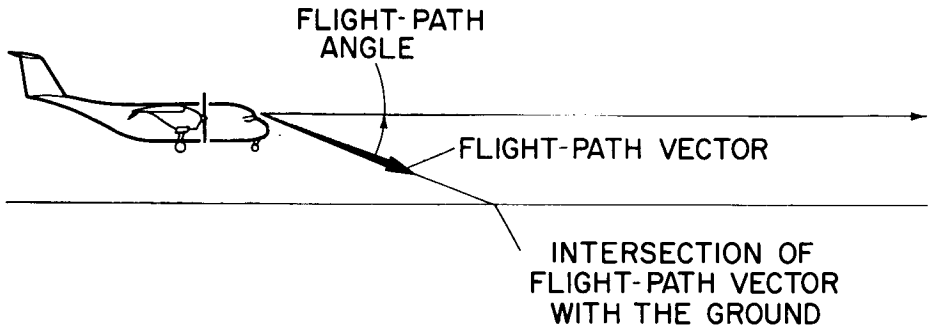

(a) Side view.

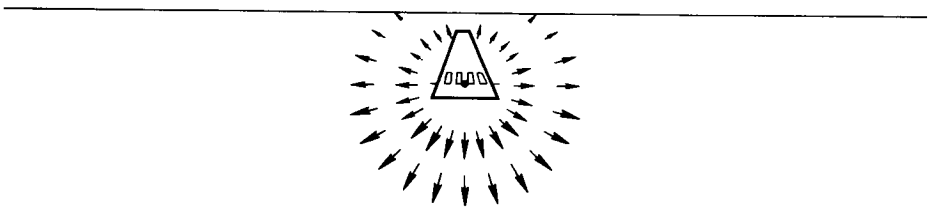

(b) Streamer's in the pilot's forward view.

Figure 3.- Visual information on the aircraft's flight-path vector.

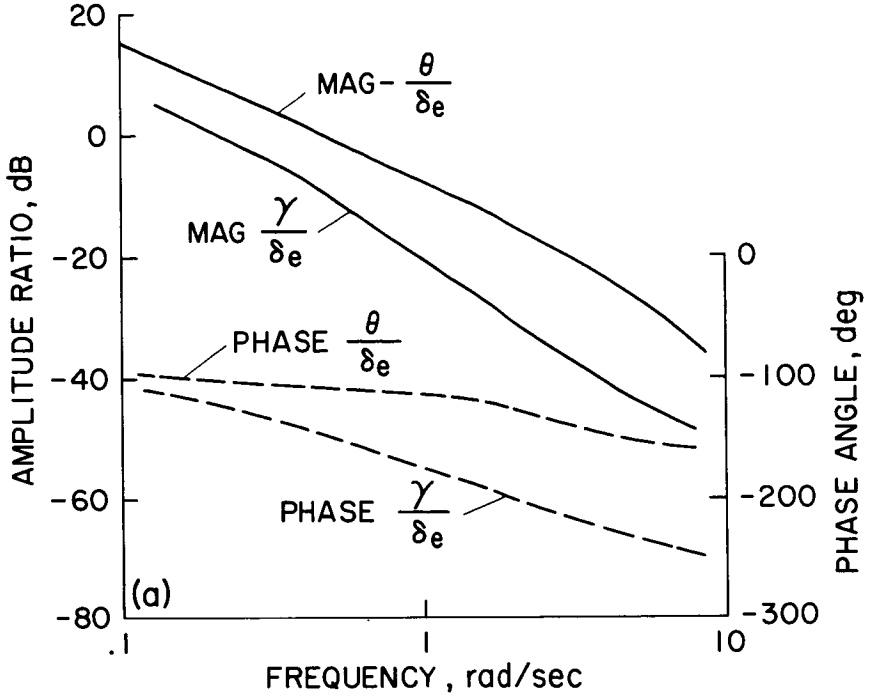

(a) Conventional control technique – flight-path angle (γ) to elevator (δ_e) and pitch (θ) to elevator (δ_e) transfer functions.

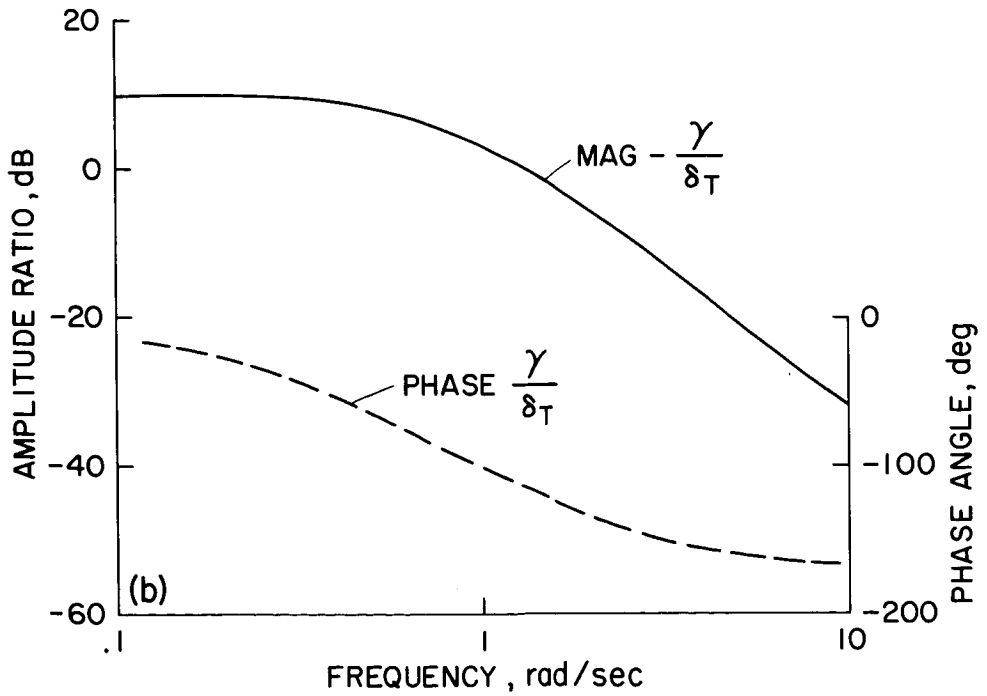

(b) Direct-lift control technique – flight-path angle (γ) to throttle (δ_T) transfer functions.

Figure 4.- Transfer functions for the two control techniques.

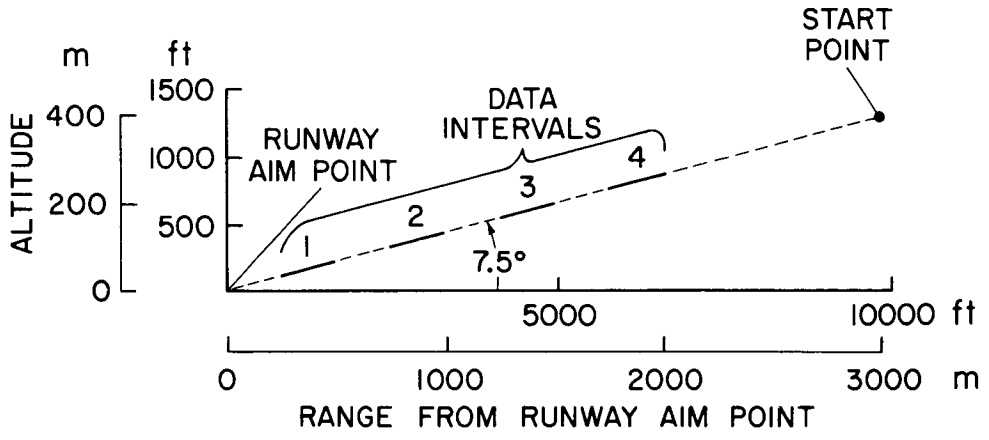

Figure 5.- Experimental task and data measurement intervals.

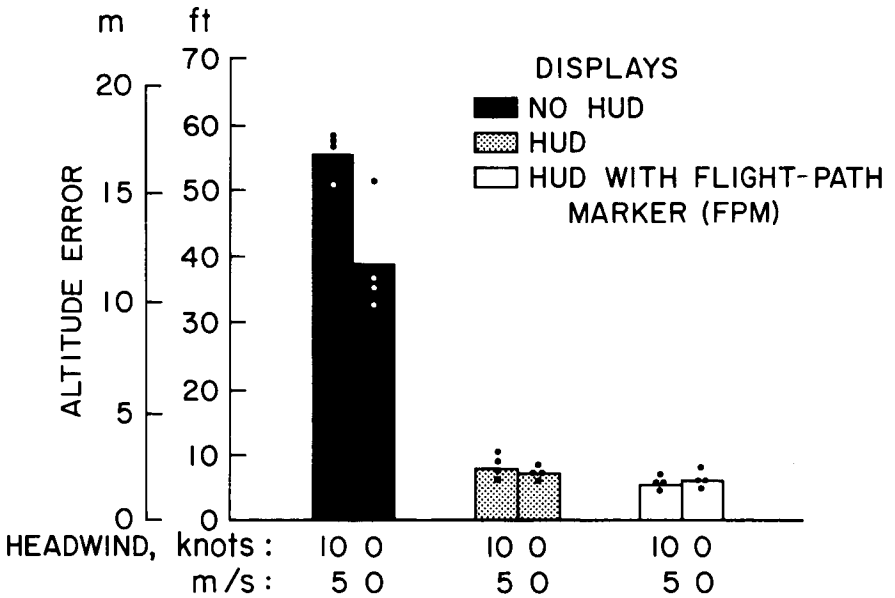

Figure 6.- Effect of displays and headwinds on average root-mean-square altitude error from a 7.5° glide slope. Dots indicate error for each pilot; 64 approaches per bar.

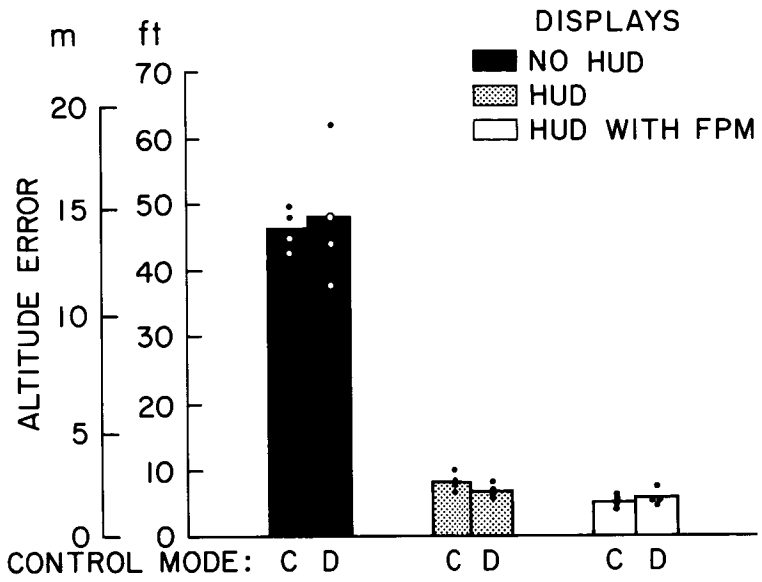

Figure 7.- Effect of displays and control technique on average root-mean-square altitude error from a 7.5° glide slope. Dots indicate error for each pilot; 64 approaches per bar.

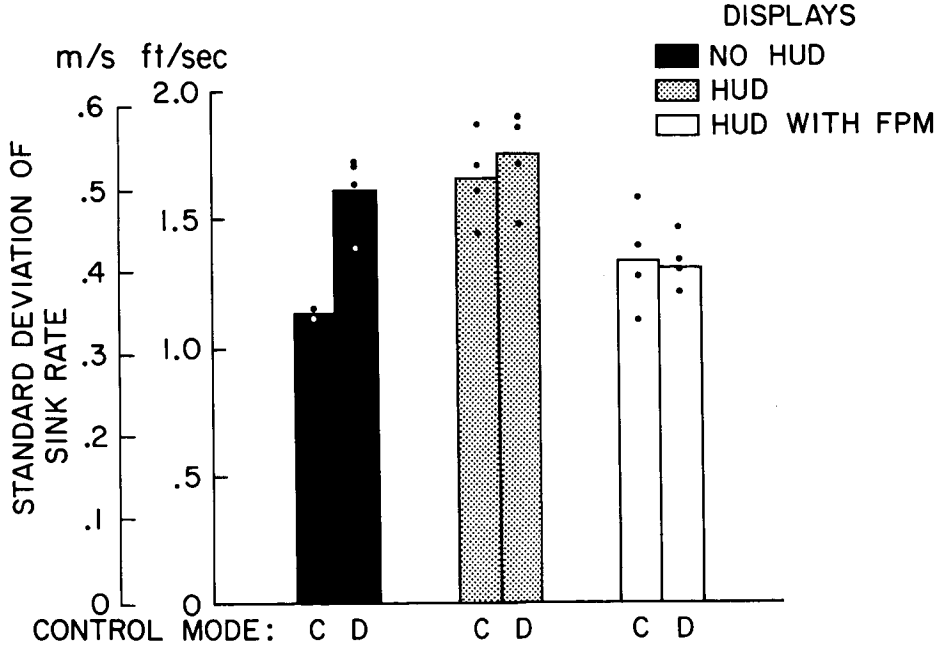

Figure 8.- Effect of displays and control technique on average standard deviation of sink rate. Dots indicate error for each pilot; 64 approaches per bar.

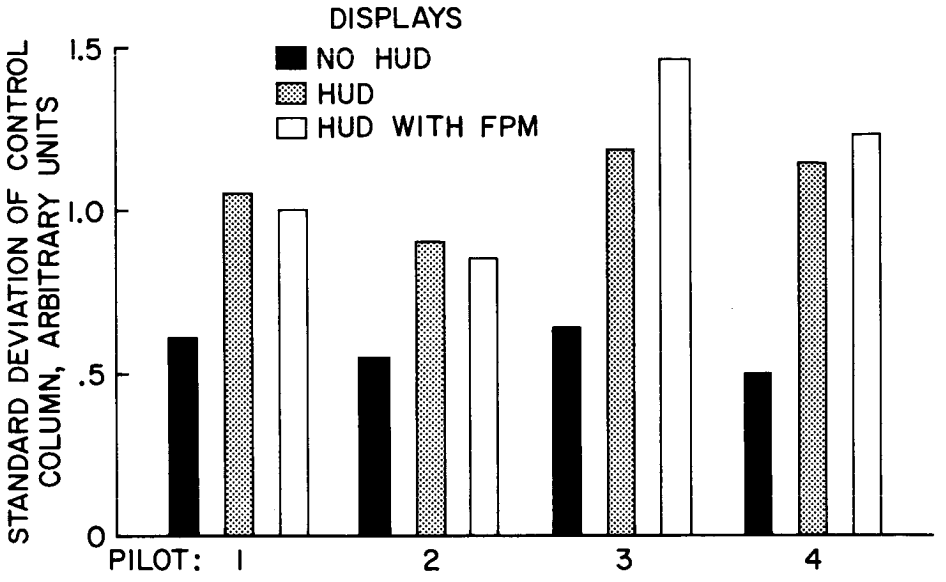

Figure 9.- Effect of displays and pilots on average standard deviation of control column. Conventional control technique; 32 approaches per bar.

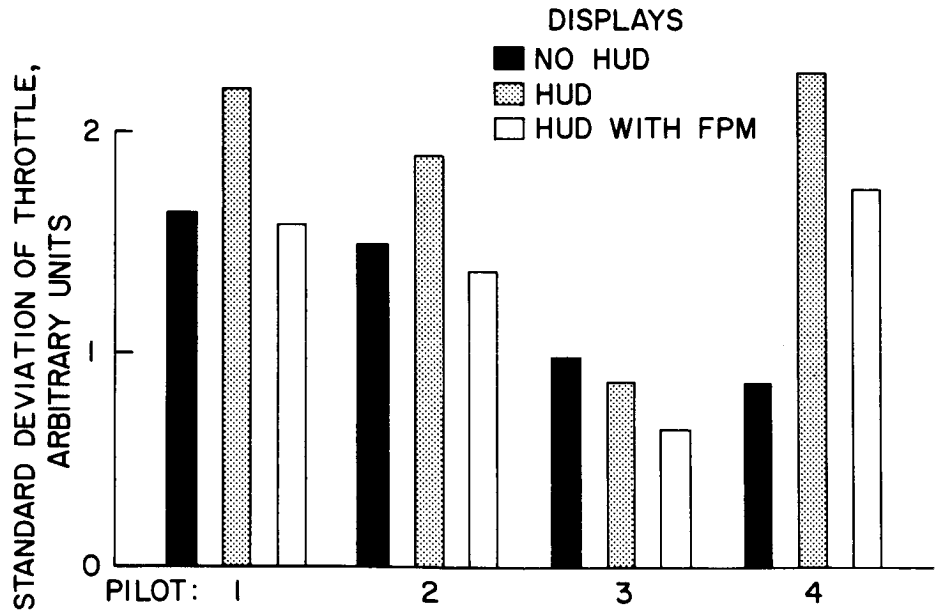

Figure 10.- Effect of displays and pilots on average standard deviation of throttle position. Direct-lift control technique; 32 approaches per bar.

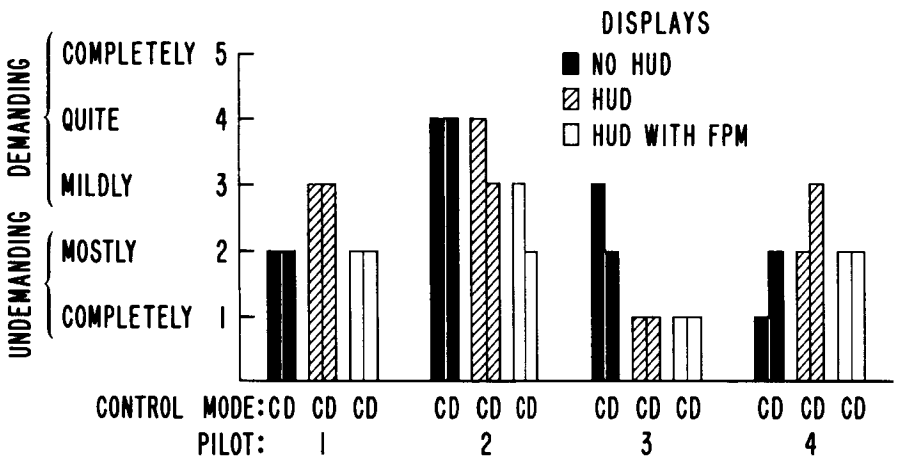

Figure 11.- Pilot ratings of display attentional workload.

A FLIGHT EVALUATION OF CURVED LANDING APPROACHES

By S. W. Gee, M. R. Barber, and T. C. McMurtry
NASA Flight Research Center

INTRODUCTION

The development of STOL technology for application to operational short-haul aircraft is accompanied by the requirement for solving problems in many areas. One of the most obvious problems is STOL aircraft operations in the terminal area. The increased number of terminal operations needed for an economically viable STOL system as compared with the current CTOL system and the incompatibility of STOL and CTOL aircraft speeds are positive indicators of an imminent problem. The high cost of aircraft operations, noise pollution, and poor short-haul service are areas that need improvement.

A potential solution to some of the operational problems lies in the capability of making curved landing approaches under both visual and instrument flight conditions.

Figure 1 illustrates STOL and CTOL traffic interspersed in the terminal area. Some of the potential benefits from curved approaches are:

(1) More efficient mix of STOL and CTOL approaches, and therefore improved utilization of airspace in the terminal area

(2) Less noise pollution by routing the traffic around critically populated areas

(3) Lower airline operating costs by more direct routing which would result in lower block time

(4) Less travel time for the traveling public

The results of many studies have emphasized the need for the development of curved-approach technology. The joint DOT-NASA CARD study (ref. 1) concluded that noise was the number 1 problem of civil aviation. One of the proposed actions for noise abatement recommended by the study is to optimize the flight path of aircraft through the use of steep descent and curved approaches. The McDonnell Douglas Corporation, in their report (ref. 2) on the operational constraints of STOL aircraft, pointed out that curved approaches and departures are essential for IFR STOL strips at major airports. In reference 3, Special Committee 117 (SC-117) of the Radio Technical Commission for Aeronautics (RTCA) recognized the need for curved approaches and made recommendations for a future guidance system to provide this capability. As a result, the FAA has undertaken a 5-year, 91 million dollar effort to comply with this recommendation, which is described in the National Plan for Development of the Microwave Landing System (ref. 4).

As a result of the foregoing, the Flight Research Center (FRC) is conducting a flight-test program to investigate the feasibility of flying IFR curved landing approaches. The objectives of the FRC program are to investigate curved patterns of different turn radii and final-approach lengths, glide slopes of 3° and 6°, different display configurations, and the effect of different flight control modes. These tests are being conducted under simulated IFR conditions, and approximately 100 approaches have been made to date.

TEST EQUIPMENT

Aircraft

The test aircraft is a twin-engine, lightweight, general-aviation airplane, the PA-30, shown in figure 2. It is utilized for the approaches because its approach speeds are sufficiently slow to allow realistic evaluation of the feasibility of flying steep curved approaches, even though its lift-drag ratio is considerably higher than that for STOL aircraft. The approach speed used during these tests is 100 knots. Also, the aircraft has the capability of being flown with advanced control-system modes as a result of earlier flight-test programs. Specifically, the advanced control-system mode utilized during the curved approaches is an attitude-command control system.

Guidance Equipment

The curved-approach mechanization scheme is illustrated in figure 3. The test aircraft's position is measured by radar. This measurement is then sent to a digital computer which compares the aircraft's position with a set of preprogramed coordinates that correspond to the curved-approach corridor. The error is then transmitted to the airplane through a digital uplink and displayed to the pilot on either a conventional ILS indicator or a flight-director display. A radial-acceleration term based on a radar-measured velocity V and the known radius R for a given approach was added in the computer. This term was required to provide bank-angle commands for the curved profile.

RESEARCH TEST VARIABLES

Curved Patterns

The curved-approach pattern shown in figure 4 is used. The 135° turn is used as a compromise for 90° and 180° approaches. Two turn radii, 1829 m (6000 ft) and 1219 m (4000 ft), have been evaluated with two final-approach straight segments of 914 m (3000 ft) and 457 m (1500 ft).

Figure 5 shows a simplified comparison of the curved-approach profile with the conventional straight-approach profile. During straight approaches, flight-director displays use runway heading as a course datum in order to compute an intercept angle and to compute steering commands about that angle. During curved approaches a course datum is undefined because the required course is continually changing in heading. Therefore, the course-datum information was deleted from the flight director and replaced by a radial-acceleration (V^2/R) term. The radial-acceleration term combines with the conventional course-deviation errors to provide the proper bank-angle commands to the pilot. That is, if the approach were flown with no deviation error, the radial-acceleration term would provide the bank angle required to maintain the curvature. When course deviations occur, they are mixed with the radial-acceleration term to provide the proper course convergence.

It should be noted that rather than using a converging corridor, the curved approaches are flown with a corridor of constant dimensions. This is done for simplicity of mechanization.

The sensitivity of the curved-approach corridor is equivalent to about 4.8 km (3 miles) from the end of the runway (8.3 km (5.2 miles) from localizer antennas) on the conventional ILS system. The straight-in approaches are flown with a glide slope γ of both 3° and 6°, and all curved approaches are flown with a 6° glide slope.

Displays

Figure 6 shows the display configurations that are evaluated during straight and curved approaches. The conventional displays are the PA-30's standard equipment instruments for attitude, heading, and localizer and glide-slope error. These displays tell the pilot what his attitude, heading, and position are, and the pilot is required to integrate this raw data mentally and then decide what he should do in order to track the ILS beam.

The other display is a Collins FD-108 flight-director display. The flight computer was modified to accept signals for curved approaches from the FRC uplink system. The computer processes the raw data and generates command signals for display. On the flight-director indicator an orange delta, which is the airplane symbol, overlays the attitude horizon. The yellow command bars provide an integrated pitch-roll command by their position relative to the airplane symbol. The commands are satisfied when the pilot takes corrective action and the airplane symbol becomes nestled between the command bars. The pilot is thus relieved from a decision-making process.

Flight-Control Modes

Since the PA-30 airplane was equipped with a special flight-control system, it was desirable to investigate the performance benefits of this system as compared with the basic airplane control system in the presence of turbulence. The attitude-command flight-control system is mechanized in the pitch and roll axes of the airplane. For simlicity, the characteristics of only the roll axis are shown in figure 7.

The pilot's wheel position is sensed by the control-position transducer (CPT), and the signal is fed to the aileron servoactuator, which causes the airplane to respond. When a bank angle that balances the control-wheel position is reached, the error signal goes to zero and the airplane stays in that attitude. Therefore, for a given control-wheel position, such as 10^{o} right, the airplane will stabilize in a 10^{o} right bank angle. Conversely, in order to maintain a given bank angle the control-wheel input must be maintained, either by a pilot effort or by trimming. This differs from the basic airplane control system, with which a given control-wheel deflection causes the airplane to roll at a constant rate.

RESULTS AND DISCUSSION

Approximately 100 approaches have been made and evaluated by research pilots. The evaluation covered curved patterns with radii of 1829 m (6000 ft) and 1219 m (4000 ft) and straight final lengths of 914 m (3000 ft) and 457 m (1500 ft). Different display modes and flight-control modes were evaluated. The 6^{o} glide-slope patterns were flown at an indicated airspeed of 100 knots under simulated IFR conditions down to a decision height of 61 m (200 ft).

Comparison of Straight and Curved Approaches

Perhaps the most significant results of the program to date are illustrated in figure 8, which presents a comparison of pilot ratings for curved and straight approaches during light and light-to-moderate turbulence. These approaches were flown with the flight-director display and the basic control system. The data for the straight approaches were taken from a previous study that was conducted at FRC (ref. 5). Since the 6^{o} straight-in approaches were not significantly more difficult to perform, the results from the 3^{o} approaches were used in this comparison.

The data show that throughout the range of turbulence of the tests, curved approaches were not significantly different from straight approaches in difficulty or workload.

The pilots commented that there was a noticeable absence of situation information during the curved approaches. This lack of information did not present a problem during the test approaches; however, for a real world situation, giving consideration to a pilot's

basic distrust of a nonredundant system, it is felt that a situation mechanism must be developed. Perhaps profile position indicators displayed in the cockpit would solve this problem.

In addition, the pilots commented that the transition from the straight to the curved segments during the roll into or out of the curve should be marked to warn the pilot of an impending transition. This problem becomes particularly important in turbulent air, but was also noted during the smooth-air approaches.

The 6^{o} glide slope used during the curved approaches presented no noticeable problem to the pilots in smooth air. However, they did comment that present-day minimum altitudes would probably have to be raised somewhat to accommodate the steeper approach.

A safety pilot was in the airplane during all the approaches and was asked to evaluate the ride qualities. Comments indicate that no discomfort due to the turning flight was noted during any of the approaches. It was concluded that in smooth air, with use of a flight-director display, curved approaches of a somewhat optimum profile are generally no more difficult than straight approaches.

Effect of Pattern Geometry

Figure 9 compares the pilot ratings for the various final-approach lengths and turn radii that have been flown to date. These data were obtained with the flight-director display and with the basic control mode for both calm air and light-to-moderate turbulence. There is no significant difference in the ratings as the final-approach segment is reduced from 914 m (3000 ft) to 457 m (1500 ft) or as the turn radius is reduced from 1829 m (6000 ft) to 1219 m (4000 ft). It is intended to carry these measurements further to determine where the ratings start to degrade as a function of the corridor characteristics, but the data have not yet been obtained. Certainly as the turn radius becomes smaller and smaller, a point will be reached where the bank angle required becomes so large that the pilots will not be able to perform the approaches satisfactorily.

Effect of Wind and Turbulence

Figure 10 provides a feel for the magnitude of the bank angles required during an approach with a 1219-m (4000-ft) radius. The top half of the figure illustrates the approach profile, and the bottom half illustrates the theoretical and flight-measured values of the bank angle required to fly the approach during light-to-moderate turbulence with a 15- to 18-knot wind from 240^{o}. Under a no-wind condition, the theoretical bank angle to maintain the profile would obviously be a constant. However, in the presence of wind the bank angle in the downwind portion of the turn is greater, because of the increased ground speed, than the bank angle in the upwind portion of the turn. Since it is desirable to land

into the wind, this situation will normally require greater than nominal bank angles during the initial portion of the turn. This effect will perhaps make down-the-runway winds a problem for curved approaches comparable to the cross-wind problem for straight approaches. However, during the approaches to date the pilots have not encountered headwinds strong enough to be a problem. The maximum winds encountered were west at 20 with gusts to 30 knots.

The flight recording superimposed on the theoretical value of bank angle illustrates two significant points. It illustrates the lack of a start-turn warning, in that the pilot initially overshot the turn and then had to utilize a steeper bank angle to return to the profile. In addition it illustrates the magnitude of the bank-angle excursions created by the light-to-moderate turbulence that will tend to add to the nominal bank angle required. This effect will become significant for approach radii that require bank angles large enough to start causing problems. It was initially believed that bank angles in the vicinity of 30^{o} would cause the pilots to degrade their ratings of the approach. However, this run resulted in a 30^{o} bank with a pilot rating of 3.5.

It was concluded that the effects illustrated in figure 10 will probably become the limiting factors. However, the program has not yet reached the limits.

Effect of Displays

Figure 11 shows the pilot ratings and root-mean-square localizer and glide-slope tracking errors resulting from use of the different displays. The data were taken for a turn of 1829-m (6000-ft) radius and a 914-m (3000-ft) straight final approach with basic control in calm air.

With the conventional displays of raw data, the pilot used a heading reference for tracking on the downwind leg. The lack of a start-turn cue and the loss of a heading reference during the turn caused a deviation from which recovery was difficult. The result was poor performance as reflected in the pilot ratings and tracking errors. While the conventional displays have been proven to be satisfactory for straight-in ILS approaches, they are not for curved approaches.

Effect of Control Modes

One of the interesting findings during the study was the effect of the control system during curved approaches. In a previous study of an advanced control system (ref. 5) it was found that during conventional straight ILS approaches with the basic aircraft control system, pilot performance was degraded in the presence of turbulence. The attitude-command system improved the airplane's stability in turbulence and the pilot's performance was significantly improved.

However, during this curved-approach study, the attitude-command system did not show an overall improvement. Figure 12 shows pilot ratings and root-mean-square localizer and glide-slope tracking errors obtained during a curved pattern of 1829-m (6000-ft) radius and a 914-m (3000-ft) straight final approach with the flight-director display in light-to-moderate turbulence. The higher pilot rating for the attitude-command system is believed to be due to a nonconstant attitude required to negotiate the turn in the presence of wind. The resulting out-of-trim condition was undesirable and caused the system to work against the pilot. Because of the changing bank angle required, it seemed easier for the pilot to work against this out-of-trim condition rather than retrim.

SUMMARY OF RESULTS

A flight-test program that investigates some of the many facets of curved approaches is currently under way. Four curved patterns with a steep glide slope, two display configurations, and two flight-control modes have been investigated thus far. Future evaluations will consist of shorter turn radii, lower approach velocities, segmented glide slopes, decelerating approaches, varying corridor size, and optimized flight-control systems.

The results obtained thus far can be summarized as follows: When using the flight-director display,

1. Curved approaches were not significantly different from straight approaches in difficulty and workload.

2. For the range of curved patterns tested, there was no significant difference in the pilot ratings.

3. The pilot ratings for curved approaches were in the satisfactory range. When using conventional displays without the flight director, the pilot ratings were in the unsatisfactory range.

4. The attitude-command system, in its present form, did not show an improvement over the basic control system during curved approaches.

REFERENCES

1. Anon.: Civil Aviation Research and Development Policy Study – Report. NASA SP-265, 1971. (Also available as DOT TST-10-4.)

2. Schaefer, R. K.; and Velten, K. R.: Operational Constraints for STOL Aircraft. AIAA Paper No. 70-1283, Oct. 1970.

3. RTCA Special Committee 117: A New Guidance System for Approach and Landing. Doc. DO-148, Radio Tech. Comm. Aeronaut., Dec. 18, 1970.

4. Anon.: National Plan for Development of the Microwave Landing System. FAA, DOD, and NASA, July 1971.

5. Loschke, P. C.; Barber, M. R.; Jarvis, C. R.; and Enevoldson, E. K.: Flight Evaluations of the Effect of Advanced Control Systems and Displays on the Handling Qualities of a General Aviation Airplane. Paper No. 720316, Soc. Automot. Eng., Mar. 1972.

INTERSPERSED STOL AND CTOL APPROACHES

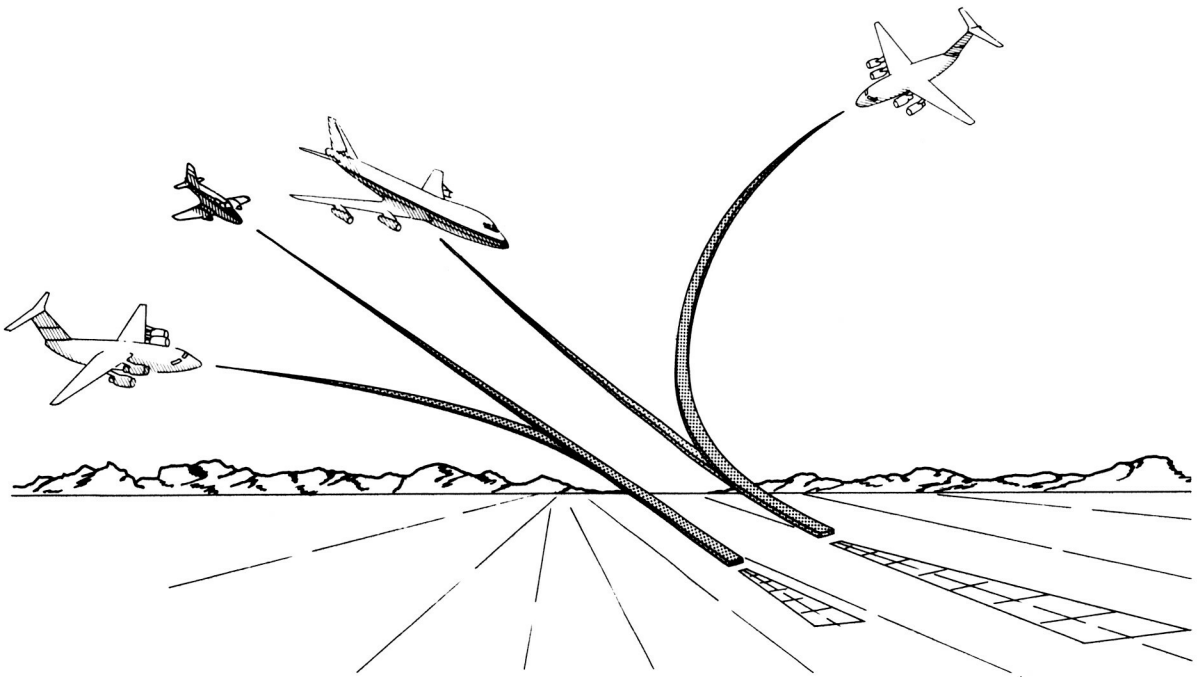

Figure 1

AIRPLANE USED IN THE STUDY

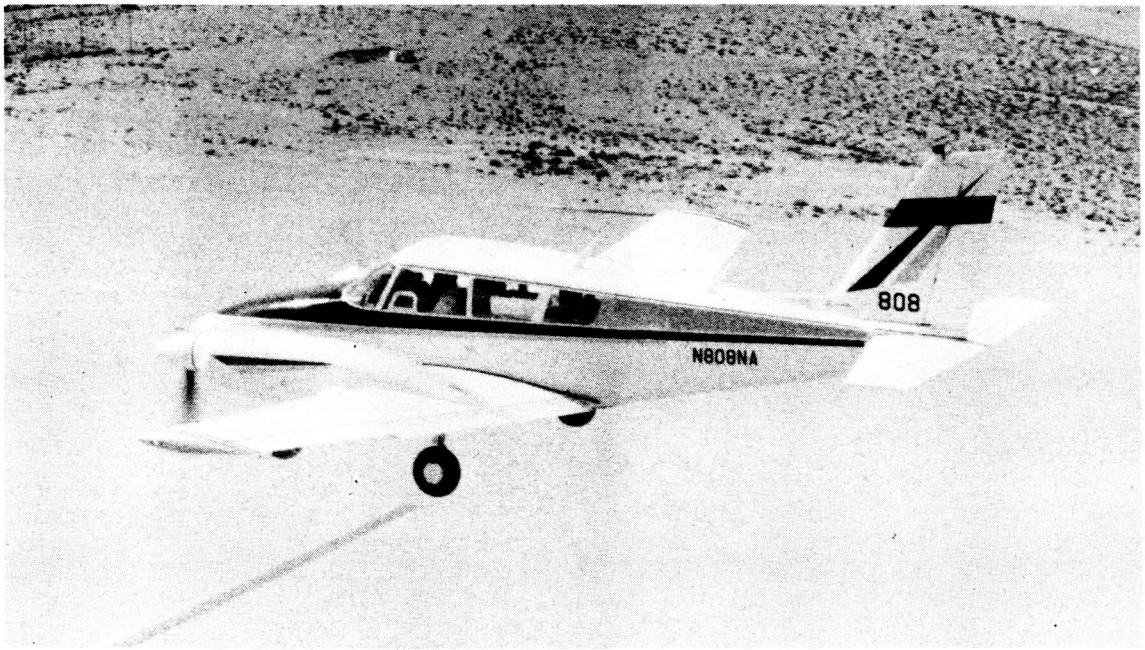

Figure 2

CURVED APPROACH MECHANIZATION SCHEME

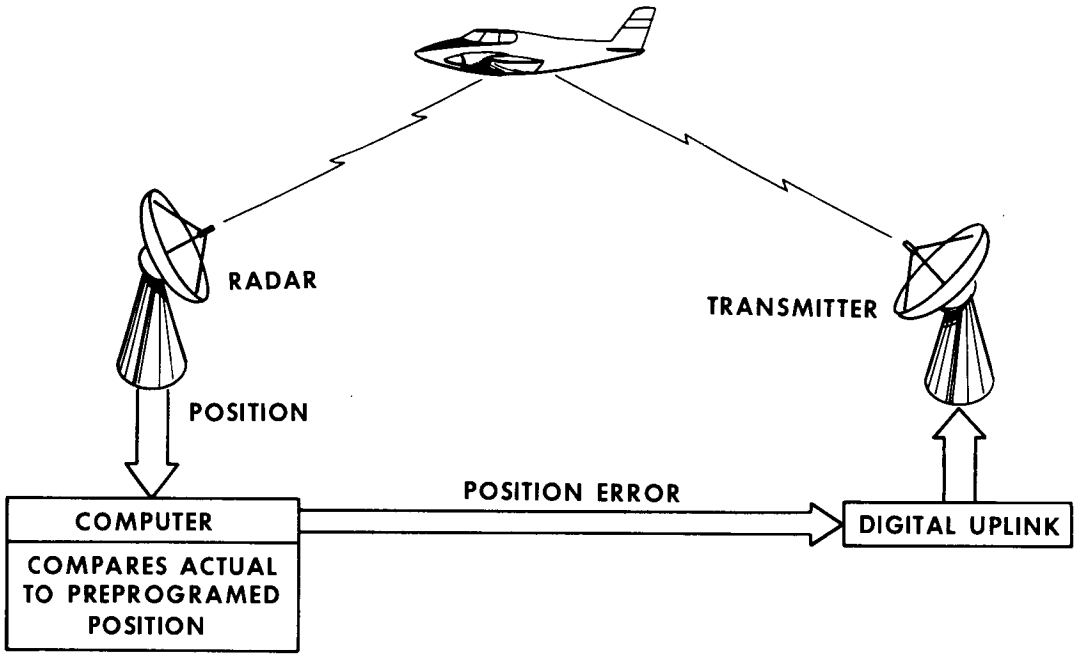

Figure 3

CURVED APPROACH PATTERN

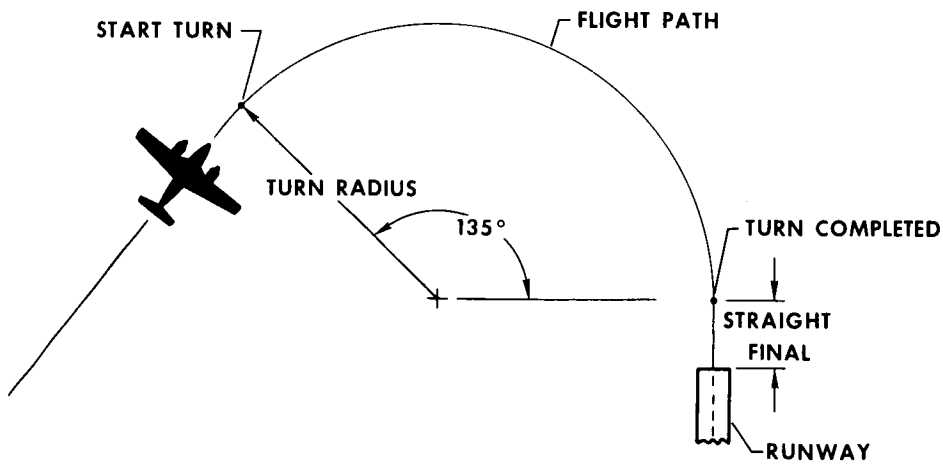

Figure 4

SIMPLIFIED COMPARISON OF CURVED AND STRAIGHT APPROACH PROFILES

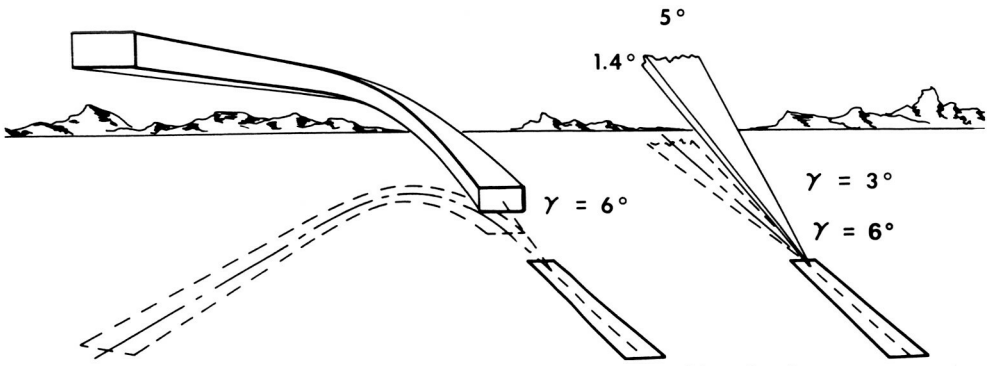

Figure 5

DISPLAYS

CONVENTIONAL

FLIGHT DIRECTOR

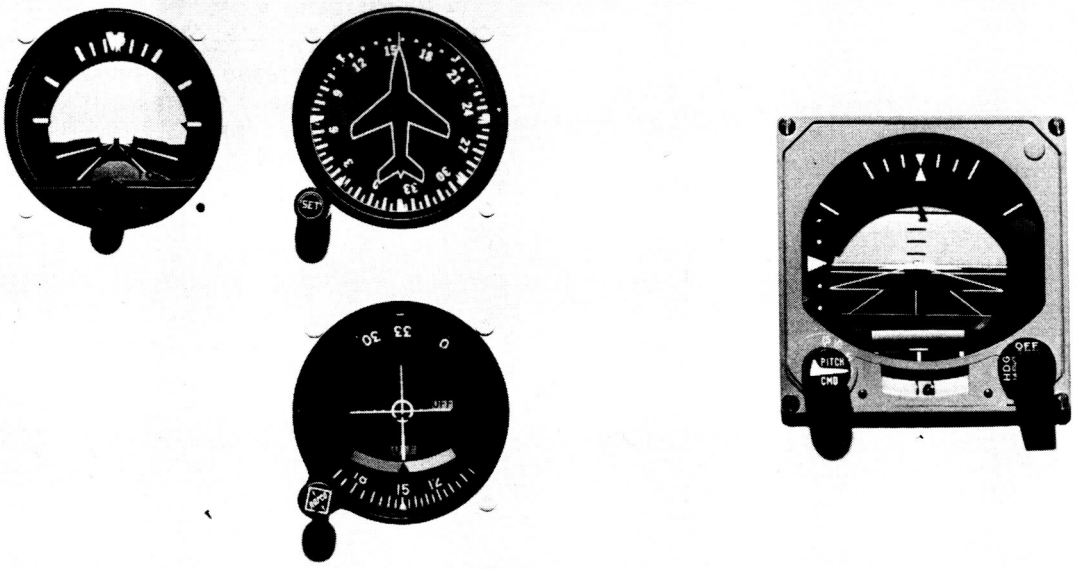

Figure 6

CHARACTERISTICS OF TEST AIRPLANE'S ROLL ATTITUDE COMMAND SYSTEM

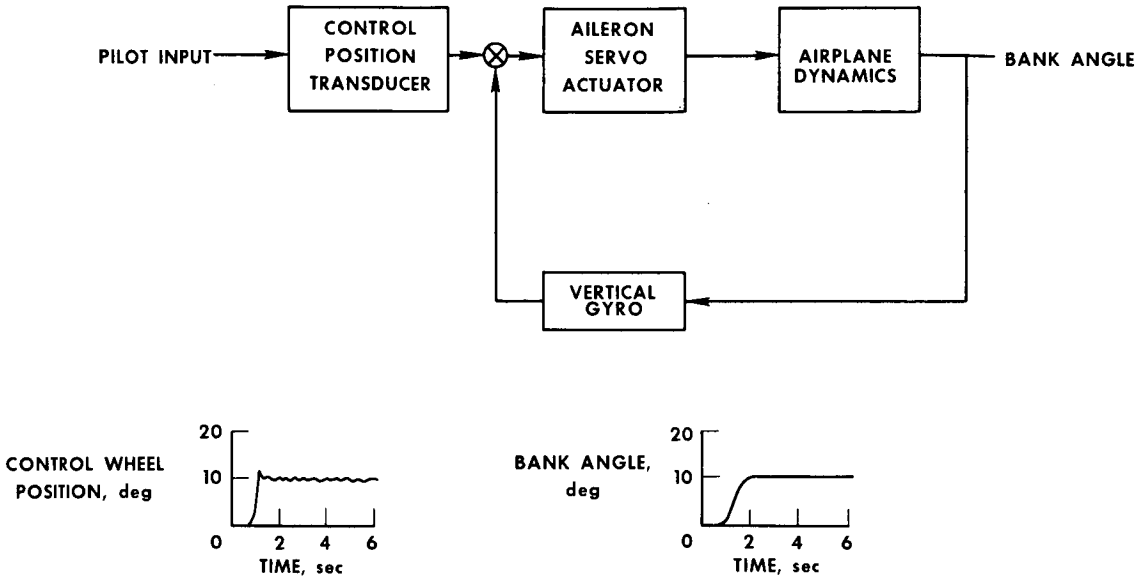

Figure 7

PILOT RATINGS FOR CONVENTIONAL ILS AND CURVED APPROACH TASKS

FLIGHT DIRECTOR WITH BASIC CONTROL

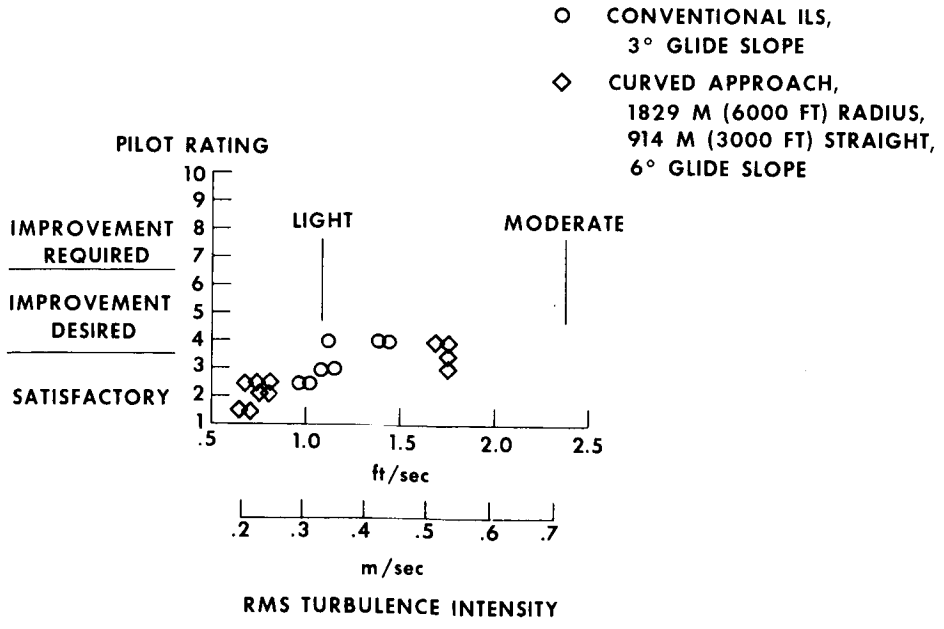

Figure 8

EFFECT OF PATTERN GEOMETRY DURING CURVED APPROACHES

FLIGHT DIRECTOR WITH BASIC CONTROL

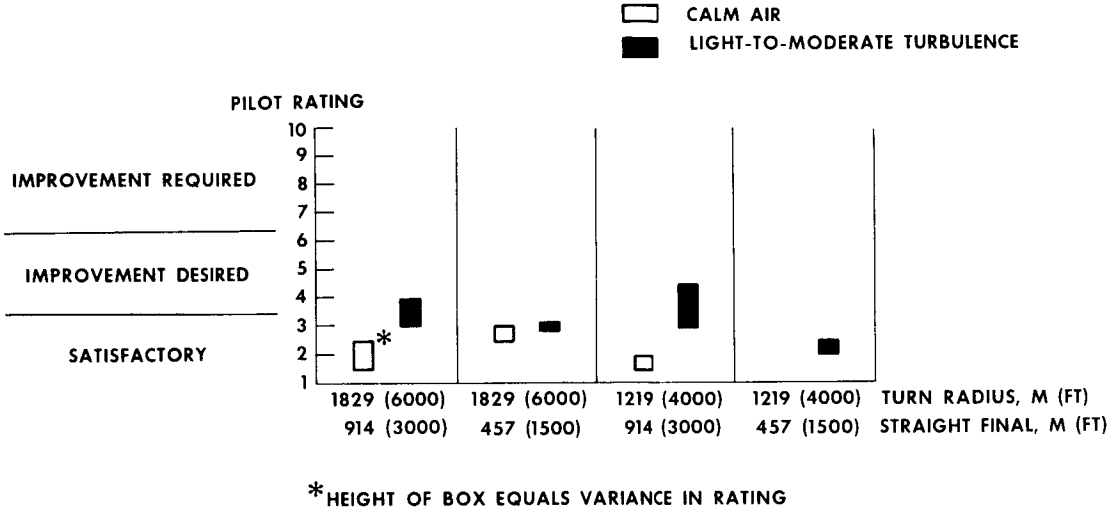

*HEIGHT OF BOX EQUALS VARIANCE IN RATING

Figure 9

EFFECT OF WIND DURING CURVED APROACHES

FLIGHT DIRECTOR, BASIC CONTROL, LIGHT-TO-MODERATE TURBULENCE

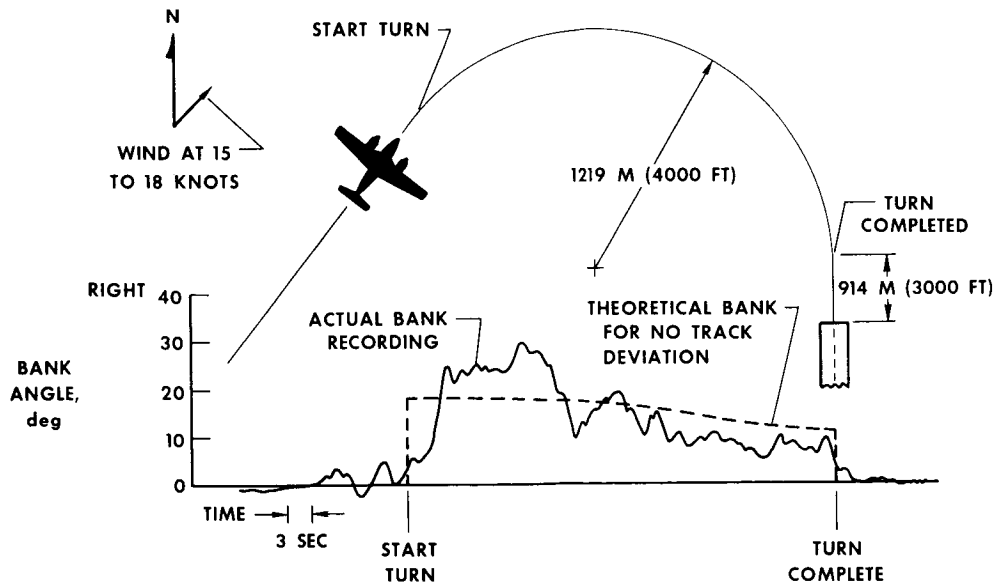

Figure 10

EFFECT OF DISPLAYS DURING CURVED APPROACHES

1829 M (6000 FT) RADIUS, 914 M (3000 FT) STRAIGHT, BASIC CONTROL, CALM AIR

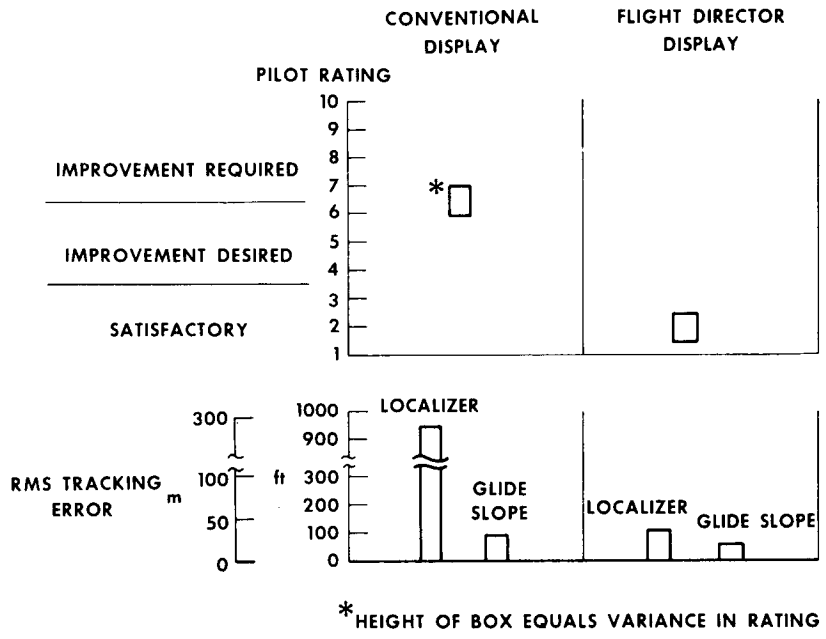

Figure 11

EFFECT OF CONTROL SYSTEM DURING CURVED APPROACHES

1829 M (6000 FT) RADIUS, 914 M (3000 FT) STRAIGHT, FLIGHT DIRECTOR, LIGHT-TO-MODERATE TURBULENCE

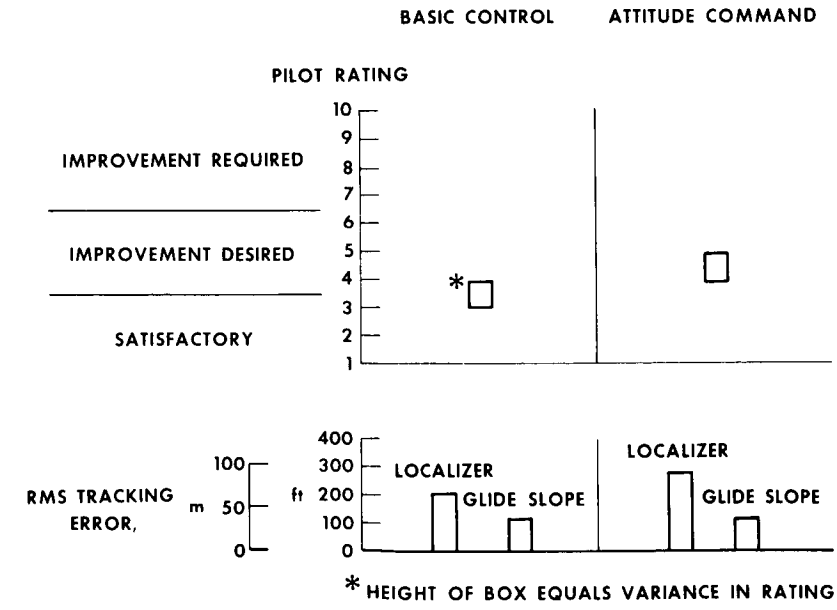

Figure 12

PRELIMINARY RESULTS OF FLIGHT TESTS OF THE AUGMENTOR-WING JET STOL RESEARCH AIRCRAFT

By Hervey C. Quigley and Richard F. Vomaske
NASA Ames Research Center

SUMMARY

The Augmentor-Wing Jet STOL Research Aircraft that has been developed jointly by NASA and the Canadian Government Department of Industry, Trade, and Commerce has started flight tests. The objectives of the program are to compare aerodynamic characteristics predicted from wind-tunnel data with data obtained in flight, to determine flight dynamic characteristics and limitations of the augmentor-wing concepts, and to contribute to the development of STOL design and operational criteria.

Initial flight test results have shown that the aerodynamic characteristics are close to values predicted from wind-tunnel tests. The lateral-directional stability and control characteristics are satisfactory for research STOL missions with stability augmentation, but the longitudinal control will require improvement. STOL take-off distance over 11 m (35 ft) is about 290 m (950 ft), and landing approach speeds are between 60 and 65 knots. The investigation of the STOL operational and performance characteristics is continuing.

INTRODUCTION

Several powered-lift concepts are being studied for use on fan jet STOL transport aircraft. The augmentor wing has been recognized by both government (ref. 1) and industry (refs. 2, 3, and 4) as one of the promising concepts for further research and development.

A cooperative NASA/Canadian Government research program on the augmentor-wing concept began in 1965. The program included analysis and small-scale static and wind-tunnel tests by De Havilland Aircraft of Canada, Ltd. (ref. 5); large-scale tests in the Ames 40- by 80-foot wind tunnel (refs. 6, 7, and 8) with a De Havilland built model; and joint design feasibility and simulator studies. The research had advanced to a point by early 1970 that a proof-of-concept aircraft was warranted to test the principle in flight. The U.S. and Canadian Governments entered into an international agreement whereby the NASA and the Canadian Department of Industry, Trade, and Commerce (DITC) would modify a De Havilland C-8A Buffalo to an augmentor-wing jet STOL research aircraft. The DITC contracted with The De Havilland Aircraft of Canada, Ltd.,

and their subcontractor Rolls Royce of Canada, Ltd., to provide the propulsion system and modify the nacelle. The NASA contracted with The Boeing Company to modify the aircraft, install the propulsion system, and perform the initial flight tests.

A De Havilland C-8A Buffalo aircraft was chosen as the aircraft to be modified into the augmentor-wing jet STOL research aircraft after a design feasibility study. The study showed that with such a modification the primary research objective could be achieved at a reasonable cost and within an acceptable time span. Also, since the C-8A has a wing planform similar to that of the large-scale model that had been tested extensively in the Ames 40- by 80-foot wind tunnel (refs. 6 and 7), a large amount of data was available for the design.

The objectives of the program are (1) to determine in flight the aerodynamic, performance, and handling qualities of a jet STOL aircraft incorporating the augmentor-wing concept, (2) to compare the results obtained in flight with characteristics predicted from wind-tunnel and simulator test results, (3) to contribute to the development of criteria for design and operation of jet STOL transport aircraft, and (4) to provide a jet STOL transport aircraft for STOL systems research and development.

The purpose of this paper is to discuss the status of the program, to present a brief description of the aircraft, and to present some preliminary data from the flight test program.

STATUS OF PROGRAM

The first flight of the aircraft was made on May 1, 1972, at Seattle, Washington. Figure 1 is a photograph of the aircraft taking off on its first flight. The initial airworthiness flight test program was conducted by The Boeing Company. The aircraft was flown within a flight envelope of from 50 to 180 knots and at load factors to demonstrate that the aircraft flight loads were within design and that the aircraft was flutter free. The aircraft was delivered to NASA on July 31, 1972, and ferried to Ames Research Center the same day. The first phase of the flight test program at Ames will include (1) measurement and documentation of the aircraft characteristics in flight, (2) determination of operational characteristics and limitations, and (3) assessment of handling qualities. After completion of these phases, STOLAND equipment will be installed and the aircraft used for a wide variety of STOL flight experiments in handling qualities, STOL operations, and terminal area guidance and navigation.

DESCRIPTION OF AIRPLANE

The De Havilland C-8A (fig. 2) is a turboprop military STOL transport aircraft. The high wing and high tail make it suitable for modification into a powered-lift jet STOL

transport. Major alterations were required to the wing to provide for the augmentor flaps.

The major modifications and additions to the aircraft are as follows:

(1) Wing span reduced from 29 to 24 m (96 to 78.8 ft)

(2) Augmentor-flap system including augmentor chokes

(3) Drooped aileron with boundary-layer control

(4) Repositioned and redesigned spoilers

(5) Fixed full-span leading-edge slats

(6) G.E. T64 turboprop engine replaced by Rolls Royce Spey split-flow fan engine

(7) Air-distribution duct system to supply fan air to the augmentor flaps, fuselage blowing, and aileron

(8) Lateral-directional stability augmentation system (SAS)

(9) Increased capacity hydraulic system

(10) Extensive flight-test instrumentation

Figure 3 is a three-view drawing of the modified aircraft and table I is a list of its major characteristics. The wing span was reduced to increase the wing loading to a value close to what would be used on a commercial or military jet STOL transport.

Augmentor Flap

A sketch of a cross section of the augmentor flaps (fig. 4) shows the general arrangement of the flap and identifies the major parts of the flap system. The flap design is the same in general as that used on the large-scale wind-tunnel model (ref. 7), but it has been scaled up for the aircraft. The flaps have a constant chord and are made in four equal spanwise sections, two on each side of the aircraft (fig. 3). The maximum flap deflection is 75°. In order to reduce the overall cost of the basic modification program, the flaps were not designed to fold in the flaps-up position as would be required in the production STOL aircraft. Preliminary design studies have shown, however, that folding the flaps can be accomplished without significant problems.

The augmentor-wing principle of achieving high lift requires that the flap system be an efficient ejector to induce flow around wings and produce an augmented thrust out the trailing edge of the flap. The critical dimensions for optimum augmentation ratio, determined from results of a 0.7-scale static model test at Boeing, are the position of the coanda surface relative to the nozzle exit, the throat to nozzle height, and the diffuser angle. The inlet door angle is also critical, as discovered in wind-tunnel tests, and must be programed with flap deflection.

The flap is supported on beams external to the wing with attaching points at the front and rear spars. Each flap is deflected by two hydraulic linear actuators also external to the wing.

Augmentor-Flap Performance

The location of the rear spar of the C-8A and the desire to make the take-off wing loading as high as possible dictated the development of an augmentor flap with a smaller ratio of flap chord to wing chord than was tested in the Ames 40- by 80-foot wind tunnel. A static test of a 0.7-scale model flap was conducted to verify the effectiveness of the new flap design (ref. 9). The results of the test to optimize the augmentation ratio (thrust at the flap trailing edge to the thrust of the nozzle alone) are shown in figure 5. An extensive study of the optimum location of the coanda surface indicated that the maximum augmentation ratio for take-off flaps $(\delta_F = 30^o)$ was 1.39 and for approach flaps $(\delta_F = 65^o)$ was 1.38. To achieve this performance on the aircraft would require that the flap system pivot about an eccentric center. It was considered highly desirable to pivot the flap about a fixed point to simplify the design of the actuating mechanism. The augmentation ratio penalty associated with choosing a fixed pivot is indicated by the dark band in the figure. Installation effects and deflections in flight result in a 2-percent loss in augmentation ratio caused by changes in the coanda position in flight. An additional 1-percent loss can be expected because under loads, the flap deflects in such a manner that the diffuser angle can vary from the optimum value of 4.75^o. These losses will vary in flight depending on the flight condition. Static tests of the wind-tunnel model (ref. 7) demonstrated the performance shown by the test points. It can thus be concluded that the wind-tunnel data are representative of the performance that can be expected from the modified C-8A.

The actual static augmentation ratio of the augmentor flap on the aircraft will be measured statically at a later date. This augmentor configuration is not necessarily optimum. Theoretically, higher augmentation ratios are possible, and NASA research is continuing to achieve better augmentor performance.

Propulsion System

The engines for the aircraft are Rolls Royce Spey MK 801 SF split-flow engines. The Spey engine has been extensively modified by Rolls Royce of Canada. Figure 6 shows the engine installed in the nacelle. The changes included a new bypass duct that collects the fan air and directs it to two 33-cm-diameter (13-in.) offtake ducts on top of the engine. Bleed valves incorporated into the fan air bypass duct maintain engine match to the duct system. A vectorable nozzle assembly from the Pegasus engine used on the Hawker Siddeley Kestrel (XV-6A) aircraft is installed in place of the tail pipe. The conical nozzles, one on each side of the nacelle, provide vectored thrust from 6^o to 104^o

below the aircraft center line. The pilot controls the nozzles by levers adjacent to the throttles in the cockpit (fig. 7). A pneumatic actuator system that uses high-pressure bleed air from the engine is used to drive the nozzles. A collander plate has been installed in front of the Pegasus nozzle divider assembly to isolate any effects on the nozzle from the hot section of the engine and to permit matching the larger area Pegasus nozzle assembly to the Spey engine. In addition, trimmers have been inserted in the Pegasus nozzles to reduce exit area. The engine has a bypass ratio of 0.6 and a fan pressure ratio of 2.5. The variation of the fan (cold) and exhaust (hot) thrust with throttle position and engine speed (rpm) is shown in figure 8. The fan thrust shown in the figure is the isentropic thrust at the engine offtake.

The installation of the engine in the nacelle is quite conventional. Because the engine is low in the nacelle, there is no place to retract the landing gear. The gear, therefore, is locked down. The engines are mounted on the same hard points as used for the T64 in the original Buffalo.

Acoustical lining is provided in the inlet and on the engine spinner as well as at the fan exit duct in the engine to reduce the fan noise. Although the augmentor-wing concept has the potential for quiet STOL transport, this aircraft is strictly a research aircraft to study the principle, and compromises, particularly in noise, had to be made in selecting the engine. The Spey MK 801 SF is basically a standard jet engine and is therefore noisy. Research for NASA (ref. 10) has shown that with properly designed engines and augmentor systems the noise of an augmentor-wing jet STOL transport could be about 95 EPNdB.

Air Distribution

An air distribution system directs the fan air from the engine to the flaps, ailerons, and body blowing nozzles. The system incorporates a crossover ducting system to accommodate engine-out operation (fig. 9). The ducting from each engine is completely separate but identical. The fan air is divided at the engine into two 33-cm (13 in.) offtake ducts on the top of the engine. Thirty-six percent of the mass flow enters the duct that goes through the nacelle to a tee at the flap nozzle inner ducts (fig. 4). This nozzle duct feeds the two flap sections on the same side of the aircraft as the eingine. Sixty-four percent of the mass flow enters the 35-cm (14 in.) duct in the leading edge of the wing. At the fuselage, a 10-cm (4 in.) duct directs 7.1 percent of the total air from one engine to the blowing nozzles on top of the fuselage at the wing leading edge. The fuselage blowing is provided by small individual nozzles that are fed alternately by ducts from the two engines.

The 35-cm (14 in.) duct enters the fuselage at the wing leading edge and is routed under the wing to the flap area on the opposite side of the aircraft. The air enters the large outer flap nozzle ducts (fig. 4) on the side opposite the engine. This nozzle duct

distributes 44 percent of the total air from one engine to the two flap sections. Another 12.9 percent of the air proceeds through the flap nozzle duct and feeds the boundary-layer control aileron nozzle. The unequal distribution of air from one engine to the flap section on each side of the aircraft and the fact that the boundary-layer control (BLC) air for the aileron comes from the engine on the opposite wing provides compensation for the initial roll and yaw associated with an engine out. Large rolling moments are associated with engine out as the result of the near 90^{o} deflection of the Pegasus nozzles on approach. The asymmetric blowing nearly compensates for this rolling moment following an engine failure on the approach. Figure 10 illustrates the design rolling-moment coefficient before and after engine failure in the approach configuration. Less than 20 percent lateral control input is required to balance the aircraft in roll following the failure, leaving a large maneuvering control margin.

At take-off the mass flow through the air distribution system is 36 kg/sec (79 lb/sec) per engine at 405 K (270^{o} F) and a pressure ratio of 2.5. The ducts were sized to keep the duct Mach number below 0.3 to minimize pressure losses. The pressure loss from the engine fan exit to the entrance to the flap duct was between 9 and 10 percent; the total pressure loss to the aileron duct near the wing tip was about 13 percent. The installation thrust losses due to pressure drops in the supply ducts to the flaps are about 5 percent of the fan thrust. An additional 7-percent loss occurs through the high-aspect-ratio nozzles and the flap ducts. This thrust loss is completely recovered by the augmentor-flap system, as is discussed later.

Control System

The elevator control, a spring tab system with no boost, is unchanged from the basic C-8A Buffalo. The rudder control consists of the basic C-8A dual irreversible hydraulic control system with the addition of a limited-authority-series stability augmentation system (SAS) with a hydraulic actuator.

The lateral control system is completely new. Three surfaces are used to produce the required rolling moments: drooped BLC ailerons, spoilers in front of the drooped aileron, and an augmentor choke (fig. 11). The ailerons are drooped mechanically as a function of the flap deflection with full droop of 30^{o} reached at flap deflection of 60^{o}. The aileron deflection is $\pm 17^{o}$ from the droop position. A large amount of blowing BLC is used on the aileron to give a large effectiveness for both the aileron and spoiler. The augmentor choke is designed to control the lift of the flap system. Although there are augmentor chokes in each section of the flap, only the choke in the outboard section of each wing is used for lateral control. All four chokes are activated on the ground after landing for lift dump.

The three lateral control surfaces are programed to give the pilot a nearly linear effectiveness with control wheel deflection (fig. 12). The maximum effectiveness of each surface is about equal. The aileron and spoiler operate from 0° wheel and the augmentor choke is phased in at 17° control wheel deflection. The spoilers are full up at 48°. A control quickener is provided by the lateral stability augmentation system which doubles the lateral control gearing for the first 3° of control wheel travel to improve the control characteristics near zero. The activating system for the lateral control surfaces consists of a central dual hydraulic power actuator that drives the aileron through a cable system. The spoilers and augmentor choke control valves are actuated by a separate cable from the central lateral power actuator. The single spoiler and choke actuators are on different hydraulic systems. Lateral control forces are low, 44 N (10 lb) maximum, and are produced by a simple spring system.

A limited-authority-series SAS that uses a hydraulic actuator is provided in the lateral control system. Both the lateral and directional SAS's have two modes of operation: a fixed gain mode that will be used for the majority of the flight tests and a variable gain mode for handling quality research where a variable stability will be required. The fixed gain lateral SAS has three inputs: (1) rolling rate for improving rolling damping, (2) yaw rate to improve spiral stability, and (3) control quickening. The yaw axis SAS has three inputs to drive the rudder (1) roll rate for turn coordination and (2) yaw rate and roll attitude for a Beta-dot Dutch roll damping.

AERODYNAMIC CHARACTERISTICS

Only a limited amount of aerodynamic data has been obtained to date on the aircraft in flight. The data presented are, therefore, only representative of the many configurations possible with this aircraft. The lift characteristics are shown in figure 13 for two flap deflections. These data are for the aircraft at power for level flight at the conditions noted in the figure. The landing approach configuration, flap deflection of 67°, is quite representative of the approach condition aerodynamically. The variation of lift coefficient with angle of attack at the test jet thrust coefficients $\left(C_j = \frac{\text{Thrust of cold (fan) air}}{\text{Dynamic pressure} \times \text{Wing area}}\right)$ agrees well with the predicted values. The predicted values are based on a similar half-scale model tested in the Ames 40- by 80-foot wind tunnel; reference 11 discusses the method used to arrive at the predicted values. In computing lift coefficient, the direct thrust component of the primary (hot) jet of the engine has been removed from the data. The cold (augmentor nozzle) thrust, however, is included and is shown in coefficient form (C_j) in the figure. In a typical STOL approach the aerodynamic lift coefficient is about 3.0 at an angle of attack of 6° and the direct hot thrust with nozzle at 70° to 80° contributes an additional 0.7 lift coefficient for an approach lift coefficient of 3.9.

Data at or near maximum lift coefficient have not been obtained in flight to date. It is estimated that the angle of attack for maximum lift coefficient will be about 20°. For the 67° flap configuration shown in figure 13, the maximum lift coefficient is estimated to be about 5.0.

The lift characteristic for the take-off flap configuration of 32° is also close to that predicted. The aerodynamic lift coefficient for a STOL take-off is about 2.5 at an angle of attack of about 10°. For take-off the nozzles are set at 6° (full up) and contribute little to the take-off lift coefficient. The drag polars (fig. 14) show the comparison of the lift and drag characteristics for the same conditions as shown in figure 13. As in the lift data, the hot thrust component of engine thrust has been removed, but the cold (fan) thrust is included. The data show fair agreement with predicted drag values particularly in the area for STOL operation. Lift coefficients are 2 to 2.5 for 32° flap deflection for take-off and 3 to 3.5 for 67° flap deflection for landing.

Operational Envelope

An operational envelope for the landing approach configuration of the aircraft is shown in figure 15. This figure shows the variation in flight-path angle with airspeed for three engine thrust settings with the flaps deflected to 67° measured in flight at the conditions noted at the top of the figure. These data show the reduction in airspeed at a constant angle of attack as thrust is increased. The airspeed decreases because of the added lift with an increase in jet thrust coefficient. For example, at an angle of attack of 12° the speed changes from 70 knots at 90 percent rpm to 58 knots at 96 percent rpm, with a corresponding decrease in flight-path angle. With the nozzles at 16° it is not possible to obtain a significant descent angle because of the large aft hot thrust component of the Spey engines. The conical nozzle must be deflected to obtain the descent angles required for STOL approaches.

The operational envelope for the aircraft at various nozzle angles is shown in figure 16. The curve for nozzle angle 16° is the same as that shown for 96-percent rpm in figure 15. The deflection of the hot thrust also produces increased lift; hence, an additional decrease in airspeed accompanies the increase in flight-path angle. A flight-path angle of -10° is achieved at 90° nozzle deflection at 60 knots. At nozzle angles of 104° the descent angle will be several more degrees.

The two operational envelopes show that the pilot has two methods for controlling flight path on the approach, the use of throttle or of nozzle. Since the throttle and nozzle control levers are adjacent to each other in the cockpit, the pilot can readily choose either method. By using power, flight-path angle can be changed with little change in pitch attitude. For example, holding 75 knots airspeed and changing power from 93 percent to 90 percent rpm produce changes of about -4° flight-path angle and +4° angle of attack;

hence, there is little attitude change. The margin from stall is, however, a function of the throttle setting in this case. With constant power and with the use of nozzles for flight-path control from a flight-path angle of about -7^{o}, the angle of attack is nearly constant when flight-path angle is changed with nozzle. The pilots have used both of these two methods for flight-path controls. They both have been found to have advantages and disadvantages and the investigation of how these controls can best be used is continuing.

Stability and Control

The stability and control characteristics of the aircraft within the flight envelope flown to date are about as predicted (ref. 12) and as flown on the simulator (refs. 13 and 14), except for the longitudinal control characteristics. The longitudinal control characteristics of the spring tab system have been problems to the pilot because of poor feel and response characteristics and reduced authority. This problem will be alleviated when the power control system is installed on the aircraft during 1973.

The lateral-directional characteristics of the aircraft with stability augmentation system (SAS) on and off are shown in table II. The functions of the SAS are as follows:

Directional axis:
- Dutch roll damping
  - Yaw rate commands rudder
  - Roll angle commands rudder
- Turn coordination
  - Roll rate commands rudder

Lateral axis:
- Roll damping
  - Roll rate commands lateral control
- Spiral stability
  - Yaw rate commands lateral control
- Control quickening
  - Small wheel deflection commands lateral control

The data in table II are marked with approximate signs because the limited data available indicate that the characteristics tend to vary with engine thrust, angle of attack, etc. The Dutch roll period is long and damping is low indicating low directional stability and damping without SAS. SAS increases the Dutch roll damping ratio to a satisfactory level of 0.3 with the Beta-dot type damper. Poor turn coordination that is associated with low directional stability and low airspeed is present, but $\Delta\beta/\Delta\phi$ is reduced to a satisfactory level of 0.3 with the rudder deflection proportioned to roll-rate SAS. The roll damping is also low with an effective time constant of 1.0 without SAS and is improved to a value of 0.5 sec with SAS. The spiral stability is quite divergent with SAS off but again is

satisfactory with SAS on. Although each of the lateral-directional characteristics are within a range that criteria have shown to be satisfactory, the pilots report that at low speed there is a tendency for the aircraft to wander in all three axes at low airspeeds. It appears that some form of attitude stability will be required under IFR conditions to reduce the pilot workload.

Lateral control quickening was incorporated to improve lateral control characteristics near zero wheel deflection. The SAS doubles the gain of the lateral control system for the first 3^{o} or 4^{o} of wheel deflection.

SAS gains are changed at flap deflections over 40^{o} and SAS is turned off at airspeeds over 100 knots.

Performance

The STOL take-off and landing performance of the aircraft has also been close to the values predicted during the design. Figure 17 is a time history of a STOL take-off showing the variation of altitude, airspeed, and distance with time. The flaps are deflected to 33^{o} and the engines are at take-off thrust (99 percent rpm). The pilot starts the take-off by setting the brake and advancing the throttle, when the engine speed reaches about 96 percent, the brakes are released and the throttle advanced to 99 percent. Rotation is initiated after about 7 seconds at 60 knots, and lift-off occurs at 72 knots at an angle of attack of about 10^{o} after about 198 m (650 ft) ground roll. The aircraft reaches an altitude of 11 m (35 ft) at 80 knots after 290 m (950 ft) total take-off distance. The climb is made at 85 to 90 knots at a climb angle of 12^{o} to 13^{o}.

The take-off is very short in both distance and time and is characterized by a rapid rotation to a high attitude angle, about 20^{o} at lift-off. The pilots have had no problems with the take-off and consider the control during take-off quite conventional. The optimum flap deflection for take-off has not been determined. The 30^{o} flap used to date was chosen as a compromise between performance and engine and climb capability.

STOL approaches and landings are illustrated in figure 18. The figure shows the variation of several items with distance from touchdown. The nominal landing configuration is with the flap deflected to 65^{o}, at an engine speed of 92 percent, and the engine nozzle positioned for the flight path desired. In a particular landing approach, shown in figure 18, the pilot chose an approach speed of 65 knots and an approach angle of 7.5^{o}. The attitude on the approach is quite flat with an angle of attack of about 2^{o}. The use of nozzle for flight-path control is illustrated by the steepening of the flight path at about 762 m (2500 ft) (see radio altitude) from touchdown when the nozzles are moved from the nominal setting of 75^{o} to about 90^{o}. The lift coefficient in this approach was 3.0 to 3.2 with a lift coefficient of about 3.8 in the flare.

The flare required a rapid rotation with about 10^{o} attitude change. The change in elevator required for the flare rotation was about 10^{o}. The pilots commented that the timing of flare must be quite precise. If the flare is a little high, the aircraft tends to float, and if too low, the touchdown tends to be firm. The poor longitudinal control feel characteristics increase the pilot's workload in the flare. The investigation of the techniques for more precise flare is continuing with consideration being given to the use of nozzle and throttle in the flare maneuver.

CONCLUSIONS

The following conclusions have been reached from the results of the initial flight tests of the augmentor-wing jet STOL research aircraft:

1. The flight-measured aerodynamic characteristics in terms of lift and drag variations with angle of attack and jet thrust coefficient at flap deflection for STOL take-off and landing are close to values predicted from the results of a similar half-scale wind-tunnel model.

2. The lateral-directional stability and control characteristics are similar to values predicted from wind-tunnel data and evaluated on the simulator before flight. With stability augmentation, the lateral-directional handling qualities are satisfactory for research STOL landing and take-off tasks performed to date.

3. The longitudinal stability and control characteristics are not as good as predicted and flown on the simulation. The stability appears to be lower for the conditions flown and the longitudinal control feel characteristics are unsatisfactory. Modification is planned to improve the longitudinal control system.

4. The take-off distance over 11 m (35 ft) with maximum take-off thrust and 30^{o} flap deflection is about 290 m (950 ft). The landing approach speed with 65^{o} flap deflection is between 60 and 65 knots.

REFERENCES

1. Wick, Bradford H.; and Kuhn, Richard E.: Turbofan STOL Research at NASA. Astronaut. & Aeronaut., vol. 9, no. 5, May 1971, pp. 32-50.

2. Whittley, D. C.: The Augmentor-Wing – A New Means of Engine Airframe Integration for STOL Aircraft. AIAA Paper No. 64-574, Aug. 1964.

3. Middlebrooks, J. E.; Tinney, H. C.; and Whittley, D. C.: The Evolutionary Development and Current Status of the Augmentor Wing Concept. [Preprint] 700812, Soc. Automot. Eng., Oct. 1970.

4. Kelley, G. S.; and Gerend, R. P.: Propulsion Systems for Commercial STOL Aircraft. AIAA Paper No. 71-746, June 1971.

5. Whittley, D. C.: The Augmentor-Wing Research Program: Past, Present and Future. AIAA Paper No. 67-741, Oct. 1967.

6. Koenig, David G.; Corsiglia, Victor R.; and Morelli, Joseph P.: Aerodynamic Characteristics of a Large-Scale Model With an Unswept Wing and Augmented Jet Flap. NASA TN D-4610, 1968.

7. Cook, Anthony M.; and Aiken, Thomas N.: Low-Speed Aerodynamic Characteristics of a Large-Scale STOL Transport Model With an Augmented Jet Flap. NASA TM X-62,017, 1971.

8. Falarski, Michael D.; and Koenig, David G.: Aerodynamic Characteristics of a Large-Scale Model With a Swept Wing and Augmented Jet Flap. NASA TM X-62,029, 1971.

9. Harkonen, D. L.; Wintermeyer, C. F.; and Wright, F. L.: Static Tests of a 0.7 Scale Augmentor Wing Flap for the Modified C-8A Airplane – Test Results and Analysis. D6-24850 (Contract NAS2-6025), Boeing Co., May 1971. (Available as NASA CR-114315.)

10. O'Keefe, J. V.; and Kelley, G. S.: Design Integration and Noise Studies for Jet STOL Aircraft. Vol. I – Program Summary. D6-40552-1 (Contract NAS2-6344), Boeing Co., May 1972. (Available as NASA CR-114471.)

11. Quigley, H. C.; Sinclair, S. R. M.; Nark, T. C., Jr.; and O' Keefe, Jack V.: A Progress Report on the Development of an Augmentor Wing Jet STOL Research Aircraft. [Preprint] 710757, Soc. Automot. Eng., Sept. 1971.

12. Spitzer, R. E.: Predicted Flight Characteristics of the Augmentor Wing Jet STOL Research Aircraft. Doc. D6-40381 (Contract No. NAS2-6025), Boeing Co., July 1972. (Available as NASA CR-114463.)

13. Rumsey, P. C.; Spitzer, R. E.; and Glende, W. L. B.: A Design Support Simulation of the Augmentor Wing Jet STOL Research Aircraft. D6-24806-1 (Contract NAS2-6025), Boeing Co., Jan. 1972. (Available as NASA CR-114435.)

14. Spitzer, R. E.; Rumsey, P. C.; and Quigley, H. C.: Use of the Flight Simulator in the Design of a STOL Research Aircraft. AIAA Paper No. 72-762, Aug. 1972.

TABLE I.- AIRCRAFT CHARACTERISTICS

Characteristics	Design	Remarks
Maximum weight, kg (lb)	20 412 (45 000)	
Maximum landing weight, kg (lb)	19 505 (43 000)	
Wing loading	49.6	19 505 kg (43 000 lb) gross weight
Nominal approach speed, knots	60 to 65	
Power on stall speed, knots	45	About one-half maximum thrust
Engine thrust:		
Primary –		
Take-off, N (lb)	27 133 (6100)	
Emergency, n (lb)	30 246 (6800)	
Fan –		
Take-off, N (lb)	15 346 (3450)	
Emergency, N (lb)	16 013 (3600)	
Maximum rate of descent at touchdown, m/sec (ft/sec)	3.7 (12.0)	19 505 kg (43 000 lb) gross weight
Limit speeds:		
Cruise, knots	160	
Dive, knots	180	
Flap up (6°), knots	160	
Flap 50°, knots	100	
Flap 75°, knots	95	
Wing:		
Area, m^2 (ft^2)	80.4 (865)	
Span, m (ft)	24 (78.75)	
Dihedral, deg	5.0	Outer wing only
Incidence, deg	2.5	
Mean aerodynamic chord, m (ft)	3.7 (12.1)	
Sweep, deg	0	
Aspect ratio	7.2	
Flaps:		
Span (each side), m (ft)	7.01 (23)	
Chord, m (ft)	1.07 (3.5)	
Deflection –		
Minimum, deg	6	
Maximum, deg	75	
Horizontal tail:		
Total area, m^2 (ft^2)	21.7 (233)	
Elevator area (aft hinge line), m^2 (ft^2)	7.6 (81.5)	
Span, m (ft)	9.75 (32.0)	
Aspect ratio	4.4	
Vertical tail:		
Total area, m^2 (ft^2)	14.1 (152)	
Rudder (aft hinge line) –		
Forward, m^2 (ft^2)	2.8 (30)	
Aft, m^2 (ft^2)	2.8 (30)	
Span, m (ft)	8.5 (28)	
Aspect ratio	1.12	

TABLE II.- LATERAL-DIRECTIONAL CHARACTERISTICS

[Flap deflection, 65°; airspeed, 60 to 65 knots]

	SAS on	SAS off
Dutch roll period	≈8.5 sec	≈6.5 sec
Dutch roll damping ratio	≈0.3	≈0.08
Effective roll time constant	≈0.5 sec	≈1.0 sec
Spiral stability	≈Neutral	≈7 sec to double
Turn coordination, $\Delta\beta/\Delta\phi$	≈0.3	≈0.7

Figure 1

UNMODIFIED C-8A AIRPLANE

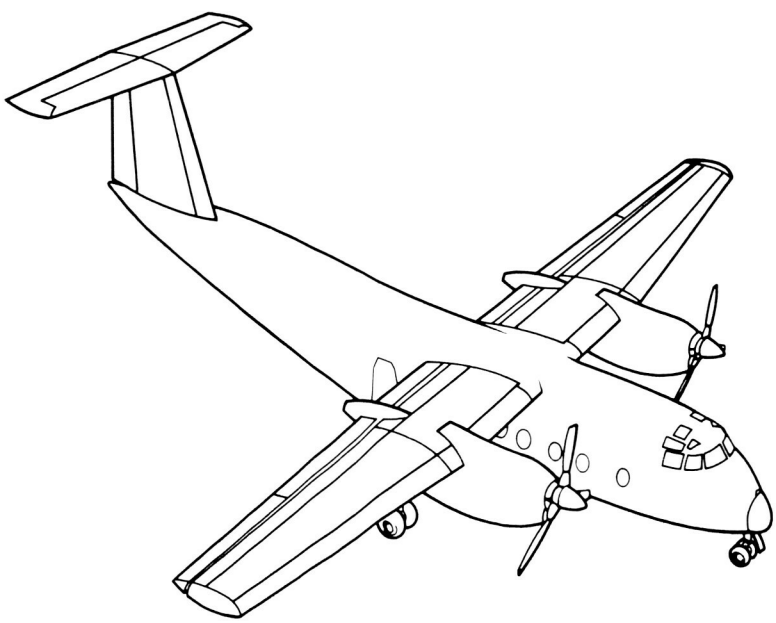

Figure 2

AUGMENTOR-WING JET STOL RESEARCH AIRCRAFT

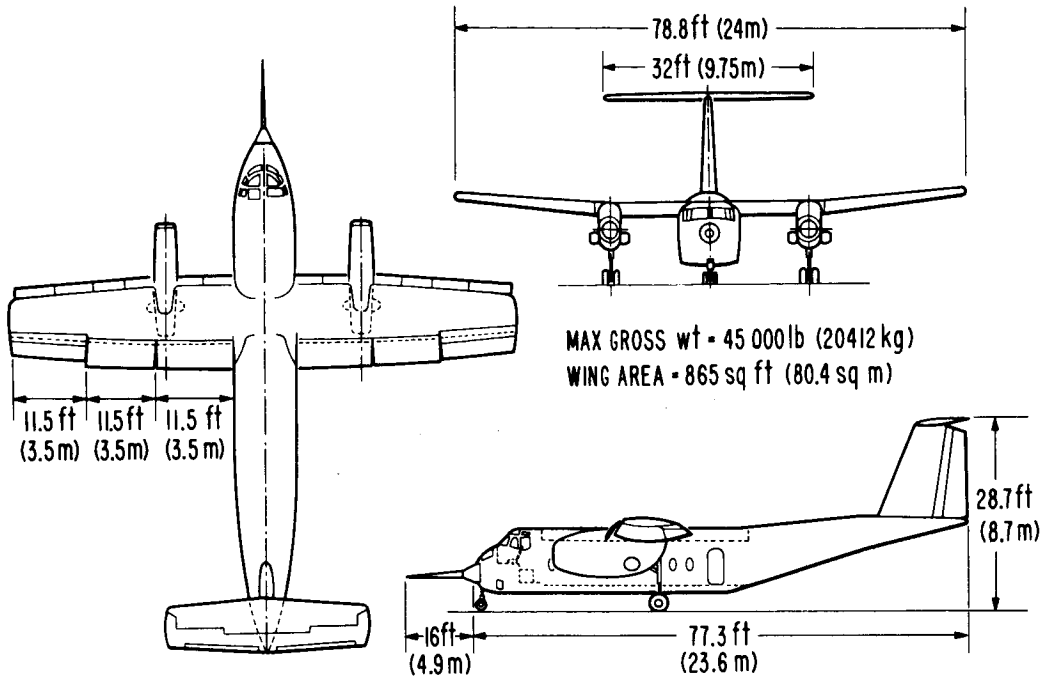

Figure 3

AUGMENTOR - WING FLAP DETAILS

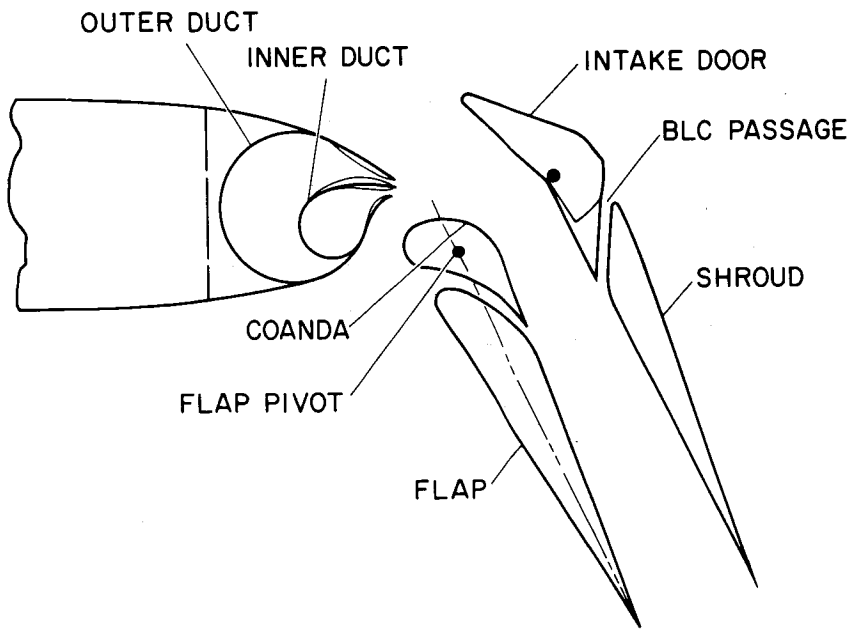

Figure 4

STATIC AUGMENTOR FLAP PERFORMANCE
0.7 – SCALE MODEL TESTS

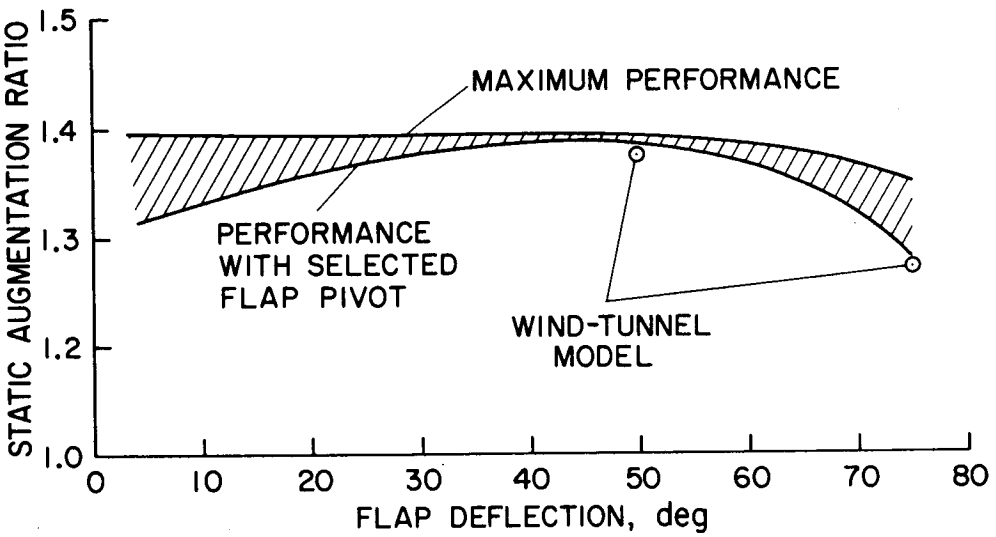

Figure 5

ROLLS ROYCE SPEY MK 801 SF ENGINE INSTALLATION

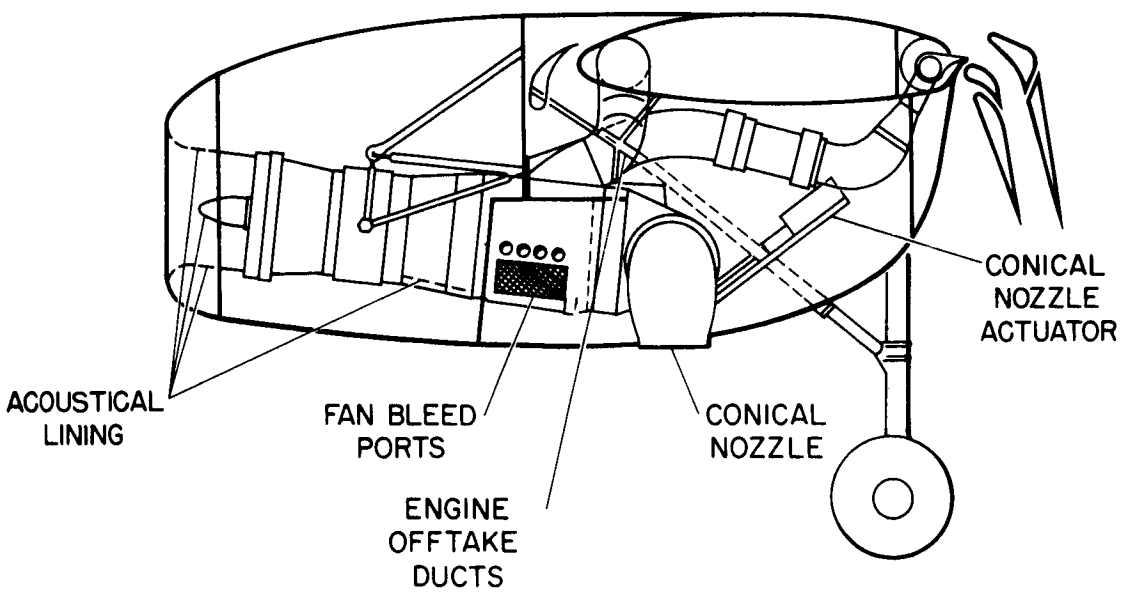

Figure 6

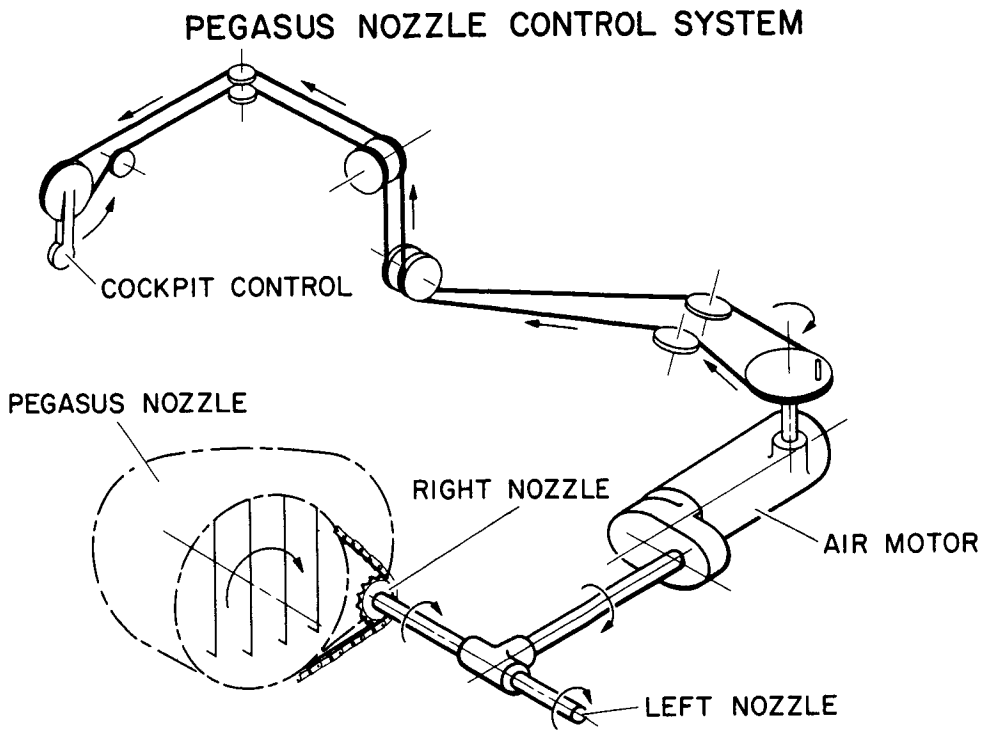

Figure 7

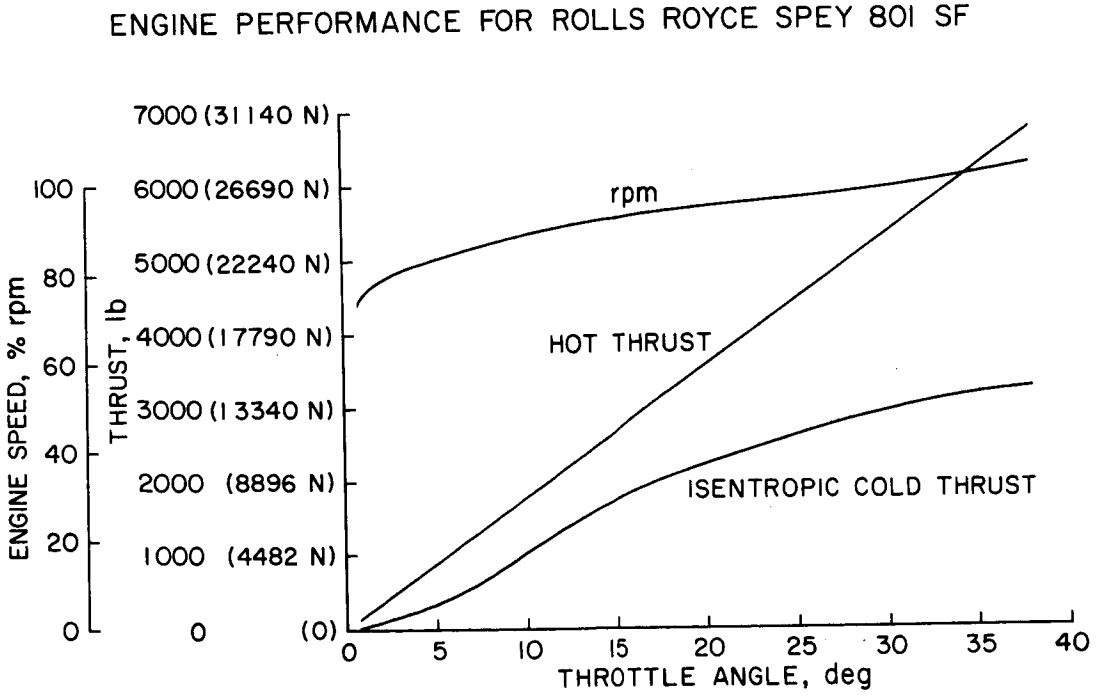

Figure 8

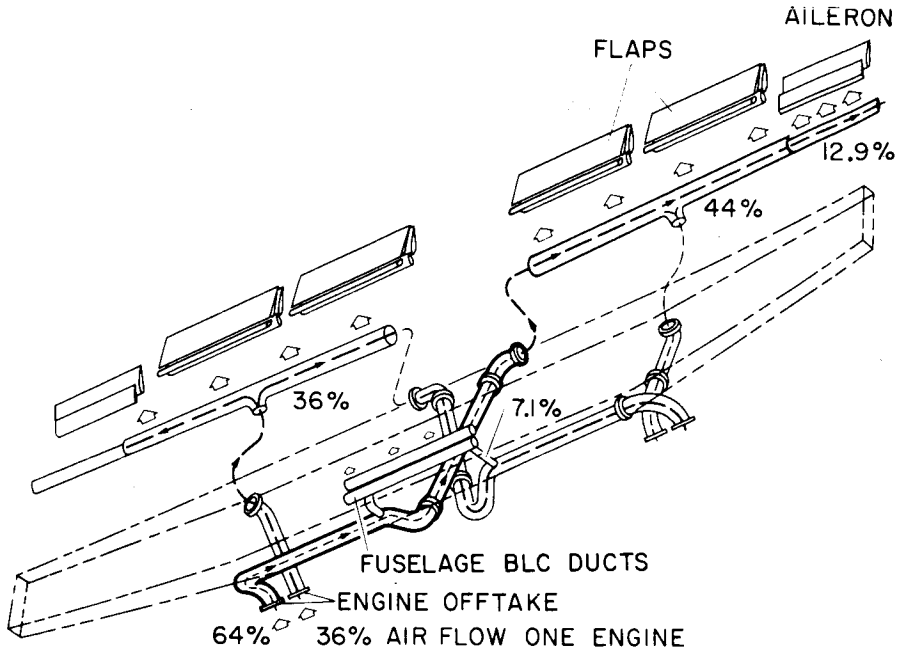

Figure 9

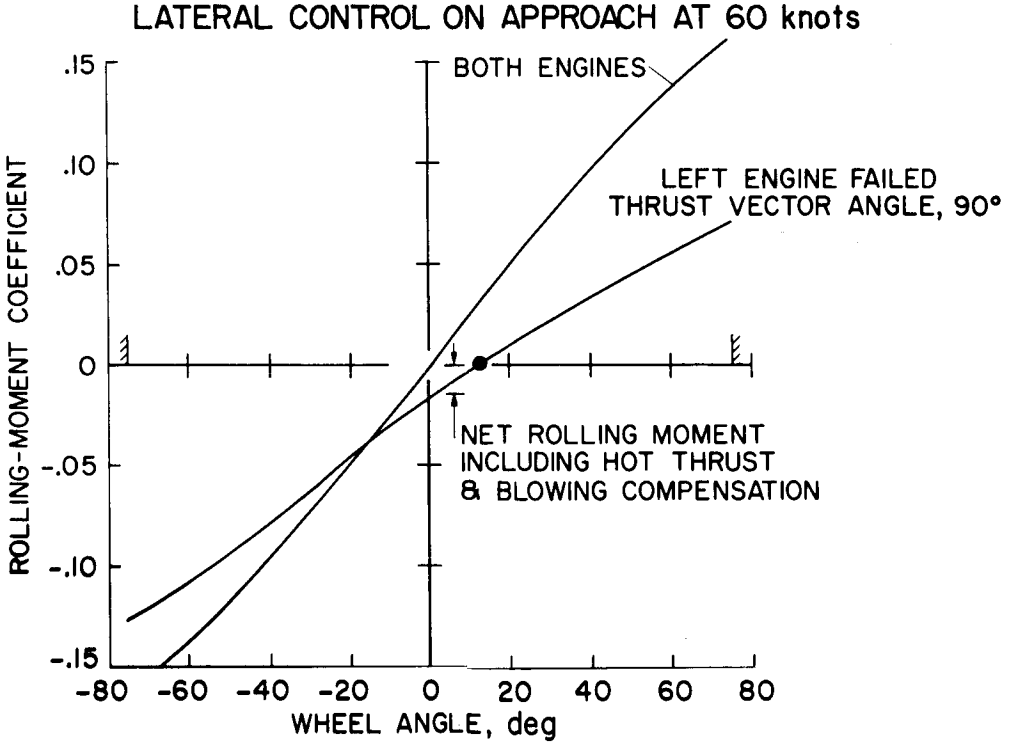

Figure 10

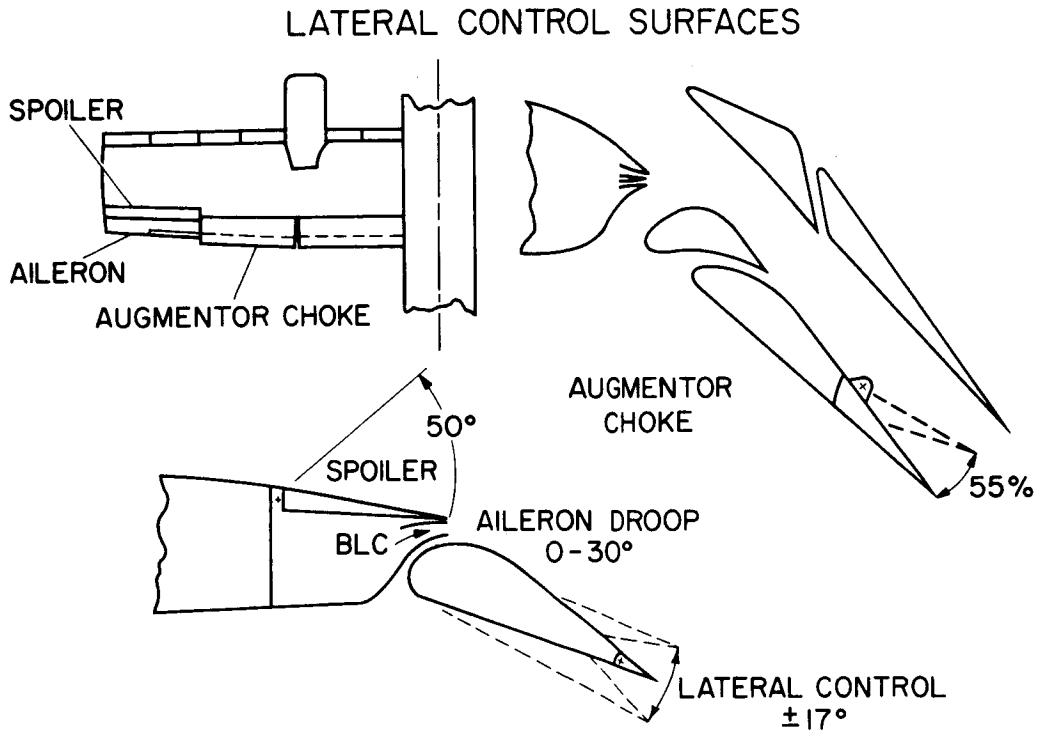

Figure 11

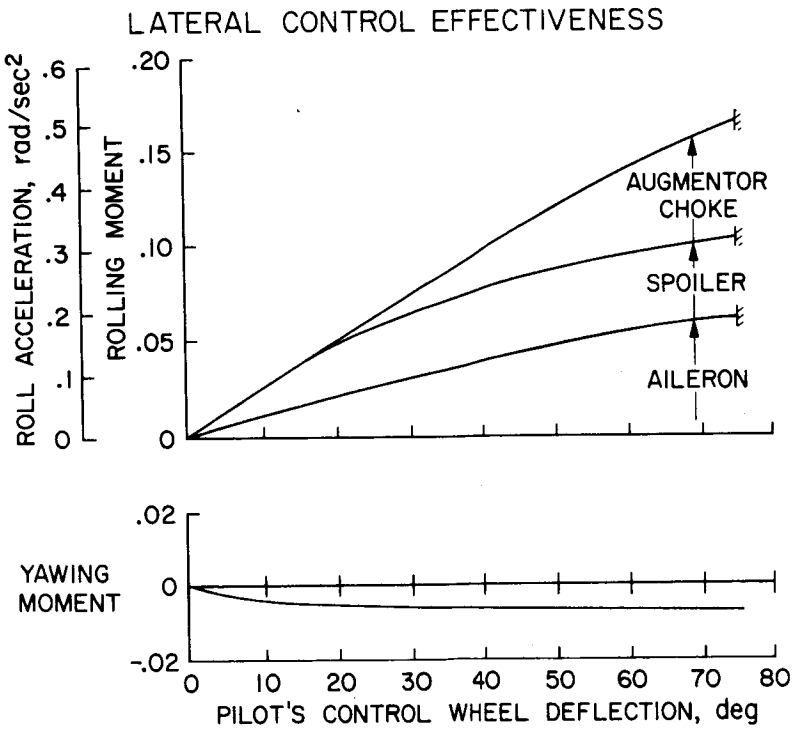

Figure 12

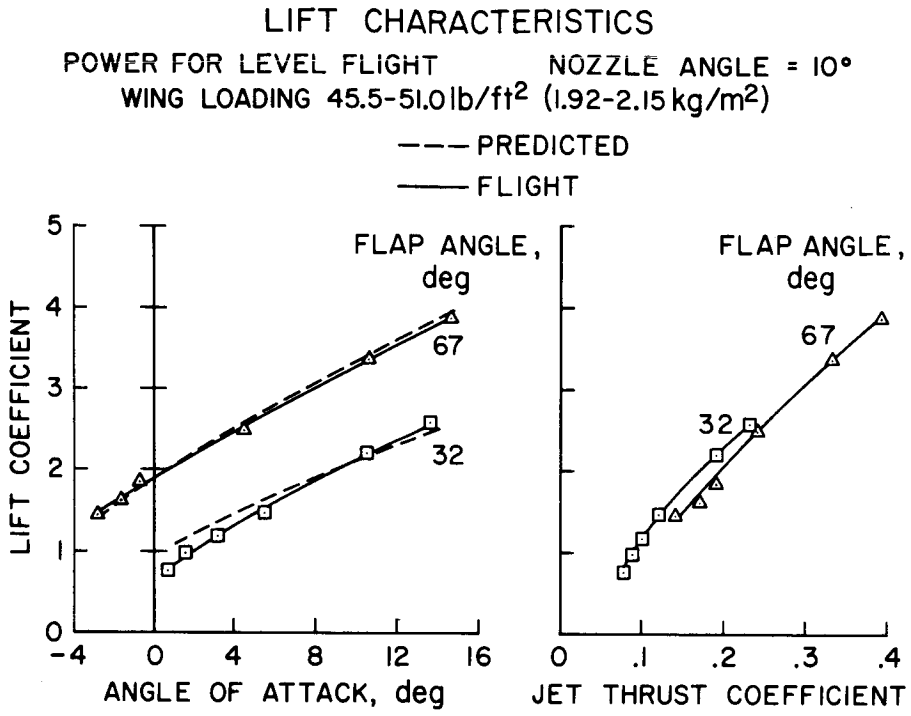

Figure 13

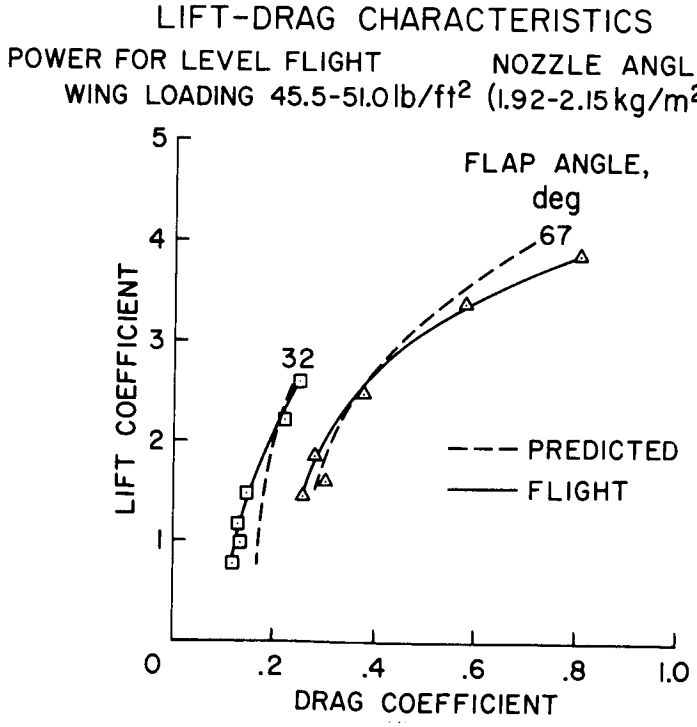

Figure 14

STOL OPERATIONAL ENVELOPE - EFFECT OF THRUST

WING LOADING 45.5 - 51.0 lb/ft^2 (1.92 - 2.15 kg/m^2)

ALTITUDE = 2 000 - 3 900 ft (609 - 1188 m)

FLAP ANGLE = 67°

NOZZLE ANGLE = 16°

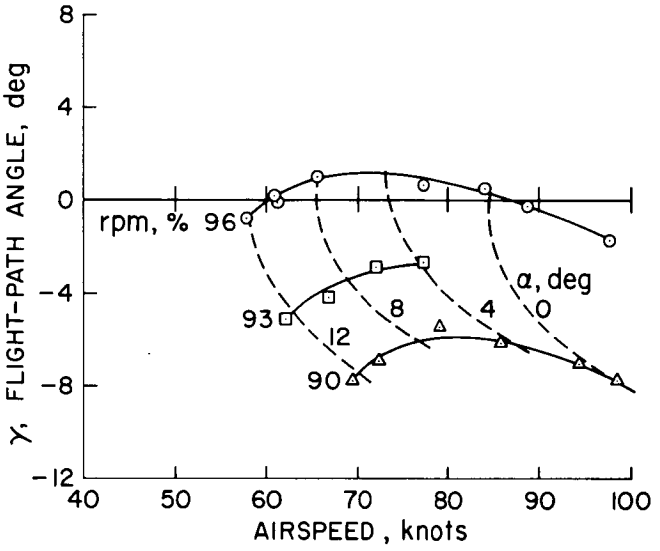

Figure 15

STOL OPERATIONAL ENVELOPE - EFFECT OF NOZZLE ANGLE

WING LOADING 45.5 - 51.0 lb/ft^2 (1.92 - 2.15 kg/m^2)

ALTITUDE = 2 000 - 3 900 ft (609 - 1188 m)

FLAP ANGLE = 67°

96% rpm

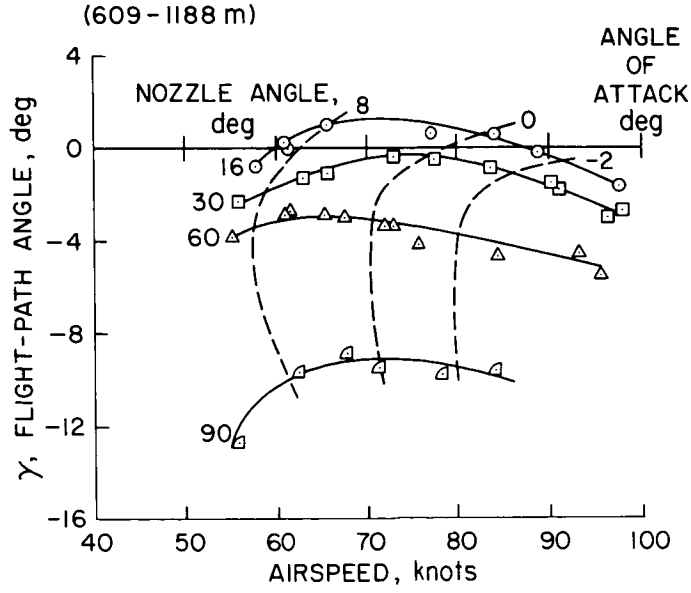

Figure 16

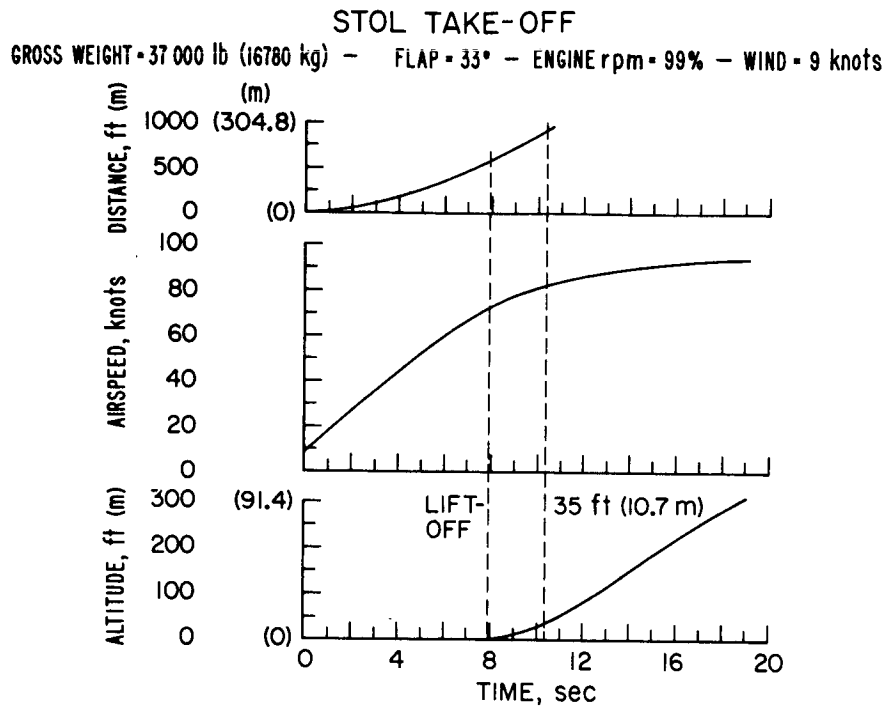

Figure 17

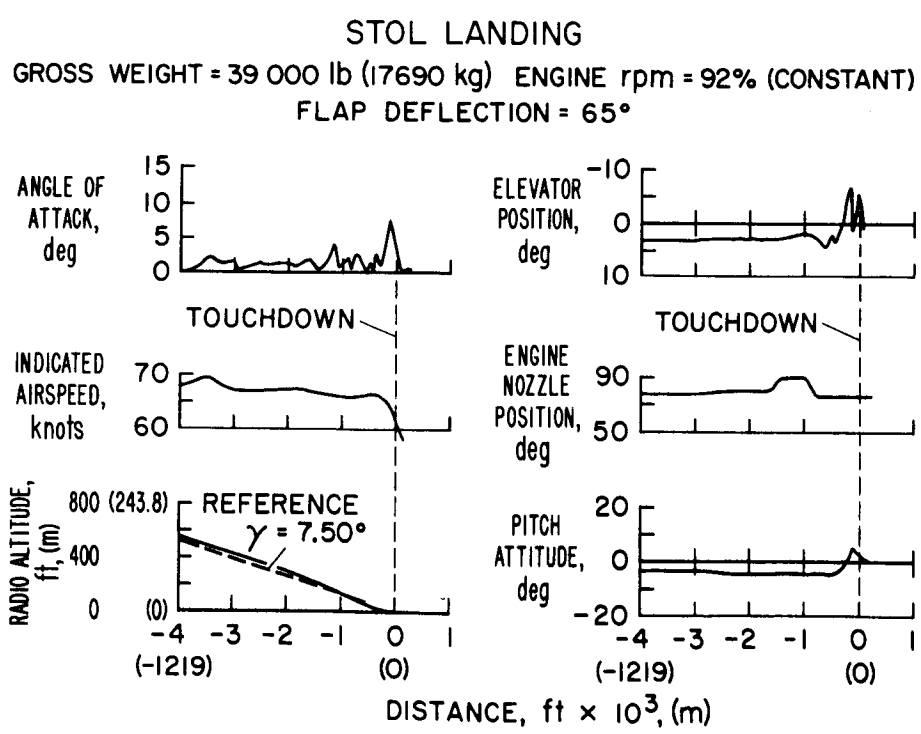

Figure 18

COMPARISONS OF SIMULATOR AND FLIGHT RESULTS ON AUGMENTOR-WING JET STOL RESEARCH AIRCRAFT

By Robert C. Innis and Seth B. Anderson
NASA Ames Research Center

INTRODUCTION

Piloted simulators have evolved in recent years to become a popularly accepted research tool for use in aircraft design. In general, acceptance by experienced test pilots of the usefulness of simulators has been mixed. In order for the pilot to have confidence in applying meaningful pilot ratings to handling qualities characteristics, for example, he must be provided with acceleration and force cues which give some reasonable representation of actual flight. For the most part this has meant that large improvements in cab motion responses and real-life visual displays have been necessary. Compare, for example, the early Link trainer (fig. 1) with the flight simulator for advanced aircraft (FSAA) (fig. 2). The former has three degrees of very limited angular cab motion and its only IFR capability consists of the most basic flight instruments. The FSAA, on the other hand has six degrees of motion freedom with a lateral movement of ±15 m (±50 ft) and a colored closed-circuit TV presentation that provides a collimated view of the real world.

Even this sophisticated simulator will not in all cases give the pilot the complete realism of actual flight. In fact, for some conditions it may be only 25-percent effective in providing the pilot the "feel" of a given aircraft. This may be true in particular for simulating pilot training missions or for certain complex research tasks where very accurate "modeling" of the characteristics of a specific aircraft is required. The need to provide representative behavior can be very important during flare in ground effect, for example.

The purpose of this paper is to show, from the test pilot's point of view, the considerations that must be taken into account to make the piloted simulator an effective research tool in the design and development of a new aircraft. Included is an assessment of the limitations of the simulator in depicting real flight as well as the problem of recognizing erroneous results when the simulator is supplied with incorrect input data.

This paper discusses only four examples of the many ways in which the simulator was used to design and develop the augmentor-wing aircraft shown in figure 3. These four examples are:

- Design: The lateral-control system to provide good feel and response.
- Investigate: Effect of engine failure during approach.
- Determine: The best technique for controlling flight-path angle during approach.
- Evaluate: The significance of lift loss in ground effect and how to cope with it.

RESULTS AND DISCUSSION

Design of Lateral-Control System

Roll control of the augmentor wing is provided by three separate surfaces on each wing, as described in more detail in paper no. 20. These consist of a drooped aileron with boundary-layer control applied to its leading edge, a spoiler directly in front of the aileron, and an augmentor choke which essentially reduces the effectiveness of the outboard augmentor flap. The rolling moments of the latter two are nonlinear; therefore, if all three surfaces were operated simultaneously, the result would be an unsatisfactory variation of rolling response with wheel deflection. The rolling moments of each of these surfaces were obtained from wind-tunnel tests and were programed separately into the simulator. A combination of mixing and gearing, shown in figure 4, was found that produced a linear response which the pilots liked. The roll acceleration resulting from this gearing is presented in figure 5. It can be seen that the augmentor choke is necessary to provide linearity at the higher wheel deflections.

In addition, evaluations were made of maximum lateral-control power, control sensitivity, rate limits, force gradients, and so forth, to tailor the characteristics for the pilots' approval. The flight tests have verified the acceptability of the lateral-control characteristics as developed on the simulator throughout the entire flight envelope; in fact, the airplane is quite maneuverable for a transport. At low approach speeds (60 to 65 knots) where turn rate is inherently large, we no longer speak of turn rate in terms of deg/sec but rather in terms of revolutions/min. The behavior of the aircraft has been examined with either the spoilers or the augmentor choke inoperative. The noticeably reduced roll rate and increased adverse yaw in turn entries convinced the pilots that these surfaces were required for satisfactory operation.

Effect of Engine Failure

In the second example, the simulator was used to examine a failure mode which cannot be safely investigated in flight – an engine failure at very low altitude during the approach to landing. The fact that this aircraft uses "powered lift" implies that if engine power is lost during this mode of flight, lift will be considerably reduced. Bear in mind that this aircraft has only two engines and uses about 50 percent of the installed thrust to

maintain an approach angle of $7\frac{1}{2}^{\circ}$. The consequences of an engine failure on the airplane were investigated on the simulator. It can be seen from the time history (fig. 6) that when the engine fails, there is an immediate increase in sink rate to something over 6 m/sec (20 ft/sec). Airspeed and angle of attack both increase as a result of the reduced lift. As a result of the cross-ducting, there is no appreciable roll or yaw asymmetry and the pilot's task of keeping the airplane straight and level is alleviated. It can be noted in the time history that the pilot responds quite rapidly to the engine failure by advancing the throttle of the good engine and rotating the nozzles to vector the thrust aft. By doing this and increasing the pitch attitude, the pilot reestablishes a reasonable enough rate of descent to accomplish a safe landing. It is quite probable, however, that the aircraft would land short of the intended touchdown spot or descend below the obstacle-clearance plane. This particular maneuver has not been duplicated in flight, but we have confirmed that single-engine asymmetric moments are small and can be easily trimmed. In essence, this means that minimum control speed is defined by the single-engine stall speed. The pilot is not concerned about losing control of the airplane when an engine fails, but he is concerned about the loss of altitude and therefore the ability to achieve a positive climb gradient with high flap deflection.

Control of Flight-Path Angle

In the third example of use of the simulator, the problem of flight-path control is addressed, using as a background paper no. 15, which is devoted entirely to this subject. There are two methods by which control of the flight path is obtained with this particular airplane. One is by modulating the position of the engine exhaust nozzles, which are normally set nearly vertical in the approach. To the pilot, this changes the longitudinal component of the thrust vector in much the same manner as the throttles do in a conventional aircraft. Of course the pitch attitude must be adjusted to maintain a constant airspeed. The second method of control is to modulate the magnitude of engine thrust. Because of the near-vertical nozzle position, this is a very powerful direct lift control with which flight path can be controlled with very little or no change in pitch attitude.

During the evaluations on the simulator, there was general agreement among the pilots that the nozzle control method was preferable, since, as previously noted, the technique was much the same as for conventional aircraft and the magnitude of control seemed adequate. This did not prove to be the case in flight, however. Although swiveling the nozzles was very effective for gross flight-path changes, the initial aircraft response to nozzle deflection was opposite to that desired. As a consequence, the pilots were reluctant to change the nozzle position when close to the ground, when small corrections were desired, or to initiate a wave-off when near the ground. Nozzle angle must be fixed prior to flare. Further, nozzle modulation proved to be very effective in controlling airspeed

(throttles fixed). Thrust modulation, on the other hand, could be used to obtain rapid aircraft response, but precision of control was not satisfactory since the aircraft response was too sensitive to small throttle inputs and the result was overcontrol. The best technique devised to control the flight-path angle incorporated both methods of control; nozzle modulation was used to make a course adjustment, such as to capture the glide path, and then fairly tight control of flight path was maintained with power changes. Now it's true that the results from flight and simulator tests were different in respect to the best technique for flight-path control, a fact which illustrated simulator deficiencies. It should be noted, however, that these differences are subtle; it is probably beyond the capabilities of this simulator to provide the proper cues with its limited vertical motion and two-dimensional display.

Flare and Touchdown Characteristics

One of the factors of greatest concern disclosed by the simulator studies was the adverse behavior of the aircraft in ground effect. Programed into the simulator were the ground-effect characteristics from theory and wind-tunnel tests, which predicted an appreciable lift loss and pitching moment. With these values it was found that the pilot could not adequately arrest the sink rate by aircraft rotation alone and had to resort to power addition or a reduction in nozzle angle to assist the flare. Even then the touchdown rate of descent was frequently greater than desired. On the basis of the simulator experience, the STOL landing was approached very cautiously in flight by increasing the steepness of the flight path and deflecting the nozzle in a more nearly vertical direction in small increments while looking for the expected nose-down pitching moment and attendant suck down. The pilot was pleasantly surprised to find that for the conditions tested no adverse ground effect was detected; in fact, some difficulty was experienced with excessive floating after the flare.

This experience, in which different results were obtained from the simulator and flight, brings out two important points: (1) Flight results showed that the data programed on the simulator were erroneous and were misleading to the pilot, and (2) it is equally important that identical test conditions be examined on the simulator and in flight. At this time it is too early to know whether the lift coefficients obtained thus far in flight are as large as those which were used in the simulator tests. Further flight tests and a more thorough analysis of flight data are needed to clarify this apparent discrepancy between flight and simulator results.

CONCLUDING REMARKS

Examples have been given of several ways in which the piloted simulator was used to aid in the design and development of the augmentor-wing jet STOL research aircraft.

As a result of the simulator studies no serious surprises were encountered in flight, and the aircraft undoubtedly was easier to fly and had pleasanter handling characteristics as a result of the many hours spent on the simulator. In particular, the ability to examine failure modes on the simulator shortened the amount of flight-test time required for flight checkout and gave the pilot more confidence by letting him know what to expect should a failure result.

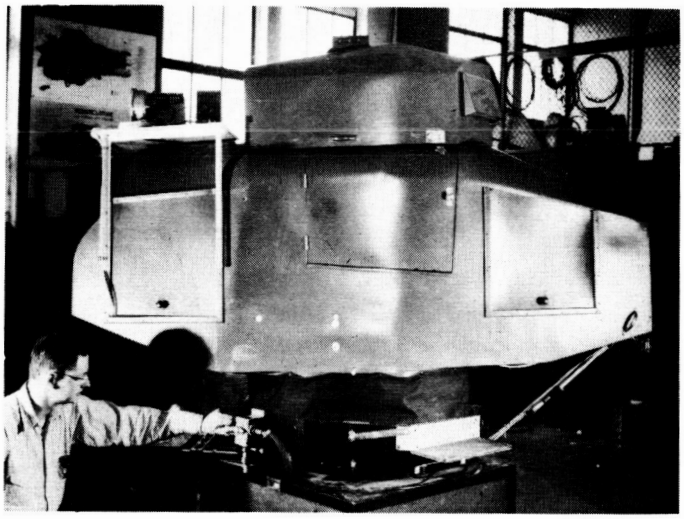

Figure 1.- View of early type of piloted simulator (Link trainer).

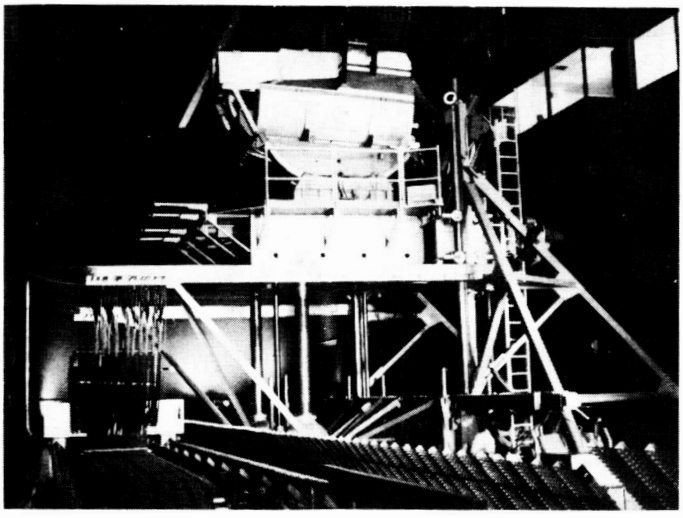

Figure 2.- Flight simulator for advanced aircraft (FSAA), which has 6 degrees of motion freedom.

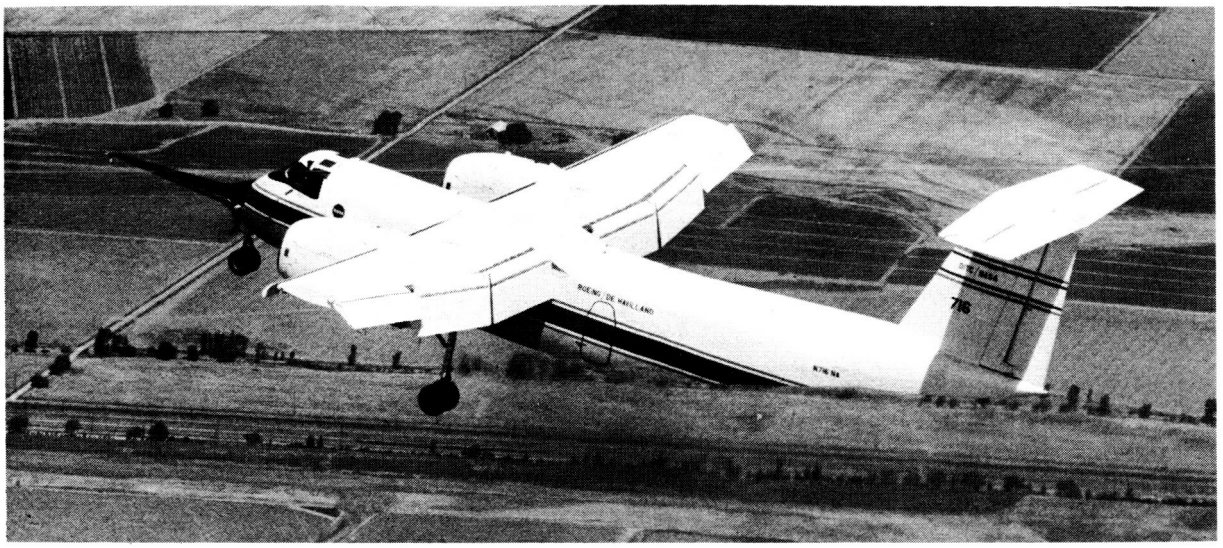

Figure 3.- In-flight view of augmentor-wing jet STOL research aircraft.

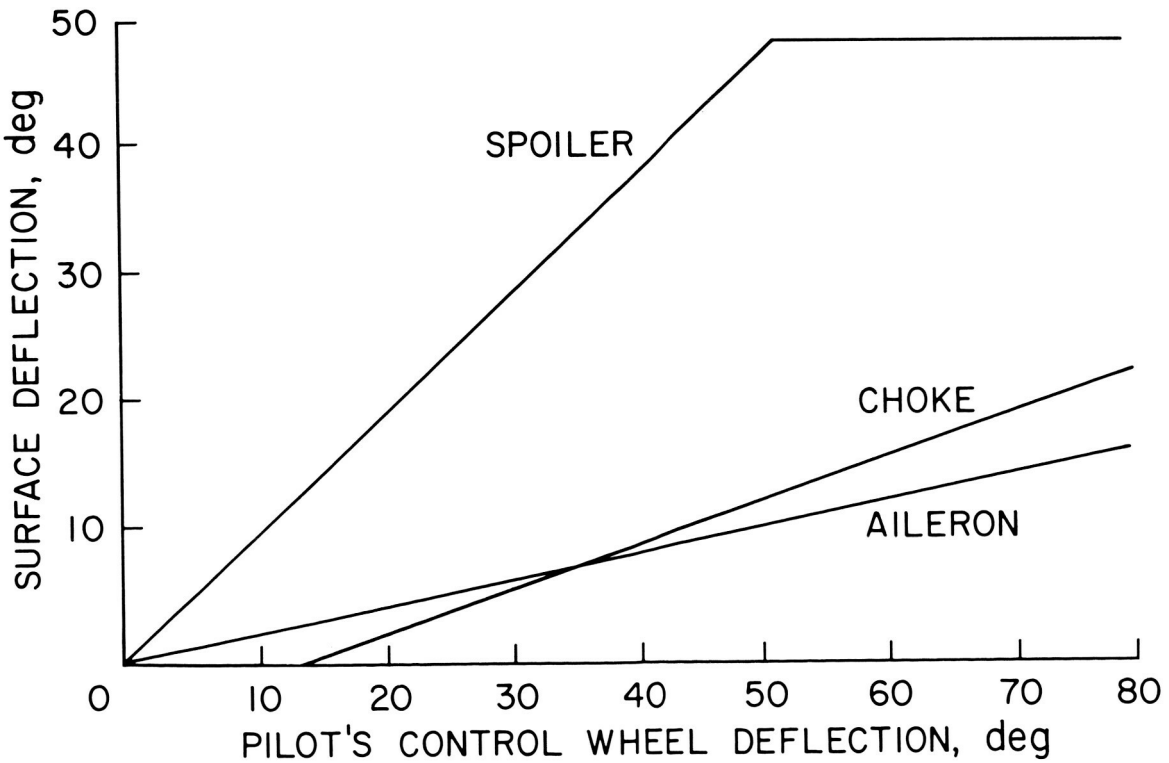

Figure 4.- Control gearing for various lateral-control devices.

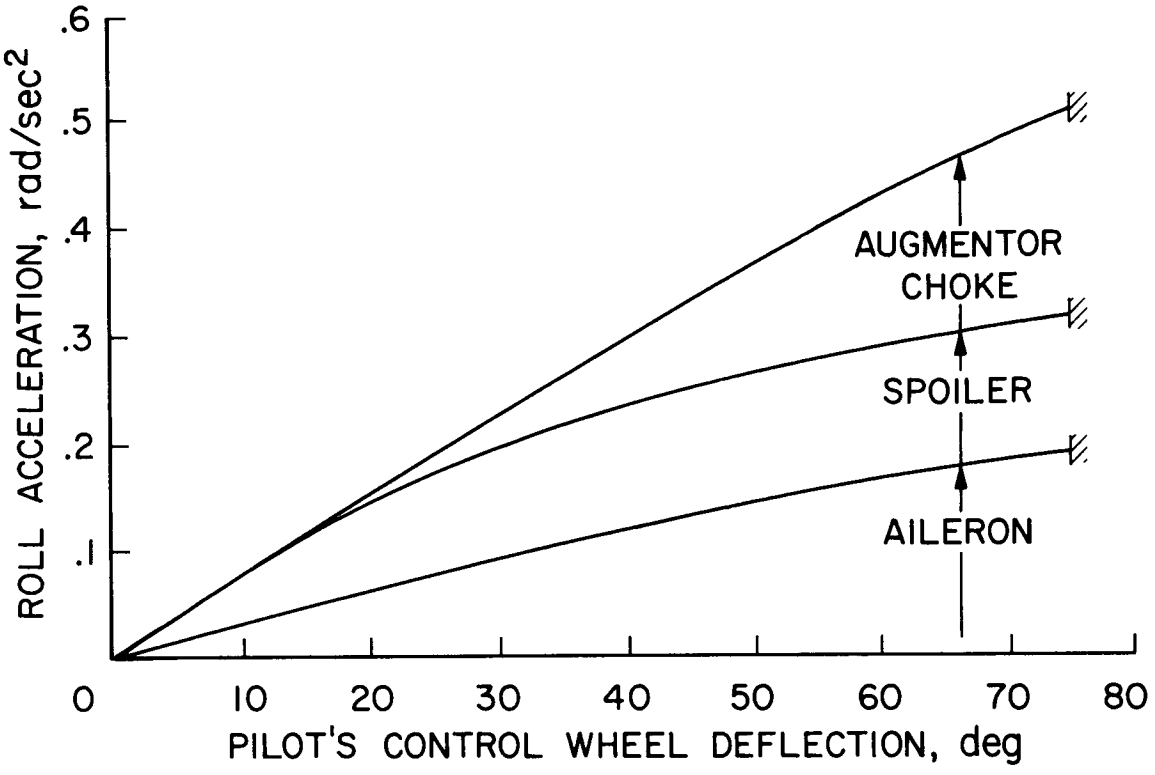

Figure 5.- Variation of roll acceleration with wheel deflection for various lateral-control devices.

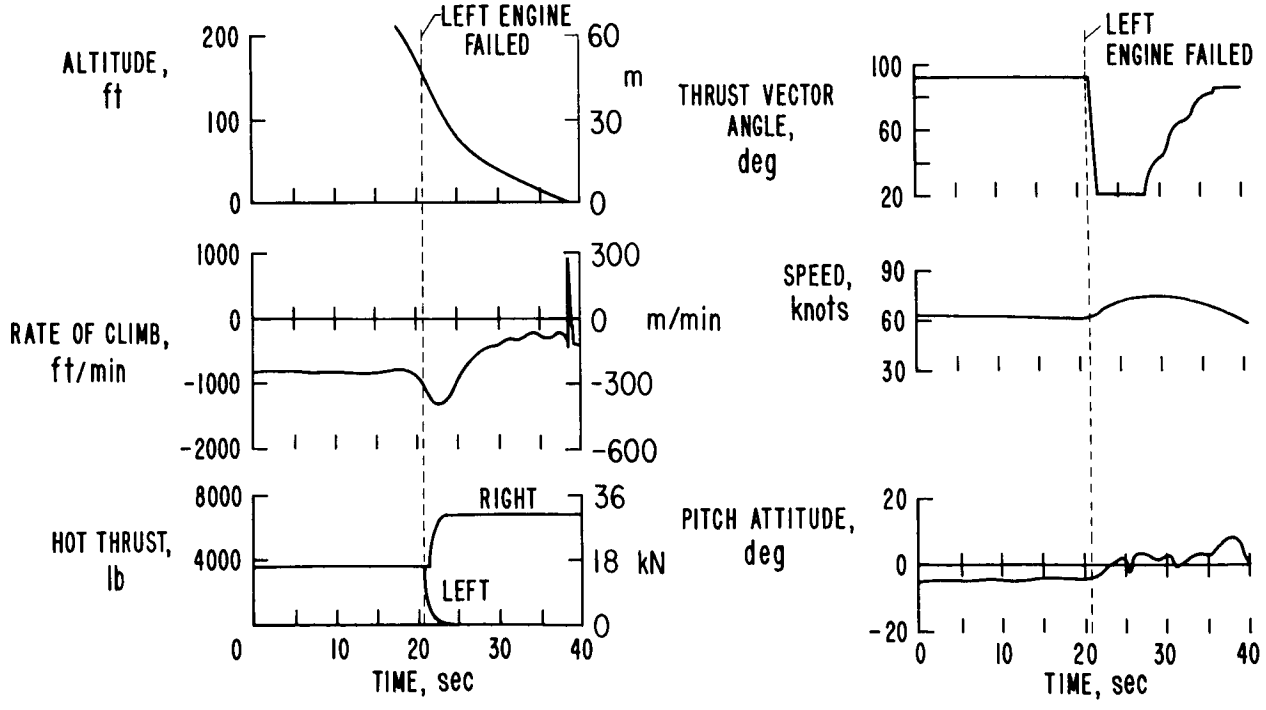

Figure 6.- Time history of engine failure in landing approach.

INTEGRATION OF STOL AIRPLANES INTO THE ATC SYSTEM

By Paul Petersen, Richard H. Sawyer,
and Milton D. McLaughlin

OBJECTIVES

The study involving the STOL airplane and air traffic control is a joint NASA/FAA effort designed to examine the effects of introducing large numbers of STOL airplanes into a high-density terminal area. Simply stated, the objectives of the study are (1) to determine the effects of the STOL airplane on the air traffic control (ATC) system and (2) to determine the effects of the ATC system on the STOL airplane. More specifically, the study seeks to determine (1) the airspace requirements and air traffic control equipment and handling techniques required to accommodate the STOL airplane in the ATC system and (2) the design characteristics, avionics equipment, and flight procedures required to operate the STOL airplane in the air traffic control system.

PART I – EFFECTS OF STOL AIRPLANES ON THE AIR TRAFFIC CONTROL SYSTEM

By Paul Petersen
Federal Aviation Administration, Washington, D.C.

This part of the paper discusses the objectives which are concerned with the air traffic control aspects of the study. From an air traffic control point of view, the major problem in the terminal area is lack of airspace for additional aircraft operations. The STOL airplane with its ability to operate at slow terminal airspeeds and execute relatively steep climb and descent profiles may provide a solution because it does not require as much operational airspace as conventional airplanes.

APPROACH

Since airspace is at such a premium, development of STOL airplane flight paths that encroach on already established conventional routes would only result in a trade-off of conventional airplane capacity for STOL airplane capacity. The approach, therefore, has been to develop air traffic control procedures and flight-path profiles tailored to the unique performance characteristics of the STOL airplane which, ideally, would enable it to operate in the terminal area independently of already established conventional airplane procedures.

In order to explore the situation in some depth, the current plan is to conduct a series of three real-time dynamic ATC simulations. These are (1) simulation of STOL operations at a downtown STOLport in a high-density terminal area, (2) simulation of STOL operations from separate runways at a busy conventional airport, and (3) a simulation including both the downtown STOLport and STOL runways at a conventional airport. The first two simulations have already been completed. The third, which will require a greater simulation capacity than that now available, has been deferred pending expansion of the simulation facility expected in 1973.

These simulations are being conducted at the FAA National Aviation Facilities Experimental Center (NAFEC) at Atlantic City, New Jersey, by means of a digital computer which can generate approximately 106 controllable radar targets on seven radar air traffic control displays or 80 targets on eight displays. (The number of displays and controllable targets is a variable which depends upon the complexities of the environment being simulated.) These simulated targets respond according to the performance criteria of the particular aircraft they represent; these criteria are programed into the computer. The targets are controlled by 24 pseudo "pilots" who react to control instructions received on interphone from the air traffic controllers by making appropriate computer keyboard entries.

In addition to the targets generated by the NAFEC computer, there is also a target input from the NASA Langley Research Center transport flight deck simulator. Telephone lines are used to convey airplane positional data and also for pilot controller communications. The Langley simulator serves as a valuable adjunct to the validity of the simulation. Operated by actual pilots and with more representative performance characteristics, it provides a degree of realism not otherwise possible as well as a potential for on-the-spot validation of procedures in use. The arrangement of the simulation facilities is depicted in figure 1.

The New York metropolitan area was selected as the site for the simulation. The three major and several peripheral airports provide a terminal air traffic environment of considerable complexity and density and the topography of this area provides most of the typical problems that can be anticipated in selecting an inner city STOLport site. Pertinent New York Common IFR Room (CIFRR) positions of operation, plus additional control positions for STOLport and STOL runway operations, were simulated. The number of controllers required for the various configurations in the first two simulations varied from 10 to 14. Controller displays were of a level of sophistication expected for the time period considered (1975-1980) with target tracking and symbology, handoff capability, and data tags consisting of identification, speed, and altitude. The air traffic environment was made up of peak day traffic samples obtained from the New York air traffic facilities and performance criteria of a family of STOL airplanes: the

De Havilland Otter, Buffalo, experimental augmentor-wing Buffalo, DHC-7, and the French Breguet. In order to keep pressure on the system, in determining capacities, the number of conventional and STOL airplanes was maintained at a level above that which could be accommodated.

The following test conditions were established:

(1) All operations were conducted under Instrument Flight Rules (IFR).

(2) The air traffic control facility had radar surveillance of, and radio communications with, traffic at all altitudes.

(3) Ninety percent of the STOL airplanes had area navigation capability.

(4) Adequate navigation aids were assumed to be available for all maneuvers required of STOL airplanes.

(5) Glide-slope angles of 7° or $7\frac{1}{2}^{\circ}$ were used for STOL airplane operations.

PHASE 1: DOWNTOWN STOLPORT

The first phase of the program was simulation of a downtown STOLport operation. The site selected was one that has been the subject of a study sponsored by the New Jersey Department of Transportation. It is located on the west bank of the Hudson River at the Morris Canal which is just about opposite the new Trade Center Building on lower Manhattan Island. (See fig. 2.) The proximity of LaGuardia, Newark, and Kennedy airports greatly restricted the airspace available for STOLport operations. Only the slow terminal speeds and steep approach/departure capability of the STOL airplanes made independent operations feasible. Independent routes (fig. 3) using relatively low arrival altitudes (1200 and 1500 m (4000 and 5000 ft)) were developed to serve the STOLport without any modification to current New York CIFRR procedures. Only a slight modification to current procedures was required to use altitudes of 2400 m (8000 ft) and above for STOL airplane arrivals.

Two methods of entering STOL airplanes into the terminal area were used. In the random entry method, the airplanes were entered on a "first come, first served" basis from the northeast and southwest. Controllers used mileage markers on the video map to determine separation between opposite direction flights. These markers were placed at 5-n. mi. intervals based on the point of convergence between the two arrival routes. They enabled the controllers to use speed control for sequencing arrivals from opposite directions. In the second method, a group of five or six airplanes was entered alternately from each direction. Although there was no significant difference in terms of capacity between the two methods, controllers preferred the second method, apparently because it eliminated the necessity for continually integrating opposite direction traffic at the

beginning of final approach. Standard separation was used between all targets except that a few additional simulation tests were made using a minimum of 2-n. mi. longitudinal separation between STOL airplanes at speeds of 120 knots or less and a minimum longitudinal separation of 1 n. mi. between departures and arrivals.

Arrival and departure configurations of the New York airports were simulated for three different wind directions. Controllers were able to maintain the independent status of the STOLport during each of these tests and achieved a relatively consistent capacity of 50 operations per hour when using standard separation criteria and 60 operations per hour when using reduced separation criteria. However, the limited available airspace did impose fairly tight restrictions on STOL airplane operations, requiring precise metering of arrivals by controllers and precise navigation and prompt response by STOL airplane pilots to control instructions.

PHASE 2: STOL OPERATIONS AT CTOL AIRPORTS

The second phase of the program was the investigation of the aspects of STOL operations at a high-density multirunway conventional take-off and landing (CTOL) airport. This second phase had two distinct parts.

In the first part of phase 2, various STOL runway configurations and placements on the CTOL airport were studied. For this experiment, which was referred to as Airport X, the Kennedy Airport runway layout (fig. 4) was used, but optimum flight paths were developed for these runways with no allowances for terrain, obstructions, noise abatement, or adjacent airports. A CTOL only operation was simulated to establish a data base of departure and arrival capacities, delays, and time in system from which to measure the impact of various STOL airplane operations. Three STOL runway configurations (fig. 5) were simulated: a 30^{o} "canted" configuration, a midfield parallel configuration, and an L-shape parallel configuration: Each configuration, with the exception of the midfield parallel, was simulated in two directions of operation. Standard separation was used except that 900 m (3000 ft) between CTOL and STOL runways on final approach paths was considered acceptable for simultaneous operations.

There was no significant adverse effect on CTOL airplane operations when the L-shape parallel configuration was used for STOL airplanes. Neither was there any significant difference in capacities when the canted runway configuration was simulated in a northwest operation. However, in a southwest operation on the canted runway, overall CTOL airplane operations were decreased 25 percent and departure delay was more than doubled. These effects were caused by the interdependency of CTOL airplane departures on runway 22R and STOL airplane arrivals on runway 16. In the simulation of the midfield parallel configuration, a trade-off developed between expeditious turnouts for

STOL airplanes and delays to CTOL airplanes. As initially simulated, STOL airplane departures to the east and south were turned left and right on course immediately after take-off (fig. 6). This procedure resulted in delays to CTOL airplane departures and arrivals. Simulation of a different procedure requiring STOL airplane departures to climb straight ahead to 1200 m (4000 ft) resulted in better operation rates for CTOL airplanes but longer time in system and greater departure delays for STOL airplanes.

In the second part of phase 2, Kennedy Airport traffic as well as pertinent traffic flows of adjacent airports were simulated (fig. 7). Again, a sufficient number of CTOL only simulations were conducted to form a data base for two different wind directions. The STOL runway configuration selected (fig. 8) was one of several that have been the subject of some study for Kennedy Airport. This particular configuration was selected because it afforded an independent IFR capability in all directions of operation (if an assumed 900 m (3000 ft) lateral separation between STOL and CTOL airplane final approach paths is acceptable).

Like the downtown STOLport operation, airspace was at a premium and STOL airplane arrivals were routed into the area from just two directions, the northeast and southwest. Although there was no significant adverse impact on CTOL airplane operations, the limited airspace remaining for STOL airplanes required precise navigation and strict metering of STOL airplane arrivals. Speed control was also used extensively. A fairly consistent rate of 45 STOL airplane operations per hour was maintained in each direction of operation.

CONCLUDING REMARKS

On the basis of simulations performed at the FAA National Aviation Facilities Experimental Center, it appears that STOL airplane operations can be accommodated in a high-density terminal area, either at an independent STOLport or at a CTOL airport. The degree of difficulty in accommodating STOL airplane operations depends upon the unique features of the specific location. Basically, accommodation seems to be a function of airspace availability and airplane performance. Relatively steep glide-slope angles (7° or more) may be required, as in the downtown STOLport and midfield parallel runway configurations. Slow terminal operating speeds to achieve optimum climb and descent profiles and small turning radii are a must in some locations. Low-altitude navigation coverage and area navigation capability may also be essential. In areas of poor radar coverage, area navigation could provide the only reasonable means of ingress or egress and, in high-density locations even with good radar coverage, can be used to significantly reduce communication and controller workload.

PART II – EFFECTS OF THE ATC SYSTEM ON THE STOL AIRPLANE

By Richard H. Sawyer and Milton D. McLaughlin
NASA Langley Research Center

The objectives of NASA in this joint program were to determine the design characteristics, avionics equipment, and flight procedures required to operate the STOL airplane in the ATC system.

TEST CONDITIONS

The test conditions of relevance to the operation of the transport flight deck simulator at the Langley Research Center are briefly discussed. For downtown operations into and out of the canted runway configuration of figure 3, the airplane simulated at Langley was the augmentor-wing Buffalo. For airport operations into and out of the three runway configurations of figure 5, the Twin Otter and standard Buffalo airplanes were simulated. In addition to the conventional flight instrumentation, single-station area navigation (RNAV) capability, a flight director programed for straight-in ILS approach, and an optical projection moving map were available for guidance. NASA and FAA pilots provided the piloting for the experimental augmentor-wing Buffalo flights and some of the Twin Otter and Buffalo flights. Most of the Twin Otter and Buffalo flights were made by pilots from two commuter airlines (Command Airways and Pilgrim Aviation and Airlines) and two trunk airlines (Eastern and American).

DOWNTOWN STOLPORT OPERATIONS

Some operating problems encountered in the downtown STOLport operations are illustrated in figure 9. The STOL airplane routes shown are somewhat different from those shown in figure 3 because this situation is for a different wind direction. Navigation in the arrival operations was initially along the low-altitude airways and followed by use of area navigation (RNAV) along transition routes to the final approach course. Conversely, departure operations were initially made along area navigation transition routes to the low-altitude airways. In the initial simulated flights, departures along the curved track (shown in fig. 9) using RNAV with way points about 3 n. mi. apart were found to be difficult to fly. The procedure used was to approximate the path by flying straight-line segments between the way points. The consensus of the pilots was that there were too many way points and that they were too close together. The procedure was changed to omit the middle way point in order to reduce the workload. Pilot opinion was that such tracks should have a rectangular shape and that way points should be at least 5 n. mi. apart.

In the initial arrivals from the southwest, the airplane was descended to 1000 m (3300 ft) and slowed only to 140 knots at the beginning of the 180° turn to final approach. (This turn had a radius of 1 n. mi.) Consequently, the airplane had to be slowed (to about 100 knots) and descended to 700 m (2300 ft) for localizer intercept in the turn. Having only RNAV and straight-in ILS guidance, the pilots simply made a standard-rate turn until a course was established to intercept the final approach course at the desired angle. The workload for these simultaneous operations of turning, descending, and speed reduction was continuously high. The procedure was first modified to slow to 100 knots for the turn. This constant speed in the turn appeared to be acceptable for this airplane which had an approach speed of 65 knots. The descending turn still proved to be difficult. The procedure was further modified to descend to 700 m (2300 ft) at the start of the turn, which then made this part of the operation feasible but only at the expense of decreasing the altitude clearance relative to the Empire State Building to less than 240 m (800 ft).

Difficulty was still experienced in the approach because the final approach distance was so short (about 3 n. mi.) that localizer intercept and glide-slope intercept occurred almost simultaneously at the end of the turn. Localizer acquisition and slowing to approach speed (which involved conversion to powered-lift flight) were difficult to accomplish. More airspace for final approach was not available without infringing on the LGA airport approach airspace. Lower intercept altitudes were not feasible because of the Empire State Building. To provide distance for localizer intercept and transition to powered flight, pilots tended to fly outbound before starting the turn; this resulted in overshoots of 1/2 to 1 n. mi. For such a limited airspace situation, the problems encountered indicate a requirement for curved descending flight-path capability in order to ensure safe altitude clearance and the precise navigation needed. Also, such a situation indicates the requirement for the capability of conversion to powered-lift flight on the glide slope.

AIRPORT OPERATIONS

The STOL operating procedures used for a canted runway configuration at Airport X are shown in figure 10. Departures were radar vectored until on course to a VHF omnirange (VOR) station or RNAV way point. Arrivals were also radar vectored to provide by use of path stretching the sequencing of the traffic from the four directions for final approach. The arrival and departure routes shown are the nominal paths.

Some operating problems encountered in Airport X operations are illustrated in figures 11, 12, and 13. Because of projected STOL airplane high rate of descent capabilities, the procedure adopted was to bring the STOL airplanes in over the CTOL airplane traffic (fig. 11). In this method, the STOL airplane arrivals from the north and east were brought in over the CTOL airplane traffic which was on simultaneous final approach to the

parallel runways at Airport X. The result was that steep descent maneuvers were required. For example, STOL airplane traffic from the east was held at 2100 m (7000 ft) over downwind CTOL airplane arrival traffic and then was allowed to descend only to 1400 m (4500 ft) while crossing the final approach traffic. Another steep descent maneuver was thus required to intercept the glide slope at 900 m (3000 ft). The controllers often requested that the descent to 900 m (3000 ft) be made at the maximum descent rate. Rates of descent up to 600 m (2000 ft) per minute were measured. Because of the critical nature of starting each descent maneuver at the proper point and ending at the designated altitude and because of the required high steepness of the descents, the pilots felt that there should be a requirement for use of three-dimensional RNAV procedures in such a situation from safety and workload considerations.

In sequencing final approach traffic from the four directions, the controllers often had to request numerous heading and speed changes in the final control area. Examples of two arrival paths are shown in figure 12. Arrival 1 from the south, an extreme example, underwent eight radar vector heading changes and six airspeed change requests in the sequencing process. Arrival 2, a more usual example, underwent four heading changes and two airspeed changes. In addition to the heading and speed change requests, up to three altitude reassignment instructions were often received in the final control area. The average number of altitude reassignments was about $1\frac{1}{2}$.

In addition to the numerous maneuvers experienced in the sequencing process, lengthy sequencing maneuvers were sometimes required. An extreme example is shown in figure 13 for an approach from the south for a wind situation requiring an approach to runway 16 of the STOL runway configuration. The time for this arrival from a point 30 n. mi. south of the airport was 22 minutes (a block speed of about 80 knots). The airplane was slowed to 140 knots adjacent to the airport on the downwind leg. The downwind leg was extended to about 10 n. mi. north of the runway. Speed was reduced to 80 knots at the turn to final approach course. The time on final approach was about 7.5 minutes. Pilot reaction was expressed as a desire for a shorter maneuver by a reduction of speed on the downwind leg, that is, more use of speed control rather than path stretching for the sequencing process.

The problems illustrated in figures 11, 12, and 13 often resulted in high crew workload situations and also resulted in increases in flight time compared with the optimum of 5 to 6 minutes on the average and up to 15 minutes occasionally. In addition to the problems illustrated, approach vertical flight-path control for the Twin Otter and Buffalo airplanes was believed to be marginal on the 7° and 7.5° glide slopes used. Once established on the glide path, the pilots could maintain the path with no external disturbances. However, it was found to be essential that the airspeed and airplane configuration be established before glide-slope intercept in order to ensure capture of glide slope.

CONCLUDING REMARKS

Both the powered-lift and turboprop STOL airplanes were successfully operated in the downtown and airport environments. Some high crew workload situations were experienced in the arrivals as well as delays averaging from 5 to 6 minutes. For routine operations in these environments, in addition to meeting the requirements for steep descent and climb capability and three-dimensional area navigation capability noted in Part I, displays for curved descending flight-path capability, development of procedures for powered-lift conversion on glide slope, automatic speed control, and excellent handling qualities appear to be requirements.

SIMULATION FACILITIES

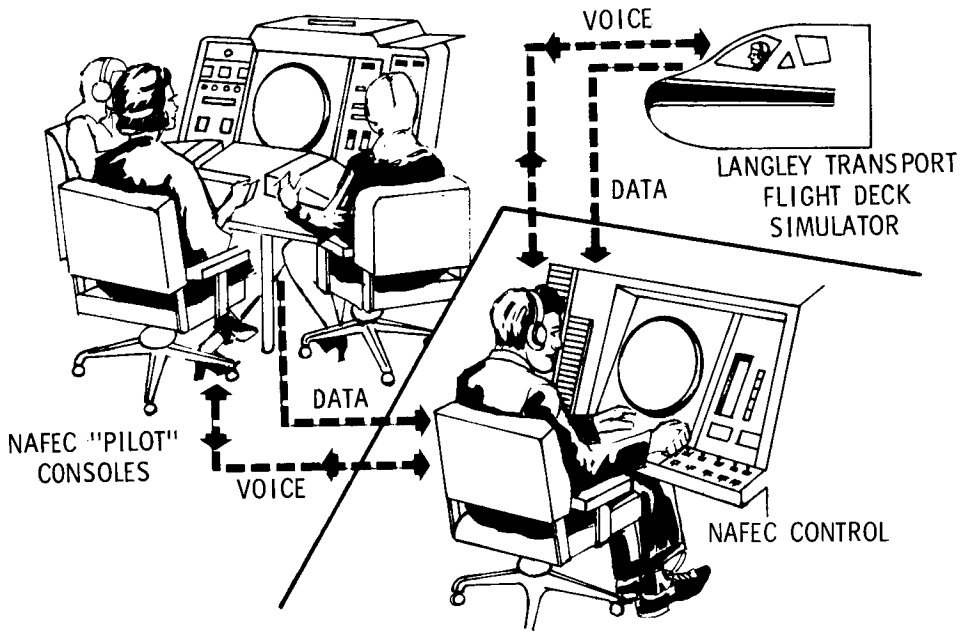

Figure 1

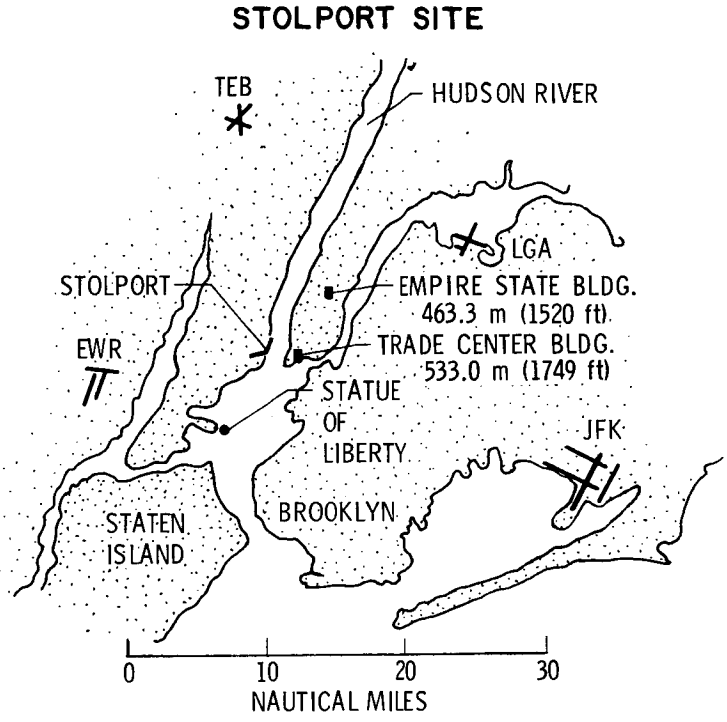

Figure 2

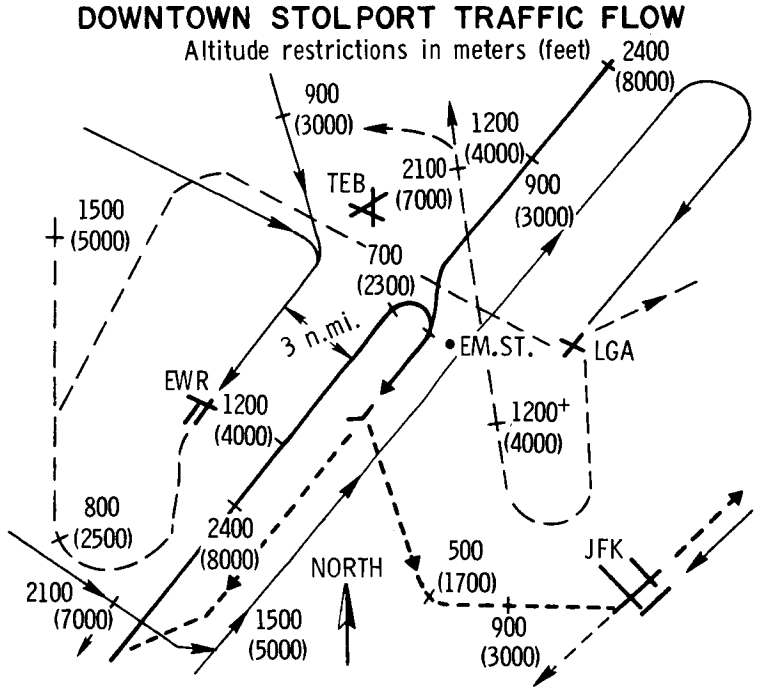

Figure 3

AIRPORT X

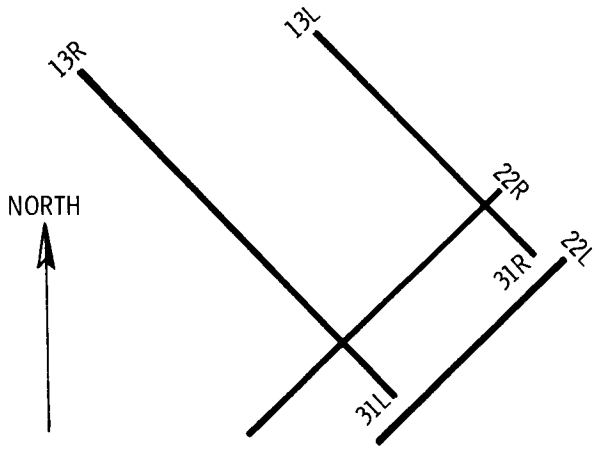

Figure 4

STOL RUNWAY CONFIGURATIONS

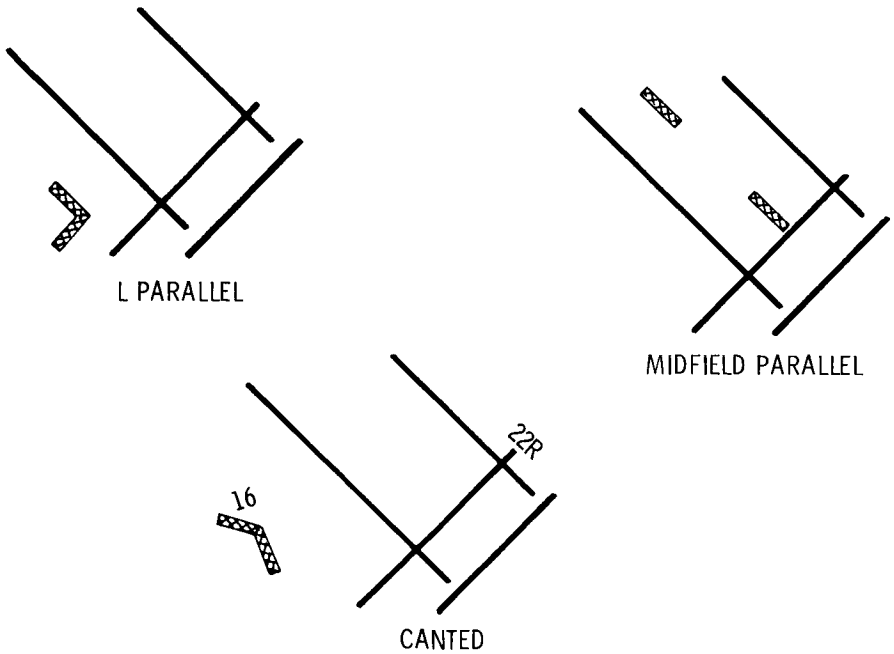

Figure 5

MIDFIELD PARALLEL

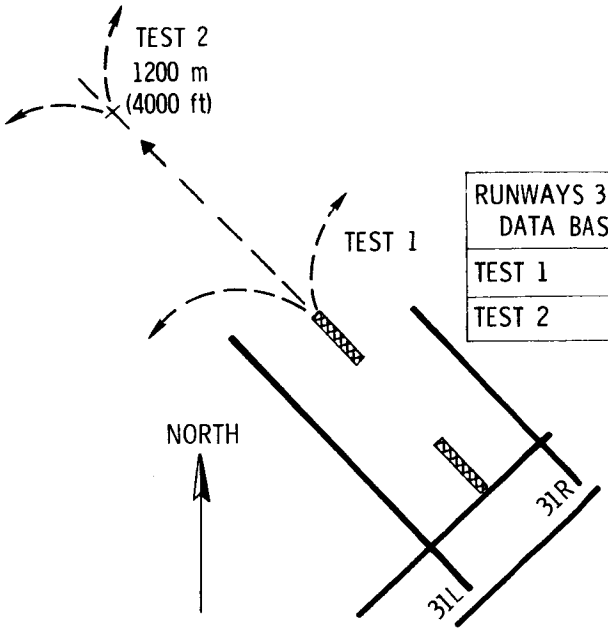

	CTOL OPERATIONS RATE PER HOUR		
	DEP.	ARR.	TOTAL
RUNWAYS 31L AND 31R DATA BASE	73	63	136
TEST 1	62	49	111
TEST 2	64	60	124

Figure 6

NEW YORK TERMINAL AREA

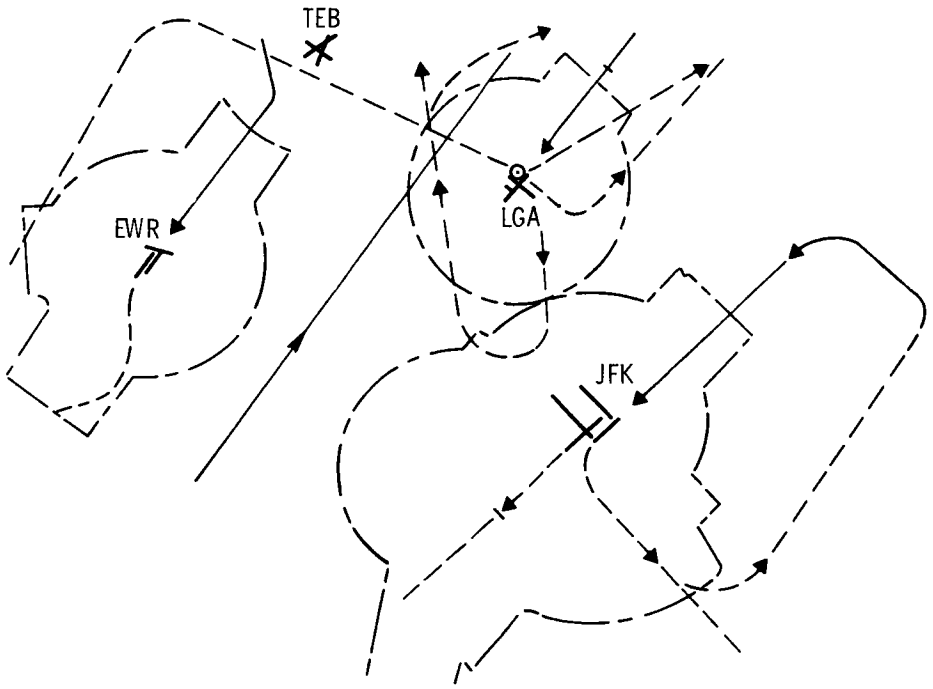

Figure 7

TEST STOL RUNWAY CONFIGURATION AT JFK AIRPORT

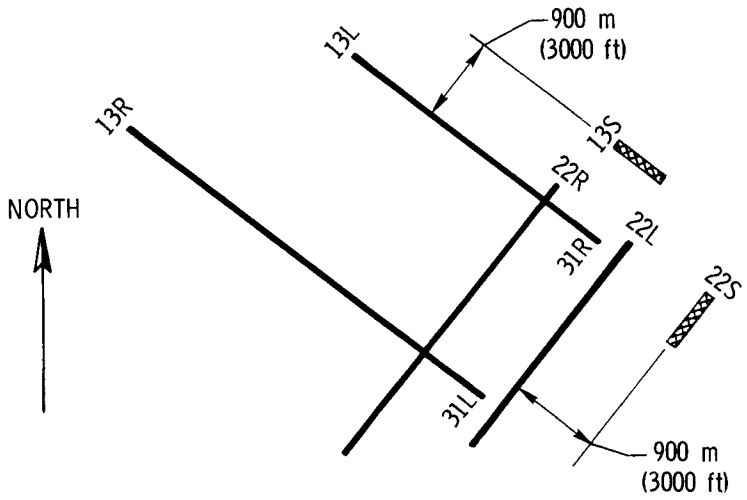

Figure 8

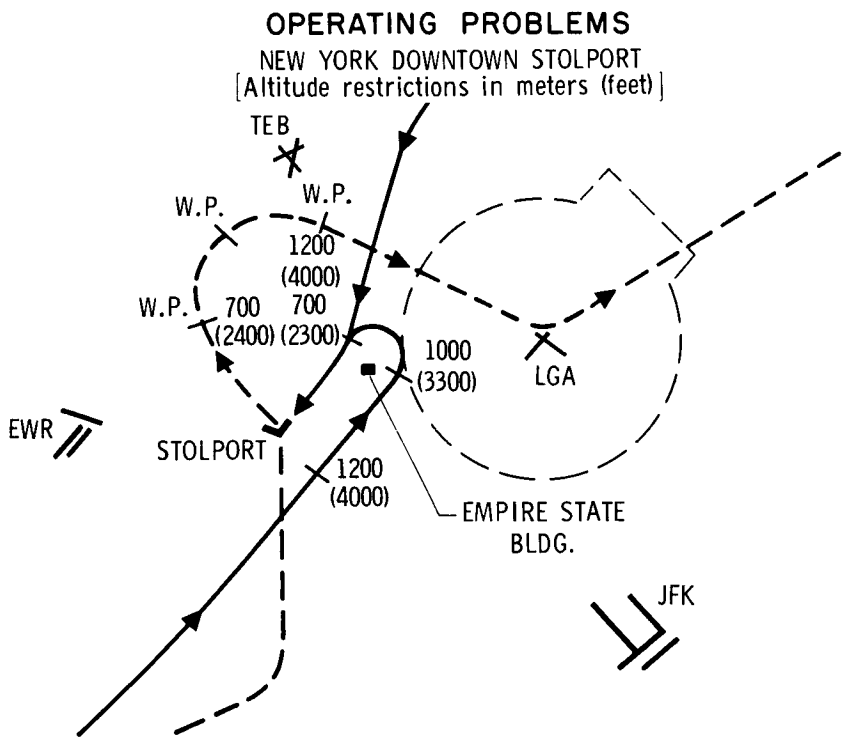

Figure 9

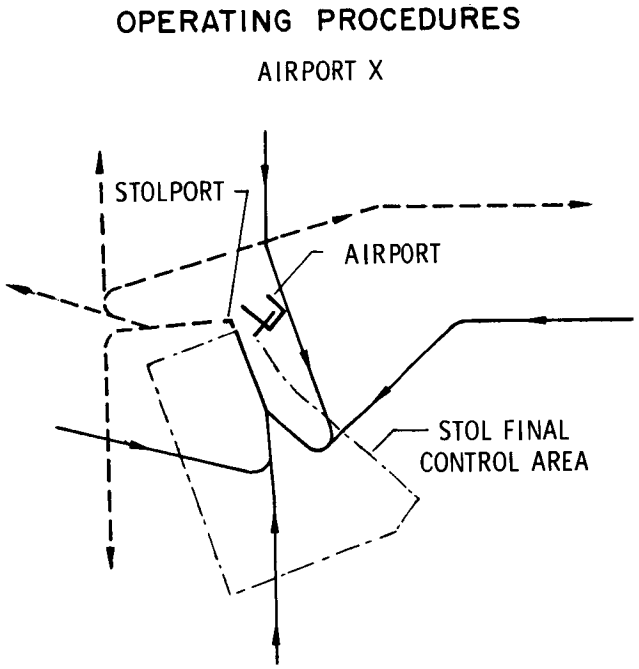

Figure 10

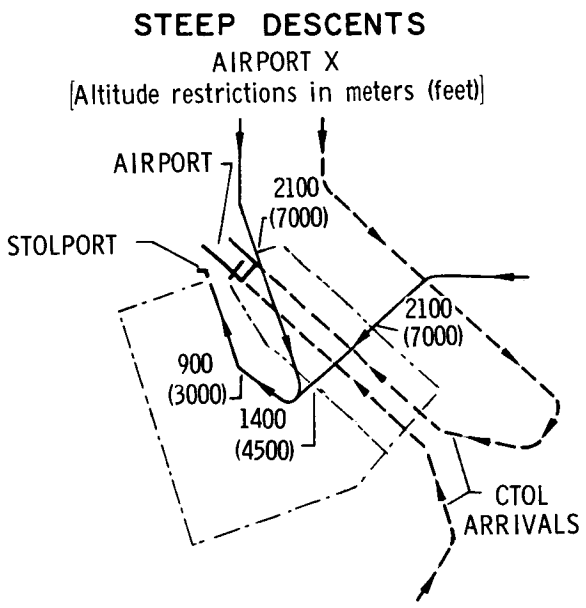

Figure 11

NUMEROUS MANEUVERS FOR SEQUENCING
AIRPORT X

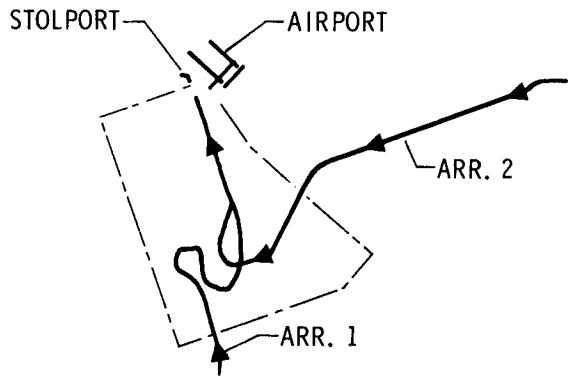

Figure 12

LENGTHY SEQUENCING MANEUVERS
AIRPORT X

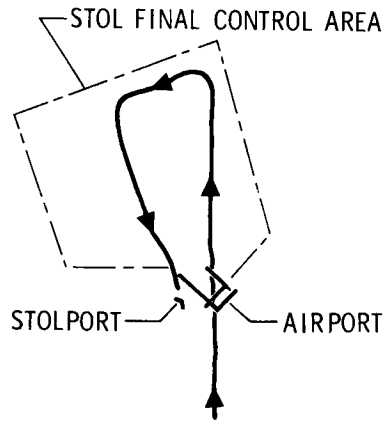

Figure 13

4-D GUIDANCE OF STOL AIRCRAFT IN THE TERMINAL AREA

By Thomas Pecsvaradi* and Heinz Erzberger
NASA Ames Research Center

SUMMARY

The primary objective of advanced STOL aircraft is the improvement of the nation's air transportation system by the elimination of delays and congestions associated with today's air travel. A new guidance technique, referred to as 4-D guidance, is being developed to achieve this objective. The 4-D guidance technique synthesizes complex three-dimensional flight paths from a minimum set of input data and flies the aircraft along the paths according to a prespecified time schedule. The two major elements of a 4-D guidance system are the trajectory synthesizer and the control law. Inputs to the trajectory synthesizer are the three-dimensional coordinates of way points, the turning radii, the speed ranges, the acceleration limits, and the arrival times at time control way points. First, the three-dimensional trajectory is computed by using circular arcs and straight lines. Then the airspeed profile, compensated for wind, is calculated to achieve the desired arrival times. The synthesized trajectory is stored as a time sequence of reference states which the aircraft is forced to track by using a linear feedback law.

INTRODUCTION

If advanced STOL aircraft are to become viable elements of the nation's air transportation network, their unique performance characteristics must be exploited to the fullest possible extent. Most notable among these characteristics are the aircraft's ability to make tight turns, steep climbouts and approaches, and to fly over a wide range of airspeeds. Consequently, STOL aircraft will possess much greater flexibility in the terminal area than CTOL aircraft. On the other hand, the performance of STOL aircraft may be limited by two important factors: the aircraft's acceleration/deceleration capability, and the effects of wind. Some existing STOL aircraft are slow to decelerate at some speeds and thus require long deceleration periods in the terminal area. Since these aircraft will be able to fly at very low speeds, on the order of 60 to 65 knots, the effects of wind can become extremely important in predicting arrival times at various key points along the route. In light of these performance characteristics and limitations, the following questions have arisen: Can STOL aircraft follow very demanding ATC instructions? Can they fly complex three-dimensional trajectories in the terminal area? Are they able to

*U.S. Army.

maintain an accurate time schedule along their flight path? To answer these questions, a technique is needed to play the characteristics of any potential STOL aircraft against these terminal operating constraints. Such a technique will enable us to determine whether a potential STOL aircraft can operate within these constraints and, if not, to identify STOL aircraft deficiencies to aircraft designers.

It seems likely that advanced short take-off and landing (STOL) aircraft will be equipped with guidance and navigation systems that satisfy far more stringent requirements than those currently used in conventional (CTOL) aircraft. Since these requirements are not yet clearly defined, investigations of the guidance problems for STOL aircraft under the most demanding circumstances were made. Although this approach places a significant burden on the aircraft and onboard guidance system, it ensures that the results obtained will not be invalidated by future developments in ground and airborne system design.

It has been assumed that STOL aircraft will (1) fly curved climbouts and approaches using a microwave landing system; (2) operate in narrow airspace corridors to avoid CTOL traffic, buildings, and other obstacles; and (3) perform noise-abatement maneuvers. The guidance system that meets these requirements is referred to as a 3-D guidance system, and it involves the precise description of complex curved flight paths and the control system to fly the aircraft along the paths.

Precise path control alone, however, is not sufficient to achieve the principal goal of a STOL transportation system, which is the elimination of, or at least the substantial reduction in, undue delays and congestions. This goal can be accomplished by increasing the landing rates at airports; this increase, in turn, implies a greater precision in delivering aircraft to the runway threshold. In the current manual system the accuracy with which aircraft can be delivered to the runway is approximately ± 15 sec. It has been suggested that this time can be reduced to about ± 2 sec by spacing aircraft accurately with less vectoring and by minimizing pilot-controller communications. Both of these requirements can be fulfilled by achieving precise time control of the aircraft along its flight path. The guidance system that accomplishes this control is referred to as 4-D guidance. It is a guidance technique consisting of two major elements: the 4-D reference trajectory synthesis, and the control law to fly the aircraft along the reference trajectory. It must be emphasized that there is a very important, intrinsic difference between these two elements. By 4-D reference trajectory synthesis is meant the generation of a precise 3-D flight path and a feasible speed profile along the path. Note that this process is a completely open-loop, or predictive, process in the sense that it takes place before the aircraft arrives at the initial point of the trajectory. The action of the control law, on the other hand, is a closed-loop process going on in real time as the aircraft is tracking the reference trajectory. It is the combined open-loop—closed-loop process that is referred to as a 4-D guidance system.

The purpose of this paper is to describe the 4-D guidance system that was developed at NASA Ames Research Center, and which will be flight tested in a STOL aircraft. Some of the crucial design considerations are discussed, and a brief description of the algorithms for trajectory synthesis and control law are given. Finally, some simulation results are presented to indicate the performance of the system.

DESIGN CONSIDERATIONS AND INTERACTION WITH AIR TRAFFIC CONTROL

Chief criteria for selecting the 3-D path are STOL terminal area maneuver requirements and simplicity of computation. These criteria are met by synthesizing the 3-D path from geometrically simple elements. In the horizontal plane these elements consist of segments of circles and straight lines. Complex flight paths are obtained by interconnecting several line segments and sections of circles with different radii. Paths constructed in this manner can yield minimum time trajectories as discussed in references 1 to 3. The vertical trajectory is synthesized from sections of constant flight-path angle. The complete three-dimensional flight path is then obtained by requiring the aircraft to fly the vertical profile along the ground track determined by the previously computed horizontal trajectory. A critical problem in implementing this synthesis procedure is minimizing the pilot work load in entering a trajectory. As explained in the next section, this problem is solved by using way points to specify the trajectory.

After the three-dimensional path has been established, the desired position of the aircraft along the path as a function of time is determined from considerations of air traffic control. Generally, more than one aircraft will be flying along the 3-D flight path or will be merging with the path at certain of its points referred to as merging points. This effect is illustrated in figure 1. Aircraft (AC) on the two approach routes merge in the vicinity of the approach gate. In the current air traffic control (ATC) system the final approach controller is responsible for merging aircraft at this point. He does this by observation of the aircraft on the ATC radar and by issuing speed and vectoring instructions to the pilots. The delays, inaccuracies, and other limitations of this manual-controller—pilot-control loop yield a broad envelope of aircraft trajectories between the feeder fix and the gate, shown as the hatched area in figure 1. This manual technique can deliver aircraft to the approach gate with a time accuracy of approximately ±15 sec. It is well-known that the time control accuracy influences the required spacing on final approach, which, in turn, determines the landing capacity of the runway (ref. 4). Through the use of 4-D guidance techniques, the accuracy of time control can be greatly increased; thus, a basis for achieving higher landing rates and greater automation in the control of terminal area traffic is provided. Instead of the controller issuing vectoring and speed commands to space aircraft, the air traffic control system specifies only the

desired arrival times at a small number of points along the terminal approach route and leaves the burden of computing aircraft control inputs to achieve these times to the onboard system.

From a knowledge of the 3-D path and the desired arrival times at specified points on the path, the 4-D guidance system computes the required airspeed profile. The airspeed computation algorithm must consider the minimum and maximum permissible airspeed, the aircraft's acceleration and deceleration capability, the landing approach speed, and the effect of winds. Also, in specifying arrival times, air traffic control will use only limited knowledge of the aircraft's performance capabilities. Therefore, the algorithm must first determine the feasibility of the specified arrival times by comparing them with the true minimum and maximum times the aircraft can achieve without deviating from the 3-D path. If the specified arrival times cannot be achieved, air traffic control must be requested to reassign arrival times or permit delaying maneuvers such as holding and/or path stretching.

In the preceding discussion of arrival time assignment, the question left unanswered was how air traffic control will generate the arrival times to be assigned to each aircraft. To clarify this question, consider an aircraft equipped with a 4-D guidance system which has just arrived at one of the feeder fixes in figure 1. It is assumed that the aircraft had previously been cleared to proceed toward the feeder fix. Those aircraft currently flying between the feeder fixes and the runway were previously assigned arrival times at the gate and the touchdown point. Given the schedules of these aircraft and, for the new aircraft, an estimate of the minimum and maximum times to the gate and from the gate to the touchdown point, a technique is needed to specify feasible times at the gate and at the touchdown point such that separation standards between aircraft are satisfied and that the aircraft lands in minimum time. A general algorithm to calculate such times has been described in reference 5. This algorithm is briefly reviewed in a later section of this paper.

SPECIFICATION OF 3-D PATH

The problem of specifying and calculating the 3-D path is divided into two problems solved in sequence. First the projection of the trajectory in a horizontal plane is computed from an analysis of the way-point coordinates and the desired turning radii (R). Then the known arc length of the horizontal trajectory together with the altitude difference between adjacent way points is used to determine the flight-path angle and, therefore, the altitude profile between adjacent way points.

A crucial part in the calculation of horizontal trajectory parameters is the interpretation of way points. This part is explained with the help of an example trajectory shown in figure 2. The trajectory begins at lift-off and terminates at touchdown, way point 7

(WP7). Although this trajectory can be flown by a STOL aircraft, its shape has no significance beyond illustrating the construction procedure. All parts of the trajectory consist of segments of straight lines and circles. The basic problem to be solved can be stated as follows: What is the essential input information that the pilot must provide to the airborne computer in order to generate this trajectory uniquely? The solution lies in the definition of two types of way points, which are referred to as the ordinary and final heading way points.

Ordinary Way Points

An ordinary way point is exemplified in figure 2 by way points 2, 4, and 5 (WP2, WP4, and WP5). Its location is defined by the intersection of two straight lines. The two lines are connected by an arc of a circle tangent to both lines. Thus, the sharp corner at the way point is rounded to obtain a trajectory the aircraft can fly. The radius of the circle used in rounding the corner can either be explicitly specified by the pilot as in this example or it can be implicitly determined from a maximum bank angle constraint ϕ_{max}. For a given ϕ_{max}, the minimum turning radius R_{min} depends on the maximum ground speed $V_{g,max}$ that can be attained in a 360^{o} turn and is

$$R_{min} = \frac{V_{g,max}^2}{g \tan \phi_{max}} \tag{1}$$

where g is the acceleration of gravity. The maximum ground speed is the sum of the maximum airspeed and the magnitude of the wind vector.

Throughout this paper, the runway-centered coordinate system is used to specify points in the plane. The origin of this system is at the touchdown point, way point 7, the X-axis points in the landing direction and the Y-axis points to the right when facing in the landing direction. Heading angles are measured clockwise from the direction of the positive X-axis.

Suppose the pilot has entered the x- and y-coordinates of a sequence of ordinary way points together with the turning radii to be used in rounding the corners at way points. From this information the onboard computer calculates various parameters defining the trajectory. It is convenient to compute these parameters successively, starting with the last way point to be flown through and ending with the first one. For this purpose figure 3 shows the trajectory between way points $i - 1$ and $i + 1$ and also defines various quantities used in the calculation. It is assumed that the calculations from way point $i + 1$ to the last way point have been completed. These calculations yielded the quantities ℓ_{i+1}, x_{i+1}, x_{Pi+1}, and ψ_{i+1} which together with x_i, y_i, R_i, x_{i-1}, and y_{i-1} are used to obtain the parameters for the ith way point. The heading of the straight-line segment

between way points $i - 1$ and i is ψ_i, given by the relation

$$\psi_i = \arctan \frac{y_i - y_{i-1}}{x_i - x_{i-1}} \qquad \left(-180^o < \psi_i \leqq 180^o\right) \tag{2}$$

The heading change ψ_{ti} in the circular segment near way point i is

$$\psi_{ti} = \frac{\text{mod}}{180^o}\left(\psi_{i+1} - \psi_i\right) \qquad \left(-180^o < \psi_{ti} \leqq 180^o\right) \tag{3}$$

where the direction of the turn is to the right for $\psi_{ti} > 0$ and to the left for $\psi_{ti} < 0$. Next, calculate the quantity b_i shown in figure 3.

$$b_i = R_i \tan \left|\frac{\psi_{ti}}{2}\right| \tag{4}$$

The length of the straight segment d_{i+1} is then

$$d_{i+1} = l_{i+1} - b_i \qquad \left(l_{i+1} \geqq 0\right) \tag{5}$$

If d_{i+1} from equation (5) is less than zero, adjacent turns overlap, the computation of the trajectory must stop, and the pilot is given a diagnostic message, such as "way points i and $i + 1$ are too close." The coordinates for the end of the turn and the center of the turn are

$$x_{Qi} = x_i + b_i \cos \psi_{i+1} \tag{6}$$

$$y_{Qi} = y_i + b_i \sin \psi_{i+1} \tag{7}$$

$$x_{Ri} = x_{Qi} \mp R_i \sin \psi_{i+1} \tag{8}$$

$$y_{Ri} = y_{Qi} \pm R_i \cos \psi_{i+1} \tag{9}$$

where the upper sign is chosen for a right turn and the lower sign for a left turn. Next, the distance l_i is calculated:

$$l_i = \sqrt{\left(x_{i-1} - x_i\right)^2 + \left(y_{i-1} - y_i\right)^2} - b_i \qquad \left(l_i \geqq 0\right) \tag{10}$$

If ℓ_i is less than zero, the calculation cannot continue and the pilot is given a diagnostic message such as "way points $i - 1$ and i are too close." If $\ell_i \geq 0$, the iteration is completed by calculating the coordinates of the beginning of the turn:

$$x_{Pi} = x_i - b_i \cos \psi_i \tag{11}$$

$$y_{Pi} = y_i - b_i \sin \psi_i \tag{12}$$

These iterations are continued until the first way point is reached. Since the way points entered do not always yield a flyable trajectory, onboard calculation of the trajectory generally will require a system that permits the pilot to correct errors after the system has issued a diagnostic message.

Final Heading Way Points

Final heading way points are illustrated in figure 2 by way points 3, 6, and 7. Instead of rounding the corner at the intersection of two lines, the trajectory for this type passes through the way point at the instant the turn toward the next way point has been completed. Thus, the aircraft begins its flight along the straight-line segment exactly over the way point. There are two reasons for introducing this type of way point. First, it simplifies the specification of some trajectory segments, such as the turn at way point 3, which contains more than 180^o. Recall that the turn at an ordinary way point is limited to less than 180^o. Second, this type is required if the arrival time at the way point is specified. Specification of arrival time at an ordinary way point lacks precision since the way-point coordinates themselves do not fall on the trajectory. By requiring all aircraft that are merging to fly through a point on the merging path with a common heading, the assignment of arrival times at the merging way point can be used to achieve precise spacing of aircraft.

In the specification of a trajectory, ordinary and final heading way points can be alternated in arbitrary fashion. The general procedure for calculating the trajectory parameters is illustrated in figure 4 with a final heading way point i embedded between way points $i - 1$ and $i + 1$ of arbitrary type. As before, the trajectory is computed backwards from the last way point. The final heading ψ_{i+1} to be achieved at way point i was previously determined in the calculation for way point $i + 1$ and is therefore a known quantity. It is evident from figure 4 that the desired final heading at way point i can be achieved with two trajectories, one ending with a left turn, the other with a right turn. The criterion for selection is to choose the one with the shorter path length between way points $i - 1$ and i. To make the selection, the coordinates of the centers of the two turns are calculated:

$$x_{Ri} = x_i - R_i \sin \psi_{i+1} \tag{13}$$

$$y_{Ri} = y_i + R_i \cos \psi_{i+1} \qquad \text{(Right turn)} \tag{14}$$

$$x_{Li} = x_i + R_i \sin \psi_{i+1} \tag{15}$$

$$y_{Li} = y_i - R_i \cos \psi_{i+1} \qquad \text{(Left turn)} \tag{16}$$

Then, the distances squared from way point $i - 1$ to each center are

$$d_{Ri}^2 = (x_{Ri} - x_{i-1})^2 + (y_{Ri} - y_{i-1})^2 \tag{17}$$

$$d_{Li}^2 = (x_{Li} - x_{i-1})^2 + (y_{Li} - y_{i-1})^2 \tag{18}$$

From the geometry of the construction in figure 4, it can be seen that the trajectory with the shorter path length also has associated with it the shorter of the two distances d_{Ri} and d_{Li}. Thus, the right-turn trajectory is chosen if d_{Ri} is greater than d_{Li}. If the way point $i - 1$ lies on the line determined by way points i and $i + 1$, both trajectories have the same length and the direction of the turn, if a turn is required, must be selected on the basis of another criterion. The next step is to determine whether way point $i - 1$ lies inside or outside the circle used to define the turn. Suppose the right turn was previously selected; then the way point lies inside if $d_{Ri}^2 < R_i^2$ and outside or on the circle if $d_{Ri}^2 \geq R_i^2$. If this former case is true, the trajectory is not feasible, further computation of the trajectory stops, and the pilot is given the message "way points i and $i - 1$ are too close." In the latter case, the calculation continues with the computation of the heading ψ_{dRi} of the directed line d_{Ri} if a right turn is required or the heading ψ_{dLi} of the directed line d_{Li} if a left turn is required:

$$\psi_{dRi} = \arctan \frac{y_{Ri} - y_{i-1}}{x_{Ri} - x_{i-1}} \qquad \text{(Right turn)} \tag{19}$$

$$\psi_{dLi} = \arctan \frac{y_{Li} - y_{i-1}}{x_{Li} - x_{i-1}} \qquad \text{(Left turn)} \tag{20}$$

Next the angle ψ_{Ri} is computed for a right turn:

$$\psi_{Ri} = \arcsin \frac{R_i}{d_{Ri}} \tag{21}$$

or ψ_{Li} for a left turn:

$$\psi_{Li} = \text{arc sin} \frac{R_i}{d_{Li}} \tag{22}$$

The heading ψ_i is then

$$\psi_i = \frac{\text{mod}}{180^o}\left(\psi_{dRi} - \psi_{Ri}\right) \tag{23}$$

if the trajectory contains a right turn and

$$\psi_i = \frac{\text{mod}}{180^o}\left(\psi_{dLi} + \psi_{Li}\right) \tag{24}$$

if it contains a left turn. The length d_i of the straight-line segment from way point $i - 1$ to the beginning of the turn is

$$d_i = \sqrt{d_{Ri}^2 - R_i^2} \qquad \text{(Right turn)} \tag{25}$$

$$d_i = \sqrt{d_{Li}^2 - R_i^2} \qquad \text{(Left turn)} \tag{26}$$

Finally, the heading change ψ_{ti} in the turn is obtained from the difference between ψ_i and ψ_{i-1}, and the coordinates of the beginning of the turn to way point i are

$$x_{Pi} = x_{i-1} + d_i \cos \psi_i \tag{27}$$

$$y_{Pi} = y_{i-1} + d_i \sin \psi_i \tag{28}$$

Further details, including flow charts for the synthesis procedures, are given in reference 6.

Technique of Flying to the First Way Point

In the preceding discussion, the trajectory from the first to the last way point was synthesized. To complete the synthesis, the trajectory from the aircraft's initial position and heading to the first way point must be constructed.

The construction procedure depends on the type of the first way point. It it is an ordinary way point, the trajectory is constructed on the basis of the rule that the aircraft will turn from its current heading toward the first way point in the direction that minimizes the total path length to the first way point. This criterion is the same as that used in

constructing the trajectory from way point $i + 1$ to way point i, where way point i is of the fixed final heading type. Thus, the procedures of the preceding section apply if the initial heading ψ_0 is identified with ψ_{i+1}, the initial position is identified with the coordinates of way point i, and the coordinates of the first way point are identified with those of way point $i - 1$, and the airplane traverses figure 4 in the opposite sense.

If, however, the first way point is the fixed final heading type, a procedure different from those discussed so far must be used. This guidance problem can be stated as follows: Determine a trajectory that starts from a given initial position and heading and leads to a position with a specified final heading. Since this problem has been dealt with extensively in references 1, 2, 3, 6, and 7, only a brief discussion of results is given here. References 1 and 2 give a minimum time solution to this problem, reference 2 deriving the optimum control law. Simplified solutions are discussed in references 3 and 6. In the simplified treatment, the required trajectory consists of a turn, a straight flight, and then another turn. The parameters of the three segments are chosen to satisfy the initial and final conditions of the problem.

Altitude Profile

The calculation of the altitude profile is simple and requires only the determination of a flight-path angle γ_i between way points $i - 1$ and i. Since the horizontal path length between way points is known, the flight-path angle γ_i is given by

$$\gamma_i = \arctan \frac{h_i - h_{i-1}}{s_i} \tag{29}$$

where s_i is the horizontal path length between way points i and $i - 1$, and h_i and h_{i-1} are the altitudes specified at way points i and $i - 1$, respectively. In order to compute s_i from the segments of turns and straight lines it is necessary to define at what point on the horizontal trajectory the specified way-point altitude is to be achieved. The rule used is that the way-point altitude must be achieved exactly at the end of the turn for a given way point. This rule is used for both ordinary and final heading way points. The last step in the altitude profile computation is to check whether each γ_i lies within the range of permissible flight-path angles for the aircraft.

It is possible and perhaps desirable to define more complicated altitude profiles between way points. Profiles that minimize a performance function such as the fuel consumed could be valuable. However, the limited size of the airborne computer to be used in flight tests of this guidance system, together with the requirement for onboard computation of the trajectory, does not permit consideration of more complex techniques at this time.

SPEED PROFILE COMPUTATION

Precise time control of aircraft is achieved by determining a feasible speed profile along the already computed 3-D trajectory. A speed profile is said to be feasible if it satisfies the following conditions:

1. The airspeed remains between the minimum and maximum airspeed restrictions imposed along the trajectory.

2. The rate of change of airspeed does not exceed the acceleration/deceleration capabilities of the aircraft.

3. The resulting ground speed yields the desired arrival times at those way points where they have been prescribed by ATC (such way points are referred to as time-controlled way points).

The first two conditions imply that the flying time between any two points on the trajectory is bounded above and below by the minimum and maximum times corresponding to the maximum and minimum airspeeds, respectively. Consequently, if arrival times at the time-controlled way points are assigned arbitrarily, then a feasible speed profile may not exist. In order to insure the existence of a feasible speed profile, ATC assigns arrival times based on the minimum and maximum possible flying times between successive pairs of time-controlled way points.

The determination of a feasible speed profile in the absence of wind would be a relatively simple task, for in this case airspeed and ground speed are identical. In the presence of wind, however, the relationship between airspeed and ground speed is highly nonlinear, and the problem becomes considerably more complex. By assuming a steady wind, the expression for the magnitude of the ground speed $V_g(t)$ at any time t is given by

$$V_g(t) = \sqrt{V_a^2(t) - V_w^2 \sin^2\psi_w(t)} + V_w \cos\psi_w(t) \tag{30}$$

where $V_a(t)$ and V_w are the magnitudes of the airspeed and windspeed, respectively, and $\psi_w(t)$ is the angle from the wind direction to the ground heading, measured positive clockwise. The differential equation governing $\psi_w(t)$ is:

$$\left|\frac{d\psi_w(t)}{dt}\right| = \begin{cases} 0 & \text{(Straight flight)} \quad (31a) \\ \frac{1}{R} V_g(t) & \text{(Circular flight)} \quad (31b) \end{cases}$$

where R is the radius of turn. Exact analytic expressions for $\psi_w(t)$ and $V_g(t)$ can be found only in the case of straight flight with constant airspeed. A considerable simplification can be made by assuming that for all t

$$\left(\frac{V_w}{V_a(t)}\right)^2 << 1 \tag{32}$$

Supporting evidence indicates that inequality (32) is a good approximation not only for CTOL but STOL aircraft operations as well. Under this assumption equation (30) can be written as

$$V_g(t) = V_a(t) + V_w \cos \psi_w(t) \tag{33}$$

Before considering the speed profiles for straight and curved flight in more detail, it is necessary to establish certain desirable characteristics for airspeed profiles. In the design of the 4-D guidance system described in this paper, the point of view was adopted that the airspeed profile should be a piecewise linear function of time, that is,

$$V_a(t) = V_a(t_k) + a_k(t - t_k) \qquad (t_k \leq t \leq t_{k+1},\ k = 0,1, \ldots) \tag{34}$$

where a_k is the constant value of acceleration/deceleration in the interval (t_k, t_{k+1}). Furthermore, changes in airspeed should occur only at a few places along the trajectory, preferably at those points where the minimum and maximum admissible airspeeds change. These requirements were dictated by considerations of passenger comfort, pilot workload, and simplicity of implementation. A typical airspeed profile possessing these characteristics is shown in figure 5.

Straight Flight

Let the desired airspeed along a straight flight segment of length d_k be given by equation (34). Then the analytic expressions for ψ_w, V_g, and t_{k+1} are

$$\psi_w(t) = \psi_w(t_k) \tag{35}$$

$$V_g(t) = V_a(t_k) + a_k(t - t_k) + V_w \cos \psi_w(t) \tag{36}$$

$$t_{k+1} = t_k + \frac{-V_g(t_k) + \sqrt{V_g^2(t_k) + 2a_k d_k}}{a_k} \tag{37}$$

Curved Flight

Let a curved flight segment consist of a circular turn of ψ_{tk} radians with turning radius R_k ($\psi_{tk} > 0$ for a right turn, $\psi_{tk} < 0$ for a left turn). If the desired airspeed along the circular arc is given by equation (34), then no analytic expressions can be found for ψ_w, V_g, and t_{k+1}. Since numerical integration for determining the speed profile would be prohibitive, a different approach is needed. It so happens that equation (31b) becomes integrable if the airspeed has the following form:

$$V_a(t) = V_a(t_k) + a_k\left(1 + \frac{V_w \cos \psi_w(t)}{V_a(t_k)}\right)(t - t_k) \qquad (t_k \leq t \leq t_{k+1}) \tag{38}$$

In this case the analytic expressions for ψ_w, V_g, and t_{k+1} are

$$\psi_w(t) = 2 \tan^{-1}\left\{\frac{C_1}{C_2} \tan\left[\tan^{-1}\left(\frac{C_2}{C_1} \tan \frac{\psi_w(t_k)}{2}\right) + \frac{C_2}{2R_k \operatorname{sgn} \psi_{tk}}\left(t + \frac{a_k}{2V_a(t_k)} t^2\right)\right]\right\} \tag{39}$$

$$V_g(t) = V_a(t_k) + a_k\left(1 + \frac{V_w \cos \psi_w(t)}{V_a(t_k)}\right)(t - t_k) + V_w \cos \psi_w(t) \tag{40}$$

$$t_{k+1} = \frac{V_a(t_k)}{a_k}\left(-1 + \sqrt{1 + \frac{2a_k}{V_a(t_k)} \bar{t}_{k+1}}\right) \tag{41}$$

where C_1, C_2, and $\bar{t}_k$ are defined by

$$C_1 = V_a(t_k) + V_w$$

$$C_2 = \sqrt{V_a^2(t_k) - V_w^2}$$

$$\bar{t}_{k+1} = \frac{2R_k \operatorname{sgn}(\psi_{tk})}{C_2}\left\{\tan^{-1}\left[\frac{C_2}{C_1} \tan\left(\frac{\psi_w(t_k) + \psi_{tk}}{2}\right)\right] - \tan^{-1}\left[\frac{C_2}{C_1} \tan\left(\frac{\psi_w(t_k)}{2}\right)\right]\right\}$$

(Note that $t_{k+1} = \bar{t}_{k+1}$ if $a_k = 0$.) Although V_a given by equation (38) is not a linear function of time, for values of $V_a(t_k)$ and V_w satisfying inequality (32), $V_a(t)$ turns out to be very nearly linear. This condition is illustrated in figure 6, which shows the airspeed and ground speed along a section of the example trajectory of figure 2.

The only remaining quantity still to be determined is the desired airspeed profile. Since the earliest and latest possible arrival times are achieved by flying the aircraft on the boundaries of the admissible speed ranges, the actual airspeed profile corresponding to an intermediate arrival time must lie between the speed boundaries. (See fig. 5.) The nonlinear relationship between arrival time and airspeed necessitates the use of an iterative procedure for the determination of the desired airspeed profile. Basically, the procedure adjusts the cruising speed level between each pair of time-controlled way points so that the prescribed arrival times are achieved. This adjustment is made by using expressions of the form of equations (37) and (41).

A final remark concerning the wind is in order. In this paper only the case of a steady wind is considered. It is well-known, however, that both the magnitude and direction of the wind are functions of the altitude. If these functions were known, they could be easily incorporated in the speed profile computation.

AN EXAMPLE OF 4-D TRAJECTORY SYNTHESIS

The preceding sections described the techniques used to calculate the two major elements of a 4-D trajectory, the 3-D path and the airspeed profile along the path. These elements must now be assembled to produce the complete reference trajectory consisting of the reference states (position, altitude, and heading) and the reference controls (turning radius, airspeed, and flight-path angle) as a function of time from initial time to final time.

The reference states and commands are calculated by a procedure which makes use of the chosen parameterization of the 4-D trajectory to minimize computer storage. The calculation is done in two steps. In the first step, the 3-D path and the airspeed acceleration time history along the path are used to construct a command table consisting of a sequence of control inputs arranged in chronological order. Since the reference controls are piecewise constant in time, the command table gives the values of the reference controls only at time instants where they change to new constant values. In the second step, the reference states between command times are computed analytically from the initial condition at the command time and the value of the controls during the command interval. Compared with the technique of storing the reference trajectory at a large number of time instants, this technique uses significantly less storage, an important consideration in implementing the technique on an airborne computer.

The example trajectory shown in figure 2 is used to illustrate the technique of 4-D trajectory synthesis described in this paper. The pilot specifies the trajectory to the system by entering the data given in table I. In the onboard system the way-point types are replaced by numerical codes. Both the initial position (lift-off) and the touchdown point are treated as final heading way points in synthesizing the trajectory. The initial heading and the runway heading associated with these way points are both 0^{o} in this case. Final heading way point 6 and the touchdown point are time control points with arrival times of 300 and 350 sec, respectively. The wind is assumed to be from 0^{o} at 25 ft/sec. The airspeed range specified for each way point in table I is valid from the end of the turn performed at that way point to the end of the turn performed at the next way point. This procedure requires choosing starting times of decelerations/accelerations such that the airspeed will fall in the next speed range at precisely the end of the turn. These fixed boundary conditions are met by synthesizing the airspeed profile backward from the last way point.

The 4-D command sequence generated for this input is given in table II. The minimum and maximum arrival times at the two time control way points (WP6 and WP7) are given in the headnote of the table. There are 17 command times in this example. Columns 3 to 8 give the states at the command times and columns 9 to 11 the piecewise constant controls between command times. Space limitations prevent giving the equations for computing the reference states between command times. For the same reason the equation for computing the instantaneous bank angle from the airspeed, heading, wind vector, and the turning radius is not given. Bank angle and flight-path angle commands are applied to the aircraft stability augmentation system (SAS) slightly in advance of those given in the table to minimize errors due to the finite rates of these quantities. Computation time of this trajectory on the IBM 360 is 0.5 sec.

PERTURBATION EQUATIONS AND CONTROL LAW

A synthesis procedure having been developed for the 4-D trajectory, which will now be referred to as the reference trajectory, the next step is to design a control law for flying it. The design of a control law for this problem, which is based on the technique described in reference 7, is accomplished by means of a perturbation method. Design of the control law for the altitude channel will not be considered here since this channel is simple with minimal coupling to the other channels.

The nonlinear dynamical equations, from which the perturbation equations are derived, are as follows:

$$\dot{X} = V_a \cos \Psi \tag{42}$$

$$\dot{Y} = V_a \sin \Psi \tag{43}$$

$$\dot{\Psi} = \frac{g(\tan \Phi)}{V_a} \tag{44}$$

where V_a is the airspeed, $\dot{X}$ and $\dot{Y}$ are components of V_a, Ψ is the heading, $\dot{\Psi}$ the heading rate, Φ the bank angle, and g the acceleration of gravity. The wind is assumed to be zero and the flight-path angle γ small so that $\cos \gamma \approx 1$.

The perturbation equations are obtained from the nonlinear equations by expansion in a Taylor series about a moving target reference system as illustrated in figure 7. The origin and positive X-axis of this system at any given time are the reference position and the direction of the aircraft flying the reference trajectory, respectively. In figure 7, X_r, Y_r, and Ψ_r refer to the reference position and heading and X_a, Y_a, and Ψ_a, to the aircraft position and heading in the runway-centered coordinate system. The linear differential equations obtained from a Taylor series expansion in the perturbed quantities X, Y, and Ψ shown in figure 7 are

$$\left.\begin{aligned} \dot{x} &= v_a + \dot{\Psi}_r y \\ \dot{y} &= V_r \psi - \dot{\Psi}_r x \end{aligned}\right\} \tag{45}$$

$$\dot{\psi} = \frac{g}{V_r}\left(\sec^2 \Phi_r\right)\phi - \frac{\dot{\Psi}_r}{V_r} v_a \tag{46}$$

where $v_a = V_a - V_r$ and $\phi = \Phi_a - \Phi_r$. The advantage of deriving the perturbation equations in this target referenced system is that terms involving $\sin \Psi_r$ and $\cos \Psi_r$, which would otherwise appear, are eliminated; thus the perturbation equations for curved trajectories are simplified. Equations (45) and (46) also show that x and y are coupled when $\dot{\Psi}_r \neq 0$, whereas the gain of the ψ channel is inversely proportional to V_r; thus, $\dot{\Psi}_r$ and V_r are parameters which depend on the reference trajectory. A control law for nulling the perturbed quantities will therefore have to contain $\dot{\Psi}_r$ and V_r as parameters.

The control variables of the aircraft for tracking the reference aircraft are the bank angle Φ_a and the speed V_a. A linear model of the combined autopilot and aircraft dynamical response for a bank angle and velocity command system can be approximated by the following equations:

$$\ddot{\phi} = \frac{1}{\tau_\phi}\left(-\dot{\phi} + k_\phi \phi - k_\phi \phi_c\right) \tag{47}$$

$$\ddot{v}_a = \frac{1}{\tau_v}\left(-\dot{v}_a + k_v v_a - k_v v_c\right) \tag{48}$$

where ϕ_c and v_c are the command inputs and ϕ and v_a are the response. The parameters in these two equations, k_ϕ, k_v, τ_ϕ, and τ_v, were deduced by matching the step responses of these equations to those of a currently in-service four-engine jet aircraft with an autopilot and autothrottle. Their numerical values are 0.375 sec^{-1}, 0.167 sec^{-1}, 1.04 sec, and 4.17 sec, respectively. The following control law is chosen for nulling the perturbed quantities x, y, and ψ:

$$\phi_c = -k_{\phi x}\dot{\psi}_r x - k_{\phi y} y - k_{\phi\psi} V_r \psi \tag{49}$$

$$v_c = -k_{vx} x - k_{vy}\dot{\psi}_r y \tag{50}$$

Note that equations (49) and (50) contain $\dot{\psi}_r$ and V_r as parameters. This parameterization has been found to be effective in achieving acceptable performance of the control law for the class of reference trajectories of interest here.

The governing factors for determining the numerical values of the five gains k_{vx}, k_{vy}, $k_{\phi x}$, $k_{\phi y}$, and $k_{\phi\psi}$ are (a) the accuracy of the navigation data, (b) the allowable bank angle and throttle activity for passenger comfort, and (c) the accuracy of following the synthesized reference trajectory. A root-locus analysis of the closed loop system indicates that a good compromise between conflicting requirements (b) and (c) is to use 0.0002 rad/ft for $k_{\phi y}$, 0.004 rad/rad (ft/sec) for $k_{\phi\psi}$, 0.0001 rad/ft (sec/rad) for $k_{\phi x}$, 0.04 (ft/sec)/ft for k_{vx}, and 0.15 (ft/sec)/ft (sec/rad) for k_{vy}. This combination of gain constants was obtained by trial and error by using a root-locus analysis of equations (45) to (50). The roots corresponding to this set of gains yield reasonable frequency and damping for all values of $\dot{\psi}_r$ from zero to 6^o/sec. A root-locus plot of equations (45) to (50) as a function of $\dot{\psi}_r$ for the choice of gains given here can be found in reference 7.

SIMULATION RESULTS

Figure 8 shows the block diagram of the simulation used to evaluate the guidance system. The general flow of computations in the trajectory synthesis algorithm is indicated inside the block drawn with dashed lines. The final product of the synthesis computations is the command schedule. The reference states and controls generator uses the command schedule, clock time, and the measured wind vector to compute the reference states and controls for each control time interval. An interval of 0.1 second was

used in the simulation. By use of the measured wind vector, ground speed and ground heading are converted to reference airspeed V_r and airspeed heading Ψ_r.

The control loop used to fly the aircraft along the reference trajectory is shown in detail. The first step is to compute the perturbed quantities x, y, z, and ψ, which are obtained in the transformations given in the bottom block. These quantities are multiplied by the appropriate gains and are added as required to form the perturbation controls v_c, ϕ_c, and z_c. They are then subtracted from the reference controls to form the autopilot and autothrottle inputs consisting of the command bank angle Φ_c, the command airspeed V_c, and the command altitude rate $\dot{Z}_c$.

A simplified model of the autopilot, autothrottle, and aircraft dynamics was developed especially for use in 4-D guidance and air traffic control simulation studies. A detailed flow chart for this model is given in reference 7. The model consists of a tenth-order dynamic system with hard limits on roll, roll rate, airspeed, airspeed acceleration, flight-path angle, and flight-path-angle rate. The actual wind vector is also an input to the model. Output quantities are the actual aircraft states. From these quantities the navigation system simulation obtains the measured aircraft states and the estimated wind vector.

A complete analysis of simulation results cannot be given within the length of this paper. Only the response of the control law to track a STOL type reference trajectory in the horizontal plane consisting of a 360^o circular segment with radius of 1220 ft and an airspeed of 135 ft/sec will be shown. The reference trajectory, which has a duration of 56.7 sec, is generated with two final heading way points located on the circle as shown in figure 9. This reference trajectory is a severe test of the control law since to fly it requires a reference bank angle of 25^o, almost equal to the bank angle limit of 30^o used in the aircraft simulation; this angle leaves little bank margin for nulling out errors. Figure 9 also shows the trajectories of the simulated aircraft for two initial conditions and an error in the wind estimate. The position of the reference aircraft and of the simulated aircraft is marked every 10 sec along the trajectories.

Starting from the two initial conditions, the simulated aircraft locks onto the reference trajectory after 30 sec of flight even though a period of bank angle limiting occurs (not shown in fig. 9) while the control law nulls the errors. To evaluate the effect of wind-estimate errors on tracking accuracy, an 8.45 ft/sec (5 knots) constant wind error was introduced. Normally, a wind estimator, which is part of the navigation system, would observe this error to a degree and refine its estimate, but in this case the estimator was disabled. The resulting tracking error is 180 ft at the end of the trajectory and indicates the importance of accurate wind estimates in precision aircraft control.

CONCLUSION

The chief advantage of the approach to 4-D guidance described here is the ability to specify and compute complex trajectories in flight. This feature is a highly desirable one from the pilot's viewpoint. Another advantage is that the technique is not strongly dependent on the aircraft type, since the only aircraft parameters used in synthesizing the trajectories are performance limitations, which are treated as parameters. Furthermore, the guidance technique can be integrated with a ground-based scheduling technique to form a complete air traffic control system. The precision of trajectory control and arrival time achieved with the system provides a solid base for reducing separation requirements and increasing landing rates in future air traffic control systems.

REFERENCES

1. Erzberger, Heinz; and Lee, Homer Q.: Optimum Horizontal Guidance Techniques for Aircraft. J. Aircraft, vol. 8, no. 2, Feb. 1971, pp. 95-101.

2. Pecsvaradi, Thomas: Optimal Horizontal Guidance Law for Aircraft in the Terminal Area. Proceedings Fifth Hawaii International Conference on System Sciences, Art Lew, ed., Jan. 1972, pp. 264-266.

3. Erzberger, Heinz; and Lee, Homer Q.: Terminal-Area Guidance Algorithms for Automated Air-Traffic Control. NASA TN D-6773, 1972.

4. Anon.: Analysis of a Capacity Concept for Runway and Final Approach Path Airspace. Rep. 10111, Nat. Bur. Standards, Nov. 1959.

5. Tobias, Leonard: Automated Aircraft Scheduling Methods in the Near Terminal Area. AIAA Paper No. 72-120, Jan. 1972.

6. Erzberger, Heinz; and Pecsvaradi, Thomas: 4-D Guidance System Design With Application to STOL Air Traffic Control. Paper presented at Joint Automatic Control Conference, Aug. 1972.

7. Lee, Homer Q.; McLean, John D.; and Erzberger, Heinz: Guidance and Control Techniques for Automated Air Traffic Control. J. Aircraft, vol. 9, no. 7, July 1972, pp. 490-496.

TABLE I.- INPUT QUANTITIES REQUIRED FOR EXAMPLE TRAJECTORY

[Initial heading, 0^{o}; runway heading, 0^{o}; airspeed acc/dec, 1.5 ft/sec^2; wind speed/direction, 25 ft/sec/0^{o}; initial airspeed, 135 ft/sec]

Way-point number	Way-point type	Way-point coordinates, ft			Turn radius, ft	Airspeed range, ft/sec	Time, sec
		x	y	h			
1	Initial position	1 000	0	0	4000	135 to 135	0
2	Ordinary	5 000	0	600	4000	203 to 304	---
3	Final heading	15 000	0	2000	4000	203 to 304	---
4	Ordinary	3 000	-3000	1500	4000	135 to 203	---
5	Ordinary	-1 500	4000	1000	3000	110 to 135	---
6	Final heading	-4 500	4000	1000	1500	110 to 135	300
7	Final heading (touchdown)	0	0	0	1500	110 to 110	350

TABLE II.- 4-D COMMAND SEQUENCE FOR EXAMPLE TRAJECTORY

[T_{min}/T_{max} to WP6 = 252/324 sec; T_{min}/T_{max} to WP7 = 295/376 sec]

Command sequence number	t, sec	States						Controls		
		x, ft	y, ft	h, ft	ψ, deg	V_g, ft/sec	V_a, ft/sec	$\dot{V}_a$, ft/sec^2	R, ft	γ, deg
1	0	1 000	0	0	0	110	135.0	1.5	Straight	6.2
2	18.2	3 249.6	0	243.2	0	137.7	162.3	1.5	4000 right	6.2
3	39.6	6 187.8	1285.9	600	47.3	174.1	191.1	1.5	Straight	3.6
4	64.1	9 383.6	4749.1	898.3	47.3	210.9	227.9	0	Straight	3.6
5	76.0	11 091.6	6594.7	1057.5	47.3	210.9	227.9	0	4000 left	3.6
6	143.7	15 000	0	2000	-166.0	252.1	227.8	0	Straight	-2.0
7	159.8	11 071.9	-979.4	1860.2	-166.0	252.1	227.8	-1.5	Straight	-2.0
⋮	⋮	⋮	⋮	⋮	⋮	⋮	⋮	⋮	⋮	⋮
14	300.3	-45 000	0	590.0	0	91.1	116.1	1.5	Straight	-7.5
15	300.5	-4 482.5	0	587.7	0	91.1	116.4	0	Straight	-7.5
16	345.4	-378.2	0	49.6	0	91.1	116.4	-1.5	Straight	-7.5
17	350.0	0	0	0	0	85.0	110.0	0	Straight	0

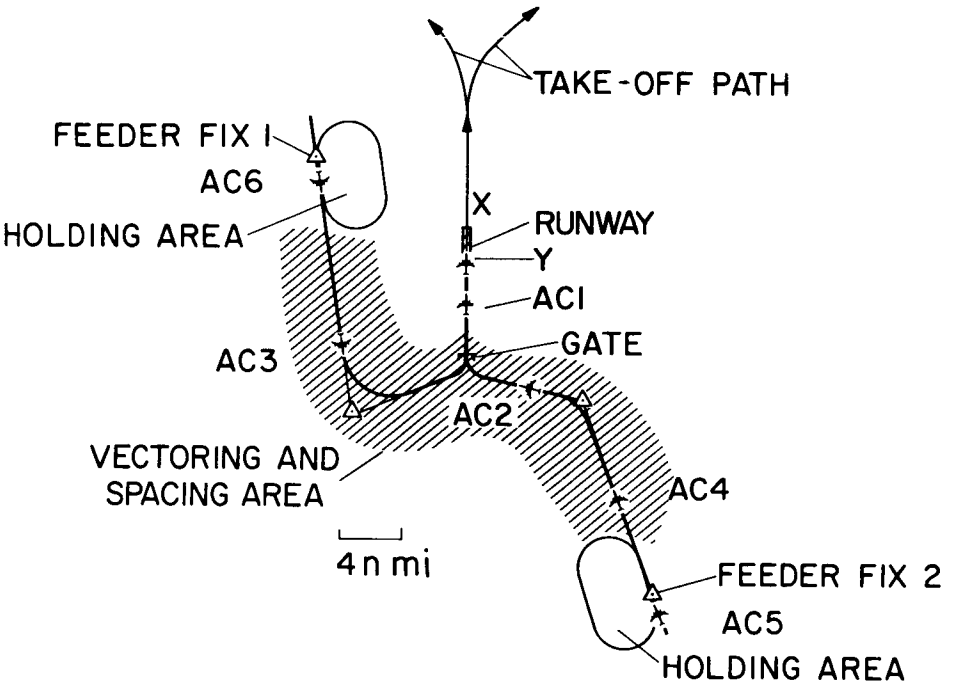

Figure 1.- Typical terminal area route structure.

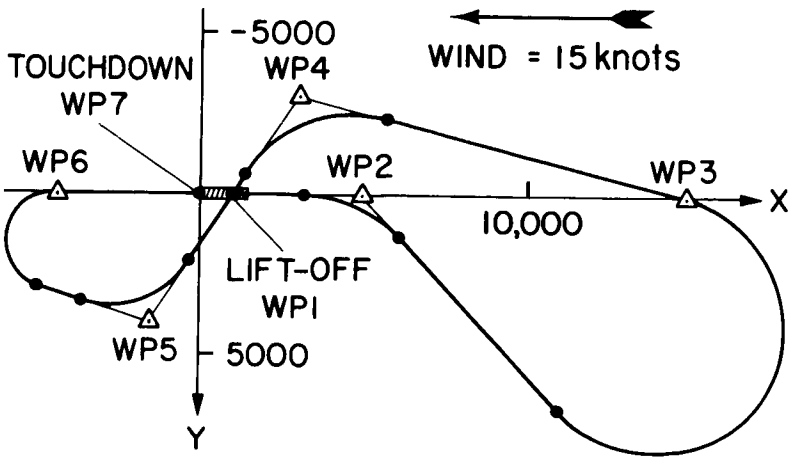

Figure 2.- Example trajectory.

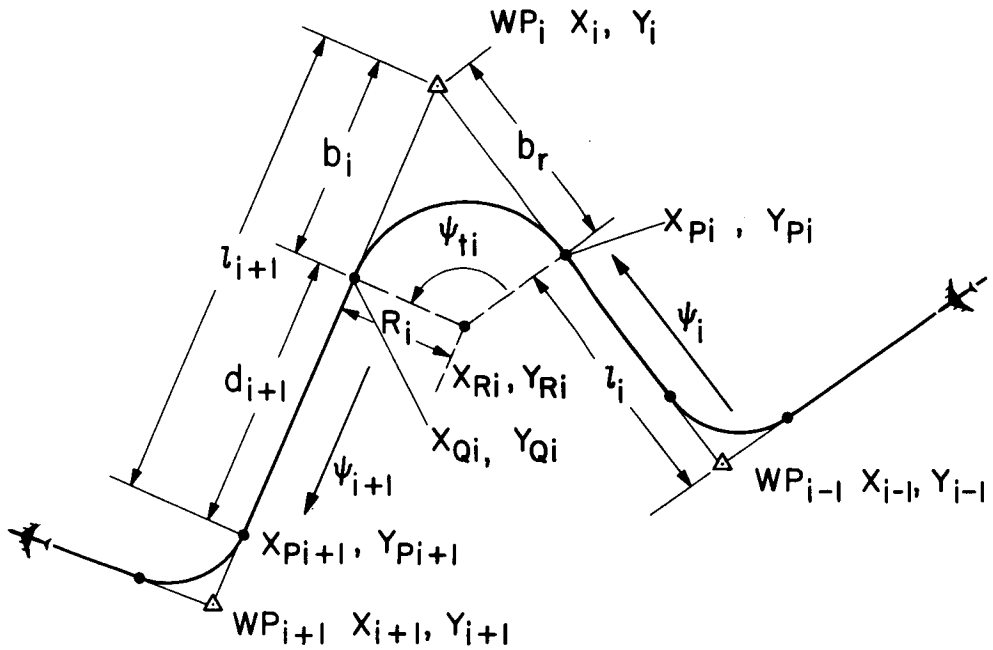

Figure 3.- Trajectory construction for ordinary way points.

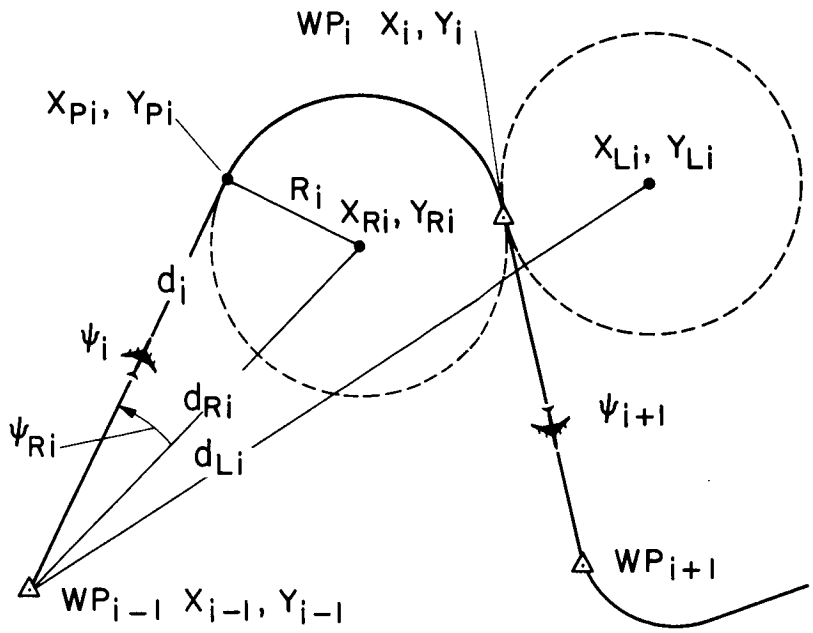

Figure 4.- Trajectory construction for final heading way points.

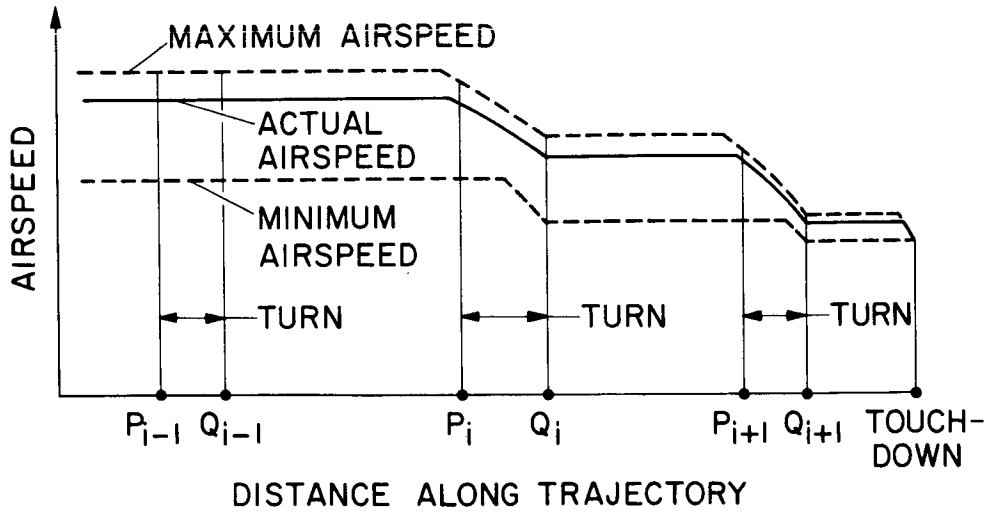

Figure 5.- Typical airspeed profile.

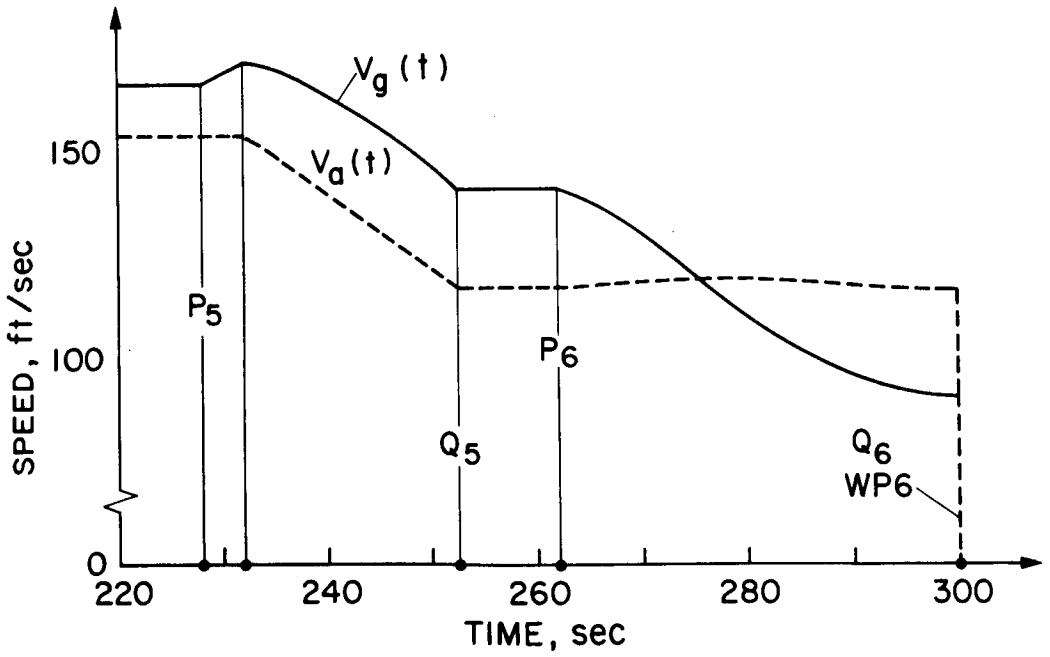

Figure 6.- Part of airspeed and ground speed time history for example trajectory. Wind speed, 25 ft/sec.

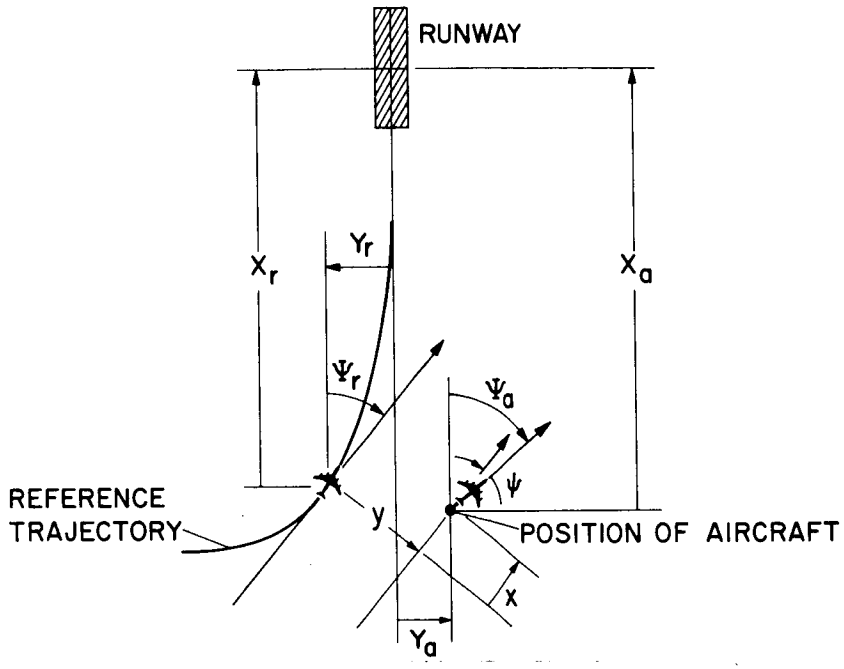

Figure 7.- Moving target reference system.

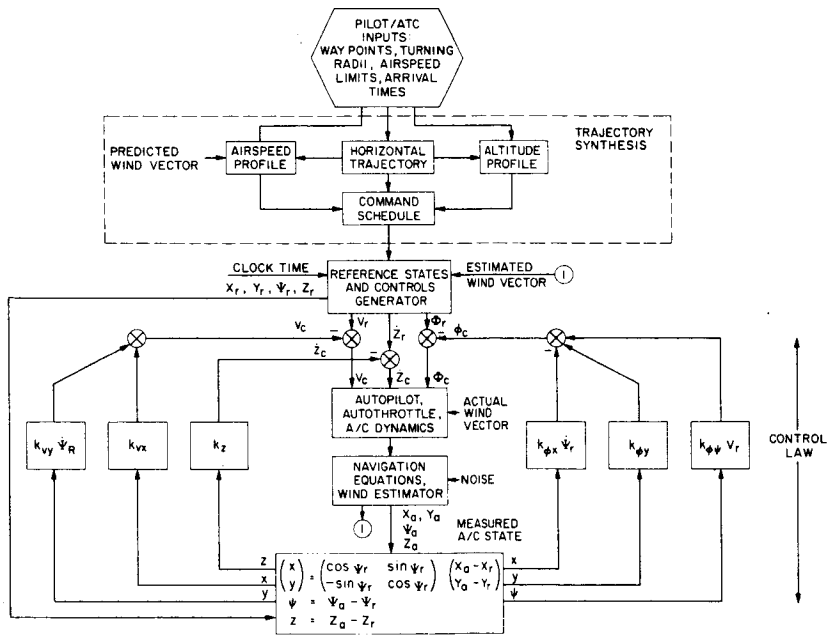

Figure 8.- Block diagram of 4-D guidance system simulation.

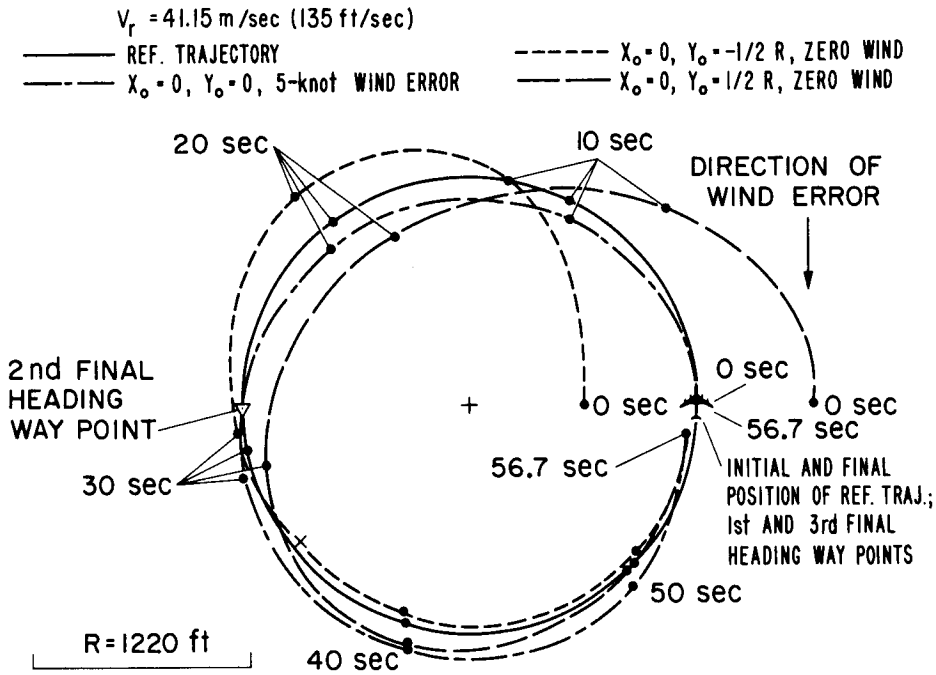

Figure 9.- Simulated flight along circular reference trajectory with initial condition errors and wind estimate error.

TERMINAL-AREA STOL OPERATING SYSTEMS EXPERIMENTS PROGRAM

By Donald W. Smith, DeLamar Watson, and Jay V. Christensen
NASA Ames Research Center

INTRODUCTION

As a result of various studies, it appears that the STOL aircraft can supply a high-speed short-haul transportation system that can operate safely into small city centers and suburban facilities. However, detailed performance data from integrated systems studies are needed to provide adequate information for a sound go-ahead decision. To meet this need, a joint Department of Transportation and National Aeronautics and Space Administration (DOT/NASA) operating systems experiments program has been initiated. This effort is focused on developing information which will aid in the choice by the U.S. Government and industry of system concepts, design criteria, operating procedures for STOL aircraft and STOLports, STOL landing guidance systems, air traffic control systems, and airborne avionics and flight control systems. Ames has developed a terminal-area STOL operating systems experiments program which is a part of the joint DOT/NASA effort.

This paper will describe briefly the Ames operating systems experiments program, its objectives, the program approach, the program schedule, typical experiments, the research facilities to be used, and the program status.

In any short-haul transportation system, there may be various levels of system complexity needed to meet traffic density and weather conditions. Simple low cost systems may be sufficient for low-density traffic conditions in good weather whereas more complex and costly automated systems may be economically justifiable in high-density traffic and poor weather.

NOMENCLATURE

C-8A	De Havilland "Buffalo" STOL aircraft
CDI	course deviation indicator
3-D	three dimensional
4-D	four dimensional
DOT	Department of Transportation

EADI electronic attitude director indicator

FAA Federal Aviation Administration

G & N guidance and navigation system

GN & C guidance, navigation, and control

HSI horizontal situation indicator

ILS instrument landing system

MFD multifunction display

MLS microwave landing system

MLS G/S microwave landing system glide slope

MLS LOC & DME microwave landing system localizer and distance measuring equipment

MODILS modular instrument landing system

NASA National Aeronautics and Space Administration

STOL short take-off and landing

STOLAND research STOL avionics system

TACAN tactical area navigation

VOR/DME very high frequency omnidirectional range/distance measuring equipment

OBJECTIVES

The overall objective of the Ames operating systems experiments program is to provide information to aid the choice of STOL terminal area GN & C systems and define operational procedures. This information will consist of system performance data as a function of the experimental variables. These variables are system complexity (for

example, raw data, flight director, standard autopilot, fully automatic flight); pilot displays and controls, operational constraints (for example, trajectories); ground navigation aids (VOR/DME, MLS, and TACAN), GN & C concepts (for example, 3-D and 4-D guidance, navigation filter techniques, etc.); and onboard sensors (for example, air data, inertial: gimbal compared with strapdown).

The Ames experiments program consists of three phases: analysis, simulation, and flight test. An advanced avionics system will be installed in two typical STOL vehicles to obtain the desired performance data in flight systems. This information will be used to establish STOL system design criteria.

PROGRAM APPROACH

The major steps to obtaining the required information are illustrated in figure 1. The first step is the definition of the experiment elements. This is a brief but intensive study based on the application and extrapolation of current knowledge and experience to define potential experiments and the number of variables possible in the flight experiments program. During this brief study, experiments with similar requirements can be identified and combined and gaps in the experiment program are defined.

From this first step comes a reasonably detailed definition of the research objectives, a preliminary definition of the experiments program and a set of specifications which are used in design and development of the STOLAND flight test system.

The main research effort consists of analytical studies and piloted closed-loop simulations. Analytical studies are carried out in-house and under contract. Piloted simulations are carried out mainly at Ames.

The analysis and simulation phases serve many purposes. In these phases of the program, the GN & C system concepts are developed in detail and system performance data are obtained. Flight experiments are refined and the flight test program is planned in detail. Every effort is made to obtain the bulk of the system performance data during these phases of the program. As a result of this approach, costs associated with flight test are minimized since flight tests are conducted chiefly to verify system performance obtained during the simulation program and to explore problem areas which cannot be adequately explored in the simulation environment.

SCHEDULE

Presented in figure 2 is a schedule for the analysis, simulation, and flight-test phases. The analysis phase has been underway since July 1971, when Sperry Flight Systems was given a contract to investigate STOL navigation, guidance, and control con-

cepts. This phase of the program will be essentially completed in mid-1973. The in-house analysis effort aimed at development of improved 4-D (time-constrained) guidance, improved automatic speed control concepts, and so forth is scheduled to continue through 1977.

The piloted/automatic flight simulations are scheduled for initiation in early 1973. As previously noted, these simulations will be utilized to define, in detail, the flight experiments and to obtain experimental results.

Flight checkout of the STOLAND system will be initiated in the Convair 340 aircraft in early 1973. The flight tests for the STOL aircraft will be initiated in the fourth quarter of 1973.

TYPICAL EXPERIMENTS

The Ames operating systems experiments program is illustrated in figure 3. Shown here is the STOL airborne/ground system configuration, the levels of G & N system automation to be investigated in the flight experiments program, and one of the flight profiles. The onboard system will allow the investigation of all the important levels of automation from a simple manual system without any augmentation to a fully automatic landing system. Time-constrained, steep, curved decelerating approaches, as well as straight-in approaches, will be investigated to obtain data on system performance. Three different ground navigation aids will be used: a microwave landing system (MODILS) provided by the FAA, VOR/DME, and TACAN. It should be emphasized that the experiments program will allow assessment of the relative merits of various levels of system sophistication in terms of system performance, system complexity, safety, and cost.

In figure 4 is illustrated one of two reference flight paths that are being flown on the simulator during system acceptance tests. This trajectory will be flown later in the flight experiments program. It incorporates a series of tasks which will provide data on system performance for many of the guidance and navigation experiments. As an example, 3-D and 4-D area navigations using VOR/DME or TACAN are evaluated for the section of the flight path in which the aircraft is climbing to altitude for the approach. Problems associated with transitioning from VOR/DME or TACAN to MLS will be investigated on passing into the zone of MLS coverage. The application of 360^{o} azimuth MLS antenna operation using a front- and rear-antenna system will be assessed. Evaluations can be made of 3-D and 4-D guidance and navigation using microwave data to establish helical approach paths, effects of winds, definition of decision height windows, definition of touchdown dispersions, pilot acceptance, and the performance of various display systems configurations.

To illustrate the proposed experiments program better, one specific experiment will be discussed in some detail.

In figure 5 is illustrated the segment of the reference flight path to be used in this specific experiment. The objectives of this experiment are to investigate the effects of variations in the radius of curved descending turns, glide-slope angle, and localizer intercept point on system performance and pilot acceptance in the automatic and flight director modes. The performance criteria to be evaluated are the errors in position and velocity along the path and the touchdown dispersion parameters of position, velocity, and aircraft attitudes.

RESEARCH FACILITIES

The flight system STOLAND is illustrated in figure 6. The system is very flexible and is consistent with the requirements of the experiments program.

The major components of the system are a Sperry 1819A general purpose digital computer and a data adapter which interfaces all the navigation aids, displays, controls, and servos with the computer. A detailed description of the STOLAND system may be found in reference 1.

Most of the STOLAND flight hardware and software will be used in the piloted flight simulation. Those functions shown in black in the STOLAND block diagram are not flight hardware and are provided by the airborne hardware simulator. The STOLAND equipment rack is installed in the simulator as shown in figure 7.

The STOLAND displays and controls are installed in the simulator cockpit as shown in figure 8.

The pilot display panel is shown in detail in figure 9. The Sperry electronic attitude director indicator (EADI) and the multifunction display (MFD) occupy the central position of the panel. A standard horizontal situation indicator (HSI) with a course deviation indicator (CDI) is located below the EADI.

The STOLAND mode select panel and MFD control panel are located adjacent to the MFD. The keyboard and status panel, not shown, are located on a pedestal to the right of the pilot.

The main features of the EADI shown here are the aircraft symbol with roll and horizon reference, the ILS window which provides the pilot with information regarding his position with respect to the MLS localizer and glide slope, the runway symbol just to the left of center, and the airspeed, vertical speed, and altitude in numeric form in the three windows at the top of the display.

The main features shown on the MFD are a reference flight path with respect to the runway at the experimental facility and the airplane symbol which is the triangular shape close to the flight path. On the top of the MFD is displayed the altitude on the left, aircraft heading in the center box, and time on the right. The scale displayed on the MFD is the aircraft heading. The details of the remainder of the STOLAND display panel can be obtained from reference 1.

The simulation allows the evaluation of GN & C and display concepts after the appropriate software has been put into the flight computer. As previously noted, the simulation will also be used for flight software validation, refinement of flight experiments, collection of experimental data, investigation of off-nominal flight conditions, and the comparative evaluation of competitive concepts.

PROGRAM STATUS

The status of the operating systems program is now presented. The GN & C operating systems experiments have been defined in some detail. The STOLAND simulator avionics system is operating at Ames Research Center. Acceptance tests of this system are scheduled for completion in November 1972. The STOLAND flight avionics system is scheduled for delivery in November 1972, with acceptance tests scheduled in December 1972. Experiments development and baseline data collection utilizing the STOLAND simulator will be initiated in January 1973. STOLAND avionics system flight checkout and preliminary data collection is scheduled on the Convair 340 aircraft in February 1973. Utilization of manual modes will be emphasized in these tests. Flight data collection utilizing the C-8A STOL and augmentor wing jet STOL aircraft is scheduled in the fourth quarter of 1973.

CONCLUDING REMARKS

A STOL GN & C operating systems experiments program has been defined to provide information for choice of STOL terminal area systems and operational procedures.

This information will allow the U.S. Government and industry to establish systems design criteria and to make trade-off studies of cost, safety, and return on investment as a function of system complexity.

A STOL simulator has been put into operation which utilizes airborne hardware and software. This simulator will be used to develop G & N system concepts, operating system experiments, and to perform other tasks in support of the program. A flight program has been developed to verify GN & C system concept performance which cannot be reliably measured by using analysis and flight simulation procedures. The flight program will

utilize the STOLAND flight avionics system in conjunction with three aircraft, the Convair 340, the C-8A STOL aircraft, and the augmentor wing jet STOL research aircraft.

REFERENCE

1. Hansen, Q. M.; Young, L. S.; Rouse, W. E.; and Osder, S. S.: Development of STOLAND, a Versatile Navigation, Guidance and Control System. AIAA Paper No. 72-789, Aug. 1972.

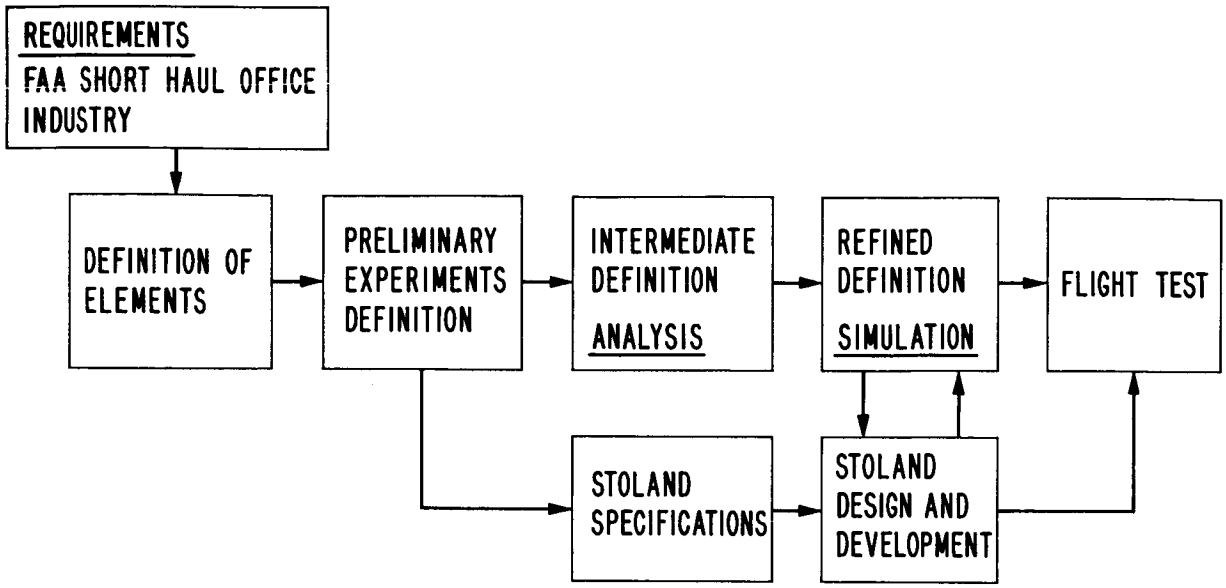

Figure 1.- Experiments approach.

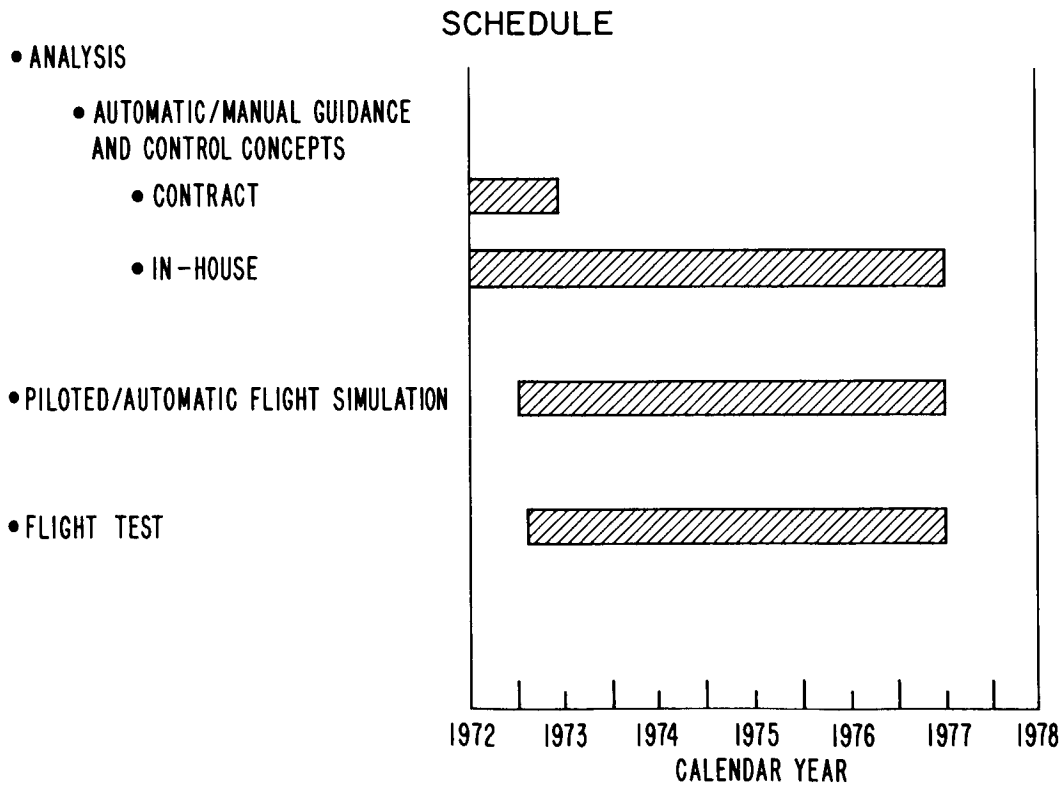

Figure 2.- STOL terminal area guidance, navigation and control operating systems experiments.

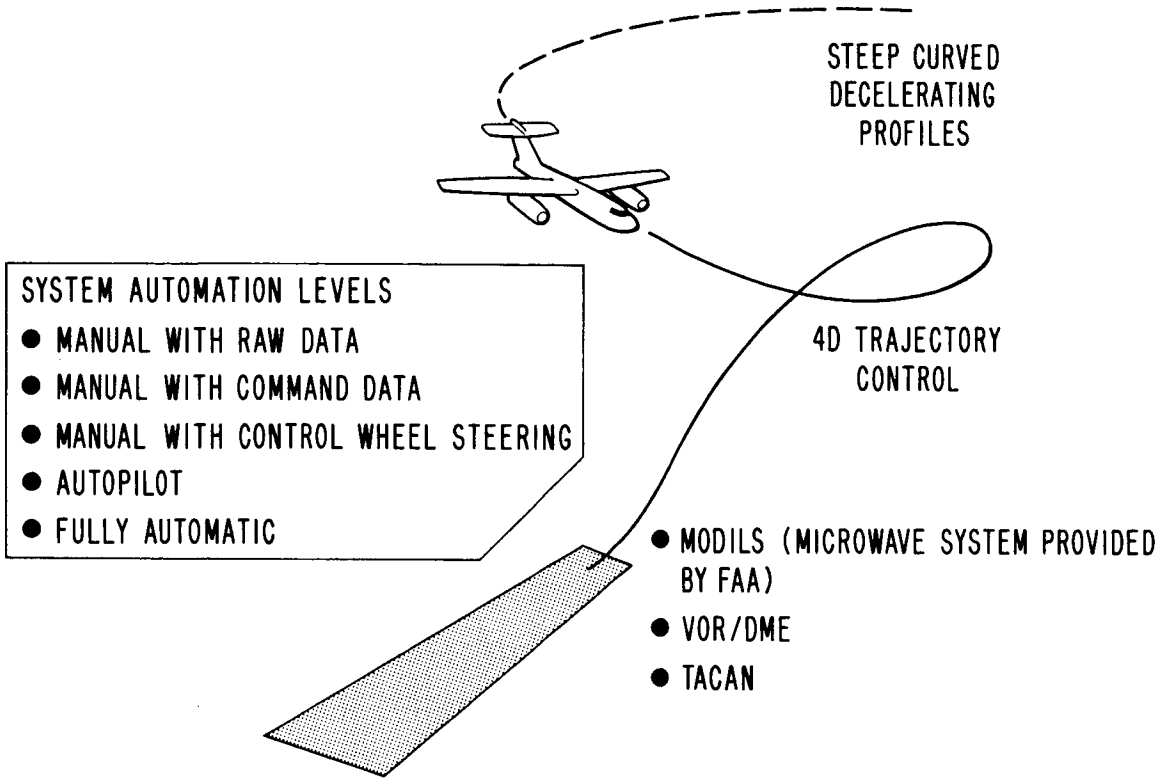

Figure 3.- STOL airborne/ground systems configuration.

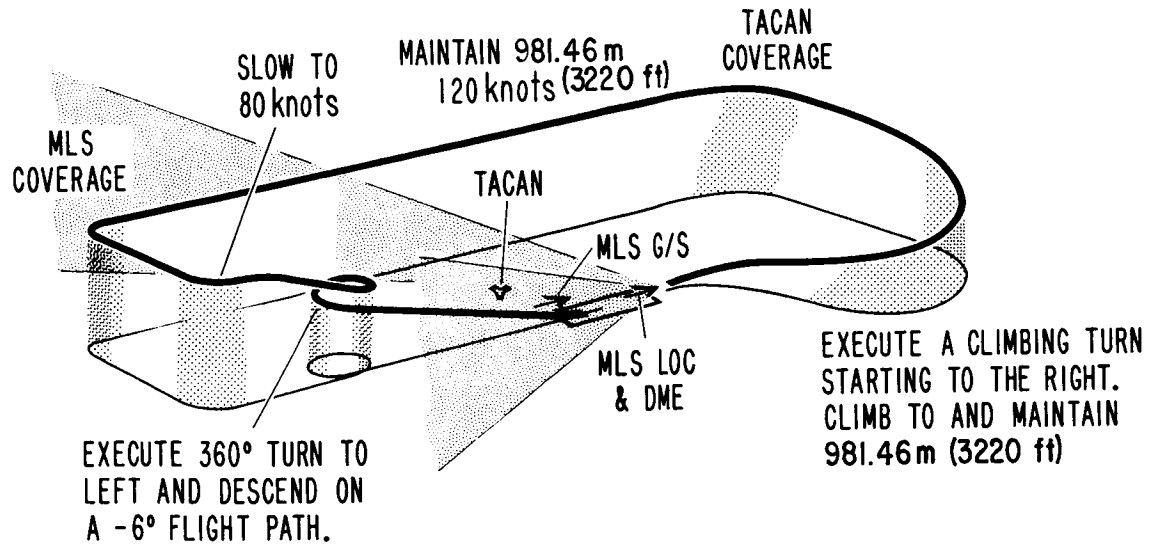

Figure 4.- Typical flight path for GN&C experiments.

- VARIABLES
  - RADIUS OF CURVED DESCENDING TURN
  - GLIDE SLOPE ANGLE
  - LOCALIZER INTERCEPT POINT LOCATION

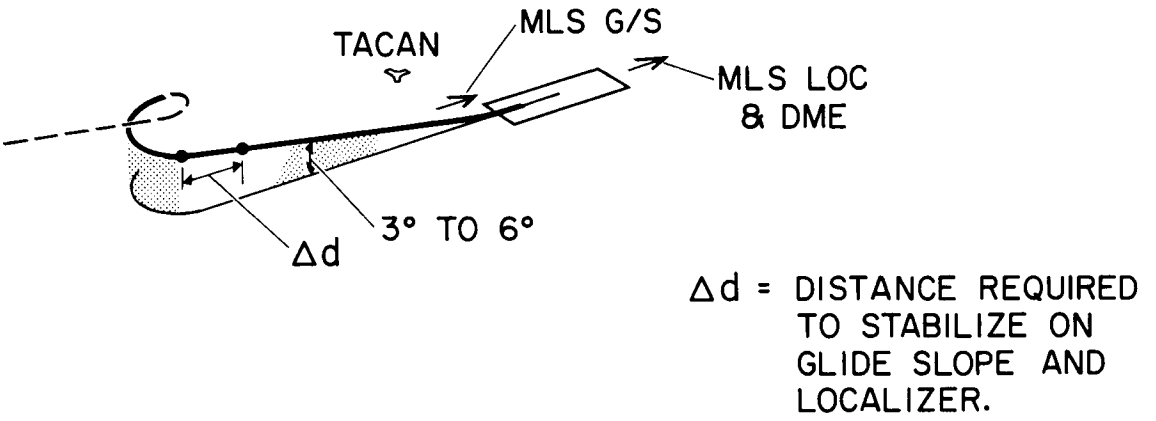

Figure 5.- Segment of flight path for a specific experiment.

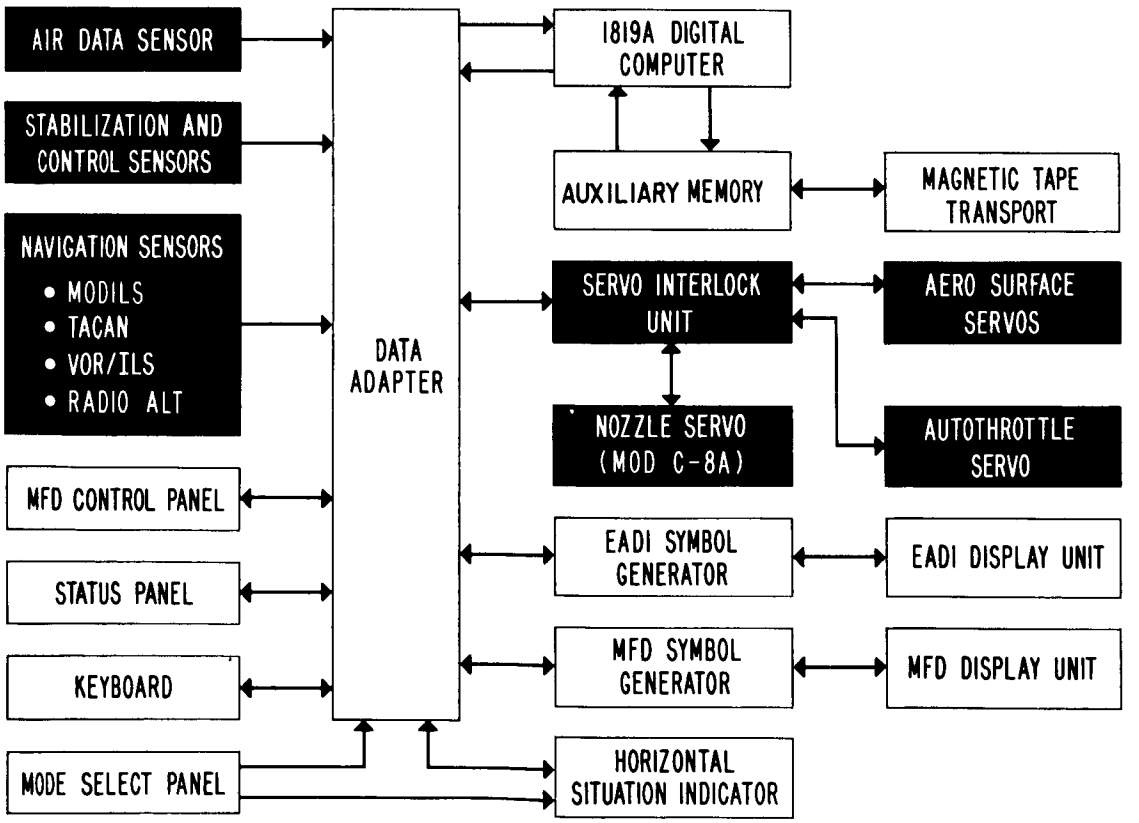

Figure 6.- STOLAND block diagram.

Figure 7.- Simulator STOLAND equipment installation.

Figure 8.- STOLAND simulation cockpit.

Figure 9.- STOLAND pilot display panel.

PROGRAM PLAN TO DEVELOP AIRWORTHINESS STANDARDS FOR STOL AIRCRAFT

By Jack E. Cayot, Robert A. Chubboy,
Federal Aviation Administration

and Charles S. Hynes
NASA Ames Research Center

SUMMARY

A program plan to develop criteria for airworthiness standards for STOL transport aircraft is presented. Initially, three different STOL concepts are to be examined with a goal to arrive at a generalized set of standards. The Breguet 941 deflected-slipstream STOL has been initially evaluated on a piloted motion simulator and in flight. Confidence in establishing criteria for airworthiness standards for STOL transport aircraft has been obtained from these studies.

25

INTRODUCTION

The fact that STOL aircraft appear to be a future mode of air transportation has prompted the Federal Aviation Administration (FAA) to examine current procedures and requirements for applicability for STOL operation. There are many aspects to be considered before this form of air transportation becomes operational – such as air traffic control, STOLport development, and airworthiness standards. The FAA has established an overall plan to aid in the development of STOL aircraft. Part of this plan is the development of airworthiness standards which include aircraft performance and related handling qualities.

The need to update airworthiness standards for STOL aircraft is outlined as follows. Current airworthiness standards for transport category airplanes – Federal Aviation Regulation (FAR) 25 (ref. 1) – do not provide credit for the performance advantages to be gained from powered-lift aircraft. For example, current CTOL performance requirements are based upon specific speed margins above demonstrated power-off stall speeds. Since powered lift implies that engine power is nominally used to augment aerodynamic lift in approach, power-off conditions would unduly penalize STOL aircraft performance. They will lose their advantage to overcome current CTOL operational limitations (i.e., to perform on steep obstacle clearance flight paths and short runways); this suggests the need to redefine the currently used minimum speed criteria as the basis for performance.

The first cut to update FAR 25 is contained in a document entitled "Tentative Airworthiness Standards for Powered-Lift Transport Category Aircraft," sometimes referred to as "Part XX" or the "Yellow Book." That document is actually a combination of applicable sections of FAR 25 (ref. 1) and FAR 29 (ref. 2, entitled "Airworthiness Standards: Transport Category Rotorcraft") and has proven very useful for discussion purposes. However, better definition is needed in many areas where technology is advancing the state of the art, such as the new concepts of powered lift that were not envisioned during development of Part XX.

This paper will discuss the plans for providing criteria for establishing airworthiness standards for STOL aircraft, the critical areas to be studied, and the current progress of the program.

RESULTS AND DISCUSSION

Joint Study Programs

The decision to conduct STOL airworthiness development studies using the Flight Simulator for Advanced Aircraft (FSAA) at Ames Research Center was a natural extension of an ongoing successful cooperative program between FAA and NASA to develop airworthiness standards for the supersonic transport. The two government agencies have overlapping interests and objectives, in that the FAA is interested in developing criteria for airworthiness standards and NASA is interested in developing aircraft design criteria. Several cooperative programs will continue in the STOL area. In addition to the FAA-NASA agreement, the partnership between the United States, United Kingdom, and French airworthiness authorities will be continued with the goal to establish a common set of international airworthiness standards. Another partnership between government agencies with common interests is in the formulative stages between the U.S. Air Force and the FAA.

Critical Areas To Be Studied

As mentioned previously, the program to define reference speed will be restricted to an examination of aircraft performance and related controllability aspects in the STOL terminal area flight regime. Five critical areas were selected for study: minimum flight-path criteria, safety margins, approach and landing performance, controllability as related to aircraft performance, and take-off performance. Initial emphasis was placed on resolving the question of whether or not to base aircraft performance on some factor of stall/minimum speed. If take-off and landing can be referenced to a specific speed, then the real question centers on the means to establish a realistic definition of the "speed" and what factors most clearly determine "speed." These points are discussed next.

The first area concerns definition of a minimum speed at which adequate control of flight-path angle can be maintained. Since, for powered-lift STOL aircraft, adjustments to flight-path angle are necessarily obtained by changing engine thrust, a power-off reference speed is not pertinent. In fact, as discussed earlier, airspeed may not be the only reference used for controlling flight path.

Safety margins are needed for several reasons. First, a margin in speed above the minimum speed is necessary to assure the pilot that the aircraft will not stall in gusty air; therefore, the aircraft must have a sufficient speed margin when maneuvering in approach and have adequate controllability in the speed range near the minimum speed. When the basis for minimum flight-path criteria has been determined, then appropriate safety margins will be established, taking into consideration the aforementioned requirements.

With regard to approach and landing performance, the reference criteria must be such that consistent air and ground distances are obtained from steep approach paths. In defining speed margins for performance measurements, evaluation will be made of angle of attack as a flight reference. Use of angle of attack has an advantage of being less sensitive to the effects of engine power setting and thereby giving the pilot a more meaningful reference from the stall.

Controllability, as related to aircraft performance, must consider several factors. First, controllability in approach is directly related to the pilot/aircraft dynamics. For example, dynamic longitudinal stability is reduced at low approach speeds which results in a longer time to damp oscillations in attitude which have resulted either from the pilot's control inputs or from gust disturbances. Further, the aircraft is more sluggish in pitch response, and the pilot usually uses large control inputs in an effort to "hurry up" the desired response. As a result, precision of control deteriorates with its attendant effect on performance. Second, configuration changes such as flaps, gear, and spoiler have an effect on precision of control. Finally, environmental aspects, turbulence, related wind shear, and cross winds have a significant effect on performance since the aircraft, by virtue of flying at low speed, is more influenced by these environmental characteristics.

The last item, take-off performance, is currently based on speed-related factors such as decision speed V_1 and rotation speed V_R. The appropriateness of these items for STOL needs to be examined in detail since, for example, with the relatively high thrust-weight ratio T/W characteristic of STOL aircraft, acceleration is very rapid and time for take-off is short, thereby making questionable the utility of using V_1 and V_R as reference since they are not sufficiently separated. Speed abuses such as over-rotation and delayed take-off have different significance for STOL aircraft because of the effect of higher T/W.

Scope of Simulator Program

The piloted simulator can be used to help establish certification criteria by studying a number of STOL concepts and thereby establishing a data base for application to advanced STOL aircraft designs. It was considered necessary to initially study different STOL concepts in order not to unduly compromise any specific type; however, the intent would be to develop generalized airworthiness standards that would apply regardless of the type of STOL concept.

Three STOL concepts chosen for initial studies on the FSAA are propeller-driven deflected slipstream, augmentor-wing jet flap, and externally blown flap. They were selected, for the most part, in the chronological order of availability for flight validation of the simulator results. Although only three STOL concepts are mentioned, other concepts such as the over-the-wing blowing may be studied at a later date to be certain that all potential problem areas are being covered.

Propeller Slipstream Study

The first concept to be studied was the Breguet 941S STOL transport. Selection of this particular aircraft had the following advantages: (1) a relatively complete data package (math model) was available based on two Ames Research Center flight test programs, (2) through the cooperation of France, the 941 aircraft was made available to United States pilots for validation, (3) the aircraft represented an advanced STOL transport concept by virtue of its completely immersed high-lift flap system and propeller interconnect setup, (4) it served to familiarize FAA and NASA pilots participating in the simulator program with recent STOL aircraft experience to help guide the simulator program, and (5) it offered the potential of gathering data to update the current math model.

Flight Program Results

In the 13 flights made in France, emphasis was given to descent performance, take-off and landing at various flight-path angles, and handling qualities which would help define the critical areas previously discussed. The results indicated three significant points. (1) Minimum flight-path reference criteria were not easily identifiable for this type of aircraft. The aircraft was flown as slow as 50 knots in approaches with no apparent undesirable characteristics. Not being able to define some limiting characteristics was somewhat disappointing; however, it was recognized beforehand that in the absence of stall, heavy buffet, or minimum control speed, the reference criteria would be elusive. (2) The 941 aircraft was found to be almost insensitive to take-off abuses, even with one engine inoperative. Because there were no asymmetries and relatively high T/W's, it was apparent that the conventionally used take-off speed criteria would not be applicable to this STOL concept. (3) The pilots were unanimous in their preference for flying rela-

tively higher approach angles. Operation at shallow approach paths was not as desirable because, with more power required, less thrust margin was available for wave-off. The pilots also preferred operating at heavier gross weights because handling qualities were better, presumably because the approach speeds were higher and offered improved controllability and damping.

Simulator Program Results

The first of a series of simulator studies was conducted on the FSAA shortly after the flight experience in France, with the definite advantage of still fresh impressions of the aircraft. Briefly, the results were as follows. First, the pilots were confident that a reasonably good representation of the aircraft had been obtained on the simulator and that it was feasible to move ahead to examine the previously mentioned critical areas. Second, some tailoring of the aircraft parameters used in simulation was necessary to provide realistic lateral-directional behavior. This was considered to be necessary since it was also the intent to arrive at demonstrable criteria as well as flight techniques or procedures to check the airworthiness standards. Third, some areas were considered to require improvement from the pilot's standpoint. In particular, ground effect appeared different on the simulator compared with flight, and environmental factors such as turbulence, wind shear, and cross wind needed further refinement for more meaningful results.

Schedule of Simulator Program

In figure 1, a schedule of the simulator program to develop airworthiness standards is shown. The propeller slipstream transport has been underway since July 1972. It can be noted that each STOL concept will be examined twice. The first part will be reserved for identifying and evaluating problem areas on a limited scale, and the second part will be a main evaluation effort by a larger selection of pilots. After examining other STOL concepts, it is expected that a review of airworthiness standards can be made in mid-1974. A final version of the standards, following the normal regulatory review process, should be available for the aircraft manufacturer in time to meet the 1980 proposed operational date for STOL aircraft.

Plans for VTOL concepts will follow, as noted, for the tilt-rotor, tilt-wing, and lift-fan transports with the same purposes in mind as for STOL.

REFERENCES

1. Anon.: Airworthiness Standards: Transport Category Airplanes. Federal Aviation Regulation Part 25, Rules Service Co. (Washington, D.C.), Feb. 1, 1965.

2. Anon.: Airworthiness Standards: Transport Category Rotorcraft. Federal Aviation Regulation Part 29, Rules Service Co. (Washington, D.C.), Feb. 1, 1965.

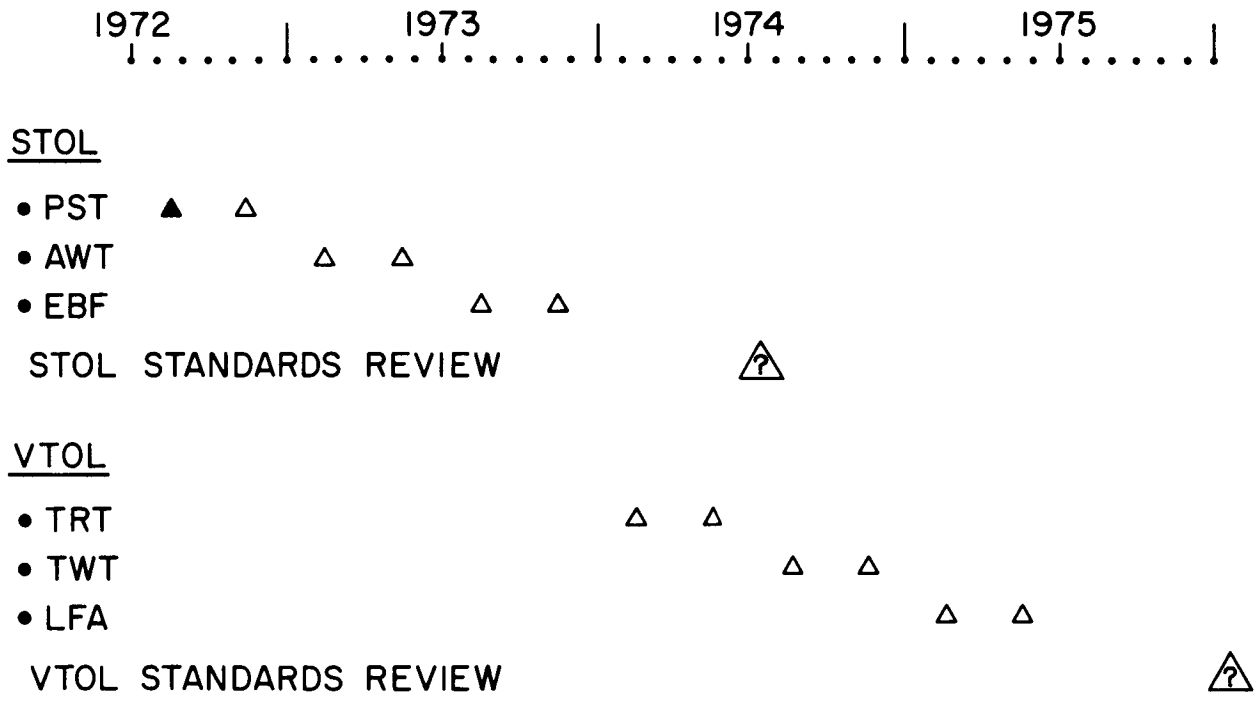

Figure 1.- Schedule of simulator program to develop STOL airworthiness standards.

FACTORS INFLUENCING PUBLIC ACCEPTANCE OF STOL NOISE

By Philip M. Edge, Jr., Jimmy M. Cawthorn, and Clemans A. Powell, Jr.
NASA Langley Research Center

INTRODUCTION

This paper is basically a review of the present knowledge of the responses of people to special noise characteristics which may be associated with STOL aircraft. In this review a progress report will be given to show the findings of recent studies which have yielded data that may be pertinent to community acceptance of STOL aircraft noise.

The scope of this paper is to present a three-step program to evaluate public acceptance of STOL noise. The three steps are (1) definition of STOL noise characteristics, (2) laboratory tests to evaluate individual responses, and (3) the use of community survey data to extrapolate CTOL experience.

The noise characteristics of a new type of aircraft are determined by its design and operational capabilities. Once these capabilities are established, the noises expected to be produced by the aircraft can be simulated for use in laboratory tests to evaluate individual responses to the noise. Finally, the results of community surveys conducted in CTOL airport communities can be extrapolated to the STOLport situation to define potential problem areas and/or areas which should be of little concern.

NOISE CHARACTERISTICS

Community Exposure Level

Dominating the noise characteristics for a STOL aircraft is the tentative requirement that its noise be 95 PNdB or less at a 152-m (500-ft) side-line distance. Some of the impact of this requirement on community noise exposure can be appreciated with the use of figure 1 where the 95-PNdB contour noise footprints of STOL and short-haul CTOL aircraft are compared. These computer-generated contours were determined on the basis of the assumption that the CTOL meets the Federal Aviation Administration FAR 36 requirements and that the STOL meets the tentative requirement of 95 PNdB at a side-line distance of 152 m (500 ft). Note that the contours are plotted for both the landing approach and the take-off ground roll and climbout. The STOL footprint is much smaller than the CTOL footprint because the STOL propulsion systems are required to be quieter and because approach and climbout associated with the STOL aircraft are steeper. The steeper approach and climbout angles result in the STOL being at a higher altitude at any given distance along the flight path, and therefore,

the noise is attenuated more than for the CTOL. The size of the STOL footprint is such that if the STOL is operated from a conventional airport, this footprint can lie entirely within the airport boundaries (ref. 1). However, when the STOL is operated from a small STOLport, which could be in a densely populated urban environment, its 95-PNdB noise will extend into the neighboring community.

Flyover Noise Duration

In addition to noise level, the special operational characteristics of low speed and steep approach and climbout will affect the characteristic of the flyover noise duration (or exposure time of the noise). Example flyover noise duration characteristics are illustrated in figure 2. On the left is a typical time history of the take-off noise exposure from a CTOL airplane at a point near the airport boundary. The duration at the 10-dB-down point is illustrated, since this duration is considered to be important and is used in computing perceived noise level. The illustration on the right is considered to be typical of a STOL aircraft at a position near the STOLport boundary.

The maximum noise level is less because of the stringent requirements which have been proposed for STOL aircraft, but the duration is longer since the STOL flies at a slower speed. Although it might be expected that the lower flight speed would always result in the STOL aircraft having a longer duration of flyover noise, this is not true. For example, if the STOL and CTOL flyover noises are of the same level, the CTOL noise duration may be equal to or even greater than that of the STOL. Related studies of duration effects are contained in reference 2.

Noise Spectra

To achieve the special STOL operational characteristics of low speed and steep approach and climbout, proposed design features include propulsion-lift systems which have important effects on the spectra of the noise generated (ref. 1). A characteristic of several of the lift augmentor systems is the generation of high levels of acoustic energy in the low frequencies below 100 Hz. As an example, in figure 3 a spectrum believed to be characteristic of an externally blown flap system is compared with a spectrum for a short-haul CTOL aircraft. The STOL spectrum shown is based on externally blown flap noise data obtained on a full-scale model. In the figure, the spectra shown are for conditions of equal perceived noise level (PNL). One-third-octave band sound pressure levels in decibels are plotted against band center frequency in hertz. It is seen that for frequencies above 200 to 300 Hz, there is very little difference between the two spectra, but in the lower frequencies (50 Hz and lower) the STOL produces significantly more energy. This low-frequency energy is believed to be due primarily to the scrubbing noise produced by the impingement of the jet exhaust on the flap surfaces. The noise contained

in these very low frequencies may be especially important since the perceived-noise-level calculation procedures do not consider any energy below 50 Hz in the calculation process. Should the low-frequency acoustic energy be significant in the responses of people to STOL noise, there may be a need to modify the present PNdB as a unit of measure or to develop a new measuring unit. Initial laboratory studies to explore this need are under way in several basic research investigations.

LABORATORY STUDIES

The noise characteristics of increased exposure duration and low-frequency spectra can be studied in the laboratory to obtain individual response data. Recent laboratory tests which are useful in evaluating public acceptance of STOL noise will be briefly described.

Both increased duration and low-frequency spectra effects were evaluated in a recent subjective judgment test at the Langley Research Center. Laboratory studies to evaluate effects of low-frequency spectra have considered the noise transmission characteristics of house structures, and tests have been directed to responses of people in the indoor situation. Some studies of the responses to indoor vibrations and to indoor noise have been accomplished.

In the Langley subjective judgment tests, the flyover duration and low-frequency spectra were incorporated into STOL noise synthesis recordings, and judgments of these STOL noises were compared with judgments of CTOL noises.

Figure 4 shows a schematic of these tests, which compared the synthesized STOL noise with the noise of several short-haul commercial airplanes. The synthesized STOL noise was produced by altering the spectrum shape and time history of a tape recording of a two-engine jet airplane under normal operating conditions. Recordings were also obtained of a three-engine jet and a two-engine turbopropeller airplane. The noises of the synthesized STOL and the three airplanes were then re-recorded at five different intensity levels for each sound for the purpose of presenting the sounds to the subjects. In figure 5 is shown the audiometric room in which the sounds were presented to the subjects over a loudspeaker system. In the foreground a test subject is shown assigning a numerical judgment of annoyance for the flyover sounds emitted from the speaker in the background. Each of 20 subjects made annoyance judgments of 119 sounds.

Some of the results of this study are illustrated in figure 6. Shown in this figure are values of EPNdB of each of the three short-haul commercial airplanes (CTOL) relative to the synthesized STOL (zero baseline) for conditions at which the subjects judged the noises to be equally annoying for take-off, landing approach, and side-line locations. The height of each bar represents the average difference obtained from 100 judgment

comparisons. It is seen that the values are generally above the zero baseline; that is, the effective-perceived-noise values of the CTOL airplanes were higher than the STOL noise values when the subjects judged them to be equally annoying. This means that the STOL was considered to be more annoying than the other airplanes, or, in other words, the subjects judged the CTOL noises to be more acceptable. The EPNL procedure is seen to do a reasonably good job of rating the STOL noises, as the agreement is fairly close when the STOL is compared with the jet-powered CTOL's. However, there are some differences and it is believed that some of these differences might be due to the low-frequency energy (below 50 Hz) contained in the STOL noise and which is not considered in the EPNL calculation procedure.

The tests just described were based on annoyance judgments. There are other measures of annoyance which are of importance – such as sleep interference, and figure 7 shows results from some recent studies of the effects of noise on sleep. These studies were conducted by Thomas E. LeVere of North Carolina State University at Raleigh under a grant from NASA Langley Research Center. In this figure, level of sleep, which is measured by the illustrated electroencephalogram (EEG) waveforms, is plotted as a function of time. At zero time in the figure a 15-sec noise stimulus was presented to a subject who was in a deep sleep stage. As a result of the noise stimulus the subject's sleep stage was shifted toward an awake condition, and the subject then gradually returned to the prestimulus sleep stage. The noise stimuli shown here were 1/3-octave bands of noise (80 dBA) at 125 Hz and 1000 Hz. As the figure shows, the subject's sleep level was more sensitive to the lower frequency noise (he was shifted to a more nearly awake condition), and it required a longer time for him to return to his prestimulus level of sleep. These results could be significant in considering nighttime operations from a STOLport in an urban environment (or daytime sleepers living in a STOLport community). Additional studies of the effects of noise on sleep are reported in references 3 to 7.

The low-frequency noise discussed herein is in the audible range; however, as mentioned previously, a STOL aircraft with a powered-lift system such as the externally blown flap could produce significant amounts of energy in the subaudible and near-subaudible portion of the frequency spectrum. Figure 8 illustrates this particular characteristic of the STOL. Community low-frequency noise levels (1 to 50 Hz) for STOL and CTOL aircraft are shown in this figure. At the top of the figure are altitude-distance profiles for a take-off operation of the two aircraft illustrating the relatively steep climbout of the STOL. In the lower portion of the figure are plotted the 1- to 50-Hz sound pressure levels (SPL) of the two aircraft as a function of distance from brake release.

If the STOL is operated from a conventional airport, it is seen that its low-frequency noise level is the same as that of the CTOL at the illustrated hypothetical airport boundary (3657 m (12 000 ft) from brake release). This is due to the fact that the more intense low-frequency levels associated with the STOL propagate from its higher altitude unattenuated by the atmosphere. When the STOL is operated from a STOLport, the low-frequency noise levels in the community near the STOLport will be considerably higher. The result is that the community neighboring the STOLport will be exposed to higher low-frequency noise levels than are presently experienced in communities neighboring conventional airports.

Important to these airport-neighboring communities are the potential effects of the low-frequency noise on the indoor environment. In figure 9 a summary of noise reduction by house structures (refs. 8 and 9) is presented. Noise reduction in decibels is plotted as a function of frequency. The data from which this plot was obtained came from a large number of houses of all types of construction and from widely scattered geographical locations. It is seen that in the frequency range below 50 Hz, there is very little noise reduction provided by the house structures. Therefore, the low-frequency noise of STOL aircraft may be expected to be readily transmitted into the indoor living area.

Some effects which this low-frequency energy (unattenuated by the house structure) will have on the indoor vibration environment are shown in figure 10. Shown in this figure are noise-induced building vibrations, with wall acceleration in g units plotted against the 1- to 50-Hz sound pressure level in decibels. The vibration data shown in the figure were obtained from a rather large variety of building structures, and, as shown, the acceleration levels range from 0.001g to 1.0g for sound pressure levels from 60 to 110 dB. Data were obtained from the literature which indicate that vibration levels of 0.001g are detectable and that levels of 1.0g are sufficient to cause structural damage. Langley in-house experience has shown that annoyance and complaint activity are associated with a rather broad range of vibration levels, as indicated in the figure. The low-frequency noise levels at hypothetical airport and STOLport boundaries are indicated in the figure by the two dashed vertical lines. It is seen that the building vibration levels which would result from the low-frequency noise of the STOL in the STOLport community lie above the detectable region but well below the structural damage region; however, they are in a range where annoyance and complaints might be expected.

In these first two sections of this paper, consideration has been given to defining STOL noise characteristics, and some results from laboratory tests of subjective individual response to STOL noise and vibration and response to low-frequency noise have been presented.

COMMUNITY SURVEYS

One further item which should be considered is community response to noise. This is shown in the following equation for the prediction of noise acceptability:

$$\text{Acceptability} \approx F_1\left(\begin{matrix}\text{Noise}\\ \text{environment}\end{matrix}\right) + F_2\left(\begin{matrix}\text{Psycho-}\\ \text{physiological}\\ \text{factors}\end{matrix}\right) + F_3\left(\begin{matrix}\text{Attitudinal}\\ \text{factors}\end{matrix}\right)$$

This equation is derived from a NASA sponsored study performed by TRACOR, Inc., in which community response surveys were conducted in nine United States cities and approximately 10 000 people were interviewed (ref. 10). It is seen that acceptability is a function of the noise environment, a function of psychophysiological factors, and a function of attitudinal factors. It should be noted that each of the modifying functions is different, but that each one is dependent on the aircraft noise exposure. Some of the parameters which are included in each factor are as follows:

Noise environment:
- Aircraft noise level
- Ambient noise level

Psychophysiological:
- Fear of aircraft crashes
- Distance from airport
- Adaptability

Attitudinal:
- Misfeasance (that is, the feeling of whether or not the authorities are doing all that they can to alleviate the noise problems)

In extending these findings to STOL, the STOL noise environment is shown to be different from that of the CTOL. Its noise exposure area should be smaller; however, the area around a STOLport might be densely populated and the ambient levels may be higher. In regard to psychophysiological factors of fear and distance from the airport, it is noted that the populace could be even nearer the STOLport than for the current conventional airports so that these could be negative factors for acceptance of STOL noise. Regarding the attitudinal factor of misfeasance, it is very important to emphasize the development of a quiet aircraft – that "quiet" is being designed into the vehicle from the outset and that a good-neighbor policy be promoted in planning its operations. Additional studies of community annoyance from V/STOL noise are reported in reference 11.

CONCLUDING REMARKS

From studies which are directed toward defining STOL noise characteristics, investigating individual responses to noise and vibration, and surveying community acceptance of aircraft noise, the following concluding remarks can be made:

1. Compared with the CTOL airplane, STOL noise exposures may be smaller in area, different in duration, and more intense in low frequencies.

2. The EPNL calculation procedure may underestimate the annoyance of STOL noise.

3. Low-frequency effects may be more significant for STOL noise annoyance.

REFERENCES

1. Hubbard, Harvey H.; Chestnutt, David; and Maglieri, Domenic J.: Noise Control Technology for Jet-Powered STOL Vehicles. ICAS Paper No. 72-50, Aug.-Sept. 1972.

2. Sternfeld, Harry, Jr.; Hinterkeuser, Ernest G.; Hackman, Roy B.; and Davis, Jerry: Acceptability of VTOL Aircraft Noise Determined by Absolute Subjective Testing. NASA CR-2043, 1972.

3. Lukas, Jerome S.; and Kryter, Karl D.: Awakening Effects of Simulated Sonic Booms and Subsonic Aircraft Noise on Six Subjects, 7 to 72 Years of Age. NASA CR-1599, 1970.

4. Lukas, Jerome S.; Dobbs, Mary E.; and Kryter, Karl D.: Disturbance of Human Sleep by Subsonic Jet Aircraft Noise and Simulated Sonic Booms. NASA CR-1780, 1971.

5. Becker, R. W.; Lukas, J. S.; Dobbs, M. E.; and Poza, F.: A Technique for Automatic Real-Time Scoring of Several Simultaneous Sleep Electroencephalograms. NASA CR-1840, 1971.

6. LeVere, T. E.; Bartus, Raymond T.; and Hart, F. D.: The Relation Between Time of Presentation and the Sleep Disturbing Effects of Nocturnally Occurring Jet Aircraft Flyovers. NASA CR-2036, 1972.

7. Lukas, Jerome S.; and Dobbs, Mary Ellen: Effects of Aircraft Noises on the Sleep of Women. NASA CR-2041, 1972.

8. Anon.: Progress of NASA Research Relating to Noise Alleviation of Large Subsonic Jet Aircraft. NASA SP-189, 1968.

9. Young, J. R.: Attenuation of Aircraft Noise by Wood-Sided and Brick-Veneered Frame Houses. NASA CR-1637, 1970.

10. Connor, William K.; and Patterson, Harrold P.: Community Reaction to Aircraft Noise Around Smaller City Airports. NASA CR-2104, 1972.

11. Johnston, G. W.: V/STOL Community Annoyance Due to Noise Proposed Indices and Levels for Toronto-York Transportation Committee. UTIAS Tech. Note No. 177, Inst. Aerosp. Studies, Univ. of Toronto, Mar. 1972.

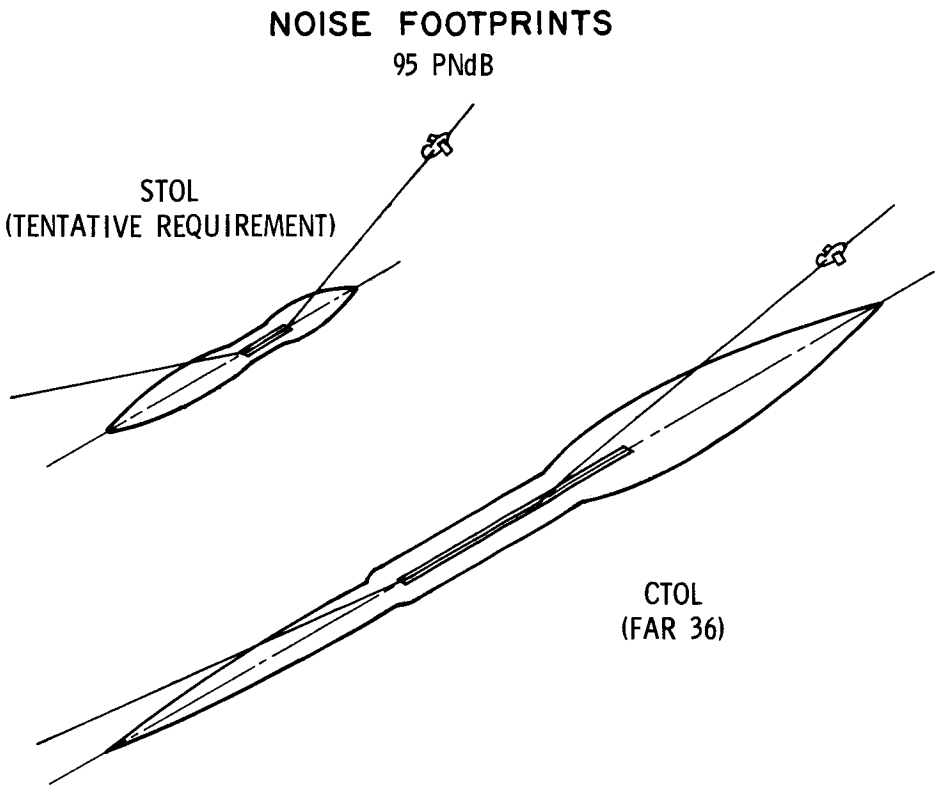

Figure 1

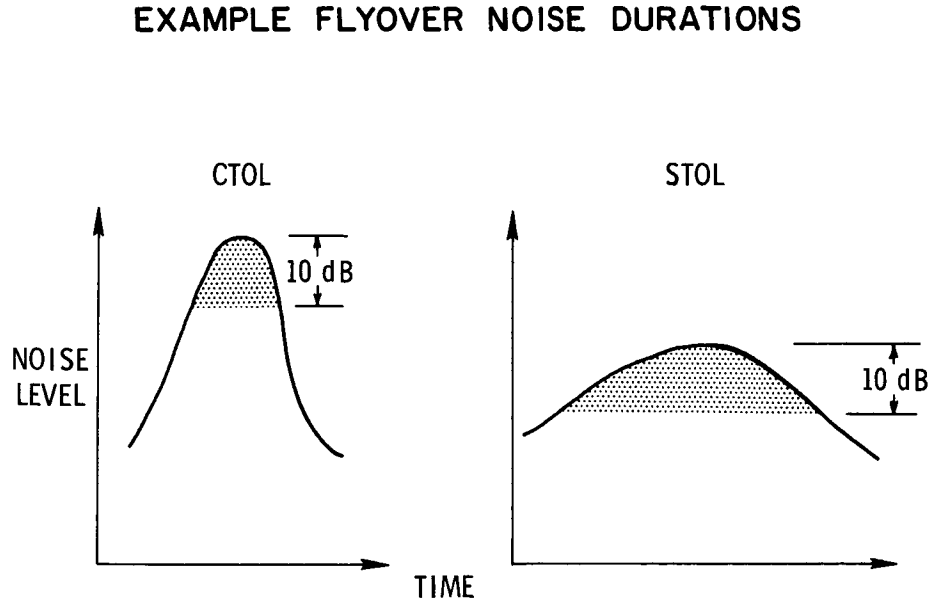

Figure 2

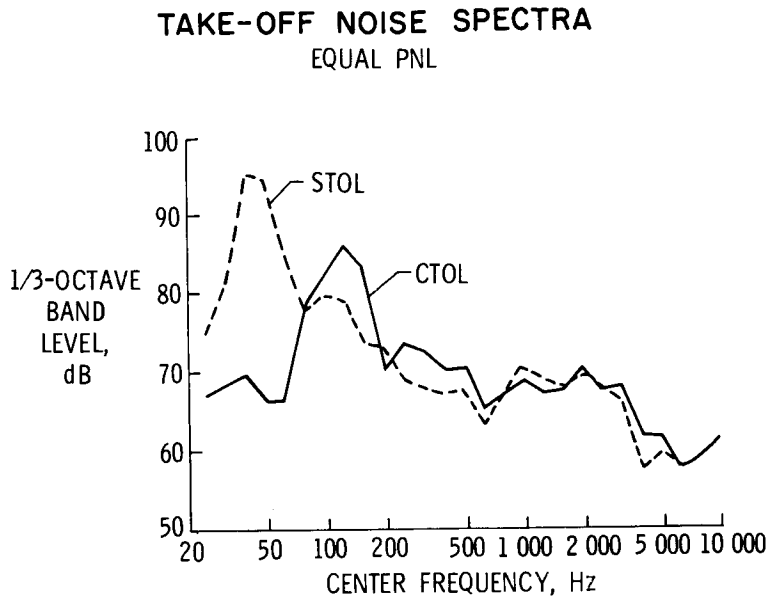

Figure 3

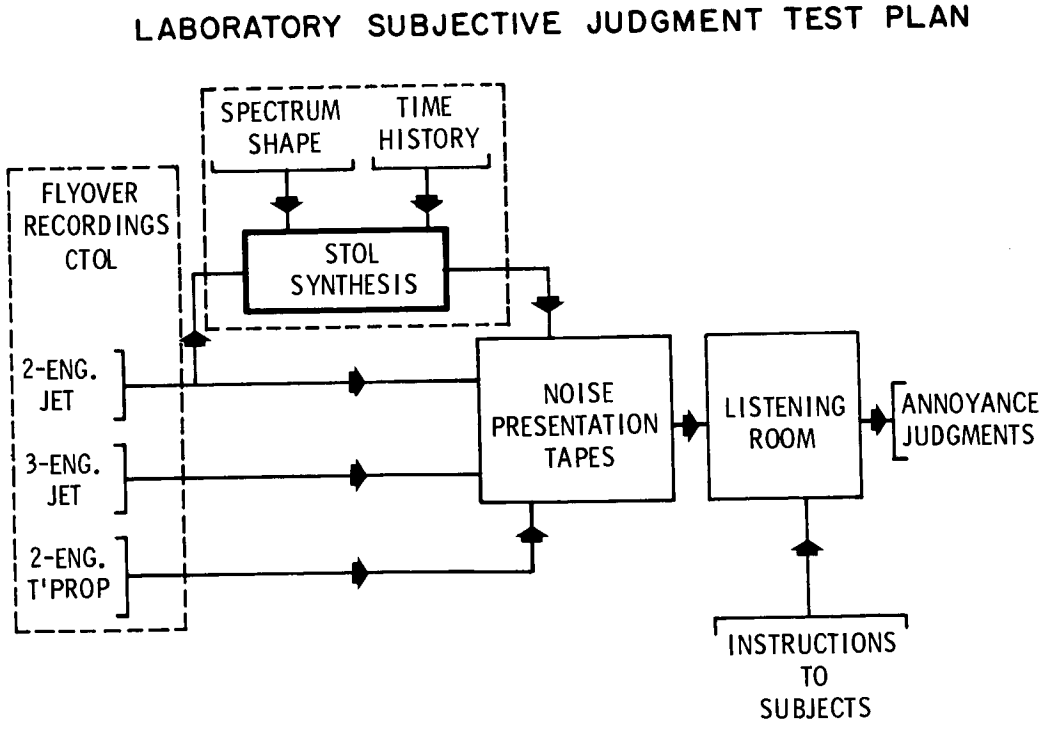

Figure 4

SUBJECTIVE JUDGMENT TEST SETUP

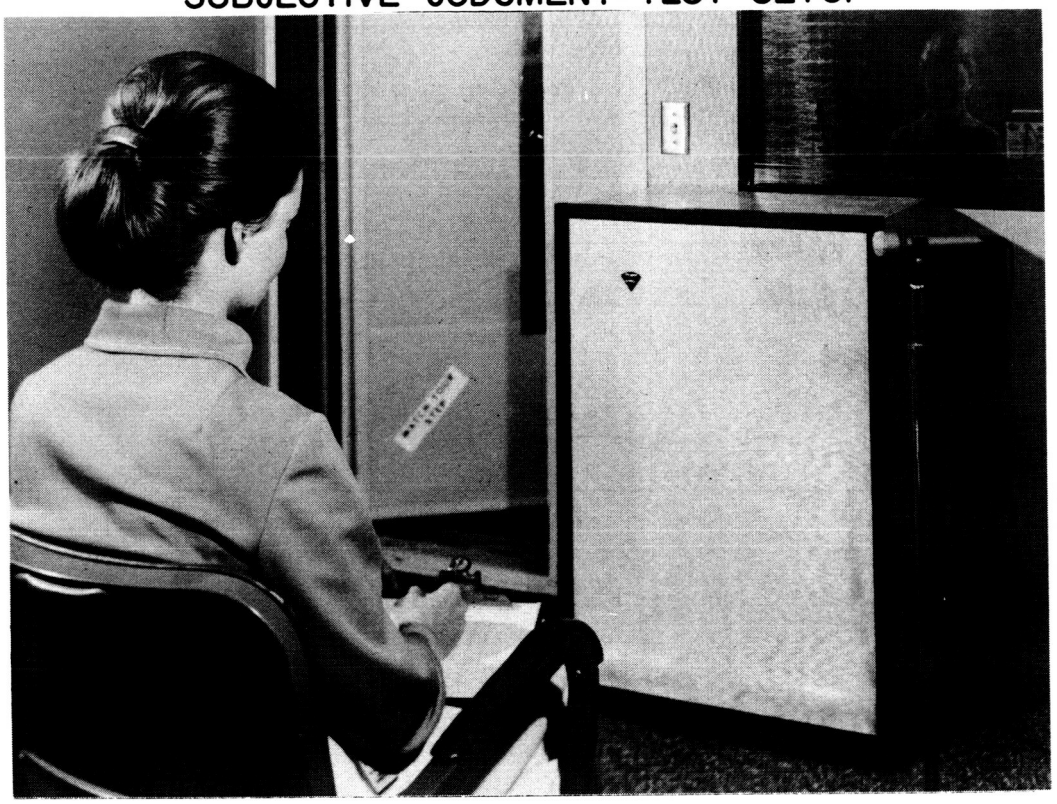

Figure 5

CONDITIONS FOR EQUAL ANNOYANCE

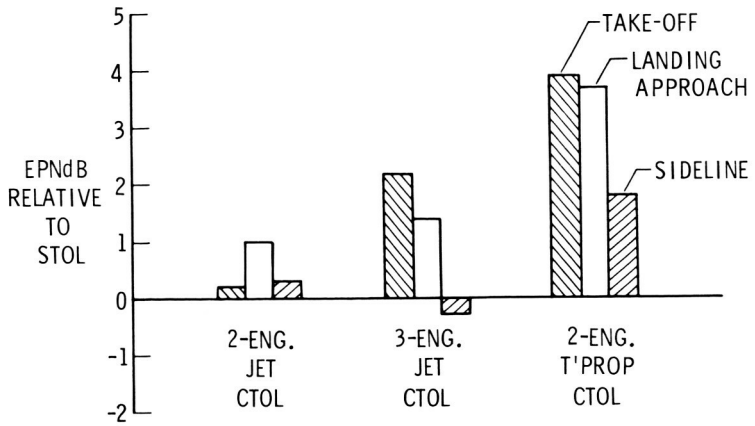

Figure 6

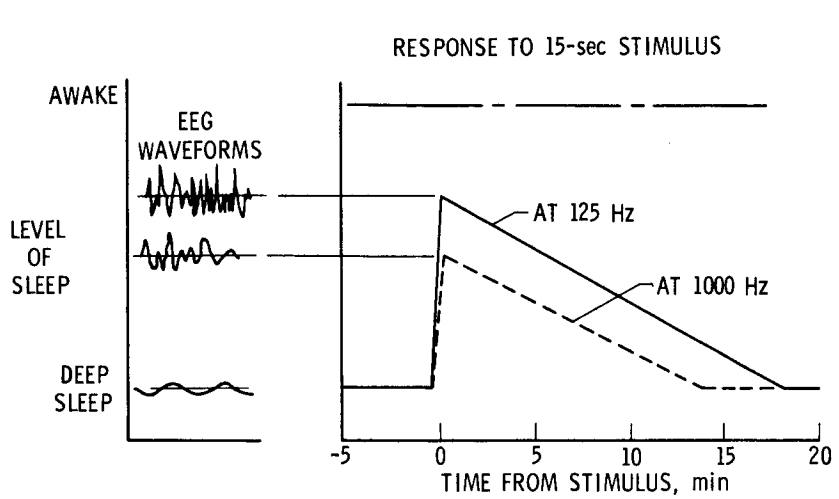

Figure 7

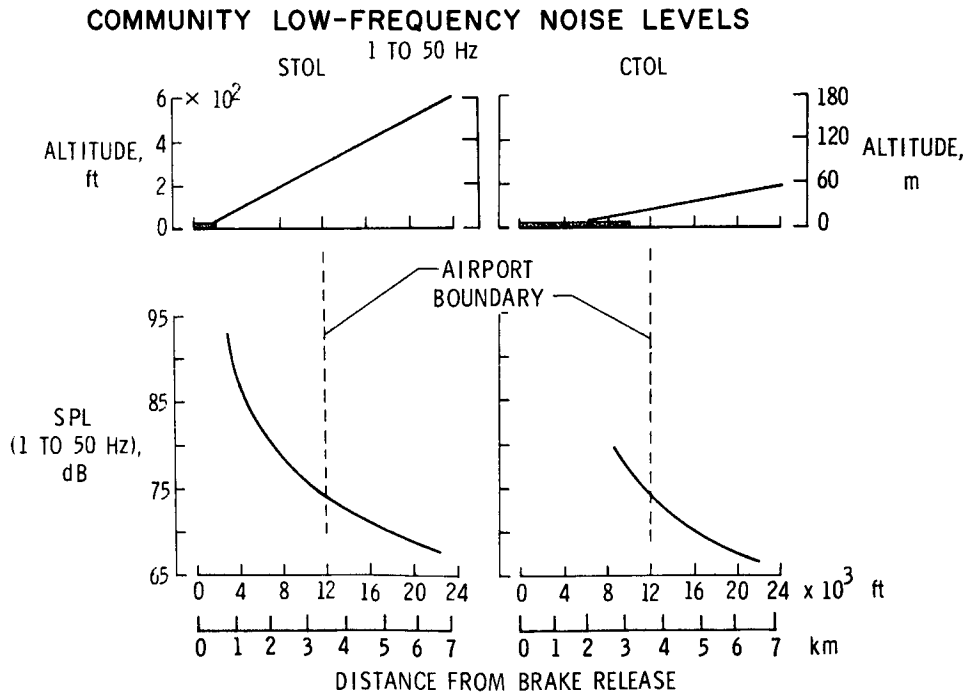

Figure 8

SUMMARY OF NOISE REDUCTION BY HOUSE STRUCTURES

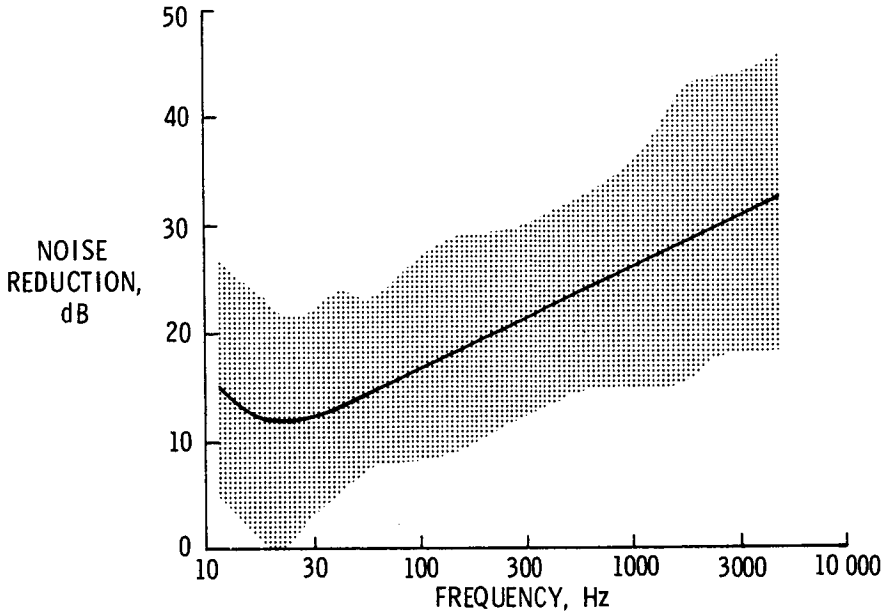

Figure 9

NOISE-INDUCED BUILDING VIBRATIONS

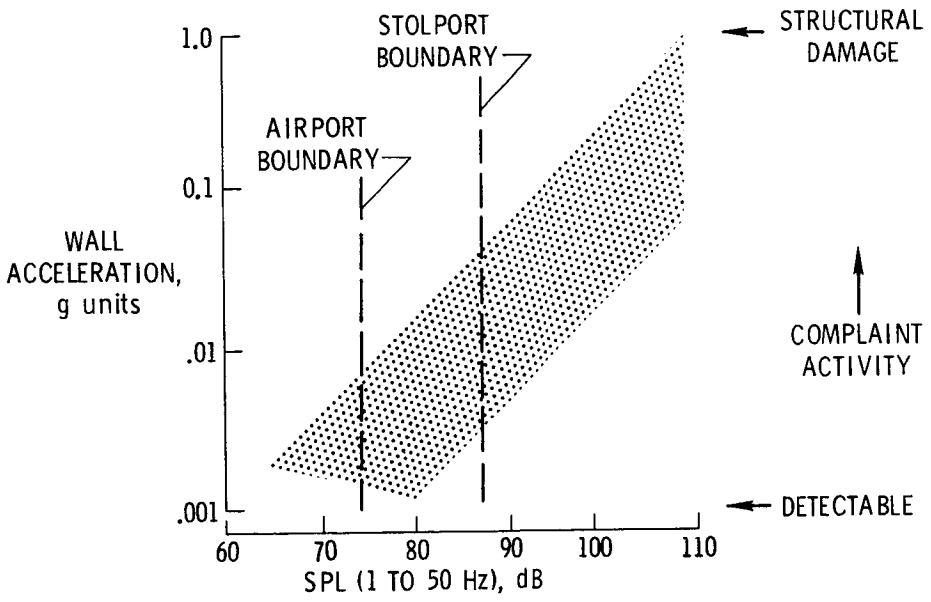

Figure 10

QUIET STOL PROPULSION SESSION

INTRODUCTORY REMARKS

By Robert W. Schroeder

NASA Lewis Research Center

In this session research activities, preliminary design activities, and system optimization studies in support of the development of advanced, quiet, clean, STOL propulsion systems will be discussed. Noise alleviation by means of controlling the source and by means of acoustical treatment will receive considerable emphasis.

A STOL airplane designed for a given payload will have essentially double the installed thrust of a comparable CTOL airplane. Unless compensated for during the design process, this alone will tend to increase the source noise by 3 dB.

Further, the propulsive lift introduces flap impingement noise or duct and flap scrubbing noise, noise sources not present in CTOL airplanes to any significant degree. These additional noise sources are illustrated by figure 1. Depending on the specific configuration, this will tend to increase the noise by several dB or more.

Although the propulsive lift characteristics of STOL airplanes will tend to increase source noise significantly, the proximity of STOL airfields to populated areas leads to STOL noise objectives considerably lower than those currently applicable to CTOL airplanes. Figure 2 illustrates the current regulatory limitation applicable to four-engine CTOL aircraft of about 150 000 pounds gross weight. It will be noted that the sideline constraint is 104 EPNdB at a sideline distance of 2100 feet. This is equivalent to 124 EPNdB at 500 feet. However, it will be noted that the tentative STOL goal is 95 EPNdB at 500 feet, a sound level almost 30 EPNdB below the current CTOL regulatory limitation. (EPNdB is a currently accepted subjective measure of noise level, and this and related terms will be discussed later.)

These comparisons are illustrated even more vividly, as shown by figure 3, by the 100 PNdB contours of the modern wide-bodied jet CTOL as compared with those of the STOL airplane just meeting the STOL objective. The modern CTOL airplane has a 100 PNdB footprint about 26 000 feet long compared with a STOL footprint about 4000 feet

long. The CTOL footprint covers an area roughly 40 times as large as the STOL footprint. This STOL objective must, of course, be achieved at acceptable operating costs and thus imposes very significant constraints on the design of the STOL propulsion systems.

Although firm EPA requirements constraining smoke and emissions have not yet been established, it is believed that STOL aircraft operating adjacent to populated areas must be as clean as is feasible, and the current pollution objectives are indicated by figure 4. It will be noted that the STOL carbon monoxide and hydrocarbon goals are appreciably lower than the current high-bypass-ratio engine emissions, and the STOL nitrogen oxide goals are more stringent by a factor of about 4.

This propulsion session will discuss three interrelated topics. The first topic will be treated by a panel that will cover engine noise technology and will discuss the identification and control of engine noise sources, as well as the application of acoustical treatment to attenuate source noise. This is basically the area to the left of the broken line of figure 1 and embraces fan and machinery noise, fan and core jet noise, and nacelle acoustical treatment. The second topic deals with the area to the right of the broken line. Four interrelated papers will discuss jet-powered-lift noise technology and will describe efforts to control the noise from duct scrubbing, wing scrubbing, flap impingement, and jet mixing.

The third topic involves the integration of these technologies into optimized STOL propulsion systems and thus will be treated by another panel discussion. The material presented by this panel will include work performed in-house as well as the efforts of a number of contractors who will be identified later.

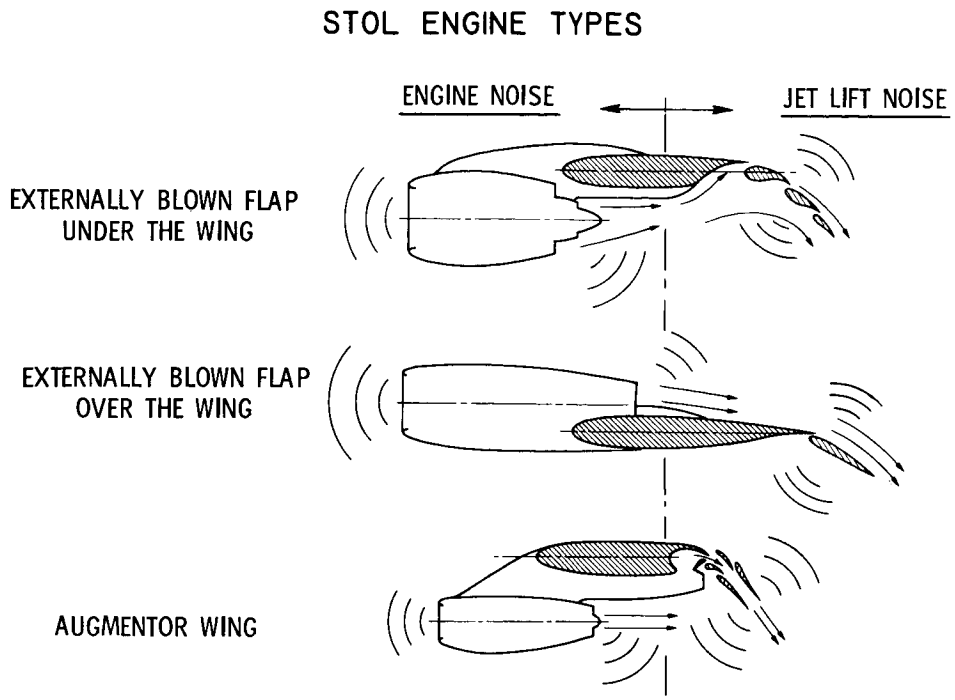

Figure 1

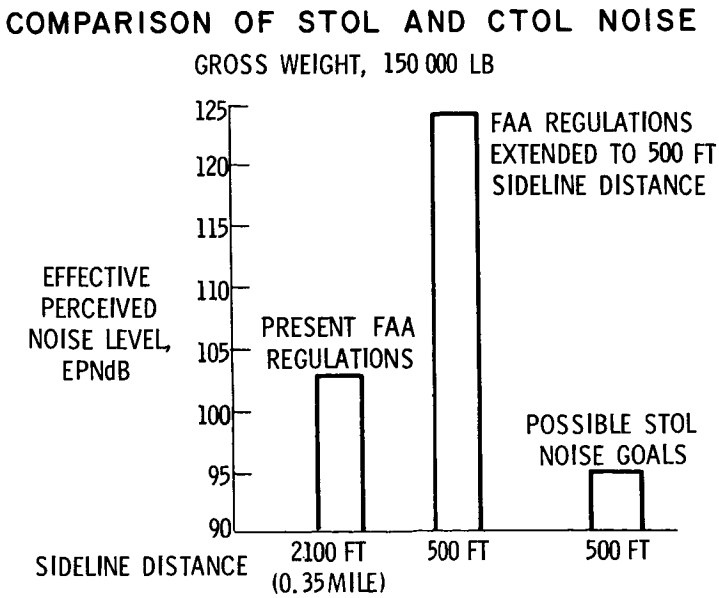

Figure 2

ESTIMATED 100 PNdB NOISE CONTOURS

MODERN WIDE BODIED JET CTOL VS STOL AIRPLANE OBJECTIVES

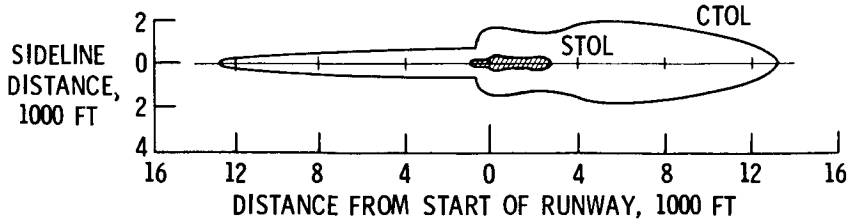

Figure 3

STOL POLLUTANT GOALS

LB POLLUTANT/1000-LB FUEL

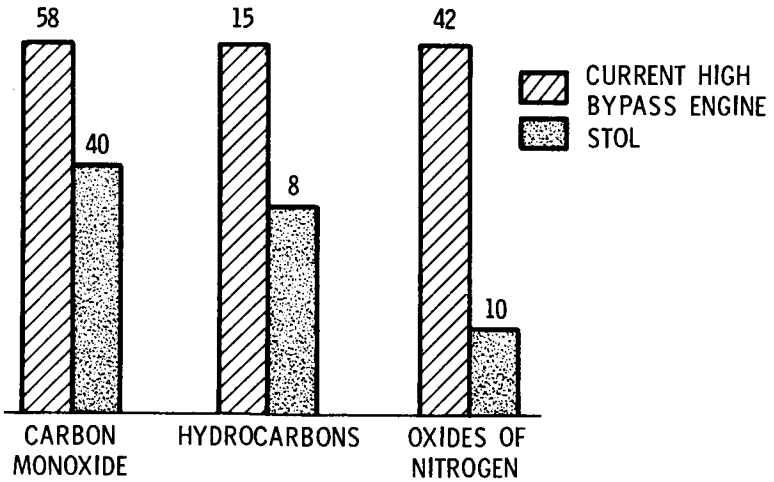

Figure 4

ENGINE NOISE TECHNOLOGY

By Roger W. Luidens, Donald R. Dietrich, James H. Dittmar, Richard G. Goldman, William A. Olsen, Jr., and Brent A. Miller

NASA Lewis Research Center

INTRODUCTION

This paper deals with engine noise technology. The reason for the emphasis on noise is that, for the current noise goals, noise is the predominant factor determining the engine design.

Because so much of the subject matter of this paper and that of the following papers is noise, noise terminology is briefly reviewed. The terms are listed in table I. Noise is defined as unwanted sound. The quantity of noise is its intensity or level. This is measured in terms of sound pressure level (SPL), the units of which are decibels, which are designated dB.

Many of the following figures present changes in sound pressure level; the units are still decibels and the symbol is now ΔdB. Many of the scales on the figures are marked in units of 10 dB, which is an easily recognizable significant change in noise.

The frequency or tone at which a noise occurs is specified in terms of hertz or cycles per second. The symbol for hertz is Hz.

When the sound pressure level is presented at each frequency over a range of frequencies, it is called a noise spectrum. Some frequencies in such a spectrum are more annoying to people than others. When the sound pressure level at each frequency is weighted by its annoyance and these values are summed over all frequencies, the resulting quantity is the perceived noise level (PNL). Its units are perceived noise decibels, and the symbol for the units is PNdB.

The annoyance of a noise is further a function of its time duration. When this is accounted for, the new quantity is called effective perceived noise level; the units are effective perceived noise decibels, which have the symbol EPNdB. The FAA regulations governing noise are written in terms of this last unit.

Finally, if the sound pressure levels themselves (rather than the annoyance-weighted sound pressure levels) are summed over all the frequencies, the resulting quantity is called the overall sound pressure level; its units are also decibels. The important point to remember is that a change in noise level of 10 dB is a significant change.

The noise technology areas that are discussed are shown on the composite engine sketch of figure 1. Discussed first are the origin and level of the noise generated by the fan. If the fan itself cannot be made quiet enough, noise suppression is required. The suppression characteristics of noise-absorbing structures, such as duct splitters, and the attenuation of sonic inlets are both described.

Next the noise generated by single and coannular jets is examined. A coannular jet is shown. Note that the core jet is surrounded by the jet from the fan duct. Finally, the performance and noise of several kinds of thrust reversers are presented. The target and cascade types are appropriate for fans which have fixed-pitch blades. Another means of thrust reversing is by reversing the fan blade pitch.

In general, for each topic the fundamental principles involved are described, and the application of these principles in the latest research experiments is illustrated. Previous surveys of engine noise technology are presented in references 1 and 2.

FAN NOISE

The internal noise sources of a typical turbofan engine are indicated in figure 2. Noise is generated by the fan, compressor, and turbine stages and by the core engine combustor. Of these sources, the fan stage is the dominant noise producer because it does work on all the engine airflow and because the noise produced has the most direct path to the atmosphere. Since the compressor and turbine noise-generation mechanisms are the same as the fan noise mechanisms and since the fan is the dominant internal noise source, only the fan noise generation will be discussed.

A typical noise spectrum for a fan is shown in figure 3. This is a plot of sound pressure level in decibels versus frequency in hertz. The spectrum consists of an underlying broadband level, a discrete tone at the rotor blade passage frequency and at its harmonics, and a cluster of multiple pure tones. These multiple pure tones are usually only present in supersonic-tip-speed fans.

The dominant noise component for subsonic-tip-speed fans is usually the blade passage frequency and its harmonics. Because of the high noise level of the tone and because it often occurs in the most sensitive region of human hearing, it is the most annoying. The chief mechanism for the generation of this blade-passage-frequency noise is the interaction of the rotor wakes with the downstream stator blades, as shown in figure 4.

As the rotor blades rotate past the stators, a stator blade first sees the flow between two rotor blades, then the flow in the rotor wake, the flow between the blades, the flow in the wake, and so on. This fluctuation in velocity presents periodically fluctuating air angles to the stator blades. These fluctuating velocities and angles of attack result in

fluctuating lift forces on the stator blades. These fluctuating forces, in turn, form pressure patterns in the duct that propagate to the far field as noise. This regular periodic variation produces blade-passage-frequency noise. More sets of blade rows, as might be found in a fan stage with inlet guide vanes or in a two-stage fan, would result in higher noise levels.

This type of noise could be reduced by decreasing the strength of the generation mechanism. For example, if the size of the rotor wake deficit striking the stator is reduced, the noise generated would be reduced. One method of accomplishing this is to increase the distance between the rotor and the stator and thus allow more time for the rotor wake to disperse.

The blade-passage-frequency noise is usually the dominant noise component for the subsonic-tip-speed fans that might be used for externally blown flap (EBF) STOL. However, supersonic-tip-speed fans that might be used for augmentor wing (AW) STOL are usually dominated by multiple pure tones. These multiple pure tones are generated by the upstream propagating Mach waves from the fan rotor blades.

In the idealized situation, shown in figure 5, these Mach waves would produce blade-passage-frequency noise which would add to the blade-passage-frequency noise which is generated by the wake interaction. The Mach waves from identical blades are equal in strength and are evenly spaced. This gives rise to evenly spaced pressure spikes that radiate as discrete tones at the rotor blade passage frequency. However, in an actual situation the rotor blades are slightly different as a result of manufacturing tolerances. This situation gives Mach waves that are different both in magnitude and periodicity, as shown in figure 6. When these waves are observed by the microphone, the pattern is only exactly repeated when that same blade comes past again on the next revolution. This pattern results in tones that are multiples of the shaft rotational frequency and are clustered about some frequency lower than the blade passage frequency. These multiple pure tones are often the dominant noise produced by supersonic-tip-speed fans.

Experimental data have been taken by NASA and others on a number of fan stages and are shown in figure 7. These results yield an indication of the measured noise of the fan in relation to the desired noise goal for a STOL airplane at a 500-foot sideline. This figure is for 90 000 pounds thrust and is a plot of noise in PNdB versus fan pressure ratio. The typical fan pressure ratio ranges for EBF and AW STOL are indicated.

To achieve the pressure ratios indicated for the AW engine, a two-stage, high-speed fan is probably required. With the two-stage fan, there are more wakes impinging on downstream blades than with a single-stage fan. This would be expected to result in more noise output. The data seem to indicate that this is indeed the case and that two-stage fans are noisier than single-stage fans. The high-speed, single-stage fans also appear to be noisier than the low-speed, single-stage fans. This is probably explained

by the presence of multiple pure tones in the spectrum of the high-speed fans.

In all cases, the noise output appears to decrease with pressure ratio. This focuses attention on the lower pressure ratios and, in particular, on the lower end of the EBF STOL pressure ratio range. To establish experimentally the noise levels in this region, two low-pressure-ratio fans were tested in the Lewis fan noise test facility shown in figure 8. In this facility, the fan is driven by electric motors which are located inside the building and which are connected to the fan by the long shaft shown entering the inlet. Both of the fans tested were 6 feet in diameter and had subsonic tip speeds. The first fan tested, pictured in figure 9, was a fixed-pitch type with 42 rotor blades. The other fan, shown in figure 10, was a variable-pitch type with 15 rotor blades and was designed by Hamilton Standard Division of United Aircraft Corporation. Both of these fans were designed to achieve approximately a 1.2 pressure ratio with tip speeds of 700 to 750 feet per second.

Typical noise spectra for each of these fans are shown in figures 11 and 12. These are plots of sound pressure level versus frequency at 120° from the fan inlet. Because of the low tip speeds, neither fan exhibits any multiple pure tones. The frequency at which the blade passage frequency occurs is lower for the variable-pitch fan because it has fewer rotor blades. This lower frequency for the blade passage tone is both an advantage and a disadvantage. Since the human ear is not as sensitive at this lower frequency, the noise will not be as annoying. However, lower frequencies require thicker structures to suppress the noise. These thicker structures may be heavier and cause higher flow losses.

The noise levels of these two fans are plotted on the curve of figure 7 and shown in figure 13. As can be seen, the data for the two fans fall approximately in the previously extrapolated regions of the curve. Both of the data points are plotted at the actual pressure ratios observed during the testing and not at the nominal 1.2 pressure ratio. The curve further indicates that the fan noise, even with extensive quieting features, is still many decibels noisier than the noise goal for a STOL airplane. For this reason, some method of attenuating the noise is necessary.

NOISE-SUPPRESSING STRUCTURES

One way to attenuate the internal noise of a jet engine is to use sound-suppressive structures. The physical mechanisms operating in such structures will be illustrated, and the result of applying these ideas to a typical jet engine will be shown.

Figure 14 shows an example of a suppressed STOL turbofan engine. The engine inlet, the aft fan duct, and the turbine exhaust duct are all lined with sound-attenuating structures. In addition, the engine inlet and the fan duct contain splitter rings each having sound-suppressive structures on both sides.

An enlarged view of a section of the suppression structure is shown in figure 15. The structure consists of rows of adjacent cavities. Holes in the facing sheet connect the flow passage with the cavity. The combination of a cavity and a hole constitutes a Helmholtz resonator. As a sound wave passes over these resonators, the high-pressure region of the wave causes a puff of gas to enter the cavity, and the low-pressure region of the wave extracts a puff of gas from the cavity. The turbulence in these small jets of gas dissipates the sound energy and, hence, reduces the noise.

There are many physical forms that these resonant structures can take. Figure 16 shows four common structures. The most common is a metallic or plastic honeycomb to provide the resonant cavities, covered with a perforated or porous facing sheet. Because the noise to be attenuated covers a wide spectrum, it is desirable to have as broad a bandwidth as possible. Broadening can be achieved, in theory at least, by a bulk absorber filling or by a double honeycomb layer where each layer is tuned to a different frequency. In the experimental installation, which will be described, both the honeycomb and the bulk-absorber types of suppression are used.

The three characteristics of a resonant structure are shown in figure 17. They are peak attenuation, frequency of peak attenuation, and bandwidth. Because engine noise has tones at different frequencies and broadband noise, all these characteristics are important. Usually, increasing the bandwidth of a suppressor with a single resonance lowers the peak attenuation. A more effective approach to broadening the bandwidth is shown in figure 18. The left sketch shows a series arrangement of linings tuned to different frequencies. The thicker linings resonate with the lower frequencies. The right sketch shows a parallel arrangement of linings with different tunings. Here the higher frequency, thinner liners are on the opposite side of the duct from the thicker, low-frequency linings. The curves show how the bandwidths of the individual sections of the lining add to give an overall broad bandwidth of absorption.

Experiments using sound-suppressive structures were performed on a modern jet engine, the TF-34. An overall view of the suppressed engine on its test stand is shown in figure 19. This engine has a thrust of about 9000 pounds and a bypass ratio of 6 to 1. It is manufactured by the General Electric Company. The tests were run at the Flight Research Center by the General Electric Company and were supervised and supported by a team of Lewis and Flight Research Center engineers.

Figure 20 shows a cross section of the TF-34 quiet-test nacelle. This is a ground-test nacelle with a bellmouth, three splitter rings in the inlet, and two splitters in the aft fan duct. Low- and high-frequency absorption is employed in the core duct as well. All aft fan duct and core linings are bulk-absorber type. The inlet treatment uses honeycomb.

The treatment of the aft fan duct is sketched in more detail in figure 21. The duct contains two splitters. The suppression consists of several thicknesses of bulk ab-

sorber designed to extend the bandwidth of the absorption. First, there is about a 1-foot length of 2-inch-thick suppression to remove low-frequency broadband noise and multiple pure tones. Next, the splitters are lined with 1/2-inch treatment which resonates at 3150 Hz, the blade passage frequency at full power. The walls are lined with 1-inch-deep treatment to extend the bandwidth of attenuation. A short section of 1/4-inch material just forward of the fan exhaust nozzle attenuates higher frequencies, such as harmonics of the blade passage frequencies.

The results of this treatment are shown in figure 22, which presents the noise spectra for the unsuppressed engine at 90° from the inlet and for the suppressed engine at 120° from the inlet. The reason for the choice of these angles will be explained later. The untreated engine exhibits a high noise level completely dominated by the fan frequency at 3150 Hz and its harmonics. The suppression treatment completely removes these pure tones; and the resulting noise is jet noise dominated, as is indicated by the peaking of the SPL curve at very low frequencies.

However, a price was paid for this noise reduction. The thrust has dropped from 9620 pounds to 8040 pounds. In analyzing this thrust loss, it was found that there was only about a 1.5-percent loss in total pressure associated with noise suppression in the inlet duct. Most of the loss occurred in the aft fan duct, and the analysis of this loss is continuing.

Figure 23 is a plot of perceived noise level as a function of angle, where 0° is the bellmouth centerline and 180° is the core exhaust centerline. The unsuppressed engine noise peaks at 90°, whereas the fully suppressed engine noise peaks at 120°. This is the reason for the selection of these two angles for the preceding figure. The shifting of the noise peak rearward is also an indication that the suppressed noise is jet dominated. The peak perceived noise level (PNL) reading has been reduced, at full rated speed (7000 rpm), from 115 PNdB to 94 PNdB, a reduction of 21 PNdB.

An interesting comparison can be made by looking at the narrowband spectra shown in figures 24 and 25. It will be remembered that the resonant linings are tuned to 3150 Hz, the blade passage frequency at full power only. At 7140 rpm, the multiple pure tones and the blade passage frequency and its harmonics are completely removed. At lower power settings, such as 5110 rpm, the blade passage frequency has shifted away from the resonant point. Consequently, although the extensive treatment still removes the fundamental tone, the higher harmonics are beginning to leak through. This illustrates the tuned nature of this type of sound suppression. Nevertheless, the overall perceived noise level at the lower power is lower than that at full power. Lower fan speeds are important because the landing approach will probably be made at some reduced power setting.

Some concern has been expressed that when the noise in the fan and inlet ducts has been completely suppressed, the core and turbine noise will become dominant. To re-

move this possibility, extensive treatment was applied to the core duct, as shown in figure 26. First, a 3-inch-thick lining was designed to remove possible combustor and low-frequency broadband noise. Second, a 1/2-inch-thick lining was tuned to remove turbine blade passage tones. The results of this treatment are plotted in figure 27. The data on the left are a plot of sound power level versus frequency in the low-frequency range. These data were obtained from an acoustic probe inserted in the core duct. The data on the right side are sound pressure levels versus frequency for the higher frequency range. These data were taken with a directional acoustic array. In each case, the instrumentation most appropriate to the frequency range shown was chosen. There is a reduction in core noise across the bands of frequencies shown of about 10 dB. This reduces the core noise to a level about equal to that for the fan and core jet noise.

In summary, the application of suppressive structures to a modern jet engine reduced the perceived noise level from 115 PNdB to 94 PNdB. This has been achieved with some reduction in thrust.

SONIC INLETS

Another way to reduce the noise emanating from the engine inlet is to use a sonic or high throat Mach number inlet. The operating principle of the sonic inlet is illustrated in figure 28. Engine noise suppression is achieved by accelerating the inlet flow to sonic or near-sonic velocity. The sonic region formed blocks the forward propagation of sound waves coming from the engine. Also, the flow velocity gradient generated within the inlet, shown by the arrows, bends the sound waves onto the wall and further reduces the engine noise.

To maintain acoustic suppression, any change in engine airflow requires a corresponding change in inlet throat area. For example, at approach to landing, where throttle setting is reduced, the engine airflow and, hence, the throat area required can be considerably less than that at takeoff. The inlets depicted schematically in figure 29 show several of the many ways that permit sonic suppression to be applied at both takeoff and approach. These inlets have a variable throat area so that a sonic inflow velocity can be maintained over a range of engine airflows. The variable area can be accomplished by one of the following means: an axial translation of the inlet centerbody; use of retracting radial vanes; contraction of the cowl wall; or variable inlet guide vanes. Scale model tests of several of these inlet concepts were recently conducted both at the Lewis Research Center and at Boeing-Seattle under contract to Lewis.

One can also conceive of inlet designs that combine the sonic inlet principle and acoustically treated splitter rings.

Figure 30 shows the translating-centerbody sonic inlet tested at Lewis. The center-

body is in the forward position. The inlet diameter is 6.5 inches. A 5.5-inch-diameter fan was used as both the suction source and the noise generator. The model was installed in the Lewis 9- by 15-foot V/STOL wind tunnel, as shown in figure 31. Both aerodynamic and acoustic data were obtained over a range of simulated flight speeds and angles of attack. The exhaust of the 5.5-inch-diameter fan was discharged into a duct carrying the flow out of the test section and into an exhaust noise muffler. The muffler was required so that the noise microphones, located ahead of the test section in a low-velocity region, could be used to measure fan noise coming through the inlet, without interference from fan noise escaping from the fan exit.

Figure 32 presents results obtained at zero tunnel velocity (ref. 3). Sound pressure level in dB is plotted versus frequency for a conventional inlet (the top line) and for the sonic inlet (the bottom line). The noise reduction obtained with the sonic inlet is simply the difference between the two lines. Note that the sonic inlet attenuates fan noise at all frequencies. This is unlike the acoustic structures described earlier, which have their maximum noise attenuation only near their tuned frequencies.

How the blade-passage-frequency noise reduction varies with inlet throat Mach number at static conditions is shown in figure 33. In this figure, both noise reduction (the top line) and inlet total pressure recovery (the bottom line) are plotted versus the normalized average throat Mach number. This is an average Mach number because, as shown in figure 28, there is a sizable velocity gradient within the inlet. A normalized Mach number of 1 was defined to exist at the highest weight flow that could be passed by the inlet. The open symbols show data obtained in the Lewis V/STOL wind tunnel at zero tunnel velocity. The solid symbols show data obtained by Boeing, under NASA contract NAS3-15574, with a similar inlet in an anechoic chamber. The data show that some noise reduction is obtained at average throat Mach numbers as low as 0.7 to 0.75. Large noise reductions, in the 30- to 40-decibel range, were obtained at the higher flow Mach numbers. The wind-tunnel-off noise floor limited the detectable fan noise suppression to 32 decibels in the Lewis test. The actual fan noise suppression obtained at a normalized average throat Mach number of 1 is probably more than the 32 decibels shown in the figure. The Boeing anechoic chamber data show a peak attenuation of 43 decibels at a normalized average throat Mach number of 1. The bottom half of the figure shows that some penalty is paid in total pressure recovery to get this noise suppression. However, at the extreme right of the figure, where the highest noise suppressions are measured, total pressure recovery is still above 98 percent.

Of major concern with this type of inlet is the effect of forward velocity and angle of attack on both the acoustic and aerodynamic performance. Figure 34 shows inlet performance obtained at a tunnel airflow velocity of 150 feet per second, at angles of attack of 0°, 20°, and 35°. Angle of attack α is defined as the angle between the free-stream velocity V and the inlet centerline. Again noise reduction and total pressure

recovery are plotted versus the normalized average throat Mach number. The wind-tunnel operating noise now limits the detectable fan noise suppression to 22 decibels. The actual noise suppression obtained at the three data points on the right side of the figure may consequently be more than the 22 decibels indicated. This is the reason for the dashed lines connecting these data points to the others. Within the limits of the data, the figure shows that angle of attack does not seriously alter the ability of the inlet to reduce fan noise. The bottom half of the figure shows that increasing incidence angle produces only a small drop in total pressure recovery. At 35° angle of attack and high average throat Mach number, total pressure recovery is considerably above 98 percent with at least 22 decibels noise reduction.

Another inlet performance parameter of importance is the inlet flow distortion, which is shown in figure 35. In this figure the total pressure distortion measured at the fan face, defined as $(p_{t,max} - p_{t,min})/p_{t,av}$ is plotted versus normalized average throat Mach number. The top half of the figure shows the distortion measured at zero tunnel velocity. Distortion increased with increasing throat Mach number, reaching a maximum value of approximately 10 percent. This is generally considered an acceptable level. The bottom half of the figure shows the distortion measured at a tunnel velocity of 150 feet per second at angles of attack of 0°, 20°, and 35°. Note the increase in distortion with increasing angle of attack. A maximum distortion of approximately 15 percent was measured at 35°. This distortion is somewhat higher than one would expect to encounter with a conventional inlet on a CTOL aircraft. However, it is less than the distortion encountered in some military applications. Also the high total pressure recovery obtained at this condition indicates that the distortion is confined to a small fraction of the fan face area.

The results of the sonic inlet tests conducted to date are encouraging. Follow-on programs are planned at Boeing, General Electric, and NASA Lewis and include more model tests at static conditions and in wind tunnels. In addition, a 6-foot-diameter sonic inlet is being designed by General Electric for test on a turbofan engine for CTOL aircraft.

If the internal noise is sufficiently low, the next problem of concern is the noise generated externally by the exhaust jet. The noise when the jet is producing forward thrust and when it is reversed to produce braking are both important. The forward-thrust jet noise is discussed in the next section.

JET NOISE

Figure 36 shows the jet mixing noise sources for a single nozzle and a coannular nozzle. The jet from a single nozzle is one of the noise sources for an augmentor-wing

type of STOL aircraft. The jets from a coannular nozzle are a noise source for the turbofan engine, which is used in the externally blown flap STOL aircraft. Both types of nozzles generate noise by the jet mixing with the external environment. For the coannular nozzle, there is the additional noise source associated with the mixing between the fan and core jets.

The noise from a single nozzle has been extensively investigated. Figure 37 was taken from reference 4. It shows the variation of the jet mixing noise with jet velocity. The data are for a large range in nozzle sizes; therefore, the data have been normalized to a nozzle exhaust area of 1 square foot. The jet total temperature also covered a large range, from ambient to about 1600° F. No correction was made to the noise to account for the temperature. At these subsonic velocities the noise varies with the eighth power of the velocity. Because of the stringent noise goal, the area of interest for STOL aircraft is in the velocity range of 500 to 800 feet per second. This is discussed in more detail in subsequent papers.

Coannular nozzle jet noise has not been as extensively investigated. Experiments on coannular nozzle jet noise were performed some time ago by T. Williams of England (ref. 5) and more recently by Boeing[1], and at the Lewis Research Center. The purpose of these experiments was to improve prediction schemes for the coannular nozzle jet noise and also to determine the effect on jet noise generation caused by variations in the nozzle geometry. One of the extensive set of coannular nozzles tested at the Lewis Research Center is shown in figure 38. This particular nozzle has a 6.7-inch outer diameter.

The Lewis coannular nozzle jet noise rig is shown in figure 39. Ambient-temperature pressurized air, free of valve noise, is supplied by two air lines to the fan and core nozzles. The noise is measured by an array of microphones in the vertical plane. This microphone arrangement and acoustic foam on the ground give noise data that are essentially free of ground reflections.

A small sample of the data obtained for coannular jets is presented in figure 40. If the two jets were separated, so that there would be no significant jet mixing, then there would be no interaction noise and the noise of the two jets would simply add. The Lewis coannular nozzle data are plotted as a change in the noise, relative to the noise from the two jets acting independently. This change is plotted against the fan-core velocity ratio for two fan-core area ratios. As the fan jet velocity is increased from zero, the noise decreases, compared with the noise from the independent separate jets. It decreases to a fan-core velocity ratio of about 0.5; and then it returns to the noise level of the independent jets at a fan-core velocity ratio of unity. The commonly used SAE pre-

[1]Unpublished Boeing/Aeritalia data.

diction for coannular nozzle jet noise assumes that the two jets generate noise independently. This prediction corresponds to the horizontal coordinate axis. The SAE prediction clearly overestimates the noise by many dB near velocity ratios of 0.5. However, the region of interest for current STOL aircraft engines is somewhere near a velocity ratio of 0.8 and an area ratio of about 3. In this region of interest the SAE prediction is slightly conservative.

In general, the agreement among the data taken at Lewis, at Boeing, and by Williams is good. For example, one sample of data from the Boeing experiment, for an area ratio of 6, is plotted as solid symbols. It is in good agreement with the Lewis data, which are plotted as open symbols.

The effect on noise generation of the variations in nozzle geometry shown in figure 41 are now considered. The core nozzle can extend well beyond the fan nozzle with only a negligible change in the noise, compared with coplanar nozzles. In the Lewis experiments the core nozzle extended up to 11 core diameters beyond the fan nozzle. Suppose instead the fan nozzle is extended beyond the core nozzle so that some internal mixing occurs. Williams showed that a small additional noise reduction could be achieved. If a centerbody is put in the core of the coannular nozzle and the centerbody is of good aerodynamic design, the resulting nozzle will be slightly quieter than a coannular nozzle without a centerbody. But if the centerbody is blunt ended, with its associated base drag, the nozzle will be noiser.

THRUST REVERSERS

Reversing the engine exhaust jet to obtain a retarding force also generates noise. The airplane studies which are discussed in paper no. 33, STOL PROPULSION SYSTEMS, suggest that thrust reversers are desirable for STOL operations in spite of STOL's slow landing speeds, about 70 knots. A retarding force of about 40 percent of the maximum forward thrust may be required. For the purpose of the present discussion, consider two possible interpretations of this reverse-thrust requirement:

(1) The engine could be operated at maximum thrust together with a 40-percent-effective thrust reverser. (By effectiveness is meant the ratio of reverse to forward thrust at the same engine throttle setting.)

(2) A 100-percent-effective thrust reverser could be assumed, in which case the engine could operate at 40-percent thrust.

From the point of view of thrust-reverser noise, the second situation is preferable. This kind of thinking is the background for the discussion that follows.

Figure 42 shows the types of thrust reversers to be discussed. There are still other types of thrust reversers, and there are many variations of the types pictured. In

the target-type thrust reverser, the engine jet impinges on a concave surface which partially reverses the jet. This reversing surface is usually stowed around the engine nacelle during forward-thrust operation. In the cascade type, a part of the cowl surface may translate aft to expose the cascade blades, which are skewed so that they pitch the flow upward as well as reverse it. A blocker door moves into place in the fan duct to force the engine flow into the cascades. In the case of the variable-pitch fan, the blade angle is changed in such a way that air is drawn into the nacelle exit and expelled through its inlet.

In figure 43, the noise characteristics of a model target-type thrust reverser are presented (ref. 6). A sketch of the model is shown in the upper corner of the figure. The model is a rough approximation of the target type shown in figure 42. Noise in dB is plotted versus the nozzle jet velocity in feet per second. The upper curve is the noise of the thrust reverser. For comparison, the lower curve gives the noise of the single forward jet that was presented earlier in figure 37 in the discussion of jet noise.

For a given jet velocity, in the range of velocities of interest for STOL, operation of the thrust reverser causes about a 10-dB increase in noise. The thrust-reverser noise decreases with nozzle velocity. If the jet velocity for reverse thrust is reduced to about 70 percent of that for forward thrust, the noises are about comparable. To achieve the desired retarding force at this reduced jet velocity requires a very high reverser effectiveness. This is the point made earlier.

Target-type reversers have only a rather modest effectiveness. However, the reverser noise they evidence is probably representative of thrust reversers in general. The following discussion deals with two thrust-reverser types that have the potential for a high reverse-thrust effectiveness and thus hopefully a low noise.

Figure 44 shows the thrust reverser model used to study reverser effectiveness. The model fan within the nacelle has a tip diameter of 5.5 inches and a pressure ratio of 1.22 at design. The top photograph shows the model which was used to determine the forward thrust. This thrust was used in calculating the ratio of reverse to forward thrust. The reverser model shown in the lower photograph has removable cascade sections and an adjustable blocker door. The blocker door was moved to maintain fan weight flow constant with different amounts of circumferential blockage. The cascade vanes turned the exhaust jet about 140^{o}, a higher turning than is used in current thrust reversers.

Figure 45 shows the results of some of these tests (ref. 7). The ordinate is the ratio of reverse thrust to static forward thrust; and the abscissa, the free-stream velocity. Data from two configurations are shown: one with approximately full circumferential emission and a second with about half circumferential, or 50 percent, emission. Also, results are shown for two yaw angles which will be considered

later. These data show a marked increase in reverser efficiency with reduced emission.

A possible explanation of this difference in efficiency is presented in figure 46. For the case of full emission, the exhaust flow is emitted from the cascades as a closed conical jet sheet that projects ahead of the inlet. The interaction between the free-stream flow and the conical jet sheet combined with the suction of the engine inlet causes the jet to bend and to be reingested. In this case, a significant amount of the fan flow exists in a recirculating pattern. The effect is that of recirculation of ambient-temperature air. This is not the hot-gas reingestion phenomenon that is observed with turbojet engines. For the case of partial emission, the upper sketch, the reversed jet does not envelope the engine. This allows the reversed jet to be swept rearward by the free-stream flow, and the air entering the inlet is free-stream air. This difference in the flow pattern accounts for the marked difference in thrust-reverser performance with emission angle. Also, the 50-percent-emission configuration shows an increase in effectiveness with free-stream velocity. This is caused largely by the ram and base drags. The peak reverse-thrust ratio at 100-foot-per-second velocity, which is about the STOL landing velocity, is approaching a value of unity. This implies the possibility of acceptable thrust reverser noise.

In addition to the previously stated requirements, a STOL aircraft must be able to land in a crosswind of as much as 35 knots (ref. 8). At forward velocity, a crosswind can be expressed as a yaw angle. The 50-percent-emission case was found to be insensitive to yaw angle. However, reverser geometries with significant side emission were found to be sensitive to yaw angle, as shown in figure 47. Wind-tunnel tests were performed with two orientations of a split 50-percent-emission reverser. The emission patterns are schematically shown. In one case the exhaust flow was emitted above and below the horizontal plane in which the yaw angle occurred. In the second orientation, the fan exhaust flow was emitted in the plane of the yaw angle. The ordinate is the relative reverse thrust, which is the reverse thrust normalized by the value at zero yaw angle. The abscissa is the yaw angle, which is defined as the angle between the fan centerline and the free-stream flow. When the emission pattern is normal to the yaw plane, the reverse thrust remains essentially constant with yaw angle. When the emission pattern is in the yaw plane, there is significant reduction in reverse thrust with yaw angle. In this case, it is hypothesized that the component of the free-stream velocity approaching the side of the windward reverse jet causes it to bend so that it is partly recirculated into the fan inlet. This is much like the situation depicted in the bottom sketch of figure 46.

The preceding results show the possibility of obtaining high ratios of reverse to forward thrust by the use of high-turning-angle cascades and properly tailored circumferential emission.

Return to figure 42, which shows the three types of thrust reversers, and consider next thrust reversing by reversing the fan blade pitch. The blade pitch must be changed so that air is drawn into the nacelle exit and exhausted from its inlet. It is assumed again that high reverser efficiency can be used to advantage in reducing noise during thrust reversing.

There are two ways to rotate the fan blade to achieve thrust reversing, as shown in figure 48. The center sketch shows a fan blade in the forward-thrust position. In this position both the blade leading edge and camber are correctly oriented for good aerodynamics. One way to rotate the blade for thrust reversing is through flat pitch, as shown on the left. In this case, the blade leading edge remains the leading edge in the flow, but now the blade camber is aerodynamically wrong. For this direction of pitch change, the leading edge of one blade must physically be able to pass the trailing edge of the adjacent blade. A second way to achieve reverse thrust is to rotate the blade through feather, as shown on the right. In this case the trailing edge of the blade becomes a leading edge in the flow, but the blade camber remains correct. For this mode the blade must pass through the stall angle to reach the reversing position.

The performance of a fan at various blade pitch angles is shown on figure 49. This experiment was performed by Hamilton Standard and is for a free-stream velocity of 110 feet per second. The thrust, presented on the ordinate, is normalized by the maximum forward thrust, also at 110-foot-per-second forward velocity. Thrust reversing is indicated by negative values. The data are plotted against the fan blade angle. The three blade angles described in figure 48 are designated by corresponding letters in this figure.

Reversing through flat pitch yields a local maximum in reverse-thrust ratio of about 0.2. Reversing through feather yields a maximum reverse-thrust ratio approaching unity. Clearly, in this case having the correct blade camber is more important than having the correct blade leading edge for achieving a high reverse thrust. The reverse-thrust ratio will also depend on the blade design, the fan pressure ratio, and many other fan and nacelle design details of a particular variable-pitch fan.

Figure 50 shows some of the research areas that must be considered for variable-pitch fans. These technology areas, which are restricted to aerodynamic considerations, include the following:

(1) The sharp-edge exit, which is appropriate for forward thrust, must be converted to a "rounded" inlet for reverse thrust. This may be done by a variable-geometry exit or by opening additional inlet doors which present rounded surfaces to the entering flow.

(2) Jet attachment to the rounded inlet will, if it occurs, reduce the reverse thrust.

(3) There must be a sufficient quantity of undistorted flow for the core during transition to reversing and during reversing operation.

(4) The core exhaust may be reingested into the core inlet.

(5) The fan flow may recirculate, as was the case with one of the cascade thrust-reverser configurations.

(6) The reversed fan jet may impinge on the ground and cause operational problems. Although these items need to be considered, continued research and development should lead to a satisfactory overall system. Paper no. 33 will show that there can be considerable merit in the use of a variable-pitch fan on a STOL airplane.

In summary, it was shown that a cowl-mounted cascade system and a reverse-pitch fan can provide high reverse-thrust ratios, which can be applied in a way to reduce noise. Programs are continuing at Lewis in the area of thrust reversers. Also, a program using a variable-pitch fan on a turbofan engine is being conducted with Hamilton Standard. This program is described in paper no. 33, STOL PROPULSION SYSTEMS.

CONCLUDING REMARKS

This paper has discussed the noise generated by engines in both forward and reverse operation and some of the means for reducing and suppressing the noise. In general, there are performance and weight penalties associated with achieving low noise. These penalties can only be evaluated in studies of a complete airplane operating in a transportation system. Thus, the information presented in this paper serves as an input to the studies, the results of which are discussed in paper no. 33, STOL PROPULSION SYSTEMS.

REFERENCES

1. Anon.: Aircraft Propulsion. NASA SP-259, 1971.
2. Anon.: Aircraft Engine Noise Reduction. NASA SP-311, 1972.
3. Miller, Brent A.; and Abbott, John M.: Aerodynamic and Acoustic Performance of Two Choked-Flow Inlets Under Static Conditions. NASA TM X-2629, 1972.
4. Von Glahn, Uwe H.: Correlation of Total Sound Power and Peak Sideline OASPL From Jet Exhaust. AIAA Paper No. 72-643, June 1972.
5. Williams, T. J.; Ali, M. R. M. H.; and Anderson, J. S.: Noise and Flow Characteristics of Coaxial Jets. J. Mech. Eng. Sci., vol. 11, no. 2, Apr. 1969, pp. 133-142.

6. Gutierrez, Orlando A.; and Stone, James R.: Preliminary Experiments on the Noise Generated by Target-Type Thrust Reverser Models. NASA TM X-2553, 1972.

7. Dietrich, Donald A.; and Luidens, Roger W.: Experimental Performance of Cascade Thrust Reversers at Forward Velocity. NASA TM X-2665, 1972.

8. Ransone, R. K.: Proposed STOL Definition and Field Length Criteria. J. Aircraft, vol. 8, no. 12, Dec. 1971, pp. 971-975.

TABLE I

NOISE TERMINOLOGY

QUANTITY	UNITS	SYMBOL FOR UNITS
NOISE OR SOUND PRESSURE LEVEL SPL	DECIBELS	dB
CHANGE IN SOUND PRESSURE LEVEL	DECIBELS	Δ dB
FREQUENCY OR TONE	HERTZ (CYCLES/SEC)	Hz
PERCEIVED NOISE LEVEL PNL	PERCEIVED NOISE DECIBELS	PNdB
EFFECTIVE PERCEIVED NOISE LEVEL EPNL	EFFECTIVE PERCEIVED NOISE DECIBELS	EPNdB
OVERALL SOUND PRESSURE LEVEL OASPL	DECIBELS	dB

TECHNOLOGY AREAS TO BE DISCUSSED

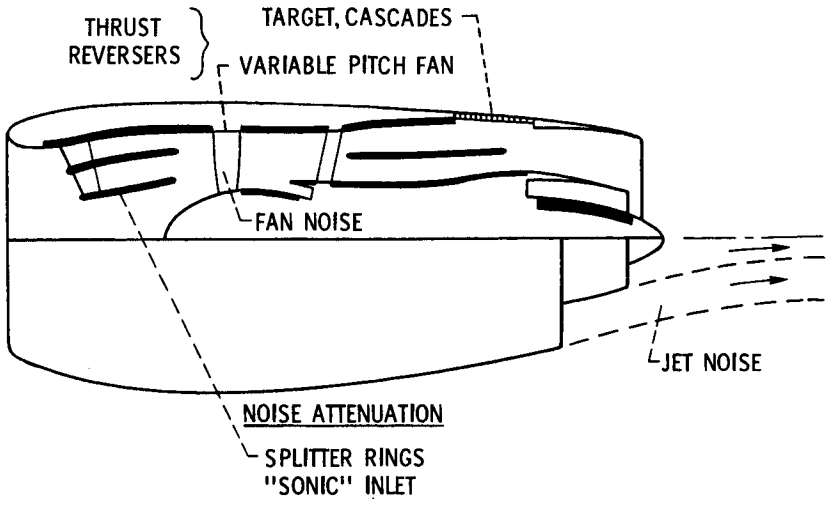

Figure 1

UNSUPPRESSED TURBOFAN ENGINE

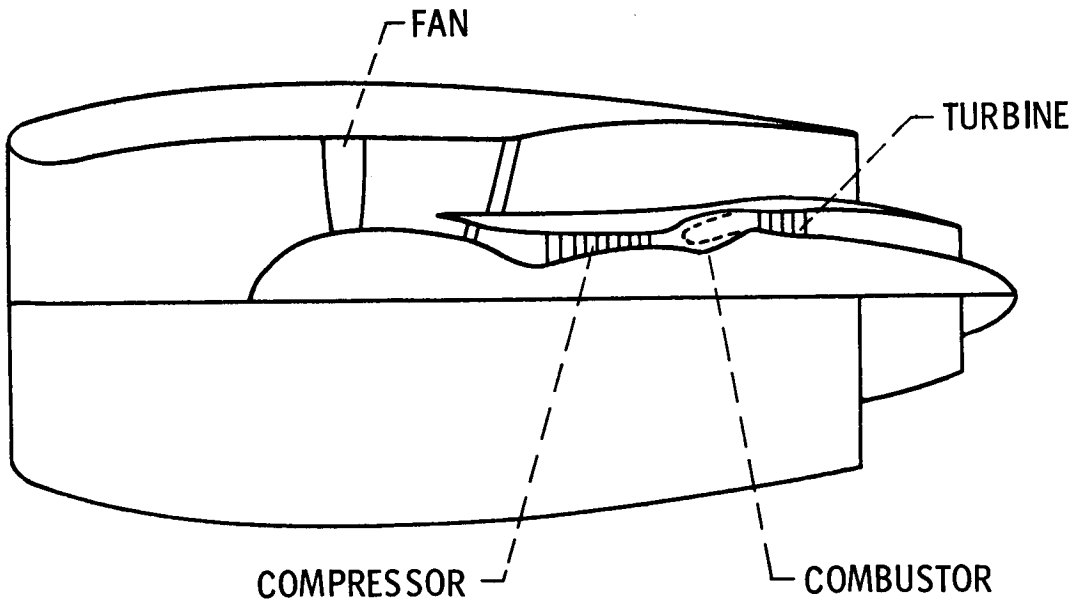

Figure 2

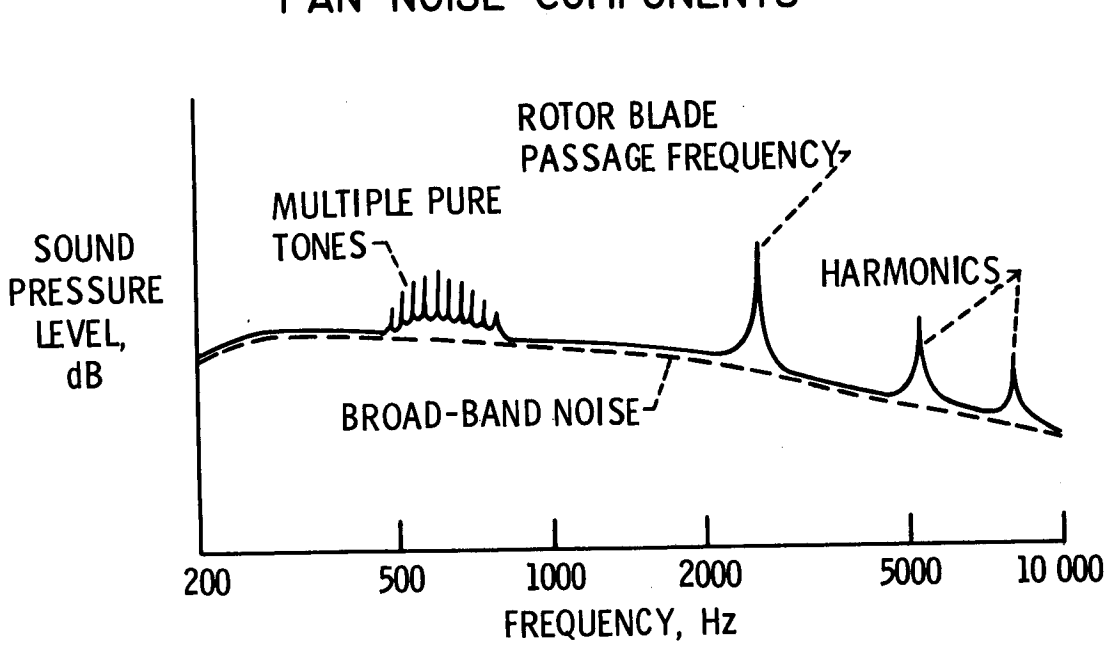

Figure 3

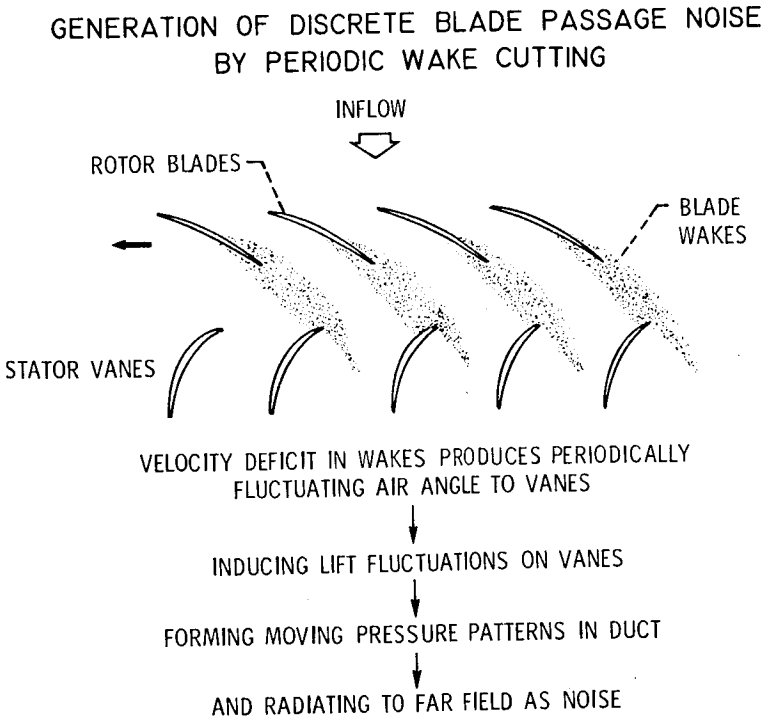

Figure 4

MULTIPLE PURE TONE NOISE AT SUPERSONIC TIP SPEEDS

IDEALIZED WAVE PATTERN

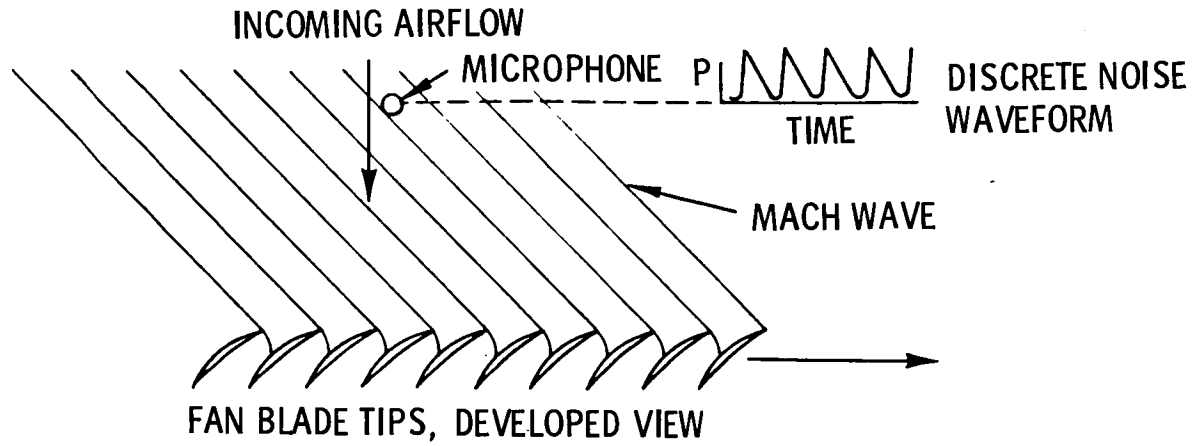

Figure 5

MULTIPLE PURE TONE NOISE AT SUPERSONIC TIP SPEEDS

ACTUAL WAVE PATTERN

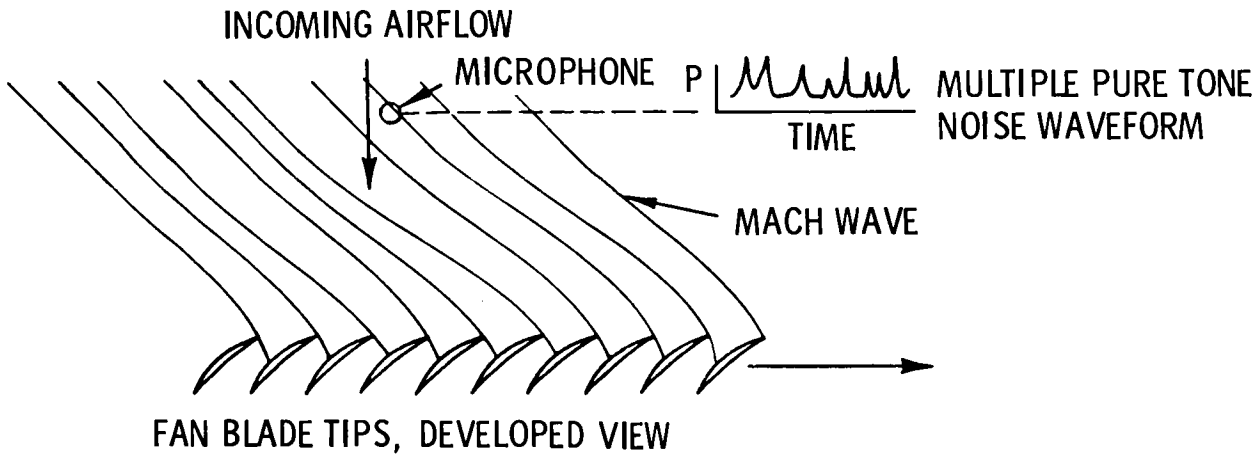

Figure 6

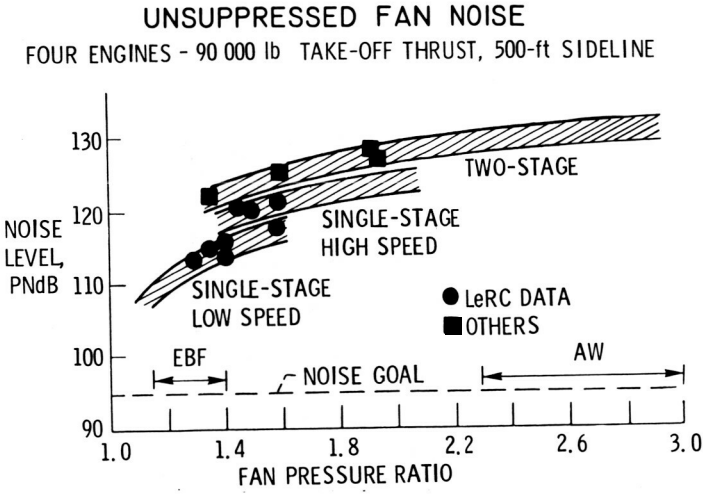

Figure 7

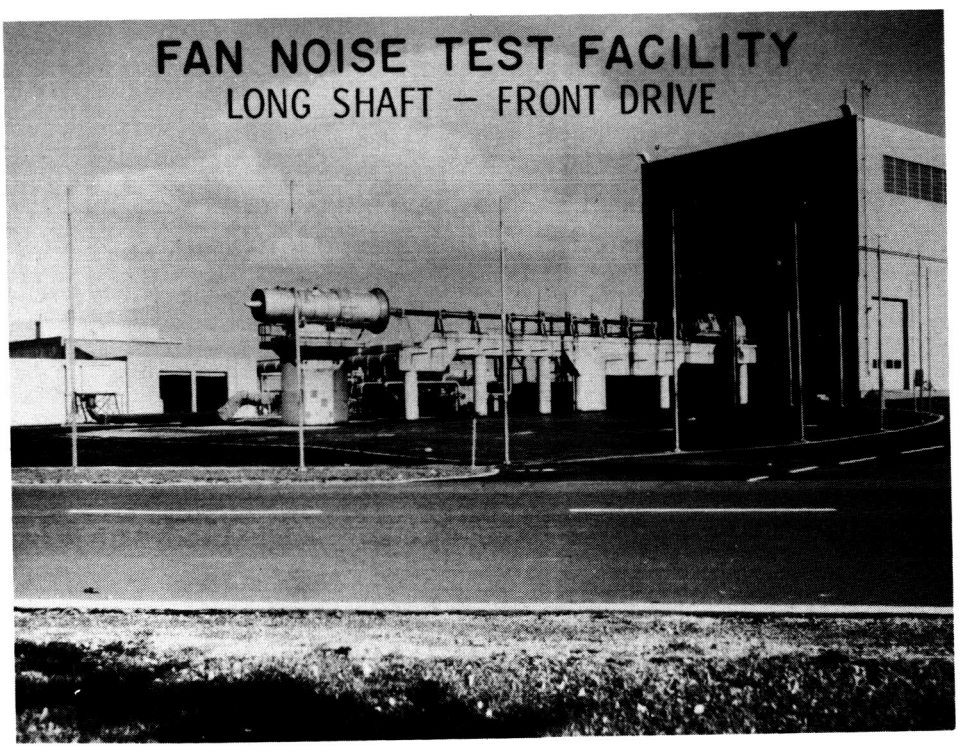

Figure 8

FIXED PITCH, 6-FT-DIAM. FAN

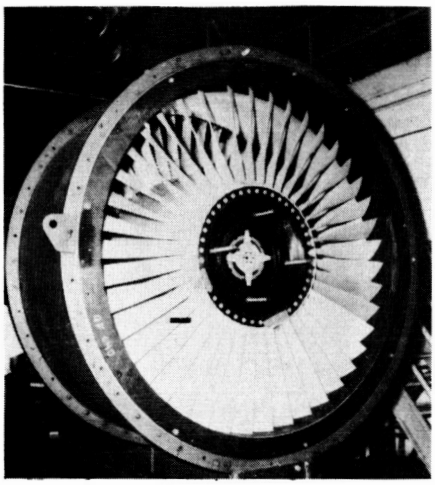

Figure 9

VARIABLE PITCH, 6-ft- DIAM. FAN

Figure 10

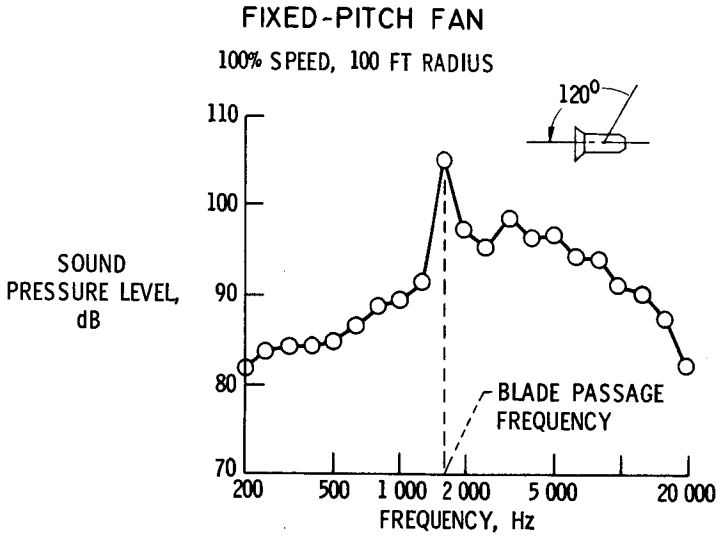

Figure 11

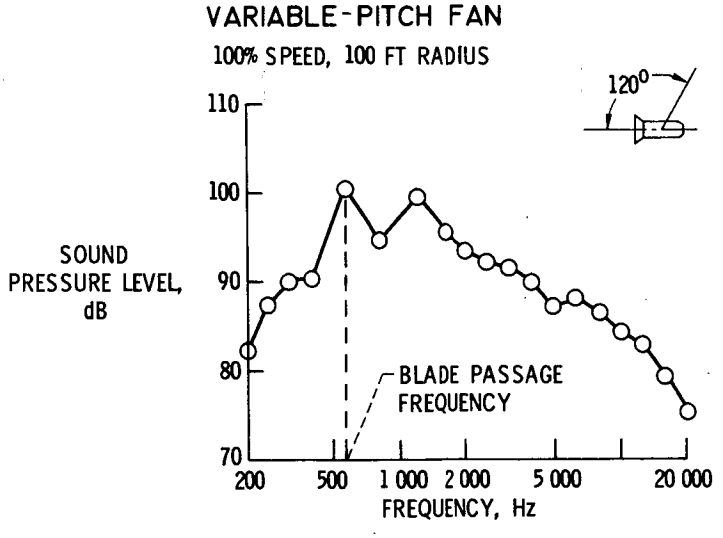

Figure 12

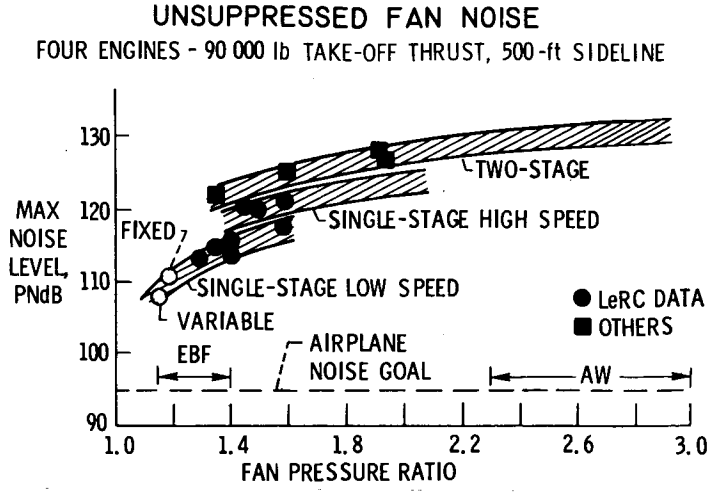

Figure 13

STOL ENGINE WITH SUPPRESSION

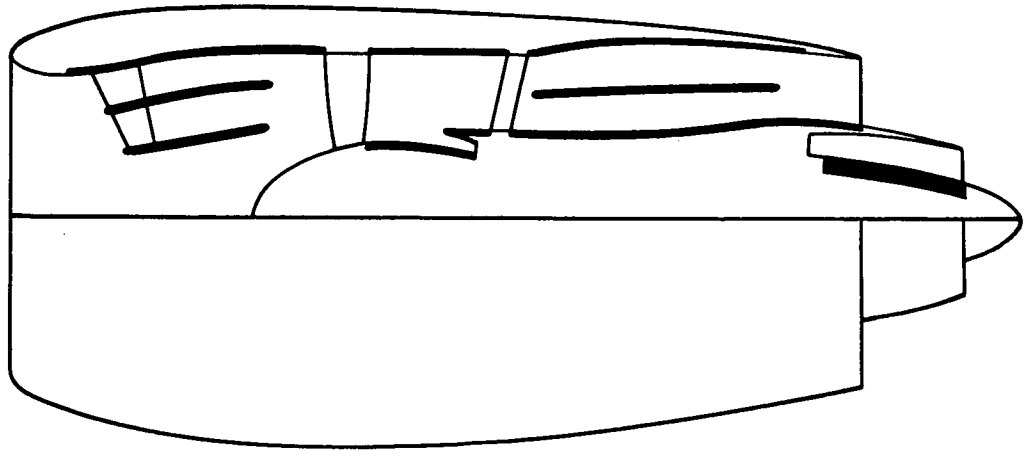

Figure 14

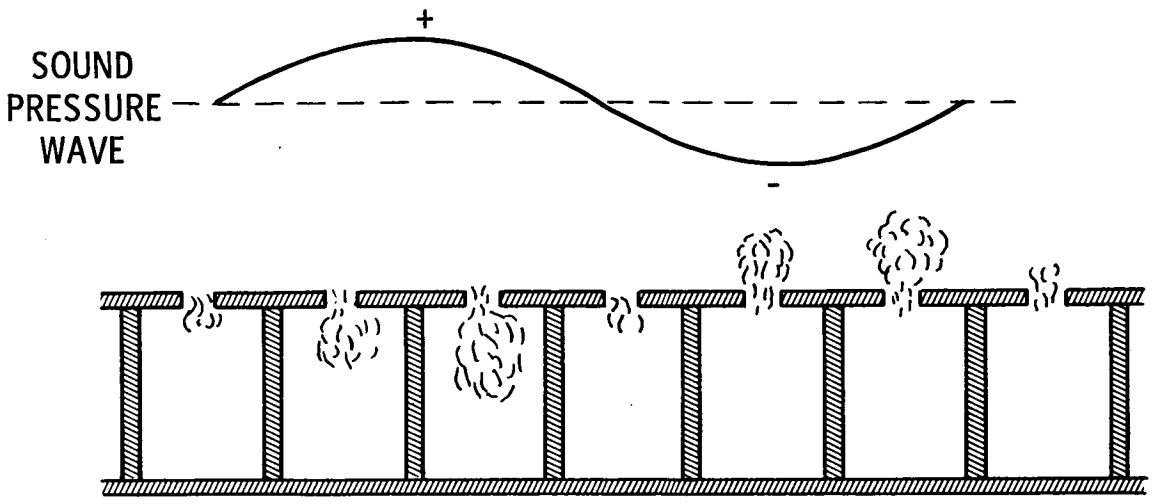

Figure 15

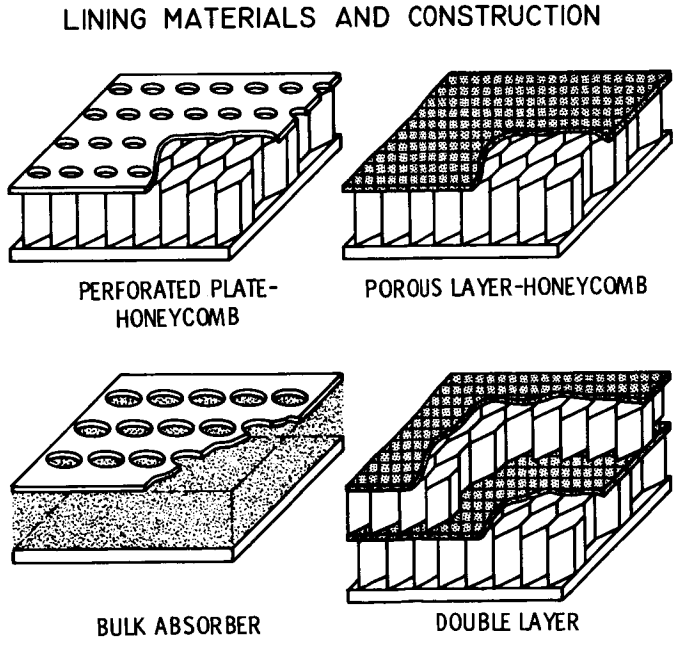

Figure 16

PARAMETERS FOR TYPICAL ATTENUATION SPECTRUM

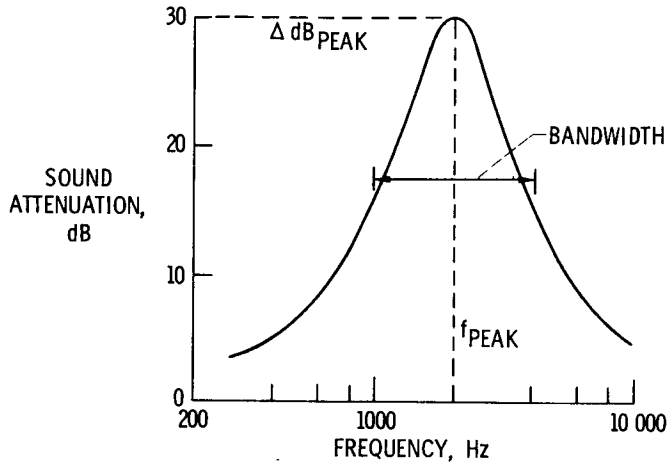

Figure 17

METHODS OF INCREASING SUPPRESSION BANDWIDTH

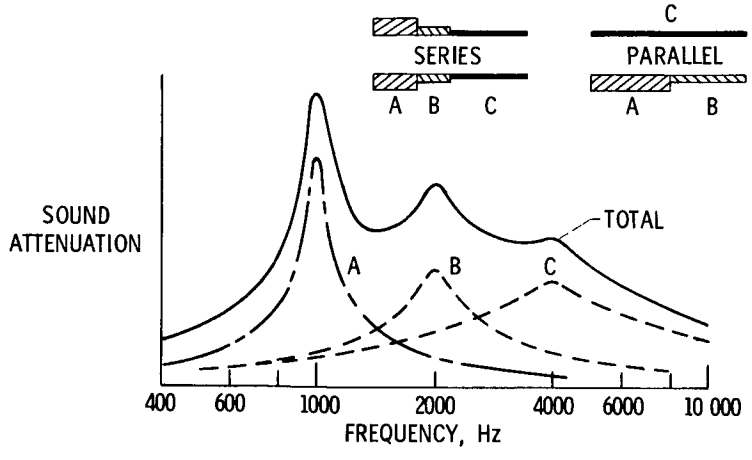

Figure 18

TEST INSTALLATION OF TF-34 AT FLIGHT RESEARCH CENTER

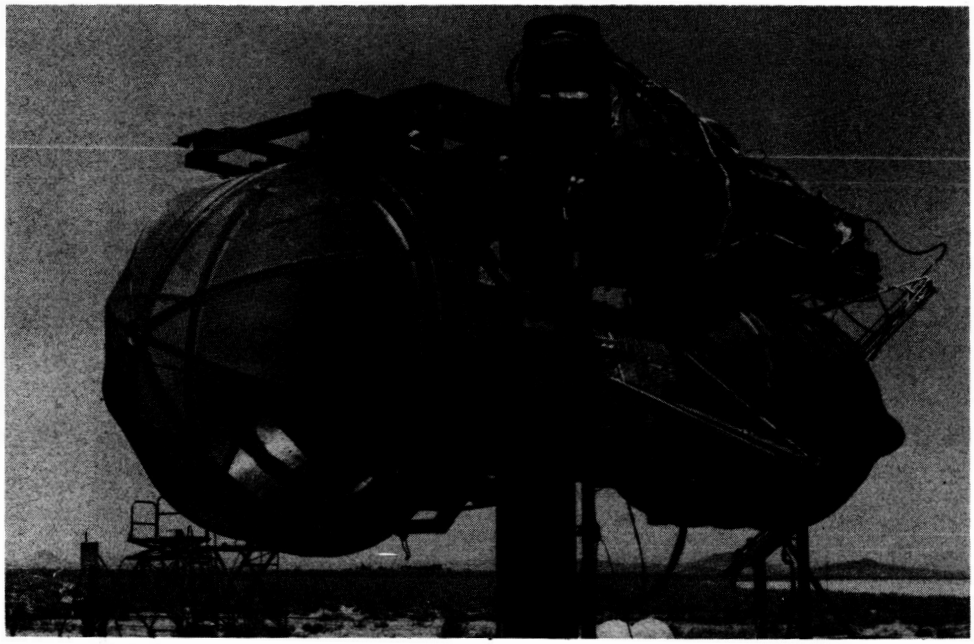

Figure 19

TF-34 WITH QUIET TEST NACELLE

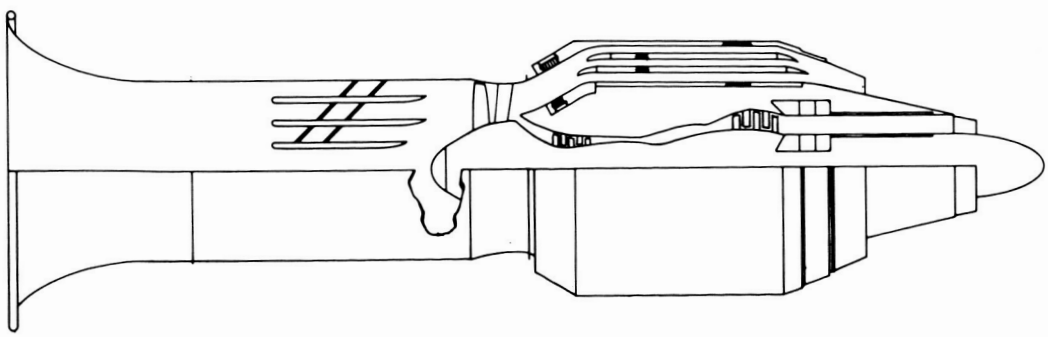

Figure 20

TF 34 FAN DUCT SUPPRESSION

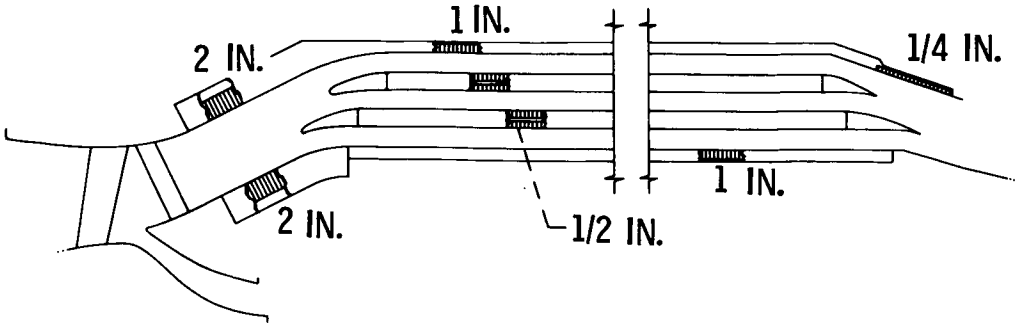

Figure 21

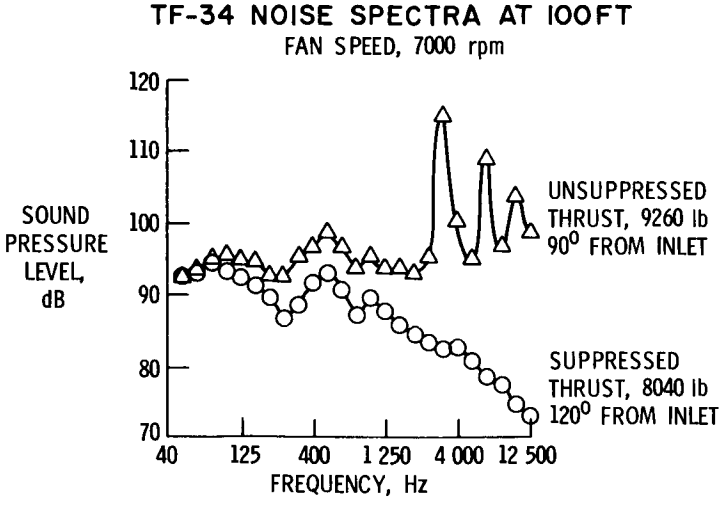

Figure 22

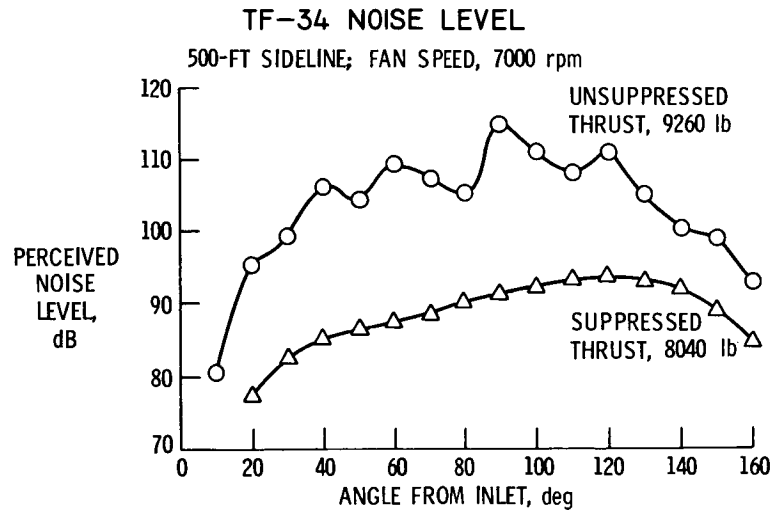

Figure 23

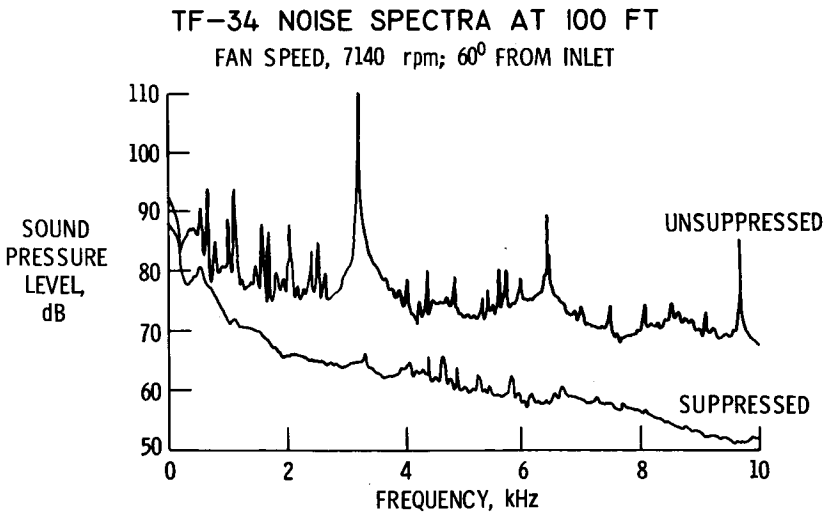

Figure 24

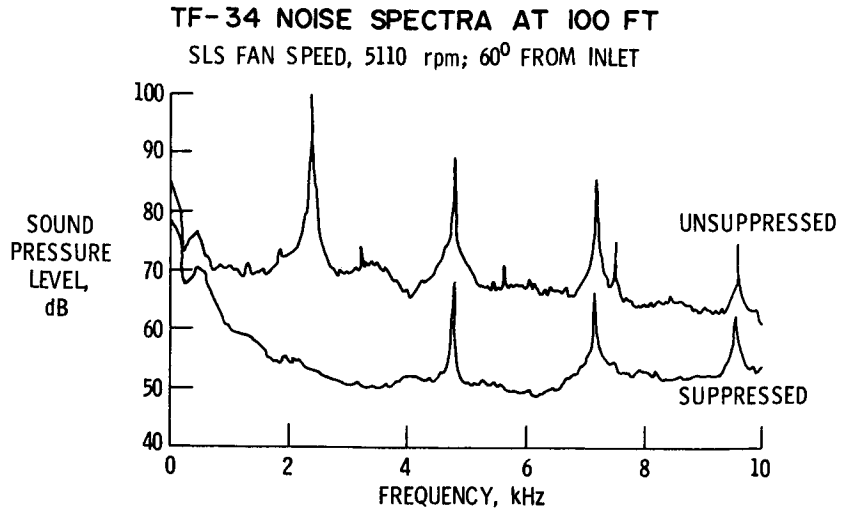

Figure 25

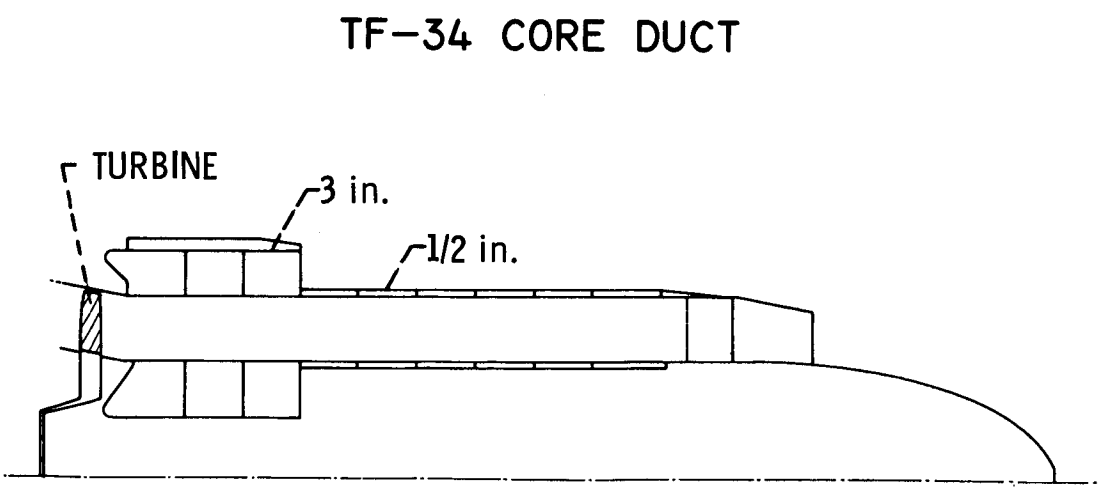

Figure 26

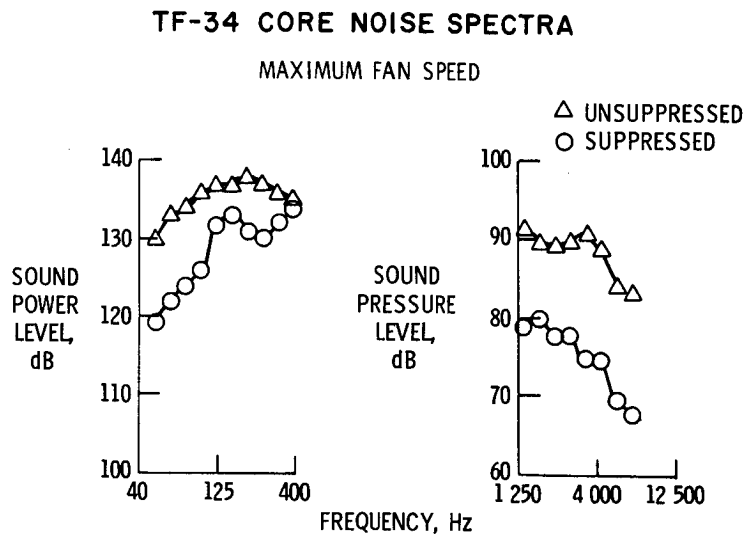

Figure 27

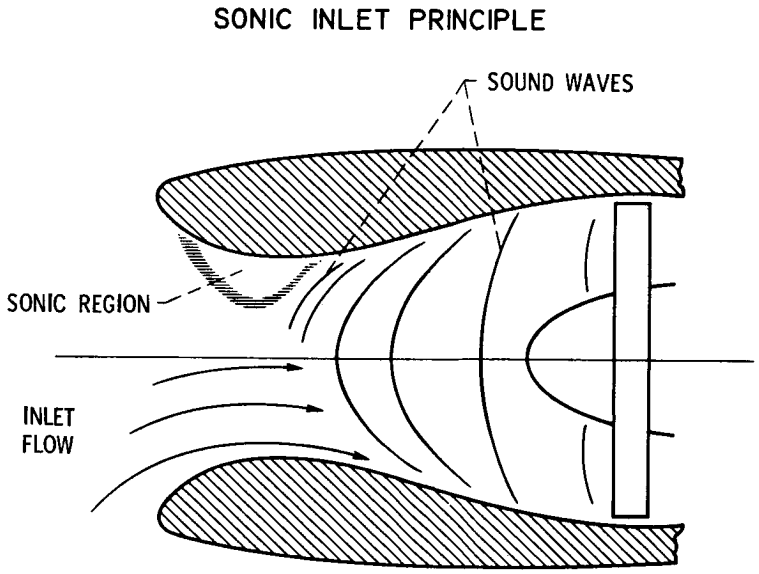

Figure 28

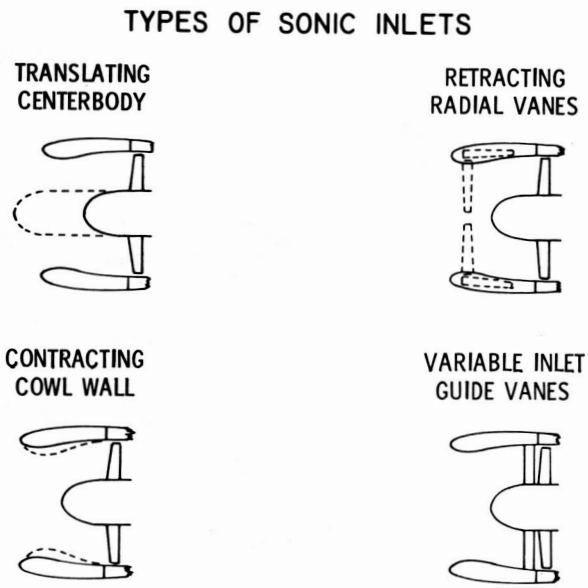

Figure 29

LEWIS SONIC INLET RESEARCH MODEL

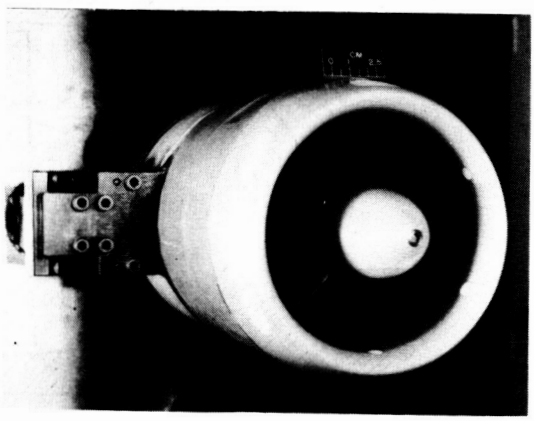

Figure 30

LEWIS SONIC INLET TEST INSTALLATION

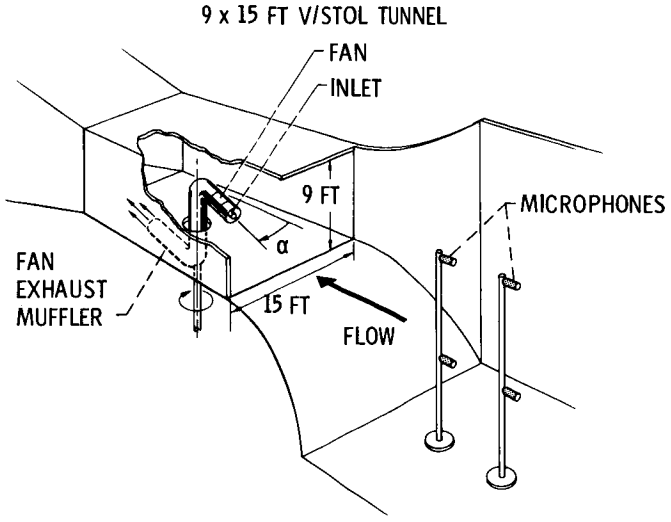

Figure 31

SONIC INLET ATTENUATES NOISE AT ALL FREQUENCIES

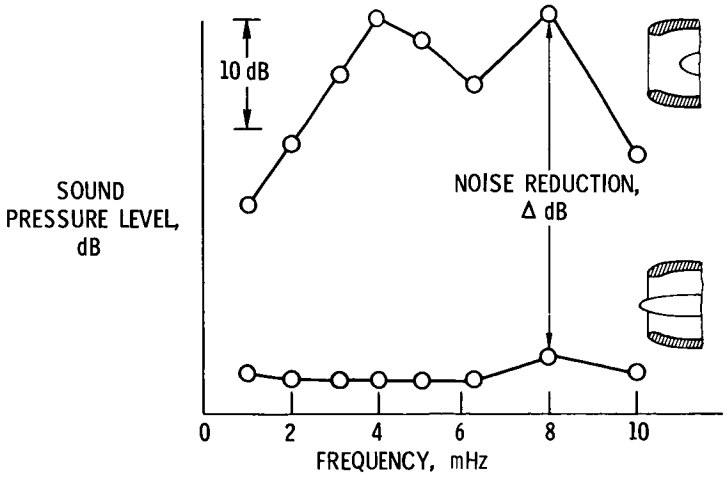

Figure 32

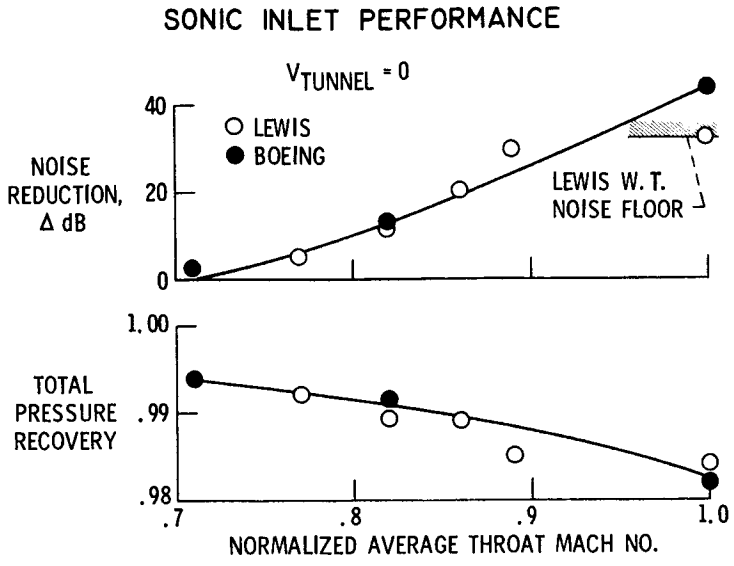

Figure 33

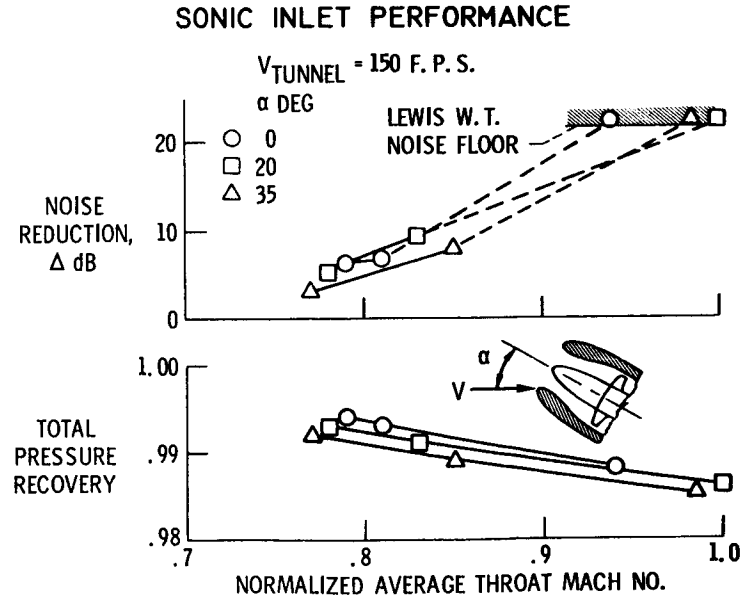

Figure 34

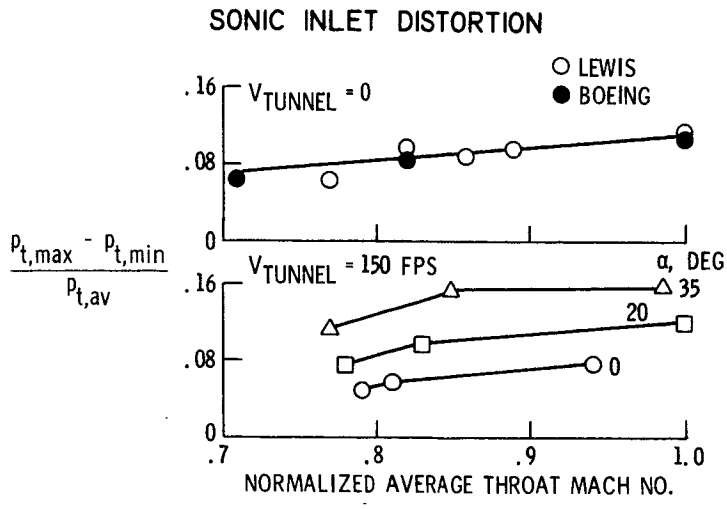

Figure 35

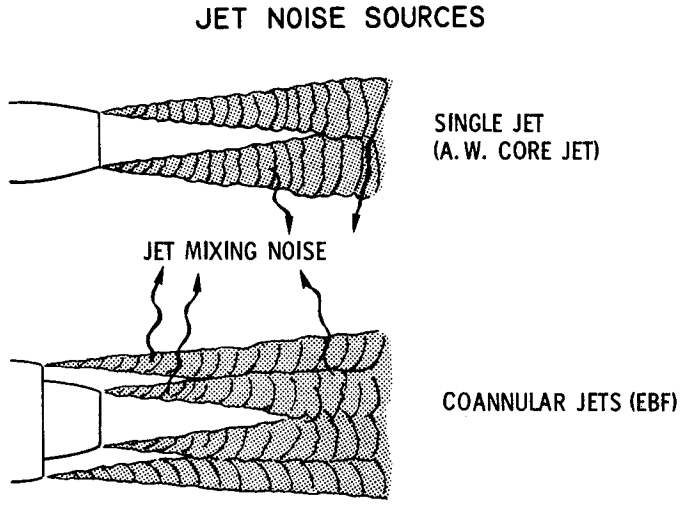

Figure 36

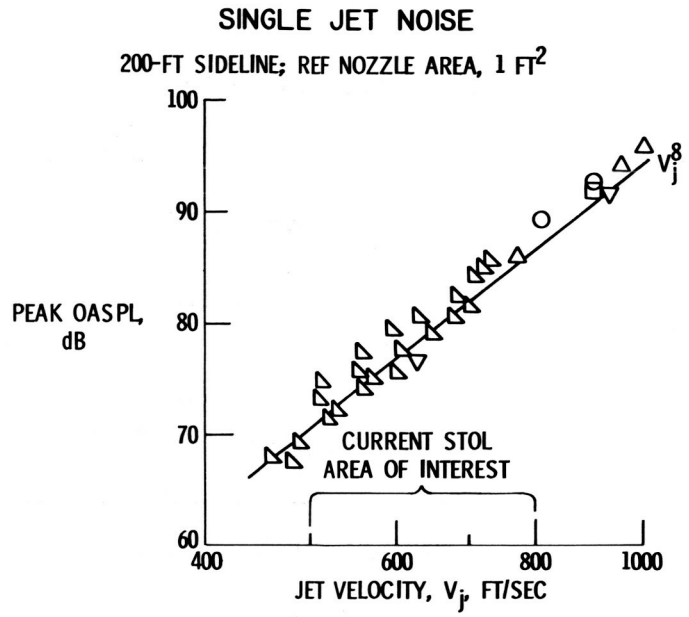

Figure 37

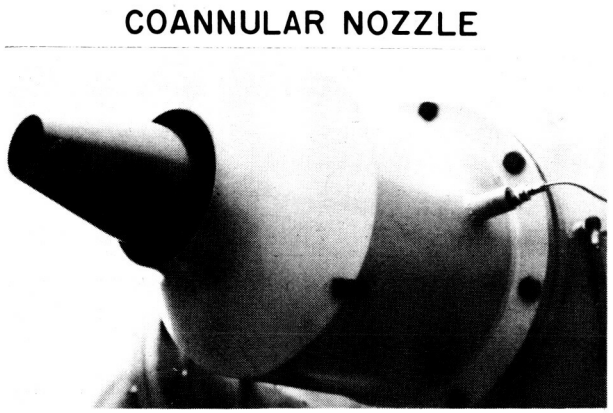

Figure 38

COANNULAR NOZZLE TEST INSTALLATION

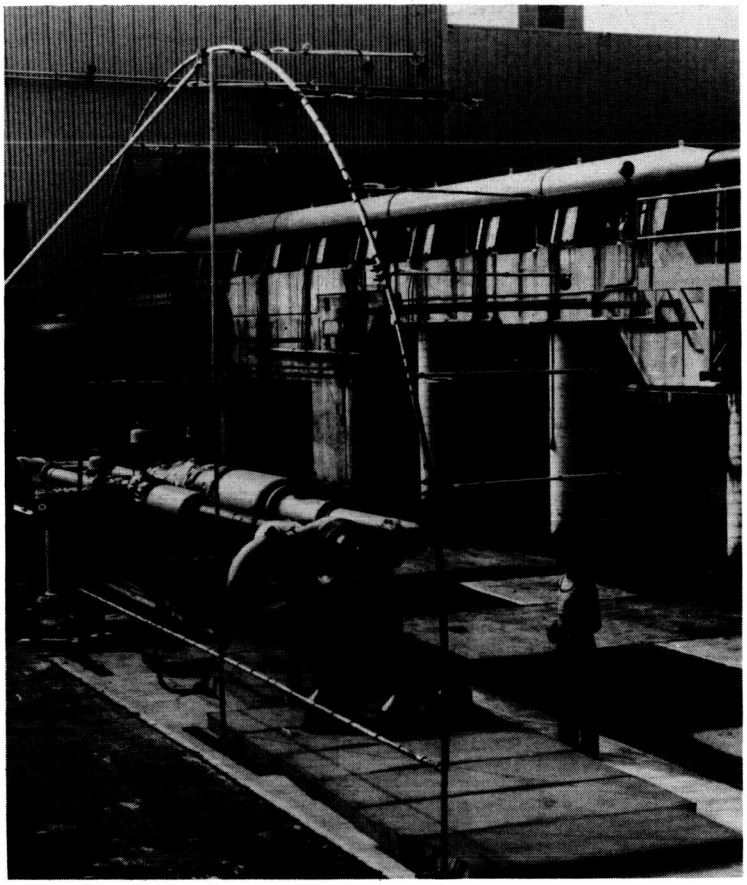

Figure 39

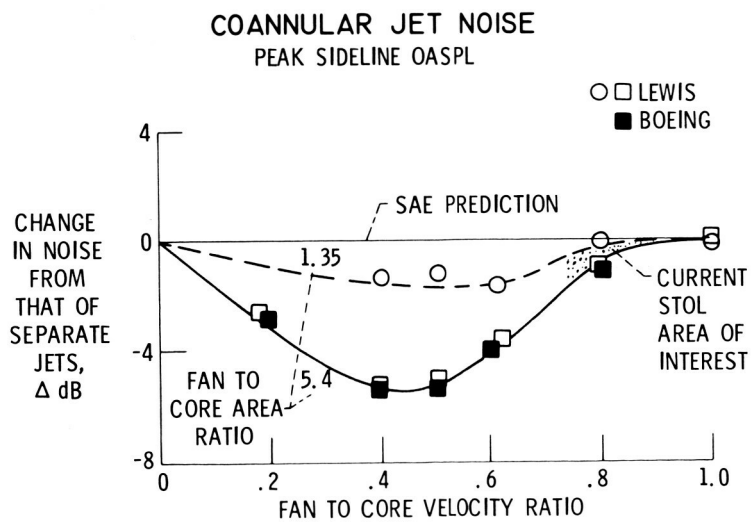

Figure 40

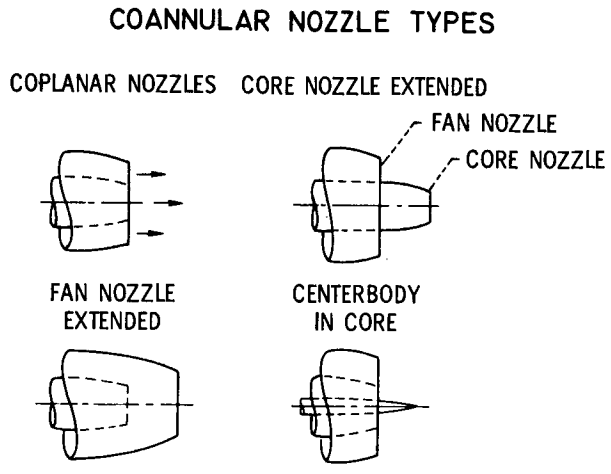

Figure 41

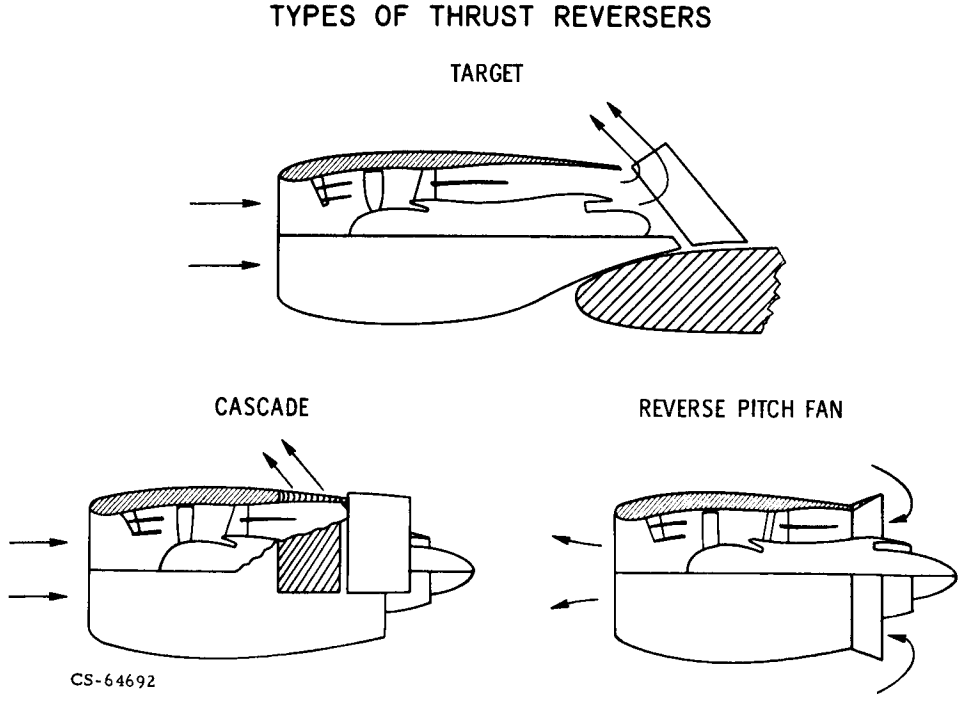

Figure 42

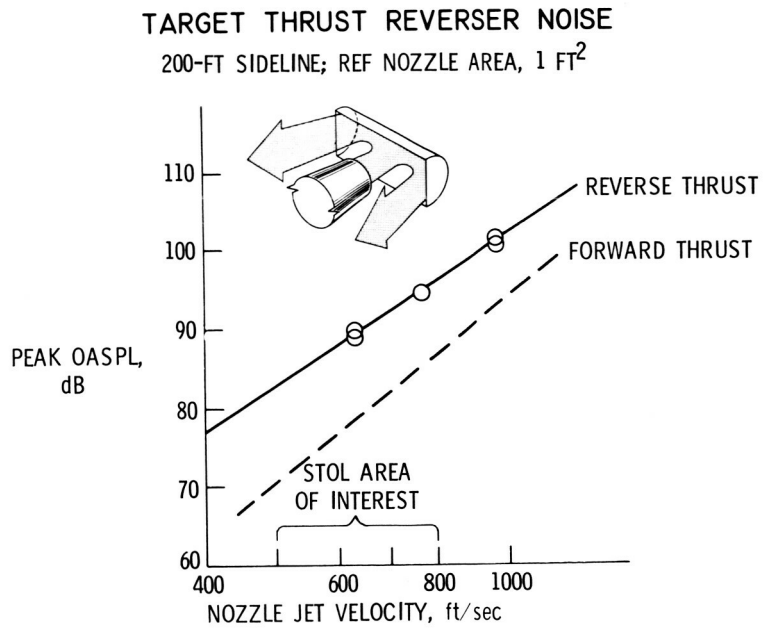

Figure 43

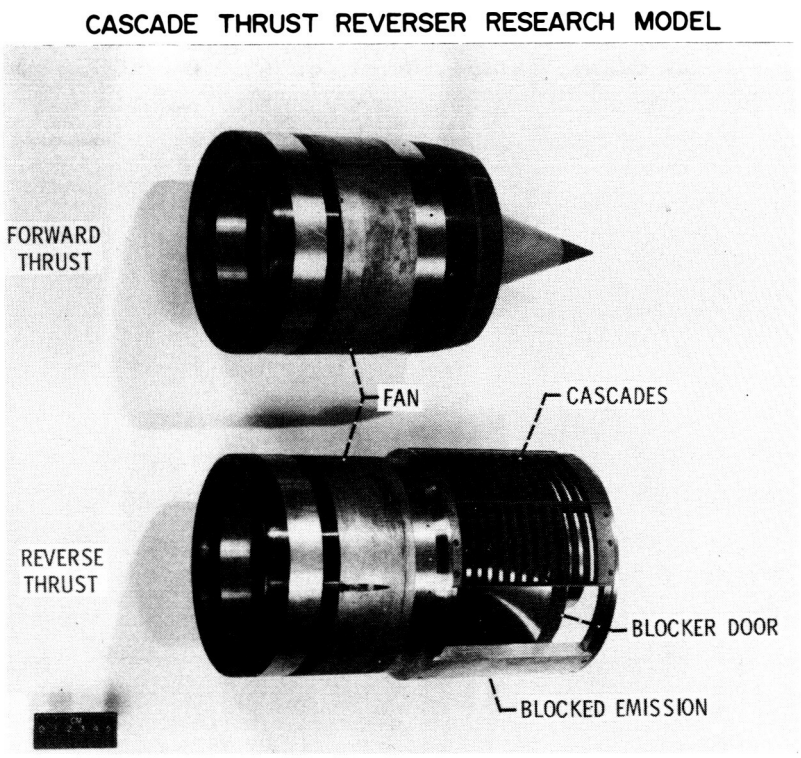

Figure 44

CASCADE THRUST REVERSER PERFORMANCE

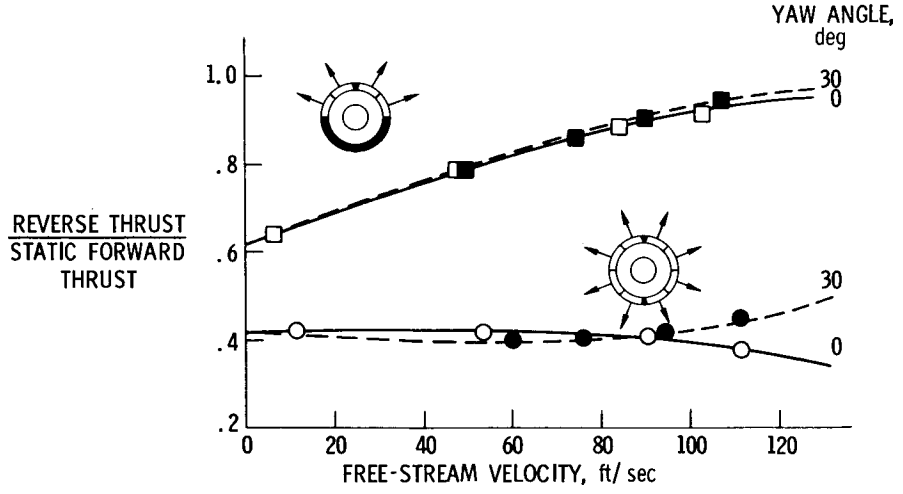

Figure 45

CASCADE THRUST REVERSER FLOW FIELDS

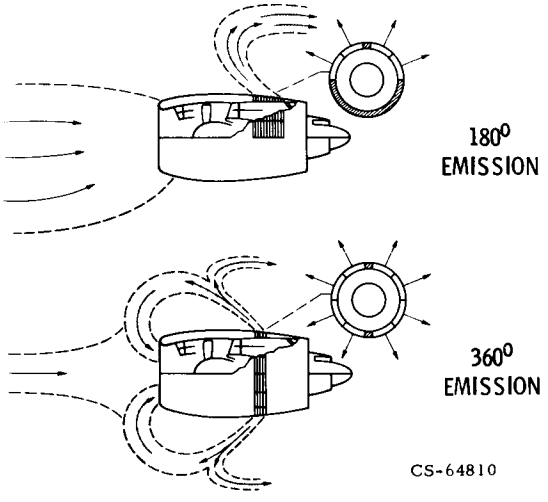

Figure 46

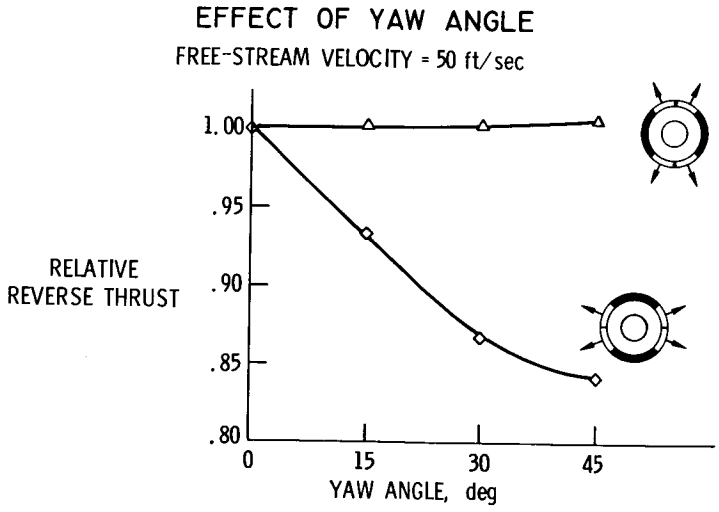

Figure 47

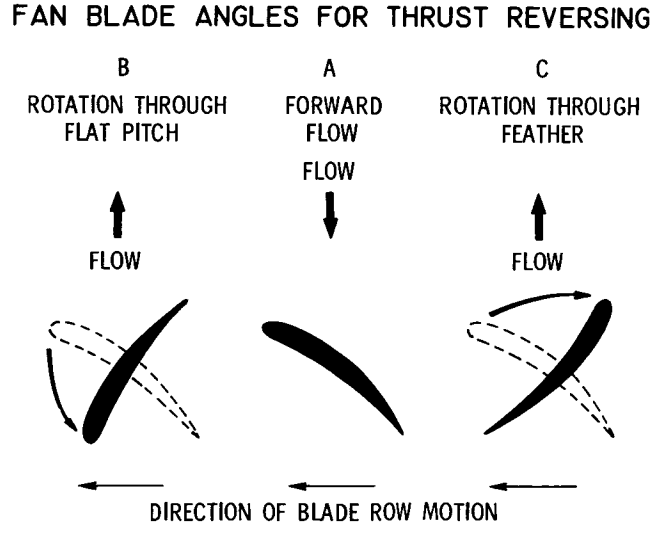

Figure 48

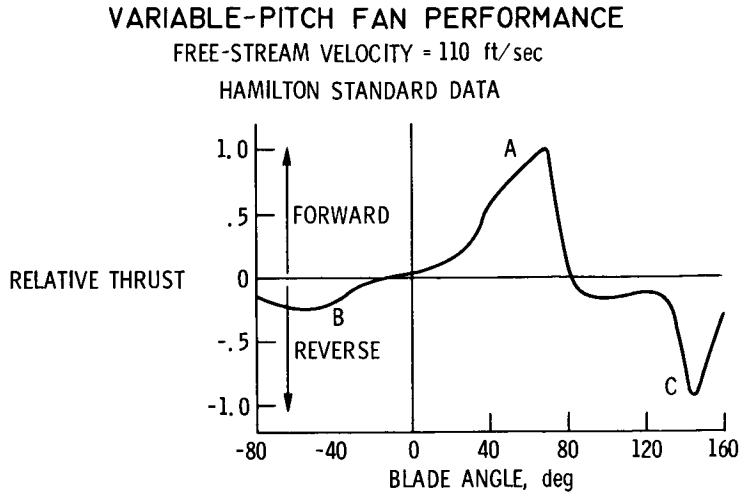

Figure 49

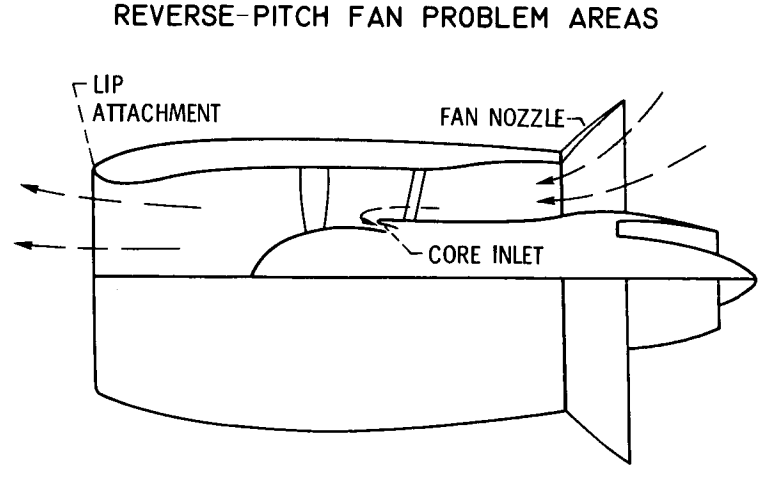

Figure 50

FLAP NOISE GENERATION AND CONTROL

By David Chestnutt, Domenic J. Maglieri,
NASA Langley Research Center

and Richard E. Hayden
Bolt Beranek and Newman Inc.

INTRODUCTION

A number of acoustic sources are found when an airstream interacts with a solid surface such as an airfoil (refs. 1 and 2). Optimal quieting of flap/nozzle systems requires a full understanding of the location and behavior of the various noise sources. Much of the discussion in this paper represents NASA coordination of work done at Bolt Beranek and Newman Inc. in a series of contract studies. Some of these studies are currently underway; therefore, this paper will serve as a status report of this research.

In figure 1 is shown a schematic diagram of the familiar jet-flap concepts being considered for integrated-powered-lift systems for STOL vehicles. Each of these concepts has in common high-velocity turbulent air flowing over relatively rigid surfaces which gives rise to what is commonly called interaction noise. This paper deals with the nature, location, and control of noise sources which involve the interactions of airflows with airfoil surfaces.

FLOW-SURFACE INTERACTIONS

Three pertinent types of flow-surface interactions are shown in figure 2. These types of interactions are categorized as inflow turbulence, in which fluctuating lift and drag forces are present wherein the high-frequency components are concentrated at the leading edge; surface impingement, where fluctuating surface pressures are present wherein the residual (uncanceled) surface pressure causes fluctuating forces on the whole surface; and trailing-edge discontinuity, where the flow may be below or above the airfoil. In the latter situation there are localized pressure and velocity fluctuations at the trailing edge which give rise to momentum fluctuations in the surrounding medium near the trailing edge. One interpretation of the significance of the trailing edge in producing noise is that sound scattering occurs at this edge. These three general categories can be further described as being affected by small-scale turbulence at the edges and larger scale turbulence over the entire airfoil (although these large-scale disturbances may originate at the leading or trailing edges).

A simplified summary of the physical quantities (ref. 3) to be considered when attempting to predict the noise generated by flow interacting with a surface in all the categories just mentioned is given by the following relationship:

$$\left[\begin{matrix}\text{Radiated}\\ \text{sound power}\end{matrix}\right] \propto \left[\begin{matrix}\text{Local mean}\\ \text{velocity}\end{matrix}\right]^6 \times \left[\begin{matrix}\text{Local turbulence}\\ \text{intensity}\end{matrix}\right]^2 \times \left[\begin{matrix}\text{Correlation lengths}\\ \text{x and y}\end{matrix}\right] \times \left[\begin{matrix}\text{Number of}\\ \text{sources}\end{matrix}\right]$$

where the fluid density and sound speed are assumed to be constant. This relationship theorizes that the radiated sound power is proportional to the local mean velocity to the sixth power, the local turbulence intensity to the second power, and the correlation lengths in the x and y directions, where correlation length is defined as that length over which the fluctuating pressures act in phase. Therefore, for minimum noise it is apparent that every effort should be made to lower the local mean velocity wherever possible. However, if this is not possible, all is not lost since reducing the local turbulence velocity and the corresponding correlation lengths should also provide a measure of noise control. Also, it should be noted that turbulence intensity and correlation length are both interrelated, that is, small values of turbulence intensity are usually accompanied by short correlation lengths in the flow fields of interest here.

FLAP SURFACE PRESSURE FLUCTUATIONS

In figure 3 are plotted spatial cross-correlation coefficients which can be used to determine the correlation lengths. This figure depicts the cross-correlation coefficients between several spanwise trailing-edge surface dynamic-pressure measurements in which one of the locations is used as a reference (zero time delay between sensors). In addition, this figure provides an indication of the source correlation area for high-frequency components and low-frequency components of noise. For high frequencies the turbulence scale (source area) is found to be small as expected, which is shown by the rapidly decreasing correlation coefficients as the distance between gages is increased. For the low frequencies, the turbulence scale is correspondingly larger as shown by the slower decrease of the correlation coefficient. Typically, it has been found that the turbulence scale for high and low frequencies at the flap edges is smaller than the jet diameter. Finally, a correlation length for a particular frequency may be obtained simply by computing the area under the curve.

Figure 4 depicts cross-correlation coefficients between chordwise dynamic surface pressures measured and the radiated sound in the far field using a retarded time corresponding to the propagation time of the sound between the two measurement points. Notice that these pressure measurements were made along the chord while in the previous figure they were made along the span. Cross correlations of this kind are useful for three reasons. First, it gives an empirical verification of the relevance of the correlation lengths shown in figure 3 as a measure of the sound-source dimensions. Second, the

cross-correlation coefficient can be used to estimate the number of independent similar noise sources contributing to the total measured radiated sound by taking the reciprocal of the square of the correlation coefficient. Finally, the data also indicate the noise-source locations since the peak correlations occur at these locations. This plot indicates that high-frequency noise sources are located closer to the edge than low-frequency noise sources since the high-frequency correlation peak is close to the edge. This in turn is another indication that trailing-edge noise is due to small-scale fluctuating pressures which tend to cancel over the whole surface except at the edge.

AIRFLOW-SURFACE NOISE CONTROL CONCEPTS

Trailing-Edge Blowing

Trailing-edge noise is noted to be common to all the STOL jet-flap concepts previously discussed. In figure 5 two possible methods of controlling noise produced at an airfoil trailing edge are shown. The sketch on the left indicates that low-velocity air may be blown from a rectangular slot along the entire airfoil span at the trailing edge (ref. 4). Alternatively, the sketch on the right indicates that the trailing edge may be modified with a porous material. Either of these methods may have some aerodynamic penalties or benefits associated with its use. However, because of the exploratory nature of this research, a thorough study of methods for alleviating aerodynamic penalties has not yet been made.

The concept of trailing-edge blowing will be discussed first. Low-velocity secondary air is blown out of the slot, this secondary air being only a very small percentage of the primary jet nozzle air. This secondary blowing serves to modify the mean shear and near-wall turbulence and produces a reduced fluctuating pressure near the edge which in turn should reduce the strength of the trailing-edge noise sources. Experiments are currently underway and preliminary data from these tests tend to verify this hypothesis. As an example, the data of figure 6 indicate the noise-reduction effects of secondary or trailing-edge blowing. Plotted are 1/3-octave spectra for a jet only, a jet plus a solid flap, and a jet plus a flap with trailing-edge blowing. These spectra are for a 4.5-cm-diameter (1.75 in.) circular nozzle with cold flow of a jet velocity of about 151 m/sec (500 ft/sec). Significant noise reductions occurred in two areas when trailing-edge blowing was used. Noise reductions were obtained primarily at the spectrum peak and in the high-frequency area. In fact, at about 10 000 Hz the amplitude for the jet plus blowing flap has reached that for the jet only. On the opposite end of the spectrum, below about 500 Hz, there was little reduction; this is consistent with figure 4 which indicated that the low-frequency noise was due to large-scale pressure fluctuations acting over the entire airfoil surface. Therefore, trailing-edge blowing should strongly influence the

high-frequency noise being generated at the trailing edge but should affect only minimally the low-frequency noise generated by large-scale pressures acting over the entire airfoil.

Porous Surface Treatment

Trailing-edge noise can also be controlled by replacing the solid edge with a porous edge. (See fig. 5.) This porous-edge type of treatment is different from that used in the augmentor-wing arrangement. These two ways in which acoustic treatment is used to reduce noise that is associated with flap systems are illustrated in figure 7. In the sketch at the top of the figure is shown the augmentor-wing jet flap with its honeycomb-backed treatment shown as darkened areas. The purpose of this type of treatment is to absorb noise after it has been generated, although some reduction of hydrodynamic pressure fluctuations may also result, and this would serve to minimize edge noise from the trailing edges of the flap channel to some extent. Duct theory is used to tune the treatment to attenuate the predominant high-frequency noise produced by the high-aspect-ratio slot nozzles. In the lower two sketches are shown an upper surface blown (USB) flap and an externally blown flap (EBF) in which noise is minimized by reducing the fluctuation pressure differences between the upper and lower surfaces before the pressure field encounters the edge. This treatment in effect prevents the generation of some noise. This reduction is accomplished by using a variable impedance (porosity) trailing edge or leading edge. The impedance (porosity) is variable in that it is lower (more porous) at the leading and trailing edges of the flap and the impedance increases (porosity decreases) toward midchord. This mechanism of noise control is not fully understood at present but is believed to prevent the generation of noise by allowing the gradual communication of fluctuating pressures between the upper and lower surfaces, thus reducing the strength of the sound source, and is also believed to decrease the magnitude of the spatial impedance gradient, thus reducing the degree of conversion of incompressible flow disturbances (turbulence) into compressible motion (sound).

In figure 8 are presented representative data on the effects of using porous edges on both the leading and trailing edges of three flaps of an externally blown flap model (ref. 3). Spectra shown are for flaps in both the take-off and landing positions. The frequency has been nondimensionalized by using the jet diameter and velocity. The solid lines indicate solid, unmodified flaps and the lower shaded region represents corresponding sound spectra from the model configuration with porous leading and trailing edges. (The width of the shaded region indicates a significant variation in amount of noise reduction observed; it was found that noise reduction was very sensitive to details of the porous flap configuration and aerodynamic losses were relatively insensitive to the same changes.) Noise reductions were obtained for the take-off flaps and for landing flaps. A significant factor is the broadband nature of the noise reduction. Since the treated area was a significant percentage of the flap areas, the treatment helped in the lower

frequency range as well as the trailing edge or high-frequency range. For this specific model the measured aerodynamic lift losses and drag increases were quite high, being of the order of 25 to 40 percent. Other porosity configurations produced noise reductions up to 12 dB with varying degrees of aerodynamic losses. However, these studies were conceptual in nature and suffered from limitations with regard to a complete understanding of the noise generation mechanisms, suitability of available materials, and sufficient information to select the appropriate material. It is thus believed that these performance losses will be reduced when a concerted effort is made to optimize the performance of the noise-reduction techniques. It bears repeating that these tests were exploratory and have indicated significant noise-reduction potential.

Upper Surface Blowing

The upper surface externally blown flap may have aerodynamic characteristics similar to the under-the-wing version of the EBF. Previous experiments on small-scale models of USB and EBF (ref. 1) and recent data on larger scale experiments (paper no. 32 by Robert Dorsch and Meyer Reshotko) have shown that, acoustically, the USB arrangements have the more favorable noise characteristics. Typical of the noise results obtained in these investigations, the noise spectra of figure 9, obtained from pilot study of noise control on the upper surface blown flaps conducted by Bolt Beranek and Newman under NASA contract, are presented. In figure 9 a comparison is made of the sound radiation from a 3-flap EBF (under wing blowing with round nozzle of 4.45-cm (1.75 in.) diameter) in the take-off setting and a single upper surface blown flap having an aspect-ratio-10 nozzle (12.7 cm (5 in.) wide by 1.27 cm (0.5 in.) high and located as shown in the insert) and a 45^{o} turning angle (relative to the wing center line). The area of the slot nozzle matched that of the round nozzle; the total flap lengths and nozzle exit velocities were comparable. No forward speed was superimposed for the data shown. It is evident from figure 9 that the USB configuration is inherently quieter than the under-wing EBF and that the sound spectrum is shifted almost a decade toward lower frequencies. This frequency shift will have a beneficial effect on subjective measures of community noise (such as PNdB or dB(A)) but could produce low-frequency noise problems related to both the airport community and noise levels inside the airplane.

The trailing-edge noise-reduction concepts involving edge porosity and edge blowing were applied to the USB configuration. In figure 10 are shown schematic diagrams of the USB flap trailing-edge modifications. The base-line flap with a solid trailing edge is illustrated in figure 10(a); the modified flap having a porous trailing edge with no backing is illustrated in figure 10(b); and the modified flap having a porous trailing edge with an air gap (air cavity) and a solid backing is illustrated in figure 10(c). The measured directivity patterns from the USB base-line flap (fig. 10(a)) and modified flap with porous edge, air gap, and solid backing (fig. 10(c)) for the 630 Hz, 1250 Hz, and 5 kHz 1/3-octave bands

are presented in figure 11. The effect of adding porous treatment to the trailing edge is to reduce the noise at essentially all angles above and below the flap and in each of the three frequency bands. A further indication of the noise reductions obtained is shown in figure 12 which contains frequency spectra, measured at an angle of 150^{o} from the jet exhaust axis for the USB configurations shown in figure 11 and including the one with porous edge and no backing. (See fig. 10(b).)

The directivity and spectra characteristics shown in figures 11 and 12, respectively, are characteristic of trailing-edge noise sources and suggest that the majority of the sound radiation below the wing of the airplane is due to the attached turbulent wall jet interaction with the trailing edge of the turning flap. The correlation measurements described earlier in this paper also confirm this hypothesis. It is also of interest to note that the configuration which produced the most noise reduction (porous flap with air gap and solid backing (fig. 10(c))) also had the least aerodynamic losses since steady-state through-flow was blocked. In addition, no significant difference in flow-turning angle was observed between the reference solid trailing-edge flap and the ones having porous edges.

Corresponding detailed data on the effect of edge blowing as a means of USB noise reduction have been acquired (ref. 4). Some results are presented in figure 13 in the form of frequency spectra for a USB arrangement with and without secondary air slot blowing at the flap trailing edge. The primary jet flow emitted from a 12.7- by 1.27-cm (5 by 0.5 in.) rectangular nozzle over the top of the flap surface at a Mach number of 0.5. It can be noted that noise reductions of the order of 3 to 6 dB were realized over a wide frequency range for relatively low secondary flow rates.

CONCLUDING REMARKS

This paper has dealt with the nature, location, and control of noise sources involving airflow and surface interactions. Results indicate that multiple noise sources are involved in flow-surface interactions of the type found in powered-lift STOL concepts. In addition, the significant factors in determining the dominant noise generation region of the airfoil are the details of the fluctuating pressure patterns on both surfaces of an airfoil. Finally, it is shown that two important factors in noise control in flow-surface interactions are trailing-edge blowing and variable porosity edges.

This paper is intended to provide a certain optimism regarding the ultimate reduction of noise due to the interaction of jets with solid surfaces. However, as the lift and drag losses have indicated, much work remains to be done. Exploratory research is continuing in all these areas and the practical limits of noise reduction are beginning to be realized.

REFERENCES

1. Dorsch, Robert G.; Lasagna, Paul L.; Maglieri, Domenic J.; and Olsen, William A.: Flap Noise. Aircraft Engine Noise Reduction. NASA SP-311, 1972, pp. 259-290.

2. Hayden, Richard E.: Noise From Interaction of Flow With Rigid Surfaces: A Review of Current Status of Prediction Techniques. NASA CR-2126, 1972.

3. Hayden, Richard E.; Kadman, Yoram; and Chanaud, Robert C.: A Study of the Variable Impedance Surface Concept as a Means for Reducing Noise From Jet Interaction With Deployed Lift-Augmenting Flaps. Rep. No. 2399 (Contract No. NAS1-9559-18), Bolt Beranek and Newman Inc., [1972]. (Available as NASA CR-112166.)

4. Hayden, R. E.; Scharton, T. D.; Kadman, Y.; Wilby, J.; and Rudd, M. J.: A Preliminary Evaluation of Noise Reduction Potential for the Upper Surface Blown Flap. Rep. No. 2478 (Contract No. NAS1-11839-5), Bolt Beranek and Newman Inc., 1973. (Available as NACA CR-112246.)

JET-FLAP CONCEPTS

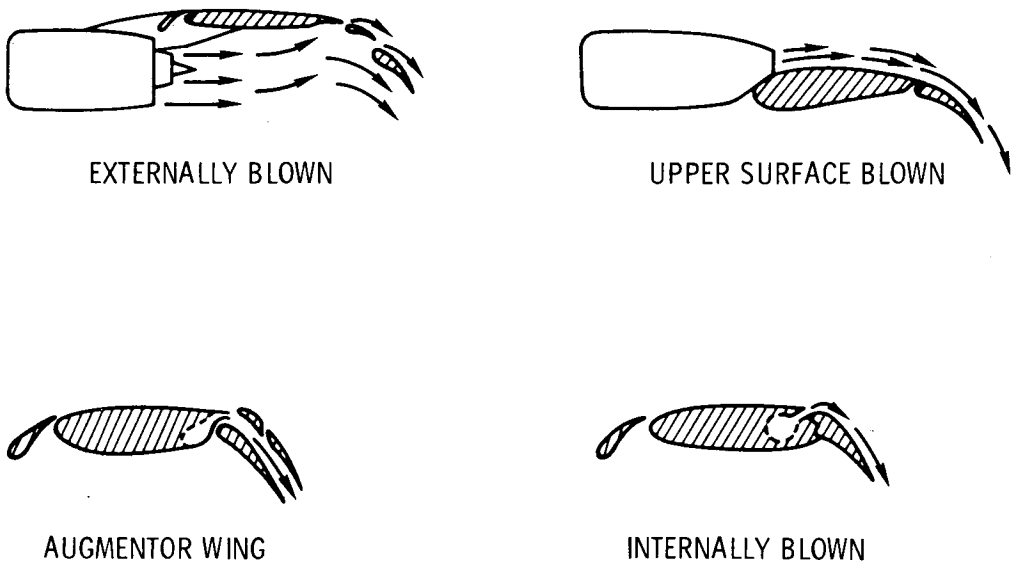

Figure 1

TYPES OF FLOW-SURFACE INTERACTION

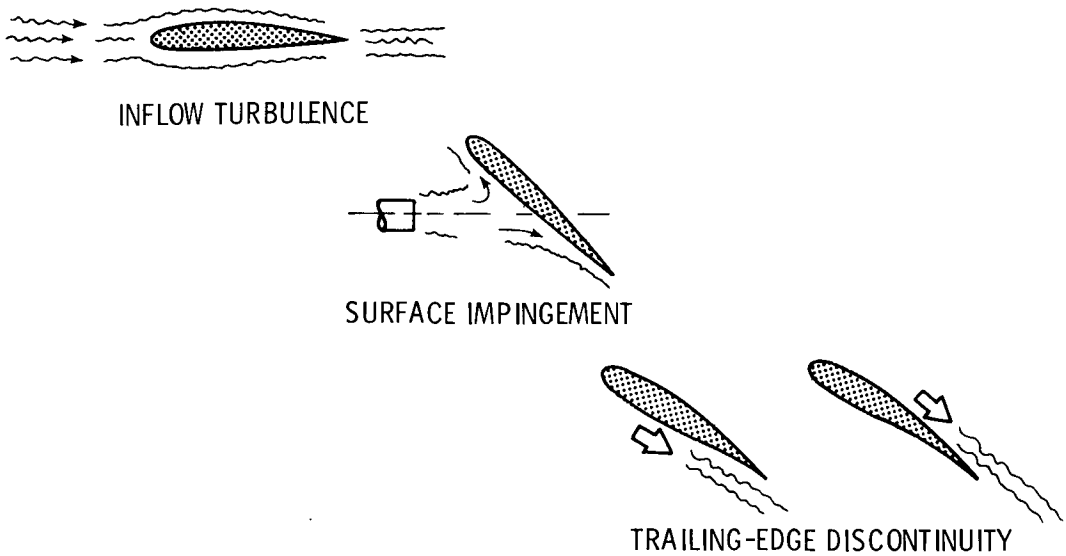

Figure 2

CORRELATION OF SPANWISE TRAILING-EDGE SURFACE PRESSURES

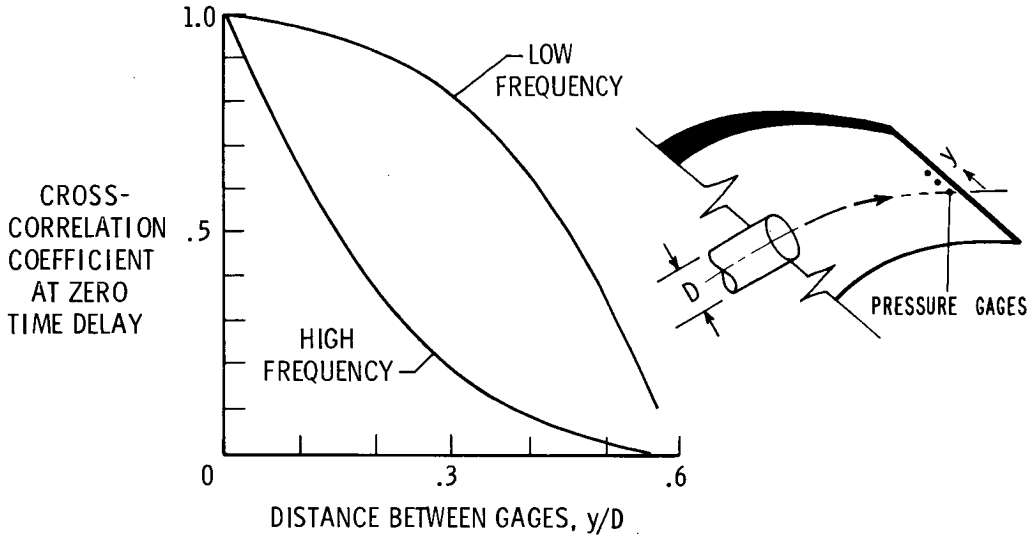

Figure 3

CORRELATION OF CHORDWISE SURFACE PRESSURES WITH FAR-FIELD RADIATED NOISE

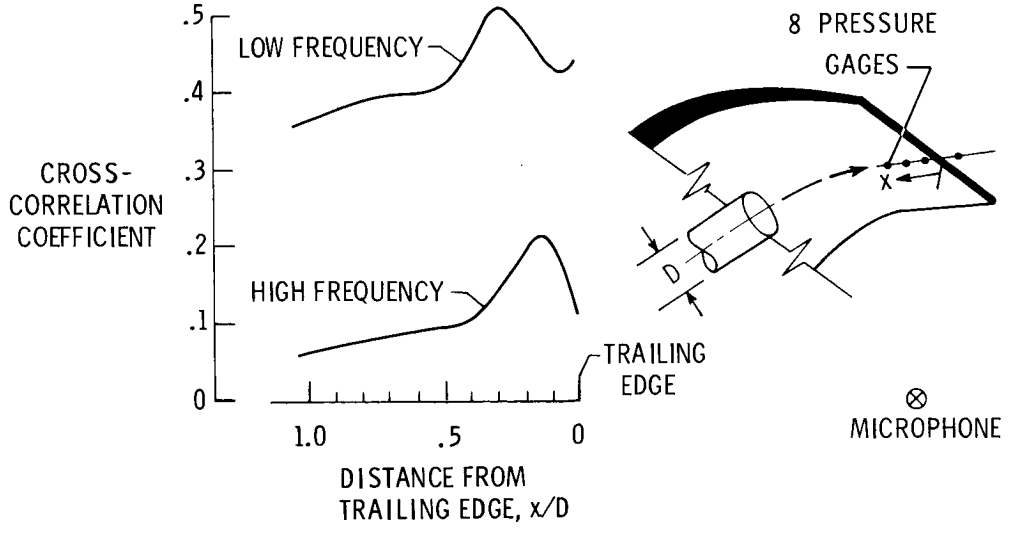

Figure 4

TRAILING-EDGE NOISE CONTROL

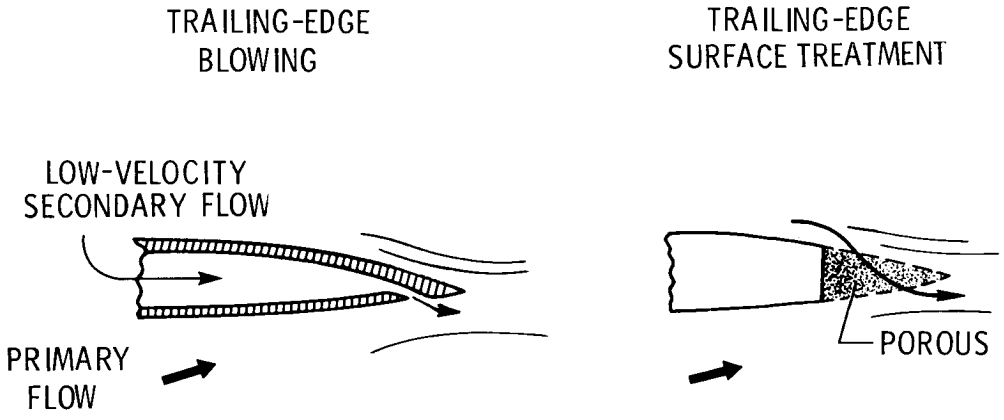

Figure 5

EFFECT OF TRAILING-EDGE BLOWING

FLAP ANGLE = 45^{0}

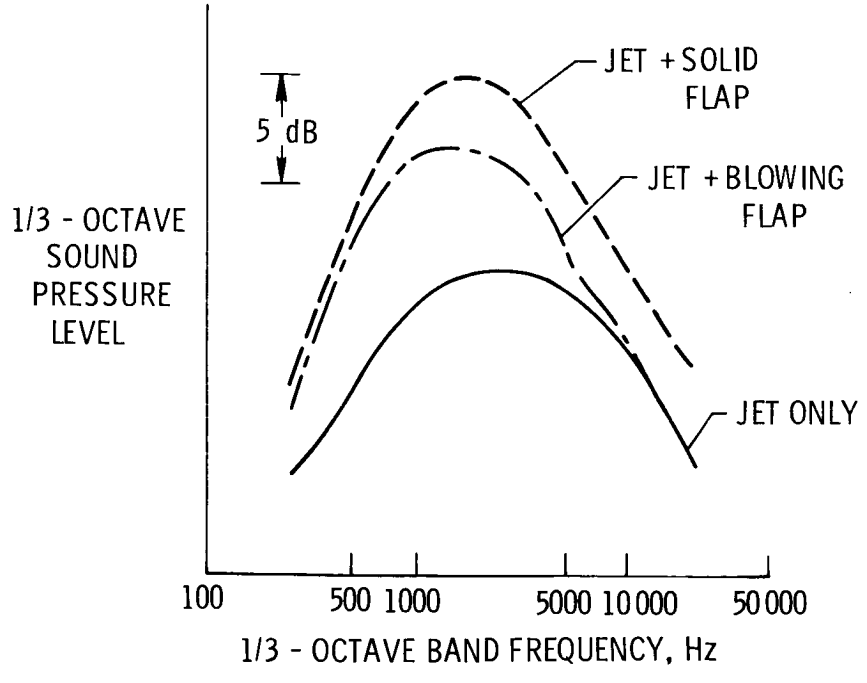

Figure 6

USE OF FLAP TREATMENT

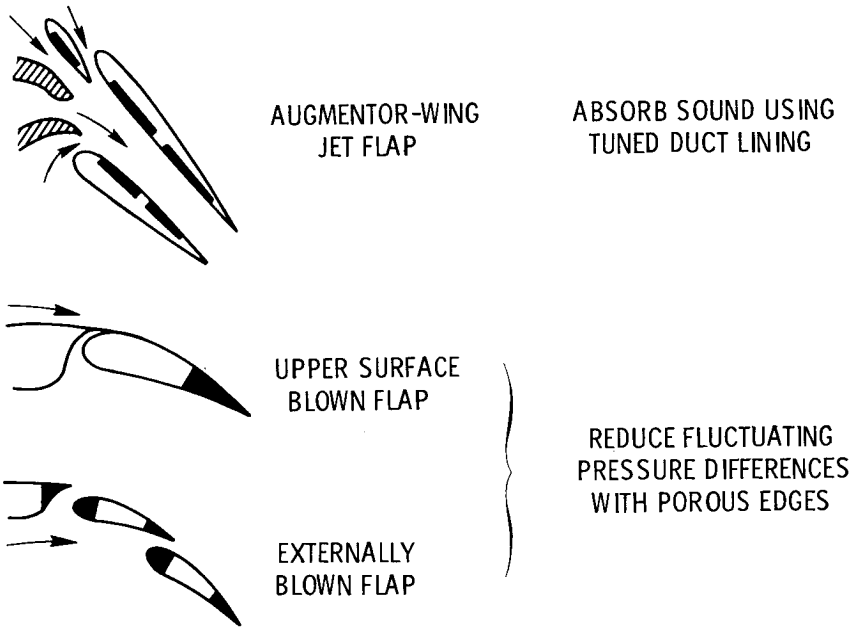

Figure 7

EFFECT OF EDGE POROSITY

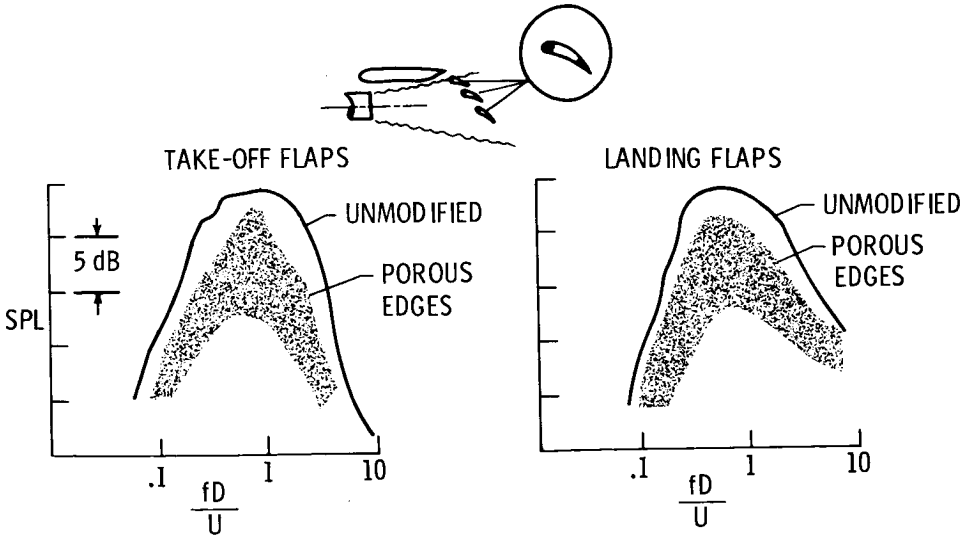

Figure 8

NOISE SPECTRA OF EBF AND USB FLAP CONFIGURATIONS

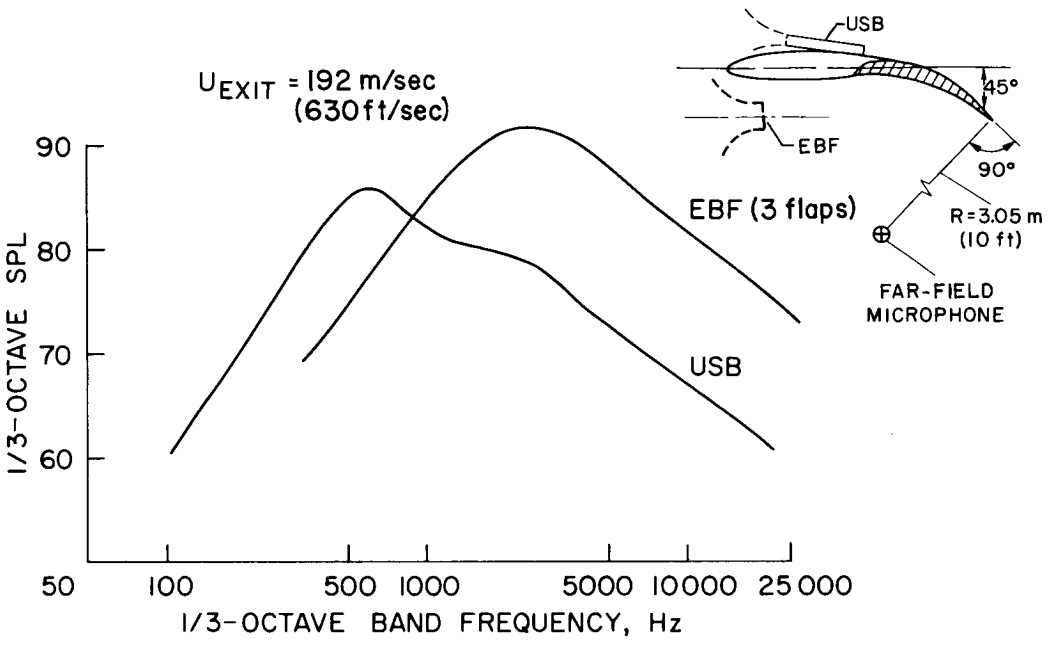

Figure 9

USB FLAP TRAILING-EDGE MODIFICATIONS

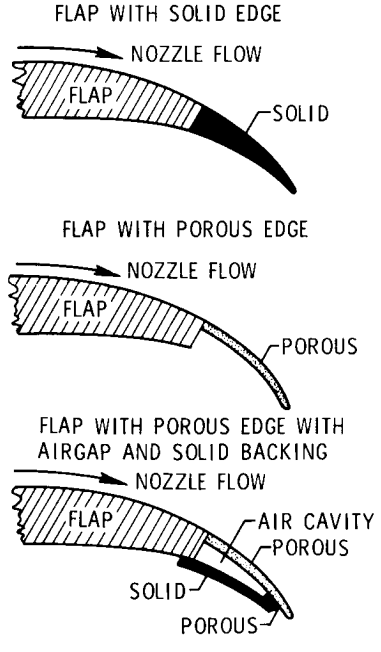

Figure 10

NOISE RADIATION PATTERNS FROM USB FLAP CONFIGURATIONS

EXIT VELOCITY = 192 m/sec (630 ft/sec)

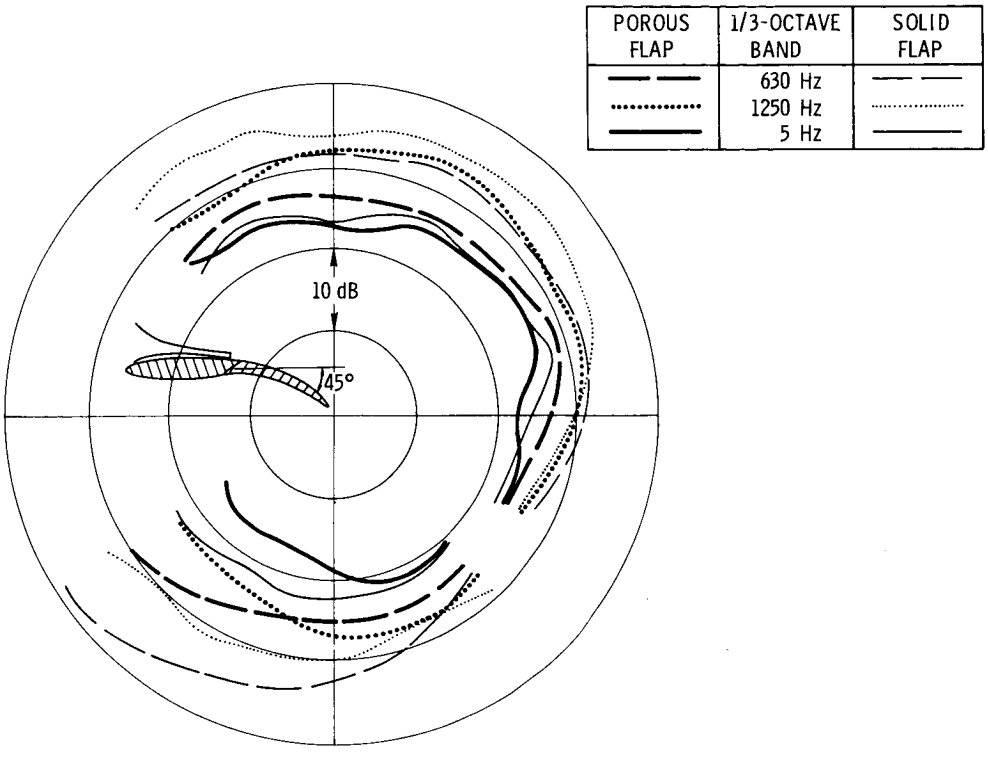

Figure 11

NOISE SPECTRA OF USB FLAP CONFIGURATIONS

EXIT VELOCITY = 192 m/sec (630 ft/sec)

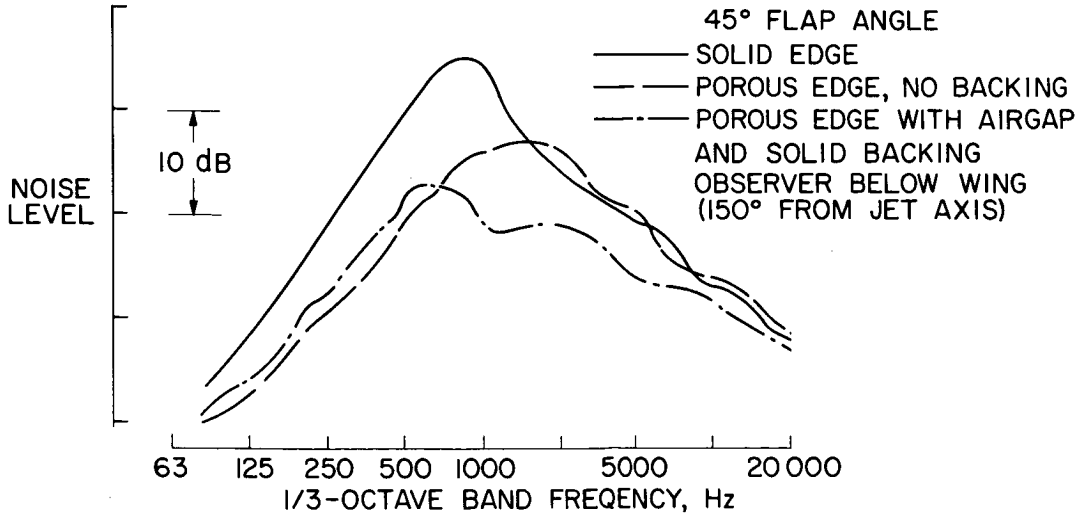

Figure 12

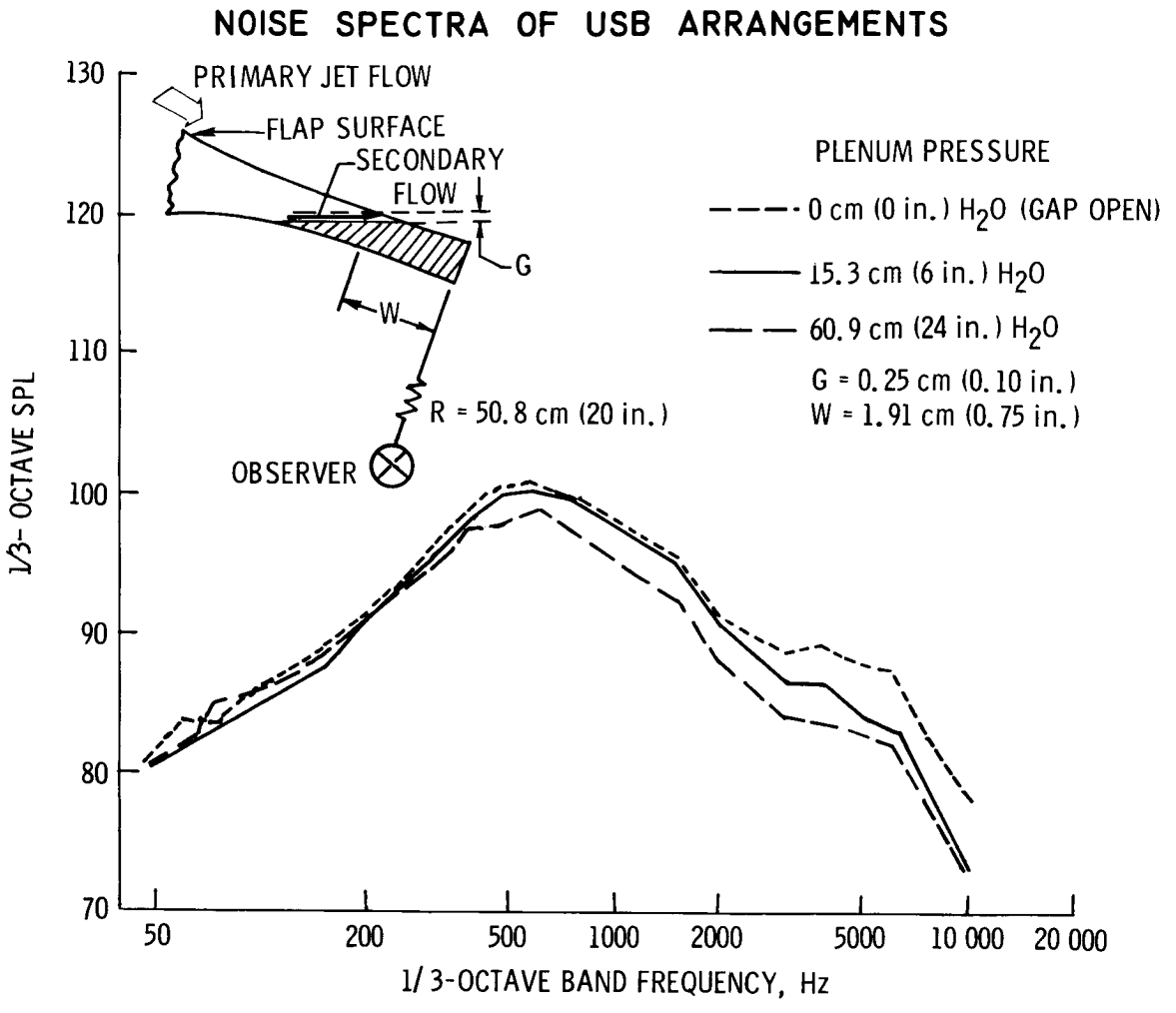
NOISE SPECTRA OF USB ARRANGEMENTS
PRIMARY JET FLOW
FLAP SURFACE
SECONDARY FLOW
G
W
R = 50.8 cm (20 in.)
OBSERVER
PLENUM PRESSURE
0 cm (0 in.) H2O (GAP OPEN)
15.3 cm (6 in.) H2O
60.9 cm (24 in.) H2O
G = 0.25 cm (0.10 in.)
W = 1.91 cm (0.75 in.)
1/3- OCTAVE SPL
130
120
110
100
90
80
70
50
200
500
1000
2000
5000
10 000
20 000
1/3-OCTAVE BAND FREQUENCY, Hz

Figure 13

EXTERNALLY BLOWN FLAP IMPINGEMENT NOISE

By Paul L. Lasagna and Terrill W. Putnam
NASA Flight Research Center

SUMMARY

Tests of the noise produced by the impingement of the jet exhaust on the wing and flap for an externally blown flap system were conducted with a CF700 turbofan engine and an F-111B wing panel. The noise produced with a daisy nozzle installed on the engine was greater than that produced by a conical nozzle at the same thrust. The presence of the wing next to the test nozzles increased the noise, as did increasing the flap deflection angle. Compared with the conical nozzle, the daisy nozzle produced slightly less noise at a flap deflection of 60^{o} but produced more noise at the lower flap deflections tested. Tests showed that the single-slotted flap deflected 60^{o} produced less noise than the double-slotted flaps. Also, maintaining the maximum distance between the exit nozzle and flap system resulted in a minor reduction in noise.

INTRODUCTION

STOL aircraft are designed to take off and land on short landing strips near heavily populated areas. The noise they generate during those operations must stay below acceptable levels. One type of a proposed STOL airplane is an externally blown flap airplane with the engines located close to the undersurface of the wing and with lower surface blowing, in which the exhaust from a fan-jet engine is directed at the flap system and is then deflected downward for lift augmentation.

The impingement of the engine exhaust jet on the flaps and the turning of the jet by the flaps create additional noise below the aircraft. The engine alone generates internal and jet-mixing noise. Internal noise comes from the engine machinery, such as the fan. Impingement of the engine exhaust jet upon the surface of the wing and flap generates additional noise, such as flap leading-edge noise, scrubbing noise, and trailing-edge noise, as illustrated in figure 1. This additional noise could be the dominant noise source of an externally blown flap airplane.

In order to evaluate the importance of noise generated from the interaction of the jet exhaust with the flaps, the NASA Flight Research Center set up a ground-test facility using an F-111B wing panel with double-slotted trailing-edge flaps and a CF700 turbofan engine. The wing and engine were positioned so that the jet exhaust would impinge on the flaps when extended. Some of the noise results have been previously reported in reference 1.

TEST APPARATUS

Test Equipment

The noise tests were conducted with a modified F-111B wing and flap system blown by the exhaust from a CF700 turbofan engine shown in the photograph of figure 2. The engine is a single-stage fan with a bypass ratio of 2. It has a rated thrust of 18 680 N (4200 lbf). At rated thrust, the turbine exhaust velocity is 457 m/sec (1500 ft/sec), and the fan air velocity is about 270 m/sec (900 ft/sec). The engine had a 3.7-m-long (12-ft) acoustically treated inlet to suppress the fan noise. A 2.7-m-long (9-ft) acoustically treated tailpipe was installed aft of the engine to remove machinery and fan noise from the engine exhaust. It also promoted mixing between the turbine and fan exhaust streams and reduced the peak jet-exit velocity. The mixed fan and core exhaust exited from the tailpipe through a 55.9-cm-diameter (22-inch) convergent nozzle or through a daisy nozzle of the same effective area and was directed at the flap system.

The F-111B wing panel was installed vertically on a table that could be actuated in either the longitudinal or transverse direction in order to vary the relative positions of the exhaust nozzle and flap system. The wing panel had double-slotted trailing-edge flaps and was designed for high dynamic pressure. Both flaps were covered with a thin stainless-steel panel to form a single-slotted flap during some of the tests. Static and dynamic pressures were measured on the undersurface of the wing and flaps. Those results were presented by Donald L. Hughes in paper no. 13.

Figure 3 is a photograph of the installed daisy nozzle used in these tests. This nozzle was designed as a jet noise suppressor to be used on the CJ805-3 turbojet engine. The daisy nozzle had eight lobes and its effective area was the same as that of the conical convergent nozzle, so that for a given corrected fan speed, both nozzles produced the same thrust.

Test Site

The tests were conducted at an engine test stand at Edwards Air Force Base, California. The test site was on the edge of Rogers Dry Lake far from any buildings or other obstructions, and the terrain surrounding the test stand consisted of hard, packed, sandy soil. The test stand consisted of a thrust-measuring platform, upon which the engine support rested, and an instrumentation and engine-control room, which was located underground.

Aerodynamic Instrumentation and Analysis

A 1.22-m-long (4-ft) aerodynamic rake (fig. 3) with elements spaced 2.54 cm (1 inch) apart was used to survey the jet exhaust axially and radially. The odd-numbered

rake elements measured total pressure and temperature, and the even-numbered elements measured static pressure. Jet-velocity profiles were calculated from these measurements and isentropic gas-dynamic relationships.

Acoustic Instrumentation and Analysis

Noise measurements were taken with 1.27-cm (0.5-inch) condenser microphones. Microphones were positioned at a radius of 30.5 m (100 ft) from the underside of the wing, as shown in figure 4. The radius was measured from the intersection of the exhaust nozzle plane with the exhaust nozzle centerline. All microphone angles are referenced to the engine inlet. The centerline of the engine exhaust nozzle was 2.7 m (9 ft) above the ground and the microphones were elevated on poles so that they were in the same horizontal plane as the engine centerline. The data were recorded with a wide-band FM tape recorder running at 76 cm/sec (30 ips). The frequency responses of the microphones, signal conditioning equipment, and recorder were determined between 20 and 20 000 hertz. Before and after each day of testing, an acoustic calibration was performed on each microphone and recorded on the data tape.

The data were reduced by using a computer-controlled real-time $\frac{1}{3}$-octave band analyzer. During data reduction, the data were properly scaled, frequency-response corrections were applied if necessary, and overall sound pressure and perceived noise levels were calculated. No corrections were applied for atmospheric absorption and no attempt was made to compensate for the ground-reflection interference observed in the data.

Test Procedure

Tests were conducted between 3 a.m. and 7 a.m. on 5 different days over a 2-week period. The tests were not started if the wind speed exceeded 2.24 m/sec (5 mph), and they were terminated if the wind speed exceeded 4.47 m/sec (10 mph). For the acoustic data points, the engine was allowed to stabilize for approximately 2 minutes, and then noise data were recorded for 1 minute. To ensure repeatability of engine thrust levels, the CF700 was always controlled by setting corrected fan speed.

The baseline tests consisted of a series of runs at various thrust levels for both the conical and daisy nozzles without the wing in position behind the engine. In this way the noise caused by each nozzle could be measured. The tests were repeated at the same thrust levels, again with both nozzles, with a velocity rake inserted in the jet exhaust at selected axial and radial positions to obtain velocity data.

After these tests the F-111B wing was installed in back of the engine at an angle of attack of 3° with respect to the jet axis and with the wing sweep at 16° as measured at the wing's rear spar. The geometric configuration used for the acoustical data to be presented is shown in figure 5. The intersection of the jet exhaust centerline and the flap

when deflected 60°, shown as x, was set at x/D = 3, 4, and 5, or at 168, 224, and 279 cm (66, 88, and 110 inches), respectively, where D is the diameter of the conical nozzle. Both the conical and daisy nozzles were positioned on the same centerline.

RESULTS AND DISCUSSION

Jet-Velocity Survey

One method to reduce flap impingement noise would be to reduce the jet velocity in the vicinity of the flap surface by the use of a velocity-decayer nozzle. Presented in figure 6 are the velocity-decay characteristics of the conical and daisy test nozzles. The ratio of the local velocity V to the maximum velocity measured V_{max} is plotted as a function of conical diameters downstream of the nozzles. The upper curve, which represents the decay characteristics of the jet exhaust with the conical nozzle, indicates that the exhaust core extends downstream of the nozzle about 3 diameters and then the peak velocity begins to decay. The daisy nozzle velocity, however, decays quite rapidly close to the exit plane and at a much slower rate at distances greater than 2 conical diameters downstream. For all distances downstream of the two nozzles, the local velocity for the daisy nozzle was less than that for the conical nozzle. This results in lower flow velocities in the vicinity of the flaps when the daisy nozzle is used. For instance, at 4 diameters downstream, the local velocity for the daisy nozzle is 35 percent less than for the conical nozzle.

Velocity profiles in the vertical plane of the jet centerline at 4 conical diameters downstream of both nozzles are shown in figure 7. Velocity is plotted against distance from the engine centerline. For both nozzles, the corrected fan speed was the same and the engine thrust was 8230 N (1850 lbf). The engine power setting at this thrust value was used for all noise contours and spectra to be presented in this paper. As can be seen, the peak velocity was 239 m/sec (785 ft/sec) for the conical nozzle and 158 m/sec (520 ft/sec) for the daisy nozzle. In comparing the conical and daisy nozzles, it is observed that the daisy nozzle reduces the peak impingement velocity by about 35 percent at 4 conical diameters downstream and also spreads out the jet flow for the equal-thrust condition.

Acoustic Results

The noise emitted by the conical and daisy nozzles was first measured without the wing present. Shown in figure 8 are the polar plots of the noise from just the engine and test nozzles. The perceived noise levels were calculated from the measured spectra in accordance with reference 2 at 30.5 m (100 ft) away from the nozzle and are plotted as a function of angle from the engine inlet. The thrust was 8230 N (1850 lbf). The daisy nozzle, which is represented by the outer set of data points, is considerably louder than the

conical nozzle even though the nozzles are producing the same thrust. At most angles, the daisy nozzle is approximately 5 PNdB louder than the conical nozzle.

Presented in figure 9 are the $\frac{1}{3}$-octave band spectra at 80° from the engine inlet for the two test nozzles at the same thrust level. The sound pressure level is shown as a function of frequency. The dips in the spectra at 315 hertz are due to ground reflection effects, which resulted in amplitude cancellation. The conical nozzle has 1 to 3 dB higher sound pressure levels than the daisy nozzle for frequencies below 200 hertz. For frequcies above 200 hertz, the daisy nozzle has significantly higher levels than the conical nozzle, which accounts for the high perceived noise levels of the daisy nozzle.

Shown in figure 10 are noise radiation patterns obtained with the conical nozzle and with the wing positioned so that for 60° flap deflection, the jet centerline intersects the flap surface at 4 conical diameters downstream (x/D = 4). Perceived noise level is given for the nozzle alone and three flap deflections. The noise level of the nozzle alone is shown by the inner set of data points. When the wing is positioned above the nozzle with the flaps retracted, the noise level increases because of reflection of the nozzle noise and impingement of the jet exhaust on the wing and flap surfaces. The level increases further as the flaps are lowered to 35° and then to 60°, the largest increases being in the forward quadrant. For example, at 120° from the engine inlet the perceived noise level has increased about 5 PNdB, but the increase at 80° is 11 PNdB. The levels at the 60° flap deflection agree with data for the $\frac{1}{2}$-scale model taken at the NASA Lewis Research Center (ref. 3), when velocity profile and flap size are considered.

The same type of trend can be seen in the $\frac{1}{3}$-octave band spectra of the sound pressure levels. Figure 11 presents the sound pressure level as a function of frequency for the conical nozzle, the 80° position from the inlet, and the same flap deflections and thrust level as in figure 10. The 80° position is shown because it is near the position of maximum noise from an externally blown flap airplane in the landing configuration heard by an observer on the ground. As the wing is brought into position, there is a large increase in the low-frequency noise, that is, 50 to 500 hertz, even with 0° flaps. When the flaps are lowered to 60°, there is an additional small increase in sound level for frequencies below 100 hertz and an increase of 4 to 12dB for all other frequencies shown.

Similar trends can be seen in the noise radiation patterns obtained with the daisy nozzle in place of the conical nozzle. Shown in figure 12 are the perceived noise levels for the daisy nozzle with the same flap positions and thrust level as were used for the conical nozzle. The noise level of the nozzle alone is represented by the inner set of data points. Again, as the wing is positioned with 0° flaps, the level increases. It increases further as the flaps are lowered to 60°. In comparing the two nozzles, it can be seen that the increase in levels due to the wing and 60° flap deflection is not as great

with the daisy nozzle. For instance, at 80° the increase with the daisy nozzle is about 6 PNdB, whereas the increase is 11 PNdB with the conical nozzle (fig. 10).

Shown in figure 13 is a comparison of the perceived noise levels of the conical and daisy nozzles with the wing in position and the flap deflected 60°. The perceived noise levels were calculated from spectra at 30.5 m (100 ft). The flaps were at 4 conical diameters downstream of the exhaust nozzle. With the 60° flap deflection, the daisy nozzle is less noisy in the forward quadrant than the conical nozzle. From 80° to 110°, which corresponds to positions below the wing, there is only a small decrease in noise level for the daisy nozzle from that for the conical nozzle. Although not shown, at flap deflections of 0° and 35° data indicate that the decrease in impingement noise due to the lower velocity of the daisy nozzle is more than offset by the noise of the daisy nozzle itself.

Shown in figure 14 are the spectra at 80° for the conical and daisy nozzles with the wing and a flap deflection of 60°. The daisy nozzle has reduced the sound pressure level in the range 80 to 315 hertz from the level for the conical nozzle. For frequencies above 315 hertz, the noise of the daisy nozzle alone, as previously shown, masks any reduction in flap impingement noise.

Now consider the effect on the noise level of changing the distance between the exhaust nozzle and the flaps. Presented in figure 15 are the perceived noise levels for the conical nozzle plotted as a function of angle from the inlet for three positions of the nozzle and the flaps at the 60° position. The engine thrust and exhaust velocity were held constant while the distance from the flap to the engine exhaust nozzle was varied from 3 to 4 and then to 5 conical diameters. The outer set of data points are for the flaps at a distance of 3 diameters downstream of the nozzle. As the flaps were moved farther from the engine, the noise decreased because of a decrease in impingement velocity on the flaps. The angles of most interest are those directly under the aircraft, that is, 70° to 100°, where the noise decreased 2 to 4 PNdB when the flap distance was varied from 3 to 5 conical diameters.

Figure 16 presents the perceived noise levels at the 80° microphone position as a function of thrust for the conical and daisy nozzles. These data were obtained with the wing positioned and with both double- and single-slotted flaps deflected 60°, which is a landing flap setting. The solid symbols represent the noise measured with the single-slotted flap. The single-slotted flap is quieter than the double-slotted flaps because it has one less slot and, hence, one less leading and trailing edge.

CONCLUDING REMARKS

The impingement of the jet exhaust on the wing and flap surface produces a significant amount of noise over and above the propulsion-system noise. Minor reductions in

the impingement noise seem possible by maintaining the maximum distance between the nozzle exit and the flap system which will still give the required powered lift. Minimizing the number of flap segments also results in only minor noise reduction. With the use of a velocity-decayer nozzle, noise reduction for a flap deflection of 60^{o} is obtained because of reduced flap interaction noise; however, there is a need for effective noise control of the mixer-nozzle noise to achieve any greater reduction in noise.

REFERENCES

1. Putnam, Terrill W.; and Lasagna, Paul L.: Externally Blown Flap Impingement Noise. AIAA Paper No. 72-664, June 1972.

2. Anon.: Definitions and Procedures for Computing the Perceived Noise Level of Aircraft Noise. ARP 865, Soc. Automot. Eng., Oct. 15, 1964.

3. Dorsch, Robert G.; Lasagna, Paul L.; Maglieri, Domenic J.; and Olsen, William A.: Flap Noise. Aircraft Engine Noise Reduction, NASA SP-311, 1972, pp. 259-290.

EXTERNALLY BLOWN FLAP NOISE SOURCES

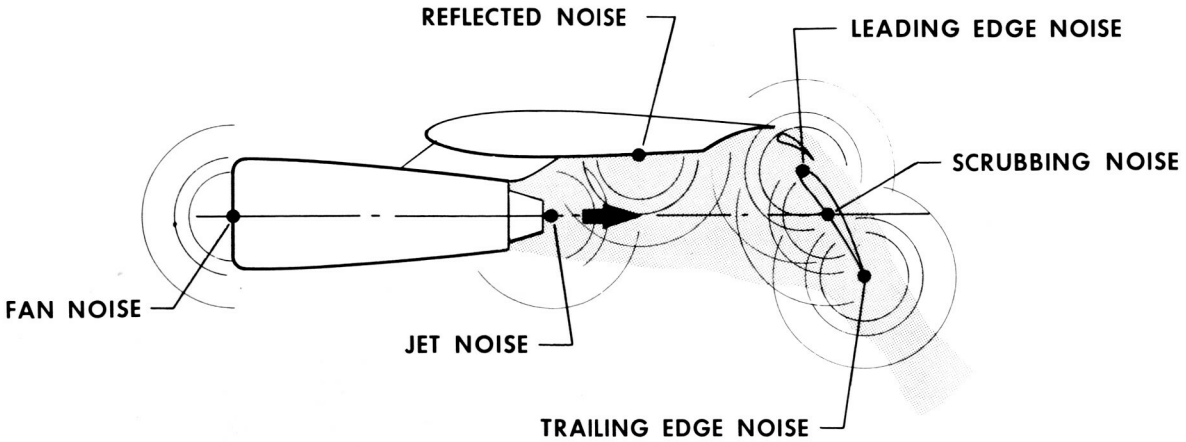

Figure 1

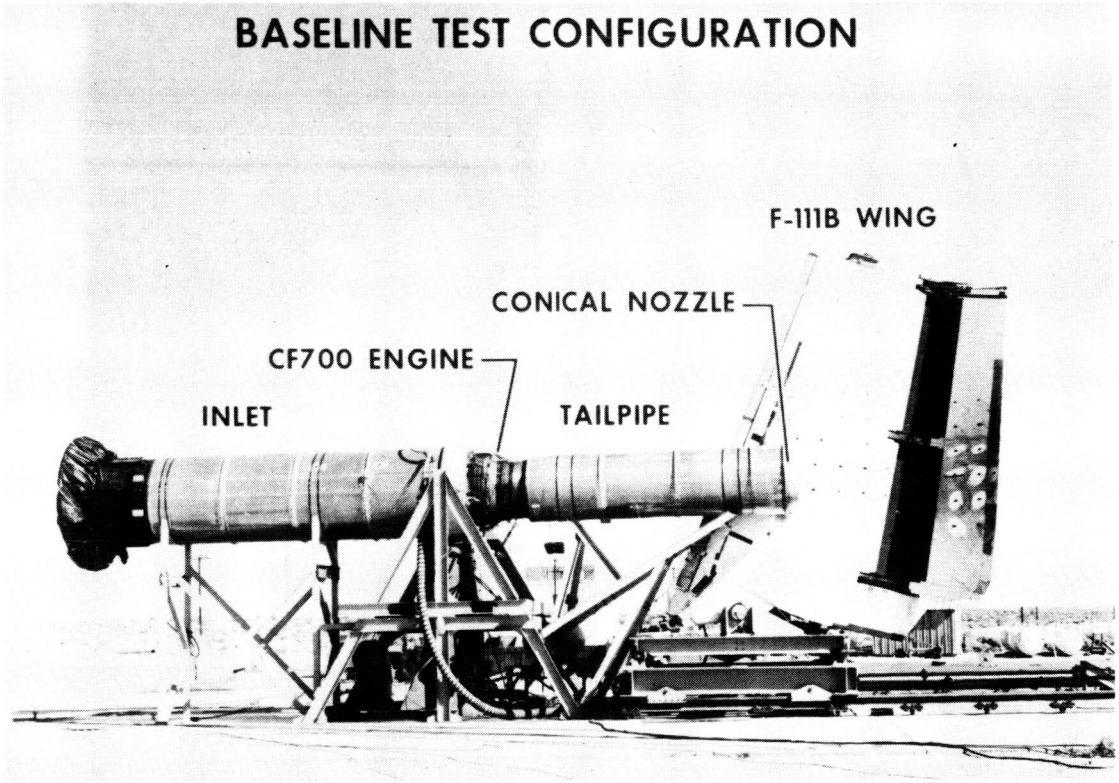

Figure 2

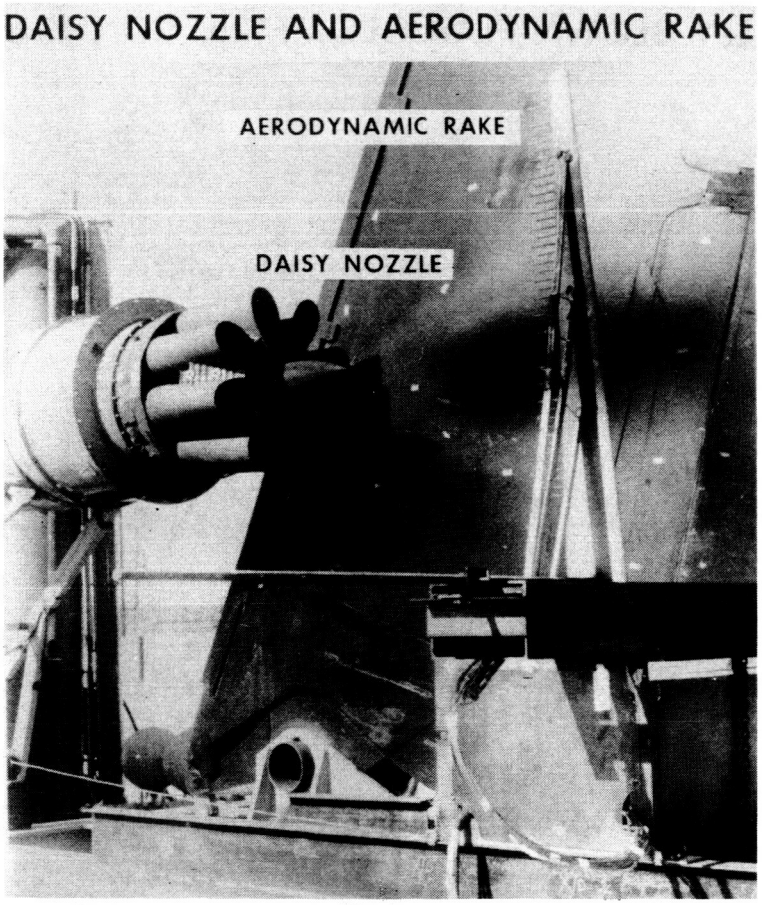

Figure 3

MICROPHONE ARRAY

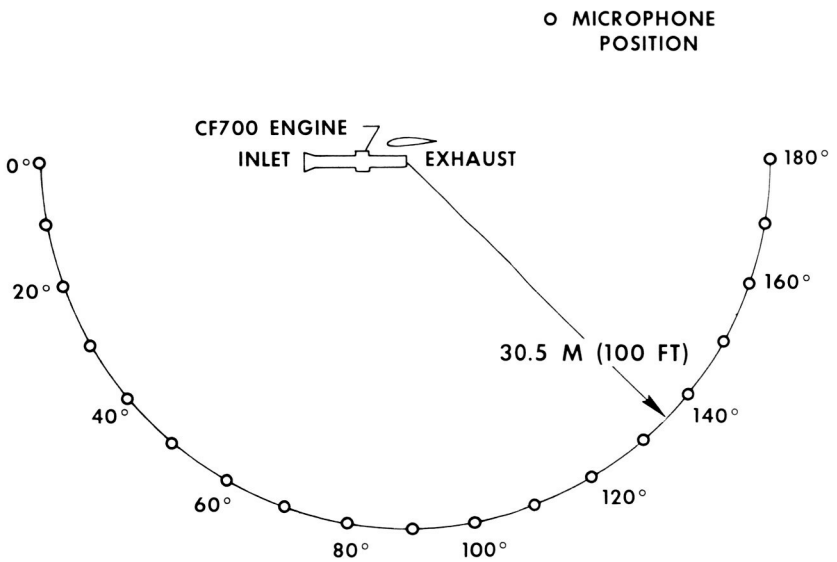

Figure 4

EXTERNALLY BLOWN FLAP GEOMETRIC CONFIGURATION

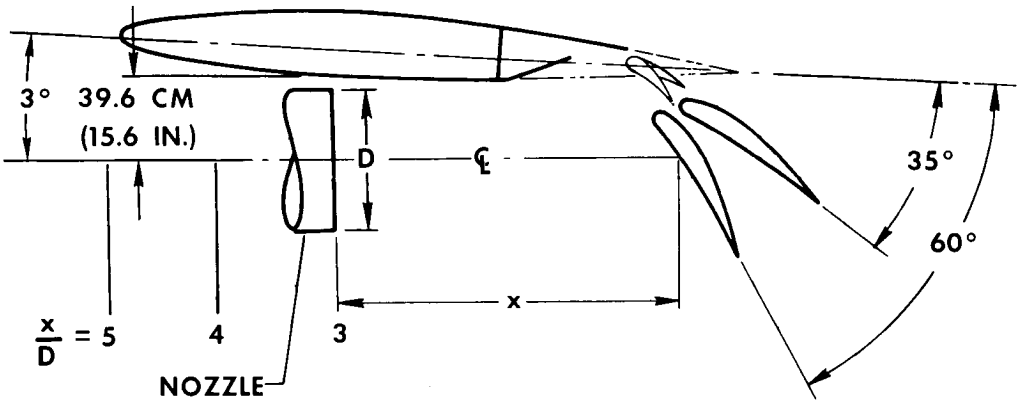

Figure 5

PEAK AXIAL VELOCITY DECAY

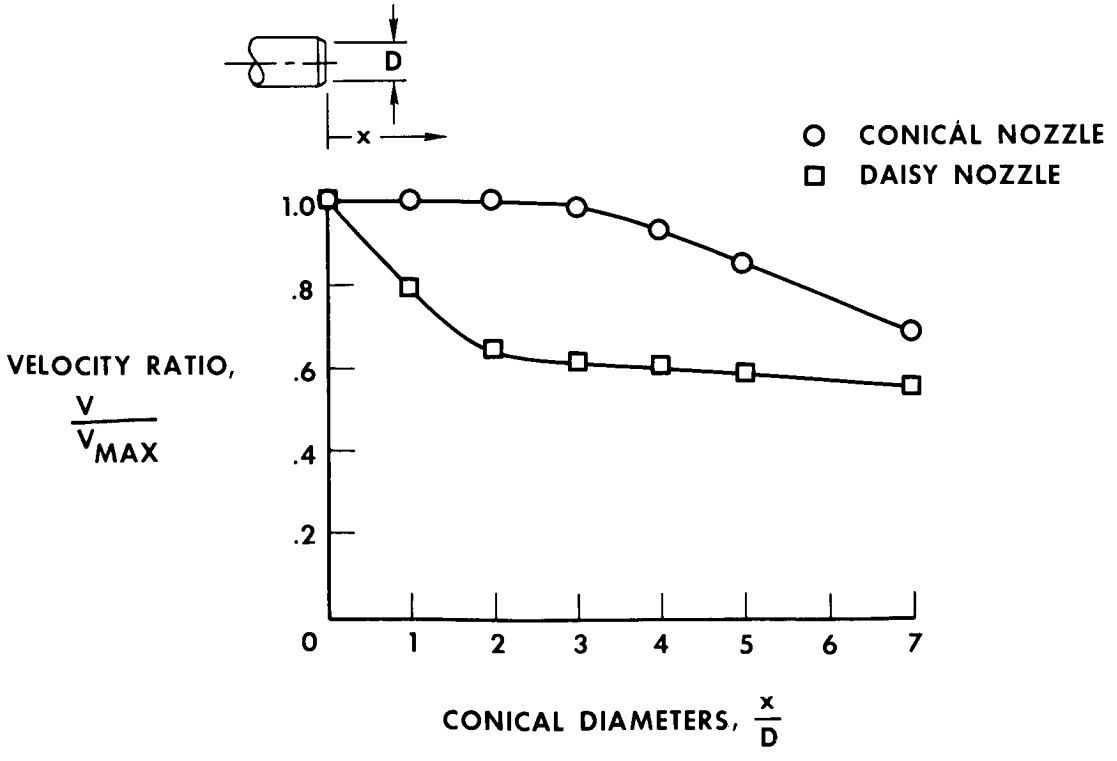

Figure 6

VELOCITY PROFILES

$\frac{x}{D}$ = 4, THRUST = 8230 N (1850 LBF)

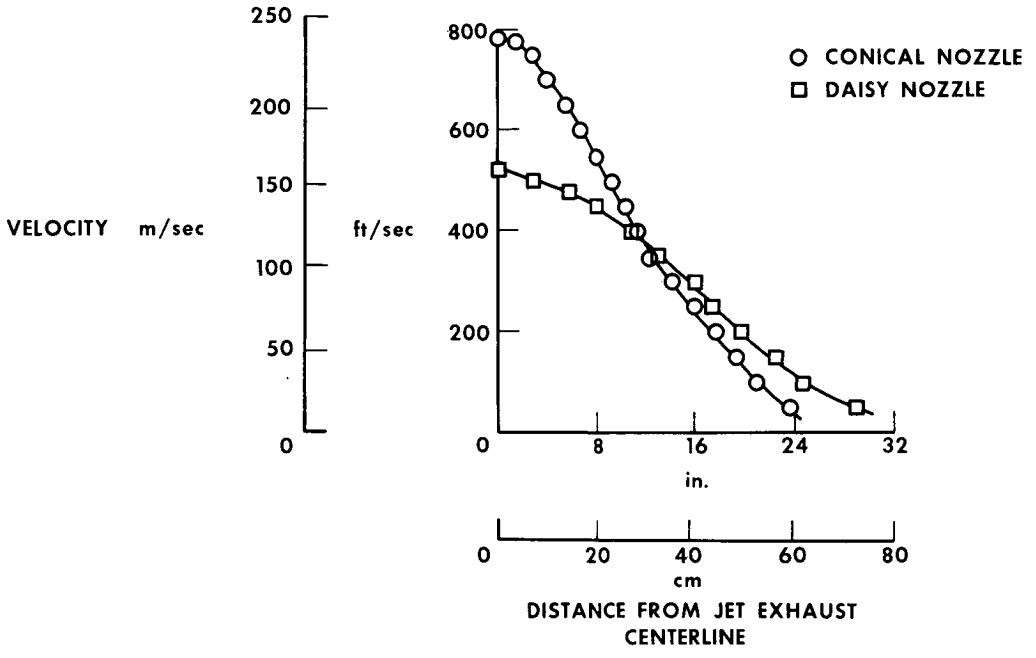

Figure 7

NOISE RADIATION PATTERNS OF CONICAL AND DAISY NOZZLES

30.5 M (100 FT) RADIUS, THRUST = 8230 N (1850 LBF)

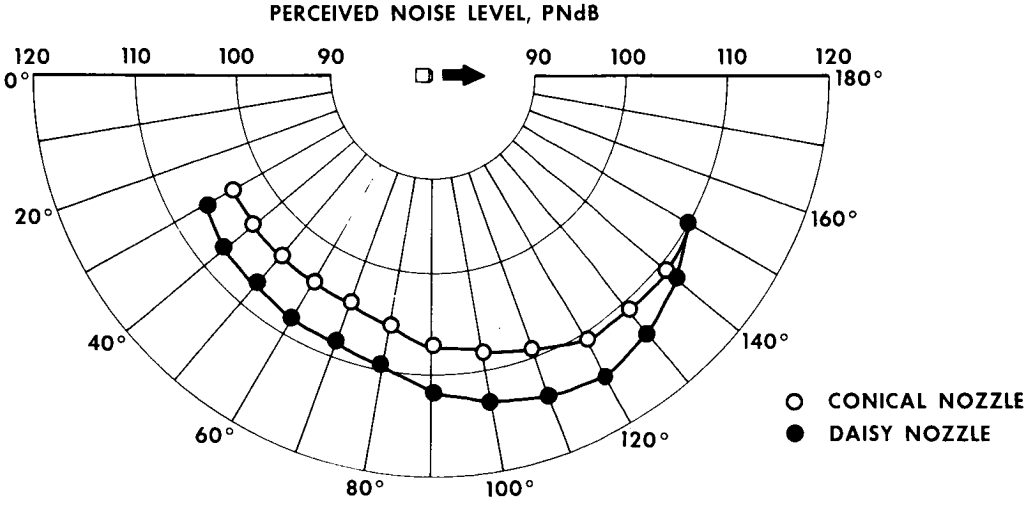

Figure 8

ONE-THIRD OCTAVE BAND SPECTRA OF CONICAL AND DAISY NOZZLES

80° FROM INLET, 30.5 M (100 FT) RADIUS, THRUST = 8230 N (1850 LBF)

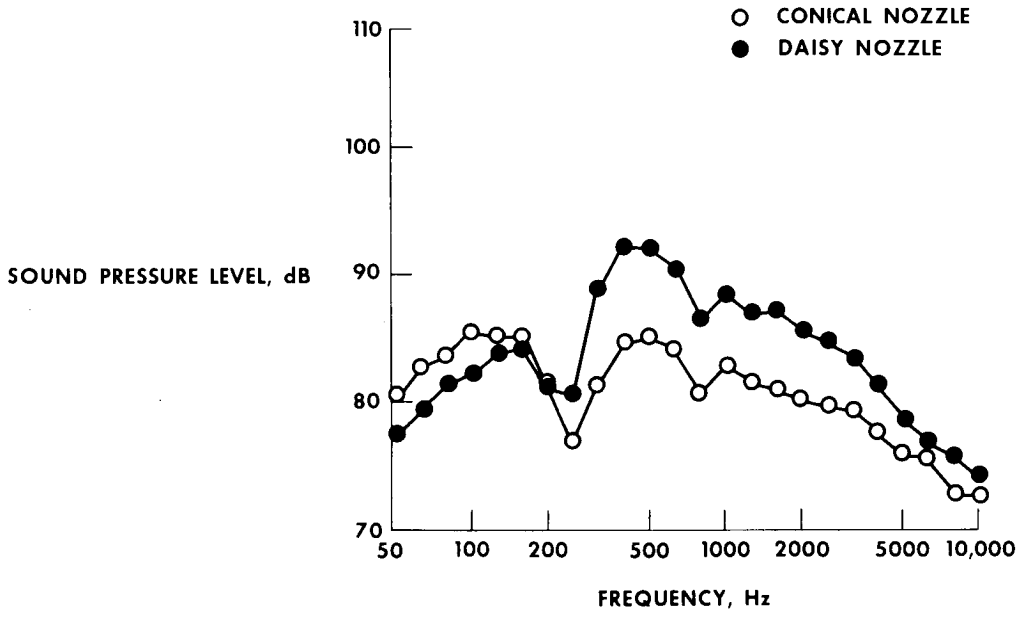

Figure 9

EFFECT OF WING AND FLAPS ON NOISE RADIATION PATTERNS

CONICAL NOZZLE, 30.5 M (100 FT) RADIUS, THRUST = 8230 N (1850 LBF), $\frac{x}{D}$ = 4

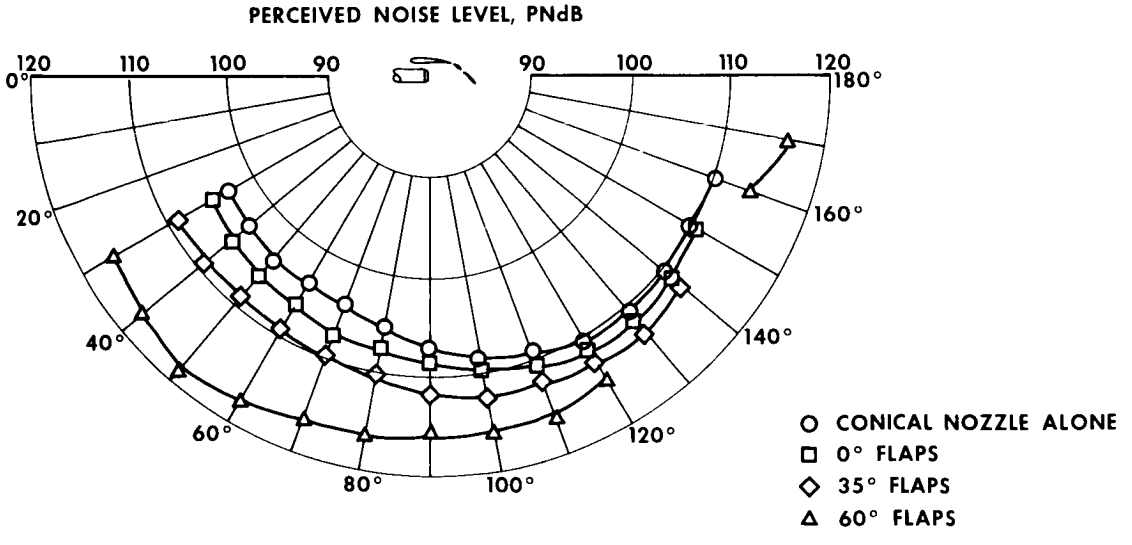

Figure 10

EFFECT OF WING AND FLAPS ON NOISE SPECTRA FOR CONICAL NOZZLE

80° FROM INLET, 30.5 M (100 FT) RADIUS, $\frac{x}{D}$ = 4, THRUST = 8230 N (1850 LBF)

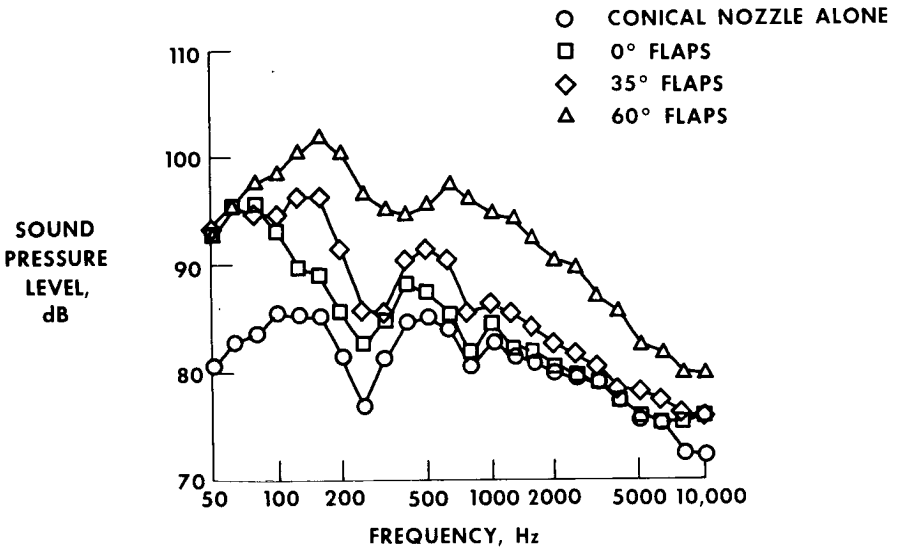

Figure 11

EFFECT OF WING AND FLAPS ON NOISE RADIATION PATTERNS

DAISY NOZZLE, 30.5 M (100 FT) RADIUS, THRUST = 8230 N (1850 LBF), $\frac{x}{D}$ = 4

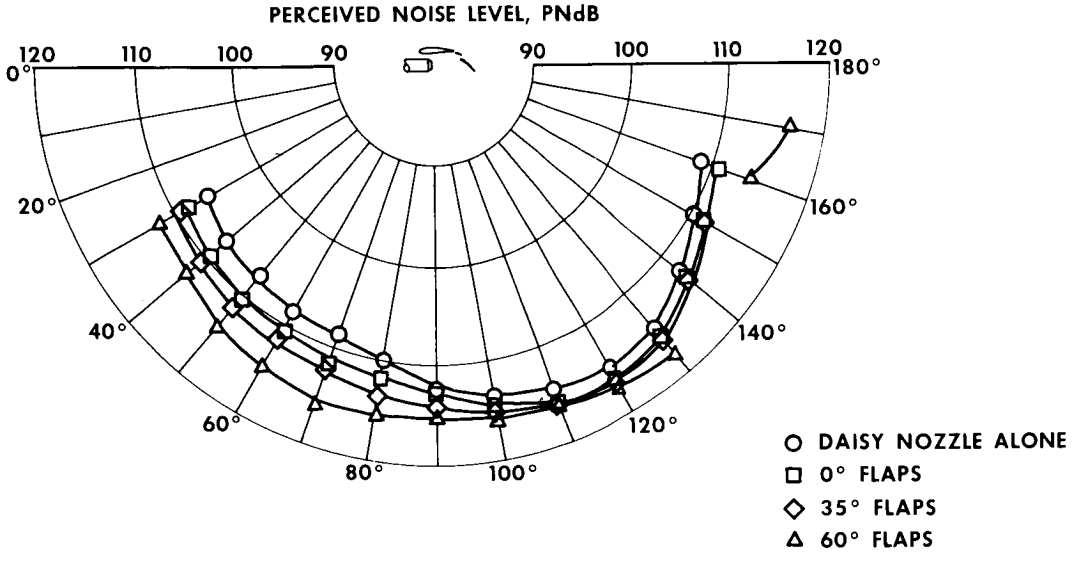

Figure 12

EFFECT OF NOZZLES ON NOISE RADIATION PATTERNS

60° FLAPS, 30.5 M (100 FT) RADIUS, THRUST = 8230 N (1850 LBF), $\frac{x}{D}$ = 4

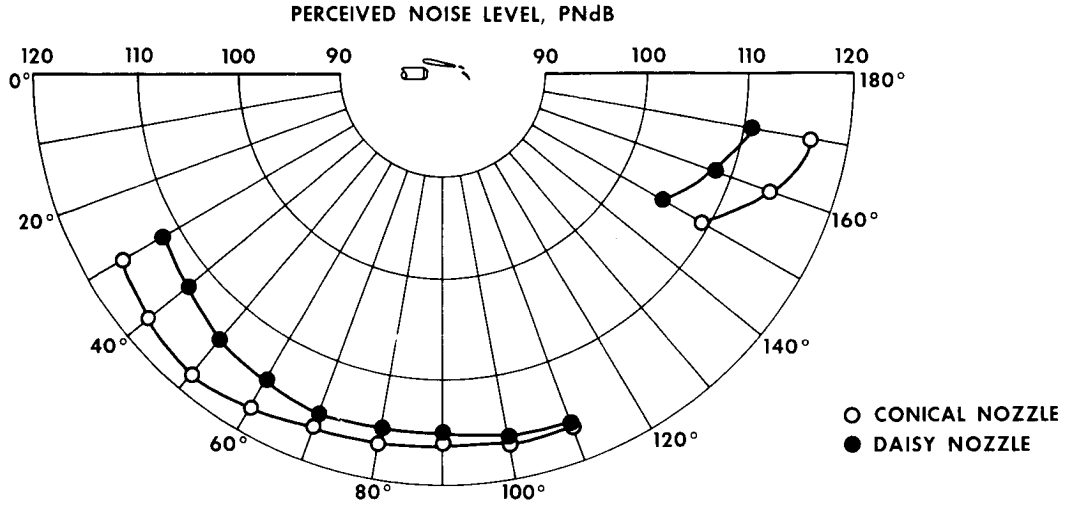

Figure 13

EFFECT OF NOZZLES ON NOISE SPECTRA

60° FLAPS, 80° FROM INLET, 30.5 M (100 FT) RADIUS, THRUST = 8230 N (1850 LBF), $\frac{x}{D}$ = 4

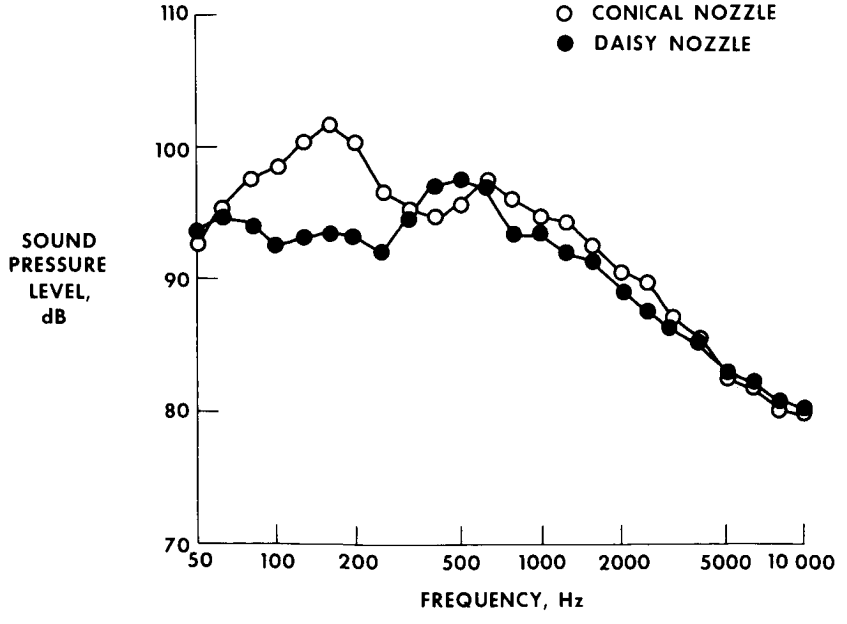

Figure 14

EFFECT OF ENGINE POSITION ON NOISE RADIATION PATTERNS

CONICAL NOZZLE, 60° FLAPS, 30.5 M (100 FT) RADIUS, THRUST = 8230 N (1850 LBF)

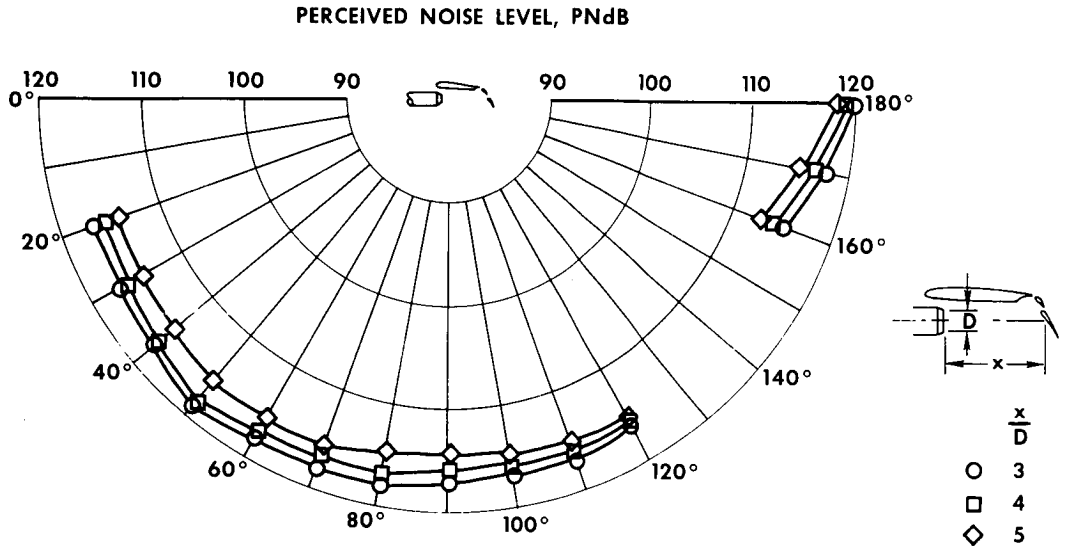

Figure 15

PERCEIVED NOISE LEVELS OF SINGLE- AND DOUBLE-SLOTTED FLAPS

60° FLAPS, 80° FROM INLET, 30.5 M (100 FT) RADIUS, $\frac{x}{D} = 4$

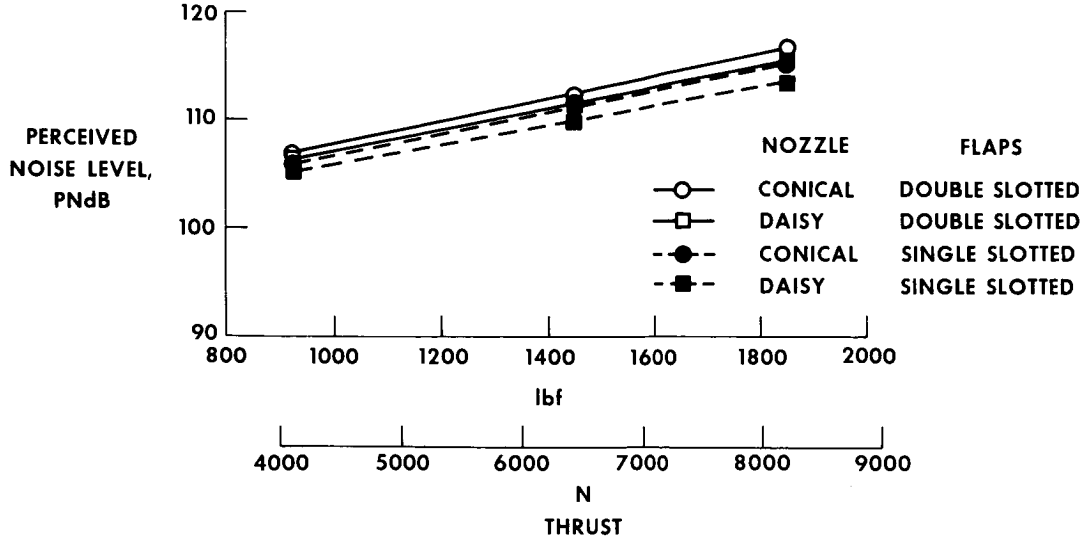

Figure 16

ACOUSTIC CHARACTERISTICS OF LARGE-SCALE STOL MODELS AT FORWARD SPEED

By Michael D. Falarski,
U.S. Army Air Mobility R&D Laboratory

Kiyoshi Aoyagi, and David G. Koenig
NASA Ames Research Center

SUMMARY

This paper presents the results of wind-tunnel investigations of the acoustic characteristics of the externally blown jet flap (EBF) and augmentor wing STOL concepts. The large-scale EBF model was equipped with a triple-slotted flap blown by four JT15D turbofan engines with circular, coannular exhaust nozzles. The large-scale augmentor wing model was equipped with an unlined augmentor blown by a slot primary nozzle.

The effects of airspeed and angle of attack on the acoustics of the EBF were small. At a forward speed of 60 knots, the impingement noise of the landing flap was approximately 2 dB lower than in the static tests. Angle of attack increased the impingement noise approximately 0.1 dB/deg.

Flap deflection had a greater effect on the acoustics of the augmentor wing than did airspeed. For a nozzle pressure ratio of 1.8, the peak perceived noise level of the landing flap was 2 to 3 PNdB higher than that of the takeoff flap. The total sound power was also significantly higher for landing indicating that turning in the augmentor generated acoustic energy. Airspeed produced a small aft shift in acoustic directivity with no significant change in the peak perceived noise levels or sound power levels.

Small-scale research of the acoustics for the augmentor wing has shown that by blowing an acoustically treated augmentor with a lobed primary nozzle, the 95-PNdB noise level goal can be achieved or surpassed.

INTRODUCTION

The acoustic characteristics of STOL aircraft are undergoing extensive investigation because of the low operating noise levels required by their operation near densely populated areas. Much of this research has been under static conditions $(V_\infty = 0)$ with small-scale models (refs. 1 and 2). This paper presents the results of wind-tunnel investigations of two STOL concepts to study the effect of airspeed and angle of attack on their noise characteristics. The investigations were performed in the Ames 40- by 80-foot wind tunnel. The STOL concepts studied were the externally blown flap

(EBF) and the augmentor wing. The models were large scale and had swept wings with spans of approximately 12 m (40 ft). The aerodynamic characteristics were also investigated and are reported in references 3 and 4.

SYMBOLS

A	engine-exhaust exit area, m^2 (ft^2)
q_{flap}	engine-exhaust dynamic pressure at the flap, N/m^2 (psf)
q_J	mean dynamic pressure at exhaust exit, $\frac{T}{2A}$, N/m^2 (psf)
q_∞	free-stream dynamic pressure, $\frac{1}{2}\rho V_\infty^2$, N/m^2 (psf)
T	turbofan gross thrust, N (lb)
V_J	mean velocity at exhaust exit, m/sec (ft/sec)
V_∞	free-stream velocity, knots
α	angle of attack with respect to the wing chord line, deg
δ_f	flap deflection, deg
ρ	air density, kg/m^3 ($slugs/ft^3$)

RESULTS AND DISCUSSION

Externally Blown Flap

The EBF model is shown in the wind tunnel in figure 1. The 57-percent chord, triple-slotted flap is immersed in the exhaust of four JT15D turbofan engines. The flap system is similar to systems being investigated by NASA Lewis and Langley Research Centers. The engine exhaust nozzles are circular coannular type with increased area to produce the required relation between engine diameter and flap chord. The nacelles were not acoustically treated for fan machinery or core engine noise. The wing had a span of 11.6 m (38 ft), a sweep of 25^o, an aspect ratio of 7, and a taper ratio of 0.4.

The model noise was measured with 1.27-cm (1/2-in.) condensor microphones equipped with windshield nose cones. The microphones were mounted along a line under the left wing tip. The noise data were reduced to one-third octave band frequency spectra

by integrating 30-sec data samples on a real-time frequency analyzer. The spectra were corrected for test-section acoustic reverberation (ref. 5) and projected to a 152.5-m (500-ft) radius by use of procedures recommended by the Society of Automotive Engineers. The perceived noise levels were computed from these data.

Effect of flap deflection.- The acoustics of the EBF model are dominated by two noise sources, the fan machinery noise and the flap impingement noise. The fan machinery noise can be seen in figure 2 as the pure tones at the blade passage frequency and its harmonics. The flap impingement noise, created by the interaction of the turbulent engine exhaust and the flap system, can be seen as the broadband noise increase with flap deflection in figure 2. The exact acoustic mechanism generating this noise is not understood. Research has shown that most of the noise is created at the flap leading and trailing edges and the noise is proportional to the sixth power of the impingement velocity.

Effect of forward speed.- Because flap impingement noise is a strong function of the velocity at the flap, any significant effect of forward speed on this velocity should change the EBF noise. Figure 3 shows the dynamic pressure distribution of the inboard JT15D turbofan exhaust near the flap (see fig. 3 inset) for several forward speeds. The general characteristics of the exhaust are not affected by forward speed although the peak dynamic pressure ratio is increased approximately 7 percent. This is a 19-percent increase in the sixth power of the flap velocity, which would tend to indicate that impingement noise would increase with forward speed.

The effect of airspeed on the frequency spectrum for the landing configuration $\left(\delta_f = 15/35/55\right)$ is shown in figure 4. The fan machinery noise decreases with forward speed because fan blade leading-edge and inlet distortion are decreased. The flap impingement noise decreased 2 dB even though the peak velocity at the flap increased. The noise may therefore also be a strong function of jet turbulence, which would be smaller at forward speed, as well as impingement velocity. A more complete investigation of the exhaust plume is required to relate the velocity to the flap noise. The reduction in flap noise with airspeed for the takeoff flap $\left(\delta_f = 0/20/40\right)$ was approximately one-half that for the landing flap.

Effect of angle of attack.- The normal flight range of angle of attack for STOL aircraft will be 0° to 10°. The frequency spectrum for the takeoff flap at $\alpha = 0^\circ$, 8°, and 20° is shown in figure 5. The results indicate an increase in flap noise of approximately 0.1 dB/deg. As shown in figure 6 this is an increase of 1 PNdB or less in perceived noise level for the operational angle-of-attack range.

The fan machinery noise is low in figure 5 because of the high free-stream velocity ratio. At lower velocity ratios, angle of attack created inlet distortion which resulted in a 2 to 3 dB increase in fan noise for an 8° increase in angle of attack.

Augmentor Wing

The acoustic characteristics of the augmentor wing at forward speed were investigated with the large-scale model having a swept augmentor wing shown in figure 7. The wing has an aspect ratio of 8, a taper ratio of 0.3, and a quarter-chord sweep of 27.5^{o}. The 70-percent span augmentor was powered by a slot primary nozzle. The high-pressure air was supplied by two modified Viper compressors driven by a J85 turbojet. The inlets of the compressors and the J85 were acoustically treated, as were the J85 residual-gas tail pipes.

The microphones and data-reduction technique were the same as described for the EBF. The augmentor-wing data have also been scaled to a 150-passenger, 91 000-kg (200 000-lb) aircraft assuming 80 percent of the installed thrust is ducted into the wing.

Effect of flap deflection.- The perceived noise level directivity patterns for the takeoff $\left(\delta_f = 40^{o}\right)$ and landing $\left(\delta_f = 70^{o}\right)$ configurations are shown in figure 8. Deflecting the flap from 40^{o} to 70^{o} while maintaining constant pressure ratio increased the noise in the forward quadrant by 3 PNdB. This trend is also evident in the total sound power level, as shown in figure 9. Since, at high flap deflections, the flap pressure ratio is reduced, this does not necessarily mean the augmentor is noisier at landing. The increase in power shows that the increased turning inside the augmentor generates acoustic energy. It has previously been assumed that any change with flap deflection was simply a redistribution of the sound energy.

Effect of forward speed.- The variation of sound power with forward speed is shown in figure 9. The results show that there is only a very small increase in sound power. The augmentor noise is dominated by the mixing noise of the primary and secondary flows. The very small change in power level indicates that the augmentor maintains the relative velocity constant with airspeed.

The perceived noise level directivity patterns for the landing and takeoff configurations at forward speed are shown in figure 10. The acoustic directivity shifted aft, reducing the front quadrant noise and increasing the aft quadrant noise by 1 to 2 PNdB. The changes in peak perceived noise levels were small: 1 PNdB decrease for takeoff and 1 PNdB increase for landing. As shown in figure 11, any change in perceived noise level results from a change in broadband frequency spectra, indicating a change in acoustic energy from the mixing of the primary and secondary flow in the augmentor.

Augmentor noise suppression.- The noise levels for the full-scale augmentor wing are much higher than the 95-EPNdB STOL noise goal. The Boeing Company, under contract to NASA, has investigated the acoustics and noise-suppression techniques for the augmentor (ref. 6). The results of this research are summarized in figure 12. The initial augmentor designs incorporated a slot primary nozzle. This was used as a baseline for the study. The spectra for this nozzle, which are typical of jet noise, produced a

perceived noise level (PNL) of 116 PNdB. A lobe-type nozzle shifted the peak noise in the spectra to a higher frequency and reduced the PNL by 6 PNdB on a 152.5-m (500-ft) sideline. Installing the untreated augmentor shroud-flap assembly shifted acoustic energy from the high- to the low-frequency bands by reducing the jet relative velocity and creating a lower frequency acoustic source at the augmentor exit. The PNL was reduced to 104 PNdB. The inside of the augmentor was then lined with acoustic absorption material which was tuned to the frequencies containing the most annoying noise. Combining the lobed nozzle with a lined augmentor reduces the noise of the augmentor wing below the 95-PNdB noise level. With this high degree of suppression, some of the characteristics noted earlier in this presentation may change. For example, if the dominant noise source is augmentor-exhaust mixing rather than mixing of the primary and secondary flow, a noise reduction with airspeed would be expected.

CONCLUDING REMARKS

Forward speed reduced the flap impingement noise of the externally blown flap model. The reduction was 2 dB for the landing flap setting and 1 dB for the takeoff flap setting. The effect of angle of attack was to increase the impingement noise by 0.1 dB/deg. From this it can be seen that the effects of flight on an EBF model that has not been acoustically treated are small. These effects apply only for the model and engine configuration discussed herein. The presence of noise-attentuating devices may significantly alter these results.

Flap deflection has a more significant effect than does airspeed on the acoustic characteristics of an augmentor wing with a slot primary nozzle. At a pressure ratio of 1.8, deflecting the flap from 40^{o} to 70^{o} increased the PNL in the forward quadrant by 3 PNdB. This does not, of course, necessarily mean that the landing flap will be noisier. In fact it will probably be quieter because of the reduced throttle setting. This increase was also evidenced in the model sound power, indicating that augmentor turning not only redistributes but also increases the total acoustic energy. Forward speed shifted the acoustic directivity aft by a small amount. The changes in peak PNL were within 1 PNdB. Small-scale static acoustic research has shown that the 95-PNdB noise level can be achieved by the augmentor wing. The augmentor is therefore no longer the dominant noise source of an augmentor wing STOL aircraft. The effect of airspeed on this acoustically treated augmentor will require further investigation.

REFERENCES

1. Dorsch, Robert G.; Kreim, Walter J.; and Olsen, William A.: Externally-Blown-Flap Noise. AIAA Paper No. 72-129, Jan. 1972.

2. Dorsch, Robert G.; Kresjsa, Eugene A.; and Olsen, William A.: Blown Flap Noise Research. AIAA Paper No. 71-745, June 1971.

3. Aoyagi, Kiyoshi; Falarski, Michael D.; and Koenig, David G.: Wind-Tunnel Investigation of a Large-Scale 25^{o} Swept-Wing Jet Transport Model With an External Blowing Triple-Slotted Flap. NASA TM X-62,197, 1972.

4. Falarski, Michael D.; and Koenig, David G.: Longitudinal and Lateral Stability and Control Characteristics of a Large-Scale Model With a Swept Wing and Augmented Jet Flap. NASA TM X-62,145, 1972.

5. Falarski, Michael D.; Koenig, David G.; and Soderman, Paul T.: Aspects of Investigating STOL Noise Using Large-Scale Wind-Tunnel Models. NASA TM X-62,164, 1972.

6. O'Keefe, J. V.; and Kelly, G. S.: Design Integration and Noise Studies for Jet STOL Aircraft. Vol. I – Program Summary. D6-40552-1 (Contract NAS2-6344), Boeing Co., May 1972. (Available as NASA CR-114471.)

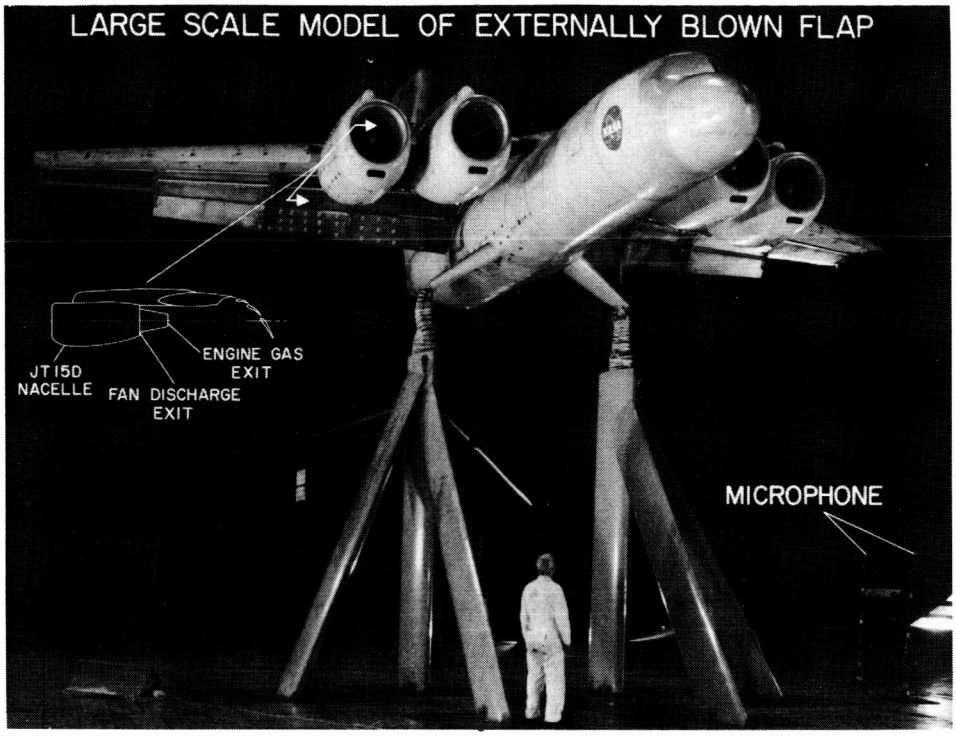

Figure 1

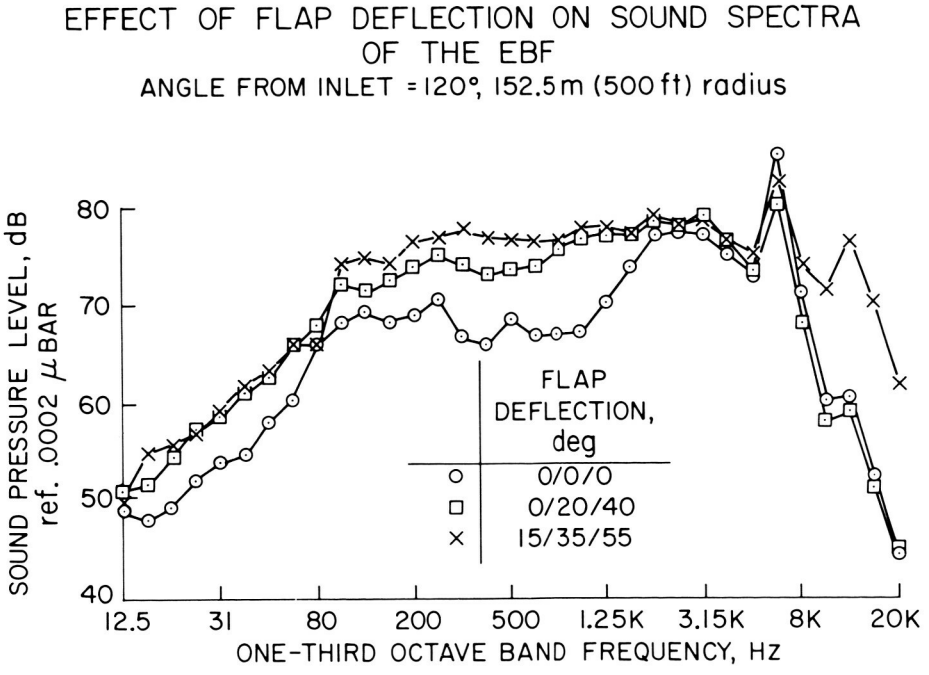

Figure 2

EXHAUST VELOCITY PROFILE AT THE FLAP OF EBF

1.65 DIA. FROM EXHAUST NOZZLE, LANDING FLAP

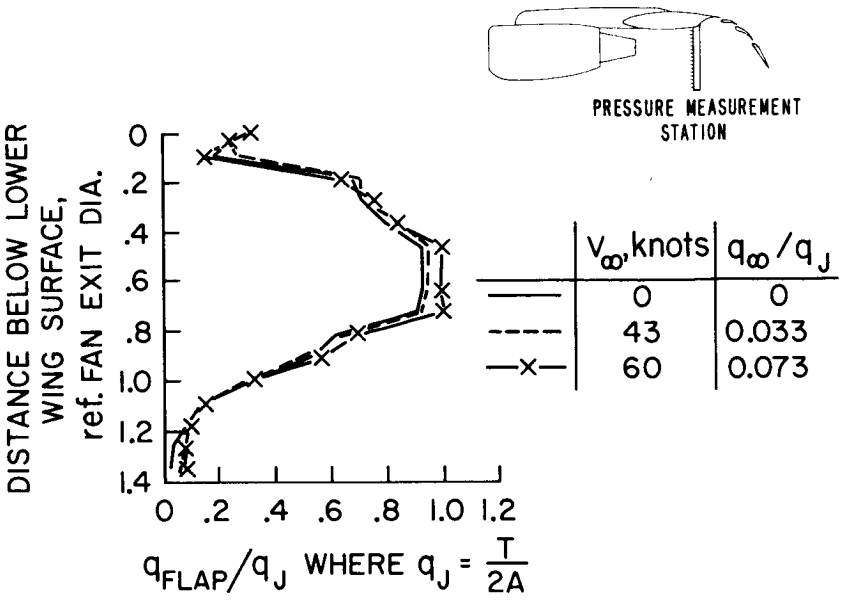

Figure 3

EFFECT OF AIRSPEED ON SOUND SPECTRA OF THE EBF

LANDING FLAP, ANGLE FROM INLET = 120°, 152.5 m (500 ft) radius

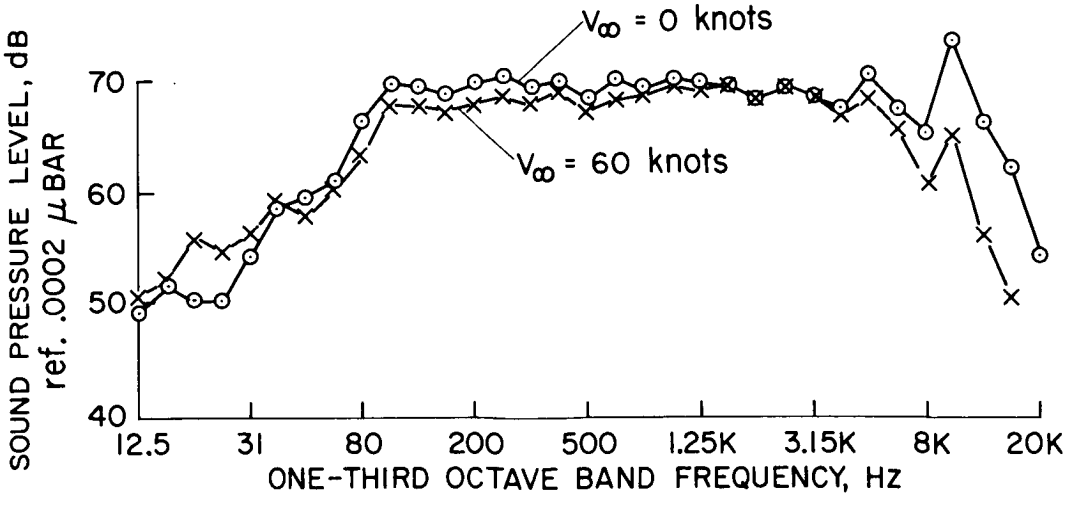

Figure 4

SOUND SPECTRA OF EBF AT SEVERAL ANGLES OF ATTACK

TAKEOFF FLAP, $V_\infty / V_J = 0.29$, 152.5 m (500 ft) radius

ANGLE FROM INLET = 120°

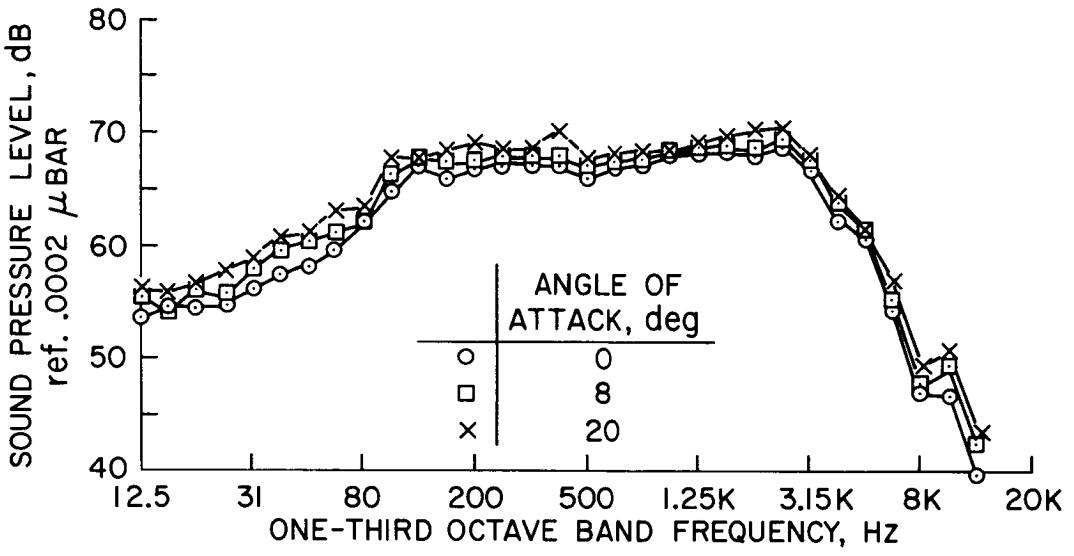

Figure 5

EFFECT OF ANGLE OF ATTACK ON PERCEIVED NOISE LEVEL OF THE EBF

TAKEOFF FLAP, $V_\infty / V_J = 0.29$, 152.5 m (500 ft) radius

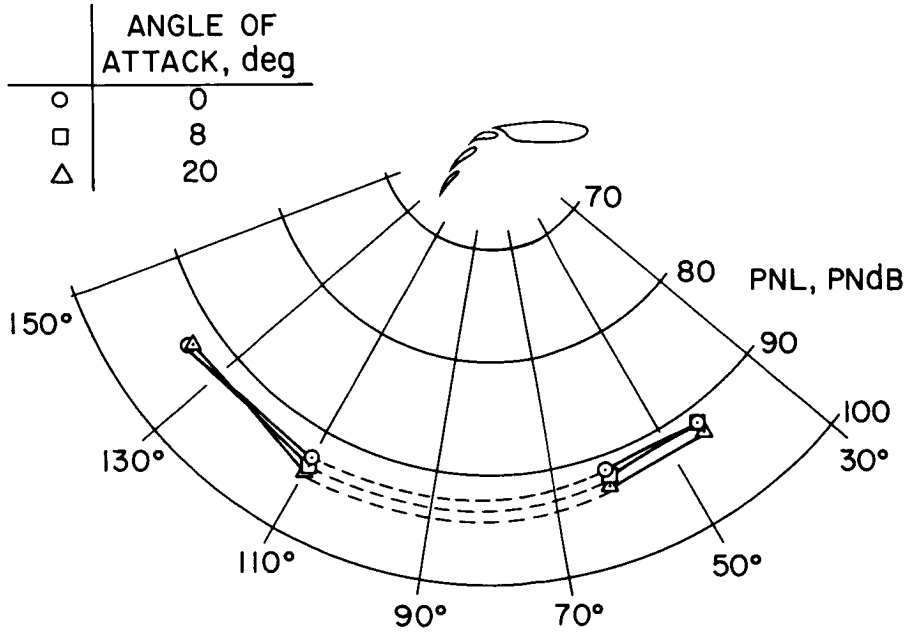

Figure 6

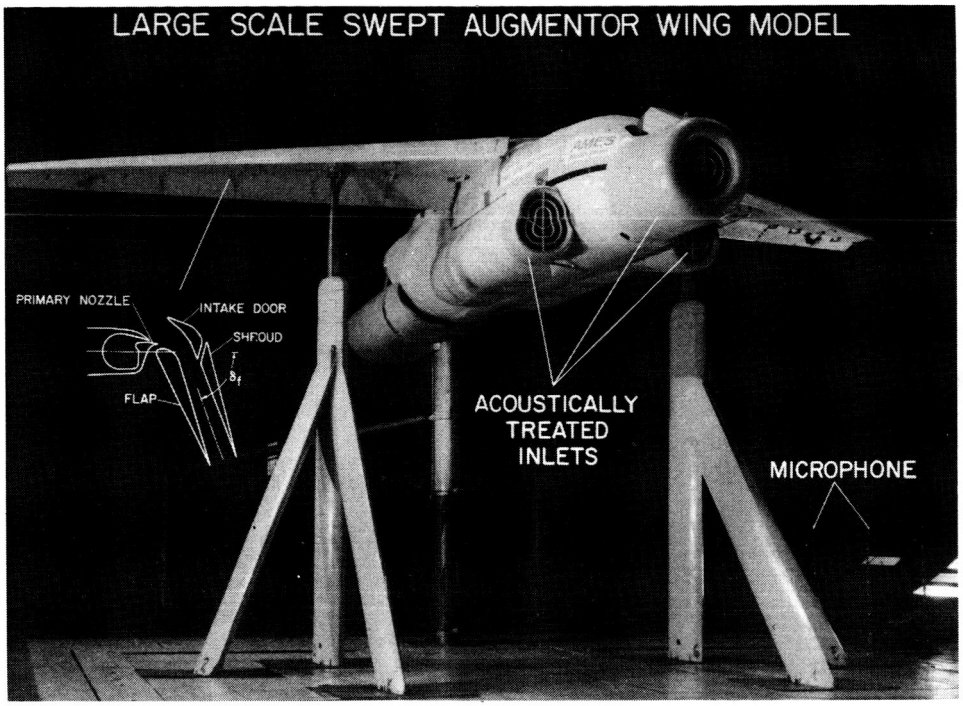

Figure 7

EFFECT OF FLAP DEFLECTION ON ACOUSTIC DIRECTIVITY OF THE AUGMENTOR WING

PRESSURE RATIO = 1.9, V_∞ = 0, 152.5 m (500 ft) FROM 150 PASSENGER AIRCRAFT

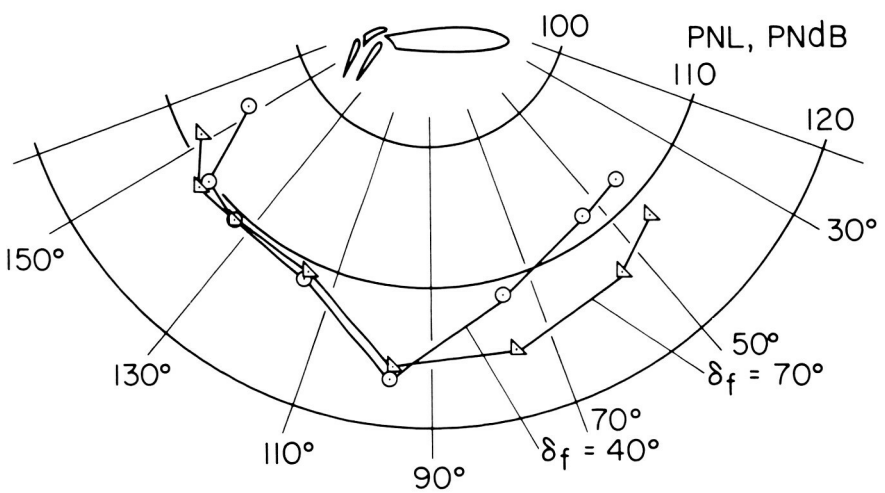

Figure 8

EFFECT OF FLAP DEFLECTION ON SOUND POWER LEVEL OF AUGMENTOR WING

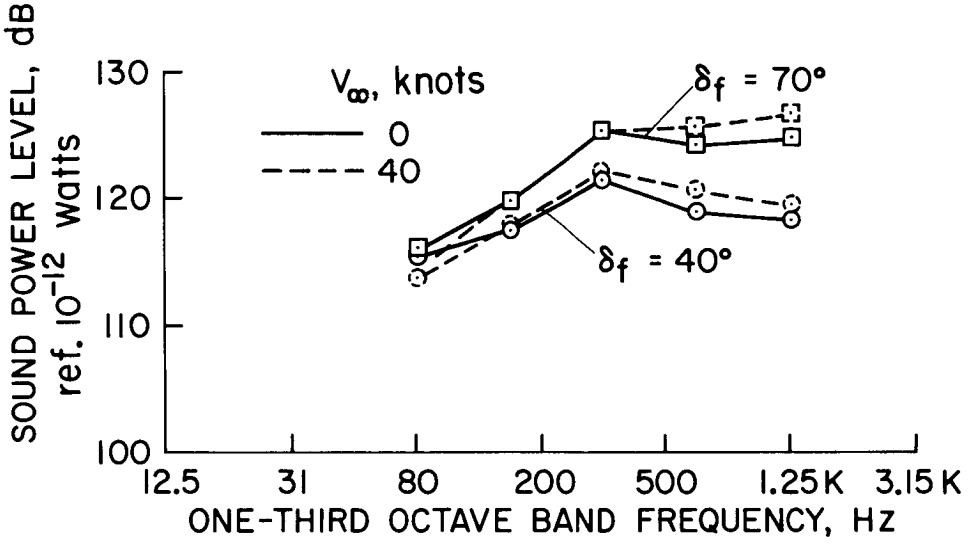

Figure 9

EFFECT OF AIRSPEED ON PERCEIVED NOISE OF THE AUGMENTOR WING
PRESSURE RATIO = 1.9, 152.5 m (500ft) FROM 150 PASSENGER AIRCRAFT

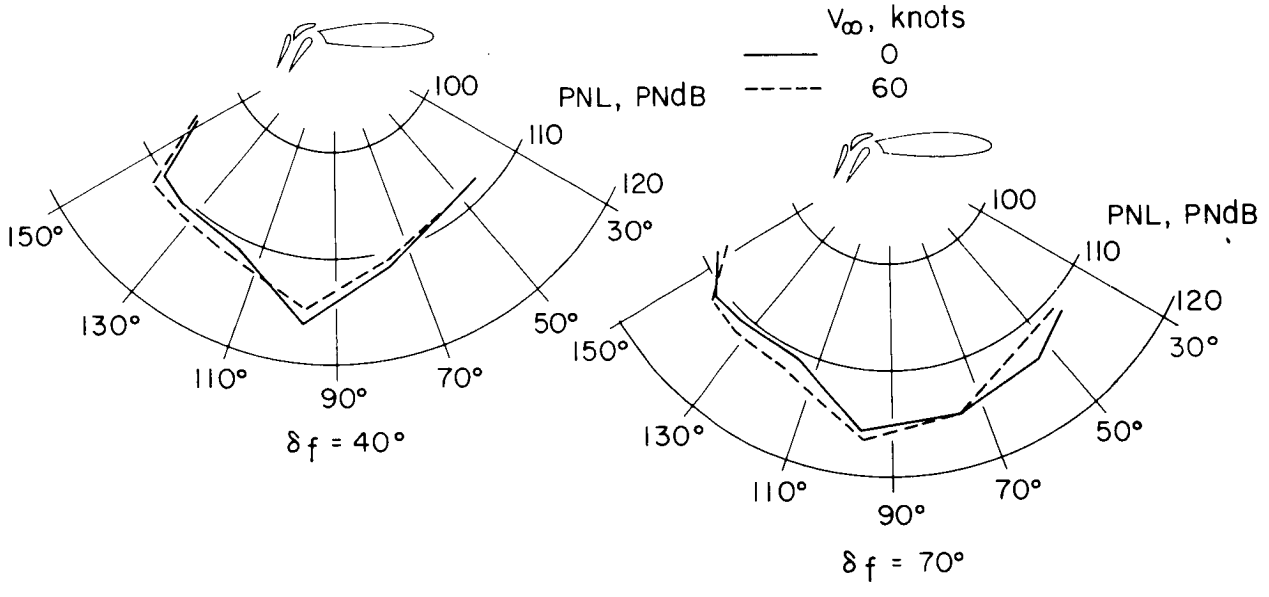

Figure 10

AUGMENTOR WING SOUND SPECTRA AT FORWARD SPEED
152.5 m (500 ft) FROM 150 PASSENGER AIRCRAFT, 83° FROM INLET

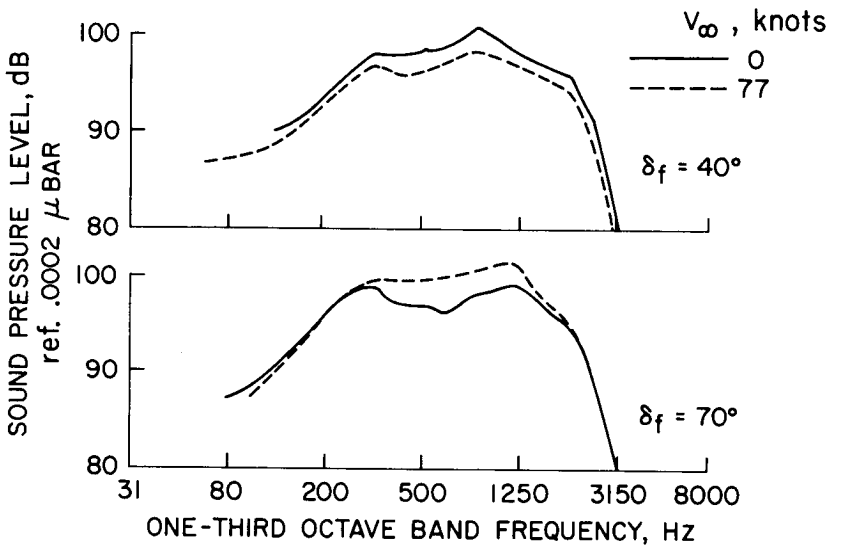

Figure 11

SUMMARY OF AUGMENTOR WING NOISE REDUCTION

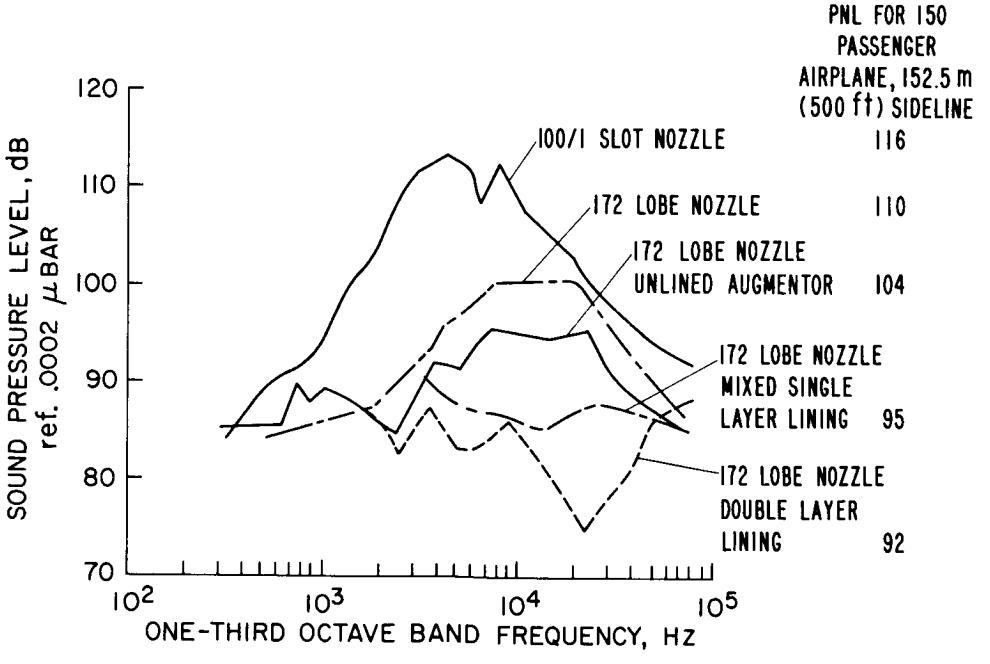

Figure 12

EBF NOISE TESTS WITH ENGINE UNDER-THE-WING AND OVER-THE-WING CONFIGURATIONS

By Robert G. Dorsch and Meyer Reshotko
NASA Lewis Research Center

INTRODUCTORY REMARKS

The contents of this paper can be summarized as follows: For the engine under-the-wing system the recent TF-34 flap-noise data are discussed first. These data are from static tests similar to those described by Paul Lasagna (paper no. 30) of Flight Research Center. Next, noise data obtained during a free-jet forward-speed-effect study are presented. These data supplement the Ames 40- × 80-foot wind tunnel results described by Michael Falarski (paper no. 31). A major shift to discussion of the engine over-the-wing system is then made. Some of the noise sources associated with this system, which employs upper surface flap blowing, were described by David Chestnutt in paper no. 29. The results of a small-scale-configuration screening study are presented first, followed by some recent large-scale-model test data. Finally, the noise data from the engine over-the-wing and the engine under-the-wing systems are compared.

ENGINE UNDER-THE-WING SYSTEMS

An under-the-wing view of the TF-34 externally blown flap (EBF) test rig located at the Flight Research Center is shown in figure 1(a). This noise test was part of the TF-34 program discussed by Richard Goldman in the Engine Noise Technology Panel Discussion (paper no. 28). The vertically mounted swept wing had a large triple-slotted-flap system. The wing chord length was 13 feet, and the section span was 11 feet. The engine centerline was located 9 feet above grade. The microphones were placed on a 100-foot semicircle in a plane parallel to the ground and passing through the engine centerline.

The rear view of the test rig (fig. 1(b)) shows the separate flow exhaust nozzle of the TF-34 engine directed at the deployed flap system. The acoustic treatment of this engine and the large amount of fan and core noise suppression achieved were described by Goldman. Flap-noise tests were run with the three flaps in the retracted position, the 0°-20°-40° takeoff position, and the 15°-35°-55° approach position.

Noise radiation patterns at 100 feet from the test rig are shown in figure 2 for a takeoff thrust level of 7760 pounds. The perceived noise level is given as a function of angle from the engine inlet. Ninety degrees is directly below the wing. Data are shown

for the engine alone, with flaps retracted, and with flaps at the 0°-20°-40° takeoff position. It is clear that there is a large increase in noise below the wing when the flaps are lowered into the engine exhaust. For example, at 90° there is an 8-perceived-noise-decibel (PNdB) increase in noise as the flaps are lowered from the retracted to the takeoff position.

This large increase in noise is clearly seen in the sound-pressure-level one-third-octave spectra (fig. 3). Data for the engine alone and for the takeoff flap setting are shown at 90° from the engine inlet for the same test conditions. The spectra show that the flap interaction noise is very broadband and peaks at about 100 hertz. The sound can best be described as a loud, low-frequency rumble.

Before the TF-34 tests, data were obtained at the Lewis Research Center with a one-half-scale model of the EBF system (fig. 4). The engine exhaust was simulated by a cold-air jet from a one-half-scale model of the TF-34 coannular nozzle. The wing section had an earlier double-slotted version of the flap system.

Because many of the early EBF noise estimates were based on the one-half-scale-model data, it is of interest to compare the results. The 500-foot perceived noise levels measured in the two tests are shown in figure 5 as a function of core-exhaust velocity. The recent TF-34 test data are shown as open symbols. The solid symbols denote the one-half-scale-model data scaled up to TF-34 size and test conditions by using simple noise scaling laws. The agreement is good – particularly at the higher exhaust velocities. At low core-exhaust velocities the TF-34 data are louder than predicted by the one-half-scale data. This results primarily from the fact that at low core velocities the TF-34 has a considerably higher ratio of fan-exhaust to core-exhaust velocity than the one-half-scale model. Thus, the new data lend credence to the early estimates that in order to meet STOL noise goals some form of flap-noise suppression will be required whenever engine-exhaust velocities are above approximately 600 feet per second.

Consider now the EBF airspeed-effect test (fig. 6). A 13-inch-diameter free jet was used to simulate airplane forward speed. A one-thirteenth-scale EBF model was mounted on the free-jet nozzle as shown (upper surface of the wing shown in photograph). The model support structure is outside the boundaries of the simulated airstream. The EBF model had a 2-inch-diameter convergent nozzle and a 13-inch wing chord.

Typical effects of airspeed on noise spectra below the wing are shown in figure 7. The spectra were measured at 100° from the inlet for a nozzle exhaust velocity of 835 feet per second. Data are shown for a 10°-20° flap setting and for the nozzle alone for both the static (or zero airspeed) condition and for an airspeed of 100 knots. The nozzle data show that the high-frequency noise is reduced by 5 or 6 decibels at 100 knots. For the EBF model the noise at 100 knots decreased by 2 to 3 decibels over much of the spectrum.

Now consider an EBF system that employs a mixer-decayer nozzle to reduce the flap-impingement velocity. In paper no. 30 Paul Lasagna presented some noise data for an EBF with a Daisy mixer nozzle. In the present test an eight-tube mixer nozzle was used. The EBF model with an eight-tube mixer nozzle is shown mounted in the free-jet test rig (fig. 8). The jet-exhaust decay characteristics of this nozzle were investigated in the Lewis 6- × 9-foot tunnel. The exhaust velocity decay ratio V/V_j is plotted against distance X from the nozzle exit plane for static conditions and for a tunnel airspeed of 100 knots (fig. 9). The distance scale is in terms of the equivalent diameter D_E of the eight-tube nozzle. The X/D_E of the EBF model at the flap station is 9.5. With zero airspeed the velocity decay is 0.35. At 100 knots the decay is changed to 0.43. In terms of the effect on flap-impingement noise, this change would predict a 5-decibel increase in flap noise at 100 knots airspeed.

Typical noise data at 100^o from the inlet are shown in figure 10. The nozzle exhaust velocity was 835 feet per second. The data for a 10^o-20^o flap setting actually show a 4-decibel decrease in high-frequency noise at 100 knots. This decrease in EBF noise is somewhat surprising in view of the fact that the eight-tube mixer nozzle has less velocity decay at 100 knots. The reduction in EBF noise with airspeed is partially related to the noise characteristics of the mixer nozzle. At static conditions the mixer nozzle installed below the wing contributes approximately one-half of the total noise at high frequencies. From the mixer-nozzle-alone data, it is seen that, because of relative velocity effects, the nozzle high-frequency noise has decreased considerably at 100 knots. This decrease in nozzle noise, however, accounts for only part of the decrease in total EBF noise. A possible explanation is that the noise generated at the flaps is lower at 100 knots because of a reduction in the turbulence intensity in the shear layer mixing region of the impinging jet or because of a reduction in the velocity gradient at the trailing edges of the flaps, or both.

The preliminary results of this airspeed-effect study indicate that an EBF airplane with conventional exhaust nozzles would be about 2 to 3 PNdB quieter at 100 knots than would be expected from static noise tests. If a mixer-decayer nozzle is used, the reduction would be about 1 PNdB. Very similar results were found in the 40 × 80 wind tunnel tests described by Falarski (paper no. 31).

ENGINE OVER-THE-WING SYSTEMS

Some possible engine over-the-wing EBF configurations are shown in figure 11. The engine over-the-wing configurations employ upper surface flap blowing. A configuration screening study was conducted with one-thirteenth-scale models having the configurations shown in this figure. The engine exhaust was simulated by an ambient-temperature air jet.

The first configuration shown is for an engine having a slot-shaped exhaust nozzle. The exhaust nozzle is located close to the wing surface to facilitate flow attachment.

The second configuration uses a conventional circular nozzle with a flow deflector to turn the flow toward the flaps. The flow deflector is retracted for cruise or CTOL flight. The flow deflector can also be designed to convert to a thrust reverser after touchdown.

The third configuration has a slot nozzle assembly that can be canted downward toward the flap system to obtain flow attachment. The nozzle is rotated back to its cruise position as the flaps are retracted.

The lower sketch in figure 11 shows a slot nozzle in combination with sideplates or wing fences to facilitate flow attachment.

Good flow attachment to the flaps is required for powered lift. The screening tests, therefore, included measurements of static turning effectiveness. A one-thirteenth-scale model with a 5 to 1 slot nozzle is shown in figure 12 suspended in the force balance of the lift-thrust rig. The lift and thrust forces were measured with load cells.

Static turning efficiencies are shown in figure 13 for the flaps in the 10^{o}-20^{o} takeoff position. The flap slots were covered in all cases shown. The ordinate is the measured lift force divided by the nozzle-alone thrust. The abscissa is the forward thrust divided by the nozzle-alone thrust. The turning angle is measured with respect to the engine axis. Data are shown for four configurations, which are listed in the same order as in figure 11. The configurations have a 10 to 1 aspect ratio slot nozzle, a circular nozzle with deflector, a canted 5 to 1 slot nozzle, and a 5 to 1 slot nozzle with sideplates. Good attachment was achieved, and the flow turned approximately 30^{o} in all cases. Static turning efficiencies between 0.77 and 0.93 are indicated. These values are similar to those obtained with various engine under-the-wing EBF models (e.g., paper no. 5).

Now look at the corresponding data for a 30^{o}-60^{o} flap position (fig. 14). This setting would be typical for landing. At this larger turning angle the circular nozzle with deflector and the canted 5 to 1 slot nozzle configurations still have very good flow attachment. The turning angle is about 60^{o}, and the efficiencies are nearly the same as for the lower flap-angle case. However, the data for the 10 to 1 slot nozzle with no attachment device and for the 5 to 1 slot nozzle with sideplates indicate that the flow attachment was not as good at this flap setting. The lift factors for these two cases, however, are roughly comparable with that for the circular nozzle with deflector case.

The turning effectiveness data in figures 13 and 14 were for configurations having the flap slots covered. In general, flow attachment under static conditions was not very sensitive to whether or not the slots were covered. The noise on the other hand was very sensitive. The effects of slot covering on the spectra below the wing at 100^{o} are shown

in figure 15. The data are for the circular nozzle with deflector configuration. The data with slots open are indicated by the solid symbols. With slots open there was a large increase in noise generation in the midfrequency range. This caused a 4.5-decibel increase in the overall sound pressure level. Because of this large effect on noise, only data for engine over-the-wing configurations having covered slots are presented from this point on.

A closer look at the noise spectra for the circular nozzle plus deflector configuration is given in figure 16. The data are at 80° from the inlet for a 30°-60° flap setting. The exhaust velocity was 585 feet per second. The lower (solid) curve is for jet noise from the 2-inch-diameter nozzle alone. When a flow deflector is attached to the nozzle, there is a large increase in noise, as can be seen from the dashed curve. When the nozzle plus deflector is placed above the wing, one obtains the spectra shown by the triangular data points. These results show that much of the high-frequency deflector noise is shielded by the wing. Further, when the exhaust flow is attached to the flap system, there is a large increase in low-frequency noise. This noise is associated with flow turning and probably originates at the flap trailing edge.

Noise spectra for the 5 to 1 slot nozzle with various attachment devices are shown in figure 17 at 120° from the inlet for the 10°-20° flap position and an exhaust velocity of 750 feet per second. The jet noise for the slot nozzle alone is given by the solid curve. With no device the flow does not attach, and the spectrum is shown by the circular data points. There is only a small increase in low-frequency noise without attachment. At high frequencies the wing shields some of the nozzle exhaust noise. Canting the nozzle toward the flaps or using sideplates resulted in flow attachment. With flow attachment there is again a large increase in low-frequency noise. The figure shows that the device used to obtain attachment has only secondary effects on the flap noise.

Flap-noise data for three good attachment cases are summarized for takeoff conditions in figure 18. The spectral data are for the circular nozzle with deflector, the 5 to 1 canted slot nozzle, and the 10 to 1 slot nozzle configurations. The spectra have generally similar shapes and levels, with the 10 to 1 slot nozzle configuration being the quietest. The data points for the circular nozzle with deflector fall in the middle and are surprisingly close to the 10 to 1 slot nozzle results.

In order to evaluate scale effects, noise tests are currently being run at Lewis with a one-half-scale engine over-the-wing model employing a circular nozzle with deflector (fig. 19). The model is geometrically identical to the one-thirteenth-scale model and is $6\frac{1}{2}$ times as large. The one-half-scale model has a wing chord length of 7 feet and a 13-inch-diameter circular nozzle. The wing section is mounted vertically and has a span of 9 feet. The flaps are shown in the 30°-60° position with the slots covered. The nozzle is supplied by dried pressurized air at ambient temperature.

Typical noise spectra at 50 feet and 90° from the inlet are shown for the one-half-scale model with the flaps in the 30°-60° position (fig. 20). The nozzle exhaust velocity was 680 feet per second. The data are for the nozzle alone, nozzle and deflector, and nozzle plus deflector and wing. As noted with the one-thirteenth-scale model, there is a large increase in noise when the deflector is added to the nozzle. However, again, the wing shields much of this noise from the ground observer at all frequencies above 400 hertz. Also, as noted with the small model there is a large increase in low-frequency noise. Thus, the large-model results are very similar to those obtained with the small model if one allows for the shift of the spectrum to lower frequencies. One-half-scale-model data are currently being obtained with smaller flap-deflection angles more typical of the takeoff setting. A preliminary analysis of data with flaps in the 10°-20° position indicates that the magnitude of the shielding effect is comparable with the 30°-60° results.

COMPARISON OF SYSTEMS

Engine over-the-wing EBF noise data are compared in figure 21 with engine under-the-wing data for the same one-half-scale wing and 13-inch-diameter convergent nozzle. The triangular symbols are the upper surface blowing data points for the nozzle with deflector over the wing. The noise data at the same test conditions with lower surface blowing are shown by the square symbols. Because of the shielding effect of the wing, upper surface blowing is about 8 decibels quieter than lower surface blowing over most of the spectrum.

The effects of shielding and reflection by the wing flap system can be seen more clearly in figure 22. The perceived-noise-level radiation patterns at 500 feet for the two systems are compared in polar form. The data points for the EBF model with upper surface blowing are shown as solid triangles. The lower surface blowing data are shown by the open squares. The engine over-the-wing system is clearly quieter below the airplane and noisier above. At 90° (or directly below the wing) the flap noise is about 8 PNdB quieter with upper surface blowing.

A comparison of perceived-noise-level data at 500 feet for the two one-half-scale EBF models as a function of nozzle exhaust velocity is presented in figure 23. The flaps were at the 30°-60° position in both tests, and the flow turning angles were comparable. The test data for lower surface blowing are given by the circular symbols. The upper surface blowing data are given by the triangles. In each case, the data are for the microphone angle which gives the maximum PNL during flyover. The two curves are nearly parallel, showing the same strong dependence of the noise level on exhaust velocity. Because of shielding, the upper surface blowing data at this flap setting are about 9 PNdB quieter over the velocity range shown. At smaller flap-angle settings the differences may be somewhat less. These test results also indicate that, although upper surface blowing

is quieter for a given exhaust velocity and flow turning angle, both EBF systems will require some form of flap-noise suppression at the higher exhaust velocities.

SUPPRESSING FLAP NOISE

The powered-lift noise test results presented in this paper and in previous papers (paper nos. 29, 30, and 31) indicate that further work is needed on flap-noise suppression. Methods of suppressing the augmentor wing noise were described by Falarski in paper no. 31.

Some possible methods of suppressing EBF noise are summarized as follows: One method is to modify the engine cycle in order to reduce engine-exhaust velocity. This requires development of very-high-bypass-ratio engines with low-pressure-ratio fans. This subject is considered in detail in paper no. 33. Another method, which is discussed in this paper and by Lasagna in paper no. 30, is to reduce the flap-impingement velocity by using a mixer-decayer nozzle. The third method is to use some form of flap surface treatment to try to reduce the noise at the source. Finally, the use of various forms of trailing-edge flap blowing is being investigated. A research study to determine the potential of the last two methods was described by Chestnutt in paper no. 29. Whatever method is tried, the object is to suppress the flap noise associated with powered lift without seriously impairing the high lift-drag ratio or the engine thrust at takeoff. In addition, the EBF system must have acceptable cruise efficiency when the flaps are retracted.

TF-34 EXTERNALLY BLOWN FLAP NOISE TEST

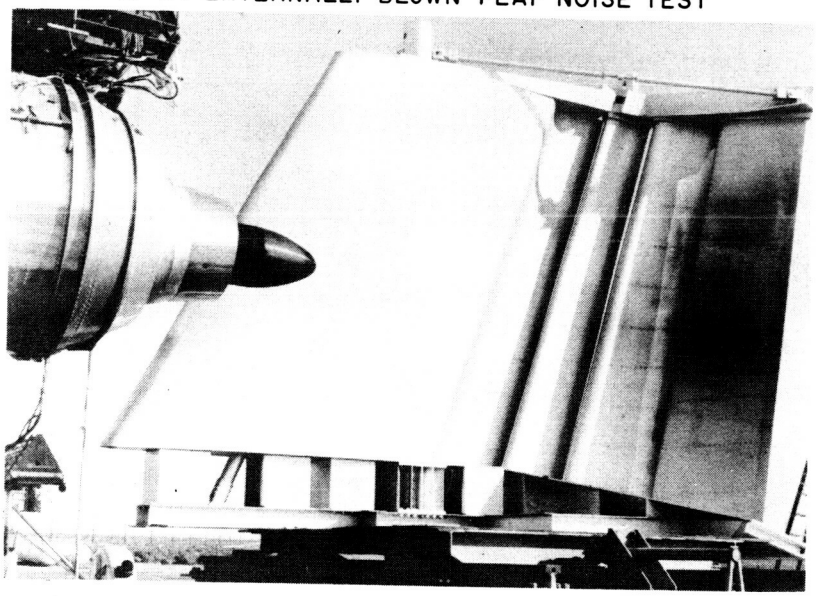

(a)

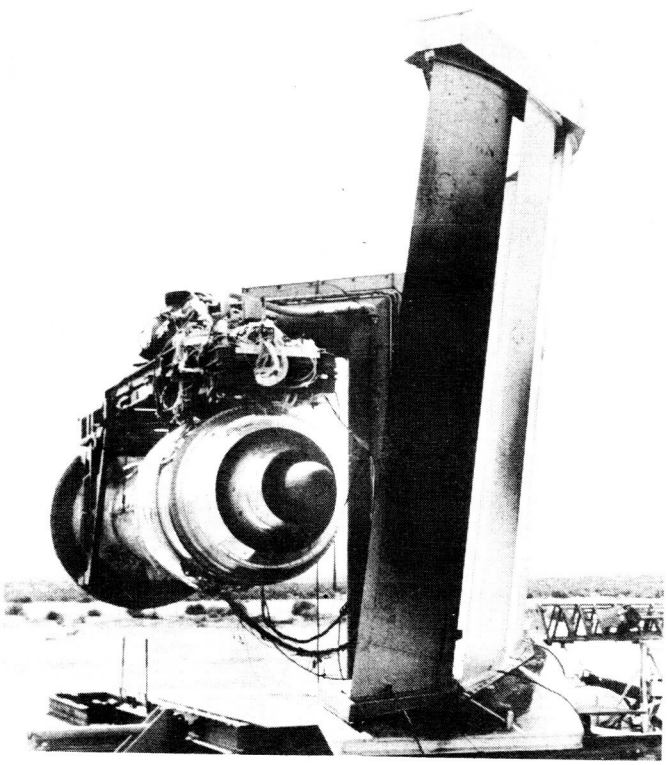

(b)

Figure 1

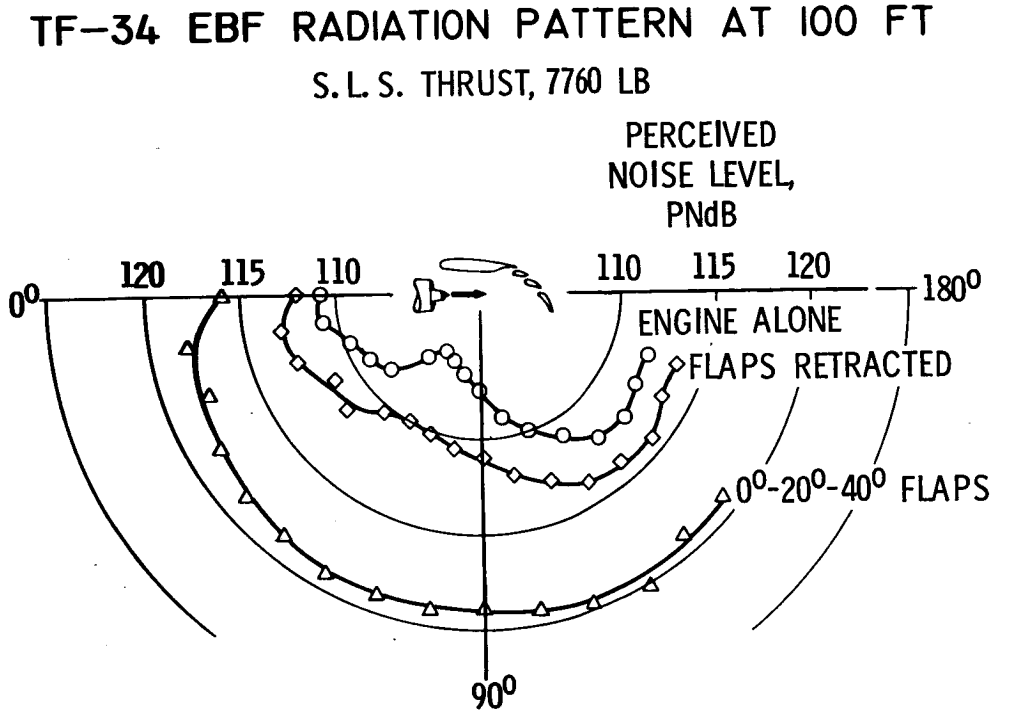

Figure 2

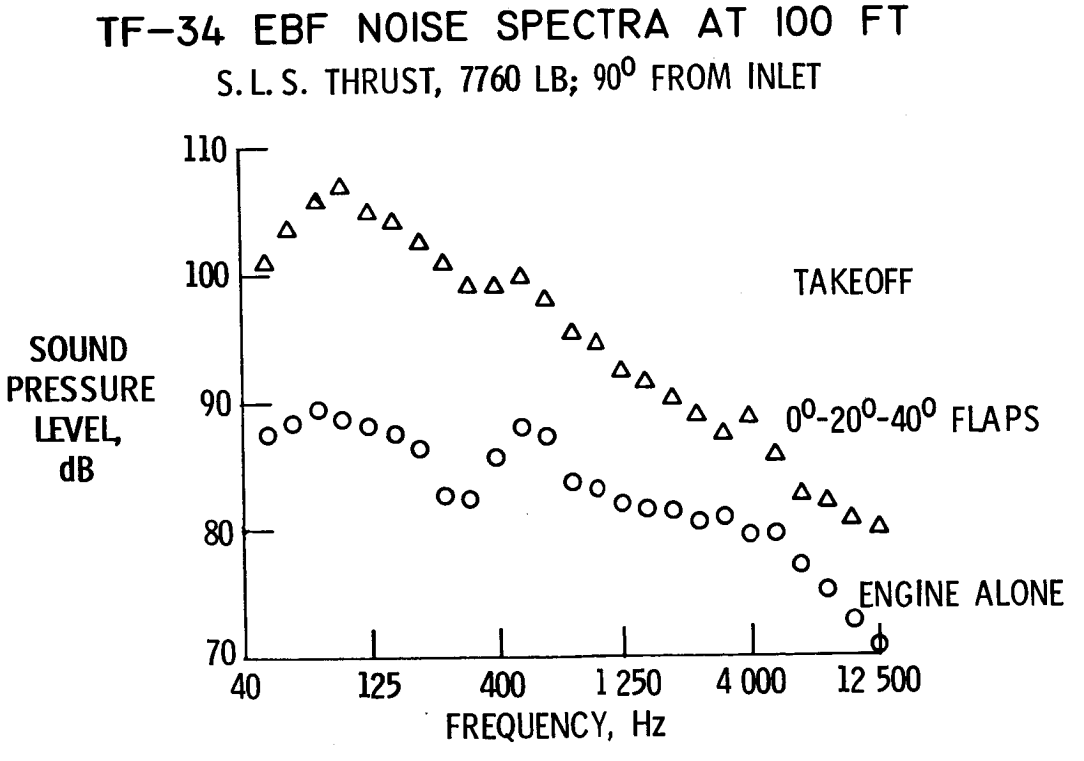

Figure 3

ONE-HALF-SCALE EXTERNALLY BLOWN FLAP MODEL

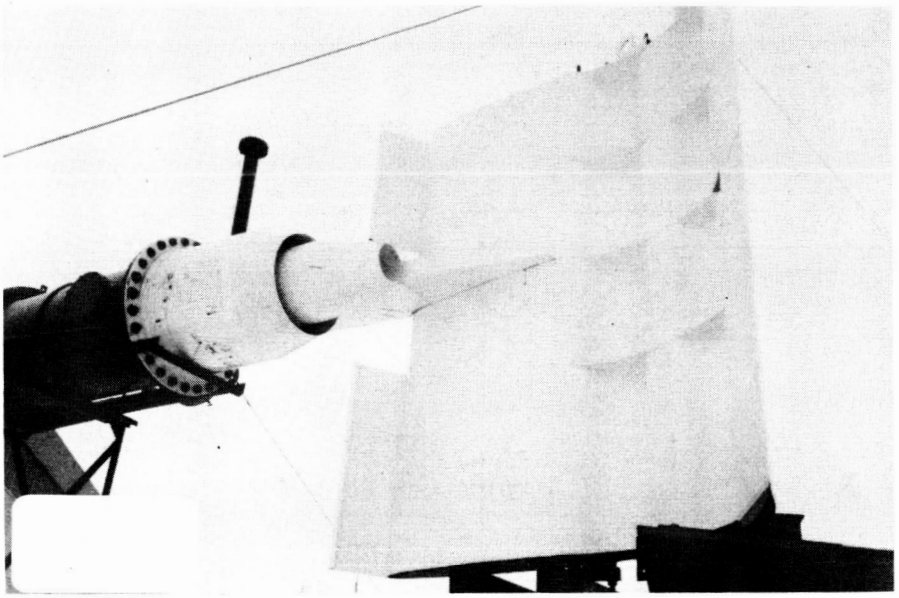

Figure 4

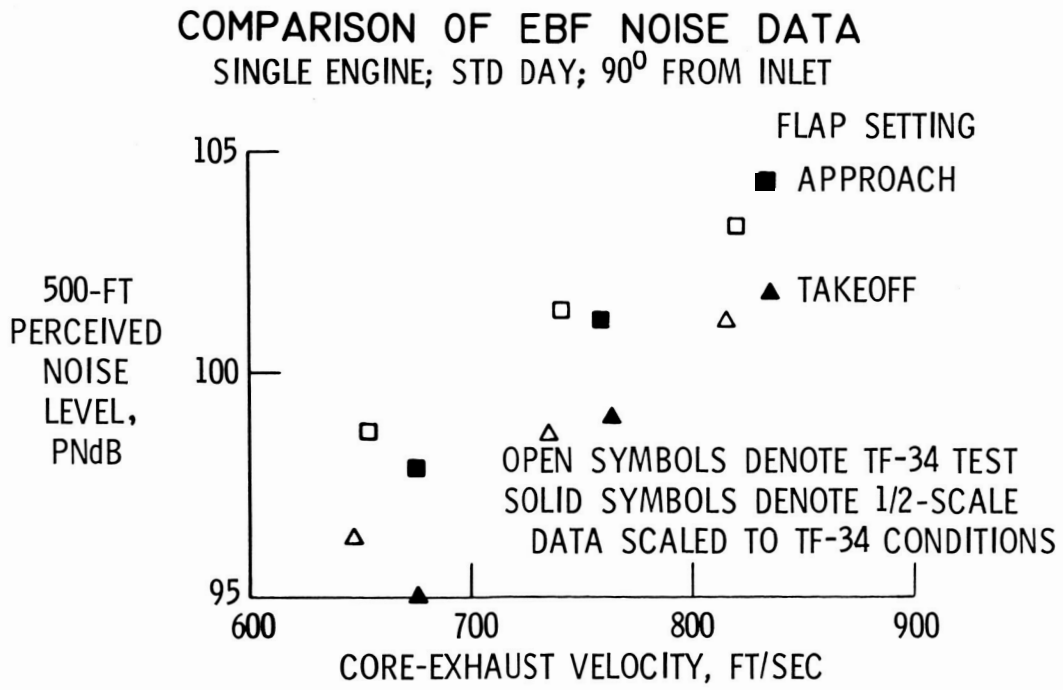

Figure 5

EXTERNALLY BLOWN FLAP AIRSPEED-EFFECT TEST

13-IN.-DIAM FREE JET; 1/13-SCALE EBF MODEL

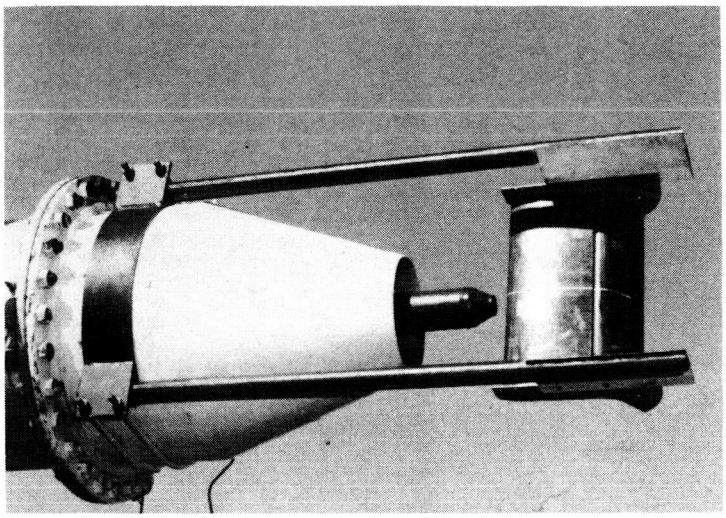

Figure 6

EFFECT OF AIRSPEED ON EBF SPECTRA AT 10 FT

2-IN.-DIAM CONVERGENT NOZZLE

100^0 FROM INLET; EXHAUST VELOCITY, 835 FT/SEC

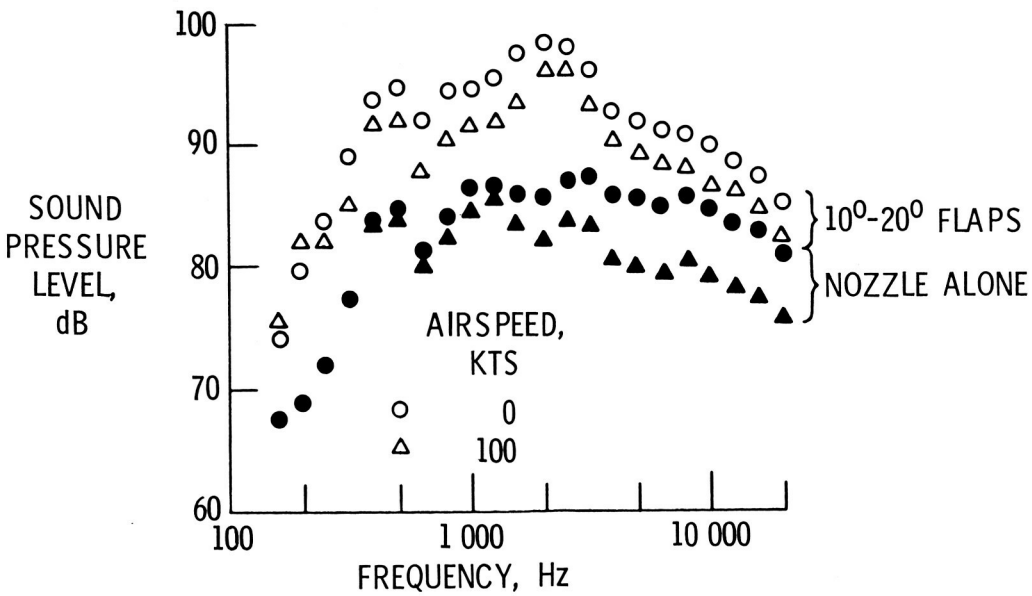

Figure 7

EXTERNALLY BLOWN FLAP AIRSPEED-EFFECT TEST

8-TUBE MIXER-NOZZLE MODEL

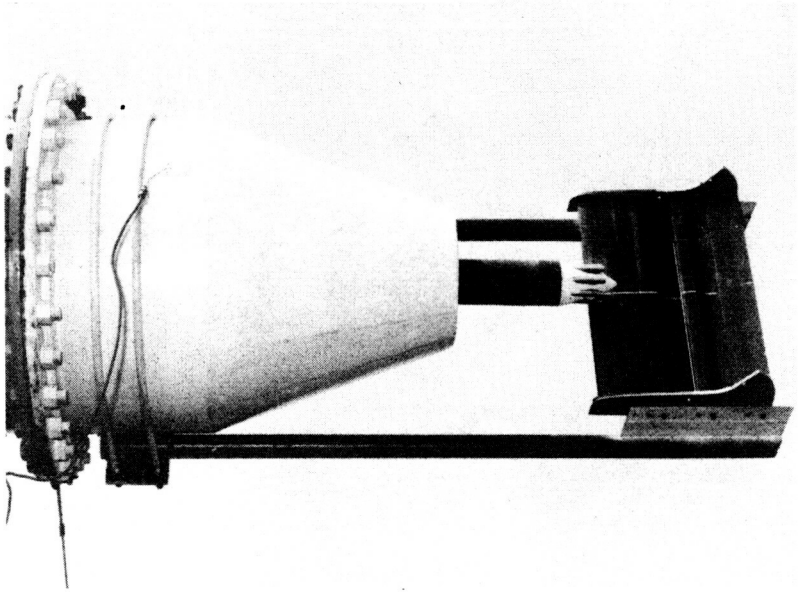

Figure 8

EFFECT OF FORWARD SPEED ON DECAY

8-TUBE MIXER NOZZLE IN 6 x 9 FT TUNNEL

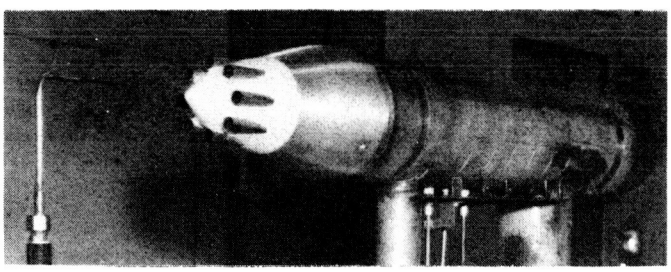

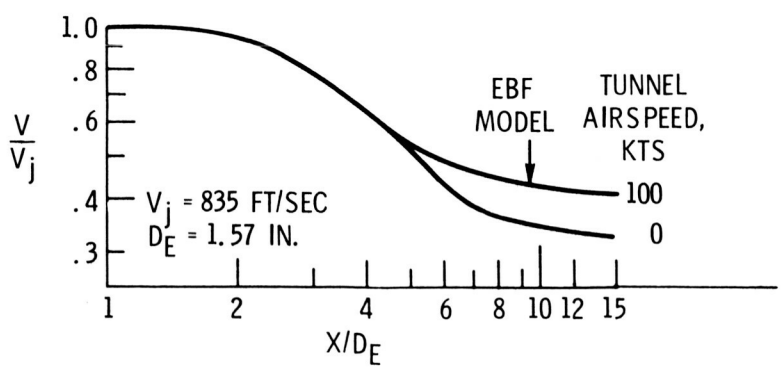

Figure 9

EFFECT OF AIRSPEED ON EBF SPECTRA AT 10 FT

8-TUBE MIXER NOZZLE (D_E = 1.57 IN.)

100^0 FROM INLET; EXHAUST VELOCITY, 835 FT/SEC

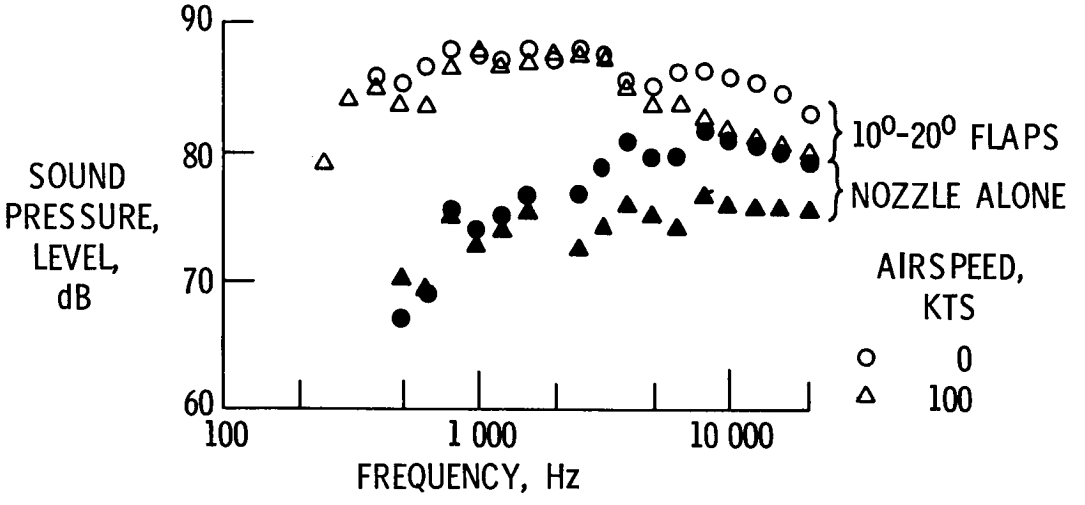

Figure 10

ENGINE OVER-THE-WING EBF CONFIGURATIONS

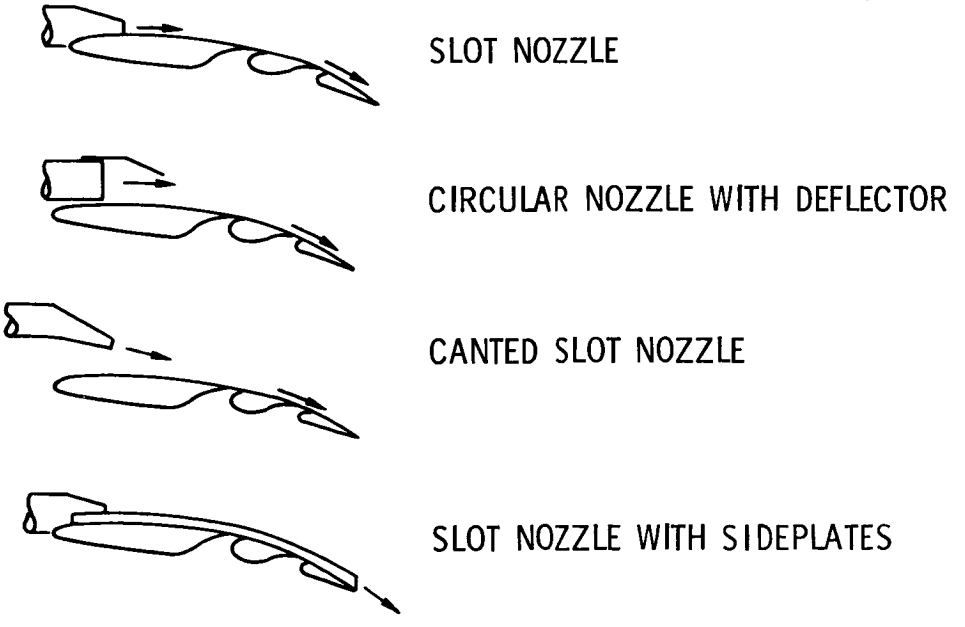

Figure 11

1/13-SCALE MODEL IN LIFT-THRUST RIG

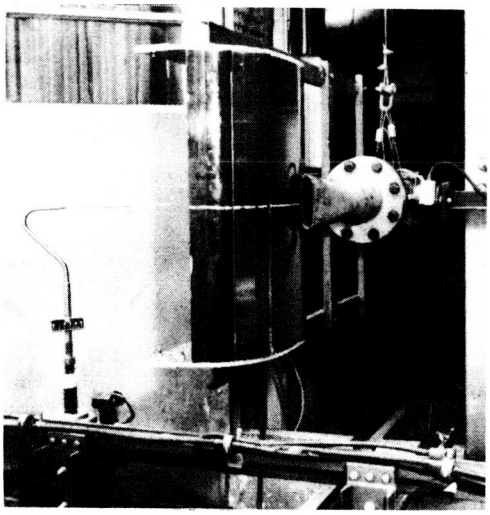

Figure 12

STATIC TURNING EFFICIENCIES

10^0-20^0 FLAP POSITION; FLAP SLOTS COVERED

NOZZLES & ATTACHMENT DEVICE

- ○ 10-1 ASPECT RATIO SLOT NOZZLE
- △ CIRCULAR NOZZLE WITH DEFLECTOR
- ◇ CANTED 5-1 SLOT NOZZLE
- □ 5-1 SLOT NOZZLE WITH SIDEPLATES

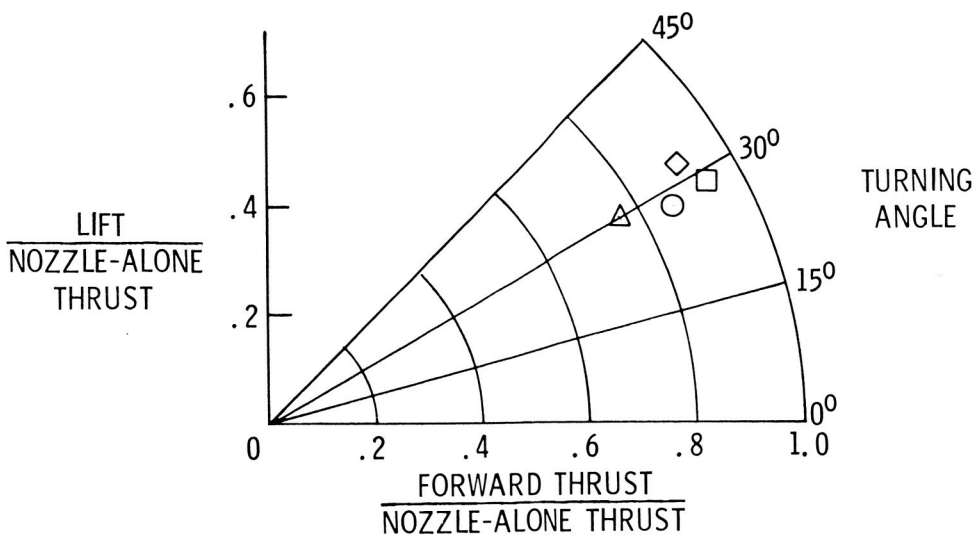

Figure 13

STATIC TURNING EFFICIENCIES

30^0-60^0 FLAP POSITION; FLAP SLOTS COVERED

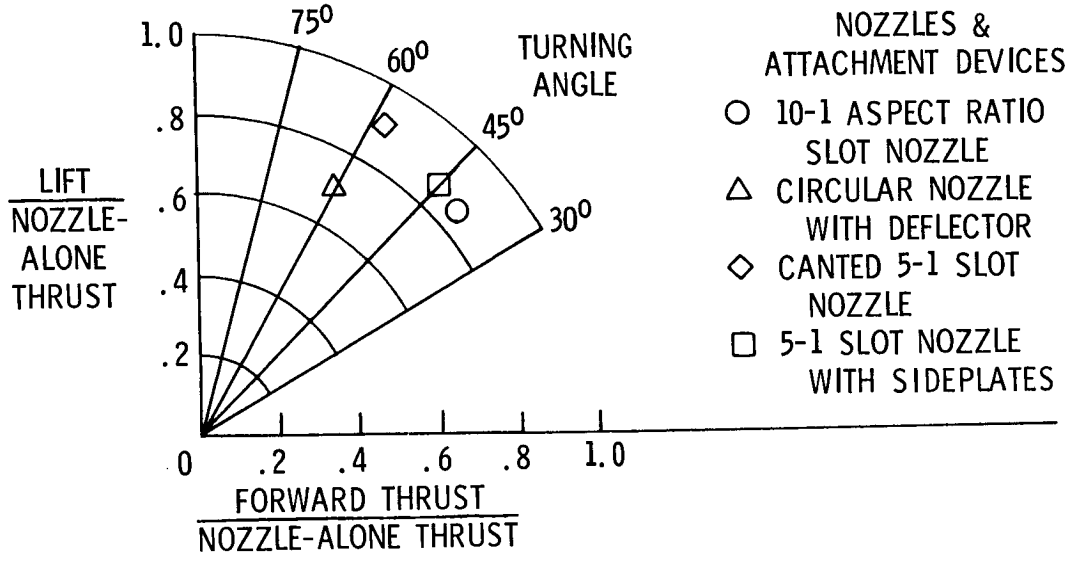

Figure 14

EFFECT OF SLOT COVERING ON NOISE SPECTRA

CIRCULAR NOZZLE DIAM, 2 IN.; 10^0-20^0 FLAP POSITION;
100^0 FROM INLET; EXHAUST VELOCITY, 750 FT/SEC

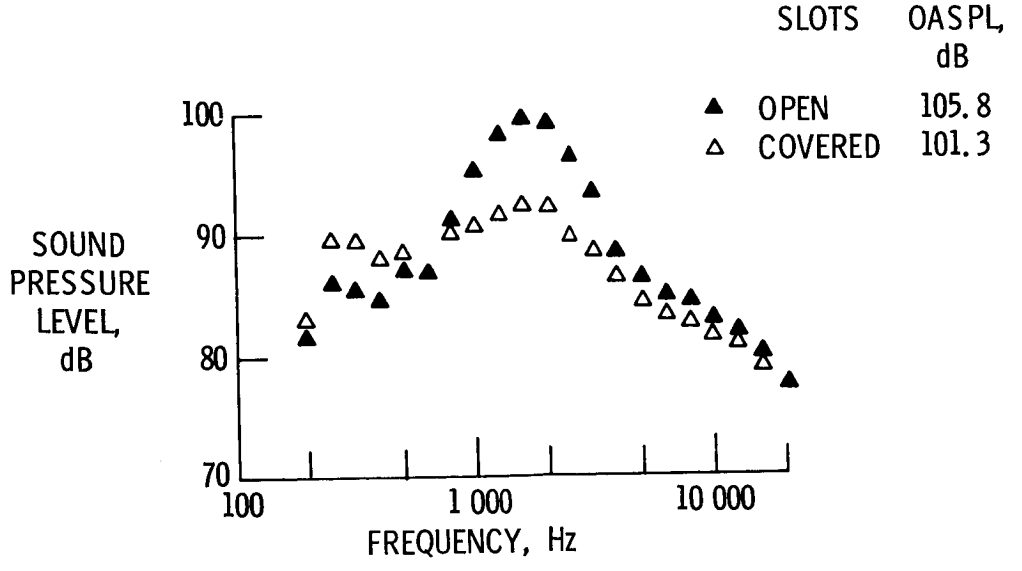

Figure 15

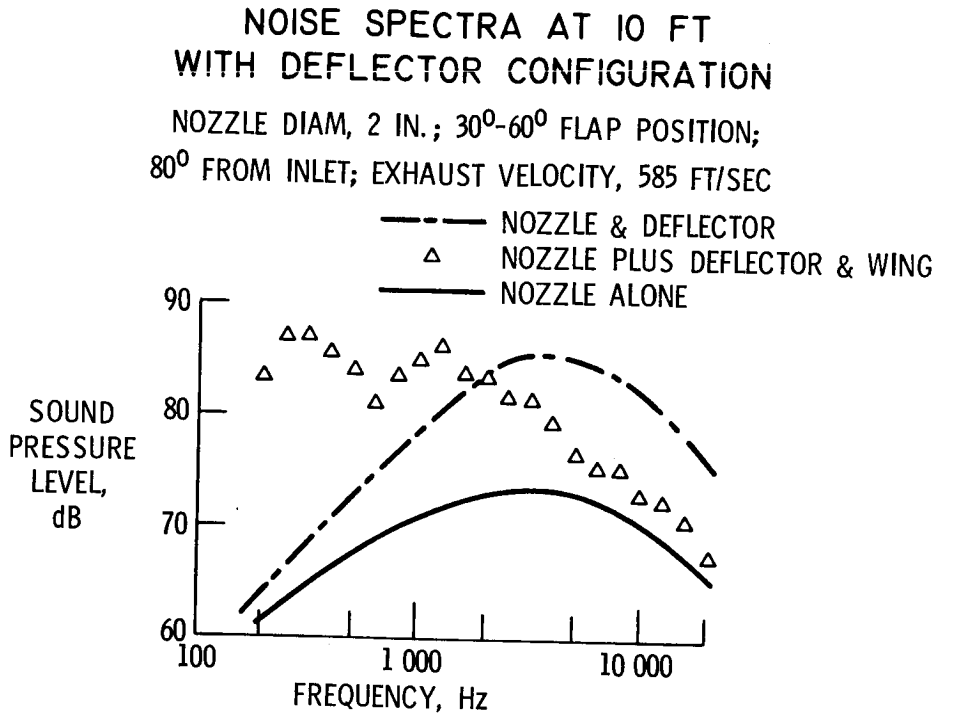

Figure 16

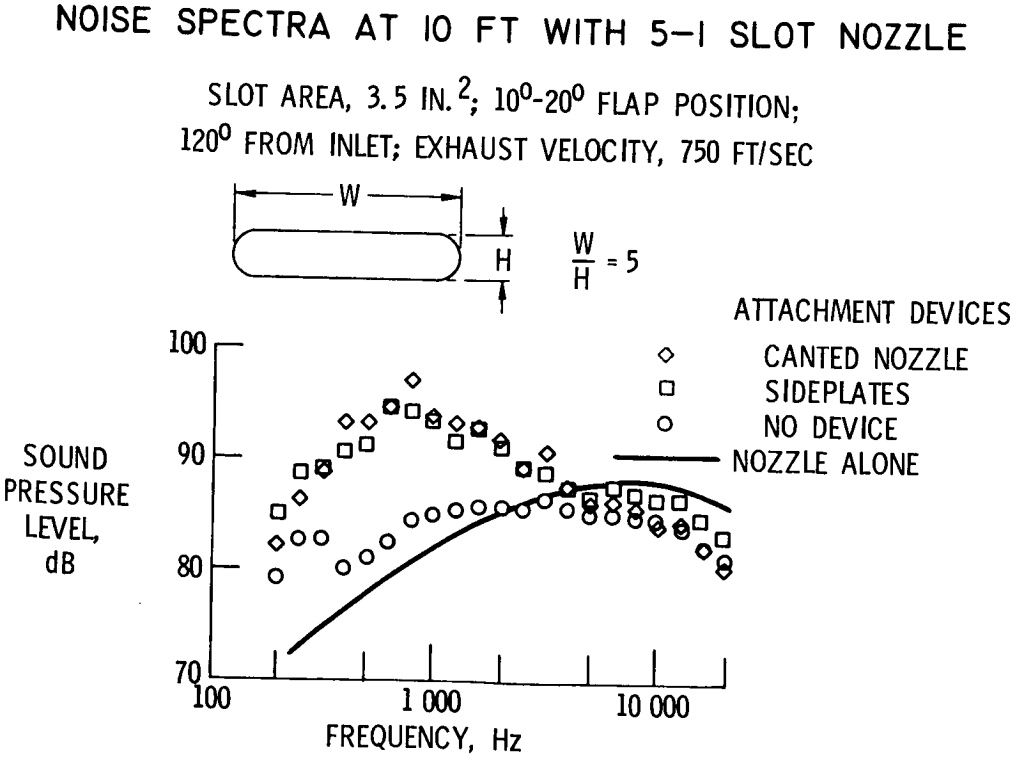

Figure 17

NOISE SUMMARY FOR GOOD ATTACHMENT CASES

NOZZLE AREA, 3.5 IN.^{2}; 10^0-20^0 FLAP POSITION;
10-FT RADIUS; 120^0 FROM INLET; EXHAUST VELOCITY, 750 FT/SEC

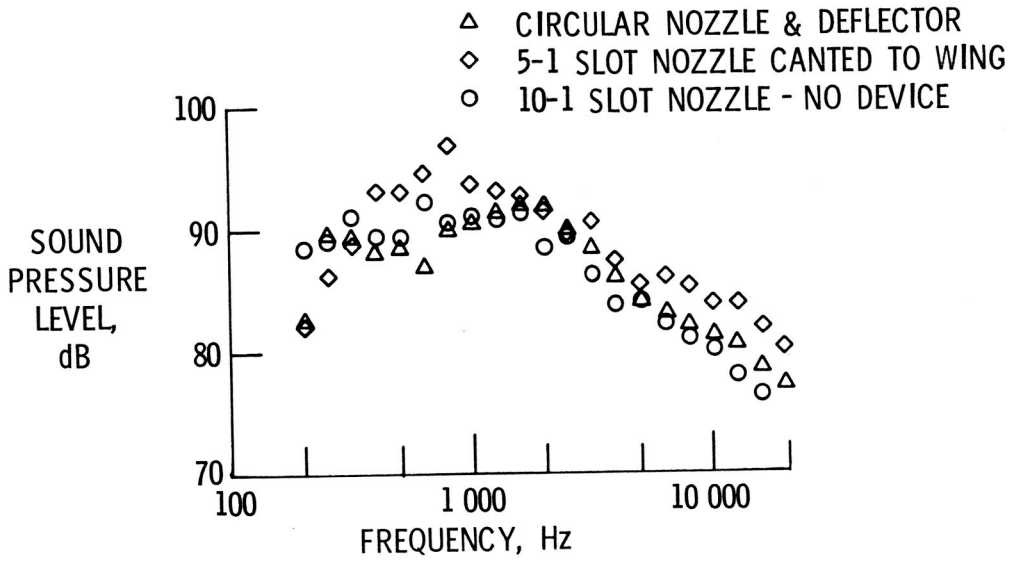

Figure 18

1/2-SCALE ENGINE OVER-THE-WING MODEL

WING CHORD LENGTH, 7 FT; 13-IN.-DIAM NOZZLE WITH DEFLECTOR

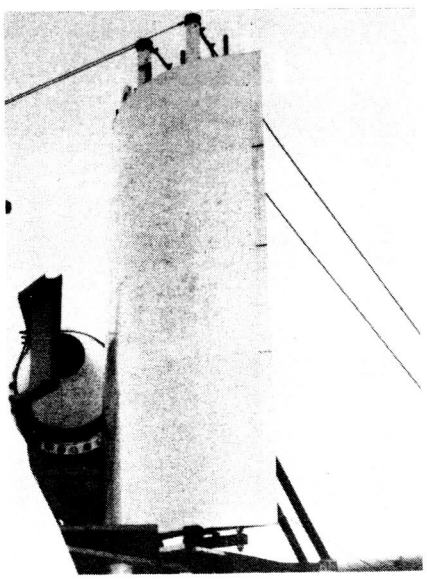

Figure 19

NOISE SPECTRA AT 50 FT WITH DEFLECTOR CONFIGURATION

NOZZLE DIAM, 13 IN.; 30^0-60^0 FLAP POSITION;
90^0 FROM INLET; EXHAUST VELOCITY, 680 FT/SEC

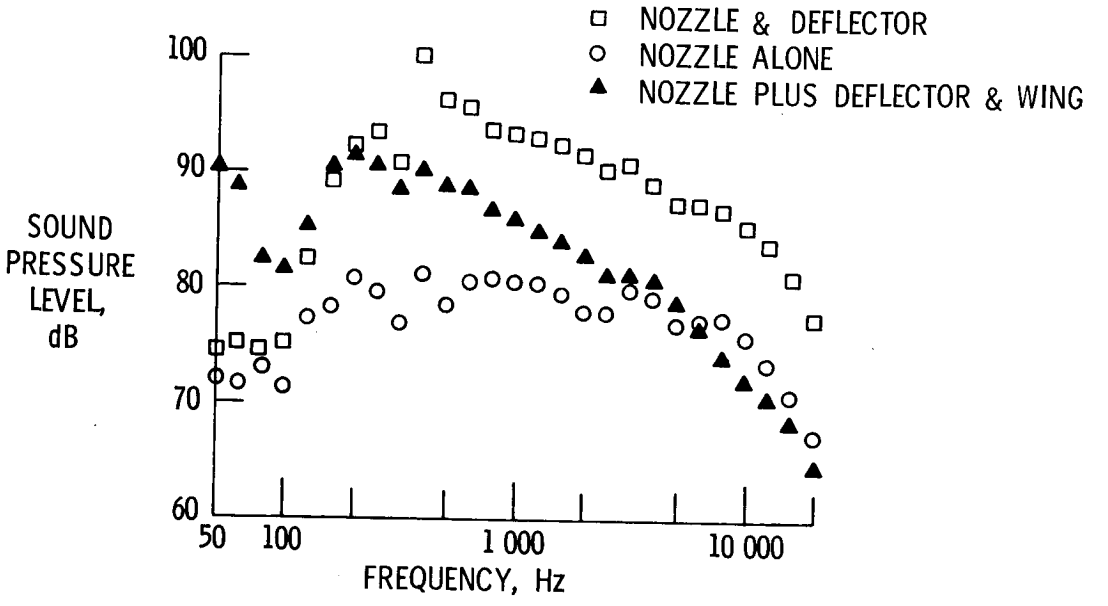

Figure 20

COMPARISON OF EBF NOISE SPECTRA AT 50 FT

90^0 FROM INLET; 30^0-60^0 FLAPS; EXHAUST VELOCITY, 680 FT/SEC

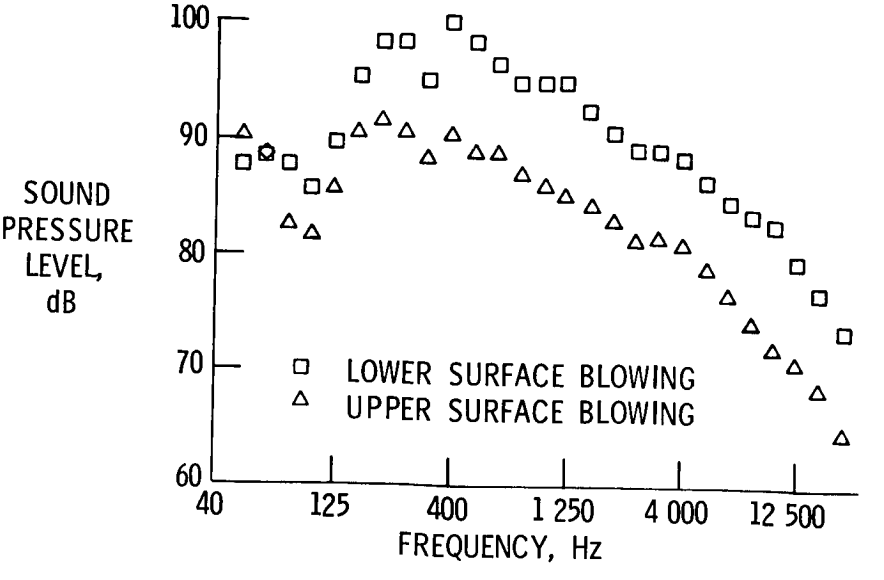

Figure 21

COMPARISONS OF EBF NOISE RADIATION PATTERNS AT 500 FT

13-IN. NOZZLE; 7-FT WING CHORD; 30-60° FLAPS;
EXHAUST VELOCITY, 680 FT/SEC

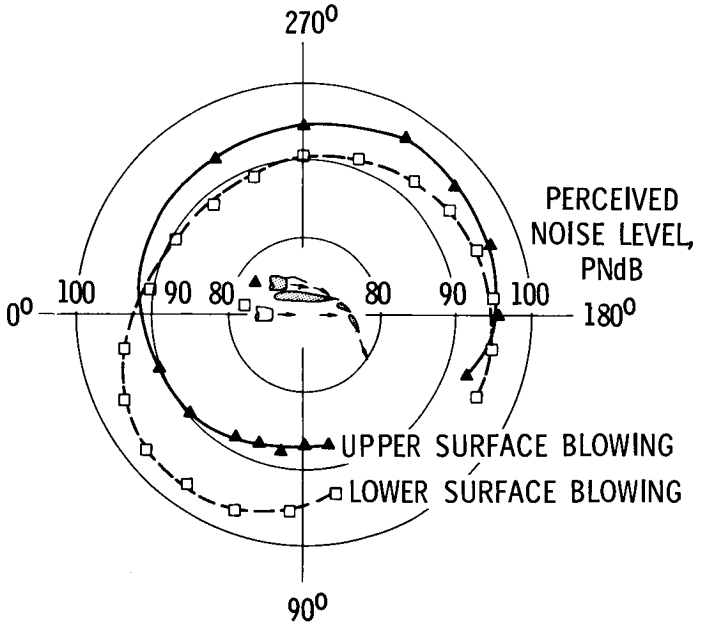

Figure 22

COMPARISON OF EBF NOISE LEVELS AT 500 FT

13-IN. NOZZLE; 7-FT WING CHORD; 30°-60° FLAPS

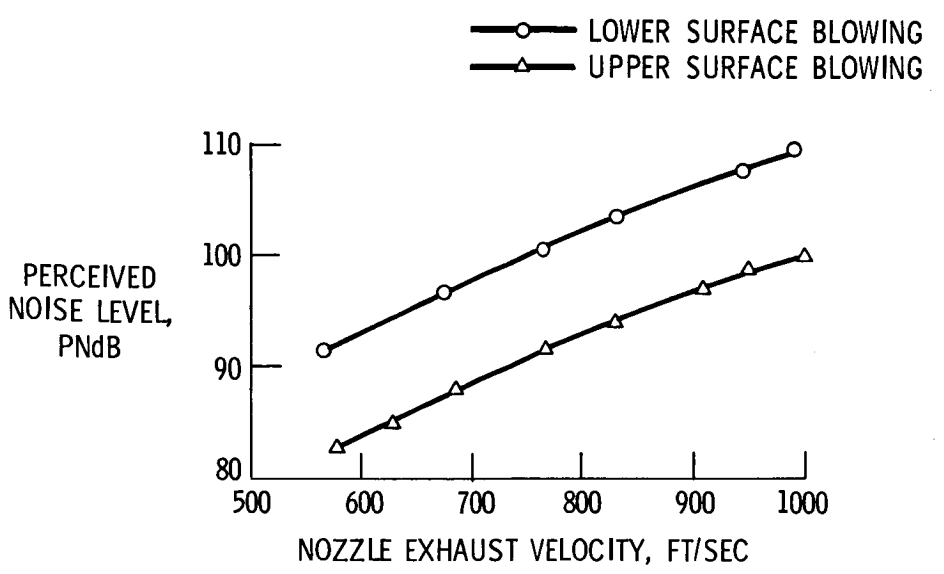

Figure 23

STOL PROPULSION SYSTEMS

By Robert J. Denington, Robert W. Koenig, Michael R. Vanco,
and David A. Sagerser

NASA Lewis Research Center

INTRODUCTION

This paper discusses the selection and the characteristics of quiet, clean propulsion systems for STOL aircraft. Engines are evaluated for augmentor wing and externally blown flap STOL aircraft with the engines located both under and over the wings. Some supporting test data are presented. Optimum engines are selected based on achieving the performance, economic, acoustic, and pollution goals presently being considered for future STOL aircraft.

The data and results presented were obtained from a number of contracted studies and some supporting NASA inhouse programs, most of which began in early 1972. The contracts (fig. 1) include (1) two aircraft and mission studies (with Douglas and Lockheed), (2) two propulsion system studies (with General Electric and Allison that provided much of the engine data on which this paper is based), (3) the experimental and analytic work on the augmentor wing (at Boeing), and (4) the experimental programs on Q-Fans (at Hamilton Standard). None of these studies is complete, so the information presented here is really a progress report.

Throughout this paper, engines are selected and discussed based on aircraft economics using the direct operating cost as the primary criterion. This cost includes the cost of the crew, fuel, aircraft, and engine maintenance and depreciation. Historically it has served as a very good criterion for commercial aircraft optimization. Common procedures and assumptions for the calculation of the direct operating cost were agreed to and have been used throughout the contracted and inhouse studies.

The direct operating costs quoted in this paper are for the STOL baseline aircraft defined in figure 2. It is a 100 passenger aircraft that meets the STOL noise goal. It has a 500-mile range and is capable of landing and taking off in a 2000-foot FAA field. Variations of these major parameters have been looked at, but, except for the noise goal, they have only a minor effect on the selection of quiet engine characteristics.

Noise

As was emphasized earlier, it is very important that STOL aircraft be accepted by the general public, thus the need for a quiet, clean propulsion system. Firm noise regulations have not been set by the Government; however, for the STOL engine and aircraft studies, 95 EPNdB at a 500-foot sideline has been selected as a representative noise goal. This goal is compared with the current FAA-FAR-36 regulations in figure 3, which shows that to meet the STOL goal of 95 EPNdB a reduction in sideline noise of about 30 PNdB relative to FAR 36 at the same sideline distance is required. This imposes severe penalties on the aircraft and engine design. The STOL aircraft and engines described are all designed to meet the 95 EPNdB design goal with the acoustic design very much dependent on the type of aircraft and installation. Some discussion of the savings associated with relaxing these noise goals is also given.

A specification on sideline noise may not be the best measure of the public's reaction to noise. Since a better criterion may be the area exposed to objectionable noise levels, footprints or noise contours are also presented for the STOL aircraft.

Pollution

The modern aircraft presently entering the commercial fleet are already fairly low in emission of pollutants and smoke. But, as shown in figure 4, significant reductions in pollutant levels for STOL are still desired. Test data from experimental combustors have already shown that the CO and HC goals can be achieved with new combustor designs and proper engine operation at idle. Meeting the NO goal, however, presents a more difficult problem.

The rate of NO generated is dependent to a large extent on combustor design and combustor inlet temperature and pressures, which are in turn a direct function of the engine cycle pressure ratio as shown in figure 5. This figure, which is a plot of analytical data of NO production against engine cycle overall pressure ratio, indicates that with an advanced combustor design the NO goal of 10 pounds per 1000 pounds of fuel can be achieved with pressure ratios of about 20 - a value slightly lower than most modern CTOL engines. Although it is not shown, the NO goal can also be met at a higher pressure ratio, with water injection, although water injection results in a more complicated aircraft and engine. Combustor exit (or turbine inlet) temperatures have a less significant effect on NO generation, although lower temperatures result in slightly lower NO production.

Direct operating cost is a good indication of the costs necessary to design engines with a low overall pressure ratio and low temperatures to reduce NO production. Figure 6 is a plot of direct operating cost against turbine inlet temperature and cycle pres-

sure ratio for a 100-passenger, four-engine externally blow flap STOL aircraft that meets the 95 EPNdB noise goal at a 500-foot sideline. The curves show that a relatively low overall pressure ratio of about 20 and a temperature in the 2300° to 2400° F range can be selected for STOL to reduce pollution and simplify the engine without significant direct operating cost penalties. This results primarily because the lower specific fuel consumption associated with higher pressure ratios and temperatures is not very important for short range STOL missions. These conclusions apply to other STOL aircraft engines, so all the engines described in the remainder of this paper are designed with overall pressure ratios of about 20 and turbine inlet temperatures of 2300° to 2400° F.

PROPULSION FOR AUGMENTOR WING STOL

The augmentor wing aircraft and its propulsion system probably have the most integrated airframe-engine combination of the STOL aircraft being considered. To understand the interaction of the engine and nacelle with the airframe, figure 7 shows a simplified schematic of an engine and wing cross section with the major noise sources. During takeoff and approach the high pressure air from the wing duct exhaust nozzle is a noise source which is propagated through the flaps and to the atmosphere. Another noise source is the machinery noise associated with the high tip speed, multistage fan which is required to compress the wing air to a suitable pressure. The only noise source from the fan is in a forward direction since the scroll and the duct system can be adequately treated to essentially eliminate the aft fan machinery noise. The other noise sources are in the back of the engine. These two sources are primary jet noise, which is a function of the core velocity, and core noise, which consists of turbine machinery combustor or other noises not associated with the jet velocity.

A unique part of this installation is the duct, which is used to direct the bypass air from the engine into the pylon. The air is then transferred from the pylon either to the wing for takeoff and landing or to a cruise nozzle for climb and cruise by diverter valves located in the ducts. Figure 8 (ref. 1) shows some of the ducting and nozzle details superimposed on a wing. Each engine feeds its own duct; appropriate crossover and nozzle locations on each side of the wing help to maintain aircraft stability during engine out operation. A cross section shows the duct locations relative to the rear wing spar, the nozzles, and the flap arrangement for exhausting the wing air. The arrows indicate the flow paths of the secondary air for the ejector type nozzle which augments the wing thrust. When the flaps are retracted, the air flow is diverted to the cruise nozzle located on the pylon.

Many factors affect the proper engine cycle selection for the augmentor wing system. The cycle selected has to meet both the aircraft and mission requirements and the noise

goal. Preliminary screening shows that a turbofan cycle best meets these requirements, although the cycle and aircraft must be optimized together because of interactions between the ducting, wing, and quieting.

The engine cycle parameters that have a significant effect on the augmentor wing propulsion system are the fan pressure ratio and bypass ratio. They affect the engine weight, blowing system weight, wing design, and noise. Once a fan pressure is selected, the bypass ratio required to meet the jet exhaust noise limit is defined. This particular noise problem is discussed later. The cycle parameters need to be selected when aircraft design, noise, and economics are all considered.

The engine system weight, which includes the engine, scroll, and nacelle, and the blowing system weight, which includes the pylon and wing ducts and nozzles, are considered a single propulsion system weight group. This weight group is shown as a function of fan pressure ratio in figure 9. Also shown is the effect of the propulsion system weight on total aircraft empty weight. The propulsion system and blowing system weights increase with increasing fan pressure ratio while the total aircraft weight decreases. A low fan pressure means a lighter engine and wing duct. However, the volume of the wing duct needs to be increased to pass the same amount of air at a lower pressure. So a larger airplane wing, either thicker or greater in area, is necessary to contain the ducts. The larger wing increases drag and requires more thrust and a heavier wing. These effects overshadow the savings in propulsion system weight.

Duct design and acoustic considerations determine the upper pressure limit. Since noise is a primary factor in fan pressure ratio selection, the effect of fan pressure ratio as a function of suppressed wing noise is shown in figure 10 for a 100 passenger augmentor wing aircraft. With a 15-percent duct pressure loss, the Boeing model tests (ref. 1) have shown that wing noise can be suppressed to about 92 PNdB for an engine designed with a 3 to 1 fan pressure ratio.

Quieting the engine to about 92 PNdB also results in a system noise level of about 95 EPNdB or slightly less when the two sources are added. Higher fan pressure ratios increase wing noise, which in turn requires unreasonable reductions in engine noise to meet a 95 EPNdB system noise goal.

A 3 to 1 fan pressure ratio looks good from an aircraft design point of view. The economics of the system also needs to be considered. Direct operating cost is shown as a function of fan pressure ratio for a 100 passenger augmentor wing aircraft in figure 11. The analysis indicates that when the fan pressure ratio is lowered, the direct operating cost rises. The direct operating cost increase is mostly from aircraft performance losses as a result of the large wing needed to meet ducting requirements. The direct operating costs indicate that a fan pressure anywhere between 2.7 and 3.0 may be used for the augmentor wing aircraft with very little to be gained or lost on an economic basis. The economics are based on an augmentor wing aircraft with a predicted sideline

noise of 95 EPNdB. The fan pressure ratio has been considered in terms of system design, economics, and wing noise suppressed to 92 PNdB. However, to meet the system noise goal of 95 EPNdB or slightly less, the remaining engine noise sources must at least be considered or suppressed at an acceptable level to meet the noise goal.

Unsuppressed and suppressed noise levels of a fan pressure ratio 3 to 1 augmentor wing engine are illustrated in figure 12. Only the major contributing noise sources are considered at a 500-foot sideline for four engines producing about 60 000 pounds of thrust. The wing noise is suppressed about 22 PNdB to achieve a 92 PNdB level. Model tests have shown that this suppression can be achieved by reasonable nozzle design and flap wall acoustic treatment. A 3 to 1 fan pressure ratio multistage, high tip speed fan is noisy. The fan inlet forward radiated noise needs to be suppressed at least 25 PNdB. The Engine Noise Technology paper (paper no. 28) indicates that small-scale tests show that a 25-PNdB suppression could be achieved with a high subsonic throat Mach number inlet. Considering the amount of forward radiated noise from the aft end, the goal could probably be achieved by suppressing the fan inlet noise to about 93 PNdB.

The unsuppressed core noise is approaching the noise goal and requires about a 6-PNdB suppression. The primary jet velocity was lowered sufficiently so that it is not a major contributor to the total noise. This was done by extracting more energy from the low pressure turbine than is common for engines of conventional takeoff and landing aircraft.

Typical cycle characteristics that evolved from this design approach are listed in figure 13. The general engine arrangement of a typical Allison augmentor wing engine is illustrated in figure 14. A three-stage fan is used in conjunction with a three-stage turbine. The engine is conventional except for the relatively high bypass ratio of 2.8 (fig. 13). This level of bypass ratio is usually not associated with a fan pressure ratio as high as 3 to 1. It results from the high energy extraction to reduce the jet noise level. The engine has an overall pressure ratio of about 22 to 1 when operating at a turbine inlet temperature of 2300° F. The thrust is about 15 000 pounds for this engine.

Two installation drawings of augmentor wing engines are illustrated in figures 15 and 16 using two approaches for suppressing fan noise. Figure 15 shows a variable area inlet to provide a sonic or near sonic throat Mach number for suppression similar to the design illustrated in the Engine Noise Technology paper. Other methods such as variable inlet guide vanes are also being investigated to achieve inlet suppression. Figure 16 illustrates a fixed area inlet using splitters and high velocity to provide the suppression. Both NASA and Boeing have shown that some suppression does occur at lower than sonic inlet flow velocities in the throat of the inlet. This particular inlet, a General Electric design, uses about a 0.78 throat Mach number to provide a 5-PNdB suppression. The remaining suppression is attributed to the long splitters. Inlet distortion, flight effects, and other problems associated with these concepts need further investigation.

Both figures 15 and 16 have core noise suppression to reduce core noise. The installations, as shown, are predicted to meet the 92 PNdB engine noise goal at a 500-foot sideline. Tests will be required to confirm these suppression predictions.

System integration problems such as the diverter valves required for changing flow passages, transient engine operation, and maintainability of the duct system are a few areas which must be investigated to determine the practicability of the augmentor wing STOL propulsion system.

EXTERNALLY BLOWN FLAP

The acoustic characteristics of the externally blown flap (EBF) aircraft and engines are discussed extensively in the previous papers. Jet flap noise was discussed in papers by Paul Lasagna of Flight Research Center and Robert Dorsch of Lewis Research Center. Fan machinery noise with its suppression and jet noise were discussed in the Engine Noise Technology paper (paper no. 28). These data together with the results of the STOL aircraft and engine studies are used herein to show how the propulsion system characteristics are selected for externally blown flap STOL aircraft with the engines located under the wing.

The noise sources for an externally blown flap aircraft are shown in figure 17. The sources are fan machinery noise, core noise, fan and core jet noise, and flap noise. The dominant noise sources are the fan noise and the flap noise. The other noise sources, namely, fan and core jet noise, are controlled by cycle selection. Core noise is reduced by wall treatment in the core duct.

The flap noise at takeoff is shown in figure 18 as a function of the installed fan nozzle exhaust velocity for a four-engine externally blown flap aircraft with 90 000 pounds of thrust. The data presented are extrapolated from Lewis experimental small-scale data. To meet the noise goal of 95 PNdB, the installed fan jet velocity must be about 600 fps or less which corresponds to a fan pressure ratio of about 1.25. For higher fan jet velocities or fan pressure ratios, a decayer must be used to reduce the velocity if the noise goal is to be met. For example, at a fan pressure ratio of 1.4, or an installed velocity of approximately 750 fps, a decayer must be used to reduce the velocity about 25 percent to meet the noise goal.

The other dominant externally blown flap noise source is fan noise. The unsuppressed fan noise is shown in figure 19 as a function of fan pressure ratio. Two sets of data are shown in this figure. The upper band is for high speed, single-stage fans with tip speeds in the 1300 to 1500 fps range. The lower band is for low speed, single-stage fans with tip speeds in the 750 to 1100 fps range. It is noted that high speed fans are noiser than low speed fans. This is due to the effect of the multiple pure tones as explained in the Engine Noise Technology paper.

If one of the dominant noise sources is close to the noise goal, the other noise source must be reduced more to achieve the system noise goal of 95 EPNdB. For example, if the flap noise is 95 PNdB, the fan noise must be suppressed to 90 PNdB to make the system noise goal of 95 EPNdB.

As shown in figures 18 and 19, several approaches can be taken to obtain a quiet externally blown flap engine. One approach is to take a very low fan pressure ratio where the flap noise is well below 95 PNdB, while a second approach would be to take a higher fan pressure ratio at which the flap noise is about 95 PNdB. A third approach would be to take a still higher fan pressure ratio and use a decayer to meet the noise goal. These three approaches are shown in figure 20. These are General Electric engines for a 100 passenger aircraft. To achieve the noise goals, these engines incorporate advanced fan technology and acoustic suppression designs.

The upper engine in figure 20 has a 1.15 pressure ratio fan. This engine has a variable pitch fan and an installed exhaust velocity of about 460 fps, which gives a flap noise below 90 PNdB. Therefore, minimum suppression is required to make the noise goal. There is one splitter and wall treatment in the inlet and one splitter and wall treatment in the fan duct. The inlet and aft fan noise are reduced about 15 dB. The core treatment shown reduces the core noise by 10 PNdB. This is a very large engine, with a nacelle diameter of about 128 inches.

The middle engine in figure 20 has a 1.25 pressure ratio variable pitch fan. The installed fan exhaust velocity of about 600 fps results in a flap noise level of about 95 PNdB. More fan suppression is needed to meet the noise goal than in the 1.15 fan pressure ratio engine mentioned previously. There are two splitters with wall treatment in the inlet and one splitter with extensive wall treatment in the aft duct. The inlet and aft fan noise are reduced about 20 dB. The core treatment shown reduces the core noise 10 dB as in the 1.15 engine. A more reasonable nacelle diameter of about 100 inches results from the higher fan pressure ratio.

The lower engine in figure 20 has a 1.30 pressure ratio fixed pitch fan with a decayer to reduce flap impingement velocity. The installed fan exhaust velocity is about 650 fps, but the decayer is designed to reduce this velocity to a level below 600 fps to meet the noise goal. Because of the higher fan pressure ratio, slightly more treatment is required in the engine. There are three splitters and wall treatment in the inlet and two splitters and wall treatment in the aft duct. The inlet and aft fan noise are reduced about 20 dB. The core nozzle is canted so that the core flow misses the flap.

Since this engine has a fixed pitch fan, a thrust reverser is needed. The lower half of the 1.30 fan pressure ratio engine installation shows the engine in the reverse thrust position. As can be seen from figure 20, the cowling is translated aft to expose the reverser. The thrust reverser shown is a cascade-type reverser with a blocker door. This type of reverser was discussed in the Engine Noise Technology paper. On the engine, the reverser is positioned so that the flow is skewed upward to avoid

reingestion and aircraft impingement. The reverser uses about 190° emission and has an estimated weight of about 1500 pounds. The 96-inch nacelle diameter is the smallest of the three engines.

The engines presented have shown three approaches to the acoustic design, but the best design has not been selected. STOL aircraft performance and economics using DOC as the primary parameter will be used to help make this selection.

The effect of fan pressure ratio on the direct operating cost for fixed and variable pitch fans is shown in figure 21 where relative direct operating cost is plotted against fan pressure ratio. The direct operating cost is seen to minimize for both the fixed and variable pitch fans at a pressure ratio of about 1.25. As the fan pressure ratio increases above 1.25 or 1.27, the direct operating cost increases sharply because of the addition of a decayer which is required to make the noise goal. Below this fan pressure ratio, the direct operating cost increases because the large nacelles increase the drag, and the low pressure ratio fans are much more sensitive to the pressure loss associated with the acoustic suppression. The variable pitch engine is 5 to 10 percent lower in direct operating cost than the fixed pitch engine because the variable pitch fan can provide reverse thrust without the use of a heavy conventional thrust reverser.

The direct operating cost trends are partially explained by the variation in engine thrust to weight ratio. The engine thrust to weight ratio is shown in figure 22 as function of fan pressure ratio. Shown in this figure are uninstalled thrust to weight ratios and installed engine thrust to weight ratios for fixed and variable pitch fans. The maximum uninstalled engine thrust to weight ratio occurs in the 1.20 to 1.35 fan pressure ratio range. The optimum fixed pitch installed engine thrust to weight is around a fan pressure ratio of 1.3 to 1.35, while that for the variable pitch fan is around 1.25. The difference between the uninstalled and installed engine thrust to weight is the weight of the nacelle and the acoustic treatment. The improvement in engine thrust to weight for the variable pitch fan over the fixed pitch fan is due to the variable pitch fan not needing a thrust reverser. This improvement accounts for the major part of the direct operating cost improvement shown in figure 21.

The other factor that affects the engine selection is the cruise Mach number capability of the aircraft and engine. A high cruise Mach number capability produces a more versatile aircraft with greater passenger appeal. The effect of fan pressure ratio on cruise Mach number is shown in figure 23, where the aircraft is optimized for minimum direct operating cost. The high drags associated with engines with fan pressure ratios below 1.25 make it uneconomical to operate at Mach numbers as high as 0.8.

Based on minimizing the direct operating cost and obtaining a cruise Mach number of about 0.8, the studies indicate that a variable pitch fan engine with a pressure ratio of about 1.25 is the best under the wing engine.

The engine characteristics for a typical 1.25 fan pressure ratio engine are shown in figure 24. The rated thrust is 22 500 pounds for a 90° day. The fan pressure ratio varies from 1.25 at takeoff to about 1.29 at cruise. The bypass ratio is 17. However, the bypass ratio can vary from 14 to 17 depending on what core flow and core exhaust velocity are used. The turbine inlet temperature is 2400° F. The uninstalled thrust to weight ratio is 6.6, and the takeoff specific full consumption is 0.23 pound of fuel per hour per pound of thrust.

An engine that meets these cycle characteristics is shown in figure 25. The Allison engine has a variable pitch fan with composite blades. The fan is driven by a low pressure, three-stage turbine through a gear train with a gear ratio of 3.0. There is a two tip aerodynamic chord spacing between the rotor and stator to reduce the noise.

An installation drawing of the Allison engine is shown in figure 26. This engine has one splitter and acoustic wall treatment in the inlet and two short splitters and wall treatment in the fan duct. A three-position fan nozzle is used to obtain optimum performance at takeoff, cruise, and in reverse thrust. The accessory gearbox is located in the nacelle for easy maintainability.

The rationale used to select the externally blown flap under the wing engine has just been described. This engine does have many new and unique features that are quite different from current CTOL engines.

Q-FAN DEMONSTRATOR

The studies have shown that variable pitch fans are best for meeting externally blown flap STOL requirements. Aero and acoustic tests are being conducted at Lewis on variable pitch fans as a component. However, little is known about the operating characteristics of a variable pitch fan and engine combination. So NASA has contracted Hamilton Standard for a test program of a variable pitch Q-Fan driven by and integrated with a turboshaft engine.

One objective of the test program is to determine the compatibility of the variable pitch fan and core engine in the forward thrust mode and especially in the reverse thrust mode, that is, to determine the core compressor inlet distortion as well as vibration and stress levels in the fan and engine. Some of the questionable areas for reverse thrust operation of variable pitch engines were discussed in the Engine Noise Technology paper (paper no. 28). It is hoped that this test program will help answer these questions.

A second objective is to measure the noise level of the fan at various speeds and blade angles both in the forward and reverse thrust modes.

Figure 27 shows a cross section of the Q-Fan engine demonstrator being tested. The fan is 55 inches in diameter and has a design pressure ratio of 1.18. There are 13 composite rotor blades and 7 stators. The fan is driven by a Lycoming T-55 shaft engine through a reduction gear.

The fan and engine are flight weight designs except for the gearbox case and the fan stators which are used to support the engine.

The compressor inlet duct and the engine exhaust duct are acoustically treated to a level sufficiently below that of the fan to allow measurement of the fan noise alone.

Figures 28 and 29 show the engine on the test stand at Hamilton Standard. The engine centerline is 20 feet above ground level to assure a relatively distortion-free inlet and not interfere with the noise measurements. Microphones will be positioned at 25- and 50-foot radii to measure far field noise. The catwalks and stairs shown next to the engine in figure 28 will be removed for the acoustic tests. The inlet shroud is removed in figure 29 exposing the 13 composite fan rotor blades.

As indicated by the bellmouth inlet, the engine will be tested only statically in this test program. However, some cross-flow tests are planned using ambient winds and a portable blower. NASA is also considering testing the engine in the 40 by 80 foot wind tunnel at Ames.

The test conditions being covered in the current program are tabulated in figure 30. For the forward thrust mode, rotor blade angles are varied from 37^{o} to 57^{o} and fan tip speeds from 400 to 810 feet per second. This includes the design takeoff angle of 52^{o} and the approach angle of 37^{o}. The maximum tip speed at a blade angle of 57^{o} is limited to about 750 feet per second by the available power from the T-55 engine. For the reverse thrust mode, rotor blade angles are varied from 134^{o} to 150^{o} and fan tip speeds from 500 to 810 feet per second.

The test program is now in progress and, as shown in figure 30, all five blade angles have been run for forward thrust performance as well as one blade angle for reverse thrust performance. Preliminary results from these tests indicate that the core compressor inlet distortion and fan blade stresses are acceptable. So far no problems have been experienced which would indicate a problem with the variable pitch fan concept.

As the engine is configured for this test program, the fan blades can be adjusted only while the engine is stopped. The fan hub can be modified, however, to accept a dynamic pitch change mechanism. This would allow the blades to be adjusted while the engine is running. A test program is currently being considered to explore the engine's performance during dynamic pitch changes. This program would include testing the engine through the thrust reversing sequence.

COMPOSITE FAN BLADE MATERIALS AND IMPACT TESTS

As mentioned earlier, the Q-Fan demonstrator has composite fan blades. The engine studies have shown a decided advantage for composite fan blade materials for the low pressure ratio, low tip speed fans. Composite blades show a 3.3-percent direct operating cost improvement and an 11-percent engine thrust to weight ratio improvement

over hollow titanium blades (fig. 31). The thrust to weight ratio advantage for composites is large compared to the direct operating cost advantage due to the high cost of composites.

Composite blades have always been susceptible to foreign object damage especially in high speed CTOL engines. However, for the low tip speeds of low pressure ratio, quiet STOL fans, foreign object damage may not be as serious a problem. NASA has contracts with Hamiliton Standard, General Electric, and Pratt & Whitney to impact test composite blades at low tip speeds with objects ranging from small nuts and bolts to 4-pound birds.

Figure 32 shows an example of one of the blades to be tested in the program. This blade, made by Hamilton Standard, is a spar-shell construction. It has an airfoil shaped shell made of a composite material. The shell is bonded to a metallic spar running down the center of the blade.

Other blades to be tested include solid composite blades as well as titanium blades for comparison. The tests are scheduled to begin in November 1972.

PROPULSION OF EXTERNALLY BLOWN FLAP STOL WITH ENGINES MOUNTED OVER THE WING

The major advantage for mounting engines over the wing (OTW) instead of under the wing (UTW) for STOL aircraft is for noise reduction by shielding the aft fan noise and reducing the flap noise. The paper by Robert Dorsch and Meyer Reshotko indicates this is the situation. If noise is not a constraint, economic studies show there are many advantages of selecting the highest possible fan pressure ratio. But flap impingement noise limits fan pressure ratio. The OTW concept appears to offer some relief of this situation. To illustrate this point, UTW and OTW flap noises are compared at takeoff for four engines producing about 90 000 pounds thrust (fig. 33). Noise is shown as a function of installed exhaust velocity with design fan pressure ratio as a secondary scale. The OTW noise data were scaled from small scale model data with a few additional points in the band obtained from the recent larger scale tests. It must be considered preliminary. The externally blown flap propulsion system for the UTW installation indicated a fuel pressure ratio of about 1.25 is required to meet the noise goal. Mounting the engines over the wing reduces the flap noise allowing higher fan pressure ratios. For the same noise level used for the engines under the wing, a fan pressure ratio of about 1.3 can be used when the engines are over the wing. Despite some shielding of the aft machinery noise by the wing, considerable fan suppression, both front and aft, is still required to meet the noise goal.

A typical OTW installation is illustrated in figure 34. The installation shown is a General Electric approach. The engine is a fixed pitch fan with a 1.3 design fan

pressure ratio. The three inlet splitters are probably needed to suppress this fan to an acceptable level for either UTW or OTW installations. When this engine was installed under the wing, it required two splitters in the fan duct. A slight shielding of the aft noise and more duct area for wall suppression means one splitter can be used instead of two to meet the noise goal when the engines are mounted over the wing. The splitter removal improves installed performance by having less pressure losses in the duct.

The engine is mounted forward of the wing for two reasons. The rotating machinery is well ahead of the wing box structure to prevent wing damage in the event of an engine failure. Also, for maintenance purposes, the engine may be removed by dropping it straight down.

In this installation, a mixed flow engine is shown. The hot core gas is mixed with the cool fan air before exhausting through a single nozzle. A separated flow system may also be used, but care must be taken to avoid the hot core gas from scrubbing directly on the upper wing surface. Much testing must still be done to answer many unknowns for this type of installation and aircraft configuration. Some questions to be answered are the following:

What is the optimum shape of an exhaust nozzle to assure that the flow attaches to the upper surface of the wing?

What are the aircraft installation penalties associated with this system at high and low speeds?

Where is the optimum span and chordwise engine location?

Tests and analysis are currently in progress in an attempt to answer these questions because the noise benefit associated with this configuration appears promising.

To illustrate the total system noise advantage of the OTW engine installation, a noise footprint of an OTW STOL aircraft is compared with that of a UTW STOL aircraft during takeoff in figure 35. The noise contours are shown at a sideline distance from the runway centerline on the abscissa and along the flight path on the ordinate. All markings are shown in thousands of feet. Both aircraft meet the 95 EPNdB sideline noise goal. The UTW footprint is about 120 acres. The aircraft with the OTW engines has a 90-acre footprint or a 25-percent decrease. A similar change is evident from the 85 EPNdB contour.

Since a primary goal for STOL is low noise and small footprints, the STOL aircraft with the engines installed over the wing appears promising.

DIRECT OPERATING COST AS FUNCTION OF NOISE

The tradeoff of noise and direct operating cost is shown in figure 36 where relative direct operating cost is plotted against noise at a 500-foot sideline. The band shown on the figure represents a family of UTW externally blown flap engines optimized for a 0.8 cruise Mach number airplane. Figure 36 shows the relatively large direct operating

cost penalty paid to achieve the 95 EPNdB goal for externally blown flap STOL as compared with a goal only a few decibels higher.

This raises the question about relaxing the noise goal a few decibels to take advantage of this dramatic improvement in direct operating cost.

It should be pointed out, however, that the shape and level of the band in figure 36 are not precisely known and should reflect the uncertainties of the noise estimates as well as the assumptions used in the studies. Also, this figure is for UTW externally blown flap airplanes, and the direct operating cost advantages shown may not be as great for augmentor wing or OTW externally blown flap airplanes.

As an example, assume that relaxing the noise goal from 95 to 97 EPNdB means a significant reduction in direct operating costs. What does this do to the engine and to the corresponding airplane footprint?

A 95 and a 97 EPNdB engine are compared in figure 37. Both have the same fan pressure ratio of 1.25; but, as can be seen the nacelles and acoustic treatment are much different. The 97 EPNdB engine requires less treatment and, therefore, has a shorter nacelle. This saves on weight and results in less drag and internal pressure losses and, therefore, improves the direct operating costs.

When a 95 EPNdB airplane is compared to a 97 EPNdB airplane, the 95 EPNdB footprint area increases from 120 to 160 acres (fig. 38). A similar increase is shown for the 85 EPNdB footprint.

Based on this example comparison, a change in the required noise level is worth further consideration for UTW externally blown flap airplanes.

CONCLUSIONS

The studies have shown that STOL propulsion systems can be designed to meet the selected STOL noise and pollution goals while still achieving acceptable performance. The noise goal was shown to be difficult to achieve and to have a dominant influence on all the engine designs.

The more promising propulsion systems, as determined from the studies, are shown in figure 39 installed on representative externally blown flap and augmentor wing STOL aircraft (all drawn to the same scale). A Boeing 737, 115 to 120 passengers, two-engine CTOL aircraft is also shown for comparison.

The augmentor wing aircraft is shown with moderate bypass engines with a fan pressure ratio of about 3. The engines and installations appear to be fairly conventional.

This augmentor wing engine was selected because its direct operating cost is relatively low, it appears to be practical to quiet it, and the pressure ratio to the wing is high enough to permit reasonable wing and duct designs. While the engine itself is fairly conventional, the installation is not. The fan inlet requires extensive acoustic treatment

at the inlet, and it probably will operate with high subsonic Mach numbers in the inlet. The fan exhaust must be collected and ducted to the wing. The ability of the fan to operate with these complex inlet and exhaust systems must still be evaluated in system tests to establish the feasibility of the quiet augmentor wing propulsion system.

An externally blown flap aircraft with the engines under the wing is shown with high bypass engines with variable pitch fans with pressure ratios of about 1.25. The nacelles are very large compared with conventional CTOL engines.

This low pressure ratio variable pitch fan engine shows the most promise for this EBF STOL, despite its size, because of the following:

1. It should meet the noise goal without a costly velocity decayer.

2. The variable pitch feature eliminates the need for an expensive, heavy thrust reverser.

3. Fan machinery acoustic suppression requirements are not excessive, although it does appear that a slight relaxation of the noise goal would be very beneficial, particularly to this suppression design.

The variable pitch fan is very new. Fan aerodynamic, acoustic, and material development are still required, and system tests to investigate the operation of the fan and core engine in all forward and reverse modes are essential before the practicality of the concept is proven.

An externally blown flap aircraft with the engines over the wing is shown with siamese engine pods.

A design with the four engines in individual pods could also have been shown, as both versions are under investigation and each appears to offer distinct advantages.

The OTW externally blown flap installation has the advantage of reducing the jet flap noise and providing some shielding of the exhaust noise. This allows the noise goal to be met with a higher fan pressure ratio, and reduced noise suppression requirements; such conditions should improve the aircraft economics. More aircraft aerodynamic data are needed, and the engine installation needs further work. NASA is particularly concerned with the cruise performance of the engines and the exhaust configuration required to turn the jet at low speeds. Propulsion system tests are essential to evaluate these problems.

The quiet, clean STOL propulsion systems described show promise, but their designs are based largely on analysis and further component engine and propulsion system development and tests are required before their practicality is assured. NASA has initiated the quiet clean STOL experimental engine (QCSEE) program to provide the component engine and installation technology needed to provide confidence that practical, quiet, clean propulsion systems can be developed for STOL. The objectives of the QCSEE program (shown in fig. 40) are to (1) develop the missing component and engine

technology, (2) investigate engine quiet nacelles and aircraft installations, and (3) demonstrate with experimental engines and nacelles that the noise, pollution, and performance goals can be met.

Component technology development in support of QCSEE is already underway. Studies of QCSEE are being completed. A contract is expected to be let in 1973 for the development of the experimental engines which will demonstrate the systems capabilities by 1976.

REFERENCE

1. Roepcke, F. A.; and Kelley, G. S.: Design Integration and Noise Studies for Jet STOL Aircraft. Volume II – System Design and Evaluation Studies. D6-40552-2 (Contract NAS2-6344), Boeing Co., May 1972. (Available as NASA CR-114472.)

SUPPORTING CONTRACTS

STOL AIRCRAFT & SYSTEM STUDIES	MCDONNELL DOUGLAS
STOL AIRCRAFT & SYSTEM STUDIES	LOCKHEED
STOL PROPULSION SYSTEM STUDIES	ALLISON
STOL PROPULSION SYSTEM STUDIES	GENERAL ELECTRIC
AUGMENTOR WING STUDIES	BOEING
Q-FAN STUDIES & TESTS	HAMILTON STANDARD

Figure 1

BASELINE AIRCRAFT FOR DIRECT OPERATING COST CALCULATIONS

100 PASSENGER STOL AIRCRAFT

2000-FT FAA FIELD LENGTH

500-MILE RANGE

FUEL RESERVES FOR 200 MILES ADDITIONAL

95 EPNdB AT 500-FT SIDELINE

Figure 2

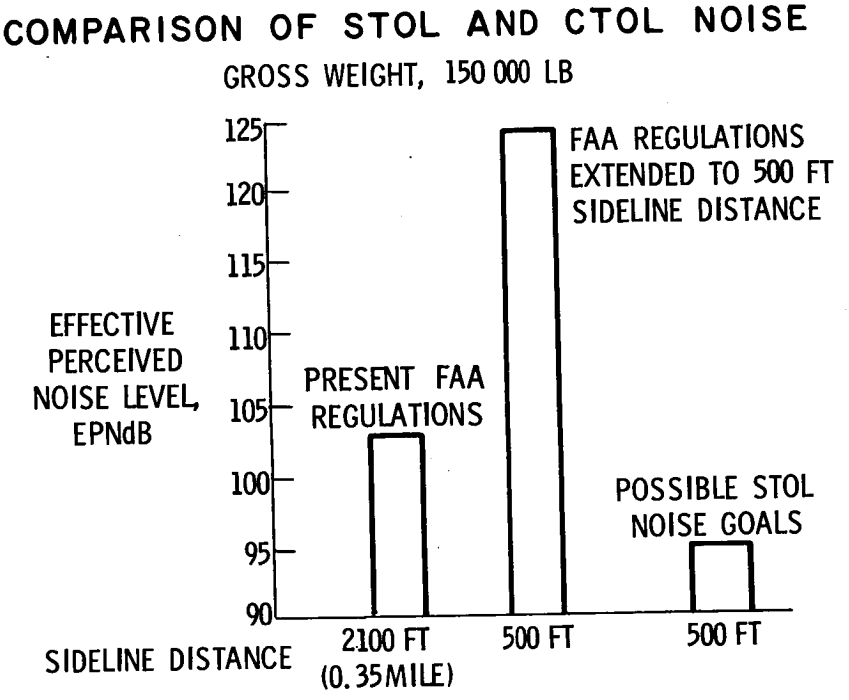

Figure 3

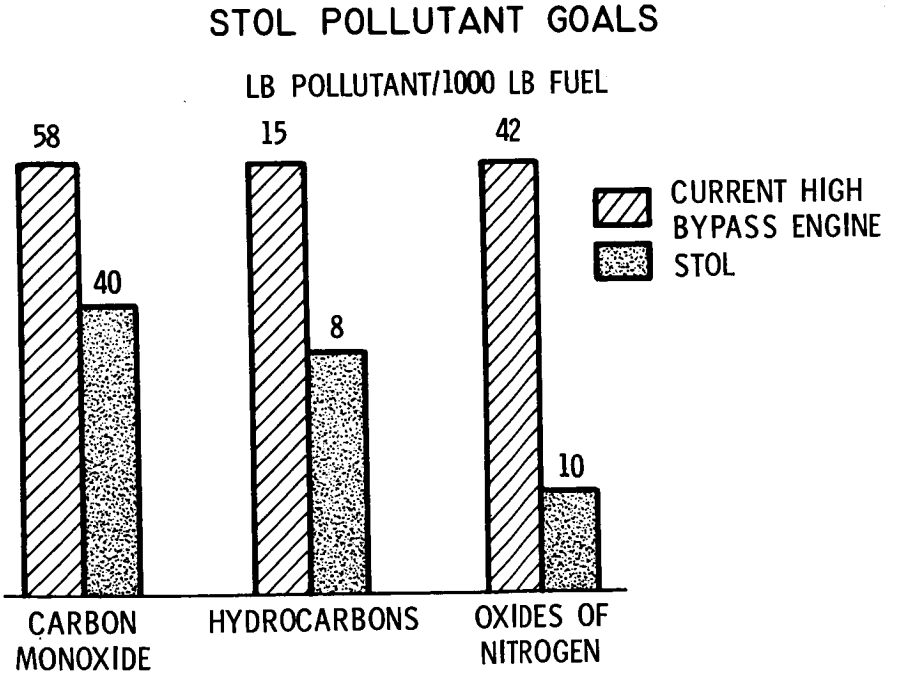

Figure 4

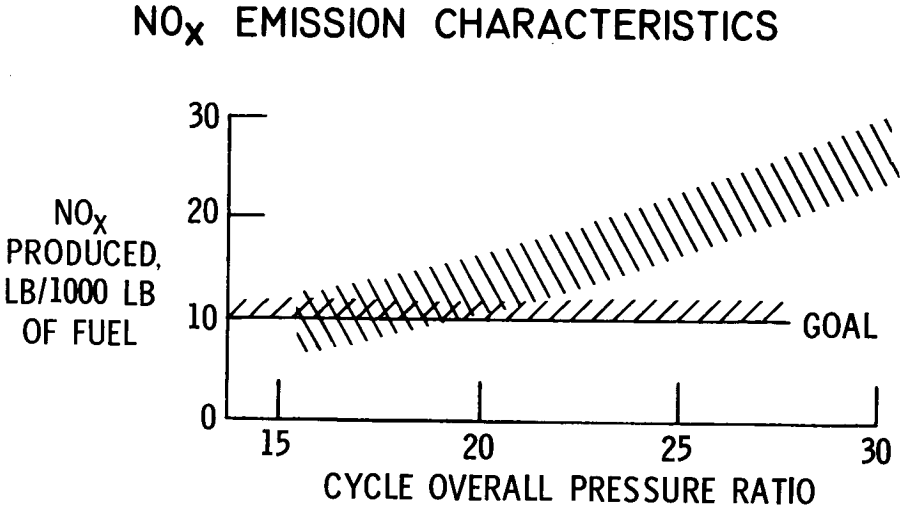

Figure 5

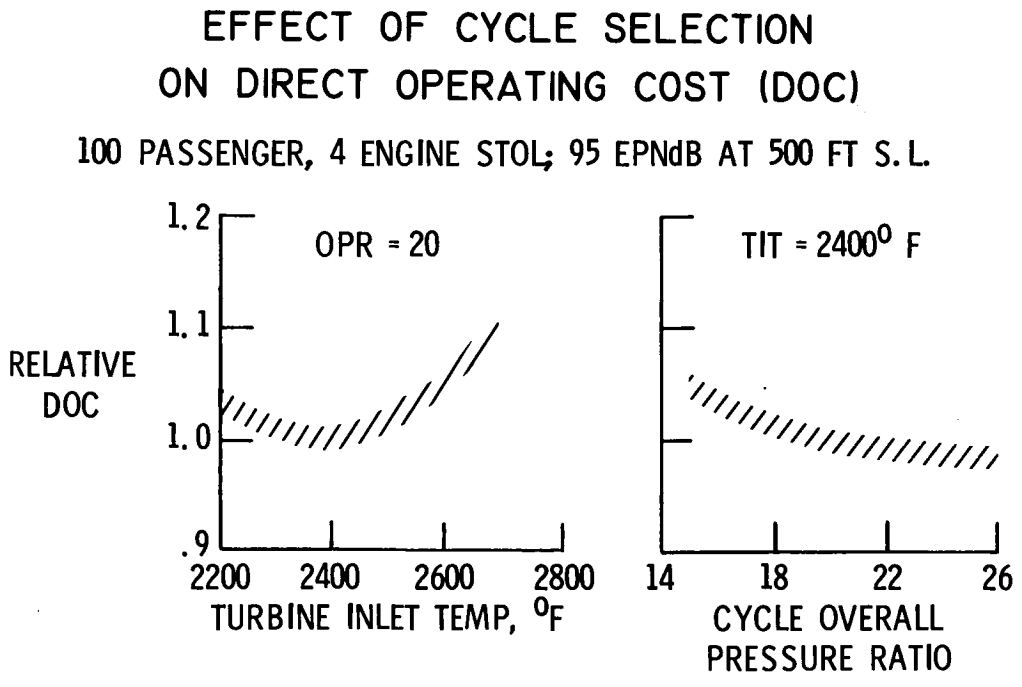

Figure 6

AUGMENTOR WING SYSTEM NOISE SOURCES

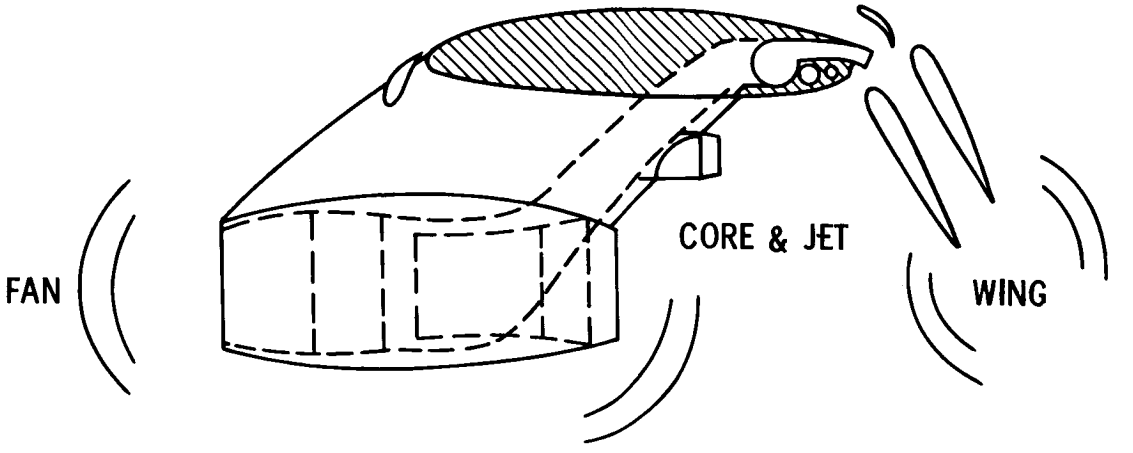

Figure 7

AUGMENTOR DUCT AND NOZZLE DETAILS

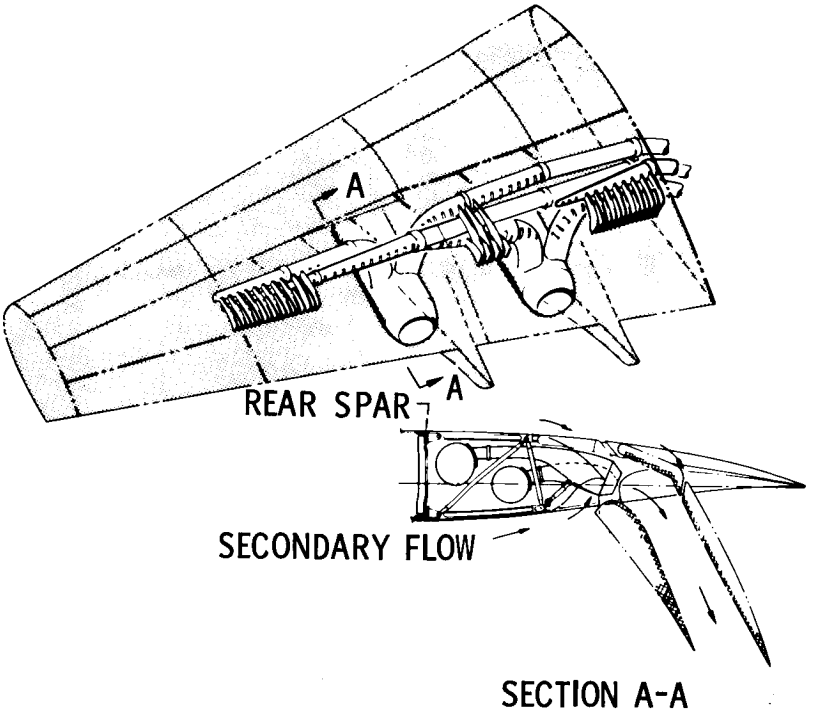

Figure 8

FAN PRESSURE RATIO AFFECTS WEIGHT

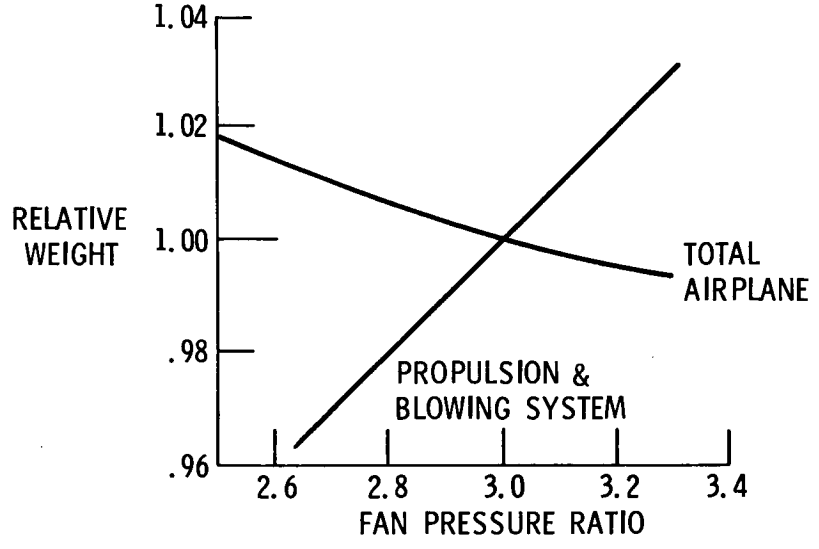

Figure 9

SUPPRESSED AUGMENTOR WING NOISE

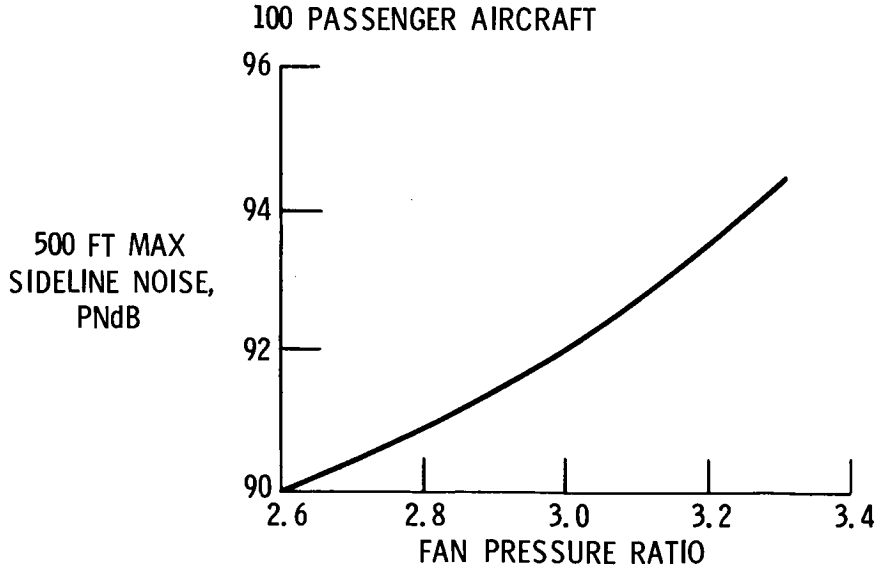

Figure 10

AUGMENTOR WING DIRECT OPERATING COSTS

100 PASSENGER AIRPLANE, 95 EPNdB

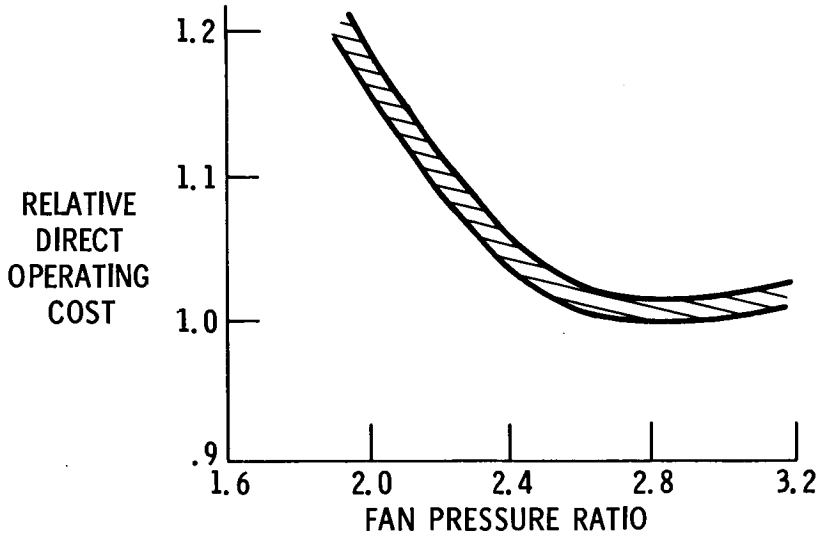

Figure 11

AUGMENTOR WING COMPONENT NOISE SOURCES

4 ENGINES, 80 KNOTS; 60 000 LB THRUST; 3.0 FAN PRESSURE RATIO

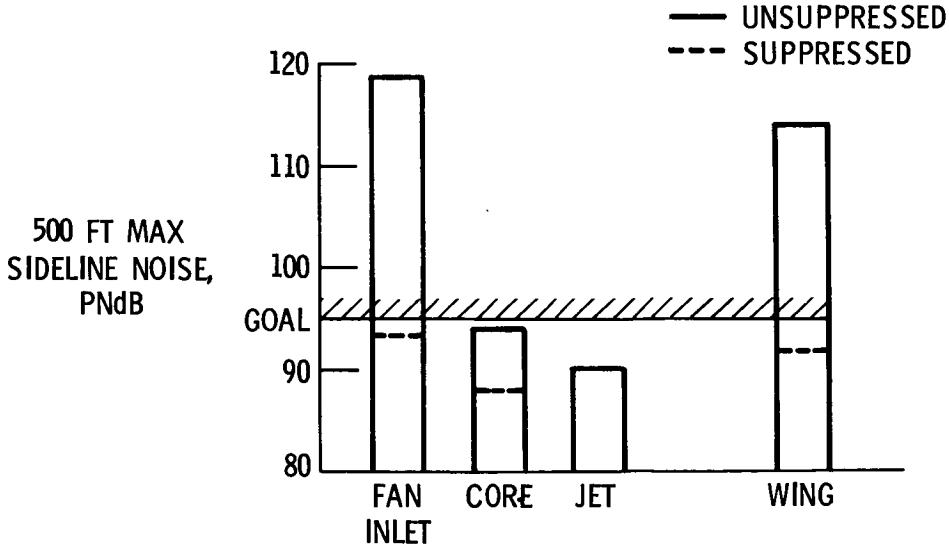

Figure 12

AUGMENTOR WING ENGINE
CYCLE CHARACTERISTICS

THRUST, LB	15 000
FAN PRESSURE RATIO	3.0
BYPASS RATIO	2.8
OVERALL PRESSURE RATIO	22
TURBINE INLET TEMP, ^{0}F	2300
THRUST TO WEIGHT	5.8
SFC AT TAKEOFF, LBF/HR/LBT	0.54

Figure 13

AUGMENTOR WING ENGINE

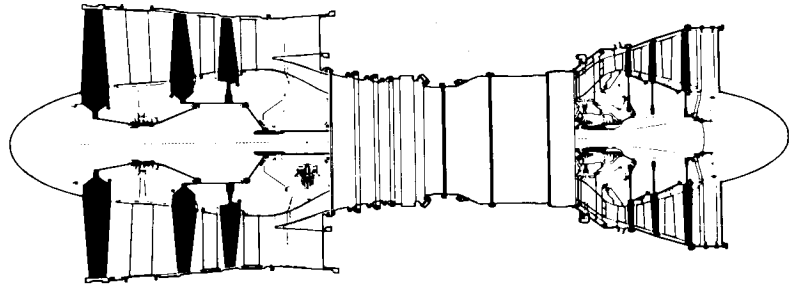

Figure 14

TYPICAL AUGMENTOR WING ENGINE

VARIABLE INLET

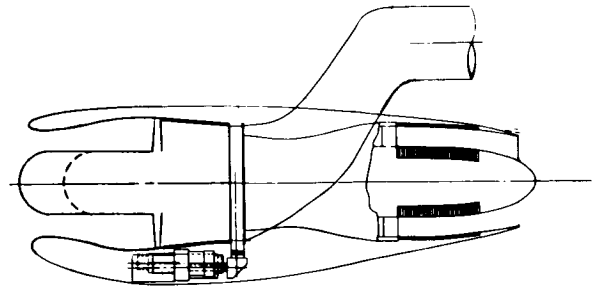

Figure 15

TYPICAL AUGMENTOR WING ENGINE

FIXED GEOMETRY INLET

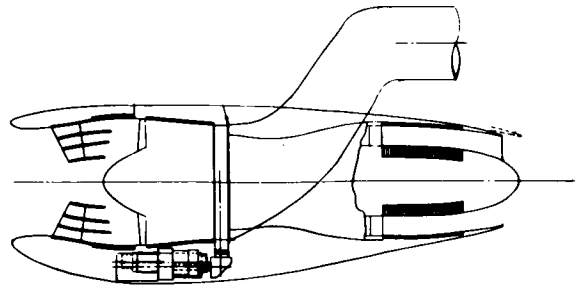

Figure 16

EBF UNDER THE WING NOISE SOURCES

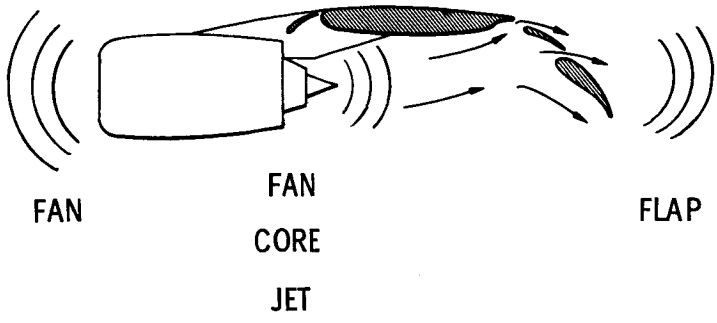

Figure 17

EBF FLAP NOISE

4 ENGINES, 90 000-LB THRUST AT TAKEOFF

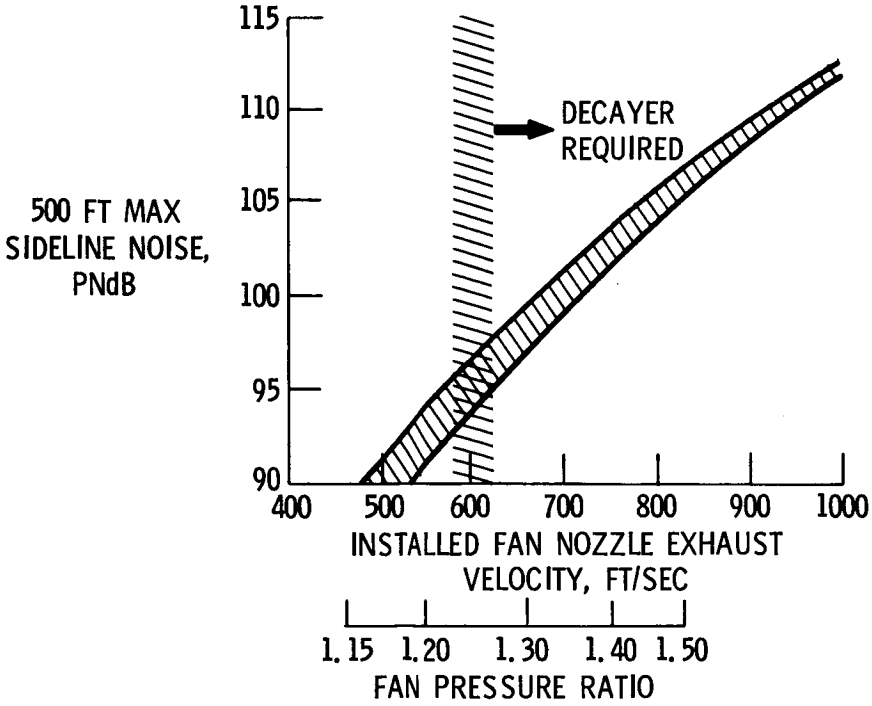

Figure 18

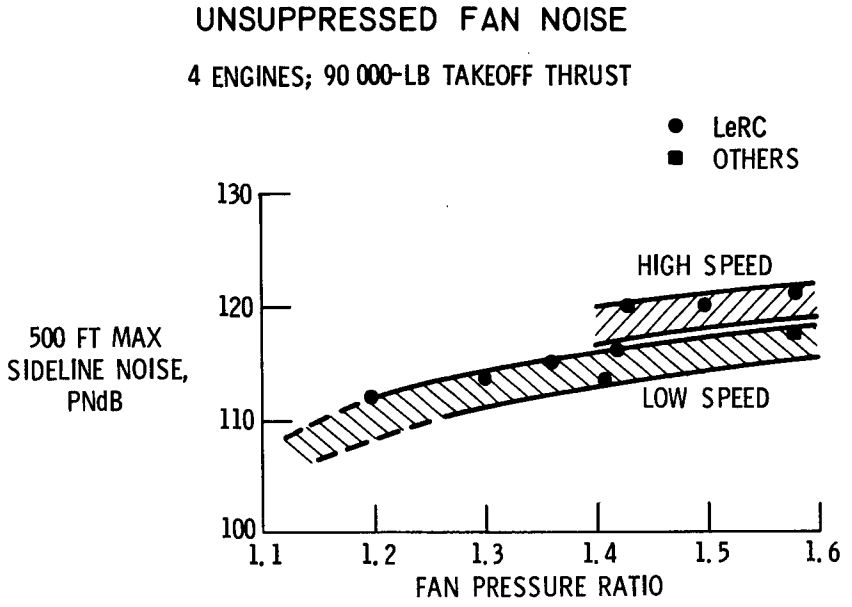

Figure 19

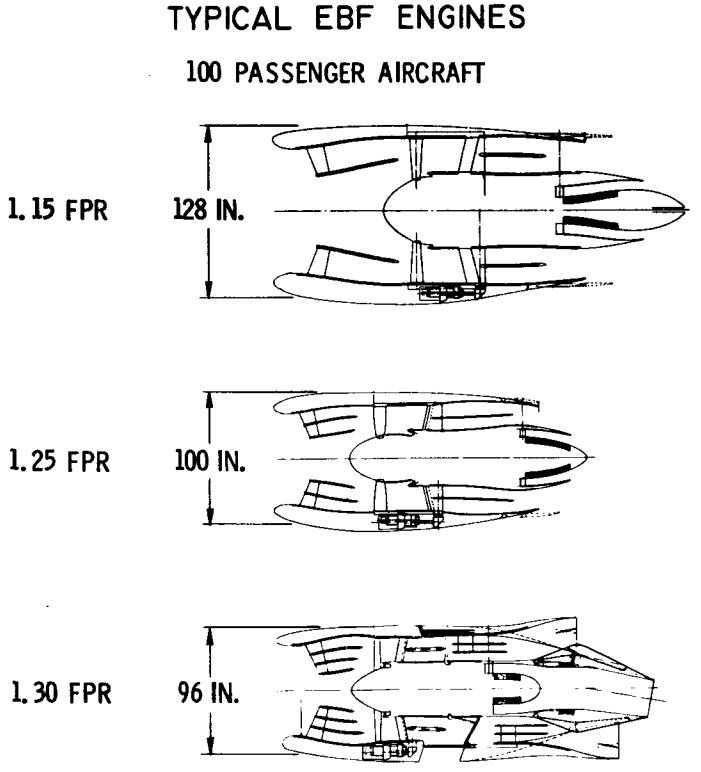

Figure 20

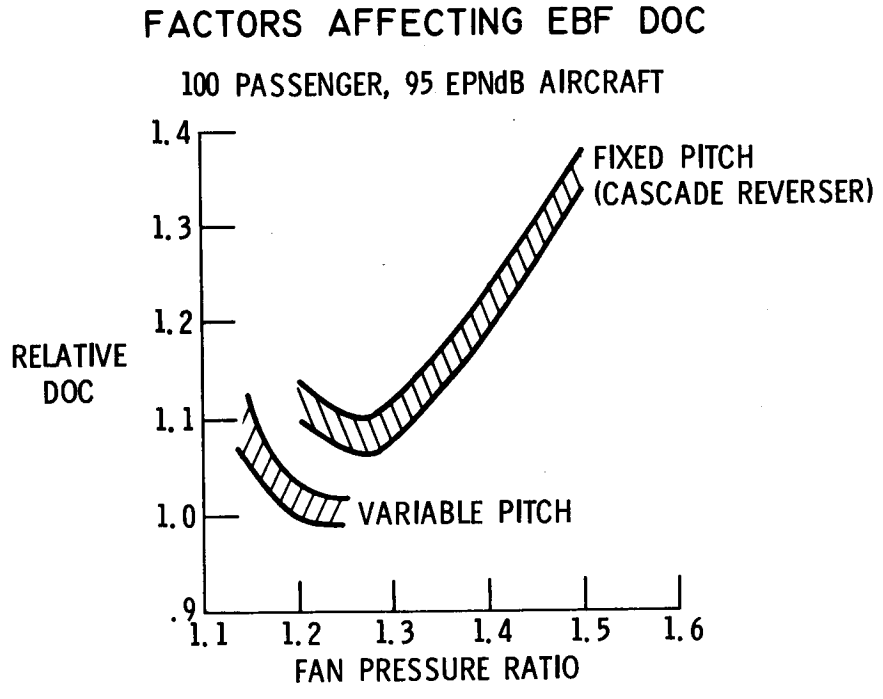

Figure 21

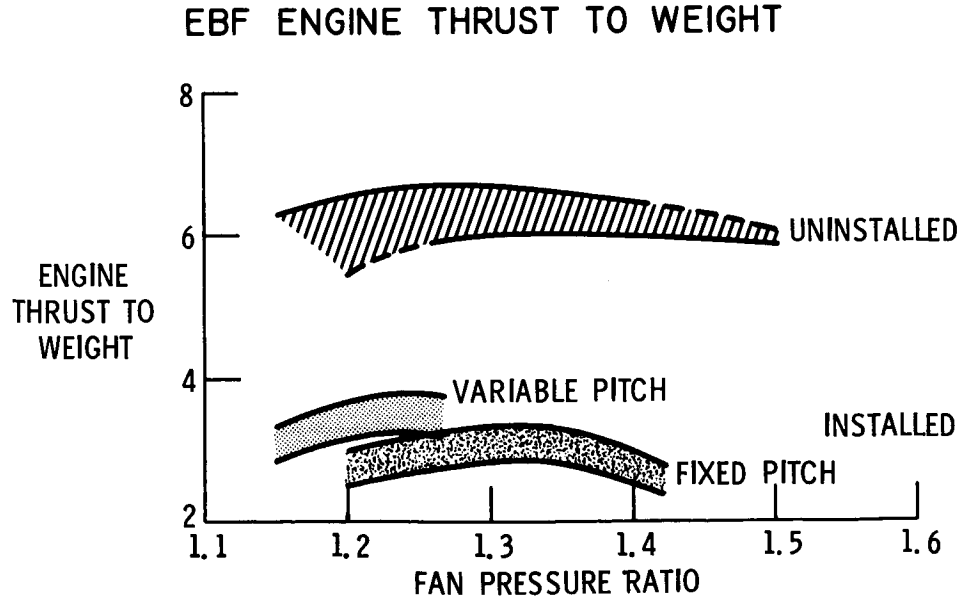

Figure 22

EBF CRUISE MACH NO. CONSTRAINT

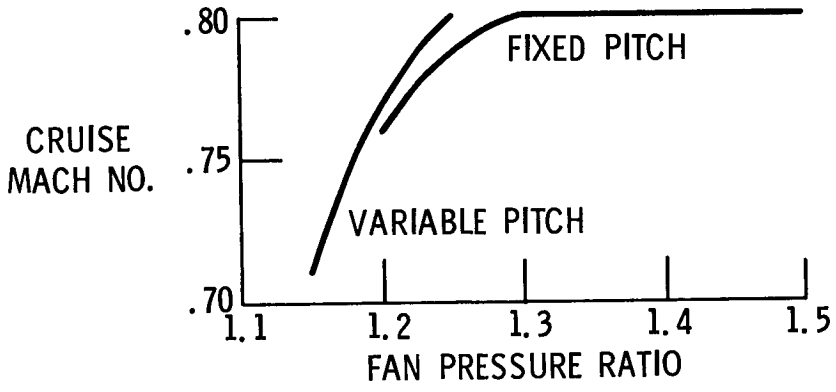

Figure 23

TYPICAL VARIABLE PITCH FAN ENGINE CYCLE CHARACTERISTICS

THRUST, LB	22 500
FAN PRESSURE RATIO	
TAKEOFF	1.25
CRUISE	1.29
BYPASS RATIO	17
OVERALL PRESSURE RATIO	20
TURBINE INLET TEMP, ^{0}F	2400
THRUST/WEIGHT	6.6
SFC AT TAKEOFF, LBF/HR/LBT	0.23

Figure 24

VARIABLE PITCH FAN ENGINE

EBF AIRCRAFT

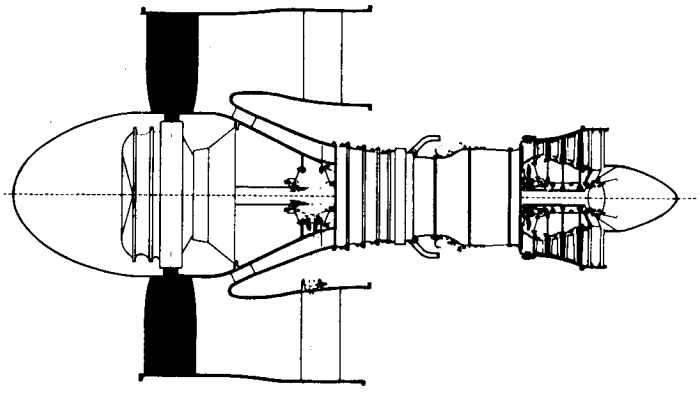

Figure 25

VARIABLE PITCH FAN ENGINE

EBF AIRCRAFT

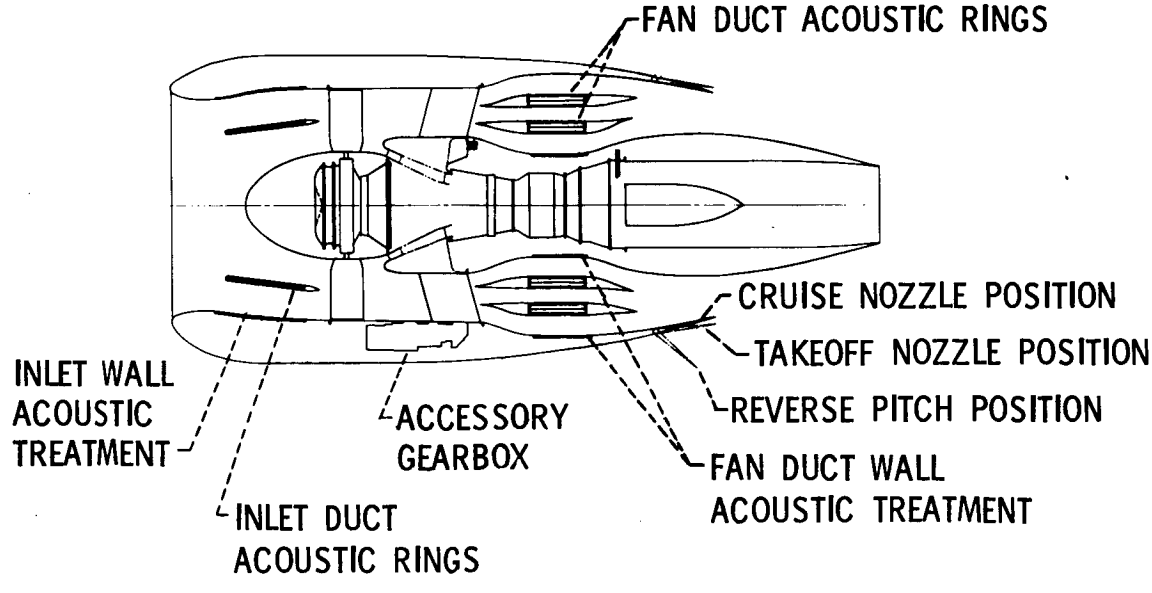

Figure 26

Q-FAN DEMONSTRATOR

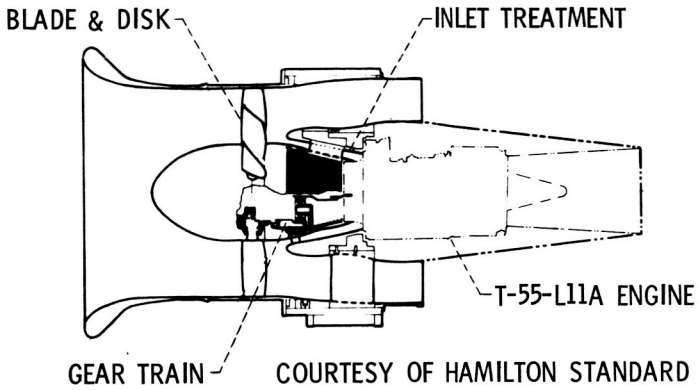

Figure 27

Q-FAN DEMONSTRATOR ON TEST STAND

Figure 28

Q-FAN DEMONSTRATOR WITHOUT INLET SHROUD

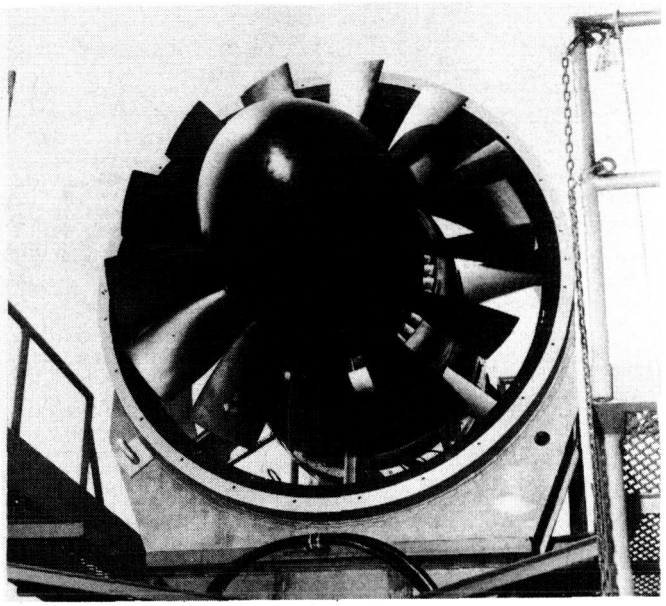

Figure 29

Q-FAN DEMONSTRATOR TEST PLAN

FORWARD THRUST MODE			
TEST CONDITIONS		TESTS COMPLETED/PLANNED	
ROTOR BLADE ANGLE, DEG	FAN TIP SPEED, FT/SEC	PERFORMANCE & STRUCTURAL	ACOUSTIC
37 (APPROACH)	400-810	●	○
42	400-810	●	○
47	400-810	●	○
52 (TAKEOFF)	400-810	●	○
57	400-750	●	○
REVERSE THRUST MODE			
134	500-810	○	○
138	500-810	○	○
142	500-810	○	○
146	500-810	○	○
150	500-810	●	○

○ PLANNED
● TESTED AS OF 10/9/72

Figure 30

BENEFITS OF COMPOSITE MATERIALS

FOR FAN BLADES

V. P. 1.25 P. R. FAN ENGINE

100 PASSENGER AIRPLANE

ΔDOC -3.3%

ΔT/W +11%

Figure 31

COMPOSITE BLADE FOR IMPACT TESTING

Figure 32

EBF FLAP NOISE AT TAKEOFF

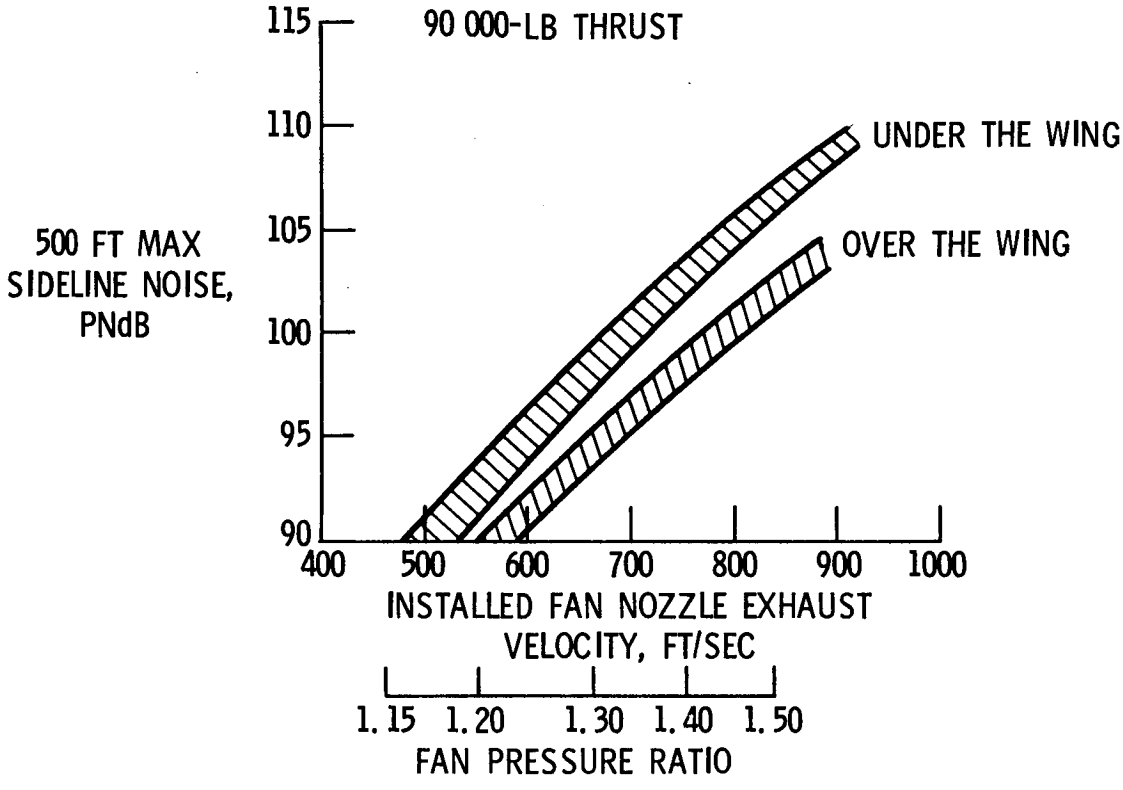

Figure 33

TYPICAL EBF ENGINE

OVER-THE-WING

1.3 FAN PRESSURE RATIO

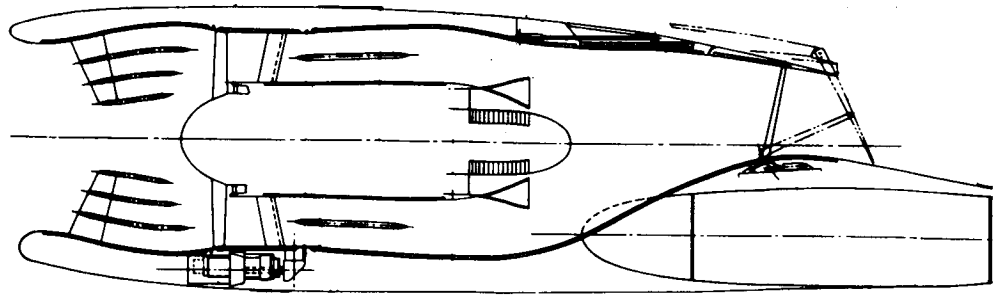

Figure 34

EBF TAKEOFF FOOTPRINT COMPARISON

FOOTPRINT AREAS
ACRES

	95 EPNdB	85 EPNdB
OTW	90	680
UTW	120	1020

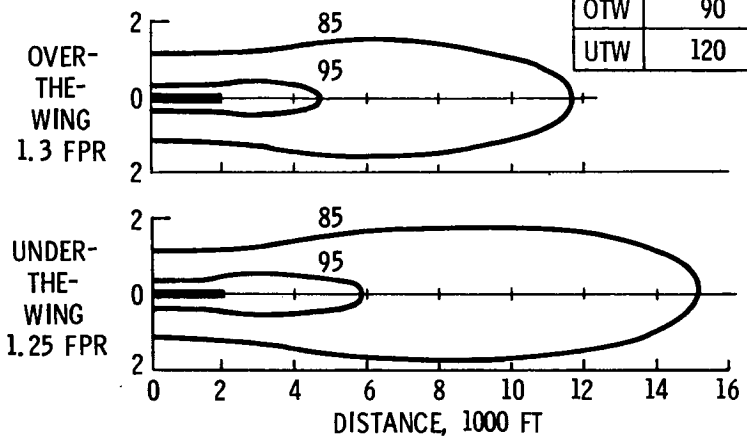

Figure 35

EFFECT OF NOISE ON DOC

EBF UNDER THE WING; 0.8 CRUISE MACH NO. AIRPLANE; 4 ENGINES, 80 KNOTS

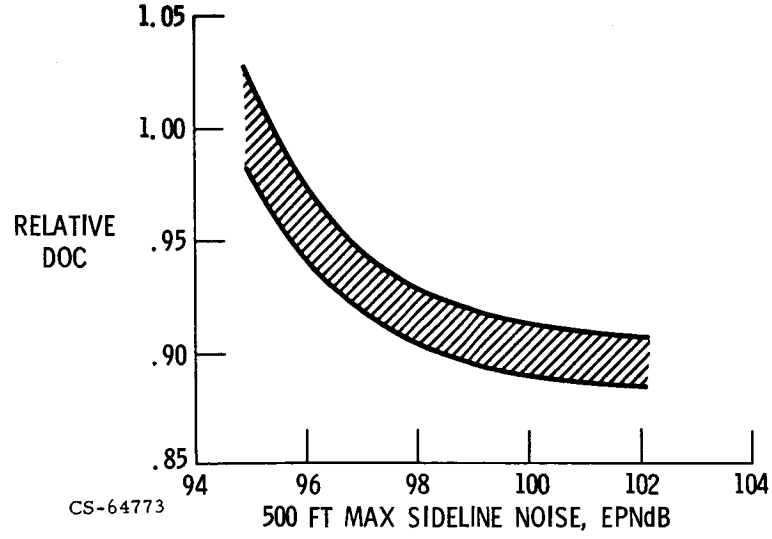

Figure 36

EFFECT OF NOISE GOAL ON ENGINE INSTALLATION

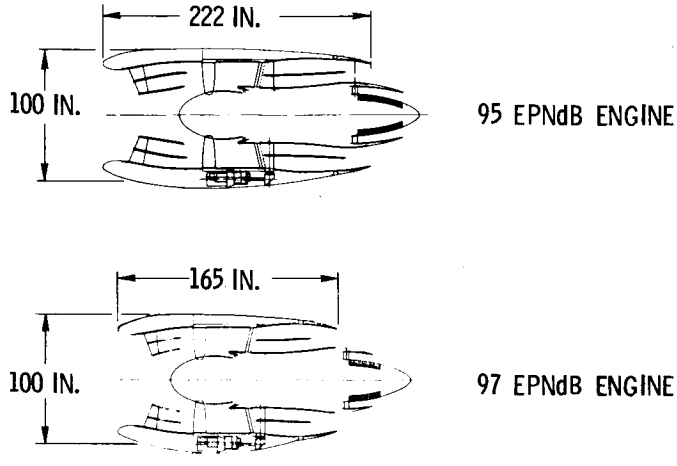

Figure 37

TAKEOFF FOOTPRINT COMPARISON OF 95 AND 97 EPNdB AIRPLANES

EBF, UNDER THE WING

FOOTPRINT AREAS, ACRES

	95 EPNdB FOOTPRINT	85 EPNdB FOOTPRINT
95 EPNdB AIRPLANE	120	1020
97 EPNdB AIRPLANE	160	1200

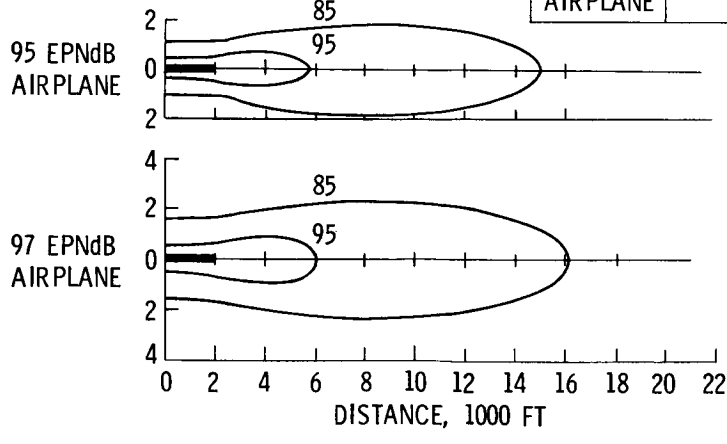

Figure 38

STOL AND CTOL AIRCRAFT

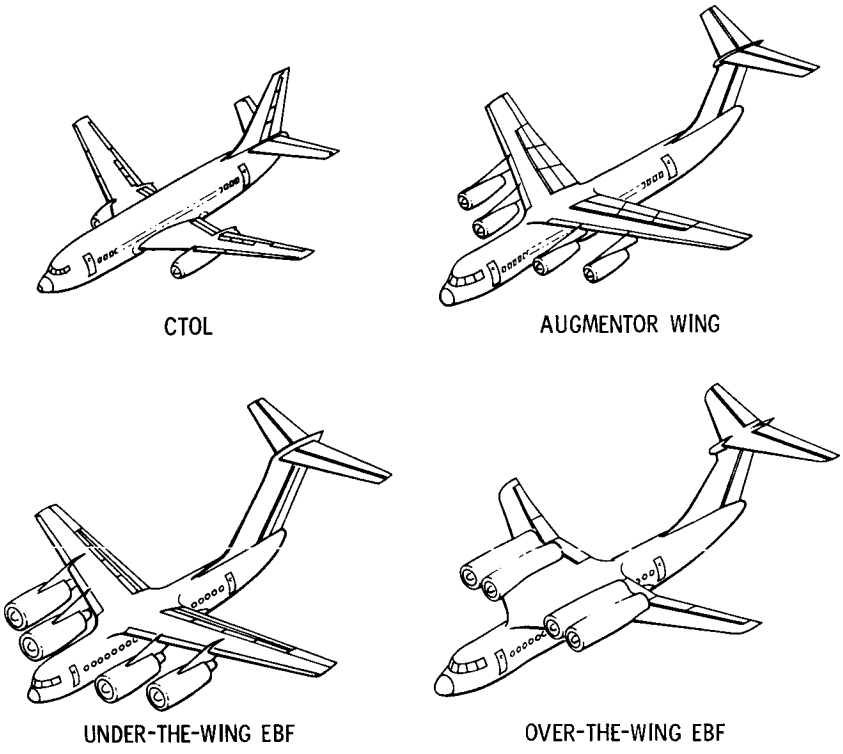

Figure 39

QUIET CLEAN STOL EXPERIMENTAL ENGINE
(QCSEE) PROGRAM
OBJECTIVES

1. DEVELOP THE MISSING PROPULSION SYSTEM TECHNOLOGY

2. INVESTIGATE STOL ENGINE INSTALLATION PROBLEMS

3. DEMONSTRATE THAT STOL NOISE, POLLUTION, & PERFORMANCE GOALS CAN BE MET

Figure 40

ERRATA

NASA Special Publication SP-320

STOL TECHNOLOGY

1972

In Paper No. 5 entitled "Aerodynamic and Performance Characteristics of Externally Blown Flap Configurations" by William G. Johnson, Jr., replace figure 5 on page 50 with the following figure:

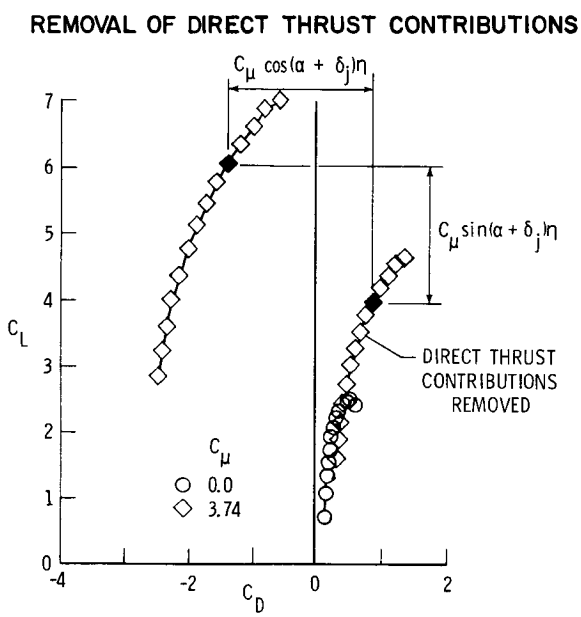

Figure 5

In Paper No. 31 entitled "Acoustic Characteristics of Large-Scale STOL Models at Forward Speed" by Michael D. Falarski, Kiyoshi Aoyagi, and David G. Koenig, the following corrections should be made:

Page 443, line 2 of third paragraph: Change "1.8" to "1.9"

Page 443, line 3 of third paragraph: Change "2 to 3" to "3 to 5"

Page 445, line 3 of third complete paragraph: Change "leading-edge" to "loading"

Page 446, line 4 of third paragraph: Change "3" to "5"

Page 447, line 3 of last paragraph: Change "1.8" to "1.9"

Page 447, line 4 of last paragraph: Change "3" to "5"